CYTOSKELETON DYNAMICS AS MASTER REGULATOR OF ORGANELLE REORGANIZATION AND INTRACELLULAR SIGNALING FOR CELL-CELL COMPETITION

EDITED BY: Noa B. Martin-Cofreces, Pedro Roda-Navarro and Francisco Sanchez-Madrid

PUBLISHED IN: Frontiers in Cell and Developmental Biology

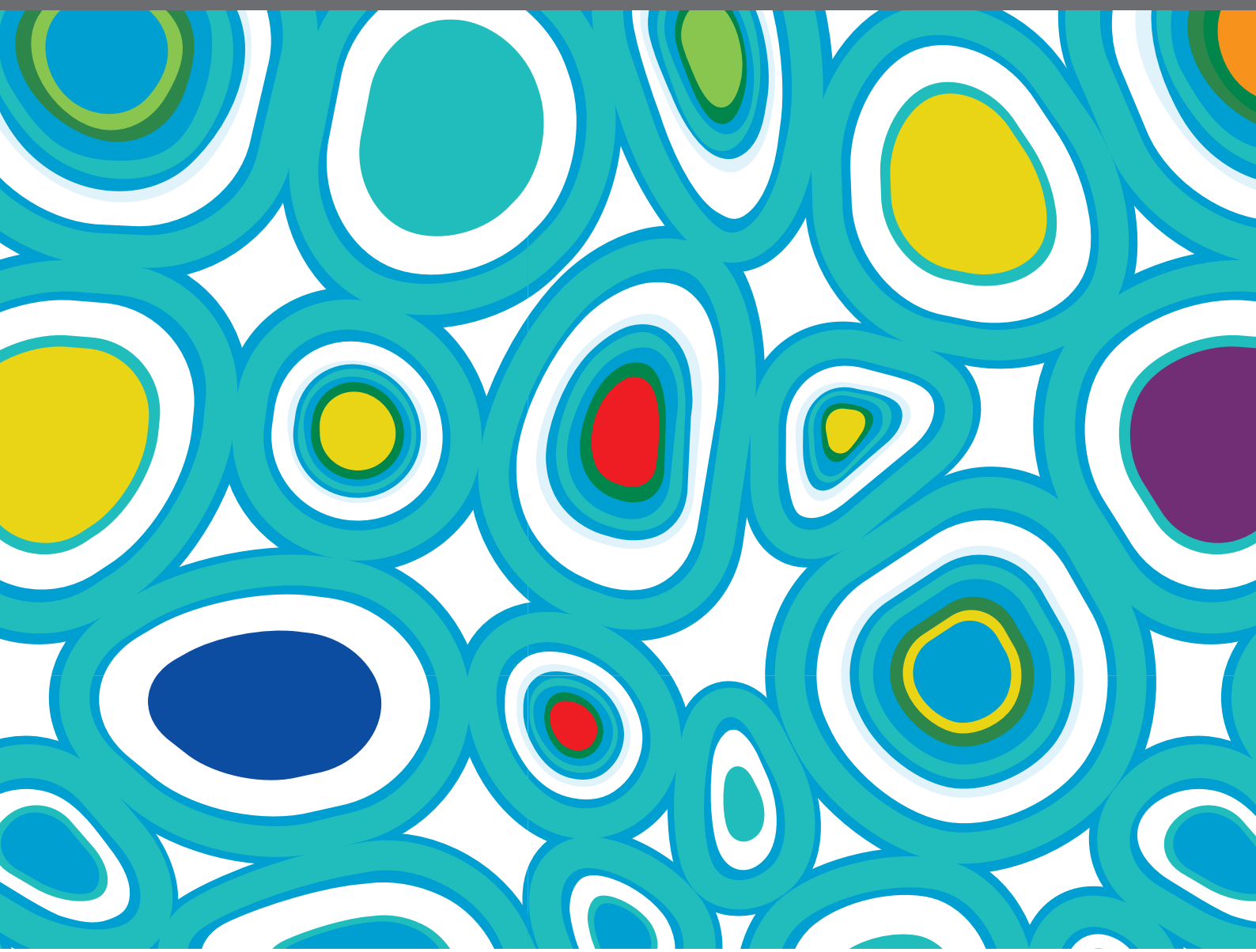

frontiers Research Topics

ISSN 1664-8714
ISBN 978-2-88971-898-6
DOI 10.3389/978-2-88971-898-6

About Frontiers

Frontiers is more than just an open-access publisher of scholarly articles: it is a pioneering approach to the world of academia, radically improving the way scholarly research is managed. The grand vision of Frontiers is a world where all people have an equal opportunity to seek, share and generate knowledge. Frontiers provides immediate and permanent online open access to all its publications, but this alone is not enough to realize our grand goals.

Frontiers Journal Series

The Frontiers Journal Series is a multi-tier and interdisciplinary set of open-access, online journals, promising a paradigm shift from the current review, selection and dissemination processes in academic publishing. All Frontiers journals are driven by researchers for researchers; therefore, they constitute a service to the scholarly community. At the same time, the Frontiers Journal Series operates on a revolutionary invention, the tiered publishing system, initially addressing specific communities of scholars, and gradually climbing up to broader public understanding, thus serving the interests of the lay society, too.

Dedication to Quality

Each Frontiers article is a landmark of the highest quality, thanks to genuinely collaborative interactions between authors and review editors, who include some of the world's best academicians. Research must be certified by peers before entering a stream of knowledge that may eventually reach the public - and shape society; therefore, Frontiers only applies the most rigorous and unbiased reviews.
Frontiers revolutionizes research publishing by freely delivering the most outstanding research, evaluated with no bias from both the academic and social point of view. By applying the most advanced information technologies, Frontiers is catapulting scholarly publishing into a new generation.

What are Frontiers Research Topics?

Frontiers Research Topics are very popular trademarks of the Frontiers Journals Series: they are collections of at least ten articles, all centered on a particular subject. With their unique mix of varied contributions from Original Research to Review Articles, Frontiers Research Topics unify the most influential researchers, the latest key findings and historical advances in a hot research area! Find out more on how to host your own Frontiers Research Topic or contribute to one as an author by contacting the Frontiers Editorial Office: frontiersin.org/about/contact

CYTOSKELETON DYNAMICS AS MASTER REGULATOR OF ORGANELLE REORGANIZATION AND INTRACELLULAR SIGNALING FOR CELL-CELL COMPETITION

Topic Editors:
Noa B. Martin-Cofreces, Princess University Hospital, Spain
Pedro Roda-Navarro, Universidad Complutense de Madrid, Spain
Francisco Sanchez-Madrid, Autonomous University of Madrid, Spain

Citation: Martin-Cofreces, N. B., Roda-Navarro, P., Sanchez-Madrid, F., eds. (2021). Cytoskeleton Dynamics as Master Regulator of Organelle Reorganization and Intracellular Signaling for Cell-Cell Competition.
Lausanne: Frontiers Media SA. doi: 10.3389/978-2-88971-898-6

Table of Contents

frontiers in Cell and Developmental Biology

EDITORIAL
published: 28 October 2021
doi: 10.3389/fcell.2021.782559

Editorial: Cytoskeleton Dynamics as Master Regulator of Organelle Reorganization and Intracellular Signaling for Cell-Cell Competition

Noa B. Martin-Cofreces[1,2,3*†], *Francisco Sanchez-Madrid*[1,2,3*†] *and Pedro Roda-Navarro*[4,5*†]

[1] Department of Immunology, Hospital Universitario de la Princesa, Universidad Autónoma de Madrid, Instituto de Investigación Sanitaria Princesa (IIS-IP), Madrid, Spain, [2] Centro de Investigación Biomédica en Red de Enfermedades Cardiovasculares (CIBERCV), Madrid, Spain, [3] Centro Nacional de Investigaciones Cardiovasculares (CNIC), Madrid, Spain, [4] Department of Immunology, Ophthalmology and ENT, School of Medicine, Universidad Complutense de Madrid, Madrid, Spain, [5] 12 de Octubre Health Research Institute (Imas12), Madrid, Spain

Keywords: cytoskeleton, actin, tubulin, cell-cell competition, adhesion, migration, post-translational modifications

OPEN ACCESS

Edited and reviewed by:
Claudia Tanja Mierke, Leipzig University, Germany

***Correspondence:**
Noa B. Martin-Cofreces
noa.martin@salud.madrid.org
Pedro Roda-Navarro
proda@med.ucm.es
Francisco Sanchez-Madrid
fsmadrid@salud.madrid.org

†These authors have contributed equally to this work

Specialty section:
This article was submitted to Cell Adhesion and Migration, a section of the journal Frontiers in Cell and Developmental Biology

Received: *24 September 2021*
Accepted: *30 September 2021*
Published: *28 October 2021*

Citation:
Martin-Cofreces NB, Sanchez-Madrid F and Roda-Navarro P (2021) Editorial: Cytoskeleton Dynamics as Master Regulator of Organelle Reorganization and Intracellular Signaling for Cell-Cell Competition. Front. Cell Dev. Biol. 9:782559. doi: 10.3389/fcell.2021.782559

Editorial on the Research Topic

Cytoskeleton Dynamics as Master Regulator of Organelle Reorganization and Intracellular Signaling for Cell-Cell Competition

The term cell-cell competition, meaning that cell growth and survival is affected by neighboring cells, was used to describe the consequences of this heterogeneous cell environment unveiled through the study of genetic mosaics of *Drosophila melanogaster* (Morata and Ripoll, 1975). In this regard, the organization of multicellular organisms relies on cell–cell interactions involving possible competition between individual somatic cells (Belardi et al., 2020). For example, many neurons compete for the same target to survive during the development of the nervous system (Buss et al., 2006) and the viability of thymocyte clones depends on the establishment of specific cell interactions for the engagement of the correct antigen (Kurd and Robey, 2016). Cell-cell competition may rely on regulators of cell signaling, gene expression or the cytoskeleton, such as vav1 (Tybulewicz et al., 2003), WASp and N-WASp (Cotta-de-Almeida et al., 2007). During the organization of the immunological synapse (IS), a proper regulation of actin and tubulin cytoskeletons is required to achieve full activation, thereby orchestrating the organization of the receptors and organelles essential for effector functions (Martín-Cófreces et al., 2011).

In this collection of articles (**Figure 1**), Lachowski et al. show that G-Protein-coupled Estrogen Receptor (GPER) activation down-regulates actin dynamics through RhoA phosphorylation at Ser188 and binding to Rho-GDI. The RhoA/mDia pathway is preferentially used by GPER, rather than ROCK/myosin-II, facilitating stress fiber and lamellipodia disorganization in fibroblasts. These data indicate that estrogens can regulate the actin cytoskeleton stiffness, modifying the cell shape and fitness, and point to differential regulation of cell adhesion and migration on different substrates depending on relative cell expression of GPER. Different receptors control actin organization and mechanotransduction in cells, which is now known to affect gene expression through factors such as MRTF/SRF (myocardin-related transcription factor/serum response factor) (Esnault et al., 2014) and YAP/TAZ [Yes-associated protein (YAP) and its homolog transcriptional co-activator with PDZ-binding motif (TAZ, also called WWTR1)] (Dupont et al., 2011). In this regard, Antón and Wandosell review the role of WIP and YAP/TAZ in the connection of the actin cytoskeleton and the development of the nervous system. The role of nuclear *vs.* cytoplasmic actin

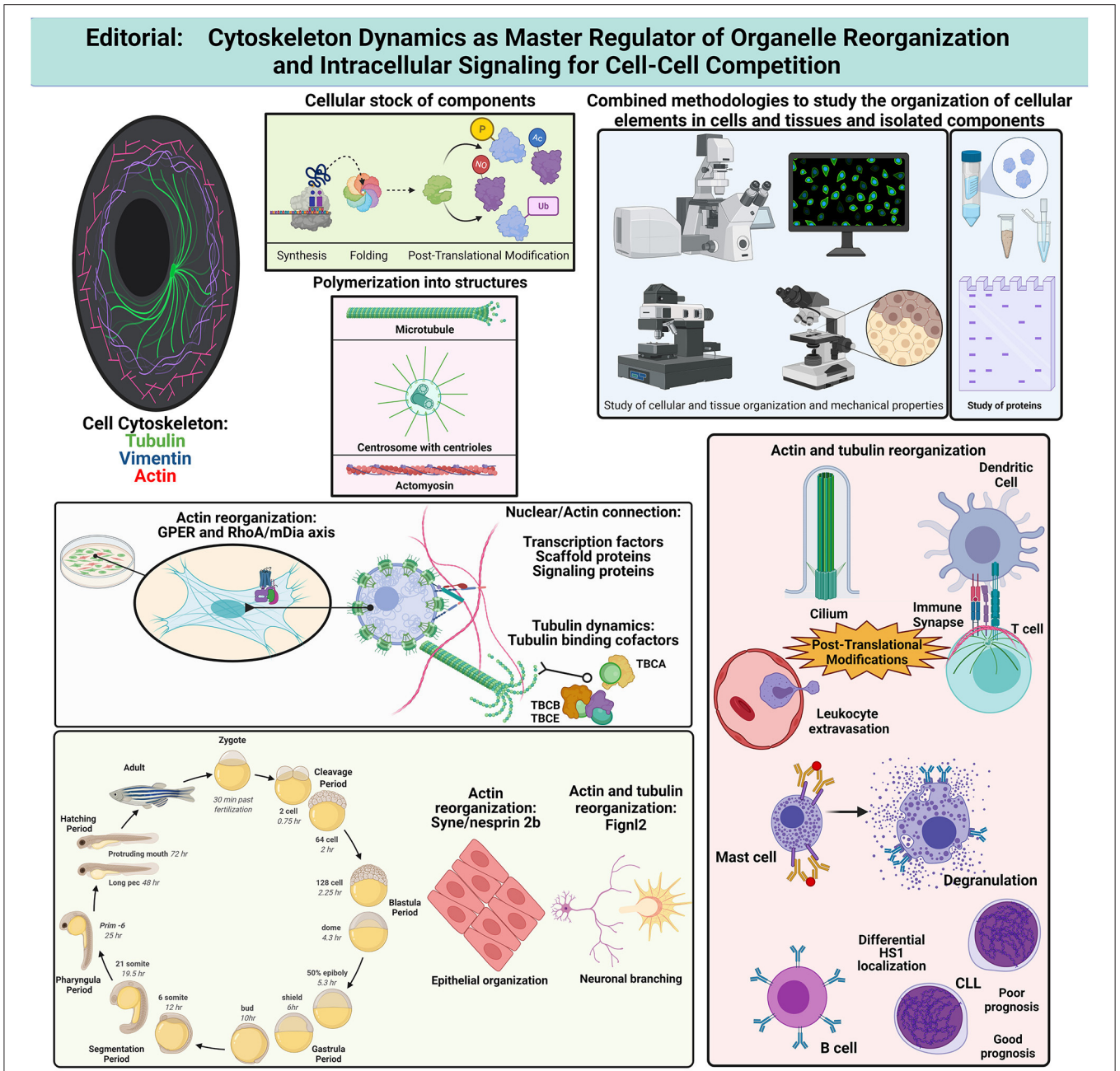

FIGURE 1 | It summarizes the concepts and findings described in the collection of articles pertaining to the Research Topic published in Frontiers in Cell and Developmental Biology, 2021. Created with BioRender.com. Ac, acetylation; CLL, chronic lymphocytic leukemia; Fignl2, fidgetin-like 2; GPER, G-Protein-coupled Estrogen Receptor; HS1, hematopoietic cell-specific lyn substrate-1; mDia, mammalian Diaphanous; NO, S-nitrosylation; P, phosphorylation; RhoA, Ras homolog family member A; TBC, tubulin-binding cofactor; Ub, ubiquitylation.

is discussed in the context of the YAP transcriptional pathway regulation during neurite development and transformation of astrocytes into glioblastoma. Authors conclude that WIP regulates nuclear shuttling of MRTF/SRF and YAP/TAP through actin polymerization, and highlight some unclear aspects of the regulation of the YAP/TAZ pathway in neurons, astrocytes and leukocytes. The connection between the actin cytoskeleton and the nuclear envelope determines cell shape (Gruenbaum et al., 2015) and regulates cell ability to migrate through constrained spaces (Lomakin et al., 2020; Venturini et al., 2020).

Li et al. address the study of the protein nesprin-2 (Syne2b), which is an outer nuclear membrane protein that interacts with actin during Zebrafish development (Davidson and Cadot, 2021). Maternal Syne2b/nesprin-2 is required to preserve the epithelial

integrity during blastoderm formation. Embryos with defective *Syne2b*/nesprin-2 show delayed progression of the epiboly due to F-actin defective organization. F-actin appears concentrated at multiple cell contacts in defective embryos instead of organizing into the usual polygonal shape. Dong et al. describe a regulatory role for the microtubule severing protein fidgetin-like 2 (Fignl2) in endothelial and neuronal cell branching during Zebrafish development. Sampietro et al. identify by STED microscopy a differential distribution of hematopoietic cortactin homolog HS1 in B cells from chronic lymphocytic leukemia (CLL) patients with poor prognosis. CLL cells show accumulation of HS1 at central regions of the cell in addition to the adhesive basal region observed in cells from healthy or CCL patients with good-prognosis. At adhesion sites, an interaction with vimentin is detected through FLIM-FRET assays. Therefore, the use of super-resolution techniques and sensors of proximity allows finding subtle, though relevant, changes in the molecular organization of the cell that might be the basis of new tumor-specific diagnosis and therapies.

Calvo and Izquierdo discuss the qualitative and quantitative differences in the organization of actin-based structures, such as actomyosin arcs, lamellipodia, or filopodia, at different areas on the T cell side of the IS in the context of secretion. During IS assembly, immune cells reorganize their membranes and organelles. The role of actin cytoskeleton in organizing the IS is still matter of study in different immune cells—T, B, or NK cells arrange their receptors and organelles for directed secretion (Soares et al., 2013; Martín-Cófreces et al., 2014). In this context, Capitani et al. recapitulate the current knowledge on the regulation of endosome function and their regulation by actin dynamics at the IS, as well as their ability to induce actin polymerization. This review article highlights the role of endosomes in the recycling of receptors, as well as in promoting long-term T cell activation.

On the other side of the IS, the actin dynamics also plays relevant roles, which are discussed by Rodríguez-Fernández and Criado-García. This review shows that the organization of the actin cytoskeleton in dendritic cells is relevant to allow correct T cell activation. Immune responses rely on the secretion of mediators, which can be pro-inflammatory. In the case of mast cell degranulation, they trigger allergic responses. In this regard, Ménasché et al. review the coordination of cytoskeletal dynamics and the secretory machinery during stress granule secretion induced by FcεR activation upon allergen engagement. FcεR signals through pathways leading to actin and microtubule reorganization, which resembles the process observed after T and B cell activation.

The regulation of actin dynamics by post-translational modifications (PTMs) is approached by Bago et al.. These authors review the role of nitric oxide and electrophilic cyclopentenone prostaglandins in PTMs of actin and actin binding proteins that facilitate actin depolymerization, ultimately reducing cell adhesion and motility. The effect of these PTMs is discussed in the context of cell-cell communication during endothelial modification to facilitate lymphocyte transmigration and IS formation. The IS and the cilia share a number of features and components (Finetti et al., 2015; Stephen et al., 2018). Primary cilia are indispensable for embryonic development and cell differentiation, which endows ciliopathies with great relevance (Reitter and Leroux, 2017). May et al. address phosphorylation and ubiquitylation of different components during cilia assembly and disassembly. K-63 linked α-tubulin poly-ubiquitylation—which takes place during microtubule de-polymerization (Wang et al., 2019), is used by IFT-A (intraflagellar transport complex A) for retrograde transport during cilia disassembly. Nolasco et al. study the effect of colchicine, a drug used to treat inflammatory diseases such as gouty arthritis and pericarditis. Tubulin binding cofactors (TBCs; TBCA, TBCB, and TBCE) are chaperones involved in the stabilization of the αβ-tubulin heterodimers. Here, authors observe that colchicine prevents the formation of β-tubulin/TBCA complexes by blocking the disassembly of TBCE/TBCB/αβ-tubulin complex. This system is key to regulate the critical concentration of αβ-tubulins needed to promote microtubule assembly. Therefore, colchicine would prevent microtubule dynamics by avoiding recycling of the αβ-tubulin heterodimers, which makes cells more dependent on new synthesis and possible metabolic constraints.

Altogether, this collection of articles summarizes part of the knowledge on cytoskeletal dynamics influencing cell-cell communication involved in sensing changes in the environment supporting development and cell responses. The underlying molecular mechanisms that account for the regulation of cell-cell competition are still barely understood. The diverse regulatory pathways exposed here support a unifying hypothesis postulating that the sensing of extracellular cues through membrane receptors stimulates changes in the cytoskeleton that eventually allow reorganizing other cellular components to adapt to the microenvironment, facilitating an accurate cell response and endurance.

AUTHOR CONTRIBUTIONS

NM-C: image composition. NM-C, PR-N, and FS-M: funding acquisition, conceptualization, and writing (original draft, review and editing). All authors contributed to the article and approved the submitted version.

FUNDING

This study was supported by grants PDI-2020-120412RB-100 to FS-M and PID2020-115444GB-100 to PR-N from the Spanish Ministry of Economy and Competitiveness (MINECO), grants INFLAMUNE-S2017/BMD-23671 (to FS-M) and Y2018/BIO-5207_SINERGY_CAM (to PR-N) from the Madrid Regional Government, a 2019 grant from the Ramón Areces Foundation Ciencias de la Vida y la Salud and a 2018 grant from Ayudas Fundación BBVA a Equipos de Investigación Científica (to FS-M) and grants PRB3 (IPT17/0019–ISCIII-SGEFI/ERDF), and La Caixa Banking Foundation (HR17-00016 to FS-M). CIBER Cardiovascular (Fondo de Investigación Sanitaria del Instituto de Salud Carlos III and co-funding by Fondo Europeo

de Desarrollo Regional FEDER). The Centro Nacional de Investigaciones Cardiovasculares (CNIC) was supported by the Spanish Ministry of Economy and Competitiveness (MINECO) and the Pro-CNIC Foundation. Funding agencies have not intervened in the design of the studies, with no copyright over the study.

ACKNOWLEDGMENTS

The professional editing service M. Gomez was used for technical preparation of the text prior to submission. We are grateful to Dr. S. Requena and C. López-Sanz for critical reading and Ms. M. Ángeles Vallejo for her helpful assistance and management.

REFERENCES

Belardi, B., Son, S., Felce, J. H., Dustin, M. L., and Fletcher, D. A. (2020). Cell-cell interfaces as specialized compartments directing cell function. *Nat. Rev. Mol. Cell Biol.* 21, 750–764. doi: 10.1038/s41580-020-00298-7

Buss, R. R., Sun, W., and Oppenheim, R. W. (2006). Adaptive roles of programmed cell death during nervous system development. *Annu. Rev. Neurosci.* 29, 1–35. doi: 10.1146/annurev.neuro.29.051605.112800

Cotta-de-Almeida, V., Westerberg, L., Maillard, M. H., Onaldi, D., Wachtel, H., Meelu, P., et al. (2007). Wiskott–Aldrich syndrome protein (WASP) and N-WASP are critical for T cell development. *Proc. Nat. Acad. Sci.* 104, 15424–15429. doi: 10.1073/pnas.0706881104

Davidson, P. M., and Cadot, B. (2021). Actin on and around the Nucleus. *Trends Cell Biol.* 31, 211–223. doi: 10.1016/j.tcb.2020.11.009

Dupont, S., Morsut, L., Aragona, M., Enzo, E., Giulitti, S., Cordenonsi, M., et al. (2011). Role of YAP/TAZ in mechanotransduction. *Nature* 474, 179–183. doi: 10.1038/nature10137

Esnault, C., Stewart, A., Gualdrini, F., East, P., Horswell, S., Matthews, N., et al. (2014). Rho-actin signaling to the MRTF coactivators dominates the immediate transcriptional response to serum in fibroblasts. *Genes Dev.* 28, 943–958. doi: 10.1101/gad.239327.114

Finetti, F., Onnis, A., and Baldari, C. T. (2015). Regulation of vesicular traffic at the T cell immune synapse: lessons from the primary cilium. *Traffic* 16, 241–249. doi: 10.1111/tra.12241

Gruenbaum, Y., Margalit, A., Goldman, R. D., Shumaker, D. K., and Wilson, K. L. (2015). The nuclear lamina comes of age. *Nat. Rev. Mol. Cell Biol.* 6, 21–31. doi: 10.1038/nrm1550

Kurd, N., and Robey, E. A. (2016). T-cell selection in the thymus: a spatial and temporal perspective. *Immunol. Rev.* 271, 114–126. doi: 10.1111/imr.12398

Lomakin, A. J., Cattin, C. J., Cuvelier, D., Alraies, Z., Molina, M., Nader, G. P. F., et al. (2020). The nucleus acts as a ruler tailoring cell responses to spatial constraints. *Science* 370:eaba2894. doi: 10.1126/science.aba2894

Martín-Cófreces, N. B., Alarcón, B., and Sánchez-Madrid, F. (2011). Tubulin and actin interplay at the T cell and antigen-presenting cell interface. *Front Immunol.* 2:24. doi: 10.3389/fimmu.2011.00024

Martín-Cófreces, N. B., Baixauli, F., and Sánchez-Madrid, F. (2014). Immune synapse: conductor of orchestrated organelle movement. *Trends Cell Biol.* 24, 61–72. doi: 10.1016/j.tcb.2013.09.005

Morata, G., and Ripoll, P. (1975). Minutes: mutants of Drosophila autonomously affecting cell division rate. *Dev. Biol.* 42, 211–221. doi: 10.1016/0012-1606(75)90330-9

Reitter, J. F., and Leroux, M. R. (2017). Genes and molecular pathways underprinting ciliopathies. *Nat. Rev. Mol. Cell Biol.* 18, 533–547. doi: 10.1038/nrm.2017.60

Soares, H., Lasserre, R., and Alcover, A. (2013). Orchestrating cytoskeleton and intracellular vesicle traffic to build functional immunological synapses. *Immunol. Rev.* 256, 118–132. doi: 10.1111/imr.12110

Stephen, L. A., ElMaghloob, Y., McIlwraith, M. J., Yelland, T., Castro Sanchez, P., Roda-Navarro, P., et al. (2018). The ciliary machinery is repurposed for T cell immune synapse trafficking of LCK. *Dev. Cell.* 47, 122–132.e4. doi: 10.1016/j.devcel.2018.08.012

Tybulewicz, V. L., Ardouin, L., Prisco, A., and Reynolds, L. F. (2003). Vav1: a key signal transducer downstream of the TCR. *Immunol. Rev.* 192, 42–52. doi: 10.1034/j.1600-065X.2003.00032.x

Venturini, V., Pezzano, F., Català Castro, F., Häkkinen, H. M., Jiménez-Delgado, S., Colomer-Rosell, M., et al. (2020). The nucleus measures shape changes for cellular proprioception to control dynamic cell behavior. *Science* 370:eaba2644. doi: 10.1126/science.aba2644

Wang, Q., Peng, Z., Long, H., Deng, X., and Huang, K. (2019). Polyubiquitylation of α-tubulin at K304 is required for flagellar disassembly in Chlamydomonas. *J. Cell Sci.* 132:jcs229047. doi: 10.1242/jcs.229047

Conflict of Interest: The authors declare that the research was conducted in the absence of any commercial or financial relationships that could be construed as a potential conflict of interest.

Publisher's Note: All claims expressed in this article are solely those of the authors and do not necessarily represent those of their affiliated organizations, or those of the publisher, the editors and the reviewers. Any product that may be evaluated in this article, or claim that may be made by its manufacturer, is not guaranteed or endorsed by the publisher.

frontiers in Cell and Developmental Biology

ORIGINAL RESEARCH
published: 22 October 2020
doi: 10.3389/fcell.2020.592628

G Protein-Coupled Estrogen Receptor Regulates Actin Cytoskeleton Dynamics to Impair Cell Polarization

Dariusz Lachowski[1†], Ernesto Cortes[1†], Carlos Matellan[1†], Alistair Rice[1], David A. Lee[2], Stephen D. Thorpe[2,3] and Armando E. del Río Hernández[1]**

[1] Cellular and Molecular Biomechanics Laboratory, Department of Bioengineering, Imperial College London, London, United Kingdom, [2] Institute of Bioengineering, School of Engineering and Material Science, Queen Mary University of London, London, United Kingdom, [3] UCD School of Medicine, UCD Conway Institute of Biomolecular and Biomedical Research, University College Dublin, Dublin, Ireland

Mechanical forces regulate cell functions through multiple pathways. G protein-coupled estrogen receptor (GPER) is a seven-transmembrane receptor that is ubiquitously expressed across tissues and mediates the acute cellular response to estrogens. Here, we demonstrate an unidentified role of GPER as a cellular mechanoregulator. G protein-coupled estrogen receptor signaling controls the assembly of stress fibers, the dynamics of the associated focal adhesions, and cell polarization *via* RhoA GTPase (RhoA). G protein-coupled estrogen receptor activation inhibits F-actin polymerization and subsequently triggers a negative feedback that transcriptionally suppresses the expression of monomeric G-actin. Given the broad expression of GPER and the range of cytoskeletal changes modulated by this receptor, our findings position GPER as a key player in mechanotransduction.

Keywords: actin cytoskeleton, focal adhesions, cell polarization, mechanosensing, RhoA, G protein-coupled receptors

OPEN ACCESS

Edited by:
Pedro Roda-Navarro, Universidad Complutense de Madrid, Spain

Reviewed by:
Javier Redondo-Muñoz, Spanish National Research Council, Spain
Mary C. Farach-Carson, University of Texas Health Science Center at Houston, United States

***Correspondence:**
Stephen D. Thorpe
stephen.thorpe@ucd.ie
Armando E. del Río Hernández
a.del-rio-hernandez@imperial.ac.uk

† These authors have contributed equally to this work

Specialty section:
This article was submitted to Cell Adhesion and Migration, a section of the journal Frontiers in Cell and Developmental Biology

Received: *07 August 2020*
Accepted: *24 September 2020*
Published: *22 October 2020*

Citation:
Lachowski D, Cortes E, Matellan C, Rice A, Lee DA, Thorpe SD and del Río Hernández AE (2020) G Protein-Coupled Estrogen Receptor Regulates Actin Cytoskeleton Dynamics to Impair Cell Polarization. Front. Cell Dev. Biol. 8:592628. doi: 10.3389/fcell.2020.592628

INTRODUCTION

The G protein-coupled estrogen receptor (GPER) belongs to the heptahelical transmembrane family of G protein-coupled receptors (GPCRs) and initiates rapid signaling cascades in response to both endogenous estrogens such as 17β-estradiol and man-made compounds (Revankar et al., 2005; Prossnitz and Barton, 2011). These GPER-mediated events may involve the generation of second messengers such as Ca^{2+}, as well as the activation of protein kinase A and tyrosine kinase receptors, among others. Given that GPER is broadly expressed in eukaryotic cells and because of its potential to regulate multiple downstream signaling, including cell survival and proliferation, GPER has attracted significant attention in biology and medicine in the last 20 years (Zimmerman et al., 2016; Barton et al., 2018; Hilger et al., 2018).

The small Rho GTPases are molecular switches downstream of GPCR that control a plethora of biological signaling in eukaryotic cells. They achieve this control by cycling between the GTP-active and GDP-inactive states (Etienne-Manneville and Hall, 2002). The RhoA GTPase (RhoA) is one of the most prominent members of the Rho GTPase family, which controls and shapes actin cytoskeleton by promoting actin polymerization *via* formins (mDia), and through actomyosin contractility by triggering the phosphorylation of the regulatory myosin light chain-2 (MLC-2) *via* Rho kinase (ROCK; Sadok and Marshall, 2014). This RhoA-dependent induction of cytoskeletal contractility is required for the nuclear translocation and activation of the transcriptional factor yes-associated protein 1 (YAP), a mechanotransducer that has cardinal roles in development, tissue homeostasis (Dupont et al., 2011), cancer (Calvo et al., 2013), and cardiovascular diseases (Wang et al., 2016). Yes-associated protein 1 activation influences further mechanical processes including genomic regulation of focal adhesion formation (Nardone et al., 2017).

The actin cytoskeleton is a complex and highly dynamic network of protein filaments that determines cell morphology, maintains the mechanical integrity of the cell, transmits forces, remodels in response to stimuli, and polarizes to enable cell migration (Krishnan et al., 2009; Pollard and Cooper, 2009; Gardel et al., 2010; Maruthamuthu et al., 2010). Actin monomers (G-actin) polymerize into actin filaments (F-actin), which in turn organize into bundles known as stress fibers (Pellegrin and Mellor, 2007). The assembly of actin filaments is controlled by two key cytoskeletal regulators, mDia and the Arp2/3 complex. The formin mDia, which is a downstream effector of RhoA, guides the formation of linear actin filaments by nucleating the polymerization of actin filaments *de novo*. Conversely, the Arp2/3 complex binds to preexisting actin filaments and nucleates the polymerization of daughter filaments at a constant 70° angle, resulting in a branched actin network (Mullins et al., 1998). The structure and assembly kinetics of actin stress fibers dominate many dynamic cellular processes such as (i) spreading, adhesion, contraction, locomotion, and mechanosensing (Tojkander et al., 2012; Murrell et al., 2015); (ii) the fate of stem cells (McBeath et al., 2004); and (iii) collective cell migration in morphogenesis and cancer (Friedl and Gilmour, 2009; Ilina and Friedl, 2009). The association of these actin stress fibers with myosin (actomyosin) constitutes the primary contractile machinery of the cell (Tojkander et al., 2012). This cytoskeletal machinery, linked to a dynamic population of focal adhesions, enables cells to sense and interact mechanically with their microenvironment (Ohashi et al., 2017).

Here, we demonstrate that RhoA-mediated GPER signaling can regulate the structure and dynamics of the actin cytoskeleton in fibroblasts. We observe that GPER activation decreases the number and thickness of stress fibers, the stiffness of the cytoskeleton, and the size and number of focal adhesions. Then, we use fluorescence recovery after photobleaching (FRAP) to quantify focal adhesion turnover and actin polymerization rates and demonstrate that GPER signaling impairs actin filament assembly as well as actin branching and cell polarization. Finally, we demonstrate that GPER downregulates actin expression in a RhoA-dependent manner.

MATERIALS AND METHODS

Cell Culture, Transfection, and Antibodies

Human foreskin fibroblasts (HFFs) were from the ATCC (catalog number SCRC-1041). Mouse embryonic fibroblasts (MEFs) were a gift from Dr. Wolfgang Ziegler and have been previously described by Xu et al. (1998). Both cell lines were maintained in high-glucose DMEM supplemented with 10% v/v FBS and 1% v/v GlutaMax (Thermo Fisher Scientific, United States), 1% v/v penicillin/streptomycin (Sigma Aldrich, P4333), and 1% v/v Fungizone/amphotericin B (Gibco, 15290-026). A humidified 37°C incubator with 5% CO_2 was used for culturing both cell lines. Cells were negative when tested for mycoplasma contamination. The primary antibodies used in the experiments were total RhoA (Millipore, 04-822, 1/1,000 dilution), pRhoA (Abcam, ab41435, 1/1,000), paxillin (BD Biosciences, 612405, 1/200), β-actin (Abcam, ab8226, 1/10,000), GPER (Abcam, ab39742, 1/100), and anti-Arp3 antibody (Abcam, ab49671, 1/100). The secondary antibodies used in the experiments were anti-mouse HRP (Invitrogen, 626580, 1/2,000), anti-rabbit HRP (Abcam, ab137914, 1/2,000), anti-mouse Alexa-488 (Invitrogen, A11029, 1/400), anti-rabbit IgG (H+L) Alexa-488 (Invitrogen, A11034, 1/400), IRDye 680RD donkey anti-mouse IgG (H+L) (LI-COR 925-68072, 1/15,000), or IRDye 800CW donkey anti-rabbit IgG (H+L) (LI-COR 925-32213, 1/15,000). siRNA targeting GPER was purchased from Santa Cruz Biotechnology (sc-60743). G protein-coupled estrogen receptor agonist (G1) and GPER antagonist (G15) were purchased from Tocris and used at 1 μM: G1 (Tocris, 2577) and G15 (Tocris, 3678) in treatments of 24 h unless specifically indicated. CellLight^{TM} Actin-GFP, BacMam 2.0 (Thermo Fisher Scientific, C10506) was used for fluorescence recovery after the photobleaching experiments. pRK GFP paxillin plasmid, also used for FRAP, was a gift from Kenneth Yamada (Addgene plasmid #50529). The constitutively active RhoA plasmid (pRK5-myc-RhoA-Q63L) was a gift from Gary Bokoch (Addgene plasmid #12964). This plasmid was used as a template to create the plasmid RhoA (S188A/Q63L) by substitution of the serine amino acid in position 188 to alanine using site-directed mutagenesis. Constitutively active mDia1 (mDia1ΔN3—an FH1-FH2 unit mutant) plasmid was a gift from Alexander Bershadsky, and GFP-cortactin was a gift from Anna Huttenlocher (Addgene plasmid #26722).

Scanning Electron Microscopy

The morphology of the cells was analyzed using scanning electron microscopy (SEM). Cells were fixed with 3% v/v EM-grade glutaraldehyde in 0.1 M PBS for 15 min at 37°C and washed with 0.1 M PBS. Following fixation, cells were lipid contrast stained using 1% w/v OsO_4 in PBS for 1 h at room temperature and dehydrated in ethanol with gradually increasing concentration. Samples were air dried overnight and coated with 10 nm of

chromium. The images were acquired using Zeiss Auriga Cross Beam SEM with 7.5 × 10^3 magnification, 5 kV. Images were analyzed using FIJI by thresholding in order to detect the outline of at least 10 cells per condition. The obtained masks were quantified using the area and roundness parameters.

Immunofluorescence Staining

Cell immunofluorescence staining was done on coverslips coated with 10 μg/ml fibronectin in PBS (Gibco, PHE0023). Following pertinent treatment, cells were fixed with 4% w/v paraformaldehyde (Sigma, P6148) in D-PBS (Sigma, D8537) for 10 min, permeabilized with 0.5% w/v saponin (Sigma, 47036), and then blocked with 1% w/v BSA (Sigma, A8022) and 22.52 mg/ml glycine (Sigma, G8898) in PBST for 30 min. After blocking, cells were incubated with primary antibodies prepared in blocking solution overnight at 4°C in a humidified chamber. Then, cells were washed in D-PBS and incubated with Alexa Fluor 488-conjugated secondary antibodies and phalloidin (Invitrogen, A22283, 1/500) prepared in PBS for 1 h at room temperature. Finally, coverslips were washed in PBS and mounted in mounting reagent with 4,6-diamidino-2-phenylindole (Invitrogen, P36931). Widefield fluorescent images were taken with Nikon Ti-e Inverted Microscope (Ti Eclipse, C-LHGFI HG Lamp, CFI Plan Fluor 40 × NA 0.6 air objective; Nikon; Neo sCMOS camera; Andor) with NIS elements AR software. Staining intensity was measured in Fiji (Schindelin et al., 2012) using the "mean gray value" parameter applied to a region of interest (ROI) created for manually segmented cells based on DIC images. Mean gray values for each image's background were subtracted for each measured staining intensity.

Ventral stress fibers were identified by overlaying widefield images of actin and paxillin, then selecting actin fibers attached to focal adhesions at both ends. Number per μm^2 was calculated by dividing manually counted number of ventral stress fibers by the cell area measured from brightfield images. The thickness of these fibers was quantified in Fiji by using the *plot profile* function for a straight line overlaid perpendicular in the middle of each ventral stress fiber and measuring the peak width of the mean gray value of actin widefield image. Arp3 edge to center staining intensity was quantified as a ratio of mean gray value (intensity) of the signal within the outer 5 μm of a whole-cell ROI and mean gray value of the signal within the inner ROI (outer 5 μm ROI subtracted from the whole-cell ROI).

Atomic Force Microscopy

Measurements of cell compliance were conducted on a Nanowizard-1 (JPK Instruments, Berlin, Germany) atomic force microscope operating in force spectroscopy mode mounted on an inverted optical microscope (IX-81; Olympus, Tokyo, Japan). Atomic force microscopy (AFM) pyramidal cantilevers (MLCT; Bruker, Camarillo, CA, United States) with a spring constant of 0.03 N/m (nominal stiffness reported by the manufacturer) were used with a 15-μm diameter polystyrene bead attached at room temperature. Before conducting measurements, cantilever sensitivity was calculated by measuring the force–distance slope in the AFM software on an empty petri dish region. Cells were seeded on fibronectin-coated glass fluorodishes and allowed to spread for >2 h. Cell attachment to the substrate was confirmed by visual inspection before conducting the nanoindentation procedure. For each cell analyzed, force curves were acquired at an approach speed of 5 μm/s and a maximum set point of 1 nN. Force curves were taken in regions distal from the cell nucleus to avoid assessing nuclear stiffness. The force–distance curves were used to calculate elastic moduli in the AFM software through the application of the Hertz contact model (Harris and Charras, 2011).

Fluorescence Recovery After Photobleaching

The FRAP experiments were conducted on glass-bottomed petri dishes (Mattek) coated with human plasma FN (10 μg/ml in PBS; Gibco, PHE0023) and incubated at 37°C. Six hours after seeding, cells were transfected either with pRK-GFP-paxillin by electroporation using the Neon Transfection system (Thermo Fisher Scientific) with one pulse of 1,300 V for 30 ms or with CellLight^{TM} actin-GFP; 2 μl of the reagent was added to 2 ml of the complete cell culture medium per dish and added to the cells. Confocal photobleaching was carried out 24 h after the transfection using an inverted microscope (Ti Eclipse, C2-SHS C2si Ready Scanner, Ti-TIRF-E Motorized TIRF Illuminator, CFI Plan Apo TIRF 60 × NA 1.49 oil objective; Nikon). Five confocal images were taken at 5 s intervals prior to bleaching for reference. Specified regions of the cells were then bleached using the confocal laser at 100% power. Images were taken at 5 s intervals for 100 s to capture fluorescent recovery. Images were analyzed with FIJI (measured mean gray value for each bleached ROI for each time point), with the fluorescent signal normalized between the prebleach intensity and background. Statistical analysis was then carried out using Prism (GraphPad). Data was pooled from repeats. Fluorescence recovery curves were compared using extra sum-of-squares *F* test on the best fit lines. Immobile fraction was calculated as 1 - plateau for each curve. Error bars represent the standard error for each plateau. Half time of recovery ($t_{1/2}$) was calculated separately for curves fit for each dataset and represented as mean for each condition with standard error bars.

RT-PCR

Total RNA was extracted using the RNeasy Mini kit (Qiagen, 74104), and 1 μg of total RNA was reverse-transcribed using the High-Capacity RNA-to-cDNA kit (Applied Biosystems, 4387406) according to the manufacturer's instructions. qPCR was performed using the SYBR Green PCR Master Mix (Applied Biosystems, 4309155) with 100 ng cDNA input in 20 μl of reaction volume. RPL0 (60S acidic ribosomal protein) expression level was used for normalization as a housekeeping gene. The primer sequences were as follows: RPLP0 (F) 5′-CGGTTTCTGATTGGCTAC-3′, RPLP0 (R) 5′-ACGATGTCACTTCCACG-3′; MLC-2: forward, 5′-ATCCACC TCCATCTTCTT-3′ and reverse, 5′-AATACACGACCTCC TGTT-3′; CTGF: forward, 5′-TTAAGAAGGGCAAAAAGTGC-3′ and reverse, 5′-CATACTCCACAGAATTTAGCTC-3′;

ANKDR1: forward, 5′-TGAGTATAAACGGACAGCTC-3′ and reverse, 5′-TATCACGGAATTCGATCTGG-3′; and ACTB (β-actin): forward, 5′-GACGACATGGAGAAAATCTG-3′ and reverse, 5′-ATGATCTGGGTCATCTTCTC-3′. All primers were used at 300 nM final concentration. The relative gene expression was analyzed by comparative $2^{-\Delta\Delta Ct}$ method.

Western Blotting

Cells were washed with chilled PBS and lysed in radio immunoprecipitation assay (RIPA) buffer containing Halt protease and phosphatase inhibitors (Thermo Fisher Scientific). Lysate was collected using a cell scraper, disrupted by repetitive trituration through a 25-gauge needle, and incubated for 30 min on ice with periodic mixing. This was followed by centrifugation at 12,000 *g* for 20 min at 4°C. The protein concentration in the supernatant was determined using a BCA protein assay kit (Fisher Scientific, 23225). Cell lysates were mixed with 4× Laemmli buffer (Bio-Rad, 1610747) including β-mercaptoethanol and denatured by heating at 95°C for 5 min. Samples were loaded into a 4–20% Mini-PROTEAN TGX Precast Gel (Bio-Rad, 4561096), and proteins were transferred to nitrocellulose membranes (Bio-Rad). Protein was stained using REVERT total protein stain (LI-COR, 926-11010) as per the manufacturer's instructions, and blots were imaged using an Odyssey infrared imaging system (LI-COR). The stain was removed using REVERT Reversal Solution (LI-COR, 926-11013), followed by washing in tris-buffered saline (TBS). The membranes were blocked in Odyssey blocking buffer (LI-COR, 927-50000) for 1 h followed by overnight incubation with primary antibodies in 0.1% v/v Tween-20 in TBS (TBST). After further washes in TBST, blots were incubated for 1 h with secondary antibodies. Membranes were washed again in TBST and imaged using an Odyssey infrared imaging system (LI-COR). Total protein for normalization and target protein expression were quantified using Image Studio Lite (Version 5.2, LI-COR). Target protein was normalized to total protein per lane and presented relative to the control group.

G-LISA Assay for RhoA

The intracellular amounts of total RhoA and RhoA-GTP were determined by using the total RhoA ELISA and G protein-linked (G-LISA) assays (Cytoskeleton, BK124) according to the manufacturer's instructions. Briefly, cells were washed with cold PBS and homogenized gently in ice-cold lysis buffer. Twenty microliters was removed for protein quantification in order to adjust sample concentration to 0.5 mg/ml. After adding an equal volume of binding buffer, triplicate assays were performed using 1.5 μg of protein per well. Samples were incubated for 30 min and then washed three times with washing buffer. Antigen-presenting buffer was added for 2 min before removal; samples were then incubated with 1/250 dilution of anti-RhoA antibody at room temperature for 45 min, washed three times, and incubated with secondary antibodies for another 45 min. HRP detection reagent was added, and signal was read by measuring absorbance at 490 nm using a microplate spectrometer.

Statistical Analysis

All statistical analyses were conducted with the Prism software (version 8, GraphPad). Data were generated from multiple repeats of different biological experiments to obtain the mean values and SEM displayed throughout. *P* values have been obtained through *t* tests on unpaired samples with parametric tests used for data with a normal distribution. ANOVA and *post hoc* Dunnett's test were used to perform multiple comparison test on normally distributed data, and Kruskal–Wallis test was used for multiple comparison of non-normally distributed data. Significance was set at $P < 0.05$ where graphs show significance through symbols (*$0.01 < P < 0.05$; **$0.001 < P < 0.01$; ***$0.0001 < P < 0.001$; ****$P < 0.0001$).

RESULTS

GPER Inhibits RhoA Activation in Fibroblasts

Previous work has demonstrated that GPER signaling can inhibit RhoA activation (Yu et al., 2017; Cortes et al., 2019c,d). We used immunoassays to measure activated (GTP-bound) and total levels of RhoA and observed a significant 40% decrease in the levels of GTP-bound (active) RhoA in HFFs treated with the selective GPER agonist (Bologa et al., 2006) G1 compared with control HFFs, whereas no significant change in total RhoA was observed between the control and G1-treated HFFs (**Figure 1A**). These results indicate that GPER activation does not affect the expression of RhoA but instead inhibits its activation. RhoA activation is regulated by a variety of factors: guanine nucleotide exchange factors (GEFs) activate RhoA by promoting the exchange of GDP by GTP, while GTPase-activating proteins (GAPs) catalyze the substitution of GTP by GDP leading to the inactivation of RhoA. Furthermore, the inactive pool of GDP-bound RhoA is sequestered in the cytosol through the formation of a complex with guanine nucleotide dissociation factors (GDIs), which prevents RhoA activation (Ellerbroek et al., 2003; Lessey et al., 2012; **Figure 1B**). Using Western blot, we confirmed that there was no change in the total levels of RhoA between the control and G1-treated HFFs, and observed around 45% increase in the levels of RhoA phosphorylated in serine 188 (pRhoA-Ser188, inactive) in G1-treated HFFs compared with control HFFs (**Figure 1C** and **Supplementary Figure 1**). It is well documented that phosphorylation of the serine residue 188 in the C-terminal tail of RhoA increases the affinity of the RhoA-GDI complex, preventing its dissociation and thereby promoting RhoA inactivation (Lang et al., 1996; Forget et al., 2002; Ellerbroek et al., 2003). Our results point toward this mechanism of RhoA inhibition mediated by RhoGDI, which is in turn consistent with the mechanism of GPER-mediated RhoA inhibition observed previously (Yu et al., 2014, 2017).

GPER Regulates Actin Cytoskeleton Organization

Given the central role of the actin cytoskeleton in cellular mechanical activity, we sought to investigate the effect of GPER

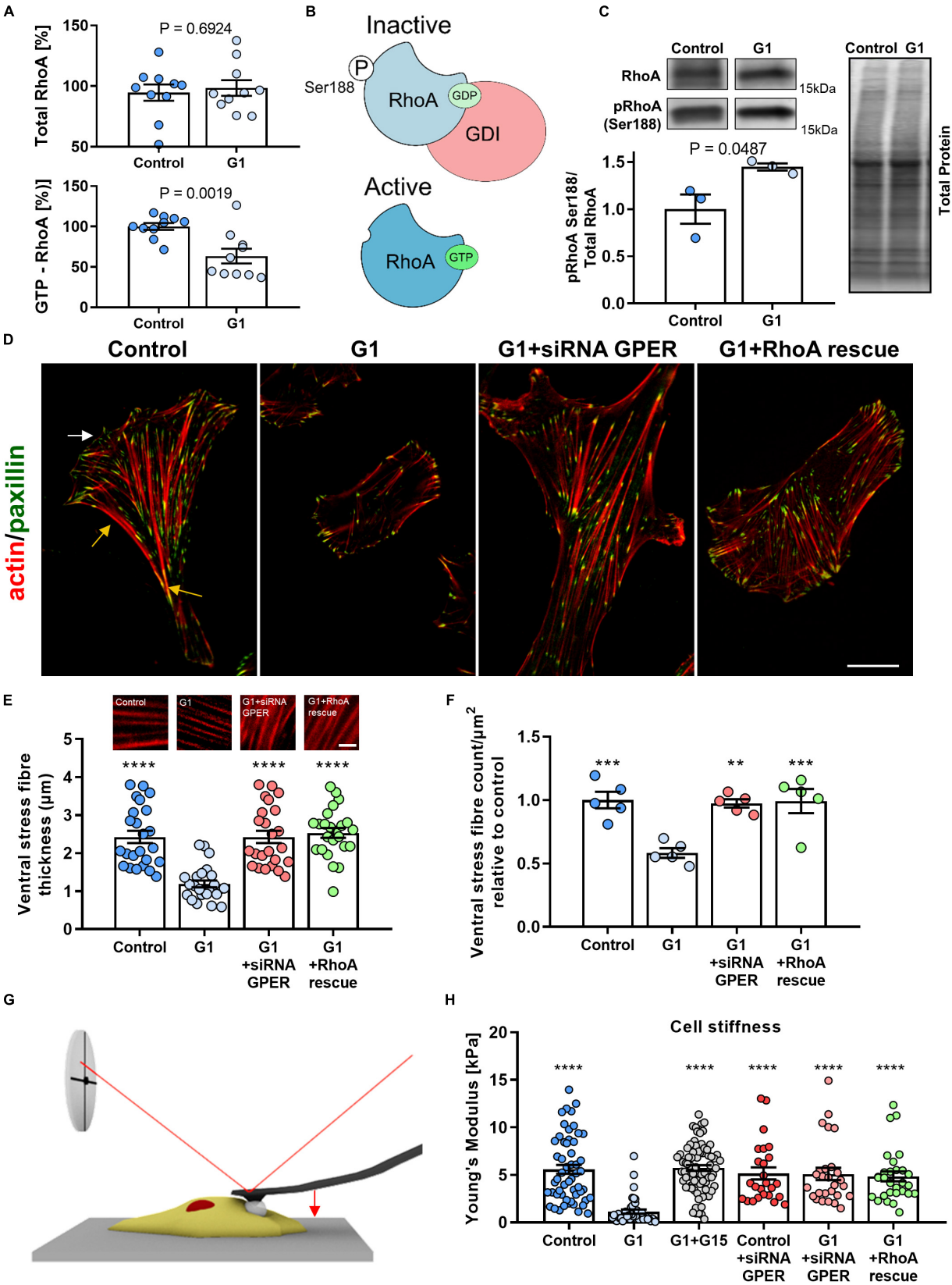

FIGURE 1 | Continued

FIGURE 1 | Actin fiber thickness and cell compliance are dependent on the G protein-coupled estrogen receptor (GPER)/RhoA GTPase (RhoA) axis. **(A)** Quantification of total and active GTP-bound RhoA, normalized to the control condition measured by G protein-linked (G-LISA) assay in human foreskin fibroblasts (HFFs) treated with GPER agonist G1 or vehicle control. **(B)** Schematics of the mechanism of RhoA regulation. Phosphorylation on the serine 188 residue increases the affinity between GDP-RhoA and guanine nucleotide dissociation factor (GDI), sequestering inactive RhoA from the cytoplasm and preventing its activation. **(C)** Western blot quantification of pRhoA Ser188 (inactive RhoA) normalized to total RhoA. Three biological samples run in triplicate. *t* test *P* values provided. **(D)** Representative images of HFFs in control, G1, G1+siRNA GPER knockdown, or G1+RhoA rescue using constitutively active RhoA (S188A/Q63L). The white arrow indicates the lamellipodium and the yellow arrows the localization of the ventral stress fibers. Scale bar is 20 μm. **(E,F)** Quantification of ventral stress fiber thickness and count per μm^2 in HFFs with representative images of actin fibers. Scale bar represents 5 μm. **(G)** Schematic image of cell cytoskeletal stiffness measurements with atomic force microscopy (AFM). **(H)** Mean cell Young's modulus as determined by AFM for control, G1, G1 + G15, control + siRNA GPER, G1 + siRNA GPER, and G1+RhoA rescue: n = 55, 41, 78, 25, 30, and 28 cells, respectively. Histogram bars represent mean ± SEM; dots represent individual data points. Three experimental replicates. Markers denote significant difference from G1 condition by ANOVA with Dunnett's *post hoc* test, $^{**}0.001 < P < 0.01$, $^{***}0.0001 < P < 0.001$, $^{****}P < 0.0001$.

activation on the assembly and organization of actin stress fibers. First, we confirmed that GPER is expressed in HFFs and MEFs (**Supplementary Figure 2A**). Then, we characterize the thickness and number (normalized by cell area to account for changes in cell morphology) of ventral stress fibers using immunofluorescence microscopy. Ventral stress fibers are a subset of actin stress fibers that attach to focal adhesions at both ends and contain myosin II, making them the primary contractile machinery of many cells. The abundance of ventral stress fibers is therefore a hallmark of highly contractile and mechanically active fibroblasts (Tojkander et al., 2012). In control HFFs, we observed numerous and thick ventral fibers, with an average of 2.4 ± 0.2 μm thickness (mean ± SEM, n = 24) (**Figures 1D,E**). These fibers were widely distributed across the entire cell body and particularly abundant in the posterior area of the well-polarized cells and less numerous at the leading edge (common localization of ventral fibers) (Tojkander et al., 2012). In contrast, G1-treated HFFs showed a more uniform distribution of stress fibers and a significant decrease in the thickness and number (normalized by cell area) of ventral fibers, with an average thickness of 1.2 ± 0.1 μm (mean ± SEM, n = 24) and an ∼40% decrease in the number of stress fibers compared with control HFFs (**Figures 1E,F**). In addition, we observed that G1 treatment did not affect the thickness and number of ventral fibers in HFFs that were previously treated with siRNA to knock down GPER expression or expressing the constitutively active form of RhoA (S188A/Q63L) (**Figures 1E,F** and **Supplementary Figure 2B**), indicating that the mechanism of stress fiber regulation is dependent on the GPER–RhoA axis. Similarly, analysis of cell morphology revealed profound changes in cell area and shape in response to GPER activation. Using SEM, we observed that G1-treated HFFs and MEFs had a significantly smaller contact area and were significantly rounder than control cells (**Supplementary Figures 3–5**). These results are consistent with the decrease in thickness and density of stress fibers and are often associated with mechanical quiescence in fibroblasts.

To further analyze the mechanical effect of the GPER-mediated decrease in actin stress fibers, we characterized cell (cytoskeletal) stiffness in response to G1 treatment. Cytoskeletal stiffness is dependent on the structure and composition of the actin cytoskeleton and a critical determinant of the cells' ability to maintain tensional homeostasis, migrate, and deform (Bruckner and Janshoff, 2015; Lautscham et al., 2015). To determine the Young's modulus of HFFs, we used AFM employing a cantilever with a 15-μm diameter polystyrene bead attached to probe cells in regions distant from the nucleus (**Figure 1G**). We observed that control HFFs showed a Young's modulus of 5.6 ± 0.5 kPa (mean ± SEM, n = 55 cells), a value within the expected range for fibroblasts (Solon et al., 2007). The Young's modulus was significantly reduced to 1.1 ± 0.2 kPa (mean ± SEM, n = 41 cells) in HFFs treated with G1. When the GPER antagonist G15 was used in conjunction with G1, the Young's modulus was significantly greater at 5.7 ± 0.3 kPa (mean ± SEM, n = 78), not significantly different from control HFFs (**Figure 1H**), indicating that GPER activation is essential in modifying the rheological properties of the cell. Knockdown of GPER *via* siRNA or expression of constitutively active RhoA similarly exhibited cytoskeletal stiffness at levels comparable to control. These results indicate that GPER modulates not only the composition of the actin cytoskeleton but also its mechanical properties.

GPER Activation Modulates Focal Adhesion Assembly and Turnover

The actomyosin cytoskeleton links to the extracellular environment through focal adhesions. These membrane-bound protein complexes are signaling hubs that allow the bidirectional communication of cells with the ECM and drive traction force generation and mechanosensing through regulation of actin polymerization, stress fiber assembly, and modulation of myosin activity (Parsons et al., 2010). Using GFP-paxillin–transfected HFFs and total internal reflection (TIRF) microscopy, we observed that focal adhesions were significantly smaller in G1-treated HFFs compared with those in control cells (**Figures 2A,C**). Similarly, the density of focal adhesions (number of focal adhesions normalized by the cell area) was significantly decreased in cells treated with G1 (**Figure 2B**), whereas siRNA knockdown of GPER or RhoA rescue abrogated the effect of G1 on both focal adhesion size and density.

Focal adhesions are highly dynamic structures, with formation, growth, and disassembly dependent on cytoskeletal properties such as mechanical tension and cell contractility (Geiger et al., 2009). The application of force to focal adhesions by the cytoskeleton promotes turnover of focal adhesion components such as paxillin (Wolfenson et al., 2010). We used the GFP-paxillin–transfected HFF cells to image focal adhesions combining TIRF with FRAP. A high-power laser is used to photobleach the GFP-paxillin fluorescence signal

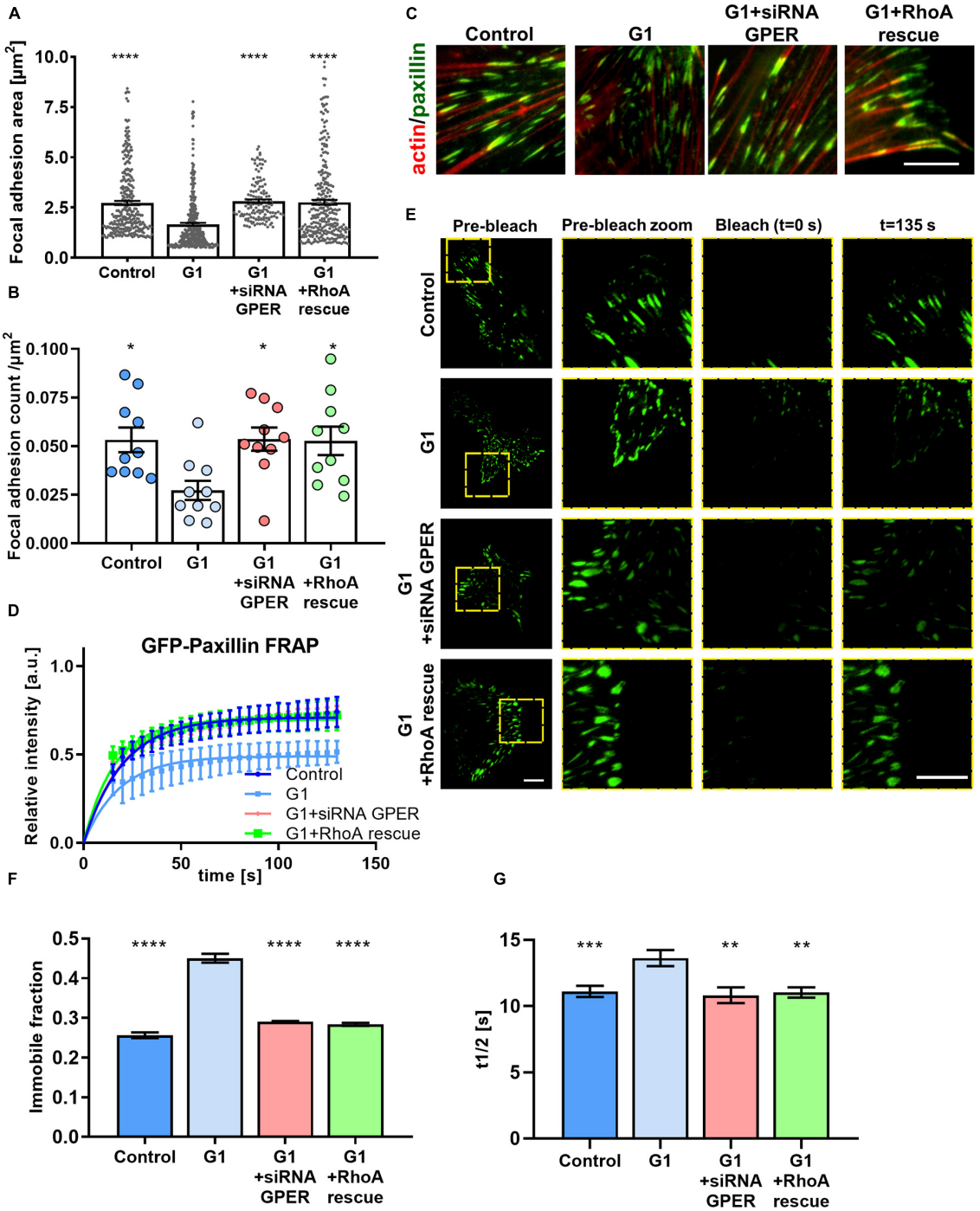

FIGURE 2 | GPER activation regulates the size and dynamics of focal adhesions in HFFs. **(A)** Quantification of paxillin-based focal adhesion area and **(B)** number (normalized by cell area in μm^2) for control, G1, G1 + siRNA GPER, and G1 + RhoA rescue with constitutively active RhoA (S188A/Q63L); n = 276, 130, 240, and 175 focal adhesions from 15, 16, 21, and 18 cells, respectively. Three experimental replicates. Markers denote significant difference from G1 condition by **(A)** Kruskal–Wallis test and **(B)** ANOVA with Dunnett's *post hoc* test. **(C)** Representative regions of interest for paxillin (immunostaining, green) and F-actin (phalloidin, red) in HFFs cultured on fibronectin-coated glass. Scale bar represents 10 µm. **(D)** FRAP curves for the recovery of GFP-paxillin in focal adhesions of HFFs; curves represent nonlinear fit, one-phase association; points and error bars represent mean ± SD. **(E)** Representative total internal reflection (TIRF)-fluorescence recovery after photobleaching (FRAP) images of GFP-paxillin focal adhesions in HFFs. Scale bar represents 10 µm. **(F)** Immobile fraction and **(G)** half time of recovery data obtained from fit of FRAP curves in panel **(D)**. For control, G1, G1 + siRNA GPER, and G1 + RhoA rescue, n = 97, 102, 47, and 47 cells, respectively. Histogram bars represent mean ± SEM, where present, dots represent individual data points. Three experimental replicates. Markers denote significant difference from G1 condition by ANOVA with Dunnett's *post hoc* test, *$0.01 < P < 0.05$, **$0.001 < P < 0.01$, ***$0.0001 < P < 0.001$, ****$P < 0.0001$.

in a ROI. As focal adhesions turn over, new GFP-paxillin is incorporated into the bleached adhesions. We observed that following photobleaching, G1-treated HFFs showed a reduced recovery rate compared with control cells, with a significant increase in the time to half recovery (the time required to recover half the final fluorescence intensity), as well as an increase in the immobile fraction (**Figures 2D–G**). In addition, knocking down GPER *via* siRNA or expression of constitutively active RhoA before G1 treatment recovered the focal adhesion dynamics seen in control HFFs, suggesting that the modulation of focal adhesion dynamics is GPER and RhoA dependent. This indicates that focal adhesion turnover is significantly reduced following G1 treatment, hampering the ability for the cell to interact mechanically with its microenvironment.

GPER Activation Regulates Actin Polymerization and Expression

The ability of cells to rapidly assemble and remodel actin filaments is critical for a variety of dynamic processes, including migration and contraction, as well as the ability to sense and respond to mechanical stimuli (mechanosensing). To assess the effect of GPER activation on actin kinetics, we used actin-GFP to visualize actin filaments in living HFFs with FRAP to quantify actin polymerization rate (**Figure 3A**).

We measured the fluorescence intensity over time and observed that the fluorescence recovery rate was significantly reduced for cells treated with G1 compared with control HFFs (**Figures 3A,B**). The time to half recovery was significantly increased from 12 ± 1 (mean ± SEM, $n = 43$) in control HFFs to 17 ± 1 s (mean ± SEM, $n = 30$) in G1-treated cells (**Figure 3D**), indicating slower recovery and impaired actin polymerization rate with GPER activation. In addition, analysis of the immobile fraction (i.e., the fraction of the fluorescence intensity that is not recovered after bleaching) revealed similar results (**Figure 3C**), with G1-treated HFFs presenting a significantly higher immobile fraction (65 ± 0.7%, mean ± SEM, $n = 43$ cells) compared with control cells (38 ± 0.6%, mean ± SEM, $n = 30$ cells). These results suggest that GPER activation impairs actin mobility and polymerization kinetics, limiting the ability for the cell to remodel its actin cytoskeleton.

To investigate if the GPER-mediated decrease in actin polymerization rate affected the overall synthesis of β-actin monomers in cells, we quantified the expression of β-actin at the protein and gene levels. β-Actin is the main monomeric form of cytosolic actin, and its expression is critical to the integrity of the cytoskeleton. Interestingly, the expression of β-actin protein was significantly downregulated in G1-treated HFF cells compared with control (**Figure 3E** and **Supplementary Figures 6A,B**), a result that was recapitulated in MEFs (**Supplementary Figures 6C–E**). We also observed a pronounced decrease in the levels of mRNA for β-actin in G1-treated HFFs compared with control (**Figure 3F**). Conversely, values comparable to controls were observed when G1 treatment was carried out in the presence of the selective GPER antagonist G15 or with siRNA knockdown of GPER (**Supplementary Figure 7**). Taken together, these results suggest that GPER activation downregulates actin expression either directly or through a negative regulatory feedback in which a reduced actin polymerization rate transcriptionally suppresses the synthesis of β-actin monomers.

GPER Modulates Cell Polarization in a mDia-Dependent Manner

Another hallmark of mechanically active fibroblasts is the development of a polarized morphology characterized by an increased aspect ratio and an asymmetric distribution of the actin cytoskeleton. Polarization is accompanied by the formation of ventral stress fibers at the trailing edge and actin-rich locomotion structures such as filopodia, lamellipodia, and invadopodia at the leading edge. These structures enable the cell to spread and to probe the mechanical properties of its microenvironment and are thus critical for directed cell migration (i.e., haptotaxis, durotaxis) and mechanosensing (Wu et al., 2012; King et al., 2016; Oakes et al., 2018).

Arp3 is an actin-binding protein that nucleates the formation of actin branches, a process required for the formation of lamellipodia (Mullins et al., 1998; Buracco et al., 2019). In polarized, mechanically active cells, Arp3 is recruited to stress fibers and localizes around the cell periphery, whereas in mechanically quiescent cells, Arp3 remains dispersed through the cytoplasm. We used immunofluorescence microscopy to assess the distribution of Arp3 and confirmed that, in control HFFs, Arp3 is primarily localized in the cell edge, with preferential distribution in one side of the cell, consistent with the asymmetric extension of lamellipodia in mechanically active cells. Conversely, in G1-treated HFFs, Arp3 localizes more uniformly across the cell body (**Figure 3G**). Quantification of Arp3 distribution revealed an ∼60% decrease in the ratio between the cell edge and cell center in G1-treated HFFs compared with control (**Figure 3H**).

Interestingly, when cells expressing a constitutively active form of mDia were treated with G1, we observed no significant change in the distribution of Arp3, which localized preferentially to the cell periphery similar to control cells (**Figures 3G,H**). These results indicate that the mechanism of GPER-mediated modulation of cell polarization is mDia dependent. A protein of the formin family and a RhoA effector, mDia catalyzes the nucleation of linear actin filaments and promotes actin polymerization. mDia and the Arp2/3 complex have been found to cooperate sequentially to generate lamellipodia by regulating the polymerization of mother actin filaments and the branching of daughter filaments, respectively (Isogai et al., 2015).

To further confirm the regulatory effect of G1 on cell polarization, we analyzed the expression of the actin-binding protein cortactin. When activated, cortactin recruits the Arp2/3 complex to mature actin filaments to promote actin branching (Kirkbride et al., 2011). Consistent with our previous results, we observed a significant (∼26%) decrease in the fluorescence intensity levels of cortactin in G1-treated HFFs compared with the control cells (**Figures 3I,J**). Taken together, these results suggest that inhibition of the RhoA/mDia axis is central to the GPER-mediated modulation of the actin cytoskeleton.

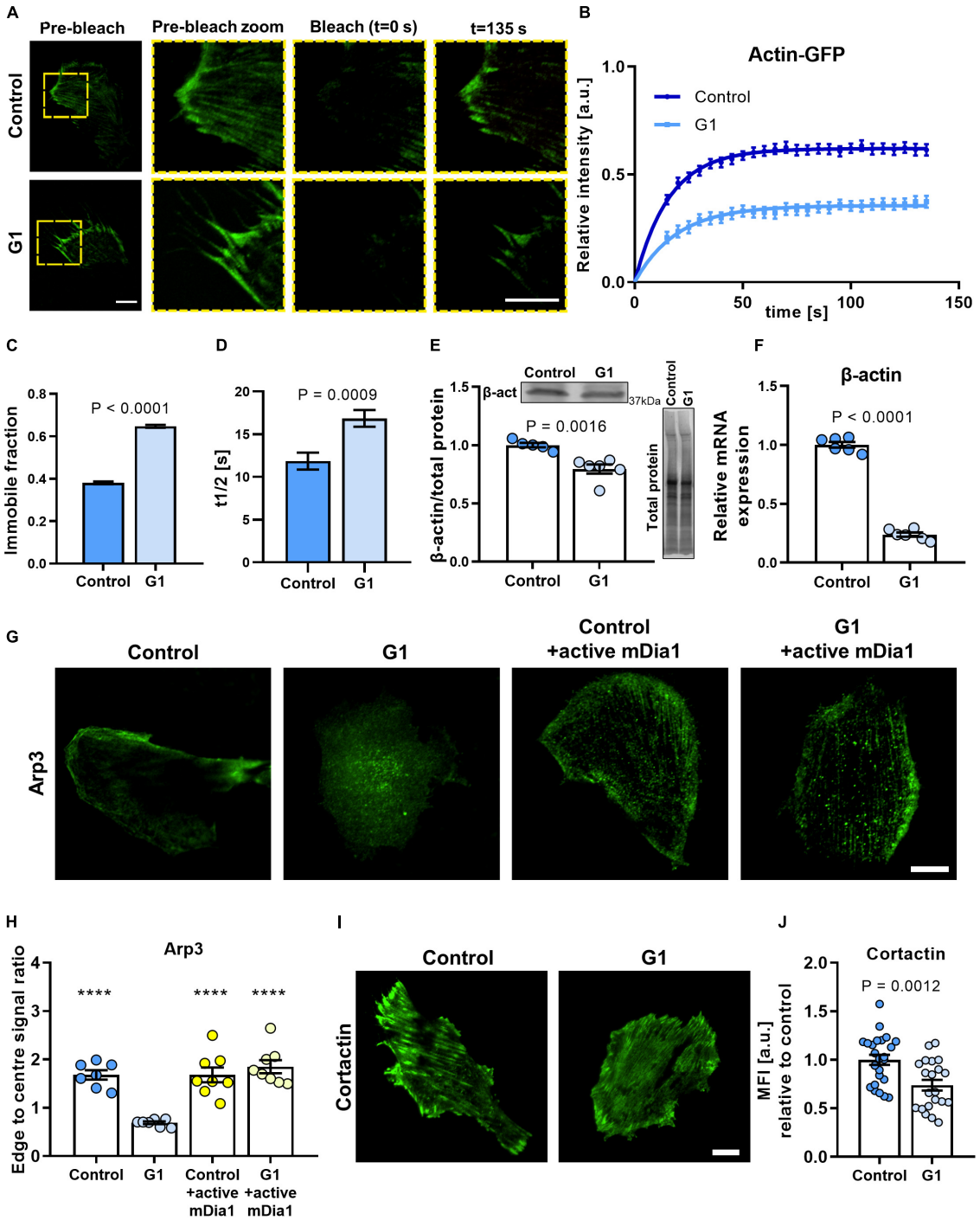

FIGURE 3 | Actin polymerization rate and cell polarization are dependent on the GPER/RhoA axis. **(A)** Representative TIRF-FRAP images of actin-GFP stress fibers in HFFs cultured on fibronectin-coated glass. Scale bar represents 10 μm. **(B)** FRAP curves for the recovery of actin-GFP in HFFs; curves represent nonlinear fit, one-phase association; points and error bars represent mean ± SEM. **(C)** Immobile fraction and **(D)** half time of recovery obtained from fit of FRAP curves in panel **(B)**. For control and G1, $n = 43$ and 30 cells, respectively. **(E)** Western blot quantification of β-actin expression in HFFs. **(F)** Quantification of mRNA levels of β-actin in HFFs. Values are relative to control and normalized to RPLP0 (60S acidic ribosomal protein). Three experimental replicates. **(G)** Representative images of HFFs immunostained for Arp3 in control or G1 conditions with or without constitutively active mDia1 expression. Scale bar is 20 μm. **(H)** Quantification of edge to center Arp3 fluorescence signal ratio. Markers denote significant difference from G1 condition by ANOVA with Dunnett's *post hoc* test, $^{****}P < 0.0001$. For control, G1, control + active mDia1, and G1 + active mDia1, $n = 31$, 30, 29, and 34 cells across seven, seven, eight, and eight experimental replicates, respectively. **(I)** Representative images of HFFs transfected with cortactin-GFP. Scale bar is 20 μm. **(J)** Quantification of cortactin-GFP. MFI, mean fluorescence intensity (expressed in arbitrary units). Scale bar = 20 μm. Histogram bars represent mean ± SEM; dots represent individual data points. $n = 25$, three experimental replicates. *t* test *P* values provided on the graphs.

DISCUSSION

The wealth of physiological and pathological roles of rapid estrogenic signaling through GPER underlies the importance of understanding its regulation and downstream signaling effects. As a member of the versatile GPCR family, GPER influences a large range of biochemical signaling pathways. A growing body of evidence highlights the emerging role of GPER-mediated mechanical pathways in health and disease (Carnesecchi et al., 2015; Wei et al., 2016; Cortes et al., 2019b,d). In this work, we present a previously unidentified biomechanical mechanism in fibroblasts by which the ubiquitous transmembrane receptor GPER controls the structure and dynamics of focal adhesion complexes and the actin stress fibers. We found that activating GPER regulates actin polymerization rate and branching through the RhoA/mDia axis and in turn modulates cell polarization in fibroblasts (**Figure 4**).

Previous studies reported that GPER can regulate cell morphology and focal adhesion size in dermal fibroblasts (Carnesecchi et al., 2015). Here, we recapitulate those results and demonstrate that GPER signaling further regulates the organization and dynamics of the actin cytoskeleton through RhoA and its downstream effector mDia. The ability to polarize in response to mechanical stimuli is fundamental for directed cell migration such as durotaxis or haptotaxis (King et al., 2016; Lachowski et al., 2017) and depends on differential, asymmetric activation of Rho GTPases such as RhoA and Rac1, which in turn orchestrate actin dynamics at the leading edge (Machacek et al., 2009; Cortes et al., 2019a). Accordingly, we found that actin polymerization and the RhoA/mDia system, which are regulated by GPER, are required for cell polarization and mechanosensing, in agreement with previous work that demonstrates that stiffness and haptotactic sensing by lamellipodia relies on RhoA-mediated actin protrusion, branching, and focal adhesion turnover (Puleo et al., 2019) independently from the ROCK/myosin-2 axis (King et al., 2016; Oakes et al., 2018; Matellan and Del Río Hernández, 2019).

The regulation of actin cytoskeletal dynamics by Rho GTPases also plays a central role in collective cell migration, a process that is fundamental in morphogenesis, wound healing, and cancer (Friedl and Gilmour, 2009). Collective cell migration requires coordinated, dynamic reorganization of the actin cytoskeleton and is characterized by the emergence of "leader cells." These leader cells present distinct lamellipodial protrusions with increased RhoA and Rac1 activity, both of which are indispensable to maintain the leading cell phenotype and to enable collective migration (Reffay et al., 2014; Yamaguchi et al., 2015). Although not analyzed here, Rac1 is another

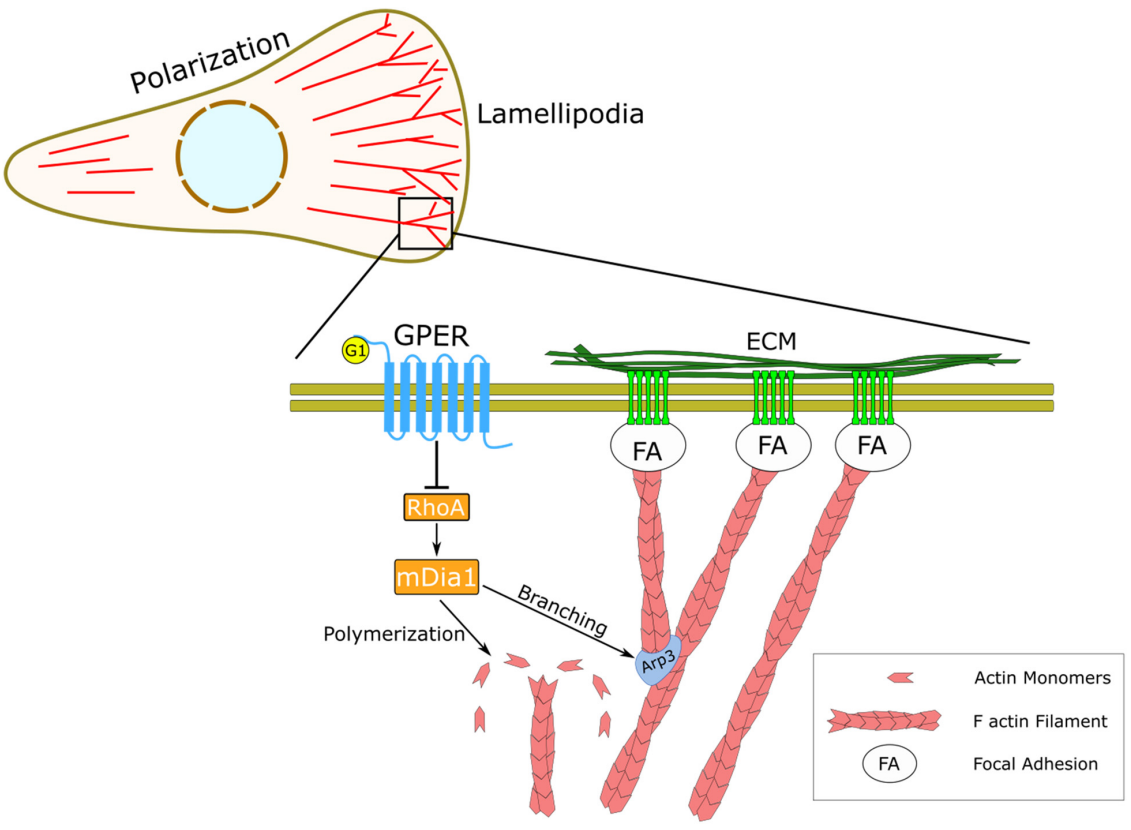

FIGURE 4 | Schematic representation of the regulatory effect of GPER on actin dynamics and mechanosensing. In HFFs, GPER signaling regulates the RhoA/mDia axis, which governs the dynamics of the actin cytoskeleton, including actin filament polymerization and actin branching through the Arp2/3 complex. At the cellular level, GPER modulates cell polarization, lamellipodia protrusion, and mechanical interaction between the cells and the ECM through focal adhesions (FA).

Rho GTPase, which plays a critical role in single and collective cell migration by modulating the formation of lamellipodia through WAVE/Arp2/3 (Ridley, 2015). While a direct effect of GPER signaling on Rac1 has not been demonstrated, Rac1 has been shown to be downregulated by GPER agonists such as 17β-estradiol and resveratrol (Laufs et al., 2003; Azios et al., 2007), suggesting that GPER signaling could act synergistically through RhoA and Rac1 to regulate actin protrusion in single and collective cell migration.

Analysis of actin polymerization rate and expression revealed that both are concomitantly reduced by GPER/RhoA signaling in fibroblasts, pointing toward an unidentified negative feedback pathway. Regulation of gene expression by RhoA-mediated actin polymerization has been previously described in proximal tubular epithelial cells through the myocardin-related transcription factor A/serum response factor (MRTF-A/SRF) axis (Giehl et al., 2015). MRTF-A is normally inactive in the cytoplasm through binding to G-actin monomers. However, when G-actin is recruited to filaments, MRTF-A translocates to the nucleus along with its binding partner SRF (Miralles et al., 2003), a transcription factor that controls the expression of a variety of cytoskeletal genes, including β-actin, talin-1, vinculin, filamin A, and integrin β1, as well as connective tissue growth factor (CTGF) and matrix metalloprotease 9 (MMP 9; Olson and Nordheim, 2010). We hypothesize that the GPER/RhoA-mediated decrease in actin polymerization leads to accumulation of G-actin monomers and inactivation of the MRTF-A/SRF system. Further experiments will be required to elucidate this mechanism and to investigate the ramifications of GPER signaling on SRF-dependent genes.

The broader implications of GPER-mediated mechanotransduction events in fibroblasts will need to be established. For example, GPER could affect actomyosin-dependent ECM remodeling directly impacting on the regulation of connective tissue homeostasis in health and disease (Scott et al., 2015). A stiff fibrotic ECM, generated by fibroblasts and fibroblast-like cells, is also a major clinical hallmark of solid tumors, often associated with aberrant mechanotransduction (Paszek et al., 2005; Jaalouk and Lammerding, 2009; Calvo et al., 2013; Chronopoulos et al., 2016; Sarper et al., 2016), and this GPER-mediated mechanism may provide a therapeutic target wherein mechanical deactivation of fibroblasts leads to a reduction in tumor-permissive desmoplasia.

The physiology of many cells depends on generation and perpetuation of a defined mechanical phenotype, which is often altered in disease and therefore targeted by therapeutics. G protein-coupled estrogen receptor, which we reveal to be a new mechanoregulator, has been investigated for its therapeutic effects in diseases such as cancer, cardiovascular disease, and atherosclerosis (Barton and Prossnitz, 2015; Feldman and Limbird, 2017), all of which have been associated with mechanical deregulation in the disease state (Paszek et al., 2005; Jaalouk and Lammerding, 2009). This suggests that therapeutics targeting GPER may also deregulate mechanopathologies in addition to influencing biomechanical signaling.

Our work positions GPER as a key player in regulating cellular mechanotransduction events in fibroblasts. Given that GPER controls the activation of RhoA, which is a molecular switch highly conserved across species that controls the dynamics of the actin cytoskeleton, and numerous transduction pathways in eukaryotic cells, our findings lay the ground for further investigation on how GPER-mediated changes in the cytoskeleton may control other processes in cells such as adhesion, spreading, migration, membrane protrusion, endocytosis, phagocytosis, and organization of the actin rings at the end of mitosis among many others.

DATA AVAILABILITY STATEMENT

The raw data supporting the conclusions of this article will be made available by the authors, without undue reservation.

AUTHOR CONTRIBUTIONS

DL and ADRH designed the project. DL, EC, and AR performed the experiments and analyzed the data. SDT performed Western blot experiments under the supervision of DAL. DL, CM, and ADRH wrote the manuscript with contributions from all authors.

FUNDING

This work has been funded by the European Research Council grant 282051 and Biotechnology and Biological Sciences Research Council (BBSRC grant no. BB/N018532/1).

ACKNOWLEDGMENTS

We are thankful to the members of CMBL Laboratory for their help with this project. We are very grateful to Alexander Bershadsky for providing us with the mDia plasmid.

SUPPLEMENTARY MATERIAL

The Supplementary Material for this article can be found online at: https://www.frontiersin.org/articles/10.3389/fcell.2020.592628/full#supplementary-material

REFERENCES

Azios, N. G., Krishnamoorthy, L., Harris, M., Cubano, L. A., Cammer, M., and Dharmawardhane, S. F. (2007). Estrogen and resveratrol regulate Rac and Cdc42 signaling to the actin cytoskeleton of metastatic breast cancer cells. *Neoplasia* 9, 147–158. doi: 10.1593/neo.06778

Barton, M., Filardo, E. J., Lolait, S. J., Thomas, P., Maggiolini, M., and Prossnitz, E. R. (2018). Twenty years of the G protein-coupled estrogen receptor GPER: Historical and personal perspectives. *J. Ster. Biochem. Mole. Biol.* 176, 4–15. doi: 10.1016/j.jsbmb.2017.03.021

Barton, M., and Prossnitz, E. R. (2015). Emerging roles of GPER in diabetes and atherosclerosis. *Trends Endocr. Metab* 26, 185–192. doi: 10.1016/j.tem.2015.02.003

Bologa, C. G., Revankar, C. M., Young, S. M., Edwards, B. S., Arterburn, J. B., Kiselyov, A. S., et al. (2006). Virtual and biomolecular screening converge on a selective agonist for GPR30. *Nat. Chem. Biol.* 2, 207–212. doi: 10.1038/nchembio775

Bruckner, B. R., and Janshoff, A. (2015). Elastic properties of epithelial cells probed by atomic force microscopy. *Biochim. Biophys. Acta* 1853, 3075–3082. doi: 10.1016/j.bbamcr.2015.07.010

Buracco, S., Claydon, S., and Insall, R. (2019). Control of actin dynamics during cell motility. *F1000Research* 8:F1000FacultyRev–977.

Calvo, F., Ege, N., Grande-Garcia, A., Hooper, S., Jenkins, R. P., Chaudhry, S. I., et al. (2013). Mechanotransduction and YAP-dependent matrix remodelling is required for the generation and maintenance of cancer-associated fibroblasts. *Nat. Cell Biol.* 15, 637–646. doi: 10.1038/ncb2756

Carnesecchi, J., Malbouyres, M., de Mets, R., Balland, M., Beauchef, G., Vié, K., et al. (2015). Estrogens induce rapid cytoskeleton re-organization in human dermal fibroblasts via the non-classical receptor GPR30. *PLoS One* 10, 120672–e120672. doi: 10.1371/journal.pone.0120672

Chronopoulos, A., Robinson, B., Sarper, M., Cortes, E., Auernheimer, V., Lachowski, D., et al. (2016). ATRA mechanically reprograms pancreatic stellate cells to suppress matrix remodelling and inhibit cancer cell invasion. *Nat. Commun.* 7:12630.

Cortes, E., Lachowski, D., Rice, A., Chronopoulos, A., Robinson, B., Thorpe, S., et al. (2019a). Retinoic Acid Receptor-β Is Downregulated in Hepatocellular Carcinoma and Cirrhosis and Its Expression Inhibits Myosin-Driven Activation and Durotaxis in Hepatic Stellate Cells. *Hepatology* 69, 785–802. doi: 10.1002/hep.30193

Cortes, E., Lachowski, D., Rice, A., Thorpe, S. D., Robinson, B., Yeldag, G., et al. (2019b). Tamoxifen mechanically deactivates hepatic stellate cells via the G protein-coupled estrogen receptor. *Oncogene* 38, 2910–2922. doi: 10.1038/s41388-018-0631-3

Cortes, E., Lachowski, D., Robinson, B., Sarper, M., Teppo, J. S., Thorpe, S. D., et al. (2019c). Tamoxifen mechanically reprograms the tumor microenvironment via HIF-1A and reduces cancer cell survival. *EMBO Rep.* 20:e46557. doi: 10.15252/embr.201846557

Cortes, E., Sarper, M., Robinson, B., Lachowski, D., Chronopoulos, A., Thorpe, S. D., et al. (2019d). GPER is a mechanoregulator of pancreatic stellate cells and the tumor microenvironment. *EMBO Rep.* 20:e46556.

Dupont, S., Morsut, L., Aragona, M., Enzo, E., Giulitti, S., Cordenonsi, M., et al. (2011). Role of YAP/TAZ in mechanotransduction. *Nature* 474, 179–183.

Ellerbroek, S. M., Wennerberg, K., and Burridge, K. (2003). Serine phosphorylation negatively regulates RhoA in vivo. *J. Biol. Chem.* 278, 19023–19031. doi: 10.1074/jbc.m213066200

Etienne-Manneville, S., and Hall, A. (2002). Rho GTPases in cell biology. *Nature* 420, 629–635.

Feldman, R. D., and Limbird, L. (2017). GPER (GPR30): A Nongenomic Receptor (GPCR) for Steroid Hormones with Implications for Cardiovascular Disease and Cancer. *Annu. Rev. Pharmacol. Toxicol.* 57, 567–584. doi: 10.1146/annurev-pharmtox-010716-104651

Forget, M. A., Desrosiers, R. R., Gingras, D., and Beliveau, R. (2002). Phosphorylation states of Cdc42 and RhoA regulate their interactions with Rho GDP dissociation inhibitor and their extraction from biological membranes. *Biochem. J.* 361, 243–254. doi: 10.1042/0264-6021:3610243

Friedl, P., and Gilmour, D. (2009). Collective cell migration in morphogenesis, regeneration and cancer. *Nat. Rev. Mole. Cell Biol.* 10, 445–457. doi: 10.1038/nrm2720

Gardel, M. L., Schneider, I. C., Aratyn-Schaus, Y., and Waterman, C. M. (2010). Mechanical integration of actin and adhesion dynamics in cell migration. *Annu. Rev. Cell Dev. Biol.* 26, 315–333. doi: 10.1146/annurev.cellbio.011209.122036

Geiger, B., Spatz, J. P., and Bershadsky, A. D. (2009). Environmental sensing through focal adhesions. *Nat. Rev. Mol. Cell Biol.* 10, 21–33. doi: 10.1038/nrm2593

Giehl, K., Christof, K., Susanne, M., and Goppelt-Struebe, M. (2015). Actin-mediated gene expression depends on RhoA and Rac1 signaling in proximal tubular epithelial cells. *PLoS One* 10: 121589–e121589. doi: 10.1371/journal.pone.0121589

Harris, A. R., and Charras, G. T. (2011). Experimental validation of atomic force microscopy-based cell elasticity measurements. *Nanotechnology* 22:345102. doi: 10.1088/0957-4484/22/34/345102

Hilger, D., Masureel, M., and Kobilka, B. K. (2018). Structure and dynamics of GPCR signaling complexes. *Nat. Struct. Mol. Biol.* 25, 4–12. doi: 10.1038/s41594-017-0011-7

Ilina, O., and Friedl, P. (2009). Mechanisms of collective cell migration at a glance. *J. Cell Sci.* 122, 3203–3208. doi: 10.1242/jcs.036525

Isogai, T., van der Kammen, R., Leyton-Puig, D., Kedziora, K. M., Jalink, K., and Innocenti, M. (2015). Initiation of lamellipodia and ruffles involves cooperation between mDia1 and the Arp2/3 complex. *J. Cell Sci.* 128, 3796–3810. doi: 10.1242/jcs.176768

Jaalouk, D. E., and Lammerding, J. (2009). Mechanotransduction gone awry. *Nat. Rev. Mol. Cell Biol.* 10, 63–73. doi: 10.1038/nrm2597

King, S. J., Asokan, S. B., Haynes, E. M., Zimmerman, S. P., Rotty, J. D., Alb, J. G. Jr., et al. (2016). Lamellipodia are crucial for haptotactic sensing and response. *J. Cell Sci.* 129, 2329–2342. doi: 10.1242/jcs.184507

Kirkbride, K. C., Sung, B. H., Sinha, S., and Weaver, A. M. (2011). Cortactin: a multifunctional regulator of cellular invasiveness. *Cell Adh. Migr.* 5, 187–198. doi: 10.4161/cam.5.2.14773

Krishnan, R., Park, C. Y., Lin, Y. C., Mead, J., Jaspers, R. T., Trepat, X., et al. (2009). Reinforcement versus Fluidization in Cytoskeletal Mechanoresponsiveness. *PLoS One* 4:e5486. doi: 10.1371/journal.pone.0005486

Lachowski, D., Cortes, E., Pink, D., Chronopoulos, A., Karim, S. A., Morton, J. P., et al. (2017). Substrate rigidity controls activation and durotaxis in pancreatic stellate cells. *Scientif. Rep.* 7, 1–12.

Lang, P., Gesbert, F., Delespine-Carmagnat, M., Stancou, R., Pouchelet, M., and Bertoglio, J. (1996). Protein kinase A phosphorylation of RhoA mediates the morphological and functional effects of cyclic AMP in cytotoxic lymphocytes. *EMBO J.* 15, 510–519. doi: 10.1002/j.1460-2075.1996.tb00383.x

Laufs, U., Adam, O., Strehlow, K., Wassmann, S., Konkol, C., Laufs, K., et al. (2003). Down-regulation of Rac-1 GTPase by Estrogen. *J. Biol. Chem.* 278, 5956–5962. doi: 10.1074/jbc.m209813200

Lautscham, L. A., Kämmerer, C., Lange, J. R., Kolb, T., Mark, C., Schilling, A., et al. (2015). Migration in confined 3D environments is determined by a combination of adhesiveness, nuclear volume, contractility, and cell stiffness. *Biophys. J.* 109, 900–913. doi: 10.1016/j.bpj.2015.07.025

Lessey, E. C., Guilluy, C., and Burridge, K. (2012). From mechanical force to RhoA activation. *Biochemistry* 51, 7420–7432. doi: 10.1021/bi300758e

Machacek, M., Hodgson, L., Welch, C., Elliott, H., Pertz, O., Nalbant, P., et al. (2009). Coordination of Rho GTPase activities during cell protrusion. *Nature* 461, 99–103. doi: 10.1038/nature08242

Maruthamuthu, V., Aratyn-Schaus, Y., and Gardel, M. L. (2010). Conserved F-actin dynamics and force transmission at cell adhesions. *Curr. Opin. Cell Biol.* 22, 583–588. doi: 10.1016/j.ceb.2010.07.010

Matellan, C., Del Río, and Hernández, A. E. (2019). Engineering the cellular mechanical microenvironment – from bulk mechanics to the nanoscale. *J. Cell Sci.* 132:jcs229013. doi: 10.1242/jcs.229013

McBeath, R., Pirone, D. M., Nelson, C. M., Bhadriraju, K., and Chen, C. S. (2004). Cell Shape, Cytoskeletal Tension, and RhoA Regulate Stem Cell Lineage Commitment. *Develop. Cell* 6, 483–495. doi: 10.1016/s1534-5807(04)00075-9

Miralles, F., Posern, G., Zaromytidou, A. I., and Treisman, R. (2003). Actin Dynamics Control SRF Activity by Regulation of Its Coactivator MAL. *Cell* 113, 329–342. doi: 10.1016/s0092-8674(03)00278-2

Mullins, R. D., Heuser, J. A., and Pollard, T. D. (1998). The interaction of Arp2/3 complex with actin: nucleation, high affinity pointed end capping, and formation of branching networks of filaments. *Proc. Natl. Acad. Sci. U S A.* 95, 6181–6186. doi: 10.1073/pnas.95.11.6181

Murrell, M., Oakes, P. W., Lenz, M., and Gardel, M. L. (2015). Forcing cells into shape: the mechanics of actomyosin contractility. *Nat. Rev. Mole. Cell Biol.* 16, 486–498. doi: 10.1038/nrm4012

Nardone, G., Oliver-De, La Cruz, J., Vrbsky, J., Martini, C., Pribyl, J., et al. (2017). YAP regulates cell mechanics by controlling focal adhesion assembly. *Nat. Commun.* 8:15321.

Oakes, P. W., Bidone, T. C., Beckham, Y., Skeeters, A. V., Ramirez-San Juan, G. R., and Winter, S. P. (2018). Lamellipodium is a myosin-independent mechanosensor. *Proc. Nat. Acad. Sci. U S A* 115, 2646–2651. doi: 10.1073/pnas.1715869115

Ohashi, K., Fujiwara, S., and Mizuno, K. (2017). Roles of the cytoskeleton, cell adhesion and rho signalling in mechanosensing and mechanotransduction. *J. Biochem.* 161, 245–254.

Olson, E. N., and Nordheim, A. (2010). Linking actin dynamics and gene transcription to drive cellular motile functions. *Nat. Rev. Mol. Cell Biol.* 11, 353–365. doi: 10.1038/nrm2890

Parsons, J. T., Horwitz, A. R., and Schwartz, M. A. (2010). Cell adhesion: integrating cytoskeletal dynamics and cellular tension. *Nat. Rev. Mol. Cell Biol.* 11, 633–643. doi: 10.1038/nrm2957

Paszek, M. J., Zahir, N., Johnson, K. R., Lakins, J. N., Rozenberg, G. I., Gefen, A., et al. (2005). Tensional homeostasis and the malignant phenotype. *Cancer Cell* 8, 241–254. doi: 10.1016/j.ccr.2005.08.010

Pellegrin, S., and Mellor, H. (2007). Actin stress fibres. *J. Cell Sci.* 120, 3491–3499. doi: 10.1242/jcs.018473

Pollard, T. D., and Cooper, J. A. (2009). Actin, a central player in cell shape and movement. *Science* 326, 1208–1212. doi: 10.1126/science.1175862

Prossnitz, E. R., and Barton, M. (2011). The G-protein-coupled estrogen receptor GPER in health and disease. *Nat. Rev. Endocrinol.* 7, 715–726.

Puleo, J. I., Parker, S. S., Roman, M. R., Watson, A. W., Eliato, K. R., Peng, L., et al. (2019). Mechanosensing during directed cell migration requires dynamic actin polymerization at focal adhesions. *J. Cell Biol.* 218, 4215–4235. doi: 10.1083/jcb.201902101

Reffay, M., Parrini, M. C., Cochet-Escartin, O., Ladoux, B., Buguin, A., Coscoy, S., et al. (2014). Interplay of RhoA and mechanical forces in collective cell migration driven by leader cells. *Nat Cell Biol.* 16, 217–223. doi: 10.1038/ncb2917

Revankar, C. M., Cimino, D. F., Sklar, L. A., Arterburn, J. B., and Prossnitz, E. R. (2005). A transmembrane intracellular estrogen receptor mediates rapid cell signaling. *Science* 307, 1625–1630. doi: 10.1126/science.1106943

Ridley, A. J. (2015). Rho GTPase signalling in cell migration. *Curr. Opin. Cell Biol.* 36, 103–112. doi: 10.1016/j.ceb.2015.08.005

Sadok, A., and Marshall, C. J. (2014). Rho GTPases: masters of cell migration. *Small GTPases* 5:e29710.

Sarper, M., Cortes, E., Lieberthal, T. J., Del Rio, and Hernandez, A. (2016). ATRA modulates mechanical activation of TGF-beta by pancreatic stellate cells. *Sci. Rep.* 6:27639.

Schindelin, J., Arganda-Carreras, I., Frise, E., Kaynig, V., Longair, M., Pietzsch, T., et al. (2012). Fiji: an open-source platform for biological-image analysis. *Nat. Methods* 9, 676–682. doi: 10.1038/nmeth.2019

Scott, L. E., Mair, D. B., Narang, J. D., Feleke, K., and Lemmon, C. A. (2015). Fibronectin fibrillogenesis facilitates mechano-dependent cell spreading, force generation, and nuclear size in human embryonic fibroblasts. *Integr. Biol.* 7, 1454–1465. doi: 10.1039/c5ib00217f

Solon, J., Levental, I., Sengupta, K., Georges, P. C., and Janmey, P. A. (2007). Fibroblast adaptation and stiffness matching to soft elastic substrates. *Biophys. J.* 93, 4453–4461. doi: 10.1529/biophysj.106.101386

Tojkander, S., Gateva, G., and Lappalainen, P. (2012). Actin stress fibers – assembly, dynamics and biological roles. *J Cell Sci.* 125, 1855–1864. doi: 10.1242/jcs.098087

Wang, L., Luo, J. Y., Li, B., Tian, X. Y., Chen, L. J., Huang, Y., et al. (2016). Integrin-YAP/TAZ-JNK cascade mediates atheroprotective effect of unidirectional shear flow. *Nature* 540(7634), 579–582. doi: 10.1038/nature20602

Wei, T., Chen, W., Wen, L., Zhang, J., Zhang, Q., Yang, J., et al. (2016). G protein-coupled estrogen receptor deficiency accelerates liver tumorigenesis by enhancing inflammation and fibrosis. *Cancer Lett.* 382, 195–202. doi: 10.1016/j.canlet.2016.08.012

Wolfenson, H., Bershadsky, A., Henis, Y., and Geiger, B. (2010). Actomyosin-generated tension controls the molecular kinetics of focal adhesions. *J. Cell Sci.* 124, 1425–1432. doi: 10.1242/jcs.077388

Wu, C., Asokan, S. B., Berginski, M. E., Haynes, E. M., Sharpless, N. E., Griffith, J. D., et al. (2012). Arp2/3 is critical for lamellipodia and response to extracellular matrix cues but is dispensable for chemotaxis. *Cell* 148, 973–987. doi: 10.1016/j.cell.2011.12.034

Xu, W. M., Baribault, H., and Adamson, E. D. (1998). Vinculin knockout results in heart and brain defects during embryonic development. *Development* 125, 327–337.

Yamaguchi, N., Mizutani, T., Kawabata, K., and Haga, H. (2015). Leader cells regulate collective cell migration via Rac activation in the downstream signaling of integrin β1 and PI3K. *Scientif. Rep.* 5:7656.

Yu, X., Li, F., Klussmann, E., Stallone, J. N., and Han, G. (2014). G protein-coupled estrogen receptor 1 mediates relaxation of coronary arteries via cAMP/PKA-dependent activation of MLCP. *Am. J. Physiol. Endocrinol. Metabol.* 307, E398–E407.

Yu, X., Zhang, Q., Zhao, Y., Schwarz, B. J., Stallone, J. N., Heaps, C. L., et al. (2017). Activation of G protein-coupled estrogen receptor 1 induces coronary artery relaxation via Epac/Rap1-mediated inhibition of RhoA/Rho kinase pathway in parallel with PKA. *PLoS One* 12:e0173085. doi: 10.1371/journal.pone.0173085

Zimmerman, M. A., Budish, R. A., Kashyap, S., and Lindsey, S. H. (2016). GPER-novel membrane oestrogen receptor. *Clin Sci.* 130, 1005–1016. doi: 10.1042/cs20160114

Conflict of Interest: The authors declare that the research was conducted in the absence of any commercial or financial relationships that could be construed as a potential conflict of interest.

frontiers in Cell and Developmental Biology

BRIEF RESEARCH REPORT
published: 18 January 2021
doi: 10.3389/fcell.2020.593234

Microtubule Severing Protein Fignl2 Contributes to Endothelial and Neuronal Branching in Zebrafish Development

*Zhangji Dong†, Xu Chen†, Yuanyuan Li†, Run Zhuo, Xiaona Lai and Mei Liu**

Key Laboratory of Neuroregeneration of Jiangsu and Ministry of Education, Co-innovation Center of Neuroregeneration, Nantong University, Nantong, China

Previously, *fidgetin* (*fign*) and its family members *fidgetin-like 1* (*fignl1*) and *fidgetin-like 2* (*fignl2*) were found to be highly expressed during zebrafish brain development, suggesting their functions in the nervous system. In this study, we report the effects of loss-of-function of these genes on development. We designed and identified single-guide RNAs targeted to generate *fign*, *fignl1*, and *fignl2* mutants and then observed the overall morphological and behavioral changes. Our findings showed that while *fign* and *fignl1* null mutants displayed no significant defects, *fignl2* null zebrafish mutants displayed pericardial edema, reduced heart rate, and smaller eyes; *fignl2* null mutants responded to the light-darkness shift with a lower swimming velocity. *fignl2* mRNAs were identified in vascular endothelial cells by *in situ* hybridization and re-analysis of an online dataset of single-cell RNAseq results. Finally, we used morpholino oligonucleotides to confirm that *fignl2* knockdown resulted in severe heart edema, which was caused by abnormal vascular branching. The zebrafish *fignl2* morphants also showed longer axonal length and more branches of caudal primary neurons. Taken together, we summarize that Fignl2 functions on cellular branches in endothelial cells and neurons. This study reported for the first time that the microtubule-severing protein Fignl2 contributes to cell branching during development.

Keywords: development, branching, neuron, vascular endothelial cells, fidgetin-like 2

OPEN ACCESS

Edited by:
Pedro Roda-Navarro, Universidad Complutense de Madrid, Spain

Reviewed by:
Srikala Raghavan, Institute for Stem Cell Science and Regenerative Medicine (inStem), India
Aurnab Ghose, Indian Institute of Science Education and Research, Pune, India

****Correspondence:***
Mei Liu
liumei@ntu.edu.cn

† These authors have contributed equally to this work

Specialty section:
This article was submitted to Cell Adhesion and Migration, a section of the journal Frontiers in Cell and Developmental Biology

Received: *10 August 2020*
Accepted: *21 December 2020*
Published: *18 January 2021*

Citation:
Dong Z, Chen X, Li Y, Zhuo R, Lai X and Liu M (2021) Microtubule Severing Protein Fignl2 Contributes to Endothelial and Neuronal Branching in Zebrafish Development. Front. Cell Dev. Biol. 8:593234. doi: 10.3389/fcell.2020.593234

INTRODUCTION

Morphology and motility of a cell are determined by the regulation of the cytoskeleton, especially microtubules. Microtubules form highly complex and dynamic arrays that play roles in various aspects of the development and function of cells. Microtubule dynamics are regulated by microtubule-associated proteins, of which microtubule severing proteins (MSPs) such as spastin, katanin, and fidgetin are key regulatory factors of microtubule dynamics (Karabay et al., 2004; Butler et al., 2010; Leo et al., 2015; Menon and Gupton, 2016). These MSPs are members of the AAA (ATPase family associated with various cellular activities) family, which is capable of severing microtubules into short fragments by forming a hexamer that consumes ATP (Sharp and Ross, 2012; McNally and Roll-Mecak, 2018).

Studies on katanin and spastin demonstrated that they primarily cut stable long microtubules into short ones for microtubule transport or elongation at new generating plus ends, while

fidgetin (Fign) and its family members may have more functions. *fign* mutation resulted in mice "fidget" behavior (Yang et al., 2005); human FIGN suppressed microtubule growth via minus-end depolymerization during cell division (Mukherjee et al., 2012); FIGNL1 is regarded to regulate DNA homologous recombination repair (Yuan and Chen, 2013; Kumar et al., 2019) or meiotic crossovers (Girard et al., 2015); Charafeddine et al. reported that Fign12 modulates orientation of cell migration by shearing microtubules (Charafeddine et al., 2015), and O'Rourke el al. showed that Fign12 affected wound healing (O'Rourke et al., 2019). We previously studied Fign's function in rat brain astrocytes and found that Fign depletion resulted in a remarkable increase in tyrosine-modified microtubules, and thus changed the microtubule orientation in the cell cortical region (Hu et al., 2017). Leo et al. reported that Fign knockout in mice neurons increased the unacetylated microtubule mass (Leo et al., 2015). However, Drosophila Fign facilitates microtubule disassembly in dendrites but not in axons after neuron injury (Tao et al., 2016). These inconsistent functional features of Fign family members in different species or cell types have aroused our interest. Therefore, we attempted to comparatively study the functions of Fign family members in one animal model.

Similar to mice, rats and humans, there are three Fign paralogues, namely Fign, Fidgetin-like 1 (Fignl1), and Fidgetin-like 2 (Fignl2) in zebrafish. In the literature on Fign family members' functions, only Fignl1 was reported to be enriched in axons and growth cones of neurons and to play roles in the motor circuit in zebrafish larvae (Fassier et al., 2018), and Fignl1 overexpressed in zebrafish embryos inhibited ciliogenesis and decreased ciliary length (Zhao et al., 2016); however, the functions of Fign and Fignl2 remain elusive. Recently, we investigated the expression patterns of *fign* and its family members, *fidgetin-like 1* (*fignl1*) and *fidgetin-like 2* (*fignl2*), during zebrafish embryonic development, and *fign* genes were found highly expressed during brain development, suggesting their functions in the nervous system (Dong et al., 2021). In this study, we aim to compare the developmental features after loss-of-function of these genes to further clarify their functions and possible mechanism.

RESULTS

Generation and Phenotype Analysis of Mutants of *fign*, *fignl1,* and *fignl2*

CRISPR/Cas9 was used to generate mutants harboring new alleles of Fign, Fignl1, and Fignl2 that contain frame-shift mutations. Selected target sites are shown in **Table 1** as sense strand genomic sequences. Incross was performed in the F1 generation to produce homozygous mutant F2 and siblings of the other two genotypes shown in this study.

fign sgRNA1-5 were able to induce ∼30% indel mutations in injected zebrafish embryos at 24 hpf. sgRNA5 was used to generate mutants for the following studies, producing mutated alleles *ntu702* and *ntu703* (**Figure 1A**), resulting in a protein completely missing the AAA domain (**Figure 1A**). *fignl1* sgRNA1 induced a mutation level of 20% in 24 hpf embryos, generating the mutated allele *ntu704* (**Figure 1A**), leading to a complete loss of the AAA-type ATPase domain. *fignl2* sgRNA1 was found to be active with a somatic mutation rate of 30–40% in the founders at 24 hpf. One mutated allele was found to have a deletion of 3 bp and an insertion of 1 bp and was named *ntu705* (**Figure 1A**), resulting in complete loss of AAA domain (**Figure 1A**).

F2 embryos were imaged for morphological changes at 4 dpf and behavioral analysis at 5 dpf and collected for genotyping to identify any phenotype caused by loss-of-function of *fignl2*. Embryos with *fignl2* mutations were found to have pericardial edema and smaller eyes, and the phenotypes were dependent on gene dose because homozygous mutants showed more severe edema and heart congestion (**Figure 1D**), while Fign and Fignl1 mutants showed no significant phenotypes in the pericardial area and the heart (**Figures 1B,C**). Cardiovascular problems may lead to embryonic death; thus, we checked the survival of embryos with mutated *fignl2*. The ratios of genotypes at 5 and 6 dpf were far from the Mendelian segregation, where the percentage of homozygous mutants was significantly reduced, demonstrating that the survival ability of mutants was weakened by the mutation and suggesting developmental abnormalities caused by loss-of-function of *fignl2* (**Figure 1E**). However, no similar reduction in the number of homozygous mutants during development was observed in *fign* or *fignl1* mutants (**Figure 1E**). Homozygous mutants had greater pericardial edema index (PEI) compared to wild type and heterozygous mutant siblings (**Figure 1F**). *fignl2* depletion leads to phenotypes with a lower heart rate and smaller eyes (**Figure 1G**), in addition to pericardial edema. Then, the mutants and wild type siblings were imaged for behavioral analysis using light stimuli. Larvae were treated with a 10-min light and 10-min darkness cycle after an initial 30-min adaptation in darkness. The *fignl2* homozygous mutants responded to the light-dark shift with a lower swimming velocity than wild type siblings (**Figure 1H**), whereas *fign* and *fignl1* knockout mutants were able to swim faster than wild type siblings.

fignl2 Is Highly Expressed in Vascular Endothelial Cells and Neuronal Cells in Zebrafish Compared With *fign and fignl1*

As the mutants had problems in the cardiovascular system, and the Fign homologs were not previously described to be expressed in the heart and vessels, we then examined the expression of *fignl2* during zebrafish development using *in situ* hybridization. At 24 hpf, *fignl2* was mainly observed in the midbrain-hindbrain boundary, hindbrain, and somites as well as in the eyes and pectoral fins. Interestingly, in the family of Fign homologs in zebrafish, only *fignl2* was detected at a low level in the caudal vessels using *in situ* hybridization (**Figure 2A**), whereas *fign* and *fignl1* were not detected.

Due to the limitation of sensitivity of *in situ* hybridization, we utilized the online resource of single-cell sequencing data of zebrafish embryos (Gene Expression Omnibus accession number GSE112294) (Wagner et al., 2018) to check the expression of *fignl2*. According to the original research, the single cells were mapped to the forebrain, midbrain, hindbrain, and other tissues. This dataset provided an abundance of resources containing

TABLE 1 | sgRNAs used in this study.

sgRNA	Gene	Position in gene	Sequence	Location in CDS	Mutation[#]
Fign-sgRNA1	*Fign* [ENSDARG00000008662]	150565–150584	CTTACAGCGGCGGTCAAAGC		∼30%
Fign-sgRNA2		150618–150637	TTGCACAGCGCTGGCCTCCT		∼30%
Fign-sgRNA3		150660–150679	CCAACCCTGGTGCCCAGCTA		∼30%
Fign-sgRNA4		150719–150738	TCCAGCAGGGTATCCCCCAC		∼30%
Fign-sgRNA5		150801–150820	TCAGGCATTGCTGCCCCCAC	785–804*	∼30%
Fignl1-sgRNA1	*fignl1* [ENSDARG00000016427]	9947–9966	GGCCTTAGAGGTCCACCTAA	1245–1264**	∼20%
Fignl2-sgRNA1	*fignl2* [ENSDARG00000057062]	99460–99479	GGCTATCAGAACAGCAGTGT	801–820***	∼40%

[#]*Mutation measured by estimation based on sequencing of amplicon containing the targeted fragment.*
**Calculated according to fign mRNA NM_001020575.*
***Calculated according to fignl1 mRNA NM_001128751.*
****Calculated according to fignl2 mRNA NM_001214908.*

the most systematic temporal expression information, and more importantly, the most in-depth sequencing, allowing analysis of genes expressed at low levels.

We then focused on verifying the expression of *fignl2*, especially in endothelial cells. We analyzed *fignl2* expression during zebrafish development (along with its two paralogues, **Figures 2Bb2–5**) and labeled cells expressing *fignl2* from the dataset (**Figure 2Bb4**). Cells expressing *fignl2* were found in all brain regions and somites. Interestingly, when we highlighted endothelial cells at 18 and 24 hpf; many of these cells showed *fignl2* expression (**Figure 2Bb4′**). According to the clustering results in the original research, cells expressing *fignl2* include neural stem cells, neurons, epithelial cells, somite cells, and endothelial cells. Further analysis of the transcript levels of *fign*, *fignl1,* and *fignl2* in the cluster of endothelial cells revealed that the transcript amount of *fignl2* is remarkably more than those of *fign* and *fignl1* (**Figures 2Bb2′–b5′**).

Using the same method, we distinguished the cluster of neuronal cells according to *elavl3* expression and displayed the neuronal cells isolated from the dataset (**Figure 2Bb1′′**). The *fign*, *fignl1*, and *fignl2* transcripts are shown in **Figures 2Bb2′′–b4′′** and a violin plot (**Figure 2Bb5′′**), and the results clearly showed that *fignl2* had significantly higher transcript levels in neuronal cells than did Fign or Fignl1. Given the *fignl2* mutants with a lower swimming velocity, we also extracted the expression data of *mnx1*-positive motor neurons and analyzed the transcript levels of *fign*, *fignl1*, and *fignl2* (**Figure 2Bb5′′′**), and the results showed that the level of *fignl2* transcripts was notably higher than those of *fign* and *fignl1*.

The above results showed that *fignl2* is expressed in more tissues with high levels than its paralogous genes, which may explain why *fignl2* null mutant zebrafish displayed serious abnormal phenotypes.

Loss of *fignl2* Caused Abnormalities in Branching in Endothelial Cells and Neurons

We then wanted to confirm whether the loss of Fignl2 indeed resulted in heart defects in zebrafish. Genomic gene defects may cause some secondary effects to alter developmental features; thus, we performed gene knockdown using morpholino oligonucleotides (MOs) to determine if similar phenotypes, that is, a phenocopy of the mutants, could be generated. Splicing-blocking MO was designed to target the splicing acceptor of intron 2 in *fignl2* (**Figure 3A**), and a series of doses of the MO were tested. The *fignl2*-MO resulted in partial (0.3 mM) or complete (0.5 and 0.6 mM) deletion of a 34 bp fragment in the coding sequence due to activation of a cryptic splice site (**Figures 3B,C**). Then, 0.5 mM splice-blocking MO was injected into 1-cell stage Tübingen (Tu) zebrafish embryos. The phenotypes observed in the *fignl2* mutants also appeared in these morphants. At 4 dpf, *fignl2* morphants displayed pericardial edema and reduced eye size. *fignl2* morphants with pericardial edema had a lower heart rate than did those injected with control MO (**Figures 3D–D′′′**). Morphants with higher levels of MO displayed more severe phenotypes (data not shown).

Pericardial edema suggested abnormalities in the cardiovascular system during development. To further understand the function of *fignl2* in zebrafish development, we generated *fignl2* morphants using MO in transgenic zebrafish *Tg(kdrl:GFP)* labeling endothelial cells (Jin et al., 2005). *fignl2* MO was injected into 1-cell stage *Tg(kdrl:GFP)* embryos, and the embryos were used for morphological observation and blood vessel imaging at 48 hpf.

Intersegmental blood vessels (ISVs) in *fignl2* morphants showed more branching and an improper direction of growth. Some ISVs were linked to a neighboring ISV to form a Y shape or a circle (**Figures 3E,E′**), which was observed in both segmental arteries and veins, identified by whether they connected to the dorsal aorta or posterior cardinal vein (Ellertsdottir et al., 2010). Fignl2 is known to be a member of the AAA-type ATPase family with microtubule-severing function, and it is involved in regulating microtubule behaviors such as cellular pseudopodia extension and branching. We injected CRISPR/Cas9 in different combinations to determine whether the *fign* family members differ in their function in regulating endothelial branching. Co-injection of Cas9 mRNA and sgRNAs targeting *fign* and *fignl1* caused minor defects in ISV branching, and in the embryos that received co-injection of CRISPR/Cas9 targeting *fign*, *fignl1*, and *fignl2*, the morphological changes seemed to be mainly contributed by mutation of *fignl2* (**Supplementary Figure 1A**).

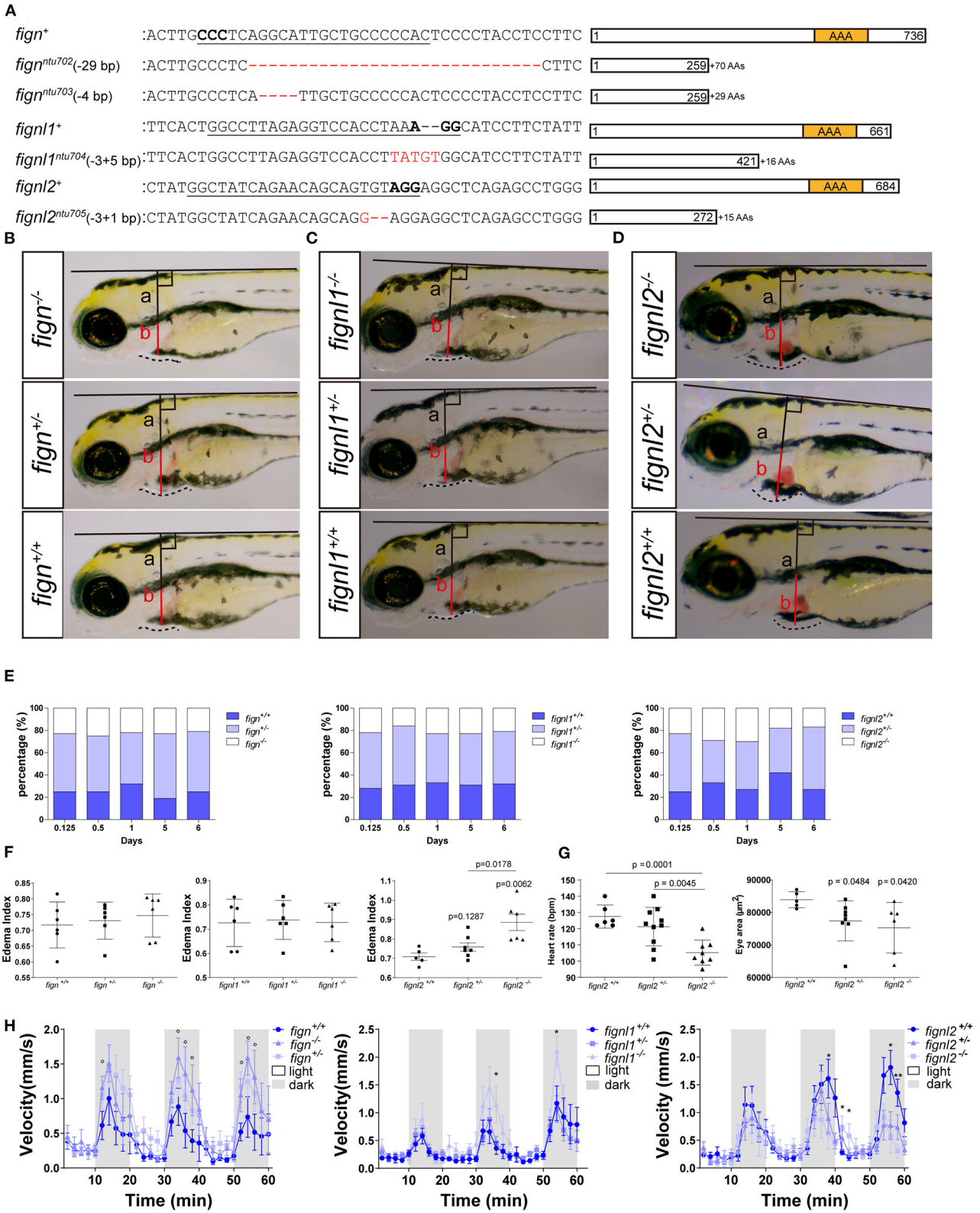

FIGURE 1 | Loss of *fignl2* leads to smaller eyes, pericardial edema, and reduced swimming velocity. **(A)** Mutated alleles generated using CRISPR/Cas9 lead to complete loss of the AAA-type ATPase domain. Underlined sequences are the CRISPR targets, wherein the bases in bold are the proto-spacer adjacent motifs

(Continued)

FIGURE 1 | (sequences are shown only on the sense strand). **(B–D)** Representative phenotype observation and edema index measurement in Fign mutants **(B)**, Fignl1 mutants **(C)**, and Fignl2 mutants **(D)** at 4 dpf. **(E)** Percentage of the filial embryos generated by crossing of *fign*$^{+/ntu702}$ × *fignl2*$^{+/ntu702}$, *fignl1*$^{+/ntu704}$ × *fignl2*$^{+/ntu704}$ and *fignl2*$^{+/ntu705}$ × *fignl2*$^{+/ntu705}$, showing partial embryonic lethality of *fignl2* loss-of-function. Significance of differences compared to the wild type group is shown as p values on top of each dataset, and those between different mutant genotypes are shown on a horizontal line indicating groups used for comparison. **(F)** Statistics of pericardial edema index (PEI), $n = (6,6,6)$ and (6,6,6) and (5,8,6); $^{*}p < 0.05$, showing that the severity of edema was negatively correlated with functional *fignl2* alleles. **(G)** Heart rate of the filial embryos generated by crossing of *fignl2*$^{+/ntu705}$ × *fignl2*$^{+/ntu705}$ showing abnormalities in the cardiovascular system in the *fignl2* mutants, $n = 6,10,8$. Eyes of the filial embryos generated by crossing of *fignl2*$^{+/ntu705}$ × *fignl2*$^{+/ntu705}$ showing abnormalities in the cardiovascular system in the *fignl2* mutants, $n = 5,8,6$. **(H)** Statistics of swimming velocity with 10-min light-dark cycle of *fign*, *fignl1*, and *fignl2* mutants at 5 dpf, $n = (12,25,9)$ and (14,22,11), and (20,19,9), showing weakened swimming ability of *fignl2* mutants. Circles indicate a $p < 0.1$, asterisks (*) indicate a $p < 0.05$, and (**) indicates a $p < 0.01$, as indicated by the Student's *t*-test between the wild type and homozygous mutant groups.

Microtubule dynamics are essential not only in endothelial branching, but also in the development of other cell types, especially in axon extension, and branching in neurons. Since the loss-of-function of Fignl2 affects branching in endothelial cells, it may cause changes in neurons where it is not only expressed but at a higher level. We performed similar treatments and observations at 28 hpf in *Tg(mnx1:GFP)* (Flanagan-Steet et al., 2005) (caudal primary neurons expressing GFP) for the effect of *fignl2* knockdown, and the loss of *fignl2* led to elongated axons and increased the number of branches in *mnx1*-expressing neurons (**Figures 3F–F′′′**) at 28 hpf and at 5 dpf (**Supplementary Figure 2**). Co-injection of Cas9 mRNA and sgRNAs targeting *fign* and *fignl1* reduced neurite length, which was consistent with the reported observation with MO targeting *fignl1* (Fassier et al., 2018). However, loss of *fignl2* resulted in longer neurites and more branching, and a similar result was observed in the embryos that received injection of CRISPR/Cas9 targeting *fign*, *fignl1*, and *fignl2* (**Supplementary Figure 2**).

Twitching of zebrafish embryos represents a type of spontaneous movement (Muto et al., 2011). We observed and recorded, and unexpectedly found that the spontaneous twitching at 28 hpf was more frequent in *fignl2* morphants (**Figure 3G** and **Supplementary Video 1**).

DISCUSSION AND CONCLUSION

As members of the AAA ATPase family, *fign* paralogous genes play various roles, and their functions are relatively poorly understood for a short research history. We previously investigated and compared the expression patterns of *fign*, *fignl1*, and *fignl2* during zebrafish development and found that Fignl2 is expressed at higher levels in the nervous system and other tissues than *fign* and *fignl1* genes, which is consistent with the result of re-analyzed online single-cell RNAseq data (GEO GSE112294) (Wagner et al., 2018). Furthermore, *fign*, *fignl1*, and *fignl2* were also shown to be expressed in zebrafish endothelial cells. However, knockout of *fign* or *fignl1* did not yield obvious phenotypes, whereas depletion of *fignl2* (at the genomic DNA level or mRNA level) caused serious zebrafish defects such as pericardial edema, reduced heart rate, and reduced swimming velocity. These hinted that Fignl2 may have some important functions, which Fign or Fignl1 fails to compensate, but not *vice versa*. We further used GFP-labeled vascular endothelial cells or motor neurons to reveal that *fignl2* knockdown resulted in abnormal vascular branching as well as longer axonal length and more branches of caudal primary neurons, clarifying that Fignl2 regulates cellular branching. The pericardial edema or the weakened reaction to the lighting shifts in Fignl2-depleted zebrafish may be due to abnormal branching in endothelial cells or neurons. Twitching behavior, the first behavior in developing zebrafish, was used to evaluate the activity of the motor circuit (Muto et al., 2011). Twitching was more frequent in the *fignl2* morphants (**Figure 3G** and **Supplementary Video 1**), suggesting that depletion of *fignl2* impaired spontaneous movement, while the decreased response after light-to-darkness shift suggested changes in vision-related circuits in the *fignl2* morphants.

Although there were some differences between the morphants and the mutants, which could have been caused by genetic compensations (Rossi et al., 2015), they exhibited similar changes after knock down or knockout. These results, together with those of the rescue experiment using *fignl2* mRNA, indicate that the phenotypes seen in the endothelial cells and *mnx1* neurons are *fignl2*-specific.

Cellular branch formation is a universal morphological change during development. In developmental processes, including angiogenesis and neurogenesis, microtubule dynamics regulates cell branching morphogenesis by mediating branch orientation or extension (Liu et al., 2010; Myers et al., 2011; Hu et al., 2012; Lyle et al., 2014; Dong et al., 2019). This study presented cellular branches alteration in morphology of ISVs and CaP neurons. Microtubule severing proteins like Fign homologs strongly affect microtubule length and direction in neurons (Leo et al., 2015; Tao et al., 2016; Fassier et al., 2018; Matamoros et al., 2019) and other cell types (Hu et al., 2017), and our study offered clear data that Fignl2 is involved in cell branching.

Our previous study showed that *fign*, *fignl1,* and *fignl2* are similar in their high expression in the central nervous system during zebrafish early development, while fignl2 is also expressed in other tissues, e.g., pronephros, where fign and fignl1 are not detectable (Dong et al., 2021). The difference in expression patterns indicate figns function during cell branching may have differentiated. Although animals with ablated *fign*, *fignl1,* and/or *fignl2* tend to swim fast under constant lighting, *fignl2* null mutants responded to "light to darkness shift" more weakly than their wildtype or heterozygous siblings, indicating this change in vision-related behavior resulted from eye defect due to *fignl2* loss of function.

In summary, this study provided comparative results of the preliminary functional analyses of *fign*, *fignl1*, and *fignl2* in one

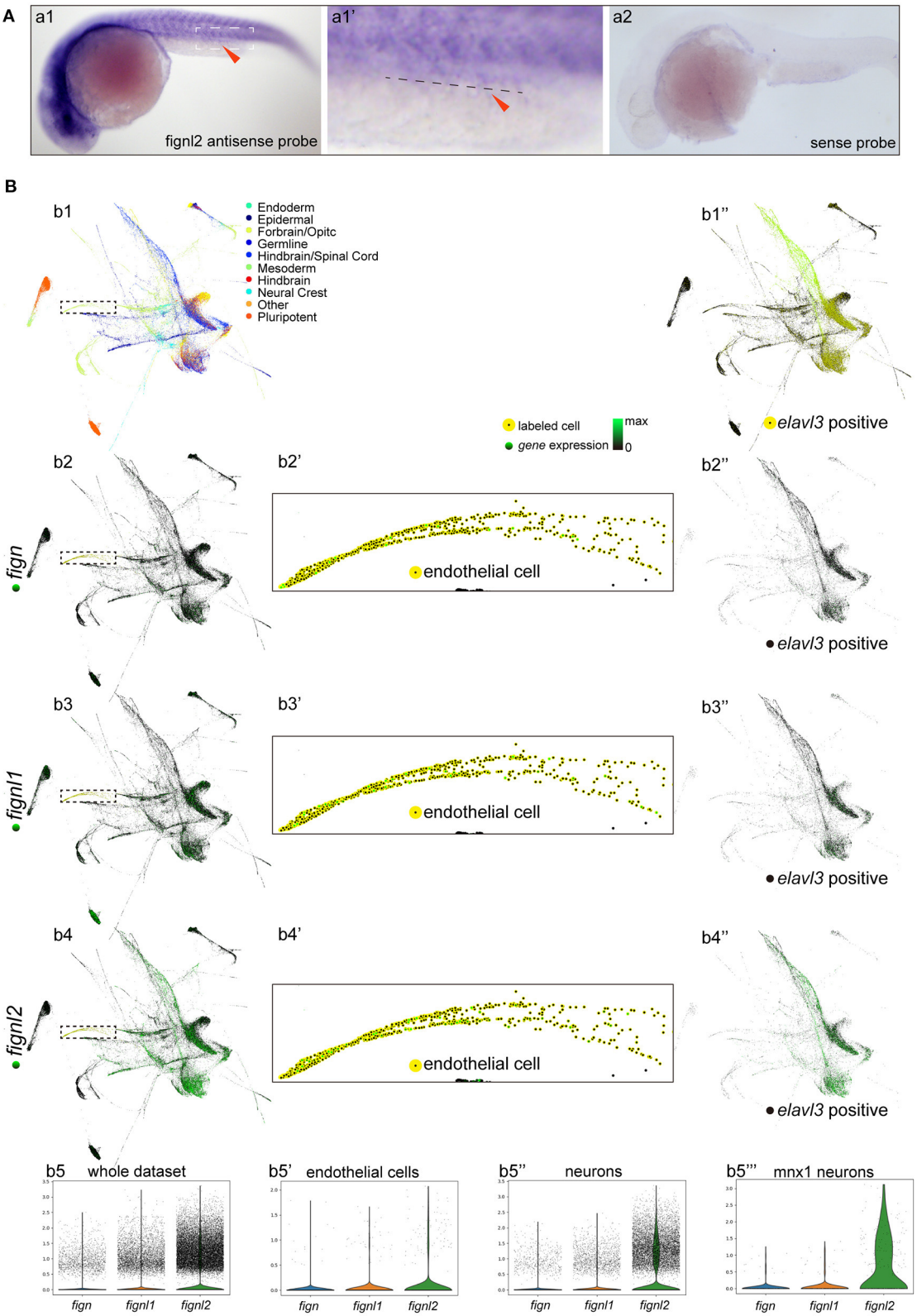

FIGURE 2 | Expression of *fign*, *fignl1,* and *fignl2* in zebrafish embryos. **(A)** Expression analysis of *fignl2* using *in situ* hybridization. (a1) *fignl2* expression is observed in the nervous system and somites at 24 hpf, and weak staining is also observed in caudal blood vessels (arrowhead) (Enlarged in **a1'**). **(a2)** *in situ* hybridization using a

(Continued)

FIGURE 2 | *fignl2* sense probe as control. **(B)** Single-cell expression analysis of *fign*, *fignl1,* and *fignl2* during zebrafish development (a re-analysis of GEO GSE112294). **(b1)** Single-cells in the dataset (4–24 hpf) are mapped to different tissues. **(b2–b4)** Expression of *fign*, *fignl1,* and *fignl2* in the single-cell dataset. **(b5)** Violin plot of *fign*, *fignl1,* and *fignl2* expression in the single-cell expression dataset of zebrafish embryos (4–24 hpf). **(b2′-b4′)** Expression of *fign*, *fignl1,* and *fignl2* in endothelial cells (18 and 24 hpf). **(b5′)** Violin plot of *fign*, *fignl1,* and *fignl2* expression in endothelial cells (18 and 24 hpf). **(b1′′)** Neuronal cells were isolated by *elavl3* expression. **(b2′′-b4′′)** Expression of *fign*, *fignl1,* and *fignl2* in *elavl3*-positive cells. **(b5′′)** Violin plot of *fign*, *fignl1,* and *fignl2* expression in *elavl3*-positive cells. **(b5′′′)** Violin plot of *fign*, *fignl1,* and *fignl2* expression in *mnx1* positive cells. Expression data for violin plots are normalized and presented as counts per 10^4.

zebrafish developmental system. Here, we report the finding that the microtubule-severing protein, Fignl2, contributes to proper cell branching during endothelial and neuronal development.

MATERIALS AND METHODS

Zebrafish Husbandry

Zebrafish were housed in the Zebrafish Center at Nantong University. Zebrafish embryos of Tübingen and *Tg(flk:GFP)* were obtained through natural mating and maintained at 28.5°C. Embryos older than 24 h post-fertilization (hpf) were treated with 0.2 mM 1-phenyl-2-thio-urea (PTU, Sigma P7629, a tyrosinase inhibitor commonly used to block pigmentation and aid visualization of zebrafish development). Breeding of *fign* mutant zebrafish was performed by Nanjing YSY Biotech Company Ltd.

Bioinformatics

The zebrafish *fignl2* genomic information was obtained from GenBank (Gene ID: 561837, mRNA NM_001214908.1, protein NP_001201837.1). Conserved domains of the *fignl2* proteins were localized according to the Ensembl database (http://www.ensembl.org/). *fignl2* sequences were aligned using Vector NTI software (http://www.thermofisher.com/). The phylogenetic tree was generated using MEGA X (https://www.megasoftware.net/) from aligned sequences generated with Clustal W (https://www.genome.jp/tools-bin/clustalw). The zebrafish embryo single-cell sequencing dataset (Wagner et al., 2018) was obtained from (https://kleintools.hms.harvard.edu/paper_websites/wagner_zebrafish_timecourse2018/mainpage.html) and visualized using SPRING (Weinreb et al., 2018). The run.py script for data preparation was modified to import original clustering results for visualization and is provided as **Supplementary Document 1**. Expression analyses were performed using Scanpy 1.5.1 (https://github.com/theislab/scanpy/) in a Python 3.8.3 environment, where neurons were extracted using the marker gene *elavl3*, and *mnx1*-positive neurons were extracted regarding *mnx1* expression. Expression data of endothelial cells were extracted according to the original clustering results provided in the dataset. The Python script is provided in **Supplementary Document 2**.

Morpholino and Microinjection

The sgRNA templates were prepared by PCR with a forward primer composed of the first 17 bases of minimum T7 promoter followed by 20 bases identical to target proto-spacer and 20 bases identical to the first 20 bases of sgRNA scaffold, a reverse primer complementary to the last 25 bases of sgRNA scaffold (**Table 2**) and a template plasmid pT7-gRNA kindly provided by Prof. Bo Zhang at Peking University. The PCR products were used as templates for *in vitro* transcription using MAXIscript T7 Kit (Invitrogen, USA) to obtain sgRNAs. Capped Cas9 mRNA was prepared by *in vitro* transcription using mMessage mMachine T7 Kit (Invitrogen, USA) with a zebrafish optimized Cas9 template plasmid pGH-T7-zCas9 (Liu et al., 2014) kindly provided by Prof. Bo Zhang at Peking University. Cas9 mRNA and sgRNA were mixed and adjusted to a final concentration of 300 ng/μl:100 ng/μl. The MOs were synthesized by Gene Tools Company. MO antisense oligomers were prepared at a stock concentration of 1 mM according to the manufacturer's protocol. The sequence of zebrafish *fignl2* splicing MO in this study was 5′-TCAGAAATGTAGCACTTACTATAGG-3′ and the standard control MO was 5′-CCTCTTACCTCAGTTACAATTTATA-3′. MOs or mixtures containing 300 ng/μl Cas9 mRNA and 100 ng/μL sgRNA were injected into *Tg(flk:EGFP)* or *Tg(mnx1:EGFP)* embryos at 1 nL of solution per embryo using borosilicate glass capillaries (Sutter, USA) pulled using a P-97 micropipette puller (Sutter, USA) and connected to an IM-400 pneumatic microinjector (Narishige, Japan).

RNA Extraction, Reverse Transcription, and RT-PCR

Tissue was homogenized and frozen in TRIzol UP (TransGen Biotech, Beijing, China) and stored at −80°C. Total RNA was extracted following the manufacturer's instructions. RNA (1 μg) was reverse-transcribed into cDNA using the HiScript II 1st Strand cDNA Synthesis Kit (Vazyme, Nanjing, China) according to the manufacturer's instructions. Synthesized cDNA was stored at −20°C.

Whole Mount *in situ* Hybridizations

The 24 hpf cDNA served as templates for cloning *fignl2* fragments to make antisense RNA probes for zebrafish *fignl2*. The *fignl2* primers for RT-PCR were: Left primer, 5′-TCCTGCTATTTGGCCCTCAA-3′; Right primer, 5′-ACAACTCCCTTTCGCTGAGA-3′; the amplicon is a 441 bp fragment in the coding sequence for *fignl2*. Digoxigenin (DIG)-labeled RNA sense and antisense probes were made from the linearized plasmids using the DIG RNA Labeling Kit (SP6/T7) (Roche). Whole mount *in situ* hybridization was performed following the methods as previously described (Schulte-Merker et al., 1992). The concentration of probes was 2 ng/μl in fresh hyb$^+$, and for blocking purpose, 2% blocking reagent (Boehringer blocking reagent, Roche), 10% sheep serum (Sigma), and 70% MAB (YSY, Nanjing, China) were used.

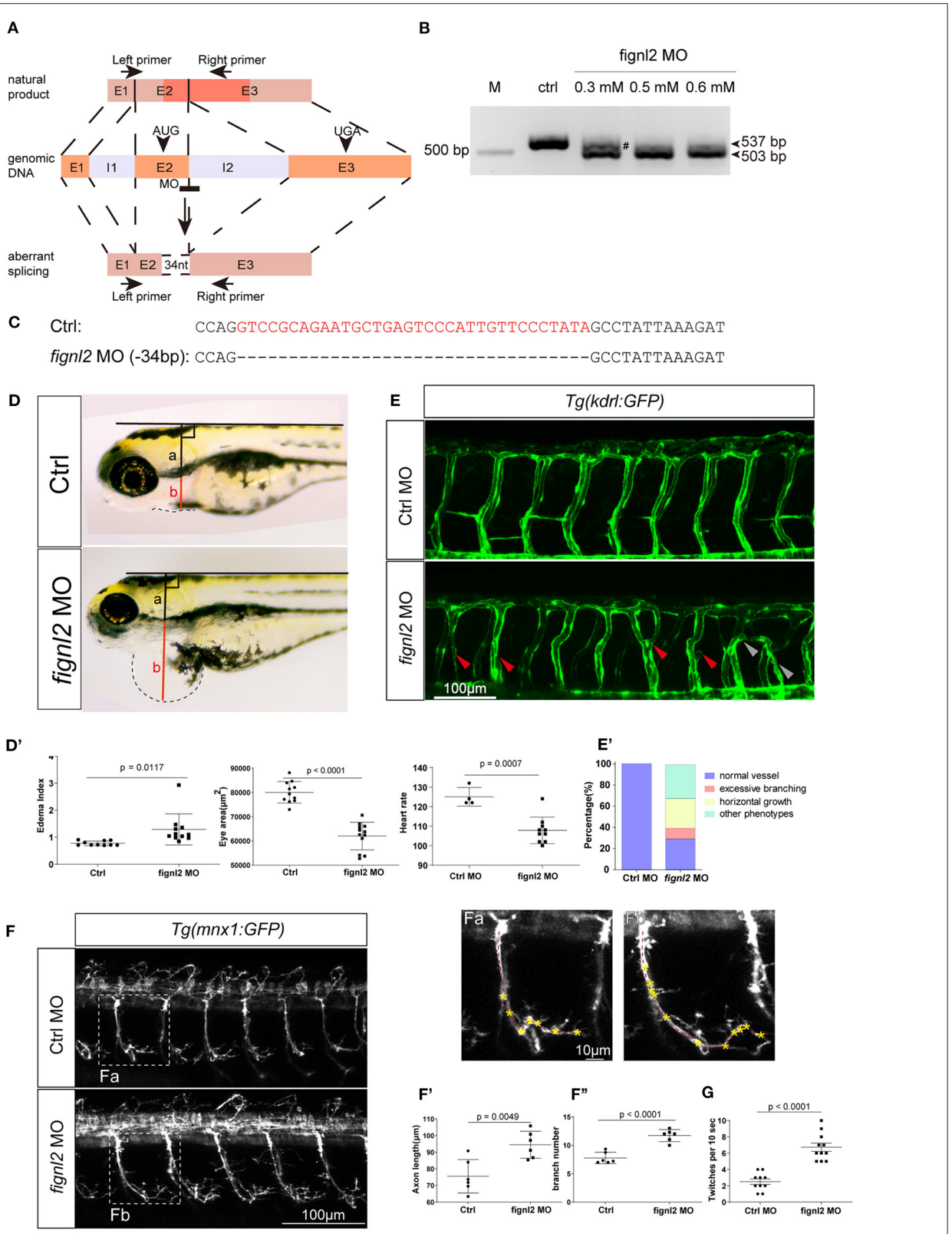

FIGURE 3 | Depletion of *fignl2* causes morphological changes in intersegmental vessels (ISVs) and caudal primary neurons. **(A)** Schematic diagram of morpholino oligonucleotide (MO) induced *fignl2* knockdown causing aberrant splicing. **(B)** MO treatment results in mRNA size change in *fignl2* RT-PCR amplicon. The pound sign

(Continued)

FIGURE 3 | (#) shows some amplicons of the original size detected after treatment with 0.3 mM MO. **(C)** MO treatment results in a 34-bp deletion in *fignl2* mRNA. **(D)** *fignl2* knockdown causes pericardial edema in developing zebrafish. Graphical representation of edema index **(D′)**, eye size **(D′′)**, heart rate **(D′′′)** in Ctrl and *fignl2* knockdown zebrafish. Ctrl MO, $n = 10$; *fignl2* MO, $n = 11$. **(E)** *fignl2* knockdown causes morphological changes in ISVs, arrows showing malformations. Graphical representation **(E′)** of the percentage of different form of ISV malformations caused by *fignl2* knockdown. Ctrl MO, $n = 10$; *fignl2* MO, $n = 11$. **(F)** *fignl2* knockdown causes morphological changes in caudal primary neurons, including greater axon length and increased branching. Representative axons were shown enlarged in (Fa) and (Fb). Graphical representation of axon length **(F′)**, primary branch numbers **(F′′)** in Ctrl and *fignl2* knockdown zebrafish. Ctrl MO, $n = 10$; *fignl2* MO, $n = 11$. **(G)** *fignl2* mutants shows more frequent twitching. Twitching was counted in 10 s. Ctrl MO, $n = 10$; *fignl2* MO, $n = 11$.

TABLE 2 | PCR primers for gRNA template preparation and genotyping of the mutants produced in this study.

Primer	Sequence (5′-3′)
T7-gRNA-primer-F	TAATACGACTCACTATA + proto spacer + GTTTTAGAGCTAGAAATAGC
gRNA-primer-R	AAAAAAAGCACCGACTCGGTGCCAC
fignl2-genotyping-F	GCAGCTCCTGCAGTGGGCCCCATTC
fignl2-genotyping-R	CTCTTCTAATGCTGCTTTAATGTG
fignl2-seq-F	TCAACCGAACCCTACACTTC
fign-genotyping-F	GCTGTGCTGCAGATGTGATT
fign-genotyping-R	GGCTTAAACGCCAAAGATGA
fign-seq-F	CACCTCCAGATGTGACAGCA
fignl1-genotyping-F	TTGAAGGACAACACACCAAAAGATA
fignl1-genotyping-R	TACAGTATAGGCCGAACC
fignl1-seq-R	TACAGTATAGGCCGAACC

Imaging

For confocal imaging of blood vessel development in *Tg(flk:GFP)* zebrafish and the neurons in *Tg(mnx1:GFP)* zebrafish, embryos were anesthetized with egg water/0.16 mg/mL tricaine (Sigma E10521)/1% 1-phenyl-2-thiourea (Sigma P7629) and embedded in 0.6% agarose. Images were taken using a Leica TCS SP5 LSM confocal microscope (Leica, Wetzlar, Germany). The analysis was performed using Imaris (http://www.bitplane.com/). For behavioral studies, zebrafish juveniles were imaged using the Noldus DanioVision system and analyzed using EthoVision XT software (https://www.noldus.com/). Animals were placed in a 48-well plate, each juvenile occupying a well. Before the beginning of detection, the light was kept off for 30 min, followed by three tandem 10 min light/10 min darkness cycles with video recording for light/dark shift behavior studies, or 15 min with the light on for spontaneous behavior observation.

Measurement and Statistics

Axon length and branching were measured and counted as previously described (Dong et al., 2019). We measured the extent of pericardial edema by defining a PEI: from the center of the pericardium (P), a perpendicular to the extended back midline was made and let the intersection be A; let the distance from P to A be a and the radius of the pericardium be b; the pericardial edema index is defined as b/(b-a). All data analysis, statistical comparisons, and graphs were generated using GraphPad Prism 5 (http://www.graphpad.com/scientific-software/prism/). Significance of differences was analyzed using Student's *t*-test. Data are expressed as mean ± S.E.M. (standard error of the mean).

DATA AVAILABILITY STATEMENT

The datasets presented in this study can be found in online repositories. The names of the repository/repositories and accession number(s) can be found in the article/**Supplementary Material**.

ETHICS STATEMENT

The animal study was reviewed and approved by Ethics Committee on Animal Experimentation of Nantong University.

AUTHOR CONTRIBUTIONS

ZD, XC, YL, RZ, and XL carried out the experiments, data collection, and analysis. ZD and ML prepared the manuscript. ZD and ML contributed to study design and management. All authors contributed to the article and approved the submitted version.

FUNDING

This study was supported from the National Natural Science Foundation of China (31701049 and 32070725), grants from Natural science foundation of Jiangsu Province (BK20150404 and BK20171253), funding from the Priority Academic Program Development (PAPD) of Jiangsu Higher Education Institutions, and the Large Instruments Open Foundation of Nantong University (KFJN2078).

SUPPLEMENTARY MATERIAL

The Supplementary Material for this article can be found online at: https://www.frontiersin.org/articles/10.3389/fcell.2020.593234/full#supplementary-material

REFERENCES

Butler, R., Wood, J. D., Landers, J. A., and Cunliffe, V. T. (2010). Genetic and chemical modulation of spastin-dependent axon outgrowth in zebrafish embryos indicates a role for impaired microtubule dynamics in hereditary spastic paraplegia. *Dis. Model. Mech.* 3, 743–751. doi: 10.1242/dmm.004002

Charafeddine, R. A., Makdisi, J., Schairer, D., O'Rourke, B. P., Diaz-Valencia, J. D., Chouake, J., et al. (2015). Fidgetin-Like 2: a microtubule-based regulator

of wound healing. *J. Invest. Dermatol.* 135, 2309–2318. doi: 10.1038/jid.2015.94

Dong, Z., Li, Y., Chen, X., Lai, X., and Liu, M. (2021). A comparative study of the expression patterns of Fign family members in zebrafish embryonic development. *Comp. Biochem. Physiol. B Biochem. Mol. Biol.* 251:110522. doi: 10.1016/j.cbpb.2020.110522

Dong, Z., Wu, S., Zhu, C., Wang, X., Li, Y., Chen, X., et al. (2019). Clustered Regularly Interspaced Short Palindromic Repeats (CRISPR)/Cas9-mediated kif15 mutations accelerate axonal outgrowth during neuronal development and regeneration in zebrafish. *Traffic* 20, 71–81. doi: 10.1111/tra.12621

Ellertsdottir, E., Lenard, A., Blum, Y., Krudewig, A., Herwig, L., Affolter, M., et al. (2010). Vascular morphogenesis in the zebrafish embryo. *Dev. Biol* 341, 56–65. doi: 10.1016/j.ydbio.2009.10.035

Fassier, C., Freal, A., Gasmi, L., Delphin, C., Ten Martin, D., De Gois, S., et al. (2018). Motor axon navigation relies on fidgetin-like 1-driven microtubule plus end dynamics. *J. Cell Biol.* 217, 1719–1738. doi: 10.1083/jcb.201604108

Flanagan-Steet, H., Fox, M. A., Meyer, D., and Sanes, J. R. (2005). Neuromuscular synapses can form *in vivo* by incorporation of initially aneural postsynaptic specializations. *Development* 132, 4471–4481. doi: 10.1242/dev.02044

Girard, C., Chelysheva, L., Choinard, S., Froger, N., Macaisne, N., Lemhemdi, A., et al. (2015). AAA-ATPase FIDGETIN-LIKE 1 and helicase FANCM antagonize meiotic crossovers by distinct mechanisms. *PLoS Genet.* 11:e1005369. doi: 10.1371/journal.pgen.1005369

Hu, J., Bai, X., Bowen, J. R., Dolat, L., Korobova, F., Yu, W., et al. (2012). Septin-driven coordination of actin and microtubule remodeling regulates the collateral branching of axons. *Curr. Biol.* 22, 1109–1115. doi: 10.1016/j.cub.2012.04.019

Hu, Z., Feng, J., Bo, W., Wu, R., Dong, Z., Liu, Y., et al. (2017). Fidgetin regulates cultured astrocyte migration by severing tyrosinated microtubules at the leading edge. *Mol. Bio. Cell* 28, 545–553. doi: 10.1091/mbc.E16-09-0628

Jin, S. W., Beis, D., Mitchell, T., Chen, J. N., and Stainier, D. Y. (2005). Cellular and molecular analyses of vascular tube and lumen formation in zebrafish. *Development* 132, 5199–5209. doi: 10.1242/dev.02087

Karabay, A., Yu, W., Solowska, J. M., Baird, D. H., and Baas, P. W. (2004). Axonal growth is sensitive to the levels of katanin, a protein that severs microtubules. *J. Neurosci.* 24, 5778–5788. doi: 10.1523/JNEUROSCI.1382-04.2004

Kumar, R., Duhamel, M., Coutant, E., Ben-Nahia, E., and Mercier, R. (2019). Antagonism between BRCA2 and FIGL1 regulates homologous recombination. *Nucleic Acids Res.* 47, 5170–5180. doi: 10.1093/nar/gkz225

Leo, L., Yu, W., D'Rozario, M., Waddell, E. A., Marenda, D. R., Baird, M. A., et al. (2015). Vertebrate fidgetin restrains axonal growth by severing labile domains of microtubules. *Cell Rep.* 12, 1723–1730. doi: 10.1016/j.celrep.2015.08.017

Liu, D., Wang, Z., Xiao, A., Zhang, Y., Li, W., Zu, Y., et al. (2014). Efficient gene targeting in zebrafish mediated by a zebrafish-codon-optimized cas9 and evaluation of off-targeting effect. *J. Genet. Genomics* 41, 43–46. doi: 10.1016/j.jgg.2013.11.004

Liu, M., Nadar, V. C., Kozielski, F., Kozlowska, M., Yu, W., and Baas, P. W. (2010). Kinesin-12, a mitotic microtubule-associated motor protein, impacts axonal growth, navigation, and branching. *J. Neurosci.* 30, 14896–14906. doi: 10.1523/JNEUROSCI.3739-10.2010

Lyle, K. S., Corleto, J. A., and Wittmann, T. (2014). Microtubule dynamics regulation contributes to endothelial morphogenesis. *Bioarchitecture* 2, 220–227. doi: 10.4161/bioa.22335

Matamoros, A. J., Tom, V. J., Wu, D., Rao, Y., Sharp, D. J., and Baas, P. W. (2019). Knockdown of fidgetin improves regeneration of injured axons by a microtubule-based mechanism. *J. Neurosci.* 39, 2011–2024. doi: 10.1523/JNEUROSCI.1888-18.2018

McNally, F. J., and Roll-Mecak, A. (2018). Microtubule-severing enzymes: From cellular functions to molecular mechanism. *J. Cell Biol.* 217, 4057–4069. doi: 10.1083/jcb.201612104

Menon, S., and Gupton, S. L. (2016). Building blocks of functioning brain: cytoskeletal dynamics in neuronal development. *Int. Rev. Cell Mol. Biol.* 322, 183–245. doi: 10.1016/bs.ircmb.2015.10.002

Mukherjee, S., Diaz Valencia, J. D., Stewman, S., Metz, J., Monnier, S., Rath, U., et al. (2012). Human Fidgetin is a microtubule severing the enzyme and minus-end depolymerase that regulates mitosis. *Cell Cycle* 11, 2359–2366. doi: 10.4161/cc.20849

Muto, A., Ohkura, M., Kotani, T., Higashijima, S., Nakai, J., and Kawakami, K. (2011). Genetic visualization with an improved GCaMP calcium indicator reveals spatiotemporal activation of the spinal motor neurons in zebrafish. *Proc. Natl. Acad. Sci. U.S.A.* 108, 5425–5430. doi: 10.1073/pnas.1000887108

Myers, K. A., Applegate, K. T., Danuser, G., Fischer, R. S., and Waterman, C. M. (2011). Distinct ECM mechanosensing pathways regulate microtubule dynamics to control endothelial cell branching morphogenesis. *J. Cell Biol.* 192, 321–334. doi: 10.1083/jcb.201006009

O'Rourke, B. P., Kramer, A. H., Cao, L. L., Inayathullah, M., Guzik, H., Rajadas, J., et al. (2019). Fidgetin-Like 2 siRNA enhances the wound healing capability of a surfactant polymer dressing. *Adv. Wound Care* 8, 91–100. doi: 10.1089/wound.2018.0827

Rossi, A., Kontarakis, Z., Gerri, C., Nolte, H., Holper, S., Kruger, M., et al. (2015). Genetic compensation induced by deleterious mutations but not gene knockdowns. *Nature* 524, 230–233. doi: 10.1038/nature14580

Schulte-Merker, S., Ho, R. K., Herrmann, B. G., and Nusslein-Volhard, C. (1992). The protein product of the zebrafish homologue of the mouse T gene is expressed in nuclei of the germ ring and the notochord of the early embryo. *Development* 116, 1021–1032.

Sharp, D. J., and Ross, J. L. (2012). Microtubule-severing enzymes at the cutting edge. *J. Cell Sci.* 125, 2561–2569. doi: 10.1242/jcs.101139

Tao, J., Feng, C., and Rolls, M. M. (2016). The microtubule-severing protein fidgetin acts after dendrite injury to promote their degeneration. *J. Cell Sci.* 129, 3274–3281. doi: 10.1242/jcs.188540

Wagner, D. E., Weinreb, C., Collins, Z. M., Briggs, J. A., Megason, S. G., and Klein, A. M. (2018). Single-cell mapping of gene expression landscapes and lineage in the zebrafish embryo. *Science* 360, 981–987. doi: 10.1126/science.aar4362

Weinreb, C., Wolock, S., and Klein, A. M. (2018). SPRING: a kinetic interface for visualizing high dimensional single-cell expression data. *Bioinformatics* 34, 1246–1248. doi: 10.1093/bioinformatics/btx792

Yang, Y., Mahaffey, C. L., Berube, N., Nystuen, A., and Frankel, W. N. (2005). Functional characterization of fidgetin, an AAA-family protein mutated in fidget mice. *Exp. Cell Res.* 304, 50–58. doi: 10.1016/j.yexcr.2004.11.014

Yuan, J., and Chen, J. (2013). FIGNL1-containing protein complex is required for efficient homologous recombination repair. *Proc. Natl. Acad. Sci. U.S.A.* 110, 10640–10645. doi: 10.1073/pnas.1220662110

Zhao, X., Jin, M., Wang, M., Sun, L., Hong, X., Cao, Y., et al. (2016). Fidgetin-like 1 is a ciliogenesis-inhibitory centrosome protein. *Cell Cycle* 15, 2367–2375. doi: 10.1080/15384101.2016.1204059

Conflict of Interest: The authors declare that the research was conducted in the absence of any commercial or financial relationships that could be construed as a potential conflict of interest.

frontiers in Cell and Developmental Biology

REVIEW
published: 04 February 2021
doi: 10.3389/fcell.2021.629097

Role of Actin Cytoskeleton Reorganization in Polarized Secretory Traffic at the Immunological Synapse

Victor Calvo[1] *and Manuel Izquierdo*[2*]

[1] *Departamento de Bioquímica, Facultad de Medicina, Instituto de Investigaciones Biomédicas Alberto Sols, Consejo Superior de Investigaciones Científicas - Universidad Autónoma de Madrid (CSIC-UAM), Madrid, Spain,* [2] *Instituto de Investigaciones Biomédicas Alberto Sols, Consejo Superior de Investigaciones Científicas - Universidad Autónoma de Madrid, Madrid, Spain*

T cell receptor (TCR) and B cell receptor (BCR) stimulation by antigen presented on an antigen-presenting cell (APC) induces the formation of the immune synapse (IS), the convergence of secretory vesicles from T and B lymphocytes toward the centrosome, and the polarization of the centrosome to the immune synapse. Immune synapse formation is associated with an initial increase in cortical F-actin at the synapse, followed by a decrease in F-actin density at the central region of the immune synapse, which contains the secretory domain. These reversible, actin cytoskeleton reorganization processes occur during lytic granule degranulation in cytotoxic T lymphocytes (CTL) and cytokine-containing vesicle secretion in T-helper (Th) lymphocytes. Recent evidences obtained in T and B lymphocytes forming synapses show that F-actin reorganization also occurs at the centrosomal area. F-actin reduction at the centrosomal area appears to be involved in centrosome polarization. In this review we deal with the biological significance of both cortical and centrosomal area F-actin reorganization and some of the derived biological consequences.

Keywords: T lymphocytes, B lymphocytes, immune synapse, actin cytoskeleton, protein kinase C δ, centrosome, multivesicular bodies, FMNL1

OPEN ACCESS

Edited by:
Pedro Roda-Navarro, Universidad Complutense de Madrid, Spain

Reviewed by:
Cosima T. Baldari, University of Siena, Italy
Enrique Aguado, University of Cádiz, Spain

***Correspondence:**
Manuel Izquierdo
mizquierdo@iib.uam.es

Specialty section:
This article was submitted to Cell Adhesion and Migration, a section of the journal Frontiers in Cell and Developmental Biology

Received: *13 November 2020*
Accepted: *11 January 2021*
Published: *04 February 2021*

Citation:
Calvo V and Izquierdo M (2021) Role of Actin Cytoskeleton Reorganization in Polarized Secretory Traffic at the Immunological Synapse. Front. Cell Dev. Biol. 9:629097. doi: 10.3389/fcell.2021.629097

INTRODUCTION

T and B lymphocyte activation by antigen-presenting cells (APC) takes place at a specialized cell to cell interface called the immunological synapse (IS). IS establishment by T and B lymphocytes is a very dynamic, plastic and critical event, acting as a tunable signaling platform that integrates spatial, mechanical and biochemical signals, involved in antigen-specific, cellular and humoral immune responses (Fooksman et al., 2010; de la Roche et al., 2016). The IS is described by the formation of a concentric, bullseye spatial pattern, termed the supramolecular activation complex (SMAC), upon cortical actin reorganization (Billadeau et al., 2007; Griffiths et al., 2010; Yuseff et al., 2013; Kuokkanen et al., 2015). This reorganization yields a central cluster of antigen receptors bound to antigen called central SMAC (cSMAC) and a surrounding adhesion molecule-rich ring, called peripheral SMAC (pSMAC), which appears to be crucial for adhesion with the APC (Monks et al., 1998; Fooksman et al., 2010). Surrounding

the pSMAC, at the edge of the contact area with the APC, is the distal SMAC (dSMAC), which consists of a circular array of dense filamentous actin (F-actin) (Griffiths et al., 2010; Le Floc'h and Huse, 2015) (**Figure 1A**).

T cell receptor (TCR) and B cell receptor (BCR) stimulation by antigen presented by APC, together with accessory molecules interaction with their ligands on the APC, induces IS formation, convergence of T and B lymphocyte secretory vesicles toward the centrosome and, almost simultaneously, centrosome polarization to the IS (Huse, 2012; de la Roche et al., 2016). This leads to polarized secretion of extracellular vesicles, lytic granules, stimulatory cytokines, or lytic proteases (**Figure 1**). The centrosome is the major microtubule organization center (MTOC) in T and B lymphocytes, and consists of two centrioles surrounded by pericentriolar material (PCM), generating a radial organization of microtubules (Sanchez and Feldman, 2017). IS formation is associated with an initial increase in cortical F-actin at the IS (Billadeau et al., 2007), followed by a decrease in F-actin density at the central region of the IS that includes the cSMAC and contains the secretory domain (Griffiths et al., 2010; Ritter et al., 2015). Subsequently, F-actin recovery at the cSMAC leads to conclusion of lytic granule secretion in cytotoxic T lymphocytes (CTL) (Ritter et al., 2017). These reversible actin cytoskeleton reorganization processes occur during lytic granule secretion in CTL and cytokine-containing vesicle secretion in T-helper (Th) lymphocytes (Na et al., 2015; Ritter et al., 2017).

IMMUNE SYNAPSE MORPHOLOGY FORMED BY DIFFERENT IMMUNE CELLS

The IS has long been characterized by the general concentric architecture that adopts during its maturation (Le Floc'h and Huse, 2015). The bullseye actin cytoskeleton architecture of the IS and the F-actin reorganization process are common to $CD4^+$ Th lymphocytes, $CD8^+$ CTL, B lymphocytes, and natural killer (NK) cells forming IS (Rak et al., 2011; Lagrue et al., 2013; Le Floc'h and Huse, 2015). However, for space reasons in this review we deal only with IS made by T and B lymphocytes. The bullseye pattern of a mature synapse includes redistribution of F-actin and surface receptors in concentric regions. In this context, radially symmetric spreading of the T lymphocyte over the surface of the APC is conducted by protrusive actin polymerization (Le Floc'h and Huse, 2015; de la Roche et al., 2016), leading to TCR-pMHC interactions at the tip of these actin-rich interdigitations (de la Roche et al., 2016). This is accompanied by the formation of TCR microclusters in the synaptic membrane that, as TCR signaling is initiated, coalesce in the center of the synapse to form the cSMAC (Le Floc'h and Huse, 2015; de la Roche et al., 2016). Thus, as the IS develops, retrograde (centripetal) F-actin flow drives TCR microclusters into the cSMAC, while F-actin intensively reorganizes into the peripheral ring that will become the dSMAC (Le Floc'h and Huse, 2015). F-actin flow within the dSMAC promotes adhesion by clustering integrins such as LFA-1 in the pSMAC (Comrie et al., 2015), that eventually will interact with ICAM-1 located on the APC (**Figure 1B**), reinforcing adhesion between these cells and amplifying TCR signaling (Le Floc'h and Huse, 2015; de la Roche et al., 2016). Remarkably, all the above mentioned immune cells share the capability to directionally secrete stimulatory cytokines, proteases, cytotoxic factors, or extracellular vesicles (including exosomes) at the IS (Calvo and Izquierdo, 2020). This F-actin structure for polarized secretion is thought to enhance the specificity and efficiency of the triggered biological responses (Le Floc'h and Huse, 2015). Although the IS formed by all these immune cells share this general F-actin pattern, important differences in terms of stability, duration but also synaptic F-actin structure exist among $CD4^+$ Th, $CD8^+$ CTL, B lymphocytes, and NK cells (Murugesan et al., 2016; Carisey et al., 2018). For instance, whereas $CD4^+$ cells form stable IS (from minutes up to several hours), that are necessary for both directional and continuous secretion of stimulatory cytokines (Ueda et al., 2011), IS made by primed CTL trigger the rapid polarization (from seconds to very few minutes) of their lytic granules or secretory lysosomes (SL) toward the IS (Griffiths et al., 2010; Huse, 2012). CTL form very transient IS, lasting only few minutes, until target cells are eliminated. Optimal CTL function is thought to require rapid and transient contacts in order to consecutively deliver as many successive lethal hits as possible to several target cells (Calvo and Izquierdo, 2020). Apart from these kinetic and stability differences, the canonical bullseye actin pattern was described in $CD4^+$ T lymphocytes using lipid bilayers or upon interaction with B cells. However, a variation of this canonical pattern was observed when $CD4^+$ T lymphocytes were challenged with dendritic cells as APC, resulting in a multifocal cell to cell IS (Brossard et al., 2005; Kumari et al., 2019). Thus, 3D spatial differences between the IS made by the same immune cell type exist. Moreover, under comparable stimulation conditions, differences in actin cytoskeleton spatial organization and dynamics among immortalized human and primary mouse and human T lymphocytes exist (Colin-York et al., 2019; Kumari et al., 2019), and there are differences in the organization and molecular mechanisms underlying these F-actin networks (Kumari et al., 2019) (**Table 1**).

Although IS architecture and dynamics are major determinants of antigen recognition and signaling by TCR and BCR, the molecular components that contribute to the

Abbreviations: 3D-SIM, 3D structured illumination microscopy; ADAP, adhesion and degranulation-adaptor protein; APC, antigen-presenting cell; BCR, B-cell receptor for antigen; ^{C}, center of mass; cSMAC, central supramolecular activation cluster; CTL, cytotoxic T lymphocytes; DAG, diacylglycerol; DGKα, diacylglycerol kinase α; DGKζ, diacylglycerol kinase ζ; Dia1, Diaphanous-1; dSMAC, distal supramolecular activation cluster; F-actin, filamentous actin; FMNL1, formin-like 1; ILPs; invadosome-like protrusions; IS, immune synapse; ITAM, immunoreceptor tyrosine-based motifs; LAT, linker activation of T cells; LFA-1, lymphocyte function-associated antigen 1; LLSM, lattice light sheet microscopy; MHC, major histocompatibility complex; MVB, multivesicular bodies; MTOC, microtubule-organizing center; NK, natural killer; NPFs, actin nucleation promoting factors; PCM, pericentriolar material; PKC, protein kinase C; PKCθ, protein kinase C θ isoform; PKD, protein kinase D; PLC, phospholipase C; PKCδ, protein kinase C δ isoform; pSMAC, peripheral supramolecular activation cluster; ROI, region of interest; SEE, staphylococcal enterotoxin E; SIM, structured illumination microscopy; SL, secretory lysosomes; SLP76, SH2 domain-containing leukocyte protein of 76 kDa; SMAC, supramolecular activation cluster; STED, stimulated emission depletion; TCR, T-cell receptor for antigen; Th, T-helper; TIRFM, total internal reflection fluorescence microscopy; WASH; Wiskott-Aldrich syndrome protein and SCAR homolog; WASp, Wiskott-Aldrich syndrome protein; ZAP70, Syk-kinase zeta chain-associated protein of 70 kDa.

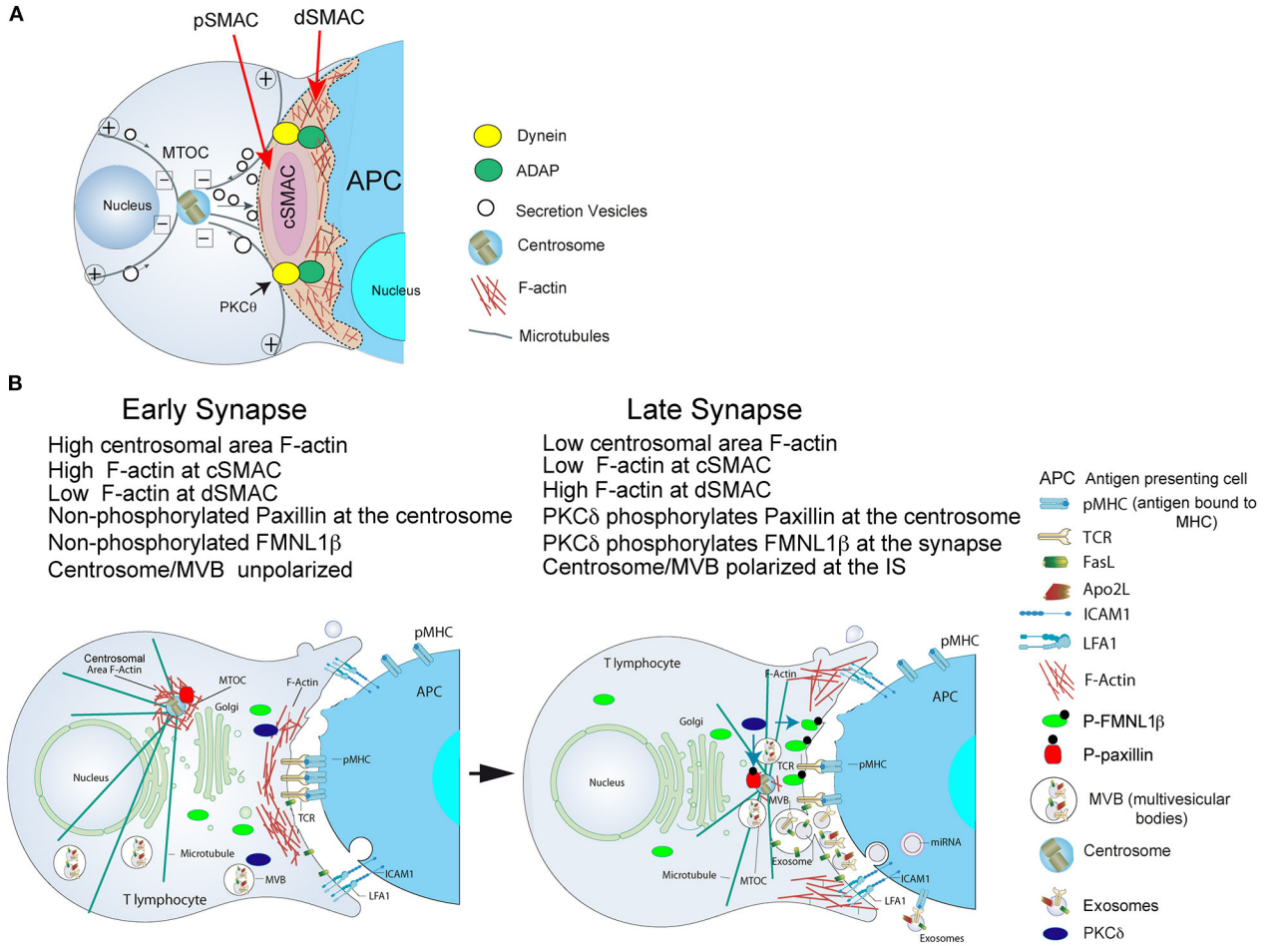

FIGURE 1 | (A) Cortical actin cytoskeleton reorganization and MTOC polarization. After the initial scanning contact of TCR with pMHC on the APC, both naive and effector T lymphocytes form mature IS with antigen-presenting cells (APC). Th IS lasts many hours during which *de novo* cytokine (i.e., IL-2, IFN-γ) production and secretion occur, that require continuous TCR signaling. Primed effector CTL establish more transient, mature IS after scanning the target cells (i.e., a virus-infected cell), and secrete lytic granules within a few minutes. Secretory vesicles (lytic granules in CTL and cytokine-containing vesicles in Th cells) are rapidly transported (several minutes for Th cells and very few minutes or seconds for effector CTL) toward the MTOC (in the minus "–" direction) and, almost simultaneously, the MTOC polarizes toward the cSMAC of the IS, a F-actin poor area that constitutes a secretory domain. MTOC translocation to the IS appears to be dependent on PKCθ-controlled dynein anchored to ADAP at the pSMAC, that pulls MTOC in the minus direction. In both types of IS, the initial F-actin reorganization in the cell-to-cell contact area, followed by a decrease in F-actin at the cSMAC and an accumulation of F-actin at the dSMAC appears to be involved in vesicle secretion. **(B)** Actin cytoskeleton reorganization events occurring at the $CD4^+$ Jurkat T lymphocyte IS model: PKCδ and MTOC/MVB polarization: both FMNL1β and paxillin are phosphorylated by PKCδ. Before forming the IS, both FMNL1β (in the cytosol) and paxillin (located at the centrosome), proteins that regulate the assembly and disassembly of F-actin, are dephosphorylated, which keeps them inactive. Left: in an early IS there is an accumulation of F-actin in the central region of the IS, while the centrosome is surrounded by a dense F-actin network that keeps it retained near the nucleus and away from the IS. Right: after PKCδ is activated by TCR stimulation at the IS, FMNL1β is phosphorylated in the C-terminal, DAD autoinhibitory domain, and is located in the IS (P-FMNL1β). In addition, paxillin is phosphorylated in Threonine 538 and remains located in the centrosome (P-paxillin). These events lead to F-actin reduction at the central region of the IS that corresponds to cSMAC, F-actin accumulation into the dSMAC and the depolymerization of F-actin surrounding the centrosome. All these processes, most probably acting in a coordinated manner, may facilitate the movement of the centrosome toward the IS and the convergence of MVB toward the F-actin depleted area in the cSMAC, which facilitates MVB fusion at the cSMAC and the subsequent secretion of exosomes (Calvo and Izquierdo, 2020) in the synaptic cleft toward the APC. For more details please refer to Herranz et al. (2019) and Bello-Gamboa et al. (2020).

distinct F-actin patterns observed in IS formed by different immune cells remain largely unknown (Kumari et al., 2019). Indeed, this knowledge is required to understand how different immune cells acquire and develop their functional specialization. It has been speculated that the actin cytoskeleton can arbitrate a force balance across the IS interface to regulate the dimensions and lifetimes of diverse subsynaptic zones that, in turn, may alter different T cell activation steps (Kumari et al., 2019). Remarkably, several F-actin regulatory proteins are different for each synapse subtype (summarized in **Table 1**), thus these differences may underlie the spatiotemporal differences in F-actin architecture

TABLE 1 | F-actin reorganization and polarized secretion events in T and B lymphocyte IS and involved proteins.

	T lymphocyte IS		B lymphocyte IS	
(*)	**CTL/APC**	**CD4$^+$ T cell /APC**	**B/APC**	**B /CD4$^+$ T cell**
F-actin reorganization at the IS	+ CDC42/WASP/ARP2/3(Billadeau et al., 2007; Sinai et al., 2010) TAGNL2 (Na et al., 2015)	+ CDC42/WASP/ARP2/3 (Chemin et al., 2012) dynamin 2 (Gomez et al., 2005) CDC42 (Stowers et al., 1995) FMNL1, Dia1 (Murugesan et al., 2016) HS1 (Gomez et al., 2006) TAGNL2 (Na et al., 2015)	+ CDC42/WASP/ARP2/3 Ezrin, Moesin(Kuokkanen et al., 2015)	+ TAGNL2(Na et al., 2016)
F-actin reduction at cSMAC and centrosome polarization	+ (Ritter et al., 2015, 2017) CDC42/IQGAP1 (Stowers et al., 1995; Stinchcombe et al., 2006)	+ PKCδ, FMNL1β(Herranz et al., 2019; Bello-Gamboa et al., 2020) Dynein(Combs et al., 2006; Liu et al., 2013; Sanchez et al., 2019)	+ dynein, proteasome(Schnyder et al., 2011; Ibanez-Vega et al., 2019)	Unknown
F-actin reduction at centrosome and centrosome polarization	Unknown	+ PKCδ, paxillin (Bello-Gamboa et al., 2020) WASH, ARP2/3(Farina et al., 2016)	+ ARP2/3(Obino et al., 2016) Proteasome(Ibanez-Vega et al., 2019)	Unknown
Lytic granules and/or Exosome secretion	+ (Peters et al., 1989)	+ (Alonso et al., 2011)	+ (Yuseff et al., 2011; Kuokkanen et al., 2015)	+ (Muntasell et al., 2007)
Centrosome polarization	+ (Stinchcombe et al., 2006)	+ (Ueda et al., 2011)	+ (Yuseff et al., 2011)	+ (Duchez et al., 2011)
Mechanisms of centrosome polarization	Paxillin (Herreros et al., 2000; Robertson and Ostergaard, 2011) FMNL1, Dia1 (Gomez et al., 2007) CDC42/IQGAP1 (Stowers et al., 1995; Stinchcombe et al., 2006)	FMNL1, Dia1 (Gomez et al., 2007) PKCθ, dynein (Quann et al., 2009) CDC42 (Stowers et al., 1995) PKCδ, paxillin(Herranz et al., 2019; Bello-Gamboa et al., 2020)	ARP2/3 (Obino et al., 2016) Proteasome(Ibanez-Vega et al., 2019)	Unknown
DAG/DGK-control of centrosome polarization.	+ (Quann et al., 2009)	+ DAG, DGKα(Quann et al., 2009; Alonso et al., 2011) DAG, dynein(Liu et al., 2013) DAG/dynein/PKC (Sanchez et al., 2019)	+ DAG, DGKζ (Merino-Cortés et al., 2020)	Unknown
PKC/PKD control of secretory granules/MVB traffic	+ PKCδ (Ma et al., 2007) PKCθ(Monks et al., 1998; Quann et al., 2011)	+ PKCδ (Herranz et al., 2019) PKD1/2 (Mazzeo et al., 2016)	+ PKCζ (Siemasko et al., 1998; Yuseff et al., 2011) PKD1/3 (Mazzeo et al., 2016)	Unknown

(*) The quoted biological response in the first column corresponds to the response of the effector, first cell type for each indicated cell-cell synapse.

existing among different IS. It is out of the scope of this review to detail these differences, please refer to some excellent reviews on this subject, that include also data on F-actin reorganization in the IS made by NK cells (Billadeau et al., 2007; Lagrue et al., 2013; Hammer et al., 2018; Li et al., 2018; Blumenthal and Burkhardt, 2020).

SIGNALS REGULATING CORTICAL ACTIN REORGANIZATION IN THE IMMUNE SYNAPSE

cSMAC, pSMAC, and dSMAC formation characterizes a mature IS and is the basis of a signaling platform that integrates signals and coordinates molecular interactions leading to both exocytic and endocytic processes, necessary for an appropriate antigen-specific immune response (Griffiths et al., 2010; Xie et al., 2013). Actin reorganization plays a central role in IS maintenance, as well as in antigen receptor-derived signaling (Billadeau et al., 2007). In brief, TCR and BCR stimulation, together with interaction of adhesion and co-stimulatory molecules at the IS, trigger early second messengers such as calcium and diacyglycerol (DAG) (Izquierdo and Cantrell, 1992). DAG regulates several protein kinase C (PKC) family members (including novel PKC members, PKCδ and PKCθ), protein kinase D (PKD1), and Ras/ERK2 pathway (Spitaler et al., 2006), leading to the activation of the two major actin regulatory pathways: the formin (FMNL1 and Dia) pathway involved in

F-actin nucleation, and the CDC42/WASP/ARP2/3 pathway involved in actin filament branching (Kühn and Geyer, 2014; Kumari et al., 2014). In the IS made by T lymphocytes, TCR engagement triggers multiple signaling pathways that regulate actin organization and rearrangements at the different F-actin networks inside and outside the IS (Billadeau et al., 2007; Kumari et al., 2014; Le Floc'h and Huse, 2015; Hammer et al., 2018). Thus, actin polymerization is a result of complex molecular interactions, and a diverse and complex set of TCR-downstream molecular pathways contributes to actin polymerization. Once the T cell is bound to the pMHC complex on the APC, the immunoreceptor tyrosine-based motifs (ITAM) in the cytosolic tail of the TCR-associated CD3 complex undergo phosphorylation, which then serve as docking sites for the Syk-kinase zeta chain-associated protein of 70 kDa (ZAP70) (Kumari et al., 2014). CD3-recruited ZAP70 then leads to phosphorylation and activation of two key adaptor molecules that associate with a variety of molecules in TCR-associated signaling complexes. First, ZAP70 phosphorylates linker activation of T cells (LAT), which in turn associates via Gads with the SH2 domain-containing leukocyte protein of 76 kDa (SLP76). SLP76 recruitment to phosphorylated LAT allows subsequent SLP76 phosphorylation by ZAP70. Phosphorylated LAT also directly interacts with PLCγ1, a major regulator of Ca2+ influx in response to TCR triggering. PLCγ is recruited via LAT interaction to the synaptic membrane and generates DAG at the IS. SLP76 acts as a scaffold for a multitude of actin effectors including Rho GTPases nucleotide exchange factor, Vav1, adaptor molecule Nck, and actin nucleation promoting factors (NPFs). Alternatively, Rho GTPases (CDC42, Rho, Rac) can also bind and activate actin NPFs (ARP2/3, WAVE), which in turn activate actin nucleation factors (ARP2/3, formins), ultimately leading to F-actin formation. In addition, PI3K activated by LAT/SLP76 activation produces PIP_3 at the plasma membrane that, by recruiting DOCK2 to the IS, activates Rac and, ultimately, WAVE/ARP2/3 (Le Floc'h and Huse, 2015). An intriguing feature of actin cytoskeleton regulation at the IS is the variety of both actin NPFs and actin nucleation factors involved in actin cytoskeleton assembly. This could be related to the complexity of the four F-actin networks contributing to the architecture of the IS described below (Hammer et al., 2018).

More recently, by using super-resolution imaging techniques, such as total internal fluorescence microscopy combined with 3D structured-illumination microscopy (TIRFM/3D-SIM) on functionalized stimulatory surfaces, it has been shown that following initial TCR-antigen interaction, at least four discrete F-actin networks form and maintain the shape and function of this canonical IS (Hammer et al., 2018; Blumenthal and Burkhardt, 2020): branched F-actin network at the dSMAC controlled by WAVE/ARP2/3 activity; actomyosin arc network at the pSMAC controlled by formin Dia1 and phosphorylated myosin; hypodense F-actin at the cSMAC controlled by ARP2/3 and probably formins such as FMNL1/Dia1; F-actin foci at the dSMAC and pSMAC controlled by WASP and HS1 (Hammer et al., 2018; Blumenthal and Burkhardt, 2020). Therefore, in the same cell type distinct regulators control discrete F-actin networks. The four F-actin networks at the T lymphocyte IS are related to the three distinct functional and signaling areas at the IS (SMACs). Thus, the outer ring of the IS, the dSMAC, corresponds to the lamellipodium region of a migrating cell and forms quickly upon TCR stimulation and contains highly-branched actin filaments generated by the ARP2/3 activator WAVE2. Radially arranged within the dSMAC are bundles of linear actin filaments, generated by formin (Dia) activity near the edge of the spreading lymphocyte, that bend as they move inward the dSMAC, forming actomyosin arcs spanning the pSMAC. Therefore, these actomyosin arcs define the pSMAC, which is enriched in integrins. Actomyosin network disassembly at the pSMAC leads to a F-actin poor region in the center of the IS known as the cSMAC. cSMAC is associated with receptor internalization and provides a site for exocytic vesicle secretion (**Figure 1**). Finally, the fourth actin network consists of dense actin foci related to protrusive structures rich in F-actin called invadosome-like protrusions (ILPs) (Hammer et al., 2018; Blumenthal and Burkhardt, 2020). Recent evidences support the view that the described F-actin network complexity is, at least in part, based on the action of different F-actin regulatory pathways. For instance, branched F-actin network at the dSMAC is controlledby PI3K-PIP3-DOCK2-WAVE/ARP2/3, whereas F-actin foci at the cSMAC is regulated by ZAP70-LAT/SLP76-VAV-CDC42-WASP-ARP2/3 (Hammer et al., 2018).

SYNAPTIC ACTIN CYTOSKELETON CONTROL OF CENTROSOME AND SECRETION VESICLES POLARIZATION: RELEASE OF EXTRACELLULAR VESICLES AND LYTIC GRANULES

Regarding the mechanisms controlling centrosome polarization and the role of cortical actin reorganization in MTOC polarization, DAG production at the IS has been shown to be important for centrosome polarization in both CTL and $CD4^+$ T lymphocytes forming IS (Quann et al., 2009). With respect to potential DAG effectors, DAG-activated PKCθ at the IS triggers the adhesion and degranulation-adaptor protein (ADAP)/dynein complex localization at the F-actin/integrin rich, pSMAC ring (**Figure 1A**). Since dynein is a minus end-directed microtubule motor, after being recruited to the IS it can bind microtubules and reorient the centrosome by minus end-directed motion (Combs et al., 2006; Quann et al., 2009, 2011; Liu et al., 2013) (**Figure 1A**). At the early stages of IS formation F-actin accumulates at the lymphocyte-APC contact area to generate filopodia and lamellipodia, that produce dynamic changes between extension and contraction in the lymphocyte over the APC surface (Le Floc'h and Huse, 2015). Subsequently, once IS growth has stabilized, cortical F-actin accumulates into the dSMAC, and F-actin reduction at the cSMAC appears to facilitate secretion toward the APC by focusing secretion vesicles on the IS (Stinchcombe et al., 2006), creating regions within the canonical bullseye IS structure (**Figure 1A**). Thus, F-actin reduction at the cSMAC does not simply allow secretion, since it apparently plays an active role in centrosome movement to the IS (Stinchcombe et al., 2006; Ritter et al., 2015; Sanchez et al., 2019). It is widely

thought that centrosome reorientation promotes cytotoxic and Th lymphocyte specificity by guiding secretory vesicles to the IS for directional secretion (Stinchcombe et al., 2006; Huse et al., 2008). However, in the context of secretory traffic at the IS, not always centrosome polarization is necessary for either secretory vesicle transport or secretion at the IS in $CD4^+$ T lymphocytes (Chemin et al., 2012) or lytic granule polarization and secretion in CTLs (Ma et al., 2007; Bertrand et al., 2013; Nath et al., 2016). For instance, it has been shown that an early and rapid secretion phase of lytic granules constitutively positioned nearby the IS precedes centrosome polarization at the CTL-target cell IS (Bertrand et al., 2013). In addition, in PKCδ-KO mouse CTL, lytic granules did not polarize to the IS and, subsequently, CTL activity and target cell death were inhibited (Ma et al., 2007). However, centrosome polarization toward the IS was not affected by the absence of PKCδ (Ma et al., 2007). In contrast, in the synapses made by $CD4^+$ Jurkat T lymphocytes, multivesicular bodies (MVB, a type of secretory vesicles involved in exosome secretion by $CD4^+$ Jurkat and primary $CD8^+$ and $CD4^+$ T lymphocytes (Alonso et al., 2005, 2011)) and centrosome always co-migrated toward the IS, and MVB and centrosome did not polarize in PKCδ-interfered $CD4^+$ Jurkat T lymphocytes and the centrosome/MTOC center of mass ($MTOC^C$) was coincident or very proximal to the MVB center of mass (MVB^C) regardless of polarization (Herranz et al., 2019; Bello-Gamboa et al., 2020). In summary, all these results broaden current views of CTL biology by revealing an extremely rapid lytic granule secretion step and by showing that centrosome polarization is dispensable for efficient lytic granule secretion. All these examples of segregation between centrosome movement and lytic granule polarization point out that centrosome repositioning, secretory vesicles traffic, and F-actin architecture and dynamics at several locations should be analyzed at the single cell level, to obtain a more complete view of the secretion process.

In addition, it has been recently described that centriole-deficient CTL exhibited reduced cytotoxicity due to an alteration in secretory granule biogenesis, although this deficient response was not due to impaired polarized secretion, since lytic granule traffic and secretion toward the IS remained unaffected (Tamzalit et al., 2020). Instead, it has been proposed that the defect was in part due to impaired F-actin reorganization at the IS produced by centriole deletion (Tamzalit et al., 2020), which points out an unexpected role of the intact centrosome in supporting synaptic F-actin architecture and dynamics. Interestingly, CTL lacking centriole formed synapses that lacked an obvious F-actin cleared region at the cSMAC, a similar phenotype to that found in PKCδ-interfered $CD4^+$ Jurkat T lymphocytes (Herranz et al., 2019; Bello-Gamboa et al., 2020). Polarized secretion is known to occur in IS domains that have been cleared of F-actin and are, thus, accessible to secretion vesicles (Griffiths et al., 2010; Huse, 2012; Ritter et al., 2015; Herranz et al., 2019).

More recently, it has been shown that PKCδ-dependent F-actin clearing at the cSMAC and PKCδ-dependent phosphorylation of formin FMNL1β at the IS, are involved in centrosome/MVB polarization leading to exosome secretion in $CD4^+$ Jurkat T lymphocytes forming IS (Herranz et al., 2019; Bello-Gamboa et al., 2020). The formins Dia and FMNL1 are constitutively inactive because they undergo intramolecular, autoinhibitory folding in the cytoplasm, which blocks their ability to nucleate and elongate actin filaments (Hammer et al., 2018). In this context, a different formin, FMNL2, is phosphorylated by PKCα and PKCδ at S1072, reversing its autoinhibition by the C-terminal, DAD auto-inhibitory domain and enhancing F-actin assembly, β1-integrin endocytosis, and invasive motility (Wang et al., 2015). In the FMNL1 isoform FMNL1β, S1086 is surrounded by a sequence displaying high homology to the one surrounding S1072 of FMNL2 (Wang et al., 2015; Bello-Gamboa et al., 2020). Our results support that IS-induced, PKCδ-dependent phosphorylation in FMNL1β C-terminal region containing the auto-inhibitory domain (possibly at S1086) activates FMNL1β and mediates centrosome polarization. Thus, PKCδ appears to regulate F-actin reorganization, most probably, by controlling FMNL1β activation through phosphorylation at S1086 (Bello-Gamboa et al., 2020), as certain PKC isoforms activate FMNL2 activity (Wang et al., 2015).

CENTROSOMAL F-ACTIN AND CENTROSOME POLARIZATION

The centrosome nucleates and anchors microtubules and is thus considered to be the principal MTOC. In addition, few years ago it was discovered that the centrosome organizes a local F-actin network and should be considered as a F-actin organizing center (Farina et al., 2016). Isolated centrosomes from Jurkat T lymphocytes efficiently nucleate actin filaments, and the centrosome is associated *in vivo* with an actin network, and these results were extended to other cell types (Farina et al., 2016; Plessner et al., 2019). Moreover, actin filament nucleation at the centrosome is mediated by the nucleation-promoting factor Wiskott-Aldrich syndrome protein (WASP) and SCAR homolog (WASH), in combination with the ARP2/3 complex (Farina et al., 2016). Pericentriolar material seems to modulate F-actin network by regulating WASH/ARP2/3 recruitment to the centrosome (Farina et al., 2016).

Centrosomal F-actin and B Lymphocytes

Centrosome-associated ARP2/3 locally nucleates F-actin, which is needed for centrosome tethering to the nucleus (Obino et al., 2016). Upon B lymphocyte activation with BCR-ligand-coated beads as a synapse model, ARP2/3 is partially depleted from the centrosome, as a result of its recruitment to the IS, where it regulates cortical F-actin. This leads to a reduction in F-actin nucleation at the centrosome and thereby allows its detachment from the nucleus and polarization to the IS (Obino et al., 2016). Thus, centrosomal F-actin depletion appears to be crucial allowing centrosome polarization toward the IS during BCR stimulation in B lymphocytes (Obino et al., 2016). Thus, both *in vitro* and living-cell experiments support this new view of centrosome as a genuine and plastic F-actin-organizing center. However, the precise function of the F-actin network at the centrosome is not well understood. In the same B lymphocyte model, F-actin depletion around the centrosome, F-actin reorganization at

the IS, and centrosome polarization depend on proteasome activity (Ibanez-Vega et al., 2019). By inhibiting proteasome activity, an inhibition of F-actin dismantling around centrosome correlated with the inhibition of centrosome polarization toward the B lymphocyte synapse (Ibanez-Vega et al., 2019). Thus, it appears that at least two mechanisms controlling centrosomal area F-actin co-exist in B lymphocytes, and both regulate centrosome polarization.

Centrosomal F-actin and T Lymphocytes

We have shown that F-actin clearing at the cSMAC and centrosomal area F-actin depletion, respectively, mediated by PKCδ-dependent phosphorylation of FMNL1β or paxillin, are associated with centrosome/MVB polarization and exosome secretion in $CD4^+$ Jurkat T lymphocytes forming IS (Herranz et al., 2019; Bello-Gamboa et al., 2020) (**Figure 1B**). Although PKCδ appeared to regulate centrosomal area F-actin, FMNL1β did not appear to participate in this regulation (Bello-Gamboa et al., 2020). A possible PKCδ downstream effector involved in centrosomal area F-actin reorganization could be the actin regulatory protein paxillin, whose phosphorylation at threonine 538 (T538) by PKCδ leads to actin cytoskeleton depolymerization and regulates integrin-mediated adhesion and migration of B lymphoid cells (Romanova et al., 2010). Moreover, the centrosome cannot polarize to the IS in paxillin-interfered CTL (Robertson and Ostergaard, 2011). In addition, paxillin phosphorylation is required for CTL lytic granule secretion (Robertson et al., 2005), and both paxillin (Herreros et al., 2000) and PKCδ (Fanning et al., 2005) are localized at the centrosome. Thus, in $CD4^+$ Jurkat T lymphocytes forming IS, we have found that PKCδ-dependent paxillin phosphorylation may govern a F-actin reorganization network different from F-actin at the IS, such as centrosomal F-actin, that may also contribute to the diminished centrosome polarization observed in PKCδ-interfered Jurkat T lymphocyte clones (**Figure 1B**). This PKCδ-dependent, paxillin-regulated mechanism for centrosomal area F-actin reorganization appears to co-exist in $CD4^+$ Jurkat T lymphocytes with the PKCδ-dependent, FMNL1β-regulated mechanism for cortical F-actin reorganization explained above. More research is necessary (i.e., experiments involving phospho-deficient and phospho-mimetic mutants of paxillin at T538 and/or FMNL1β at S1086) to establish the relative contribution of these mechanisms to the polarization processes.

In addition, impaired F-actin reorganization at the IS was produced by centriole deletion in CTL (Tamzalit et al., 2020), which points out an unexpected role for the intact centrosome and/or centrosomal F-actin in supporting synaptic F-actin architecture and dynamics. Moreover, lower centrosomal actin filament densities enhanced microtubule growth at the centrosome (Inoue et al., 2019), that decisively affected cell adhesion and spreading. These results, together with the fact that ARP2/3 is partially depleted from the centrosome as a result of its recruitment to the IS (Farina et al., 2016), suggest an unsuspected direct or indirect interaction (i.e., competition for F-actin regulators such as ARP2/3), between cortical and centrosomal area F-actin networks, that in turn may regulate tubulin cytoskeleton at different subcellular locations. The distinct F-actin networks may be functionally interconnected by coordinated activation of different actin assembly factors (Bello-Gamboa et al., 2020) (**Figure 1B**), competition for the same regulatory factor (Obino et al., 2016) and/or actin monomer availability (Suarez and Kovar, 2016). Pericentriolar material seemed to modulate the centrosomal F-actin network by regulating ARP2/3 and WASH recruitment to the centrosome (Farina et al., 2016). Since F-actin reorganization at the remaining proteinaceous pericentriolar material (PCM) area, containing pericentrin and γ-tubulin, was not analyzed in centriole-deficient CTL (Tamzalit et al., 2020), it will be interesting to study pericentriolar area F-actin in detail in these cells. In addition, considering that PKCδ is located in the centrosome (Fanning et al., 2005; Ma et al., 2008a), but also in lytic granules in CTL (Ma et al., 2008b), it is conceivable that PKCδ, directly or indirectly, may coordinately regulate both centrosomal area and synaptic F-actin networks.

CURRENT RESEARCH GAPS

Lipid Bilayer Synapse Model

Most of what we know about the formation, organization, and dynamics of the four described F-actin and actomyosin networks at the IS results from high spatio-temporal resolution image analysis of T cells engaged with activating surfaces such as coated glass and planar lipid bilayers, which position these networks in the ideal imaging plane, avoiding the Z spatial dimension (Hammer et al., 2018). This approach is certainly somewhat reductionist since it is not possible to guarantee that all the molecular interactions occurring in a real, cell to cell synapse will also occur upon interaction with the coated glass or the lipid bilayer (Fooksman et al., 2010). In fact, supported lipid bilayers do not completely imitate the complex and irregular surface of an APC or target cell, possibly causing non-physiological interactions in the IS (Bertolet and Liu, 2016). Thus, although studies using supported planar bilayers are powerful in terms of resolution and sensitivity, it is important to test the predictions of these model systems using *in vitro* or *in vivo* cell–cell systems in order to extend the results to a more physiologic scenario (Dustin, 2009).

Actin Cytoskeleton in Primary vs. Immortalized T Cells and Different Synapse Subtypes

Striking differences in F-actin architecture and dynamics at the IS have been found between human primary $CD4^+$ and immortalized $CD4^+$ T lymphocytes, such as Jurkat cells, under comparable activation conditions on lipid bilayers (Colin-York et al., 2019; Kumari et al., 2019). In contrast, no major differences were found between the synaptic architecture of Jurkat cells and mouse $CD8^+$ primary CTLs (Murugesan et al., 2016) on stimulatory lipid bilayers. F-actin network dynamics and mechanics are likely to be different in these cells, and influence how T cells employ mechanical cues in different ways during antigen recognition (Kumari et al., 2019). Thus, caution should be taken when generalizing the cellular mechanisms underlying

the variety of IS patterns and motility behaviors to specific T cell subtypes and across different species (Kumari et al., 2019). It is conceivable that these differences also exist in different real cell-cell synapses, although they have not been observed yet (Colin-York et al., 2019; Kumari et al., 2019). In addition, while PKCδ regulates centrosomal area F-actin upon IS formation by $CD4^+$ Jurkat cells (Bello-Gamboa et al., 2020), more research is necessary to extend these results to both $CD8^+$ and $CD4^+$ primary T lymphocytes forming IS. While TIRFM combined with super-resolution 3D-SIM provided probably the best live-cell images of synapses on lipid bilayer models (Murugesan et al., 2016; Colin-York et al., 2019), the best live-cell images of F-actin architecture and dynamics within T cells engaged with an APC were obtained using high temporal resolution, lattice light sheet microscopy (LLSM) in a diffraction-limited mode (Ritter et al., 2015; Fritzsche et al., 2017). An option to improve the image spatial resolution is taking advantage of the better XY resolution of microscopes with respect to the axial (Z) resolution (Calvo and Izquierdo, 2018), by using LLSM combined with 3D-SIM. Other options are placing the T lymphocyte on top of an APC by using "pairing and coupling" microfluidic devices (Jang et al., 2015), or on a very flat APC in which the IS is located in the XY optical plane (Wang et al., 2018). These last two options will indeed provide real cell-cell synapse models. While LLSM images in a diffraction-limited mode (Ritter et al., 2015; Fritzsche et al., 2017) showed with remarkable definition the branched F-actin network dynamics in the dSMAC, including its contribution to a flow of F-actin up the sides of the APC-bound T cell, none of the four F-actin networks observed by TIRFM combined with 3D-SIM in lipid bilayers were visible using LLSM (Hammer et al., 2018). These latter F-actin networks, all of which are much fainter F-actin structures than those observed in the dSMAC (Hammer et al., 2018), will probably become discernible in the future by using one or more of the cell setups and super-resolution imaging methods described above.

Centrosomal F-actin Network Characterization and Measurements

Although in the original publication the authors defined the existence of a "centrosomal" F-actin network, it should be underlined this is an operative definition that does not specify the extension and/or the limits of such a network (Farina et al., 2016). In fact, the authors arbitrarily defined a 2 μm-diameter region of interest (ROI) including the centrosome for F-actin fluorescence intensity measurements. Subsequent publications have incorporated for centrosomal F-actin measurements the use of a 1.6–2 μm diameter, centrosome-centered ROI (Obino et al., 2016; Ibanez-Vega et al., 2019; Bello-Gamboa et al., 2020). However, a more appropriate term could be "centrosomal area" F-actin, to remark that measures were referred to an area centered at the centrosome and surely larger than the centrosome itself. Indeed, this is a more accurate term that includes the complexity of organelle interconnection. This is an important issue for centrosomal area F-actin evaluation, since the imaging techniques used in these publications (confocal microscopy, TIRFM, epifluorescence microscopy plus deconvolution) do not allow enough resolution to sustain that F-actin assembles at the pericentrosomal matrix instead of other membrane-bound organelles included in this area (Obino et al., 2016; Bello-Gamboa et al., 2019; Ibanez-Vega et al., 2019). Since interphase centrosomes are smaller than mitotic centrosomes (Decker et al., 2011) and cells may be at any cell cycle phase, it is difficult to establish a fixed centrosomal diameter. If a 2 μm-diameter centrosomal area ROI is analyzed, it cannot be ruled out that other F-actin-regulating organelles are included in this area, such as the Golgi, endosomes, or MVB (Colon-Franco et al., 2011; Bello-Gamboa et al., 2020). MVB are also involved in actin polymerization at the IS during intracellular reorganization (Calabia-Linares et al., 2011). Electron microscopy images show that vesicles and endosomes are located nearby the centrosomes (Ueda et al., 2011). The use of a pericentriolar marker, together with new imaging super-resolution techniques, would facilitate the study of the centrosomal area and the specific localization and dynamics of centrosomal F-actin. Indeed, in the future, emerging and promising techniques, such as LLSM (Ritter et al., 2015; Fritzsche et al., 2017), combined with non-diffraction limited, super-resolution microscopy (Fritzsche et al., 2017; Calvo and Izquierdo, 2018), may help to a better definition of centrosomal area F-actin structure and function, as it occurred for the four recently defined, synaptic F-actin networks that contribute to maintain the shape and function of the canonical IS (Section Signals Regulating Cortical Actin Reorganization In The Immune Synapse). In this context, TIRFM or TIRFM combined with 3D-SIM are exceptionally useful imaging techniques to study both F-actin cytoskeleton and secretion vesicle degranulation on the XY plane of coated glass or lipid bilayer (Rak et al., 2011; Murugesan et al., 2016; Sinha et al., 2016; Carisey et al., 2018), due to its high signal-to-noise ratio and improved spatial resolution below the diffraction limit (Calvo and Izquierdo, 2018). However, this procedure is somewhat limited since only an illuminated homogeneous surface can be used to stimulate cells and TIRFM would dismiss subcellular structures (i.e., centrosome) or molecules located beyond a minor Z distance from the stimulatory surface (>200–300 nm). Thus, centrosome movement in the Z dimension from distal subcellular locations cannot be imaged, although its last stages approaching the IS can be properly imaged. One possibility to circumvent this problem is to limit centrosome movement in the Z dimension by using the cell setups explained above. Indeed, other techniques as the already mentioned diffraction-limited LLSM, combined with 2D or 3D stimulated emission depletion (STED) super-resolution microscopy (Fritzsche et al., 2017), may provide in the future new tools to address the study of centrosomal area F-actin organization and dynamics at the nanoscale level.

POTENTIAL FUTURE DEVELOPMENTS IN THE FIELD. IMAGING THE IMMUNOLOGICAL SYNAPSE

For adequate IS imaging by fluorescence microscopy, harmonizing temporal and spatial resolutions, overcoming

spatial constraints due to imaging in Z optical axis, improving signal-to-noise ratio, and solving the photobleaching and cytotoxicity inherent to any live cell imaging, are required (Combs and Shroff, 2017; Calvo and Izquierdo, 2018). Please refer to some excellent reviews dealing with the more relevant fluorescence microscopy techniques used in cell biology in general (Combs and Shroff, 2017; Lambert and Waters, 2017; Sahl et al., 2017), and specifically for IS imaging (Rossy et al., 2013; Calvo and Izquierdo, 2018; Herranz et al., 2019), since it is out of the scope of this review to deal with these relevant technical issues. In this context, it is remarkable that to date difficulties in visualization of both primary and transformed T lymphocyte models at high spatio-temporal resolution have somewhat limited our understanding of the principles underlying T lymphocyte subtype-specific activation (Kumari et al., 2019). However, visualization and quantification of actin cytoskeleton and the underlying patterns and dynamics has evolved to a significant degree due to the advances in microscopy regarding spatiotemporal resolution (Kumari et al., 2019). Currently, we only have a limited knowledge of how actin cytoskeleton organization affects distinct synaptic patterning and signaling. This is due to several facts, including the low transfection efficiency of F-actin reporters in primary lymphocytes, the rapid kinetics of changes, the reduced area of cell-cell synapses, and the active, highly plastic and irregular cell-cell synaptic interface that precludes image capture at high spatiotemporal resolution (Kumari et al., 2019; Blumenthal and Burkhardt, 2020). In the future, the development of emerging and promising techniques such as LLSM (Ritter et al., 2015) and new 3D live-cell super-resolution microscopy (Fritzsche et al., 2017), combined with some useful probes for F-actin in living cells (Lukinavicius et al., 2013, 2014; Bello-Gamboa et al., 2020) will transform how we image cellular and protein dynamics during IS interactions. These advances will indeed shed more light into our knowledge of these processes.

Thus, some techniques of choice have been specifically used for IS imaging and to overcome the mentioned caveats. Planar lipid bilayers and coverslips or beads-coated with surface proteins or agonistic antibodies are good options. These approaches reduce a 3D complex structure such a cell-cell IS to only two dimensions (XY), enabling high-resolution imaging techniques such as TIRFM (Huppa and Davis, 2003) and, since stimulation occurs at a homogenous, well-defined Z position, image capture at high spatial resolution becomes feasible. If the imaged cell is flat enough, or the Z dimension-restricted cell setups described above are used, secretory vesicle movement at the XY focus plane is a centripetal convergence toward the cSMAC area and can be conveniently imaged and analyzed (Fooksman et al., 2010; Sinha et al., 2016). Using this technique for some structures contained and reorganizing within the IS (i.e., F-actin), the images obtained by using anti-TCR-coated coverslips and lipid bilayers and TIRFM and TIRFM-SIM combination probably exhibit, by far, the highest definition and spatial resolution obtained to date (Murugesan et al., 2016; Sinha et al., 2016). The opportunity to change the composition of the lipid bilayer or the stimulatory antibodies by loading antigens, accessory molecules, changing lipids, etc., allows for reconstitution approaches, increasing the flexibility of this strategy (Huppa and Davis, 2003), although centrosomal area F-actin imaging in living cells will require to develop alternative strategies such as LLSM combined with super-resolution imaging techniques (i.e., STED, 3D-SIM), harboring higher temporal resolution and full competence in the Z dimension.

Apart of the described role of F-actin regions and SMACs in vesicle secretion obtained by high-resolution microscopy, emerging evidences obtained thanks to high-resolution live imaging microscopy support that F-actin-driven and maintained structures such as T cell microvilli, acting as finger-like membrane protrusions or invadosome-like protrusions, may participate in sensing pMHC on APCs, acting as bona fide "synaptosomes" (Sage et al., 2012; Kim et al., 2018; Kim and Jun, 2019), or acting as interfacial protrusions at the IS contact area to facilitate lytic granule secretion and CTL activity (Tamzalit et al., 2019). The formation, maintenance and activity of the later protrusions, as SMACs architecture and functions, both depend on WASP and ARP2/3 activity. The fact that some of the IS actin networks consist of dense actin foci related to protrusive structures rich in F-actin, called invadosome-like protrusions (ILPs) (Hammer et al., 2018; Blumenthal and Burkhardt, 2020), supports that these protrusions should also be analyzed in the IS and actin cytoskeleton studies. Moreover, T lymphocyte microvilli should also be considered not only as structures involved in surveying antigen on APCs or target cells, but also in signaling to APCs or target cells. Thus, these structures are related with relevant immune regulation mechanisms previously discovered (Kim and Jun, 2019). More research involving state-of-the-art microscopy techniques is necessary to understand the mechanisms controlling their generation and function.

CONCLUDING REMARKS

Cells precisely control the formation and the dynamics of both tubulin and actin cytoskeleton networks to coordinate important processes, including motility, cell division, endocytosis and polarized secretion. In addition, cells coordinate the formation of distinct F-actin networks from a general cytosolic pool of actin monomers (Suarez and Kovar, 2016). The available literature concerning the centrosomal subcellular localization and actin cytoskeleton dynamics described here and elsewhere (Dogterom and Koenderink, 2019) demonstrate the existence of a relevant connection between tubulin and actin cytoskeletons and centrosome/MVB polarized traffic and function. Although these links between F-actin and microtubule dynamics are intriguing, very little is known about their molecular bases and functional relevance (Le Floc'h and Huse, 2015). In addition, recent evidences demonstrate that the different F-actin networks appear to be co-ordinately regulated and interconnected. Close coordination between centrosome and centrosomal area F-actin with synaptic F-actin could facilitate the efficient organization of synaptic responses in space and time (Tamzalit et al., 2020). In addition, inhibitor studies indicate that the four discrete cortical actin networks more recently described at the IS (Section Signals Regulating Cortical Actin Reorganization In The Immune

Synapse) largely function independently of one another, although there is some coordinate control due to competition for free actin monomer (Hammer et al., 2018). How these distinct cortical and non-cortical networks are regulated, how they interact with the TCR signaling network, as well as their interconnections constitute an intriguing and challenging issue to be addressed in the future. The application of super-resolution microscopy in this context will enable, together with conventional biochemistry techniques, to tackle some of these issues through directly analyzing the interactions between the cytoskeletons and other cell proteins at immune synapses.

AUTHOR CONTRIBUTIONS

VC and MI: conceived the manuscript, writing of the manuscript, approved its final content, conceptualization, and writing—review and editing. MI: writing original draft preparation. Both authors contributed to the article and approved the submitted version.

FUNDING

This research was funded by grants from the Spanish Ministerio de Economía y Competitividad (MINECO), Plan Nacional de Investigación Científica (SAF2016-77561-R and PID2020-114148RB-I00) to MI, which was in part granted with FEDER funding (EC), corresponding to the Programa Estatal de Investigación, Desarrollo e Innovación Orientada a los Retos de la Sociedad.

ACKNOWLEDGMENTS

The authors apologize for not including some relevant references due to space limitations. We acknowledge all the past and present members of the lab for their generous contribution. We acknowledge the support of the publication fee by the CSIC Open Access Publication Support Initiative through its Unit of Information Resources for Research (URICI).

REFERENCES

Alonso, R., Mazzeo, C., Rodriguez, M. C., Marsh, M., Fraile-Ramos, A., Calvo, V., et al. (2011). Diacylglycerol kinase alpha regulates the formation and polarisation of mature multivesicular bodies involved in the secretion of Fas ligand-containing exosomes in T lymphocytes. *Cell Death Differ*. 18, 1161–1173. doi: 10.1038/cdd.2010.184

Alonso, R., Rodriguez, M. C., Pindado, J., Merino, E., Merida, I., and Izquierdo, M. (2005). Diacylglycerol kinase alpha regulates the secretion of lethal exosomes bearing Fas ligand during activation-induced cell death of T lymphocytes. *J. Biol. Chem*. 280, 28439–28450. doi: 10.1074/jbc.M501112200

Bello-Gamboa, A., Izquierdo, J. M., Velasco, M., Moreno, S., Garrido, A., Meyers, L., et al. (2019). Imaging the human immunological synapse. *J. Vis. Exp*. 154:e60312. doi: 10.3791/60312

Bello-Gamboa, A., Velasco, M., Moreno, S., Herranz, G., Ilie, R., Huetos, S., et al. (2020). Actin reorganization at the centrosomal area and the immune synapse regulates polarized secretory traffic of multivesicular bodies in T lymphocytes. *J. Extracell. Vesicles* 9:1759926. doi: 10.1080/20013078.2020.1759926

Bertolet, G., and Liu, D. (2016). The planar lipid bilayer system serves as a reductionist approach for studying NK cell immunological synapses and their functions. *Methods Mol. Biol*. 1441, 151–165 doi: 10.1007/978-1-4939-3684-7_13

Bertrand, F., Muller, S., Roh, K. H., Laurent, C., Dupre, L., and Valitutti, S. (2013). An initial and rapid step of lytic granule secretion precedes microtubule organizing center polarization at the cytotoxic T lymphocyte/target cell synapse. *Proc. Natl. Acad. Sci. U. S. A*. 110, 6073–6078 doi: 10.1073/pnas.1218640110

Billadeau, D. D., Nolz, J. C., and Gomez, T. S. (2007). Regulation of T-cell activation by the cytoskeleton. *Nat. Rev. Immunol*. 7, 131–143. doi: 10.1038/nri2021

Blumenthal, D., and Burkhardt, J. K. (2020). Multiple actin networks coordinate mechanotransduction at the immunological synapse. *J. Cell Biol*. 219:e201911058. doi: 10.1083/jcb.201911058

Brossard, C., Feuillet, V., Schmitt, A., Randriamampita, C., Romao, M., Raposo, G., et al. (2005). Multifocal structure of the T cell - dendritic cell synapse. *Eur. J. Immunol*. 35, 1741–1753. doi: 10.1002/eji.200425857

Calabia-Linares, C., Robles-Valero, J., de la Fuente, H., Perez-Martinez, M., Martin-Cofreces, N., Alfonso-Perez, M., et al. (2011). Endosomal clathrin drives actin accumulation at the immunological synapse. *J. Cell Sci*. 124 (Pt 5), 820–830 doi: 10.1242/jcs.078832

Calvo, V., and Izquierdo, M. (2018). Imaging polarized secretory traffic at the immune synapse in living T lymphocytes. *Front. Immunol*. 9:684. doi: 10.3389/fimmu.2018.00684

Calvo, V., and Izquierdo, M. (2020). Inducible polarized secretion of exosomes in T and B lymphocytes. *Int. J. Mol. Sci*. 21:2631. doi: 10.3390/ijms21072631

Carisey, A. F., Mace, E. M., Saeed, M. B., Davis, D. M., and Orange, J. S. (2018). Nanoscale dynamism of actin enables secretory function in cytolytic cells. *Curr. Biol*. 28, 489–502.e9. doi: 10.1016/j.cub.2017.12.044

Chemin, K., Bohineust, A., Dogniaux, S., Tourret, M., Guegan, S., Miro, F., et al. (2012). Cytokine secretion by CD4+ T cells at the immunological synapse requires Cdc42-dependent local actin remodeling but not microtubule organizing center polarity. *J. Immunol*. 189, 2159–2168. doi: 10.4049/jimmunol.1200156

Colin-York, H., Kumari, S., Barbieri, L., Cords, L., and Fritzsche, M. (2019). Distinct actin cytoskeleton behaviour in primary and immortalised T-cells. *J. Cell Sci*. 133:jcs232322. doi: 10.1242/jcs.232322

Colon-Franco, J. M., Gomez, T. S., and Billadeau, D. D. (2011). Dynamic remodeling of the actin cytoskeleton by FMNL1gamma is required for structural maintenance of the Golgi complex. *J. Cell Sci*. 124 (Pt 18), 3118–3126 doi: 10.1242/jcs.083725

Combs, C. A., and Shroff, H. (2017). Fluorescence microscopy: a concise guide to current imaging methods. *Curr. Protoc. Neurosci*. 79, 2.1.1–2.1.25. doi: 10.1002/cpns.29

Combs, J., Kim, S. J., Tan, S., Ligon, L. A., Holzbaur, E. L., Kuhn, J., et al. (2006). Recruitment of dynein to the Jurkat immunological synapse. *Proc. Natl. Acad. Sci. U. S. A*. 103, 14883–14888. doi: 10.1073/pnas.0600914103

Comrie, W. A., Babich, A., and Burkhardt, J. K. (2015). F-actin flow drives affinity maturation and spatial organization of LFA-1 at the immunological synapse. *J. Cell Biol*. 208, 475–491. doi: 10.1083/jcb.201406121

de la Roche, M., Asano, Y., and Griffiths, G. M. (2016). Origins of the cytolytic synapse. *Nat. Rev. Immunol*. 16, 421–432. doi: 10.1038/nri.2016.54

Decker, M., Jaensch, S., Pozniakovsky, A., Zinke, A., O'Connell, K. F., Zachariae, W., et al. (2011). Limiting amounts of centrosome material set centrosome size in *C. elegans* embryos. *Curr. Biol*. 21, 1259–1267 doi: 10.1016/j.cub.2011.06.002

Dogterom, M., and Koenderink, G. H. (2019). Actin–microtubule crosstalk in cell biology. *Nat. Rev. Mol. Cell Biol*. 20, 38–54 doi: 10.1038/s41580-018-0067-1

Duchez, S., Rodrigues, M., Bertrand, F., and Valitutti, S. (2011). Reciprocal polarization of T and B cells at the immunological synapse. *J. Immunol*. 187, 4571–4580 doi: 10.4049/jimmunol.1100600

Dustin, M. L. (2009). Supported bilayers at the vanguard of immune cell activation studies. *J. Struct. Biol*. 168, 152–160. doi: 10.1016/j.jsb.2009.05.007

Fanning, A., Volkov, Y., Freeley, M., Kelleher, D., and Long, A. (2005). CD44 cross-linking induces protein kinase C-regulated migration of human T lymphocytes. *Int. Immunol*. 17, 449–458. doi: 10.1093/intimm/dxh225

Farina, F., Gaillard, J., Guerin, C., Coute, Y., Sillibourne, J., Blanchoin, L., et al. (2016). The centrosome is an actin-organizing centre. *Nat. Cell Biol.* 18, 65–75 doi: 10.1038/ncb3285

Fooksman, D. R., Vardhana, S., Vasiliver-Shamis, G., Liese, J., Blair, D. A., Waite, J., et al. (2010). Functional anatomy of T cell activation and synapse formation. *Annu. Rev. Immunol.* 28, 79–105. doi: 10.1146/annurev-immunol-030409-101308

Fritzsche, M., Fernandes, R. A., Chang, V. T., Colin-York, H., Clausen, M. P., Felce, J. H., et al. (2017). Cytoskeletal actin dynamics shape a ramifying actin network underpinning immunological synapse formation. *Sci. Adv.* 3:e1603032. doi: 10.1126/sciadv.1603032

Gomez, T. S., Hamann, M. J., McCarney, S., Savoy, D. N., Lubking, C. M., Heldebrant, M. P., et al. (2005). Dynamin 2 regulates T cell activation by controlling actin polymerization at the immunological synapse. *Nat. Immunol.* 6, 261–270. doi: 10.1038/ni1168

Gomez, T. S., Kumar, K., Medeiros, R. B., Shimizu, Y., Leibson, P. J., and Billadeau Daniel, D. (2007). Formins regulate the actin-related protein 2/3 complex-independent polarization of the centrosome to the immunological synapse. *Immunity* 26, 177–190. doi: 10.1016/j.immuni.2007.01.008

Gomez, T. S., McCarney, S. D., Carrizosa, E., Labno, C. M., Comiskey, E. O., Nolz, J. C., et al. (2006). HS1 functions as an essential actin-regulatory adaptor protein at the immune synapse. *Immunity* 24, 741–752. doi: 10.1016/j.immuni.2006.03.022

Griffiths, G. M., Tsun, A., and Stinchcombe, J. C. (2010). The immunological synapse: a focal point for endocytosis and exocytosis. *J. Cell Biol.* 189, 399–406. doi: 10.1083/jcb.201002027

Hammer, J. A., Wang, J. C., Saeed, M., and Pedrosa, A. T. (2018). Origin, organization, dynamics, and function of actin and actomyosin networks at the T cell immunological synapse. *Annu. Rev. Immunol.* 37, 201–224. doi: 10.1146/annurev-immunol-042718-041341

Herranz, G., Aguilera, P., Davila, S., Sanchez, A., Stancu, B., Gomez, J., et al. (2019). Protein kinase C delta regulates the depletion of actin at the immunological synapse required for polarized exosome secretion by T cells. *Front. Immunol.* 10:851. doi: 10.3389/fimmu.2019.00851

Herreros, L., Rodriguez-Fernandez, J. L., Brown, M. C., Alonso-Lebrero, J. L., Cabanas, C., Sanchez-Madrid, F., et al. (2000). Paxillin localizes to the lymphocyte microtubule organizing center and associates with the microtubule cytoskeleton. *J. Biol. Chem.* 275, 26436–26440. doi: 10.1074/jbc.M003970200

Huppa, J. B., and Davis, M. M. (2003). T-cell-antigen recognition and the immunological synapse. *Nat. Rev. Immunol.* 3, 973–983. doi: 10.1038/nri1245

Huse, M. (2012). Microtubule-organizing center polarity and the immunological synapse: protein kinase C and beyond. *Front. Immunol.* 3:235. doi: 10.3389/fimmu.2012.00235

Huse, M., Quann, E. J., and Davis, M. M. (2008). Shouts, whispers and the kiss of death: directional secretion in T cells. *Nat. Immunol.* 9, 1105–1111. doi: 10.1038/ni.f.215

Ibanez-Vega, J., Del Valle Batalla, F., Saez, J. J., Soza, A., and Yuseff, M. I. (2019). Proteasome dependent actin remodeling facilitates antigen extraction at the immune synapse of B cells. *Front. Immunol.* 10:225. doi: 10.3389/fimmu.2019.00225

Inoue, D., Obino, D., Pineau, J., Farina, F., Gaillard, J., Guerin, C., et al. (2019). Actin filaments regulate microtubule growth at the centrosome. *EMBO J.* 38:e99630. doi: 10.15252/embj.201899630

Izquierdo, M., and Cantrell, D. A. (1992). T-cell activation. *Trends Cell Biol.* 2, 268–271. doi: 10.1016/0962-8924(92)90199-W

Jang, J. H., Huang, Y., Zheng, P., Jo, M. C., Bertolet, G., Zhu, M. X., et al. (2015). Imaging of cell-cell communication in a vertical orientation reveals high-resolution structure of immunological synapse and novel PD-1 dynamics. *J. Immunol.* 195, 1320–1330. doi: 10.4049/jimmunol.1403143

Kim, H. R., and Jun, C. D. (2019). T cell microvilli: sensors or senders? *Front. Immunol.* 10:1753. doi: 10.3389/fimmu.2019.01753

Kim, H. R., Mun, Y., Lee, K. S., Park, Y. J., Park, J. S., Park, J. H., et al. (2018). T cell microvilli constitute immunological synaptosomes that carry messages to antigen-presenting cells. *Nat. Commun.* 9:3630. doi: 10.1038/s41467-018-06090-8

Kühn, S., and Geyer, M. (2014). Formins as effector proteins of Rho GTPases. *Small GTPases* 5:e29513. doi: 10.4161/sgtp.29513

Kumari, S., Colin-York, H., Irvine, D. J., and Fritzsche, M. (2019). Not all T cell synapses are built the same way. *Trends Immunol.* 40, 977–980. doi: 10.1016/j.it.2019.09.009

Kumari, S., Curado, S., Mayya, V., and Dustin, M. L. (2014). T cell antigen receptor activation and actin cytoskeleton remodeling. *Biochim. Biophys. Acta* 1838, 546–556. doi: 10.1016/j.bbamem.2013.05.004

Kuokkanen, E., Sustar, V., and Mattila, P. K. (2015). Molecular control of B cell activation and immunological synapse formation. *Traffic* 16, 311–326. doi: 10.1111/tra.12257

Lagrue, K., Carisey, A., Oszmiana, A., Kennedy, P. R., Williamson, D. J., Cartwright, A., et al. (2013). The central role of the cytoskeleton in mechanisms and functions of the NK cell immune synapse. *Immunol. Rev.* 256, 203–221. doi: 10.1111/imr.12107

Lambert, T. J., and Waters, J. C. (2017). Navigating challenges in the application of superresolution microscopy. *J. Cell Biol.* 216, 53–63. doi: 10.1083/jcb.201610011

Le Floc'h, A., and Huse, M. (2015). Molecular mechanisms and functional implications of polarized actin remodeling at the T cell immunological synapse. *Cell. Mol. Life Sci.* 72, 537–556. doi: 10.1007/s00018-014-1760-7

Li, J., Yin, W., Jing, Y., Kang, D., Yang, L., Cheng, J., et al. (2018). The coordination between B cell receptor signaling and the actin cytoskeleton during B cell activation. *Front. Immunol.* 9:3096. doi: 10.3389/fimmu.2018.03096

Liu, X., Kapoor, T. M., Chen, J. K., and Huse, M. (2013). Diacylglycerol promotes centrosome polarization in T cells via reciprocal localization of dynein and myosin II. *Proc. Natl. Acad. Sci. U. S. A.* 110, 11976–11981. doi: 10.1073/pnas.1306180110

Lukinavicius, G., Reymond, L., D'Este, E., Masharina, A., Gottfert, F., Ta, H., et al. (2014). Fluorogenic probes for live-cell imaging of the cytoskeleton. *Nat. Methods* 11, 731–733. doi: 10.1038/nmeth.2972

Lukinavicius, G., Umezawa, K., Olivier, N., Honigmann, A., Yang, G., Plass, T., et al. (2013). A near-infrared fluorophore for live-cell super-resolution microscopy of cellular proteins. *Nat. Chem.* 5, 132–139. doi: 10.1038/nchem.1546

Ma, J. S., Haydar, T. F., and Radoja, S. (2008b). Protein kinase C delta localizes to secretory lysosomes in CD8+ CTL and directly mediates TCR signals leading to granule exocytosis-mediated cytotoxicity. *J. Immunol.* 181, 4716–4722. doi: 10.4049/jimmunol.181.7.4716

Ma, J. S., Monu, N., Shen, D. T., Mecklenbrauker, I., Radoja, N., Haydar, T. F., et al. (2007). Protein kinase Cdelta regulates antigen receptor-induced lytic granule polarization in mouse CD8+ CTL. *J. Immunol.* 178, 7814–7821. doi: 10.4049/jimmunol.178.12.7814

Ma, W., Koch, J. A., and Viveiros, M. M. (2008a). Protein kinase C delta (PKCdelta) interacts with microtubule organizing center (MTOC)-associated proteins and participates in meiotic spindle organization. *Dev. Biol.* 320, 414–425. doi: 10.1016/j.ydbio.2008.05.550

Mazzeo, C., Calvo, V., Alonso, R., Merida, I., and Izquierdo, M. (2016). Protein kinase D1/2 is involved in the maturation of multivesicular bodies and secretion of exosomes in T and B lymphocytes. *Cell Death Differ.* 23, 99–109. doi: 10.1038/cdd.2015.72

Merino-Cortés, S. V., Gardeta, S. R., Roman-Garcia, S., Martínez-Riaño, A., Pineau, J., Liebana, R., et al. (2020). Diacylglycerol kinase ζ promotes actin cytoskeleton remodeling and mechanical forces at the B cell immune synapse. *Sci. Signal.* 13:eaaw8214. doi: 10.1126/scisignal.aaw8214

Monks, C. R. F., Freiberg, B. A., Kupfer, H., Sciaky, N., and Kupfer, A. (1998). Three-dimensional segregation of supramolecular activation clusters in T cells. *Nature* 395, 82–86. doi: 10.1038/25764

Muntasell, A., Berger, A. C., and Roche, P. A. (2007). T cell-induced secretion of MHC class II-peptide complexes on B cell exosomes. *EMBO J.* 26, 4263–4272. doi: 10.1038/sj.emboj.7601842

Murugesan, S., Hong, J., Yi, J., Li, D., Beach, J. R., Shao, L., et al. (2016). Formin-generated actomyosin arcs propel T cell receptor microcluster movement at the immune synapse. *J. Cell Biol.* 215, 383–399. doi: 10.1083/jcb.201603080

Na, B.-R., Kim, H.-R., Piragyte, I., Oh, H.-M., Kwon, M.-S., Akber, U., et al. (2015). TAGLN2 regulates T cell activation by stabilizing the actin cytoskeleton at the immunological synapse. *J. Cell Biol.* 209, 143–162. doi: 10.1083/jcb.201407130

Na, B. R., Kwon, M. S., Chae, M. W., Kim, H. R., Kim, C. H., Jun, C. D., et al. (2016). Transgelin-2 in B-cells controls T-cell activation by stabilizing T cell - B cell conjugates. *PLoS One* 11:e0156429. doi: 10.1371/journal.pone.0156429

Nath, S., Christian, L., Tan, S. Y., Ki, S., Ehrlich, L. I. R., and Poenie, M. (2016). Dynein separately partners with NDE1 and dynactin to orchestrate T cell focused secretion. *J. Immunol.* 197, 2090–2101. doi: 10.4049/jimmunol.1600180

Obino, D., Farina, F., Malbec, O., Saez, P. J., Maurin, M., Gaillard, J., et al. (2016). Actin nucleation at the centrosome controls lymphocyte polarity. *Nat. Commun.* 7:10969. doi: 10.1038/ncomms10969

Peters, P. J., Geuze, H. J., Van der Donk, H. A., Slot, J. W., Griffith, J. M., Stam, N. J., et al. (1989). Molecules relevant for T cell-target cell interaction are present in cytolytic granules of human T lymphocytes. *Eur. J. Immunol.* 19, 1469–1475. doi: 10.1002/eji.1830190819

Plessner, M., Knerr, J., and Grosse, R. (2019). Centrosomal actin assembly is required for proper mitotic spindle formation and chromosome congression. *iScience* 15, 274–281. doi: 10.1016/j.isci.2019.04.022

Quann, E. J., Liu, X., Altan-Bonnet, G., and Huse, M. (2011). A cascade of protein kinase C isozymes promotes cytoskeletal polarization in T cells. *Nat. Immunol.* 12, 647–654. doi: 10.1038/ni.2033

Quann, E. J., Merino, E., Furuta, T., and Huse, M. (2009). Localized diacylglycerol drives the polarization of the microtubule-organizing center in T cells. *Nat. Immunol.* 10, 627–635. doi: 10.1038/ni.1734

Rak, G. D., Mace, E. M., Banerjee, P. P., Svitkina, T., and Orange, J. S. (2011). Natural killer cell lytic granule secretion occurs through a pervasive actin network at the immune synapse. *PLoS Biol.* 9:e1001151. doi: 10.1371/journal.pbio.1001151

Ritter, A. T., Asano, Y., Stinchcombe, J. C., Dieckmann, N. M., Chen, B. C., Gawden-Bone, C., et al. (2015). Actin depletion initiates events leading to granule secretion at the immunological synapse. *Immunity* 42, 864–876. doi: 10.1016/j.immuni.2015.04.013

Ritter, A. T., Kapnick, S. M., Murugesan, S., Schwartzberg, P. L., Griffiths, G. M., and Lippincott-Schwartz, J. (2017). Cortical actin recovery at the immunological synapse leads to termination of lytic granule secretion in cytotoxic T lymphocytes. *Proc. Natl. Acad. Sci. U. S. A.* 114:201710751. doi: 10.1073/pnas.1710751114

Robertson, L. K., Mireau, L. R., and Ostergaard, H. L. (2005). A role for phosphatidylinositol 3-kinase in TCR-stimulated ERK activation leading to paxillin phosphorylation and CTL degranulation. *J. Immunol.* 175, 8138–8145. doi: 10.4049/jimmunol.175.12.8138

Robertson, L. K., and Ostergaard, H. L. (2011). Paxillin associates with the microtubule cytoskeleton and the immunological synapse of CTL through its leucine-aspartic acid domains and contributes to microtubule organizing center reorientation. *J. Immunol.* 187, 5824–5833. doi: 10.4049/jimmunol.1003690

Romanova, L. Y., Holmes, G., Bahte, S. K., Kovalchuk, A. L., Nelson, P. J., Ward, Y., et al. (2010). Phosphorylation of paxillin at threonine 538 by PKCdelta regulates LFA1-mediated adhesion of lymphoid cells. *J. Cell Sci.* 123 (Pt 9), 1567–1577. doi: 10.1242/jcs.060996

Rossy, J., Pageon, S. V., Davis, D. M., and Gaus, K. (2013). Super-resolution microscopy of the immunological synapse. *Curr. Opin. Immunol.* 25, 307–312. doi: 10.1016/j.coi.2013.04.002

Sage, P. T., Varghese, L. M., Martinelli, R., Sciuto, T. E., Kamei, M., Dvorak, A. M., et al. (2012). Antigen recognition is facilitated by invadosome-like protrusions formed by memory/effector T cells. *J. Immunol.* 188, 3686–3699. doi: 10.4049/jimmunol.1102594

Sahl, S. J., Hell, S. W., and Jakobs, S. (2017). Fluorescence nanoscopy in cell biology. *Nat. Rev. Mol. Cell Biol.* 18, 685–701. doi: 10.1038/nrm.2017.71

Sanchez, A. D., and Feldman, J. L. (2017). Microtubule-organizing centers: from the centrosome to non-centrosomal sites. *Curr. Opin. Cell Biol.* 44, 93–101. doi: 10.1016/j.ceb.2016.09.003

Sanchez, E., Liu, X., and Huse, M. (2019). Actin clearance promotes polarized dynein accumulation at the immunological synapse. *PLoS ONE* 14:e0210377. doi: 10.1371/journal.pone.0210377

Schnyder, T., Castello, A., Feest, C., Harwood, N. E., Oellerich, T., Urlaub, H., et al. (2011). B cell receptor-mediated antigen gathering requires ubiquitin ligase Cbl and adaptors Grb2 and Dok-3 to recruit dynein to the signaling microcluster. *Immunity* 34, 905–918. doi: 10.1016/j.immuni.2011.06.001

Siemasko, K., Eisfelder, B. J., Williamson, E., Kabak, S., and Clark, M. R. (1998). Cutting edge: signals from the B lymphocyte antigen receptor regulate MHC class II containing late endosomes. *J. Immunol.* 160, 5203–5208.

Sinai, P., Nguyen, C., Schatzle, J. D., and Wülfing, C. (2010). Transience in polarization of cytolytic effectors is required for efficient killing and controlled by Cdc42. *Proc. Natl. Acad. Sci.* 107:11912. doi: 10.1073/pnas.0913422107

Sinha, S., Hoshino, D., Hong, N. H., Kirkbride, K. C., Grega-Larson, N. E., Seiki, M., et al. (2016). Cortactin promotes exosome secretion by controlling branched actin dynamics. *J. Cell Biol.* 214, 197–213. doi: 10.1083/jcb.201601025

Spitaler, M., Emslie, E., Wood, C. D., and Cantrell, D. (2006). Diacylglycerol and protein kinase D localization during T lymphocyte activation. *Immunity* 24, 535–546. doi: 10.1016/j.immuni.2006.02.013

Stinchcombe, J. C., Majorovits, E., Bossi, G., Fuller, S., and Griffiths, G. M. (2006). Centrosome polarization delivers secretory granules to the immunological synapse. *Nature* 443, 462–465. doi: 10.1038/nature05071

Stowers, L., Yelon, D., Berg, L. J., and Chant, J. (1995). Regulation of the polarization of T cells toward antigen-presenting cells by Ras-related GTPase CDC42. *Proc. Natl. Acad. Sci.* 92:5027. doi: 10.1073/pnas.92.11.5027

Suarez, C., and Kovar, D. R. (2016). Internetwork competition for monomers governs actin cytoskeleton organization. *Nat. Rev. Mol. Cell Biol.* 17, 799–810. doi: 10.1038/nrm.2016.106

Tamzalit, F., Tran, D., Jin, W., Boyko, V., Bazzi, H., Kepecs, A., et al. (2020). Centrioles control the capacity, but not the specificity, of cytotoxic T cell killing. *Proc. Natl. Acad. Sci. U. S. A.* 117, 4310–4319. doi: 10.1073/pnas.1913220117

Tamzalit, F., Wang, M. S., Jin, W., Tello-Lafoz, M., Boyko, V., Heddleston, J. M., et al. (2019). Interfacial actin protrusions mechanically enhance killing by cytotoxic T cells. *Sci. Immunol.* 4:eaav5445. doi: 10.1126/sciimmunol.aav5445

Ueda, H., Morphew, M. K., McIntosh, J. R., and Davis, M. M. (2011). CD4+ T-cell synapses involve multiple distinct stages. *Proc. Natl. Acad. Sci. U. S. A.* 108, 17099–17104. doi: 10.1073/pnas.1113703108

Wang, J. C., Bolger-Munro, M., and Gold, M. R. (2018). "Imaging the interactions between B cells and antigen-presenting cells," in *B Cell Receptor Signaling: Methods and Protocols*, ed C. Liu (New York, NY: Springer New York), 131–161.

Wang, Y., Arjonen, A., Pouwels, J., Ta, H., Pausch, P., Bange, G., et al. (2015). Formin-like 2 promotes β1-integrin trafficking and invasive motility downstream of PKCα. *Dev. Cell* 34, 475–483. doi: 10.1016/j.devcel.2015.06.015

Xie, J., Tato, C. M., and Davis, M. M. (2013). How the immune system talks to itself: the varied role of synapses. *Immunol. Rev.* 251, 65–79. doi: 10.1111/imr.12017

Yuseff, M. I., Pierobon, P., Reversat, A., and Lennon-Dumenil, A. M. (2013). How B cells capture, process and present antigens: a crucial role for cell polarity. *Nat. Rev. Immunol.* 13, 475–486. doi: 10.1038/nri3469

Yuseff, M. I., Reversat, A., Lankar, D., Diaz, J., Fanget, I., Pierobon, P., et al. (2011). Polarized secretion of lysosomes at the B cell synapse couples antigen extraction to processing and presentation. *Immunity* 35, 361–374. doi: 10.1016/j.immuni.2011.07.008

Conflict of Interest: The authors declare that the research was conducted in the absence of any commercial or financial relationships that could be construed as a potential conflict of interest.

frontiers in Cell and Developmental Biology

REVIEW
published: 16 March 2021
doi: 10.3389/fcell.2021.652077

Cytoskeletal Transport, Reorganization, and Fusion Regulation in Mast Cell-Stimulus Secretion Coupling

Gaël Ménasché[1], Cyril Longé[1], Manuela Bratti[2,3] and Ulrich Blank[2,3]**

[1] *Laboratory of Molecular Basis of Altered Immune Homeostasis, Imagine Institute, INSERM UMR 1163, Université de Paris, Paris, France,* [2] *Centre de Recherche sur l'Inflammation, INSERM UMR 1149, CNRS ERL8252, Faculté de Médecine site Bichat, Université de Paris, Paris, France,* [3] *Laboratoire d'Excellence Inflamex, Université de Paris, Paris, France*

Mast cells are well known for their role in allergies and many chronic inflammatory diseases. They release upon stimulation, e.g., via the IgE receptor, numerous bioactive compounds from cytoplasmic secretory granules. The regulation of granule secretion and its interaction with the cytoskeleton and transport mechanisms has only recently begun to be understood. These studies have provided new insight into the interaction between the secretory machinery and cytoskeletal elements in the regulation of the degranulation process. They suggest a tight coupling of these two systems, implying a series of specific signaling effectors and adaptor molecules. Here we review recent knowledge describing the signaling events regulating cytoskeletal reorganization and secretory granule transport machinery in conjunction with the membrane fusion machinery that occur during mast cell degranulation. The new insight into MC biology offers novel strategies to treat human allergic and inflammatory diseases targeting the late steps that affect harmful release from granular stores leaving regulatory cytokine secretion intact.

Keywords: mast cells, signaling, cytoskeleton, actin, microtubule, degranulation, secretory granule transport, secretory granule fusion

OPEN ACCESS

Edited by:
Noa B. Martin-Cofreces, Hospital Universitario Princess, Spain

Reviewed by:
Eric Espinosa, Université de Toulouse, France
Ronit Sagi-Eisenberg, Tel Aviv University, Israel

****Correspondence:***
Gaël Ménasché
gael.menasche@inserm.fr
Ulrich Blank
ulrich.blank@inserm.fr

Specialty section:
This article was submitted to Cell Adhesion and Migration, a section of the journal Frontiers in Cell and Developmental Biology

Received: *11 January 2021*
Accepted: *03 February 2021*
Published: *16 March 2021*

Citation:
Ménasché G, Longé C, Bratti M and Blank U (2021) Cytoskeletal Transport, Reorganization, and Fusion Regulation in Mast Cell-Stimulus Secretion Coupling. Front. Cell Dev. Biol. 9:652077. doi: 10.3389/fcell.2021.652077

INTRODUCTION

Mast cells (MC) are granulated cells of the hematopoietic lineage in tissues that localize in large numbers, especially under epithelial and mucosal surfaces exposed to the external environment such as the skin, the airways, and the intestine. This widespread distribution throughout the body attributes them the role of sentinel cells at the interface between innate and adaptive immunity (Beghdadi et al., 2011; Galli et al., 2020). Despite their undeniable role in the regulation of immune responses, MC are best-known as effector cells of allergic diseases after stimulation through their high-affinity IgE receptors (FcεRI). Within minutes after the crosslinking of FcεRI-bound IgE by a specific antigen/allergen, the MC degranulate and release a variety of inflammatory mediators contained in secretory granules (SG) including proteases, proteoglycans, lysosomal enzymes such as β-hexosaminidase, and vasoactive amines such as histamine and serotonin. This is followed (within 15 to 30 min) by the synthesis of lipid mediators, such as leukotrienes and prostaglandins, and (after several hours) by the *de novo* synthesis and secretion of cytokines and chemokines that mediate and

regulate the inflammatory response (Blank and Rivera, 2004; Blank et al., 2014; Wernersson and Pejler, 2014).

The earliest signaling event in response to FcεRI crosslinking is the phosphorylation of the immunoreceptor tyrosine-based activation motifs (ITAM) in the cytoplasmic tails of FcεRIβ and disulfide-linked FcεRIγ subunits and the activation of two Src-family protein tyrosine kinases (PTK) Fyn and Lyn followed by recruitment of the PTK Syk to the phosphorylated FcεRIγ ITAM (Rivera et al., 2008; Metcalfe et al., 2009). Activated PTK (in particular Fyn and Syk) then induce the phosphorylation of multiple intracellular adaptor proteins including growth-factor-receptor bound protein 2 (Grb2), Grb2-related adaptor protein (Gads), Grb2-associated binding protein 2 (Gab2), SH2 domain-containing leukocyte phosphoprotein of 76 kDa (SLP-76), and the transmembrane adapter protein linker for activation of T cells (LAT) (Alvarez-Errico et al., 2009). Phosphorylated LAT then enables the plasma membrane (PM) recruitment and activation of phospholipase Cγ (PLCγ) generating diacylglycerol (DAG) and inositol 1,4,5-trisphosphate (IP3) that activate, respectively, protein kinase C (PKC) and Ca2+ influx signaling (Rivera et al., 2008; Metcalfe et al., 2009). Signaling is further enhanced by the TEC family kinase BTK recruited to the PM via phosphatidylinositol (3,4,5)-trisphosphate (PIP3) generated by Gab2 activated phosphatidyl inositol-3 kinase (PI3K) (Metcalfe et al., 2009; Zorn et al., 2018). The release of Ca2+ from the endoplasmic reticulum (ER) induces the stromal interaction molecule 1 (STIM-1) recruitment to the Ca2+ release activated channel (CRAC) Ca2+ release-activated Ca2+ channel protein1 (ORAI1) leading to extracellular Ca2+ influx (Ma and Beaven, 2009; Holowka et al., 2012). Additionally, the transient potential Ca2+ channel 1 (TRPC1) amplifies the Ca2+ influx across the PM leading to an enhancement of the free cytoplasmic Ca2+ concentration, propagating further signaling events (**Figure 1**; Suzuki et al., 2010).

Early signal transduction downstream of FcεRI is accompanied by several changes in cell morphology based on cytoskeleton reorganization allowing MC degranulation (Draber et al., 2012). Several lines of evidence have shown that the Ca2+ response is crucial to regulate actin remodeling (Koffer et al., 1990) and the later stages of SG fusion with the PM by controlling the soluble N-ethylmaleimide sensitive fusion (NSF) attachment protein receptor (SNARE) complex formation (Blank and Rivera, 2004; Holowka et al., 2012). Gab2 phosphorylation by Fyn has been shown to be critical for the recruitment and activation of phosphatidyl inositol-3 kinase (PI3K) and the small GTPase Ras homology family member A (RhoA), which are required for microtubule formation and SG translocation in a Ca2+-independent manner (**Figure 1**; Gu et al., 2001; Parravicini et al., 2002; Nishida et al., 2005; Nishida et al., 2011).

Thus, the degranulation process requires the extensive reorganization of the cytoskeleton associated with membrane ruffling and cell spreading, the anterograde movement of SG and their fusion with the PM that leads to the release of inflammatory mediators. Research in recent years on the interplay between the secretory and cytoskeletal machinery that occurs during MC degranulation has highlighted complex processes that are tightly regulated by proximal signaling events downstream of the FcεRI. In this review, we will discuss the molecular processes that regulate stimulus-secretion coupling during MC degranulation highlighting molecular events that regulate the cytoskeleton and transport machinery in conjunction with the membrane fusion machinery.

MICROTUBULE DYNAMICS DURING MC DEGRANULATION

Microtubule Organization and Dynamics

MC activation by FcεRI aggregation induces increased formation of microtubules leading to microtubule-containing PM protrusions (Nishida et al., 2005; Draber et al., 2012). Microtubules are hollow tubular structures constituted of heterodimers of globular α- and β-tubulin subunits assembled into 13 linear protofilaments. New microtubules are nucleated from a central Microtubule Organizing Center (MTOC) also called centrosome. The minus-ends are capped and anchored to the MTOC with a slow-growing activity exposing α-tubulin subunits while the plus-ends generally are localized to the cell periphery with a fast-growing activity exposing β-tubulin subunits. Hence, microtubules are polarized. At the minus-end, γ-tubulin contributes to microtubule nucleation and stabilization by associating with γ-tubulin complex proteins (GCPs) to form a ring complex named the γ-tubulin ring complex (γ-TuRC) (Oakley et al., 2015). Microtubules undergo phases of growth, pause, and shrinkage, separated by rescue (transition from depolymerization to growth) or catastrophe (transition from growth to depolymerization) events. This microtubule behavior was called "dynamic instability" (Desai and Mitchison, 1997) and was observed *in vitro* and *in vivo* (Schulze and Kirschner, 1986; Burbank et al., 2006). Initiation of the microtubule polymerization requires addition of GTP-bound tubulin subunits at the plus-end of microtubules. Growing microtubule sheets create a cap of GTP-tubulin with stabilizing properties. Cap loss induces rapid depolymerization of microtubules. Microtubule dynamics is also coordinated by external regulators such as stabilizing factors (microtubules plus-end tracking proteins [+Tips], microtubule-associated proteins [MAPs], minus-end capping proteins) and destabilizing factors (depolymerizing kinesins, stathmin and severing proteins) (Akhmanova and Steinmetz, 2015).

Modulation of Microtubules by Drugs

Microtubule assembly is susceptible to drugs. Taxol is a natural product, and its derivatives induce microtubule assembly by stabilizing microtubules whereas nocodazole, colchicine, vinblastine, and vincristine destabilize microtubules. In MC, treatment with nocodazole and taxol suppressed FcεRI-mediated degranulation and translocation of SG to the PM demonstrating the role of tubulin dynamics in MC degranulation (Nielsen and Johansen, 1986; Martin-Verdeaux et al., 2003; Smith et al., 2003). More recently, miltefosine, a derivative of plasmalogen phospholipids used to treat MC-driven diseases, was described to inhibit the formation of microtubule protrusions on activated

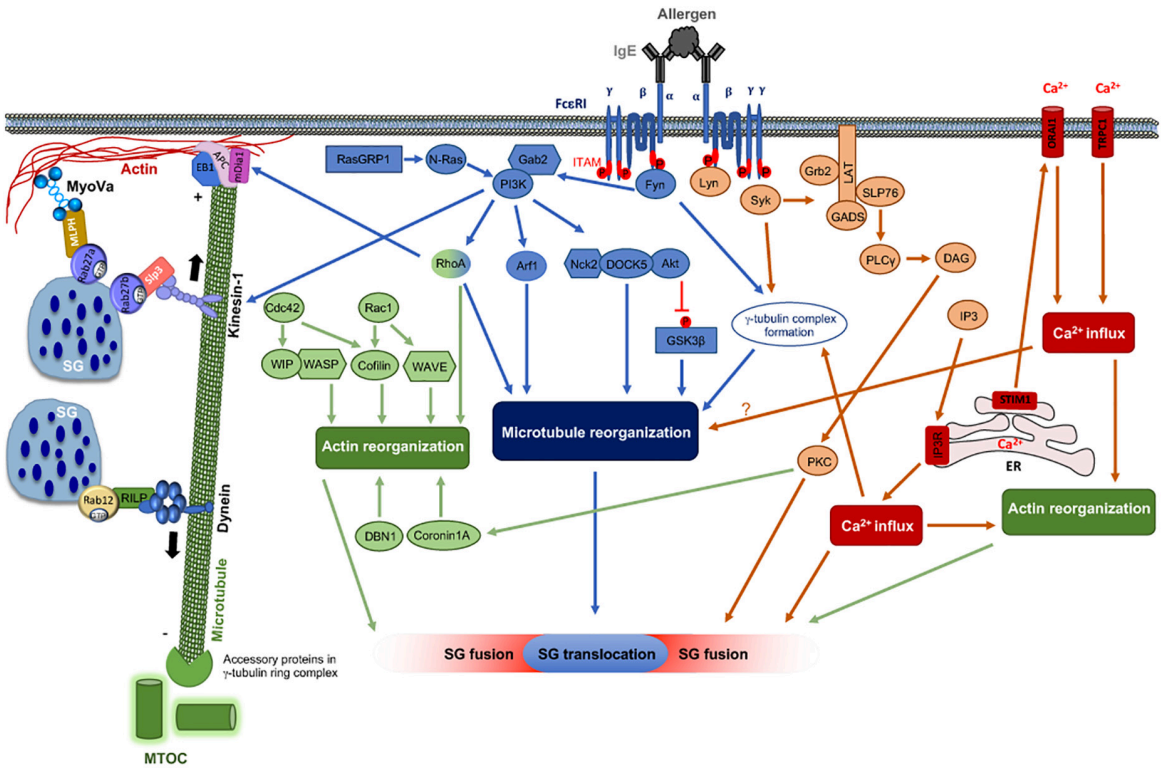

FIGURE 1 | FcεRI signaling pathways involved in cytoskeleton reorganization required for SG transport and fusion. The aggregation of the FcεRI by the IgE-allergen complex leads to phosphorylation of the ITAMs and the PTK (Fyn, Lyn, and Syk). They participate in the phosphorylation of multiple adapter proteins (Grb2, Gab2, SLP76, LAT), which generate additional signalosomes further propagating the signal. FcεRI-mediated signaling can be partitioned into Ca2+-dependent (LAT, SLP76; PLCγ, DAG, IP3, PKC) and Ca2+-independent pathways (Fyn, Gab2, PI3K, RhoA, RasGRP1, Arf1, Nck2, DOCK5, Akt) that mediate microtubule and actin reorganization necessary for SG transport and fusion. Actin dynamics in MC is also regulated by several actors including RhoA, Cdc42, Rac1, WIP, WASP, WAVE, Coronin1A, DBN1, and Cofilin. Microtubule dynamics is regulated by stabilization at the plus-end extremity by the trimeric protein complex EB1/APC/mDia1 and by a crosstalk between Fyn, Syk, and γ-tubulin signaling that may lead to microtubule nucleation at the MTOC or to enhanced non-centrosomal microtubule nucleation. Microtubule-mediated SG retrograde transport on microtubule is mediated by Rab12 that recruits the RILP-dynein complex. SG anterograde transport requires PI3K activation that allows kinesin-1's accessibility to the cargo receptor Slp3. The SG switch from microtubules to cortical actin is regulated by the Rab27a/Mlph/MyoVa complex. Thin arrows indicate direct effects on signaling cascades, cytoskeleton reorganization, SG translocation, and fusion events.

MC through the inhibition of DAG-regulated conventional PKC activity (Rubikova et al., 2018).

Signaling Events Downstream FcεRI Regulating Microtubule Dynamics

Genetic studies in mice were employed to dissect more precisely the molecular mechanisms required for cytoskeletal rearrangement in the degranulation process. It was reported that Fyn-deficient bone marrow-derived MC (BMMC) are defective in degranulation, albeit the Ca2+ influx was intact (Parravicini et al., 2002). Further analysis showed that microtubule formation was impaired in Fyn- and Gab2-deficient BMMC upon FcεRI activation (Nishida et al., 2005). In addition, activation of the small GTPase RhoA, known to regulate cytoskeletal reorganization, was significantly decreased in Gab2-deficient BMMC after FcεRI stimulation (Nishida et al., 2005). Thus, these reports identified a Fyn/Gab2/RhoA proximal FcεRI signaling pathway required for microtubule-dependent SG translocation to the PM (**Figure 1**). Inhibitors targeting PI3K and genetic inactivation of the p110δ catalytic subunit of PI3K also abrogated SG translocation (Barker et al., 1995; Ali et al., 2004). Activation of PI3K depends on recruitment of its p85 subunit to Gab2 (Gu et al., 2001) and knock-in mice expressing Gab2 mutated for the PI3K binding site were deficient in SG translocation (Nishida et al., 2011). This study also identified the small GTPase, ADP-ribosylation factor 1 (ARF1), as the downstream target of PI3K involved in SG translocation. ARF1 activation depends on Fyn, Gab2, and the Gab2 interaction with PI3K highlighting that the Fyn/Gab2/PI3K/ARF1 signaling pathway is required for FcεRI-mediated SG translocation (**Figure 1**; Nishida et al., 2011). By contrast this pathway controlling microtubule formation and SG translocation was not required for Ca2+ influx and F-actin disassembly (**Figure 1**). Another downstream target of PI3K is DOCK5, an atypical guanine nucleotide exchange factor (GEF) for Rac that was shown to regulate microtubule dynamics during MC degranulation independently of its Rac GEF activity (Ogawa et al., 2014). DOCK5 interacts with Nck2 and Akt promoting the phosphorylation and subsequent inactivation of the serine/threonine kinase GSK3β, which negatively regulates

microtubule dynamics and MC degranulation (**Figure 1**; Zhou and Snider, 2005; Ogawa et al., 2014). The Ras guanyl nucleotide-releasing protein 1 (RasGRP1), in parallel to Gab2, also participated to the activation of RhoA and PI3K through the activation of N-Ras (**Figure 1**; Liu et al., 2007). Genetic inactivation of RasGRP1 was associated in MC with a profound defect in microtubule formation and SG translocation to the PM (Liu et al., 2007).

The formation of microtubules upon FcεRI stimulation could potentially require (i) stabilization of the plus-end extremity of the microtubules, (ii) regulation of the microtubule nucleation at the minus-end of microtubules at the MTOC, or alternatively (iii) enhancement of non-centrosomal microtubule nucleation. Several signaling molecules involved in FcεRI-mediated microtubule reorganization could play a role in these three ways of microtubule nucleation. Activated RhoA was found to regulate microtubule formation upon FcεRI stimulation downstream of Fyn/Gab2 (Nishida et al., 2005). It could act by stabilizing the plus-end extremity of microtubules through the recruitment of mammalian diaphanous-related formin 1 (mDia1) promoting its binding to microtubule plus-end tracking proteins (+Tips), end-binding protein 1 (EB1), and adenomatous polyposis coli (APC) (Palazzo et al., 2001; Wen et al., 2004; Wojnacki et al., 2014). This trimeric protein complex functions as a microtubule plus cap, which prevents heterodimer exchange, thereby stabilizing microtubules at the PM (**Figure 1**). In addition, several evidences show a crosstalk between Fyn, Syk, and γ-tubulin-signaling complexes. This could lead, in activated MC, to microtubule nucleation at the MTOC or to enhanced non-centrosomal microtubule nucleation (Sulimenko et al., 2006). Work from the same team showed that in differentiating P19 embryonal carcinoma cells, γ-tubulin was recruited to the PM through a direct interaction with PI3K enabling non-centrosomal microtubule nucleation (Macurek et al., 2008). Moreover, microtubule nucleation in BMMC has recently been shown to involve proteins that are associated with γ-tubulin, such as p21-activated kinase interacting exchange factor β (βPIX, also known as Rho guanine exchange factor 7) and G protein-coupled receptor kinase-interacting protein 1 (GIT1) (Sulimenko et al., 2015). βPIX and GIT1, in association with centrosomes, have opposite function on microtubule nucleation, affecting either negatively or positively microtubule growth. Surprisingly, the interaction between GIT1 and γ-tubulin was Ca2+-dependent, suggesting a role of Ca2+ leading to microtubule nucleation in activated MC (**Figure 1**; Sulimenko et al., 2015). Recently, protein tyrosine phosphatases were also found to be important for the regulation of microtubule nucleation. Indeed, the Src homology 2 domain-containing protein tyrosine phosphatase 1 (SHP-1) is present in complexes containing γ-tubulin, GCP2, GCP4, and Syk and modulates negatively microtubule nucleation from the centrosomes of BMMC (Klebanovych et al., 2019).

While several studies showed the role of Ca2+ in the regulation of microtubule remodeling (Hajkova et al., 2011; Cruse et al., 2013; Sulimenko et al., 2015) another study that used Ca2+-free medium or medium containing EGTA with or without xestospongin (IP3 receptor inhibitor) found that these conditions did not inhibit FcεRI-induced microtubule formation (Nishida et al., 2005). This discrepancy may be attributable to differences in cell activation and various methods of sample preparation. Another explanation is that initial steps of microtubule formation and granule displacement could be Ca2+-independent, whereas later steps of MC activation and protrusion formation could be dependent on calcium influx (Draber et al., 2012). A truncated splice variant of the FcεRIβ subunit, t-FcεRIβ, known to bind to Gab2, Fyn, and calmodulin, could act to propagate Ca2+ signaling for microtubule nucleation in human LAD-2 MC. After MC activation t-FcεRIβ localized to the Golgi in close contact with the pericentrosomal region and hence may involve the Golgi complex to regulate Ca2+-dependent microtubule formation required for MC degranulation (Cruse et al., 2013). STIM-1 is one of the key components that regulates the influx of extracellular Ca2+ mediated by the opening of store-operated channels (SOCs). Interestingly, STIM-1 was also described as a microtubule-tracking protein that interacts with EB1 (Grigoriev et al., 2008). Knockdown approaches identified STIM1 as being required for the formation of microtubule protrusions (Hajkova et al., 2011; Cruse et al., 2013). By contrast, intact microtubules were not required for STIM-1 aggregation and recruitment beneath the PM to support opening of CRAC channels.

Although the complexity of signaling leading to the regulation of microtubule dynamics upon MC activation starts to be described (**Figure 1**), further studies are still required to understand the full complexity of the coordination of microtubule dynamics and secretion regulation in MC.

ACTIN DYNAMICS DURING MC DEGRANULATION

Actin Organization and Regulation

Actin is highly abundant, comprising 1 to 5% of the total cellular proteins. It exists as a monomer called G-actin (globular) that can polymerize into long helical F-actin (filamentous) microfilaments (Pollard, 2016). They can be held together by crosslinking proteins to form actin bundles and networks (e.g., α-actinin, fimbrin, fascin, filamin, spectrin, dystrophin) or branch using specific effectors (e.g., actin-related proteins 2/3, [Arp2/3] complex) (Broderick and Winder, 2005; Zhou et al., 2010; Liem, 2016; Pollard, 2016; Machnicka et al., 2019). Actin interacts with a substantial number of proteins that contribute to maintain a pool of actin monomers, initiate polymerization, constrain the length of actin microfilaments, regulate their assembly and turnover, or crosslink them into bundles or networks (dos Remedios et al., 2003; Pollard, 2016). The actin cytoskeleton consists of structurally and biochemically different actin filament arrays. Although still poorly defined, the one attached to the membrane, called cortical actin, is planar forming a web beneath the PM (Svitkina, 2020), while within the cell the actin cytoskeleton is three-dimensional providing the cytosol with gel-like properties (Pollard, 2016). The actin cortex is attached to the membrane involving other proteins of the ERM (Ezrin, Radixin, Moesin) family and the spectrin network, all of which may contribute to signaling functions (Machnicka et al., 2014; Garcia-Ortiz and Serrador, 2020). The actin cytoskeleton provides a framework

for cell shape, yet an important characteristic is that it is highly dynamic thereby (i) facilitating the transduction of mechanical signals, (ii) generating forces that allow cell motility, cell division, cytokinesis, and (iii) allow vesicular trafficking and muscle contraction (Svitkina, 2018), (iv) contribute to the formation and maintenance of cell junctions (Zhang et al., 2005), and (v) participate in cell signaling (Draber et al., 2012; Mattila et al., 2016). Actin dynamics is regulated by small GTPases of the Rho family (Rho, Rac, Cdc42) in response to external signals. Rho activates the formation of stress fibers and focal adhesions, Rac enables formation of lamellipodia and membrane ruffles and Cdc42 activates the formation of filopodia (Hall, 1998; Heasman and Ridley, 2008). Rho family GTPases act as molecular switches that enable either directly or indirectly the activation of multiple downstream signaling effectors of actin dynamics including kinases (p21-activated kinase [PAK]); Rho-associated coiled-coil kinase (ROCK); LIM-motif containing kinase (LIMK); myosin light chain phosphatase (MLCP); myosin light chain kinase (MLCK); as well as nucleation and branching promoting factors (mDia); Wiskott-Aldrich syndrome protein (WASP); Wiskott-Aldrich syndrome protein-family verprolin homologous protein (WAVE); Arp2/3 complex (Heasman and Ridley, 2008; Draber et al., 2012).

Actin Dynamics in MC

MC signaling is accompanied by important changes in the actin cytoskeleton. Initial data showed that FcεRI-mediated stimulation in rat basophilic leukemia (RBL) MC promotes a decrease in cellular F-actin content during the first 10–30 s followed by a rapid increase within 1 min. This coincided with the transformation of the surface topography to a less dense actin cortex and formation of lamellar actin ruffles at the cell surface as well as cell spreading (Pfeiffer et al., 1985; Frigeri and Apgar, 1999; Wilson et al., 2016). This was confirmed in cultured primary and *ex vivo* isolated MC (Pendleton and Koffer, 2001; Tumova et al., 2010). Additional data showed that during stimulation the cortical actin becomes fragmented and disassembled (Koffer et al., 1990; Narasimhan et al., 1990) in a Ca2+ and calmodulin-dependent manner strongly correlating with secretion (Sullivan et al., 2000; Nishida et al., 2005). This supported earlier data in other cells (Orci et al., 1972; Cheek and Burgoyne, 1986) indicating that the actin web could represent a physical barrier for secretion with its disassembly representing a terminal step in exocytosis. In agreement with the assumption that actin remodeling is necessary for secretion to occur, addition to MC of Jasplakinolide, a drug that stabilizes F-actin polymers, inhibited MC degranulation (Nishida et al., 2005; Wilson et al., 2016), while Cytochalasin D and Latrunculin A, which inhibit actin polymerization thereby disrupting microfilaments, enhanced MC secretion (Narasimhan et al., 1990; Pierini et al., 1997; Frigeri and Apgar, 1999; Martin-Verdeaux et al., 2003).

Yet, data accumulated to date show that the signal-induced changes in the actin cytoskeleton are far more complex relating to both early and late signaling events. Studies with actin disrupting agents showed that they promoted an increased and prolonged phosphorylation response including that of the FcεRI β and γ subunits (Frigeri and Apgar, 1999; Holowka et al., 2000; Tolarova et al., 2004; Torigoe et al., 2004) and an increase in intracellular Ca2+ levels (Oka et al., 2002). Fluorescence localization microscopy and pair-correlation analysis indicated that this was associated with an enhanced colocalization of IgE-FcεRI, Lyn, and a lipid anchor probe of Lyn in ordered lipid regions. This supports that the actin cytoskeleton might regulate this functional interaction by influencing the organization of membrane lipids (Shelby et al., 2016). In addition to its barrier function, the actin cortex also acts as a carrier for myosin V actin motors to capture and transport vesicles to membrane fusion sites, thereby playing a role in corraling and docking SG at the PM (Elstak et al., 2011; Wollman and Meyer, 2012; Singh et al., 2013). Based on these evidences, MC activation was clearly associated with signaling of actin remodeling.

Signaling Events Downstream FcεRI Regulating Actin Dynamics

Early studies showed that the GTPase Rho participated in actin polymerization, while Rac favored reorientation of microfilaments, and both proteins were implicated in secretion in rat peritoneal MC (Norman et al., 1994, 1996; Price et al., 1995). In RBL MC, activated Cdc42 participated in the formation of cell adhesions while Rac1 played a role in FcεRI-mediated membrane ruffling. Expression of trans-dominant inhibitory forms of both Cdc42 or Rac1 significantly inhibited antigen-induced degranulation (Guillemot et al., 1997). Recent studies using specific inhibitors confirmed that Rac proteins triggered F-actin-mediated protrusions and flattening of the cell periphery to create an active degranulation zone, whereas RhoA participated in ruffle formation also controlling granule motility (Sheshachalam et al., 2017). The involved actin remodeling plays a role in FcεRI early signaling and Ca2+ responses possibly via by its effect on the activation of cofilin (see also below) (Oka et al., 2004; Ang et al., 2016). Indeed, when receptors were desensitized through repeated stimulation with increasing doses of antigen, dynamic reorganization of the actin cytoskeleton is inhibited. This is associated with an inhibition of the cofilin dephosphorylation/phosphorylation cycle regulating actin dynamics (Ang et al., 2016). Regarding downstream signaling of Rho GTPases, genetic knockout (KO) and knockdown (KD) as well as inhibitor approaches identified a Pak1 kinase-dependent interaction with protein phosphatase 2 (PP2A) promoting dephosphorylation of Thr567 of Ezrin/Radixin/Moesin (ERM) proteins. This uncouples the PM from the actin cytoskeleton prior to F-actin clearing and degranulation. Absence of this axis led to defective F-actin rearrangement, impaired degranulation, and systemic histamine release (Staser et al., 2013). Other important downstream targets of Rho GTPases are WASP (downstream of Cdc42) and Wave (downstream of Rac) proteins promoting the association with the Arp2/3 complex to create a nucleation core for actin branching (**Figure 1**; Moller et al., 2019). In WASP-deficient BMMC actin polymerization, cell spreading, formation of ruffles, and degranulation was inhibited after FcεRI stimulation (Pivniouk et al., 2003). Likewise, although some pleiotropic actions including on early signaling responses were observed, the Wiskott-Aldrich syndrome protein interacting

protein (WIP), which holds WASP in an inactive state, was found to play a role in degranulation and generation of actin filaments in FcεRI-stimulated BMMC (**Figure 1**; Kettner et al., 2004). All these data strongly indicate that Rho GTPase family members and their effectors have a major role in organization of microfilaments and degranulation responses in activated MC. Drebrin (DBN) is another actin-associated protein able to crosslink F-actin bundles, thereby stabilizing the actin network (**Figure 1**). In DBN1-KO MC, histamine and *in vivo* passive systemic anaphylactic responses are inhibited, indicating a positive regulatory role (Law et al., 2015). Further analysis showed that DBN1-KO MC exhibited defects in actin organization with actin bundles accumulating in the cytoplasm and a delay in F-actin clearance in stimulated cells. The effect on degranulation could be rescued by the actin depolymerizing drug Latrunculin B. The DBN1-KO MC also showed a defect in intracellular Ca2+ influxes after stimulation, as was also observed in WASP- (Pivniouk et al., 2003) and WIP-KO MC (Kettner et al., 2004), again supporting a role of the actin network in Ca2+ responses. In contrast, the actin-binding protein Coronin1A, which binds to F-actin via its WD40 repeat domain, was reported to negatively regulate exocytosis (**Figure 1**; Foger et al., 2011). In its absence degranulation was enhanced mimicking the effects of actin depolymerizing drugs, whereas cytokine secretion (but not production) was inhibited. FcεRI stimulation phosphorylated Coronin1A on the PKC substrate Ser2 promoting its relocation from the cortex to the cytoplasm and cortical F-actin disassembly, hence providing genetic evidence for its function as a physical barrier. The positive action on cytokine secretion of Coronin1A points to a role of F-actin cytoskeleton remodeling in the egress of transport vesicles from the trans-Golgi. A recent study points to the contribution of the actin-severing protein cofilin in cortical actin depolymerization/polymerization in MC (Suzuki et al., 2021). Following receptor crosslinking with a hapten-antigen, cofilin becomes rapidly dephosphorylated promoting cortical actin disassembly. When disaggregating receptors with the free hapten, cofilin rephosphorylates, thereby restoring the cortical actin barrier. The actin polymerizing effector mDia1, when activated through chemokine receptors, but not by FcεRI, was shown to participate in the buildup of pericentral actin clusters that converge the SG to the cell center, preventing them to undergo secretion (Klein et al., 2019). The formation of these clusters presents therefore a mechanism to favor migration over secretion in cells stimulated via chemokine receptors. Interestingly, mDia1 has been reported to generate actin filaments that are resistant to the action of cofilin (Mizuno et al., 2018). The filaments generated by this formin may also play a role in the terminal trafficking steps close to the cortex that could depend on actin as shown in pancreatic acinar cells (Geron et al., 2013). However, presently this has not been investigated in MC.

Actin Facilitating SG Secretion

Although it was proposed that the cortical actin ring may act as a physical barrier in MC (Koffer et al., 1990), observations in other cells are also compatible with the assumption that microfilaments provide tracks for myosin-dependent SG mobility (Oheim and Stuhmer, 2000). This process may involve actin coating of SG as shown in pancreatic acinar cells favored by the release of Rab3D GTPase from them (Valentijn et al., 1996, 1999). Actin coating and myosin may also serve as mechanical forces for the expulsion of granular content and/or eventually stabilize fusing granules (Nightingale et al., 2012). Although it was found that Rab3D can regulate SG fusion in MC (Roa et al., 1997; Tuvim et al., 1999), its possible involvement in actin granule coating has not been investigated in these cells, yet. The Rab GTPase Rab27a has also been proposed to play a role in coupling SG to the actin cytoskeleton (Fukuda, 2013). In MC, Rab27a regulates cortical actin integrity limiting secretion by restricting the access of SG to the PM. It functions likely together with its interacting partners Melanophilin and Myosin Va as mice deficient in these proteins similarly show a slightly hypersecretory phenotype (**Figure 1** and **Table 1**; Singh et al., 2013). Comparison of the secretory phenotype of Rab27b-KO and Rab27a/b double KO indicated that Rab27a may also play a positive role acting in concert with Rab27b to facilitate degranulation (Mizuno et al., 2007; Singh et al., 2013). This involves the switching of SG from a microtubule-dependent movement to an F-actin-dependent movement, finally allowing to corral and dock motile SG at the PM in conjunction with Munc13-4 (Elstak et al., 2011; Singh et al., 2013). As shown in neutrophils, Rab27a action on the actin cytoskeleton may also involve another effector of the Synaptotagmin-like protein (Slp) family such as Slp1 shown to bind to the PM via its C2A domain. This promotes the interaction with the Rho GAP Gem-interacting protein (GIMP) leading to the inhibition of RhoA, thereby facilitating actin depolymerization (Johnson et al., 2012; Ramadass and Catz, 2016). Besides Rab27a, Rab11 may represent another Rab protein regulating actin dynamics. Rab11 localizes to recycling endosomes (RE) in MC. Expression of a dominant negative form (S25N) inhibited antigen stimulated exocytosis of vesicles emanating from the RE, which was rescued in the presence of actin depolymerizing drugs. Further mechanistic studies indicated that PM-recruited Rab11 played a role in the regulation of actin depolymerization when activated through its GTPase activating protein p50RhoGAP (Wilson et al., 2016).

The possible simultaneous function of the actin cortex as a release barrier and as a carrier for vesicle transport to the PM in the terminal steps in MC secretory signaling has been investigated in more detail with advanced imaging approaches. Using a variety of biosensors (actin, Ca2+, PIP2, N-WASP, Dextran) Wollman and Meyer found that actin remodeling during secretion in RBL MC is tightly coupled to Ca2+ oscillations (Wollman and Meyer, 2012). FcεRI stimulation induced waves of intracellular Ca2+ and PIP2 lipid levels that, in turn, regulate cyclic recruitment of WASP and cortical actin assembly/disassembly. Dextran labeled granules get captured by actin when cortical F-actin levels are high, followed by vesicle passage through the cortex when F-actin starts to disassemble with vesicle fusion at the PM taking place at Ca2+ peak values. Likewise, TIRF image analysis of the cortical actin skeleton in RBL MC revealed a highly orchestrated series of events (Colin-York et al., 2019). Stimulation initially induced cell spreading. Then at the contact interface, the central F-actin network of the cortex exhibiting bright cluster-like actin plaques underwent a symmetry break associated with disassembly of

TABLE 1 | Proteins implicated in SG fusion.

Protein (Hu/mo gene name)	Functional domains	Role in MC exocytosis
SNAP-23 = Synaptosomal-associated protein 23 (*SNAP23/Snap23*)	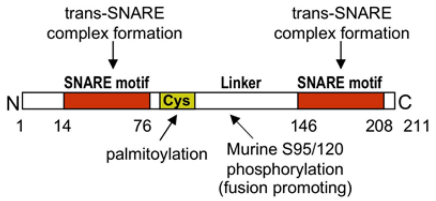	PM-localized t-SNARE; enhanced trans-SNARE complex formation and cytoplasmic relocation along degranulation channels (SG and SG-PM fusion) in stimulated MC; Inhibition of stimulated exocytosis in KD MC and after introduction of blocking Abs
STX3 = Syntaxin 3 (*STX3/Stx3*)	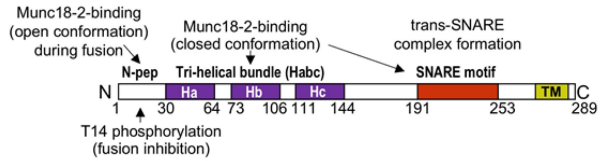	SG-localized t-SNARE; enhanced trans-SNARE complex formation and PM relocation (SG-SG and SG-PM fusion) in stimulated MC; inhibition of stimulated exocytosis in KO/KD MC
STX4 = Syntaxin 4 (*STX4/Stx4*)	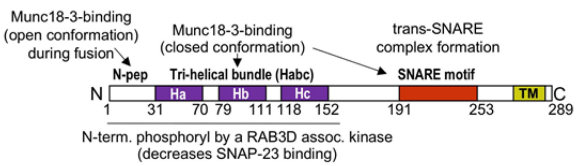	PM-localized t-SNARE; enhanced trans-SNARE complex formation upon stimulation (role in SG-PM fusion?); no inhibition of stimulated exocytosis in KO MC; partial inhibition in KD MC
STX11 = Syntaxin 11 (*STX11/Stx11*)	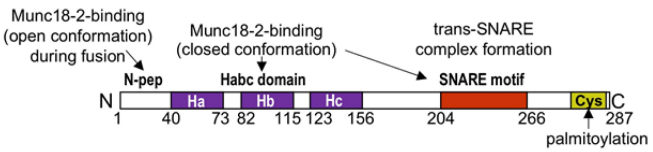	Expression upregulated upon IgE/Ag and LPS stimulation; no inhibition of stimulated exocytosis in KO MC; plays a role in lytic granule exocytosis in NK and T cells
VAMP8 = Vesicle-associated membrane protein-8, also endobrevin (*VAMP8/Vamp8*)	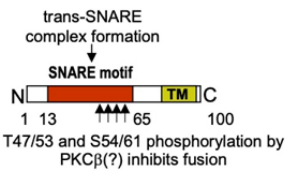	Endosomal, lysosomal and SG-localized v-SNARE; enhanced trans-SNARE complex formation in stimulated MC (role in SG and SG-PM fusion); partial inhibit of stimulated exocytosis in KO and KD MC; one manuscript reports specific effect on β-hexosaminidase but not histamine secretion
VAMP7 = vesicle-associated membrane protein 7, also Tetanus Insensitive Ti-VAMP (*VAMP7/Vamp7*)	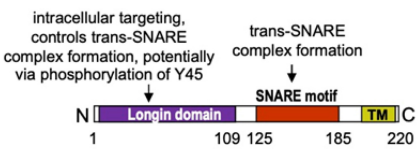	Punctuate staining pattern in resting hu MC (SG?), PM relocation in stimulated primary hu MC; enhanced trans-SNARE complexes upon stimulation in hu MC; inhibition of stimulated exocytosis In KD MC and after introduction of blocking Abs
VAMP2 = vesicle associated membrane protein 2, also Synaptobrevin-2 (*VAMP2* or *SYB2/Vamp2* or *Syb2*)	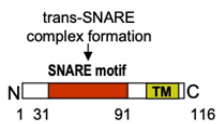	Transfected (but not endogenous) fluorescent VAMP2 showed cytoplasmic (SG?) staining; PM translocation in transfected, stimulated RBL cells, enhanced trans-SNARE complexes in stimulated VAMP8 KO but not in WT BMMC; no inhibition of stimulated exocytosis in KO BMMC, inhibition with blocking Abs in RBL but not hu MC
SYT2 = Synaptotagmin-2 (*SYT2/Syt2*)	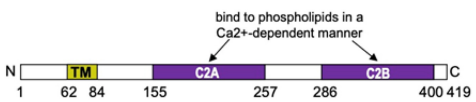	SG-localized Ca2+ sensor; inhibition of stimulated exocytosis in KO MC
CPLX2 = Complexin 2, also Complexin II or Synaphin-1 (*CPLX2/Cplx2*)	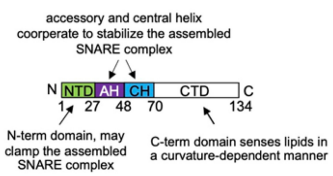	Punctuate cytoplasmic staining; PM translocation in stimulated RBL cells, pulldown assay reveals binding to an assembled STX3 (not STX4)/SNAP-23/VAMP2 or VAMP8 SNARE complex; stimulated exocytosis is inhibited in KD RBL cells, Ca2+ titration experiments show that CPLX2 increases Ca2+ sensitivity

(Continued)

TABLE 1 | Continued

Protein (Hu/mo gene name)	Functional domains	Role in MC exocytosis
Munc13-4 = mammalian uncoordinated protein 13-4, also protein unc-13 homolog D (*UNC13D/unc13d*)	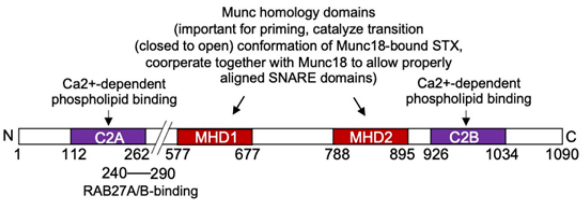	Interacts with SG localized Rab27a or b? through a non-canonical motif, the Rab27/Munc13-4 complex is necessary to dock SG at the PM; substantial inhibition of stimulated exocytosis in KO MC; in neuronal cells Munc13 homologues promote disassembly of the closed Munc18/STX complex; assures together with Munc18 proper parallel SNARE zippering
DOC2α = Double C2-like domain-containing protein alpha (*DOC2A/Doc2a*)	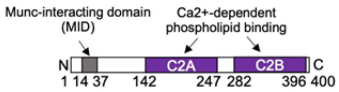	Interacts with Munc13-4 on SG via N-terminal MID and C-terminal C2B domain, colocalizes with SG, partial inhibition of stimulated exocytosis in KD and KO MC
Munc18-2/Munc18b = mammalian uncoordinated protein 18-2/18b, also syntaxin binding protein 2 (STXBP2) or protein unc-18 homolog 2/b (*STXBP2/Stxbp2*)	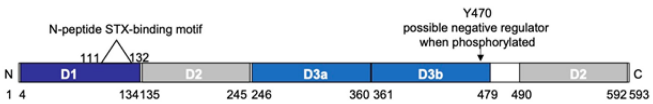	Interacts with SG-localized STX3, Munc18 has two binding modes: binding in closed conformation to a STX SNARE blocks SNARE zippering; binding in an open conformation to STX SNARE (implicating N-terminal peptide) enables zippering; assures together with Munc13-4 proper parallel SNARE zippering
SCAMP2 = Secretory carrier-associated membrane protein 2 (*SCAMP2/Scamp2*)	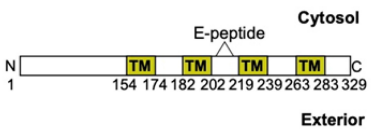	A tetraspanin that may participate in organizing the phospholipid composition for fusion pore formation by coupling Arf6-stimulated PLD generating PIP2; implicates a peptide (E-peptide) as its expression inhibits stimulated exocytosis in MC
STXBP5 = Syntaxin binding protein 5 or tomosyn-1 or Lethal(2) giant larvae protein homolog 3 (*STXBP5/Stxbp5*)		Binds to STX3 and STX4; acts as a fusion clamp as stimulated exocytosis is enhanced in KD MC; STX4 binding decreases and STX3 increases after stimulation in MC; STXBP5 becomes phosphorylated on multiple S/T residues during stimulation promoting STX3 association and STX4 dissociation
Rab3D = Ras-related protein Rab3D (*RAB3D/Rab3d*)	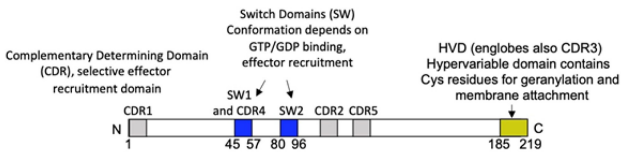	SG-localized; transient PM relocation upon stimulation; "GTP-bound" mutant inhibits exocytosis; no effect in KO MC (compensatory mechanism?); role in actin coating of SG?
RAB5 = Ras-related protein Rab5 (*RAB5/rab5*)	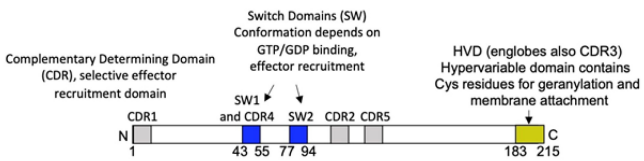	Role in SG maturation mediating SG fusion during biogenesis; role in stimulated exocytosis favoring SG recruitment of SNAP-23 and SG-SG fusion; In KD MC balance is shifted from compound to full exocytosis with SG-PM fusion only
RAB27A = Ras-related protein Rab27A (*RAB27A/Rab27a*)	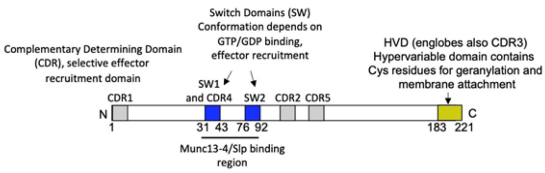	SG-localized; regulates cortical actin integrity; switches SG from microtubule-dependent movement to F-actin-dependent docking; enhanced stimulated exocytosis in KO MC; but facilitates stimulated exocytosis together with Rab27b and Munc13-4 (Rab27a magnifies inhibitory effect of Rab27b on stimulated exocytosis in DKO MC)

(Continued)

TABLE 1 | Continued

Protein (Hu/mo gene name)	Functional domains	Role in MC exocytosis
RAB27B = Ras-related protein Rab27B (*RAB27B/Rab27b*)	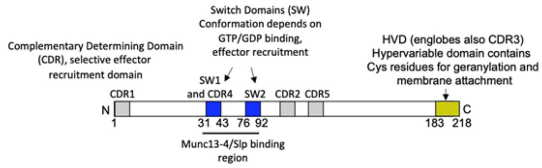	SG-localized; regulates microtubule-dependent movement of SG connecting via Slp3 to the kinesin-1 motor; inhibition of stimulated exocytosis in KO MC, may act partly together with Rab27a as inhibition of stimulated exocytosis is magnified in DKO MC
RAB37 = Ras-related protein Rab37 (*RAB37/Rab37*)	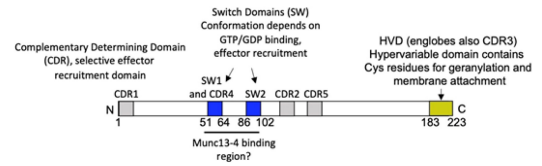	SG-localized, GTP-bound Rab37 interacts with Munc13-4 in a trimeric complex containing Rab27 and Munc13-4; KD MC and transfected GTP-bound Rab37 exhibit hypersecretory phenotypes; Rab37 may counteract the Rab27/Munc13-4-dependent docking/priming step

the actin cortex before reassembling again at later time points. These processes appeared intimately linked to the formation of distinct nanoscale F-actin architectures (asters, vortices) that only form in activated cells and were driven by Arp2/3 nucleation. Myosin II motor protein did not colocalize with these patterns, but accumulated in structures around, finally promoting their disassembly supporting an important role in pattern maturation and disassembly. Extrusion of granular content (as measured by appearance of Annexin V staining) was prominent at the contact interface and was closely related to actin dynamics with the dense mesh abruptly forming a small (∼1 μm) circular opening, which remained stable during extrusion. Another study using combined atomic force and laser scanning confocal microscopy in BMMC again showed that stimulation is associated with important changes in F-actin structures with the cell forming lamellipodia and ruffles when adhering to poly-lysine coated surfaces (Deng et al., 2009). As observed in the above study, the cortical F-actin moves to the periphery removing the barrier, thereby favoring permanent fusion as compared to kiss-and-run fusion observed in cells where surfaces were not coated with poly lysine and where actin clearing is much less prominent. The granule extrusion sites appear as craters and are clearly excluded from the F-actin ruffles at the cell surface as observed previously (Martin-Verdeaux et al., 2003).

Taken together, the results accumulated over many years show a tight connection between actin remodeling and secretory functions. How these complex and highly dynamic events are controlled by upstream signaling molecules remains still a puzzle that now, however, can be approached through modern imaging techniques.

MOLECULAR MECHANISMS REGULATING SG TRAFFICKING IN MC SECRETION

Rab GTPase proteins are well known to regulate and coordinate discrete vesicular trafficking steps along the endocytic and exocytic pathway in all cell types. Rab GTPases function as molecular switches that alternate between the GTP-bound "on" form and the GDP-bound "off" form (Stenmark, 2009). More than 60 Rab family members have been identified from mammalian species and each localizes to a particular membrane compartment. Using a functional screening assay of 44 Rab proteins, 30 of them were identified with a potential role as regulators of MC SG trafficking and exocytosis (Azouz et al., 2012). The Rab27a and Rab27b are both expressed in BMMC and localize to SG (**Table 1**). The use of single murine KO for Rab27a or Rab27b and the double KO of Rab27a/b demonstrated that the Rab27 family and particularly Rab27b plays a crucial role in MC degranulation (**Figure 1**; Mizuno et al., 2007). Indeed, as explained above, Rab27a and Rab27b have distinct and opposing roles, Rab27a acts as a negative regulator through its action on actin (**Figure 1**), whereas both Rab27a and Rab27b act as positive regulators through their interaction with Munc13-4 (**Figure 2**; Singh et al., 2013). Another Rab GTPase that acts as a negative regulator of MC degranulation is Rab12 described to mediate microtubule-dependent retrograde transport of SG (Efergan et al., 2016). Rab12 transports SG toward the minus-end on microtubules to the perinuclear region upon MC activation by interacting with Rab-interacting lysosomal protein (RILP) within the RILP-dynein complex (**Figure 1**; Efergan et al., 2016). Indeed, in MC SG were shown to move bidirectionally on the microtubule network (Smith et al., 2003; Nishida et al., 2005; Brochetta et al., 2014). More recently, the plus-end directed microtubule-dependent transport of SG was attributed to the archetypal member of the kinesin superfamily, kinesin-1 (Munoz et al., 2016). Kinesin-1 is composed of two heavy chains (KIF5A, KIF5B, or KIF5C) and two light chains (KLC1, KLC2, KLC3, or KLC4) with KIF5B and KLC1 being the main isoforms present in BMMC. The use of a conditional murine model lacking *Kif5b* in MC demonstrated that kinesin-1 regulates SG transport toward the secretion site during FcεRI activation (Munoz et al., 2016). Upon stimulation, kinesin-1 couples to Slp3 known to interact through its Slp homology domain (SHD) with Rab27b on SG (**Figure 1**). The stimulation-induced coupling required PI3K activity highlighting that activation regulates

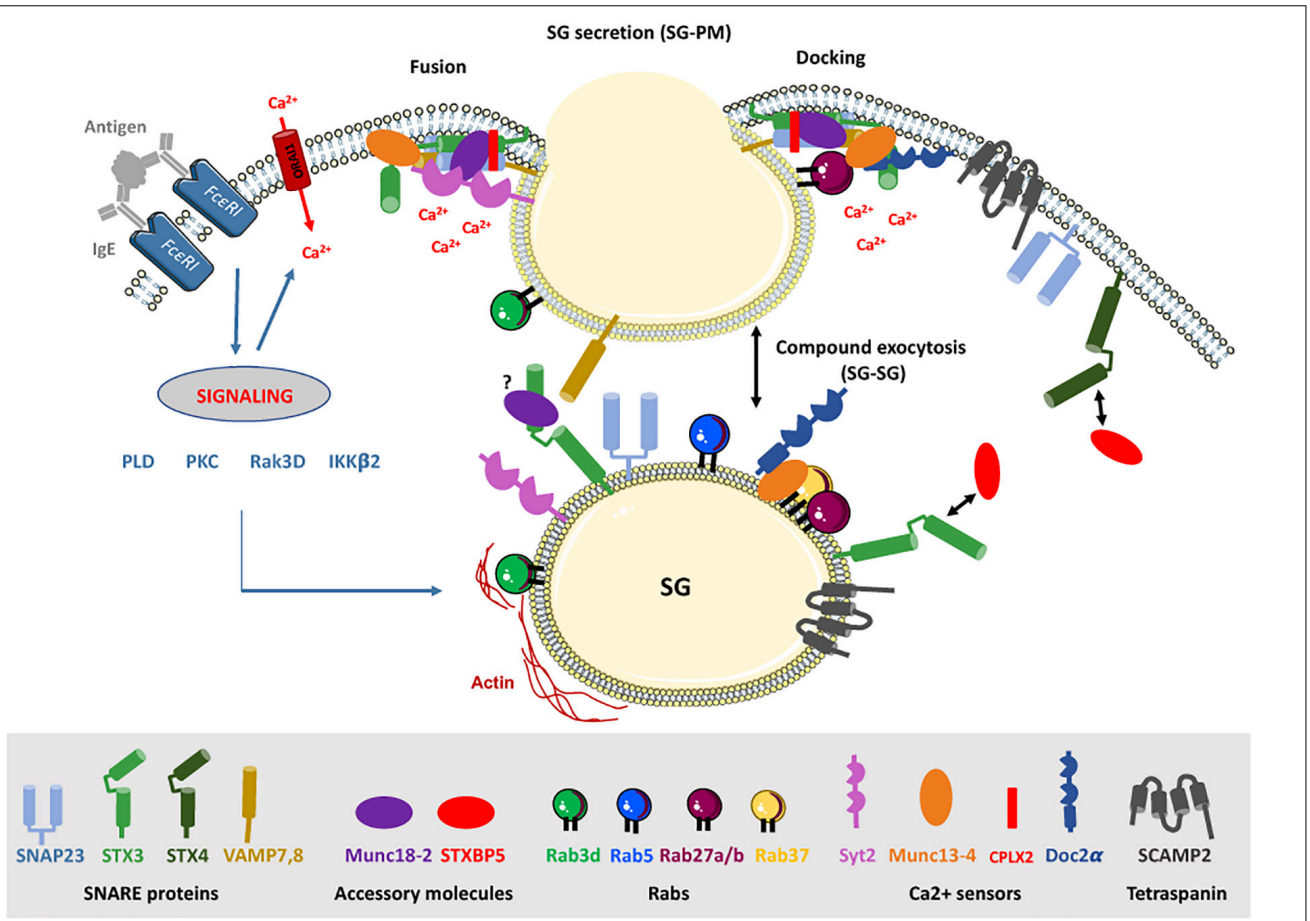

FIGURE 2 | The docking/fusion machinery in MC degranulation. FcεRI aggregation initiates proximal signaling that lead to increases of intracellular Ca2+ levels and the activation of PKC, PLD, Rak3D, and IKKβ2. These signaling events enable SG docking at the PM and their fusion to release granular content. In MC, fusion occurs also between SG, a process known as compound exocytosis, enabling massive release of inflammatory mediators. For simplicity the docking and fusion steps are detailed only at the PM. Note, however, that because of the compound exocytosis mechanisms, many of the molecular effectors are localized on SG eventually redistributing and serving also at the PM after stimulation (see text of **Table 1** for further details). In addition, some effectors (e.g., SNAP-23) reversely relocate to SG to serve in the SG fusion process. This process has been shown to be regulated by Rab5 and Ikkβ2. Membrane fusion involves SNARE proteins that lie on opposing membranes. In MC, they include the t-SNARE SNAP-23, STX 3 and 4, and the v-SNAREs VAMP 7 and 8 (see text and **Table 1** for further details). Fusion involves formation of a tetrameric trans-SNARE complex that is regulated by numerous accessory proteins allowing SG to dock at the PM or between themselves (not shown) and to facilitate their fusion. Docking involves a complex between Rab27, Munc13-4, and Doc2α and the Ca2+-activated phospholipid binding of Munc13-4 and Doc2α C2 domains. The formation of the docking complex is prevented by Rab37 when bound in a tripartite complex with Rab27 and Munc13-4. SNARE complex formation and fusion is regulated by the concerted action of Munc18-2 and Munc13-4 that allow the proper alignment of SNARE helices and is further assisted by CPLX2 and the Ca2+ sensor Syt2 that triggers fusion at high Ca2+ levels. STXBP5/tomosyn-1, by binding to its STX partner (STX3/4) in a manner regulated by PKCδ, controls the availability of fusion-competent SNARE proteins available for fusion. SCAMP2 may participate in the generation of an appropriate phospholipid composition through the coupling of Arf6-stimulated PLD activity. Rab3D, besides regulating Rak3D activity known to phosphorylate STX4 and inhibit SNAP-23 binding, may have a possible role in actin coating of SG supporting terminal transport and SG content extrusion.

kinesin-1 accessibility to the cargo receptor Slp3 (**Figure 1**). Interestingly, this coupling occurred even in the absence of assembled microtubules in cells treated with nocodazole (Munoz et al., 2016). Rab44, an atypical Rab GTPase, has recently been shown to be involved in MC degranulation and IgE-mediated anaphylaxis (Kadowaki et al., 2020). Rab44 belongs to the family of large Rab proteins that include the founder member CRACR2A and Rab45 (Srikanth et al., 2016). Their carboxy-terminal Rab domain is linked to additional domains, including an EF-hand domain, a coiled-coil domain, and a proline-rich domain that (in CRACR2A) interacts, respectively, with Ca2+, ORAI1/STIM1, and VAV1. In T lymphocytes, CRACR2A is recruited to the immunological synapse through its interaction with VAV-1, where it facilitates CRAC channel function by stabilizing the ORAI1-STIM1 interaction in response to TCR stimulation (Srikanth et al., 2010, 2016). Interestingly, CRACR2A is also able to interact with dynein to regulate endocytic trafficking in a Ca2+ dependent manner (Wang et al., 2019). Although CRACR2A links vesicular trafficking and signaling pathways upon TCR stimulation in T cells, it is not clear whether Rab44 is involved in Ca2+ signaling or other signaling pathways in MC to induce SG secretion.

In addition to Rab GTPases and molecular motors, the mammalian uncoordinated18 (Munc18) isoform 2 (Munc18-2) (**Table 1**), besides acting as fusion accessory protein, may also act in SG translocation (Brochetta et al., 2014). Treatment with the microtubule-destabilizing drug nocodazole induced redistribution of Munc18-2 from a granular to a diffuse cytosolic location, indicating that its recruitment/docking to SG was dependent on microtubules. Munc18-2 localized to SG, and upon stimulation Munc18-2 was translocated to the periphery into forming lamellipodia along microtubules remaining associated with large (fused) SG (Brochetta et al., 2014). During stimulation, the interaction of Munc18-2 with β-tubulin was downmodulated, indicating a possible dynamic functional interaction with the microtubule cytoskeleton. In agreement, KD of Munc18-2 affected SG translocation and docking at the PM with SG appearing stationary docked along microtubules inside the cell. This suggests that Munc18-2 could dynamically dock SG during microtubular transport, eventually in conjunction with the kinesin1/Slp3/Rab27b transport mechanism described above (Brochetta et al., 2014). In this context, neuronal Munc18-1 was demonstrated to bind to the kinesin-1 adaptor protein, fasciculation, and elongation protein zeta 1 (FEZ1 or zygin) to mediate axonal transport along microtubules, providing a link to microtubule-dependent vesicular transport (Chua et al., 2012).

Although some clues have been obtained how the molecular machinery of SG transport gets linked to signaling pathways downstream of FcεRI, much work remains to be done to understand further the complex signaling pathways of SG trafficking.

FUSION MACHINERY IN MC SECRETION

The terminal step in MC degranulation is the fusion of the SG membrane with the PM to release stored inflammatory mediators into the surrounding environment (Lorentz et al., 2012; Blank et al., 2014). In MC this generally involves, besides the release of soluble mediators, the extrusion of the granular proteoglycan core to which inflammatory compounds are bound via electrostatic interactions (Lawson et al., 1975; Nitta et al., 2009). The change in pH (from acidic to neutral) allows their diffusion into the surrounding environment (Wernersson and Pejler, 2014). MC perform multigranular or compound exocytosis characterized, respectively, by the extrusion of the content of multiple intracellularly fused SG or sequential fusion of SG from the periphery into the interior (**Figure 2**; Röhlich et al., 1971; Alvarez, de Toledo and Fernandez, 1990). This enables MC to secrete up to 100% of granular content in one single stimulatory event. Under certain conditions of activation MC are also able to perform piecemeal degranulation (PMD) characterized by the gradual emptying of SG content without any evidences for fusion events (Dvorak et al., 1994; Crivellato et al., 2003). Early ultrastructural analysis indicated that this could be due to the budding of intravesicular tubular compartments moving toward the PM (Dvorak et al., 1980; Melo et al., 2005). However, another possibility could be that PMD is the result of transient fusion events also called "kiss-and-run fusion," which are readily observed in MC (Williams and Webb, 2000). New studies also indicate that MC can change their degranulation pattern from a unit mode to a multigranular/compound mode depending on the type of stimulus (e.g., MRGPRX2 versus FcεRI) and the involved signaling pathways (Gaudenzio et al., 2016; Espinosa and Valitutti, 2018). Furthermore, a detailed spatiotemporal analysis of the dynamics of MC degranulation following exposure to large antigens targeted by IgE/IgG revealed that MC are able to form a unique immunological synapse called antibody-dependent degranulatory synapse (ADDS), which may be relevant to increase the local concentration of inflammatory mediators for example to fight parasite pathogens inactivated by proteases (Joulia et al., 2015; Espinosa and Valitutti, 2018).

SNARE Proteins

MC degranulation relies on the evolutionary conserved membrane fusion machinery implicating Soluble N-ethyl-maleimide-sensitive factor Attachment protein Receptor (SNARE) proteins (Hong, 2005; Sudhof and Rothman, 2009; Jahn and Fasshauer, 2012). SNARE lie on opposing intracellular membranes and through their SNARE helical motif of about 60 aa can form a stable multimeric complex that catalyzes fusion (**Figure 2**). A typical SNARE complex at the PM includes a vesicular SNARE (v-SNARE) such as a vesicle associated membrane protein (VAMP) family member that pairs with two target SNARE (t-SNARE) such as synaptosome-associated protein (SNAP) of 23, 25, 29, 47 kDa (SNAP-23/25/29/47) and a Syntaxin (STX) family member (Hong, 2005; Sudhof and Rothman, 2009; Jahn and Fasshauer, 2012). SNAP-23 was the first functional t-SNARE described in MC exocytosis (**Figure 2** and **Table 1**). Introduction of Abs against SNAP-23 into permeabilized rat peritoneal MC (RPMC) blocked stimulus-secretion coupling (Guo et al., 1998). During stimulation SNAP-23 relocated into the interior of the cell forming degranulation channels, a feature compatible with the compound mode of exocytosis. The implication of SNAP-23 in compound exocytosis and its association with SG was found to depend on the endosomal GTPase Rab5 and SNAP-23 phosphorylation on Ser95 and Ser120 mediated by IκB kinase 2/β (IKKβ2) (Klein et al., 2017). Treatment with an inhibitor of IKKβ2 (BMS-345541) switched the degranulation pattern from a compound mode to a unit mode (Gaudenzio et al., 2016). The role of SNAP-23 as an essential SNARE protein was confirmed by others including in mature human MC (Vaidyanathan et al., 2001; Sander et al., 2008; Woska and Gillespie, 2011). SNAP-23 formed complexes with both t-SNARE (STX4, STX3) and v-SNARE (VAMP2, VAMP7, VAMP8) and complexes with VAMP7 and VAMP8 were enhanced after stimulation (**Figure 2**; Paumet et al., 2000; Sander et al., 2008; Tiwari et al., 2008). Concerning STX family members, siRNA-mediated KD or introduction of an inhibitory peptide of PM-localized STX4 inhibited IgE-mediated degranulation (Woska and Gillespie, 2011; Brochetta et al., 2014; Yang et al., 2018; **Table 1** and **Figure 2**). Like for SNAP-23, STX4 showed an enhanced formation of complexes with VAMP8 after stimulation (Tiwari et al., 2008). The implication of STX4 was recently put into question as MC obtained from STX4 conditional KO mice degranulated normally (Sanchez et al., 2019). However, it is not

yet clear whether other STX family members could compensate for the loss of STX4. Indeed, in the same study complete genetic deficiency of STX3 largely blunted degranulation (Sanchez et al., 2019) confirming in this case results from siRNA experiments or experiments with STX3 mutants that indicated an important role of STX3 (Brochetta et al., 2014; Tadokoro et al., 2016; Sanchez et al., 2019; **Table 1** and **Figure 2**). In contrast to STX4, STX3 is mainly located on SG but relocates to the PM upon stimulation, taking the opposite direction to SNAP-23 (**Figure 2**; Guo et al., 1998; Brochetta et al., 2014; Munoz et al., 2016). This suggests that STX3 could be a component of SNARE complexes both for the fusion between SG but also with the PM, which again is compatible with the compound mode of MC exocytosis. Another t-SNARE, STX11, a lipid anchored t-SNARE, has been proposed to be implicated in MC exocytosis based on its interaction with Munc18-2, a known regulator of MC degranulation (Gutierrez et al., 2018), and its ability to support fusion in other hematopoietic cells (CD8 T and NK cells, neutrophils) (Cote et al., 2009; D'Orlando et al., 2013; **Table 1**). However, studies with STX11-deficient BMMC did not reveal a MC degranulation defect (D'Orlando et al., 2013).

Concerning v-SNARE, several studies reported a role of VAMP8 (**Figure 2** and **Table 1**). Both native and transduced forms of VAMP8 colocalized with SG in the RBL MC line and primary mature MC (Paumet et al., 2000; Tiwari et al., 2008; Horiguchi et al., 2016). One study (Tiwari et al., 2008) showed that VAMP8-deficient BMMC released less histamine and β-hexosaminidase while cytokine/chemokine secretion was intact. Introduction of soluble recombinant VAMP8 'or siRNA-mediated KD in RBL MC also inhibited β-hexosaminidase (Lippert et al., 2007) or β-hexosaminidase and histamine release (Woska and Gillespie, 2011). A study performed in pancreatic acinar cells proposed that VAMP8 may serve only in SG fusion, however, in MC VAMP8 readily gets recruited to the PM in stimulated cells (Tiwari et al., 2008; Horiguchi et al., 2016; Malmersjo et al., 2016; Wilson et al., 2016). Another study reported that VAMP8 deficiency only affects β-hexosaminidase but not histamine release, suggesting that these mediators might be stored in different granule compartments (Puri and Roche, 2008). However, this was not observed by others and is incompatible with data that VAMP8 KO mice also exhibited reduced passive anaphylactic responses *in vivo*, which is dependent on histamine (Tiwari et al., 2008; Woska and Gillespie, 2011). Several other v-SNARE were also analyzed for their role in MC degranulation (**Table 1**). Introduction of blocking Abs to VAMP7 and its siRNA-mediated KD inhibited secretion, respectively, in primary human MC and RBL MC (Sander et al., 2008; Woska and Gillespie, 2011). VAMP7 translocated to the PM upon stimulation forming enhanced complexes with SNAP-23 and STX4 (Sander et al., 2008; Woska and Gillespie, 2011). Presently, however, no clear localization of VAMP7 to SG has been demonstrated in MC and initial studies, contrary to VAMP8, did not show a colocalization of VAMP7 with the SG compartment in RBL cells (Paumet et al., 2000). Concerning VAMP2 (also called synaptobrevin), initial studies showed that a VAMP2 fluorescent probe transfected into RBL MC readily translocated to the PM upon stimulation (Miesenbock et al., 1998). Some studies showed evidence for a role of VAMP2 in fusion using blocking agents introduced into permeabilized RBL cells (Yang et al., 2018) while others using primary human MC did not (Sander et al., 2008). Importantly, BMMC cultured from VAMP2-KO mice did not show a degranulation defect (Puri and Roche, 2008). Furthermore, localization studies with Abs to endogenous VAMP2 did not reveal colocalization with SG, albeit some interaction with SNAP-23 was detectable (Paumet et al., 2000; Tiwari et al., 2008). While this interaction did not increase after stimulation, it did so in VAMP8-deficient BMMC, opening up the possibility that VAMP2 may replace VAMP8 as a relevant v-SNARE under particular circumstances (Tiwari et al., 2008). Yet another study reported increased association even in the presence of VAMP8 (Suzuki and Verma, 2008). In VAMP8-deficient BMMC VAMP3 also formed enhanced complexes with SNAP-23. However, these complexes decreased upon stimulation, suggesting that VAMP3 may play a role in constitutive fusion mechanisms, which get downregulated during stimulation (Tiwari et al., 2009). In agreement, no evidence for an implication of VAMP3 in MC degranulation was found as VAMP3-deficient BMMC had no defect in SG release (Puri and Roche, 2008). Nonetheless, in macrophages, an important role of VAMP3 was reported in cytokine secretion with VAMP3-containing recycling endosomes serving as an intermediate sorting compartment once cytokines have exited the trans-Golgi (Manderson et al., 2007). However, in MC no effect of VAMP3 inhibition (using blocking Abs) was seen on chemokine secretion while several other SNAREs (STX3, SNAP-23, and for some chemokines VAMP8, STX4, and STX6) were shown to play a role (Frank et al., 2011).

Regulation of SNARE Complex Formation by Phosphorylation

Although SNARE complexes may support membrane fusion spontaneously (Weber et al., 1998), in living cells this process is highly regulated, implying multiple upstream signaling pathways and accessory proteins (Sudhof and Rothman, 2009). In MC, it has been known for many years that increases in intracellular Ca2+ levels, activation of Ca2+-dependent and independent PKC isoforms (PKCβ, PKCδ), and many other effectors represent essential early signaling intermediates of MC degranulation (Blank and Rivera, 2004; **Figures 1**, **2**). However, the connection to the late signaling events regulating the last steps of the exocytotic process is still incompletely worked out. Phosphorylation of cognate SNARE proteins could represent an important regulatory step. It was reported that murine SNAP-23 was phosphorylated on Ser95 and Ser120 in the cys-rich linker region between its two SNARE domains. Phosphorylated SNAP-23 was enriched in SNARE complexes present in stimulated cells, indicating that this modification directly supports fusion (Hepp et al., 2005; Suzuki and Verma, 2008). In particular, phosphorylation of SNAP-23 may be relevant for compound mode of exocytosis enabling, together with Rab5, its relocation to SG (Klein et al., 2017). Although it was initially reported that SNAP-23 phosphorylation involved PKC (Hepp et al., 2005), later studies reported that this was mediated by IKKβ2 (**Figure 2**;

Suzuki and Verma, 2008). Yet, this was not confirmed in another study, leaving open the possibility of phosphorylation through PKC (Peschke et al., 2014). Concerning STX family members, *in vitro* studies showed that STX4 (but not STX2 and 3) was phosphorylated in its N-terminal regulatory domain by a Rab3D associated kinase (Rak3D), preventing its interaction with SNAP-23 (**Figure 2**). Phospho-STX4 could be found in living cells. As Rak3D dissociated from Rab3D in a Ca2+-dependent manner, STX4 phosphorylation could be a negative regulator of fusion in resting MC (Pombo et al., 2001). Likewise, STX3 was found to be constantly phosphorylated on Thr14 in the N-terminal peptide domain (**Table 1**). Mutating this residue enhanced degranulation, indicating a negative regulatory role (Tadokoro et al., 2016). As STX3 phosphorylation inhibited binding to Munc18-2, the inhibitory effect was attributed to its diminished ability to interact with an essential SNARE accessory protein Munc18-2. Concerning v-SNARE family members, it was found that non-neuronal v-SNAREs (e.g., VAMP4, 5, 7, and 8) contain between one to four phosphorylation sites for PKCβ, with VAMP8 containing four (Thr47/53; Ser54/61) located at the interface for SNARE zippering. Phosphomimetic mutants of each individual residue prevented fusion both in *in vitro* liposome fusion assays and in living cells albeit vesicle docking was maintained suggesting that it is the SNARE complex formation that is blocked (Malmersjo et al., 2016).

Calcium Sensors in MC Fusion

Concerning the role of Ca2+ in MC secretion, several molecular targets of the membrane fusion process have been identified. These include a synaptotagmin (Syt) family member. Syts are transmembrane anchored proteins containing tandem C2 domains (C2A and C2B), which display Ca2+-dependent phospholipid binding (Pinheiro et al., 2016; Brunger et al., 2019). Although initially reported to be a negative regulator in RBL MC (Baram et al., 2002), newer studies using MC from KO animals clearly attributed a positive role of the perigranular localized calcium sensor Syt2 in MC exocytosis (Melicoff et al., 2009; **Table 1** and **Figure 2**). Absence of Syt2 inhibited both histamine and β-hexosaminidase release by close to 70% in BMMC exposed to IgE/Ag. Syt2-KO animals also exhibited a reduced passive cutaneous anaphylaxis responses (PCA) (Melicoff et al., 2009). Likewise, *in vitro* liposome fusion of a MC-relevant SNARE complex (SNAP-23/STX3/VAMP8) was clearly enhanced by the addition of Syt2 and Ca2+ (Nagai et al., 2011). However, little is known about the mechanism of action of Syt2 in MC. Syt action has been mostly worked out for the asynchronous release at the synapse in neuronal cells. In these cells, according to a new "*release of inhibition* model" based on 3D structural data (Brunger et al., 2019), fusion is triggered very fast (within milliseconds) from a primed state where two neuronal Syt1 molecules interact with a preassembled SNARE prefusion complex that also contains complexin (CPLX) (see below). Arrival of Ca2+ dislodges Syt, thereby unlocking the prefusion complex to allow SNARE zippering. This pulls the membranes together, likely assisted by the parallel induced phospholipid binding of Syt1 (and eventually other effectors such as CPLX, Munc13-4, Doc2α; see below) that favor docking and membrane curvature. Together, this fusion machinery may comprise an assembly of a multiprotein complex forming a buttressed ring that acts as a work station for SNAREpin assembly, clamping, and release (**Figure 2**; Rothman et al., 2017). As MC exocytosis usually takes minutes and not milliseconds, it is presently unclear whether such a priming mechanism also applies to MC exocytosis. Yet, based on the described positive role of Syt2 and CPLX (see below) it is possible that the prefusion complex just represents a short-lived intermediate state during exocytosis. It is also not clear how Syt2, which like Syt1 is a Ca2+ sensor of low affinity (Pinheiro et al., 2016), couples to Ca2+ in MC as the required Ca2+ concentration for secretion is an order of magnitude lower than in neurons (1 versus 20 μM; Blank and Rivera, 2004), although high local concentration at fusion sites may still be relevant.

In this scenario another effector, CPLX, is also relevant as it enables Syt binding to the ternary SNARE complex (Brunger et al., 2019). CPLX is a small (13 kDa) cytoplasmic protein, which exists in several isoforms, with CPLX1 being exclusively neuronal while CPLX2 being expressed in MC lines (RBL, PT18, expression in primary MC has not been investigated) (**Table 1**). CPLX is composed of short N- and C-terminal sequences that in neurons support, respectively, fast Ca2+-triggered release and membrane lipid binding. It also contains two central α-helices the N-terminal one may regulate neuronal spontaneous exocytosis while the central domain is the one interacting with the preassembled (non-zippered) trans-SNARE complex and Syt (Maximov et al., 2009; Sudhof and Rothman, 2009; Brunger et al., 2019). In RBL MC siRNA-mediated KD of CPLX2 indicated a positive regulatory role in exocytosis. It also translocated from a punctuate cytoplasmic (probably granular) staining pattern to a PM location (Tadokoro et al., 2005). In pulldown experiments CPLX2 preferentially interacted with a complex containing STX3/SNAP-23/VAMP2/8 present in RBL cell lysates, while no STX4 containing complex was detectable (Tadokoro et al., 2010). Together, these results could be in agreement with a role of CPLX2 supporting Syt2 binding and Ca2+ sensitivity of the fusion machinery (**Figure 2**).

Another important Ca2+ sensor in MC is mammalian uncoordinated 13-4 (Munc13-4) protein, a member of the invertebrate/mammalian Unc13/Munc13s family of proteins involved in vesicle docking and priming (Palfreyman and Jorgensen, 2017; Brunger et al., 2019; **Table 1** and **Figure 2**). Munc13 proteins are large multi-domain proteins. While Munc13-4 shares the two characteristic Munc Homology Domains (MHD) as well as C2A and C2B domains with the neuronal isoforms Munc13-1, 2, and 3, it does not contain the calmodulin and DAG binding sites of other members of this family (Pinheiro et al., 2016; Bin et al., 2018). In neuronal cells the MHD domains are important for the priming function as they allowed the transition of the closed Munc18-1-bound conformation of STX1 to the open conformation involving N-terminal peptide binding, which can engage in SNARE complex formation (Brunger et al., 2019). Munc13-4 was initially described as the mutated effector responsible for familial hemophagocytic lymphohistiocytosis type 3 (FHL3), where patients fail to exocytose docked cytotoxic granules in cytotoxic T cells (Feldmann et al., 2003). Studies in MC using

Munc13-4 (or Unc13d or jinx) KO animals showed a severe degranulation defect (Singh et al., 2013; Rodarte et al., 2018). Further functional assessment indicated that in MC, like in T cells, Munc13-4 interacts with SG-localized Rab27a (Neeft et al., 2005; Singh et al., 2013) contributing together with the, respectively, SNARE and phospholipid binding C2A and C2B domains (both of which get activated by Ca2+) (Boswell et al., 2012; Woo et al., 2017; Bin et al., 2018) to the bridging of opposing membranes. This may also support membrane curvature, which in MC may occur both between SG membranes and between SG membrane and the PM (**Figure 2**; Elstak et al., 2011; Woo et al., 2017). Bridging may further imply a Rab27 binding Slp (PCR data show expression of Slp2 and Slp3 in BMMC; Munoz et al., 2016) molecule as demonstrated in neutrophils and T cells, although this has yet to be shown for MC (Ramadass and Catz, 2016). The corralling of SG beneath the PM, and hence fusion, is lost in cells expressing point mutants of Munc13-4 that do not bind Rab27 (Elstak et al., 2011). As deduced from single molecule FRET studies in liposome fusion assays with neuronal SNAREs, another important function of Munc13-4, executed together with Munc18 proteins, is to control the correct assembly of parallel alpha-helices of the SNARE complex (Lai et al., 2017; Brunger et al., 2019).

Another calcium sensor Doc2α may further participate in this docking and priming process (**Table 1**). Doc2 are small cytoplasmic proteins, which contain the brain specific isoform DOC2α, and the ubiquitous isoforms Doc2β and Doc2γ (Orita et al., 1997). Doc2 proteins possess an N-terminal Munc13-interacting (Mid) domain and tandem C2A and C2B domains with the C2A domain exhibiting phospholipid binding in a Ca2+-dependent manner (Orita et al., 1996). Strikingly, it was found that MC express the brain specific DOC2α isoform and that MC degranulation was reduced in BMMC from Doc2α-KO mice (Higashio et al., 2008). In RBL MC, Doc2α colocalized with Munc13-4 on SG and interacted with Munc13-4 through its N-terminal Munc13-interacting domain and the C-terminal C2B domain (Higashio et al., 2008). Hence, it was proposed that Doc2α represents an additional Ca2+ sensor assisting to anchor Munc13-4 at the PM to fulfill its priming function (**Figure 2**; Elstak et al., 2011).

SM Family Proteins

Sec1/Munc18 (SM) family proteins are crucial effectors in membrane trafficking and exocytosis. Three family members, neuronal Munc18-1, as well as ubiquitously expressed Munc18-2 and Munc18-3, play a role in regulated exocytosis. The predominant isoforms expressed in MC are Munc18-2 and Munc18-3 (**Table 1**). Munc18 proteins bind to STX t-SNAREs (hence they are also called STXBP1, 2, and 3) with a certain degree of specificity: Munc18-1 preferentially binding to STX1, 2, and 3 (Hata and Südhof, 1995), Munc18-2 to STX1 and 3 (Hata and Südhof, 1995; Martin-Verdeaux et al., 2003), Munc18-3 to STX2 and 4 (Tellam et al., 1995; Martin-Verdeaux et al., 2003). Crystal structure analysis showed that Munc18-1 binds to its STX1 partner in a closed conformation unable to undergo fusion. However, this may not be the case for Munc18-2, which like shown in the structure analysis of Munc18-3 could prefer binding to its STX partner in an open conformation driven by N-peptide binding (Hu et al., 2007; Christie et al., 2012). Independent of these structural considerations, Munc18 proteins are crucial effectors of the fusion process. In animals deficient for Munc18-1 neuronal synaptic transmission was completely abolished (Verhage et al., 2000). Likewise, in MC absence of the STX3-binding, Munc18-2 strongly inhibited homo- and heterotypic fusion both in BMMC and in *ex vivo* derived RPMC (Gutierrez et al., 2018) confirming earlier results obtained in RBL cells or BMMC using KD experiments (Tadokoro et al., 2007; Bin et al., 2013; Brochetta et al., 2014). This concurs also with results indicating that STX3 is a major t-SNARE in MC exocytosis. Munc18-2 KD also affects secretion in other hematopoietic cells, being responsible for the secretory defect in FLH5 patients carrying different mutations (Cote et al., 2009; Cardenas et al., 2019). By contrast, no roles for Munc18-1 and Munc18-3 could be delineated in MC, although Munc18-3 seemed to play a role in neutrophil exocytosis (Martin-Verdeaux et al., 2003; Brochetta et al., 2008; Gutierrez et al., 2018). It is likely that mechanistically Munc18-2 plays a similar role than the neuronal isoform Munc18-1 in membrane fusion as already described above (Brunger et al., 2019). However it is possible that Munc18-2 may already in unstimulated cells bind in an open fusion-competent conformation to a single STX3 molecule as reported for Munc18-3 and STX4 (Hu et al., 2007; Christie et al., 2012) prior to the stimulation-induced binding to the assembled SNARE complex (**Figure 2**). Both Munc18-2 and Munc13-4 act then together as assembly factors in a coordinated fashion to enable proper structural alignment of a primed and Syt bound ternary SNARE complex (**Figure 2**; Brunger et al., 2019). Contrary to neurons, where vesicles need to be ready to fuse within milliseconds, the primed complex in MC may represent a short-lived intermediate state.

Biochemical studies in MC showed a differential STX3 and Munc18-2 distribution into rafts (Pombo et al., 2003). Likewise, functional data supported additional effects on exocytosis (Brochetta et al., 2014), suggesting that Munc18-2, besides assembling the fusion complex, might have supplementary functions. These could relate to a functional SG docking. In chromaffin cells a docking defect of SG at the PM was observed in the absence of neuronal Munc18-1, a property that may depend on its ability to interact with Rab3a (Voets et al., 2001; van Weering et al., 2007). Likewise, a Munc18-1-dependent docking for SG in insulin secreting cells with stable docking being promoted by formation of clusters of STX1/Munc18-1 at the nascent granule docking site being further supported by Rab3a known to be expressed on SG and able to interact with Munc18 (Gandasi and Barg, 2014). Indeed, interactions of Rab3 proteins with Munc18 isoforms have been proposed before to be relevant for the fusion process, but this awaits further studies in MC (Graham et al., 2008; Gandasi and Barg, 2014). Based on this it seems possible that besides its role in fusion, Munc18-2, like Munc18-1, may also dynamically regulate docking, which, in the case of Munc18-2, may also involve docking at the microtubule cytoskeleton. Munc18 proteins are also known to represent a downstream target of kinases. Thus, tyrosine phosphorylation by neuronal Src family kinases (SFK) of Munc18-1 at Y473

(a site conserved in Munc18-2) prevents its ability to promote fusion and was proposed as a powerful mechanism to block synaptic transmission (Meijer et al., 2018). Likewise, PKC- and CDK5-dependent phosphorylation favored, respectively, vesicle pool replenishment in neurons and enhanced insulin secretion in pancreatic β cells (Lilja et al., 2004; Nili et al., 2006). However, a regulatory role of phosphorylation of Munc18-2 has not yet been reported in MC.

SCAMP

Another family of fusion accessory proteins are secretory carrier membrane proteins (SCAMP). These are tetraspanins with major isoforms expressed in MC being SCAMP1 and SCAMP2 (**Table 1**). Both SCAMP 1 and 2 in MC localize to SG, but a small fraction is also found at the PM where they co-localize with STX4 and SNAP-23 (**Figure 2**). Both isoforms can also be co-immunoprecipitated with SNAP-23. Expression of a peptide (E-peptide), within the second and third transmembrane (TM) domain, potently inhibits exocytosis in permeabilized RPMC (Guo et al., 2002) with the peptide derived from SCAMP2 being an order of magnitude more potent than SCAMP1, suggesting that this isoform represents the major regulator of the fusion process (**Table 1**). SCAMP2 may act at a late step that couples Arf6-stimulated phospholipase D (PLD) activity to the formation of fusion pores. PLD catalyzes the hydrolysis of phosphatidylcholine to generate the lipid second messenger, phosphatidate (PA), important in the regulation of the membrane phospholipid PIP2 that is important at fusion sites. This could be in agreement with the proposed implication of PLD isozymes (granular localized PLD1 and PM localized PLD2) as regulators of MC exocytosis (**Figure 2**; Cockcroft et al., 2002).

Tomosyn-1 (STXBP5)

Tomosyn is encoded by two related genes, tomosyn-1 (STXBP5) and tomosyn-2 (STXBP5L). MC express high amounts of tomosyn-1 mRNA encoding a large (∼130 kDa) protein with a C-terminal v-SNARE domain and 14 N-terminal tryptophan-aspartic acid (WD) 40 repeats forming propeller-like structures as protein interaction platforms (Hattendorf et al., 2007; **Table 1**). Both domains are reported to participate in inhibiting vesicle membrane fusion (Pobbati et al., 2004; Bielopolski et al., 2014) either by preventing access to the cognate v-SNARE or by promoting fusion-incompetent ternary SNARE complex oligomerization. Studies in different cells showed that tomosyn binds STX and inhibits secretory events including in non-neuronal cells where it restricts insulin secretion (Zhang et al., 2006) and endothelial cell exocytosis (Zhu et al., 2014). However, positive regulatory actions have been also reported in pancreatic β cells, platelets, and in yeast expressing the homologue Sro7, the latter of which, however, lacks the C-terminal v-SNARE domain (Cheviet et al., 2006; Hattendorf et al., 2007; Ye et al., 2014). A positive regulatory role was also attributed to a C-terminal tail region preceding the tomosyn v-SNARE domain that upon interaction with its STX partner may then serve as a facilitator for cognate v-SNARE interaction (Yamamoto et al., 2010). This may suggest that tomosyn has more complex roles. Studies in MC showed that tomosyn-1/STXBP5 acts as a fusion clamp as specific KD enhances degranulation (Madera-Salcedo et al., 2018). Further analysis revealed that it binds to STX4 in resting cells but dissociates after stimulation, which could explain the fusion clamp mechanism (**Figure 2**). Dissociation was mediated by stimulation-induced Ser and Thr phosphorylation, implicating the Ca2+-independent PKCδ isoform as KD of the latter prevented dissociation. Increased phosphorylation was notably observed in the regulatory second loop region and tail region preceding the v-SNARE domain (Yamamoto et al., 2009; Madera-Salcedo et al., 2018). Strikingly, the situation was different for STX3 as stimulation rather induced its phosphorylation-dependent association with tomosyn-1/STXBP5. Although the functional significance of the increased association with STX3 remains unclear, it was proposed that this STX binding switch may act as a feedback mechanism at the membrane once STX3 gets translocated to gradually block membrane fusion to limit eventually life-threatening anaphylactic reaction due to excessive MC activation (Madera-Salcedo et al., 2018).

Rab Proteins

Among the sixty Rab expressed in mammals, several of them have been already mentioned above as they regulate important trafficking steps, coupling granule trafficking to the microtubule and actin cytoskeleton (**Figure 1**). We will only discuss briefly the implication of those that may directly be implicated in the membrane fusion process. One candidate is Rab3D found to be the most prevalent Rab3 isoform expressed in MC (Roa et al., 1997; Tuvim et al., 1999; **Table 1** and **Figure 2**). It partially localized to SG in RBL MC, but fully in PMC and transiently translocated to the PM upon exocytosis. Overexpression of a constitutively active mutant blocked secretion (Roa et al., 1997; Tuvim et al., 1999). A MC effect was not confirmed in Rab3D-KO mice, although these mice exhibited increases in the size of SG in both the exocrine pancreas and the parotid gland but not in MC, which suggested a role in SG maturation (Riedel et al., 2002). However, potential compensatory mechanisms by other isoforms (Rab3A, Rab3B, and Rab3C) have not been investigated in this study (Riedel et al., 2002). Rab37 was also found highly expressed in BMMC and able to interact in a GTP-independent manner with Munc13-4 in a trimeric complex containing Rab27 and Munc13-4 (Masuda et al., 2000; Higashio et al., 2016; **Table 1** and **Figure 2**). This trimeric complex formation (Rab37-Munc13-4-Rab27) negatively regulates MC degranulation through a probable inhibition of the SG docking/priming step with the PM (Higashio et al., 2016). Rab5 may also play an important role in the fusion process favoring compound/multigranular exocytosis (**Table 1**). Indeed, based on studies with constitutively active mutant forms and KD experiments, Rab5 was attributed a key role in SG maturation mediating SG fusion during biogenesis controlling the amount and composition of the SG content (Azouz et al., 2014). Additional studies then showed that Rab5 also directly regulates SNAP-23-mediated SG-SG fusion during stimulation.

The above data clearly show that in living cells the fusion process is regulated, besides cognate SNARE proteins, by a

multitude of molecular effectors that can be connected to upstream signals such as Ca2+ influx and phosphorylation and which may vary from cell type to cell type. It becomes thus clear that this multitude of molecular actors further increases the complexity of the molecular interactions and regulatory steps to be worked out.

CONCLUDING REMARKS

MC signaling dowstream the FcεRI stimulation has been widely studied during the last 20 years. However, it is not entirely clear how the molecular processes governing the cytoskeleton reorganization and the SG translocation and fusion are connected to upstream signaling pathways upon MC activation. Decoding new effectors involved in their interplay will unveil new knowledge into MC biology. This field of research will also benefit from the advances that will be made in other cell types of immune or non-immune origin, which are capable of regulated secretion and share the same molecular machineries that regulate cargos translocation and fusion. In addition to FcεRI, MC express many other receptors (Toll-like receptors, complement receptors, neuropeptide and neurotransmitter receptors, lipid mediator receptors, etc.) able to respond to a highly diverse array of products (including neuropeptides, complement fragments, cationic compounds, environmental substances, and other inflammatory mediators) and trigger SG release (Redegeld et al., 2018). While these receptors contribute to the sentinel function of MC, they may also cause their inappropriate activation in an inflammatory setting, thereby participating to chronic activation, for example, during the allergic response. Hence, it will be important to further progress in the understanding of the crosstalk between signaling pathways and MC degranulation to delineate all involved effector mechanisms to design novel therapeutic approaches for controlling allergic reactions.

AUTHOR CONTRIBUTIONS

GM and UB contributed equally in writing and editing the manuscript. GM, CL, MB, and UB created the figures. All authors corrected the manuscript and approved the submitted version.

FUNDING

This work was supported by "le Fonds de Recherche en Santé respiratoire sous le haut patronage de la Fondation du Souffle" 2018 to GM, SFA 2014 and 2016 (promotion D.A. Moneret-Vautrin) to UB and GM, the Investissements d'Avenir program (Grant: ANR-10-IAHU-01), ANR-19-CE15-0016 IDEA and ANR-11-IDEX-0005-02 (Sorbonne Paris Cite, Laboratoire d'excellence INFLAMEX). CL received a doctoral fellowship from the Ministère de l'Education Nationale de la Recherche et de la Technologie and the FRM for the 4-year Ph.D. fellowship. MB received a doctoral Inflamex fellowship.

ACKNOWLEDGMENTS

We would like to thank Marc Benhamou for critical reading and constructive comments on our manuscript.

REFERENCES

Akhmanova, A., and Steinmetz, M. O. (2015). Control of microtubule organization and dynamics: two ends in the limelight. *Nat. Rev. Mol. Cell Biol.* 16, 711–726. doi: 10.1038/nrm4084

Ali, K., Bilancio, A., Thomas, M., Pearce, W., Gilfillan, A. M., Tkaczyk, C., et al. (2004). Essential role for the p110delta phosphoinositide 3-kinase in the allergic response. *Nature* 431, 1007–1011. doi: 10.1038/nature02991

Alvarez, de Toledo, G., and Fernandez, J. M. (1990). Compound versus multigranular exocytosis in peritoneal mast cells. *J. Gen. Physiol.* 95, 397–409. doi: 10.1085/jgp.95.3.397

Alvarez-Errico, D., Lessmann, E., and Rivera, J. (2009). Adapters in the organization of mast cell signaling. *Immunol. Rev.* 232, 195–217. doi: 10.1111/j.1600-065X.2009.00834.x

Ang, W. X., Church, A. M., Kulis, M., Choi, H. W., Burks, A. W., and Abraham, S. N. (2016). Mast cell desensitization inhibits calcium flux and aberrantly remodels actin. *J. Clin. Invest.* 126, 4103–4118. doi: 10.1172/JCI87492

Azouz, N. P., Matsui, T., Fukuda, M., and Sagi-Eisenberg, R. (2012). Decoding the regulation of mast cell exocytosis by networks of Rab GTPases. *J. Immunol.* 189, 2169–2180. doi: 10.4049/jimmunol.1200542

Azouz, N. P., Zur, N., Efergan, A., Ohbayashi, N., Fukuda, M., Amihai, D., et al. (2014). Rab5 is a novel regulator of mast cell secretory granules: impact on size, cargo, and exocytosis. *J. Immunol.* 192, 4043–4053. doi: 10.4049/jimmunol.1302196

Baram, D., Peng, Z., Medalia, O., Mekori, Y., and Sagi-Eisenberg, R. (2002). Synaptotagmin II negatively regulates MHC class II presentation by mast cells. *Mol. Immunol.* 38:1347. doi: 10.1016/S0161-5890(02)00086-X

Barker, S. A., Caldwell, K. K., Hall, A., Martinez, A. M., Pfeiffer, J. R., Oliver, J. M., et al. (1995). Wortmannin blocks lipid and protein kinase activities associated with PI 3-kinase and inhibits a subset of responses induced by Fc epsilon R1 cross-linking. *Mol. Biol. Cell* 6, 1145–1158. doi: 10.1091/mbc.6.9.1145

Beghdadi, W., Madjene, L. C., Benhamou, M., Charles, N., Gautier, G., Launay, P., et al. (2011). Mast cells as cellular sensors in inflammation and immunity. *Front. Immunol.* 2:37. doi: 10.3389/fimmu.2011.00037

Bielopolski, N., Lam, A. D., Bar-On, D., Sauer, M., Stuenkel, E. L., and Ashery, U. (2014). Differential interaction of tomosyn with syntaxin and SNAP25 depends on domains in the WD40 beta-propeller core and determines its inhibitory activity. *J. Biol. Chem.* 289, 17087–17099. doi: 10.1074/jbc.M113.515296

Bin, N. R., Jung, C. H., Piggott, C., and Sugita, S. (2013). Crucial role of the hydrophobic pocket region of Munc18 protein in mast cell degranulation. *Proc. Natl. Acad. Sci. U.S.A.* 110, 4610–4615. doi: 10.1073/pnas.1214887110

Bin, N. R., Ma, K., Tien, C. W., Wang, S., Zhu, D., Park, S., et al. (2018). C2 domains of Munc13-4 are crucial for Ca(2+)-dependent degranulation and cytotoxicity in NK cells. *J. Immunol.* 201, 700–713. doi: 10.4049/jimmunol.1800426

Blank, U., Madera-Salcedo, I. K., Danelli, L., Claver, J., Tiwari, N., Sanchez-Miranda, E., et al. (2014). Vesicular trafficking and signaling for cytokine and chemokine secretion in mast cells. *Front. Immunol.* 5:453. doi: 10.3389/fimmu.2014.00453

Blank, U., and Rivera, J. (2004). The ins and outs of IgE-dependent mast-cell exocytosis. *Trends Immunol.* 25, 266–273. doi: 10.1016/j.it.2004.03.005

Boswell, K. L., James, D. J., Esquibel, J. M., Bruinsma, S., Shirakawa, R., Horiuchi, H., et al. (2012). Munc13-4 reconstitutes calcium-dependent SNARE-mediated membrane fusion. *J. Cell Biol.* 197, 301–312. doi: 10.1083/jcb.201109132

Brochetta, C., Suzuki, R., Vita, F., Soranzo, M. R., Claver, J., Madjene, L. C., et al. (2014). Munc18-2 and syntaxin 3 control distinct essential steps in mast cell degranulation. *J. Immunol.* 192, 41–51. doi: 10.4049/jimmunol.1301277

Brochetta, C., Vita, F., Tiwari, N., Scandiuzzi, L., Soranzo, M. R., Guerin-Marchand, C., et al. (2008). Involvement of Munc18 isoforms in the regulation of granule exocytosis in neutrophils. *Biochim. Biophys. Acta* 1783, 1781–1791. doi: 10.1016/j.bbamcr.2008.05.023

Broderick, M. J., and Winder, S. J. (2005). Spectrin, alpha-actinin, and dystrophin. *Adv. Protein Chem.* 70, 203–246. doi: 10.1016/S0065-3233(05)70007-3

Brunger, A. T., Choi, U. B., Lai, Y., Leitz, J., White, K. I., and Zhou, Q. (2019). The pre-synaptic fusion machinery. *Curr. Opin. Struct. Biol.* 54, 179–188. doi: 10.1016/j.sbi.2019.03.007

Burbank, K. S., Groen, A. C., Perlman, Z. E., Fisher, D. S., and Mitchison, T. J. (2006). A new method reveals microtubule minus ends throughout the meiotic spindle. *J. Cell Biol.* 175, 369–375. doi: 10.1083/jcb.200511112

Cardenas, E. I., Gonzalez, R., Breaux, K., Da, Q., Gutierrez, B. A., Ramos, M. A., et al. (2019). Munc18-2, but not Munc18-1 or Munc18-3, regulates platelet exocytosis, hemostasis, and thrombosis. *J. Biol. Chem.* 294, 4784–4792. doi: 10.1074/jbc.RA118.006922

Cheek, T. R., and Burgoyne, R. D. (1986). Nicotine-evoked disassembly of cortical actin filaments in adrenal chromaffin cells. *FEBS Lett.* 207, 110–114. doi: 10.1016/0014-5793(86)80022-9

Cheviet, S., Bezzi, P., Ivarsson, R., Renstrom, E., Viertl, D., Kasas, S., et al. (2006). Tomosyn-1 is involved in a post-docking event required for pancreatic beta-cell exocytosis. *J. Cell Sci.* 119, 2912–2920. doi: 10.1242/jcs.03037

Christie, M. P., Whitten, A. E., King, G. J., Hu, S. H., Jarrott, R. J., Chen, K. E., et al. (2012). Low-resolution solution structures of Munc18:syntaxin protein complexes indicate an open binding mode driven by the Syntaxin N-peptide. *Proc. Natl. Acad. Sci. U.S.A.* 109, 9816–9821. doi: 10.1073/pnas.1116975109

Chua, J. J., Butkevich, E., Worseck, J. M., Kittelmann, M., Gronborg, M., Behrmann, E., et al. (2012). Phosphorylation-regulated axonal dependent transport of syntaxin 1 is mediated by a Kinesin-1 adapter. *Proc. Natl. Acad. Sci. U.S.A.* 109, 5862–5867. doi: 10.1073/pnas.1113819109

Cockcroft, S., Way, G., O'luanaigh, N., Pardo, R., Sarri, E., and Fensome, A. (2002). Signalling role for ARF and phospholipase D in mast cell exocytosis stimulated by crosslinking of the high affinity FcepsilonR1 receptor. *Mol. Immunol.* 38, 1277–1282. doi: 10.1016/S0161-5890(02)00075-5

Colin-York, H., Li, D., Korobchevskaya, K., Chang, V. T., Betzig, E., Eggeling, C., et al. (2019). Cytoskeletal actin patterns shape mast cell activation. *Commun. Biol.* 2:93. doi: 10.1038/s42003-019-0322-9

Cote, M., Menager, M. M., Burgess, A., Mahlaoui, N., Picard, C., Schaffner, C., et al. (2009). Munc18-2 deficiency causes familial hemophagocytic lymphohistiocytosis type 5 and impairs cytotoxic granule exocytosis in patient NK cells. *J. Clin. Invest.* 119, 3765–3773. doi: 10.1172/JCI40732

Crivellato, E., Nico, B., Mallardi, F., Beltrami, C. A., and Ribatti, D. (2003). Piecemeal degranulation as a general secretory mechanism? *Anat. Rec. A Discov. Mol. Cell. Evol. Biol.* 274, 778–784. doi: 10.1002/ar.a.10095

Cruse, G., Beaven, M. A., Ashmole, I., Bradding, P., Gilfillan, A. M., and Metcalfe, D. D. (2013). A truncated splice-variant of the FcepsilonRIbeta receptor subunit is critical for microtubule formation and degranulation in mast cells. *Immunity* 38, 906–917. doi: 10.1016/j.immuni.2013.04.007

D'Orlando, O., Zhao, F., Kasper, B., Orinska, Z., Muller, J., Hermans-Borgmeyer, I., et al. (2013). Syntaxin 11 is required for NK and CD8(+) T-cell cytotoxicity and neutrophil degranulation. *Eur. J. Immunol.* 43, 194–208. doi: 10.1002/eji.201142343

Deng, Z., Zink, T., Chen, H. Y., Walters, D., Liu, F. T., and Liu, G. Y. (2009). Impact of actin rearrangement and degranulation on the membrane structure of primary mast cells: a combined atomic force and laser scanning confocal microscopy investigation. *Biophys. J.* 96, 1629–1639. doi: 10.1016/j.bpj.2008.11.015

Desai, A., and Mitchison, T. J. (1997). Microtubule polymerization dynamics. *Annu. Rev. Cell. Dev. Biol.* 13, 83–117. doi: 10.1146/annurev.cellbio.13.1.83

dos Remedios, C. G., Chhabra, D., Kekic, M., Dedova, I. V., Tsubakihara, M., Berry, D. A., et al. (2003). Actin binding proteins: regulation of cytoskeletal microfilaments. *Physiol. Rev.* 83, 433–473. doi: 10.1152/physrev.00026.2002

Draber, P., Sulimenko, V., and Draberova, E. (2012). Cytoskeleton in mast cell signaling. *Front. Immunol.* 3:130. doi: 10.3389/fimmu.2012.00130

Dvorak, A. M., Hammond, M. E., Morgan, E., Orenstein, N. S., Galli, S. J., and Dvorak, H. F. (1980). Evidence for a vesicular transport mechanism in guinea pig basophilic leukocytes. *Lab. Invest.* 42, 263–276.

Dvorak, A. M., Tepper, R. I., Weller, P. F., Morgan, E. S., Estrella, P., Monahan-Earley, R. A., et al. (1994). Piecemeal degranulation of mast cells in the inflammatory eyelid lesions of interleukin-4 transgenic mice. Evidence of mast cell histamine release in vivo by diamine oxidase-gold enzyme-affinity ultrastructural cytochemistry. *Blood* 83, 3600–3612. doi: 10.1182/blood.V83.12.3600.3600

Efergan, A., Azouz, N. P., Klein, O., Noguchi, K., Rothenberg, M. E., Fukuda, M., et al. (2016). Rab12 regulates retrograde transport of mast cell secretory granules by interacting with the RILP-dynein complex. *J. Immunol.* 196, 1091–1101. doi: 10.4049/jimmunol.1500731

Elstak, E. D., Neeft, M., Nehme, N. T., Voortman, J., Cheung, M., Goodarzifard, M., et al. (2011). The munc13-4-rab27 complex is specifically required for tethering secretory lysosomes at the plasma membrane. *Blood* 118, 1570–1578. doi: 10.1182/blood-2011-02-339523

Espinosa, E., and Valitutti, S. (2018). New roles and controls of mast cells. *Curr. Opin. Immunol.* 50, 39–47. doi: 10.1016/j.coi.2017.10.012

Feldmann, J., Callebaut, I., Raposo, G., Certain, S., Bacq, D., Dumont, C., et al. (2003). Munc13-4 is essential for cytolytic granules fusion and is mutated in a form of familial hemophagocytic lymphohistiocytosis (FHL3). *Cell* 115, 461–473. doi: 10.1016/S0092-8674(03)00855-9

Foger, N., Jenckel, A., Orinska, Z., Lee, K. H., Chan, A. C., and Bulfone-Paus, S. (2011). Differential regulation of mast cell degranulation versus cytokine secretion by the actin regulatory proteins Coronin1a and Coronin1b. *J. Exp. Med.* 208, 1777–1787. doi: 10.1084/jem.20101757

Frank, S. P., Thon, K. P., Bischoff, S. C., and Lorentz, A. (2011). SNAP-23 and syntaxin-3 are required for chemokine release by mature human mast cells. *Mol. Immunol.* 49, 353–358. doi: 10.1016/j.molimm.2011.09.011

Frigeri, L., and Apgar, J. R. (1999). The role of actin microfilaments in the down-regulation of the degranulation response in RBL-2H3 mast cells. *J. Immunol.* 162, 2243–2250.

Fukuda, M. (2013). Rab27 effectors, pleiotropic regulators in secretory pathways. *Traffic* 14, 949–963. doi: 10.1111/tra.12083

Galli, S. J., Gaudenzio, N., and Tsai, M. (2020). Mast cells in inflammation and disease: recent progress and ongoing concerns. *Annu. Rev. Immunol.* 38, 49–77. doi: 10.1146/annurev-immunol-071719-094903

Gandasi, N. R., and Barg, S. (2014). Contact-induced clustering of syntaxin and munc18 docks secretory granules at the exocytosis site. *Nat. Commun.* 5:3914. doi: 10.1038/ncomms4914

Garcia-Ortiz, A., and Serrador, J. M. (2020). ERM proteins at the crossroad of leukocyte polarization, migration and intercellular adhesion. *Int. J. Mol. Sci.* 21:1502. doi: 10.3390/ijms21041502

Gaudenzio, N., Sibilano, R., Marichal, T., Starkl, P., Reber, L. L., Cenac, N., et al. (2016). Different activation signals induce distinct mast cell degranulation strategies. *J. Clin. Invest.* 126, 3981–3998. doi: 10.1172/JCI85538

Geron, E., Schejter, E. D., and Shilo, B. Z. (2013). Directing exocrine secretory vesicles to the apical membrane by actin cables generated by the formin mDia1. *Proc. Natl. Acad. Sci. U.S.A.* 110, 10652–10657. doi: 10.1073/pnas.1303796110

Graham, M. E., Handley, M. T., Barclay, J. W., Ciufo, L. F., Barrow, S. L., Morgan, A., et al. (2008). A gain-of-function mutant of Munc18-1 stimulates secretory granule recruitment and exocytosis and reveals a direct interaction of Munc18-1 with Rab3. *Biochem. J.* 409, 407–416. doi: 10.1042/BJ20071094

Grigoriev, I., Gouveia, S. M., Van Der Vaart, B., Demmers, J., Smyth, J. T., Honnappa, S., et al. (2008). STIM1 is a MT-plus-end-tracking protein involved in remodeling of the ER. *Curr. Biol.* 18, 177–182. doi: 10.1016/j.cub.2007.12.050

Gu, H., Saito, K., Klaman, L. D., Shen, J., Fleming, T., Wang, Y., et al. (2001). Essential role for Gab2 in the allergic response. *Nature* 412, 186–190. doi: 10.1038/35084076

Guillemot, J., Montcourrier, P., Vivier, E., Davoust, J., and Chavrier, P. (1997). Selective control of membrane ruffling and actin plaque assembly by the Rho GTPases Rac1 and CDC42 in FceRI-activated rat basophilic leukemia (RBL-2H3) cells. *J. Cell Sci.* 110, 2215–2225.

Guo, Z., Liu, L., Cafiso, D., and Castle, D. (2002). Perturbation of a very late step of regulated exocytosis by a secretory carrier membrane protein (SCAMP2)-derived peptide. *J. Biol. Chem.* 277, 35357–35363. doi: 10.1074/jbc.M202259200

Guo, Z., Turner, C., and Castle, D. (1998). Relocation of the t-SNARE SNAP-23 from lamellipodia-like cell surface projections regulates compound exocytosis in mast cells. *Cell* 94, 537–548. doi: 10.1016/S0092-8674(00)81594-9

Gutierrez, B. A., Chavez, M. A., Rodarte, A. I., Ramos, M. A., Dominguez, A., Petrova, Y., et al. (2018). Munc18-2, but not Munc18-1 or Munc18-3, controls compound and single-vesicle-regulated exocytosis in mast cells. *J. Biol. Chem.* 293, 7148–7159. doi: 10.1074/jbc.RA118.002455

Hajkova, Z., Bugajev, V., Draberova, E., Vinopal, S., Draberova, L., Janacek, J., et al. (2011). STIM1-directed reorganization of microtubules in activated mast cells. *J. Immunol.* 186, 913–923. doi: 10.4049/jimmunol.1002074

Hall, A. (1998). Rho GTPases and the actin cytoskeleton. *Science* 279, 509–514. doi: 10.1126/science.279.5350.509

Hata, Y., and Südhof, T. (1995). A novel ubiquitous form of Munc-18 interacts with multiple syntaxins. *J. Biol. Chem.* 270, 13022–13028. doi: 10.1074/jbc.270.22.13022

Hattendorf, D. A., Andreeva, A., Gangar, A., Brennwald, P. J., and Weis, W. I. (2007). Structure of the yeast polarity protein Sro7 reveals a SNARE regulatory mechanism. *Nature* 446, 567–571. doi: 10.1038/nature05635

Heasman, S. J., and Ridley, A. J. (2008). Mammalian Rho GTPases: new insights into their functions from in vivo studies. *Nat. Rev. Mol. Cell Biol.* 9, 690–701. doi: 10.1038/nrm2476

Hepp, R., Puri, N., Hohenstein, A. C., Crawford, G. L., Whiteheart, S. W., and Roche, P. A. (2005). Phosphorylation of SNAP-23 regulates exocytosis from mast cells. *J. Biol. Chem.* 280, 6610–6620. doi: 10.1074/jbc.M412126200

Higashio, H., Nishimura, N., Ishizaki, H., Miyoshi, J., Orita, S., Sakane, A., et al. (2008). Doc2 alpha and Munc13-4 regulate Ca(2+) -dependent secretory lysosome exocytosis in mast cells. *J. Immunol.* 180, 4774–4784. doi: 10.4049/jimmunol.180.7.4774

Higashio, H., Satoh, Y., and Saino, T. (2016). Mast cell degranulation is negatively regulated by the Munc13-4-binding small-guanosine triphosphatase Rab37. *Sci. Rep.* 6:22539. doi: 10.1038/srep22539

Holowka, D., Calloway, N., Cohen, R., Gadi, D., Lee, J., Smith, N. L., et al. (2012). Roles for ca(2+) mobilization and its regulation in mast cell functions. *Front. Immunol.* 3:104. doi: 10.3389/fimmu.2012.00104

Holowka, D., Sheets, E. D., and Baird, B. (2000). Interactions between Fc(epsilon)RI and lipid raft components are regulated by the actin cytoskeleton. *J. Cell Sci.* 113(Pt 6), 1009–1019.

Hong, W. (2005). SNAREs and traffic. *Biochim. Biophys. Acta* 1744, 120–144. doi: 10.1016/j.bbamcr.2005.03.014

Horiguchi, K., Yoshikawa, S., Saito, A., Haddad, S., Ohta, T., Miyake, K., et al. (2016). Real-time imaging of mast cell degranulation in vitro and in vivo. *Biochem. Biophys. Res. Commun.* 479, 517–522. doi: 10.1016/j.bbrc.2016.09.100

Hu, S. H., Latham, C. F., Gee, C. L., James, D. E., and Martin, J. L. (2007). Structure of the Munc18c/Syntaxin4 N-peptide complex defines universal features of the N-peptide binding mode of Sec1/Munc18 proteins. *Proc. Natl. Acad. Sci. U.S.A.* 104, 8773–8778. doi: 10.1073/pnas.0701124104

Jahn, R., and Fasshauer, D. (2012). Molecular machines governing exocytosis of synaptic vesicles. *Nature* 490, 201–207. doi: 10.1038/nature11320

Johnson, J. L., Monfregola, J., Napolitano, G., Kiosses, W. B., and Catz, S. D. (2012). Vesicular trafficking through cortical actin during exocytosis is regulated by the Rab27a effector JFC1/Slp1 and the RhoA-GTPase-activating protein Gem-interacting protein. *Mol. Biol. Cell* 23, 1902–1916. doi: 10.1091/mbc.e11-12-1001

Joulia, R., Gaudenzio, N., Rodrigues, M., Lopez, J., Blanchard, N., Valitutti, S., et al. (2015). Mast cells form antibody-dependent degranulatory synapse for dedicated secretion and defence. *Nat. Commun.* 6:6174. doi: 10.1038/ncomms7174

Kadowaki, T., Yamaguchi, Y., Kido, M. A., Abe, T., Ogawa, K., Tokuhisa, M., et al. (2020). The large GTPase Rab44 regulates granule exocytosis in mast cells and IgE-mediated anaphylaxis. *Cell. Mol. Immunol.* 17, 1287–1289. doi: 10.1038/s41423-020-0413-z

Kettner, A., Kumar, L., Anton, I. M., Sasahara, Y., De La Fuente, M., Pivniouk, V. I., et al. (2004). WIP regulates signaling via the high affinity receptor for immunoglobulin E in mast cells. *J. Exp. Med.* 199, 357–368. doi: 10.1084/jem.20030652

Klebanovych, A., Sladkova, V., Sulimenko, T., Vosecka, V., Capek, M., Draberova, E., et al. (2019). Regulation of microtubule nucleation in mouse bone marrow-derived mast cells by protein tyrosine phosphatase SHP-1. *Cells* 8:345. doi: 10.3390/cells8040345

Klein, O., Krier-Burris, R. A., Lazki-Hagenbach, P., Gorzalczany, Y., Mei, Y., Ji, P., et al. (2019). Mammalian diaphanous-related formin 1 (mDia1) coordinates mast cell migration and secretion through its actin-nucleating activity. *J. Allergy Clin. Immunol.* 144, 1074–1090. doi: 10.1016/j.jaci.2019.06.028

Klein, O., Roded, A., Zur, N., Azouz, N. P., Pasternak, O., Hirschberg, K., et al. (2017). Rab5 is critical for SNAP23 regulated granule-granule fusion during compound exocytosis. *Sci. Rep.* 7:15315. doi: 10.1038/s41598-017-15047-8

Koffer, A., Tatham, P. E., and Gomperts, B. D. (1990). Changes in the state of actin during the exocytotic reaction of permeabilized rat mast cells. *J. Cell Biol.* 111, 919–927. doi: 10.1083/jcb.111.3.919

Lai, Y., Choi, U. B., Leitz, J., Rhee, H. J., Lee, C., Altas, B., et al. (2017). Molecular mechanisms of synaptic vesicle priming by Munc13 and Munc18. *Neuron* 95, 591.e10–607.e10. doi: 10.1016/j.neuron.2017.07.004

Law, M., Lee, Y., Morales, J. L., Ning, G., Huang, W., Pabon, J., et al. (2015). Cutting edge: drebrin-regulated actin dynamics regulate IgE-dependent mast cell activation and allergic responses. *J. Immunol.* 195, 426–430. doi: 10.4049/jimmunol.1401442

Lawson, D., Fewtrell, C., Gomperts, B., and Raff, M. (1975). Anti-immunoglobulin-induced histamine secretion by rat peritoneal mast cells studied by immunoferritin electron microscopy. *J. Exp. Med.* 142, 391–402. doi: 10.1084/jem.142.2.391

Liem, R. K. (2016). Cytoskeletal integrators: the spectrin superfamily. *Cold Spring Harb. Perspect. Biol.* 8:a018259. doi: 10.1101/cshperspect.a018259

Lilja, L., Johansson, J. U., Gromada, J., Mandic, S. A., Fried, G., Berggren, P. O., et al. (2004). Cyclin-dependent kinase 5 associated with p39 promotes Munc18-1 phosphorylation and Ca(2+)-dependent exocytosis. *J. Biol. Chem.* 279, 29534–29541. doi: 10.1074/jbc.M312711200

Lippert, U., Ferrari, D. M., and Jahn, R. (2007). Endobrevin/VAMP8 mediates exocytotic release of hexosaminidase from rat basophilic leukaemia cells. *FEBS Lett.* 581, 3479–3484. doi: 10.1016/j.febslet.2007.06.057

Liu, Y., Zhu, M., Nishida, K., Hirano, T., and Zhang, W. (2007). An essential role for RasGRP1 in mast cell function and IgE-mediated allergic response. *J. Exp. Med.* 204, 93–103. doi: 10.1084/jem.20061598

Lorentz, A., Baumann, A., Vitte, J., and Blank, U. (2012). The SNARE machinery in mast cell secretion. *Front. Immunol.* 3:143. doi: 10.3389/fimmu.2012.00143

Ma, H. T., and Beaven, M. A. (2009). Regulation of Ca2+ signaling with particular focus on mast cells. *Crit. Rev. Immunol.* 29, 155–186. doi: 10.1615/CritRevImmunol.v29.i2.40

Machnicka, B., Czogalla, A., Hryniewicz-Jankowska, A., Boguslawska, D. M., Grochowalska, R., Heger, E., et al. (2014). Spectrins: a structural platform for stabilization and activation of membrane channels, receptors and transporters. *Biochim. Biophys. Acta* 1838, 620–634. doi: 10.1016/j.bbamem.2013.05.002

Machnicka, B., Grochowalska, R., Boguslawska, D. M., and Sikorski, A. F. (2019). The role of spectrin in cell adhesion and cell-cell contact. *Exp. Biol. Med.* 244, 1303–1312. doi: 10.1177/1535370219859003

Macurek, L., Draberova, E., Richterova, V., Sulimenko, V., Sulimenko, T., Draberova, L., et al. (2008). Regulation of microtubule nucleation from membranes by complexes of membrane-bound gamma-tubulin with Fyn kinase and phosphoinositide 3-kinase. *Biochem. J.* 416, 421–430. doi: 10.1042/BJ20080909

Madera-Salcedo, I. K., Danelli, L., Tiwari, N., Dema, B., Pacreau, E., Vibhushan, S., et al. (2018). Tomosyn functions as a PKCdelta-regulated fusion clamp in mast cell degranulation. *Sci. Signal.* 11:eaan4350. doi: 10.1126/scisignal.aan4350

Malmersjo, S., Di Palma, S., Diao, J., Lai, Y., Pfuetzner, R. A., Wang, A. L., et al. (2016). Phosphorylation of residues inside the SNARE complex suppresses secretory vesicle fusion. *EMBO J.* 35, 1810–1821. doi: 10.15252/embj.201694071

Manderson, A. P., Kay, J. G., Hammond, L. A., Brown, D. L., and Stow, J. L. (2007). Subcompartments of the macrophage recycling endosome direct the differential secretion of IL-6 and TNFalpha. *J. Cell Biol.* 178, 57–69. doi: 10.1083/jcb.200612131

Martin-Verdeaux, S., Pombo, I., Iannascoli, B., Roa, M., Varin-Blank, N., Rivera, J., et al. (2003). Analysis of Munc18-2 compartmentation in mast cells reveals a role for microtubules in granule exocytosis. *J. Cell. Sci.* 116, 325–334. doi: 10.1242/jcs.00216

Masuda, E. S., Luo, Y., Young, C., Shen, M., Rossi, A. B., Huang, B. C., et al. (2000). Rab37 is a novel mast cell specific GTPase localized to secretory granules. *FEBS Lett.* 470, 61–64. doi: 10.1016/S0014-5793(00)01288-6

Mattila, P. K., Batista, F. D., and Treanor, B. (2016). Dynamics of the actin cytoskeleton mediates receptor cross talk: an emerging concept in tuning receptor signaling. *J. Cell Biol.* 212, 267–280. doi: 10.1083/jcb.201504137

Maximov, A., Tang, J., Yang, X., Pang, Z. P., and Sudhof, T. C. (2009). Complexin controls the force transfer from SNARE complexes to membranes in fusion. *Science* 323, 516–521. doi: 10.1126/science.1166505

Meijer, M., Dorr, B., Lammertse, H. C., Blithikioti, C., Van Weering, J. R., Toonen, R. F., et al. (2018). Tyrosine phosphorylation of Munc18-1 inhibits synaptic transmission by preventing SNARE assembly. *EMBO J.* 37, 300–320. doi: 10.15252/embj.201796484

Melicoff, E., Sansores-Garcia, L., Gomez, A., Moreira, D. C., Datta, P., Thakur, P., et al. (2009). Synaptotagmin-2 controls regulated exocytosis but not other secretory responses of mast cells. *J. Biol. Chem.* 284, 19445–19451. doi: 10.1074/jbc.M109.002550

Melo, R. C., Perez, S. A., Spencer, L. A., Dvorak, A. M., and Weller, P. F. (2005). Intragranular vesiculotubular compartments are involved in piecemeal degranulation by activated human eosinophils. *Traffic* 6, 866–879. doi: 10.1111/j.1600-0854.2005.00322.x

Metcalfe, D. D., Peavy, R. D., and Gilfillan, A. M. (2009). Mechanisms of mast cell signaling in anaphylaxis. *J. Allergy Clin. Immunol.* 124, 639–646; quiz 647–638. doi: 10.1016/j.jaci.2009.08.035

Miesenbock, G., De Angelis, D. A., and Rothman, J. E. (1998). Visualizing secretion and synaptic transmission with pH-sensitive green fluorescent proteins. *Nature* 394, 192–195. doi: 10.1038/28190

Mizuno, H., Tanaka, K., Yamashiro, S., Narita, A., and Watanabe, N. (2018). Helical rotation of the diaphanous-related formin mDia1 generates actin filaments resistant to cofilin. *Proc. Natl. Acad. Sci. U.S.A.* 115, E5000–E5007. doi: 10.1073/pnas.1803415115

Mizuno, K., Tolmachova, T., Ushakov, D. S., Romao, M., Abrink, M., Ferenczi, M. A., et al. (2007). Rab27b regulates mast cell granule dynamics and secretion. *Traffic* 8, 883–892. doi: 10.1111/j.1600-0854.2007.00571.x

Moller, L. L. V., Klip, A., and Sylow, L. (2019). Rho GTPases-emerging regulators of glucose homeostasis and metabolic health. *Cells* 8:434. doi: 10.3390/cells8050434

Munoz, I., Danelli, L., Claver, J., Goudin, N., Kurowska, M., Madera-Salcedo, I. K., et al. (2016). Kinesin-1 controls mast cell degranulation and anaphylaxis through PI3K-dependent recruitment to the granular Slp3/Rab27b complex. *J. Cell Biol.* 215, 203–216. doi: 10.1083/jcb.201605073

Nagai, Y., Tadokoro, S., Sakiyama, H., and Hirashima, N. (2011). Effects of synaptotagmin 2 on membrane fusion between liposomes that contain SNAREs involved in exocytosis in mast cells. *Biochim. Biophys. Acta* 1808, 2435–2439. doi: 10.1016/j.bbamem.2011.07.003

Narasimhan, V., Holowka, D., and Baird, B. (1990). Microfilaments regulate the rate of exocytosis in rat basophilic leukemia cells. *Biochem. Biophys. Res. Commun.* 171, 222–229. doi: 10.1016/0006-291X(90)91380-B

Neeft, M., Wieffer, M., De Jong, A. S., Negroiu, G., Metz, C. H., Van Loon, A., et al. (2005). Munc13-4 is an effector of rab27a and controls secretion of lysosomes in hematopoietic cells. *Mol. Biol. Cell* 16, 731–741. doi: 10.1091/mbc.e04-10-0923

Nielsen, E. H., and Johansen, T. (1986). Effects of dimethylsulfoxide (DMSO), nocodazole, and taxol on mast cell histamine secretion. *Acta Pharmacol. Toxicol.* 59, 214–219. doi: 10.1111/j.1600-0773.1986.tb00157.x

Nightingale, T. D., Cutler, D. F., and Cramer, L. P. (2012). Actin coats and rings promote regulated exocytosis. *Trends Cell. Biol.* 22, 329–337. doi: 10.1016/j.tcb.2012.03.003

Nili, U., De Wit, H., Gulyas-Kovacs, A., Toonen, R. F., Sorensen, J. B., Verhage, M., et al. (2006). Munc18-1 phosphorylation by protein kinase C potentiates vesicle pool replenishment in bovine chromaffin cells. *Neuroscience* 143, 487–500. doi: 10.1016/j.neuroscience.2006.08.014

Nishida, K., Yamasaki, S., Hasegawa, A., Iwamatsu, A., Koseki, H., and Hirano, T. (2011). Gab2, via PI-3K, regulates ARF1 in FcepsilonRI-mediated granule translocation and mast cell degranulation. *J. Immunol.* 187, 932–941. doi: 10.4049/jimmunol.1100360

Nishida, K., Yamasaki, S., Ito, Y., Kabu, K., Hattori, K., Tezuka, T., et al. (2005). Fc{epsilon}RI-mediated mast cell degranulation requires calcium-independent microtubule-dependent translocation of granules to the plasma membrane. *J. Cell Biol.* 170, 115–126. doi: 10.1083/jcb.200501111

Nitta, N., Aoki, Y., Isogawa, Y., Tsuchiya, T., and Kanegasaki, S. (2009). Image analysis of mast cell degranulation in a concentration gradient of stimuli formed in the channel between a glass plate and a silicon substrate. *Eur. J. Cell Biol.* 88, 541–549. doi: 10.1016/j.ejcb.2009.03.004

Norman, J., Price, L., Ridley, A., and Koffer, A. (1996). The small GTP-binding proteins, Rac and Rho, regulate cytoskeletal organization and exocytosis in mast cells by parallel pathways. *Mol. Biol. Cell* 7, 1429–1442. doi: 10.1091/mbc.7.9.1429

Norman, J. C., Price, L. S., Ridley, A. J., Hall, A., and Koffer, A. (1994). Actin filament organization in activated mast cells is regulated by heterotrimeric and small GTP-binding proteins. *J. Cell Biol.* 126, 1005–1015. doi: 10.1083/jcb.126.4.1005

Oakley, B. R., Paolillo, V., and Zheng, Y. (2015). gamma-Tubulin complexes in microtubule nucleation and beyond. *Mol. Biol. Cell* 26, 2957–2962. doi: 10.1091/mbc.E14-11-1514

Ogawa, K., Tanaka, Y., Uruno, T., Duan, X., Harada, Y., Sanematsu, F., et al. (2014). DOCK5 functions as a key signaling adaptor that links FcepsilonRI signals to microtubule dynamics during mast cell degranulation. *J. Exp. Med.* 211, 1407–1419. doi: 10.1084/jem.20131926

Oheim, M., and Stuhmer, W. (2000). Tracking chromaffin granules on their way through the actin cortex. *Eur. Biophys. J.* 29, 67–89. doi: 10.1007/s002490050253

Oka, T., Hori, M., Tanaka, A., Matsuda, H., Karaki, H., and Ozaki, H. (2004). IgE alone-induced actin assembly modifies calcium signaling and degranulation in RBL-2H3 mast cells. *Am. J. Physiol. Cell. Physiol.* 286, C256–C263. doi: 10.1152/ajpcell.00197.2003

Oka, T., Sato, K., Hori, M., Ozaki, H., and Karaki, H. (2002). FcepsilonRI cross-linking-induced actin assembly mediates calcium signalling in RBL-2H3 mast cells. *Br. J. Pharmacol.* 136, 837–846. doi: 10.1038/sj.bjp.0704788

Orci, L., Gabbay, K. H., and Malaisse, W. J. (1972). Pancreatic beta-cell web: its possible role in insulin secretion. *Science* 175, 1128–1130. doi: 10.1126/science.175.4026.1128

Orita, S., Naito, A., Sakaguchi, G., Maeda, M., Igarashi, H., Sasaki, T., et al. (1997). Physical and functional interactions of Doc2 and Munc13 in Ca2+-dependent exocytotic machinery. *J. Biol. Chem.* 272, 16081–16084. doi: 10.1074/jbc.272.26.16081

Orita, S., Sasaki, T., Komuro, R., Sakaguchi, G., Maeda, M., Igarashi, H., et al. (1996). Doc2 enhances Ca2+-dependent exocytosis from PC12 cells. *J. Biol. Chem.* 271, 7257–7260. doi: 10.1074/jbc.271.13.7257

Palazzo, A. F., Cook, T. A., Alberts, A. S., and Gundersen, G. G. (2001). mDia mediates Rho-regulated formation and orientation of stable microtubules. *Nat. Cell Biol.* 3, 723–729. doi: 10.1038/35087035

Palfreyman, M. T., and Jorgensen, E. M. (2017). Unc13 Aligns SNAREs and superprimes synaptic vesicles. *Neuron* 95, 473–475. doi: 10.1016/j.neuron.2017.07.017

Parravicini, V., Gadina, M., Kovarova, M., Odom, S., Gonzalez-Espinosa, C., Furumoto, Y., et al. (2002). Fyn kinase initiates complementary signals required for IgE-dependent mast cell degranulation. *Nat. Immunol.* 3, 741–748. doi: 10.1038/ni817

Paumet, F., Le Mao, J., Martin, S., Galli, T., David, B., Blank, U., et al. (2000). Soluble NSF attachment protein receptors (SNAREs) in RBL-2H3 mast cells: functional role of syntaxin 4 in exocytosis and identification of a vesicle-associated membrane protein 8-containing secretory compartment. *J. Immunol.* 164, 5850–5857. doi: 10.4049/jimmunol.164.11.5850

Pendleton, A., and Koffer, A. (2001). Effects of latrunculin reveal requirements for the actin cytoskeleton during secretion from mast cells. *Cell Motil. Cytoskelet.* 48, 37–51. doi: 10.1002/1097-0169(200101)48:1<37::AID-CM4>3.0.CO;2-0

Peschke, K., Weitzmann, A., Heger, K., Behrendt, R., Schubert, N., Scholten, J., et al. (2014). IkappaB kinase 2 is essential for IgE-induced mast cell de novo cytokine production but not for degranulation. *Cell Rep.* 8, 1300–1307. doi: 10.1016/j.celrep.2014.07.046

Pfeiffer, J. R., Seagrave, J. C., Davis, B. H., Deanin, G. G., and Oliver, J. M. (1985). Membrane and cytoskeletal changes associated with IgE-mediated serotonin release from rat basophilic leukemia cells. *J. Cell Biol.* 101, 2145–2155. doi: 10.1083/jcb.101.6.2145

Pierini, L., Harris, N. T., Holowka, D., and Baird, B. (1997). Evidence supporting a role for microfilaments in regulating the coupling between poorly dissociable IgE-Fc epsilonRI aggregates downstream signaling pathways. *Biochemistry* 36, 7447–7456. doi: 10.1021/bi9629642

Pinheiro, P. S., Houy, S., and Sorensen, J. B. (2016). C2-domain containing calcium sensors in neuroendocrine secretion. *J. Neurochem.* 139, 943–958. doi: 10.1111/jnc.13865

Pivniouk, V. I., Snapper, S. B., Kettner, A., Alenius, H., Laouini, D., Falet, H., et al. (2003). Impaired signaling via the high-affinity IgE receptor in Wiskott-Aldrich syndrome protein-deficient mast cells. *Int. Immunol.* 15, 1431–1440. doi: 10.1093/intimm/dxg148

Pobbati, A. V., Razeto, A., Boddener, M., Becker, S., and Fasshauer, D. (2004). Structural basis for the inhibitory role of tomosyn in exocytosis. *J. Biol. Chem.* 279, 47192–47200. doi: 10.1074/jbc.M408767200

Pollard, T. D. (2016). Actin and actin-binding proteins. *Cold Spring Harb. Perspect. Biol.* 8:a018226. doi: 10.1101/cshperspect.a018226

Pombo, I., Martin-Verdeaux, S., Iannascoli, B., Le Mao, J., Deriano, L., Rivera, J., et al. (2001). IgE receptor type I-dependent regulation of a Rab3D-associated kinase. A possible link in the calcium-dependent assembly of SNARE complexes. *J. Biol. Chem.* 12:12. doi: 10.1074/jbc.M103527200

Pombo, I., Rivera, J., and Blank, U. (2003). Munc18-2/syntaxin3 complexes are spatially separated from syntaxin3-containing SNARE complexes. *FEBS Lett.* 550, 144–148. doi: 10.1016/S0014-5793(03)00864-0

Price, L., Norman, J., Ridley, A., and Koffer, A. (1995). The small GTPases rac and rho as regulators of secretion in mast cells. *Curr. Biol.* 5, 68–73. doi: 10.1016/S0960-9822(95)00018-2

Puri, N., and Roche, P. A. (2008). Mast cells possess distinct secretory granule subsets whose exocytosis is regulated by different SNARE isoforms. *Proc. Natl. Acad. Sci. U.S.A.* 105, 2580–2585. doi: 10.1073/pnas.0707854105

Ramadass, M., and Catz, S. D. (2016). Molecular mechanisms regulating secretory organelles and endosomes in neutrophils and their implications for inflammation. *Immunol. Rev.* 273, 249–265. doi: 10.1111/imr.12452

Redegeld, F. A., Yu, Y., Kumari, S., Charles, N., and Blank, U. (2018). Non-IgE mediated mast cell activation. *Immunol. Rev.* 282, 87–113. doi: 10.1111/imr.12629

Riedel, D., Antonin, W., Fernandez-Chacon, R., Alvarez, De Toledo, G., Jo, T., et al. (2002). Rab3D is not required for exocrine exocytosis but for maintenance of normally sized secretory granules. *Mol. Cell Biol.* 22, 6487–6497. doi: 10.1128/MCB.22.18.6487-6497.2002

Rivera, J., Fierro, N. A., Olivera, A., and Suzuki, R. (2008). New insights on mast cell activation via the high affinity receptor for IgE. *Adv. Immunol.* 98, 85–120. doi: 10.1016/S0065-2776(08)00403-3

Roa, M., Paumet, F., Lemao, J., David, B., and Blank, U. (1997). Involvement of the ras-like GTPase rab3d in RBL-2H3 mast cell exocytosis following stimulation via high affinity IgE receptors (Fc epsilon RI). *J. Immunol.* 159, 2815–2823.

Rodarte, E. M., Ramos, M. A., Davalos, A. J., Moreira, D. C., Moreno, D. S., Cardenas, E. I., et al. (2018). Munc13 proteins control regulated exocytosis in mast cells. *J. Biol. Chem.* 293, 345–358. doi: 10.1074/jbc.M117.816884

Röhlich, P., Anderson, P., and Uvnäs, B. (1971). Electron microscope observation on compoun 48/80-induced degranulation in mast cells. *J. Cell Biol.* 51, 465–483. doi: 10.1083/jcb.51.2.465

Rothman, J. E., Krishnakumar, S. S., Grushin, K., and Pincet, F. (2017). Hypothesis - buttressed rings assemble, clamp, and release SNAREpins for synaptic transmission. *FEBS Lett.* 591, 3459–3480. doi: 10.1002/1873-3468.12874

Rubikova, Z., Sulimenko, V., Paulenda, T., and Draber, P. (2018). Mast cell activation and microtubule organization are modulated by miltefosine through protein Kinase C inhibition. *Front. Immunol.* 9:1563. doi: 10.3389/fimmu.2018.01563

Sanchez, E., Gonzalez, E. A., Moreno, D. S., Cardenas, R. A., Ramos, M. A., Davalos, A. J., et al. (2019). Syntaxin 3, but not syntaxin 4, is required for mast cell-regulated exocytosis, where it plays a primary role mediating compound exocytosis. *J. Biol. Chem.* 294, 3012–3023. doi: 10.1074/jbc.RA118.005532

Sander, L. E., Frank, S. P., Bolat, S., Blank, U., Galli, T., Bigalke, H., et al. (2008). Vesicle associated membrane protein (VAMP)-7 and VAMP-8, but not VAMP-2 or VAMP-3, are required for activation-induced degranulation of mature human mast cells. *Eur. J. Immunol.* 38, 855–863. doi: 10.1002/eji.200737634

Schulze, E., and Kirschner, M. (1986). Microtubule dynamics in interphase cells. *J. Cell Biol.* 102, 1020–1031. doi: 10.1083/jcb.102.3.1020

Shelby, S. A., Veatch, S. L., Holowka, D. A., and Baird, B. A. (2016). Functional nanoscale coupling of Lyn kinase with IgE-FcepsilonRI is restricted by the actin cytoskeleton in early antigen-stimulated signaling. *Mol. Biol. Cell* 27, 3645–3658. doi: 10.1091/mbc.e16-06-0425

Sheshachalam, A., Baier, A., and Eitzen, G. (2017). The effect of Rho drugs on mast cell activation and degranulation. *J. Leukoc. Biol.* 102, 71–81. doi: 10.1189/jlb.2A0616-279RRR

Singh, R. K., Mizuno, K., Wasmeier, C., Wavre-Shapton, S. T., Recchi, C., Catz, S. D., et al. (2013). Distinct and opposing roles for Rab27a/Mlph/MyoVa and Rab27b/Munc13-4 in mast cell secretion. *FEBS J.* 280, 892–903. doi: 10.1111/febs.12081

Smith, A. J., Pfeiffer, J. R., Zhang, J., Martinez, A. M., Griffiths, G. M., and Wilson, B. S. (2003). Microtubule-dependent transport of secretory vesicles in RBL-2H3 cells. *Traffic* 4, 302–312. doi: 10.1034/j.1600-0854.2003.00084.x

Srikanth, S., Jung, H. J., Kim, K. D., Souda, P., Whitelegge, J., and Gwack, Y. (2010). A novel EF-hand protein, CRACR2A, is a cytosolic Ca2+ sensor that stabilizes CRAC channels in T cells. *Nat. Cell Biol.* 12, 436–446. doi: 10.1038/ncb2045

Srikanth, S., Kim, K. D., Gao, Y., Woo, J. S., Ghosh, S., Calmettes, G., et al. (2016). A large Rab GTPase encoded by CRACR2A is a component of subsynaptic vesicles that transmit T cell activation signals. *Sci. Signal.* 9:ra31. doi: 10.1126/scisignal.aac9171

Staser, K., Shew, M. A., Michels, E. G., Mwanthi, M. M., Yang, F. C., Clapp, D. W., et al. (2013). A Pak1-PP2A-ERM signaling axis mediates F-actin rearrangement and degranulation in mast cells. *Exp. Hematol.* 41, 56.e2–66.e2. doi: 10.1016/j.exphem.2012.10.001

Stenmark, H. (2009). Rab GTPases as coordinators of vesicle traffic. *Nat. Rev. Mol. Cell Biol.* 10, 513–525. doi: 10.1038/nrm2728

Sudhof, T. C., and Rothman, J. E. (2009). Membrane fusion: grappling with SNARE and SM proteins. *Science* 323, 474–477. doi: 10.1126/science.1161748

Sulimenko, V., Draberova, E., Sulimenko, T., Macurek, L., Richterova, V., Draber, P., et al. (2006). Regulation of microtubule formation in activated mast cells by complexes of gamma-tubulin with Fyn and Syk kinases. *J. Immunol.* 176, 7243–7253. doi: 10.4049/jimmunol.176.12.7243

Sulimenko, V., Hajkova, Z., Cernohorska, M., Sulimenko, T., Sladkova, V., Draberova, L., et al. (2015). Microtubule nucleation in mouse bone marrow-derived mast cells is regulated by the concerted action of GIT1/betaPIX proteins and calcium. *J. Immunol.* 194, 4099–4111. doi: 10.4049/jimmunol.1402459

Sullivan, R., Burnham, M., Torok, K., and Koffer, A. (2000). Calmodulin regulates the disassembly of cortical F-actin in mast cells but is not required for secretion. *Cell Calc.* 28, 33–46. doi: 10.1054/ceca.2000.0127

Suzuki, K., and Verma, I. M. (2008). Phosphorylation of SNAP-23 by IkappaB kinase 2 regulates mast cell degranulation. *Cell* 134, 485–495. doi: 10.1016/j.cell.2008.05.050

Suzuki, R., Inoh, Y., Yokawa, S., Furuno, T., and Hirashima, N. (2021). Receptor dynamics regulates actin polymerization state through phosphorylation of cofilin in mast cells. *Biochem. Biophys. Res. Commun.* 534, 714–719. doi: 10.1016/j.bbrc.2020.11.012

Suzuki, R., Liu, X., Olivera, A., Aguiniga, L., Yamashita, Y., Blank, U., et al. (2010). Loss of TRPC1-mediated Ca2+ influx contributes to impaired degranulation in Fyn-deficient mouse bone marrow-derived mast cells. *J. Leukoc. Biol.* 88, 863–875. doi: 10.1189/jlb.0510253

Svitkina, T. (2018). The actin cytoskeleton and actin-based motility. *Cold Spring Harb. Perspect. Biol.* 10:a018267. doi: 10.1101/cshperspect.a018267

Svitkina, T. M. (2020). Actin cell cortex: structure and molecular organization. *Trends Cell Biol.* 30, 556–565. doi: 10.1016/j.tcb.2020.03.005

Tadokoro, S., Kurimoto, T., Nakanishi, M., and Hirashima, N. (2007). Munc18-2 regulates exocytotic membrane fusion positively interacting with syntaxin-3 in RBL-2H3 cells. *Mol. Immunol.* 44, 3427–3433. doi: 10.1016/j.molimm.2007.02.013

Tadokoro, S., Nakanishi, M., and Hirashima, N. (2005). Complexin II facilitates exocytotic release in mast cells by enhancing Ca2+ sensitivity of the fusion process. *J. Cell Sci.* 118, 2239–2246. doi: 10.1242/jcs.02338

Tadokoro, S., Nakanishi, M., and Hirashima, N. (2010). Complexin II regulates degranulation in RBL-2H3 cells by interacting with SNARE complex containing syntaxin-3. *Cell Immunol.* 261, 51–56. doi: 10.1016/j.cellimm.2009.10.011

Tadokoro, S., Shibata, T., Inoh, Y., Amano, T., Nakanishi, M., Hirashima, N., et al. (2016). Phosphorylation of syntaxin-3 at Thr 14 negatively regulates exocytosis in RBL-2H3 mast cells. *Cell Biol. Int.* 40, 589–596. doi: 10.1002/cbin.10600

Tellam, J., Mcintosh, S., and James, D. (1995). Molecular identification of two novel munc-18 isoforms expressed in non-neuronal tissues. *J. Biol. Chem.* 270, 5857–5863. doi: 10.1074/jbc.270.11.5857

Tiwari, N., Wang, C. C., Brochetta, C., Ke, G., Vita, F., Qi, Z., et al. (2008). VAMP-8 segregates mast cell-preformed mediator exocytosis from cytokine trafficking pathways. *Blood* 111, 3665–3674. doi: 10.1182/blood-2007-07-103309

Tiwari, N., Wang, C. C., Brochetta, C., Scandiuzzi, L., Hong, W., and Blank, U. (2009). Increased formation of VAMP-3-containing SNARE complexes in mast cells from VAMP-8 deficient cells. *appetite. Inflamm. Res.* 58(Suppl. 1), 13–14. doi: 10.1007/s00011-009-0645-y

Tolarova, H., Draberova, L., Heneberg, P., and Draber, P. (2004). Involvement of filamentous actin in setting the threshold for degranulation in mast cells. *Eur. J. Immunol.* 34, 1627–1636. doi: 10.1002/eji.200424991

Torigoe, C., Song, J., Barisas, B. G., and Metzger, H. (2004). The influence of actin microfilaments on signaling by the receptor with high-affinity for IgE. *Mol. Immunol.* 41, 817–829. doi: 10.1016/j.molimm.2004.03.033

Tumova, M., Koffer, A., Simicek, M., Draberova, L., and Draber, P. (2010). The transmembrane adaptor protein NTAL signals to mast cell cytoskeleton via the small GTPase Rho. *Eur. J. Immunol.* 40, 3235–3245. doi: 10.1002/eji.201040403

Tuvim, M. J., Adachi, R., Chocano, J. F., Moore, R. H., Lampert, R. M., Zera, E., et al. (1999). Rab3D, a small GTPase, is localized on mast cell secretory granules and translocates to the plasma membrane upon exocytosis. *Am. J. Resp. Cell Mol. Biol.* 20, 79–89. doi: 10.1165/ajrcmb.20.1.3279

Vaidyanathan, V. V., Puri, N., and Roche, P. A. (2001). The last exon of SNAP-23 regulates granule exocytosis from mast cells. *J. Biol. Chem.* 276, 25101–25106. doi: 10.1074/jbc.M103536200

Valentijn, J., Sengupta, D., Gumkowski, F., Tang, L., Konieczko, E., and Jamieson, J. (1996). Rab3D localizes to secretory granules in rat pancreatic acinar cells. *Eur. J. Cell Biol.* 70, 33–41.

Valentijn, K., Valentijn, J. A., and Jamieson, J. D. (1999). Role of actin in regulated exocytosis and compensatory membrane retrieval: insights from an old acquaintance. *Biochem. Biophys. Res. Commun.* 266, 652–661. doi: 10.1006/bbrc.1999.1883

van Weering, J. R., Toonen, R. F., and Verhage, M. (2007). The role of Rab3a in secretory vesicle docking requires association/dissociation of guanidine phosphates and Munc18-1. *PLoS One* 2:e616. doi: 10.1371/journal.pone.0000616

Verhage, M., Maia, A. S., Plomp, J. J., Brussaard, A. B., Heeroma, J. H., Vermeer, H., et al. (2000). Synaptic assembly of the brain in the absence of neurotransmitter secretion. *Science* 287, 864–869. doi: 10.1126/science.287.5454.864

Voets, T., Toonen, R. F., Brian, E. C., De Wit, H., Moser, T., Rettig, J., et al. (2001). Munc18-1 promotes large dense-core vesicle docking. *Neuron* 31, 581–591. doi: 10.1016/S0896-6273(01)00391-9

Wang, Y., Huynh, W., Skokan, T. D., Lu, W., Weiss, A., and Vale, R. D. (2019). CRACR2a is a calcium-activated dynein adaptor protein that regulates endocytic traffic. *J. Cell Biol.* 218, 1619–1633. doi: 10.1083/jcb.201806097

Weber, T., Zemelman, B. V., Mcnew, J. A., Westermann, B., Gmachl, M., Parlati, F., et al. (1998). Snarepins - minimal machinery for membrane fusion. *Cell* 92, 759–772. doi: 10.1016/S0092-8674(00)81404-X

Wen, Y., Eng, C. H., Schmoranzer, J., Cabrera-Poch, N., Morris, E. J., Chen, M., et al. (2004). EB1 and APC bind to mDia to stabilize microtubules downstream of Rho and promote cell migration. *Nat. Cell Biol.* 6, 820–830. doi: 10.1038/ncb1160

Wernersson, S., and Pejler, G. (2014). Mast cell secretory granules: armed for battle. *Nat. Rev. Immunol.* 14, 478–494. doi: 10.1038/nri3690

Williams, R. M., and Webb, W. W. (2000). Single granule pH cycling in antigen-induced mast cell secretion [In Process Citation]. *J. Cell Sci.* 113, 3839–3850.

Wilson, J. D., Shelby, S. A., Holowka, D., and Baird, B. (2016). Rab11 regulates the mast cell exocytic response. *Traffic* 17, 1027–1041. doi: 10.1111/tra.12418

Wojnacki, J., Quassollo, G., Marzolo, M. P., and Caceres, A. (2014). Rho GTPases at the crossroad of signaling networks in mammals: impact of Rho-GTPases on microtubule organization and dynamics. *Small GTPases* 5:e28430. doi: 10.4161/sgtp.28430

Wollman, R., and Meyer, T. (2012). Coordinated oscillations in cortical actin and Ca2+ correlate with cycles of vesicle secretion. *Nat. Cell Biol.* 14, 1261–1269. doi: 10.1038/ncb2614

Woo, S. S., James, D. J., and Martin, T. F. (2017). Munc13-4 functions as a Ca(2+) sensor for homotypic secretory granule fusion to generate endosomal exocytic vacuoles. *Mol. Biol. Cell* 28, 792–808. doi: 10.1091/mbc.e16-08-0617

Woska, J. R. Jr., and Gillespie, M. E. (2011). Small-interfering RNA-mediated identification and regulation of the ternary SNARE complex mediating RBL-2H3 mast cell degranulation. *Scand. J. Immunol.* 73, 8–17. doi: 10.1111/j.1365-3083.2010.02471.x

Yamamoto, Y., Fujikura, K., Sakaue, M., Okimura, K., Kobayashi, Y., Nakamura, T., et al. (2010). The tail domain of tomosyn controls membrane fusion through tomosyn displacement by VAMP2. *Biochem. Biophys. Res. Commun.* 399, 24–30. doi: 10.1016/j.bbrc.2010.07.026

Yamamoto, Y., Mochida, S., Kurooka, T., and Sakisaka, T. (2009). Reciprocal intramolecular interactions of tomosyn control its inhibitory activity on SNARE complex formation. *J. Biol. Chem.* 284, 12480–12490. doi: 10.1074/jbc.M807182200

Yang, Y., Kong, B., Jung, Y., Park, J. B., Oh, J. M., Hwang, J., et al. (2018). Soluble N-ethylmaleimide-sensitive factor attachment protein receptor-derived peptides for regulation of mast cell degranulation. *Front. Immunol.* 9:725. doi: 10.3389/fimmu.2018.00725

Ye, S., Huang, Y., Joshi, S., Zhang, J., Yang, F., Zhang, G., et al. (2014). Platelet secretion and hemostasis require syntaxin-binding protein STXBP5. *J. Clin. Invest.* 124, 4517–4528. doi: 10.1172/JCI75572

Zhang, J., Betson, M., Erasmus, J., Zeikos, K., Bailly, M., Cramer, L. P., et al. (2005). Actin at cell-cell junctions is composed of two dynamic and functional populations. *J. Cell Sci.* 118, 5549–5562. doi: 10.1242/jcs.02639

Zhang, W., Lilja, L., Mandic, S. A., Gromada, J., Smidt, K., Janson, J., et al. (2006). Tomosyn is expressed in beta-cells and negatively regulates insulin exocytosis. *Diabetes* 55, 574–581. doi: 10.2337/diabetes.55.03.06.db05-0015

Zhou, A. X., Hartwig, J. H., and Akyurek, L. M. (2010). Filamins in cell signaling, transcription and organ development. *Trends Cell Biol.* 20, 113–123. doi: 10.1016/j.tcb.2009.12.001

Zhou, F. Q., and Snider, W. D. (2005). Cell biology. *GSK*-3beta and microtubule assembly in axons. *Science* 308, 211–214. doi: 10.1126/science.1110301

Zhu, Q., Yamakuchi, M., Ture, S., De La Luz, Garcia-Hernandez, M., Ko, K. A., et al. (2014). Syntaxin-binding protein STXBP5 inhibits endothelial exocytosis and promotes platelet secretion. *J. Clin. Invest.* 124, 4503–4516. doi: 10.1172/JCI71245

Zorn, C. N., Simonowski, A., and Huber, M. (2018). Stimulus strength determines the BTK-dependence of the SHIP1-deficient phenotype in IgE/antigen-triggered mast cells. *Sci. Rep.* 8:15467. doi: 10.1038/s41598-018-33769-1

Conflict of Interest: The authors declare that the research was conducted in the absence of any commercial or financial relationships that could be construed as a potential conflict of interest.

GLOSSARY

ADDS, Antibody-dependent degranulatory synapse; APC, Adenomatous polyposis coli; Arp2/3, Actin-related proteins 2/3; BMMC, Bone marrow-derived MC; CPLX, Complexin; CRAC, Ca2+ release activated channel; DAG, Diacylglycerol; DBN, Drebrin; EB1, End-binding protein 1; ER, Endoplasmic reticulum; ERM, Ezrin Radixin Moesin; FEZ1, Fasciculation and elongation protein zeta 1; FHL, Familial hemophagocytic lymphohistiocytosis; Gab2, Grb2-associated binding protein 2; Gads, Grb2-related adaptor protein; GCPs, γ-tubulin complex proteins; GEF, Guanine nucleotide exchange factor; GIMP, Gem-interacting protein; GIT1, G protein-coupled receptor kinase-interacting protein 1; Grb2, Growth-factor-receptor bound protein 2; IKKβ2, IκB kinase 2/β; IP3, Inositol 1,4,5-trisphosphate; ITAM, Immunoreceptor tyrosine-based activation motifs; KD, Knockdown; KO, Genetic knockout; LAT, Linker for Activation of T cells; LIMK, LIM-motif containing kinase; MAPs, Microtubule-associated proteins; MC, Mast cells; mDia1, Mammalian diaphanous-related formin 1; Mid, Munc13-interacting domain; MHD, Munc Homology Domains; MLCK, Myosin light chain kinase; MLCP, Myosin light chain phosphatase; MTOC, Microtubule Organizing Center; Munc13-4, Mammalian uncoordinated 13-4; ORAI1, Ca2+ release-activated Ca2+ channel protein1; PA, phosphatidate; PAK, p21-activated kinase; PCA, Passive cutaneous anaphylaxis responses; PI3K, Phosphatidyl inositol-3 kinase; PIP3, Phosphatidylinositol (3,4,5)-trisphosphate; βPIX, p21-activated kinase interacting exchange factor β; PKC, Protein kinase C; PLCγ, Phospholipase Cγ; PLD, Phospholipase D; PM, Plasma membrane; PMD, Piecemeal degranulation; PP2A, Protein phosphatase 2; PTK, Protein tyrosine kinases; RasGRP1, Ras guanyl nucleotide-releasing protein 1; RBL, Rrat basophilic leukemia; RE, Recycling endosomes; RhoA, Ras homology family member A; RILP, Rab-interacting lysosomal protein; ROCK, Rho-associated coiled-coil kinase; RPMC, Rat peritoneal MC; SCAMP2, Secretory carrier membrane protein 2; SFK, Src family kinases; SG, Secretory granules; SHP-1, Src homology 2 domain-containing protein tyrosine phosphatase 1; SLP-76, SH2 domain-containing leukocyte phosphoprotein of 76 kDa; SM, Sec1/Munc18; SNAP, Synaptosome-associated protein; SNARE, Soluble N-ethyl-maleimide-sensitive factor Attachment protein Receptor; SOCs, Store-operated channels; STIM-1, Stromal interaction molecule 1; STX, Syntaxin; STXBP, Syntaxin binding protein; Syt, Synaptotagmin; TM, Transmembrane; +Tips, Microtubules plus-end tracking protein; TRPC1, Transient potential Ca2+ channel 1; γ-TuRC, γ-tubulin ring complex; VAMP, Vesicle associated membrane protein; WASP, Wiskott-Aldrich syndrome protein; WAVE, Wiskott-Aldrich syndrome protein-family verprolin homologous protein; WIP, Wiskott-Aldrich syndrome protein interacting protein.

frontiers in Cell and Developmental Biology

MINI REVIEW
published: 12 April 2021
doi: 10.3389/fcell.2021.664279

Phosphorylation and Ubiquitylation Regulate Protein Trafficking, Signaling, and the Biogenesis of Primary Cilia

Elena A. May[1,2†], *Tommy J. Sroka*[1,2†] *and David U. Mick*[1,2*]

[1] Center of Human and Molecular Biology (ZHMB), Saarland University School of Medicine, Homburg, Germany, [2] Center for Molecular Signaling (PZMS), Department of Medical Biochemistry and Molecular Biology, Saarland University School of Medicine, Homburg, Germany

The primary cilium is a solitary, microtubule-based membrane protrusion extending from the surface of quiescent cells that senses the cellular environment and triggers specific cellular responses. The functions of primary cilia require not only numerous different components but also their regulated interplay. The cilium performs highly dynamic processes, such as cell cycle-dependent assembly and disassembly as well as delivery, modification, and removal of signaling components to perceive and process external signals. On a molecular level, these processes often rely on a stringent control of key modulatory proteins, of which the activity, localization, and stability are regulated by post-translational modifications (PTMs). While an increasing number of PTMs on ciliary components are being revealed, our knowledge on the identity of the modifying enzymes and their modulation is still limited. Here, we highlight recent findings on cilia-specific phosphorylation and ubiquitylation events. Shedding new light onto the molecular mechanisms that regulate the sensitive equilibrium required to maintain and remodel primary cilia functions, we discuss their implications for cilia biogenesis, protein trafficking, and cilia signaling processes.

Keywords: primary cilia, post-translational modification, cell signaling, ciliogenesis, Hedgehog signaling, phosphorylation, ubiquitylation

OPEN ACCESS

Edited by:
Francisco Sanchez-Madrid, Autonomous University of Madrid, Spain

Reviewed by:
Cosima T. Baldari, University of Siena, Italy
Miguel Angel Alonso, Consejo Superior de Investigaciones Científicas (CSIC), Spain

****Correspondence:***
David U. Mick
david.mick@uks.eu

† These authors have contributed equally to this work

Specialty section:
This article was submitted to Cell Adhesion and Migration, a section of the journal Frontiers in Cell and Developmental Biology

Received: *04 February 2021*
Accepted: *09 March 2021*
Published: *12 April 2021*

Citation:
May EA, Sroka TJ and Mick DU (2021) Phosphorylation and Ubiquitylation Regulate Protein Trafficking, Signaling, and the Biogenesis of Primary Cilia. Front. Cell Dev. Biol. 9:664279. doi: 10.3389/fcell.2021.664279

INTRODUCTION

Primary cilia are dynamic cellular signaling compartments of the plasma membrane (Garcia et al., 2018; Anvarian et al., 2019) composed of a membrane-surrounded microtubule core, termed the axoneme. The axoneme emerges from a matured mother centriole, the so-called basal body, that connects to the plasma membrane via distinct appendages, the transition fibers (see **Figure 1**). Primary cilia are indispensable for embryonic development and cell differentiation. Consequently, defective primary cilia give rise to severe human diseases, known as ciliopathies, that are commonly caused by aberrant ciliary signaling processes (Baker and Beales, 2009; Reiter and Leroux, 2017). On a molecular level, observed defects comprise not only signaling components but also the protein machinery that is required to build and maintain cilia (Sánchez and Dynlacht, 2016; Breslow and Holland, 2019). Therefore, ciliopathy genes also include protein trafficking components, such as the cilia-specific intraflagellar transport (IFT) complexes, IFT-A and IFT-B

(Webb et al., 2020), and all eight subunits of the BBSome, defects of which cause Bardet–Biedl Syndrome (Jin et al., 2010; Forsythe et al., 2018). IFT complexes transport cargoes along the axoneme in an anterograde and retrograde fashion with the help of specific kinesin and dynein motors, respectively (Satir and Christensen, 2007). The ciliary membrane does not fully enclose the ciliary compartment at the proximal end, where it is separated from the cytosol by the transition zone (Yang et al., 2015). A concerted interplay of IFT complexes, the BBSome, transition fibers, and the transition zone enables select proteins to enter or exit the cilium (Garcia-Gonzalo and Reiter, 2017; Gonçalves and Pelletier, 2017).

Post-translational modification (PTM) is a fundamental principle in molecular biology referring to the modulation of protein properties by covalent attachment of small molecules. PTMs are catalyzed by various antagonistic enzymatic activities that modify target proteins at specific locations (Vu et al., 2018). For instance, phosphorylation can modulate interaction surfaces or lead to intramolecular rearrangements that alter enzymatic activities. Protein kinases phosphorylate their substrates at specific consensus sites consisting of only a few amino acids. Moreover, they are often targets of phosphorylation themselves, which results in phosphorylation cascades that are typically found in cellular signaling processes (Miller and Turk, 2018). Opposingly, protein phosphatases act on hundreds of different substrates to revert phosphorylations (Bertolotti, 2018). Compared to phosphorylation, ubiquitylation requires a more elaborate machinery. Ubiquitin is a small, 8.5-kDa protein that is usually attached to lysine residues of target proteins (Swatek and Komander, 2016; Yau and Rape, 2016). The enzymatic cascade of ubiquitylation involves E1 activating, E2 conjugating, and E3 ligating enzymes. While the E1 and E2 enzymes supply reactive ubiquitin molecules, the vast number of different E3 ubiquitin ligases determines substrate specificity. Similarly, deubiquitylating enzymes (DUBs) are highly specific with only a few substrates per enzyme (Clague et al., 2019). Ubiquitin contains seven lysine residues, to which further ubiquitin molecules can be added to generate poly-ubiquitin chains. Depending on the lysine residue, ubiquitin chains are differentiated into several linkage types that have been implicated in specific functions. K48- and K29-linked ubiquitins, for example, are the main linkage types associated with proteasomal degradation of target proteins, while the K63 chains and mono-ubiquitin are often times involved in protein trafficking events (Swatek and Komander, 2016).

The dynamic nature of PTMs is critical for most cellular processes and is extensively studied in protein trafficking and cell signaling (Patwardhan et al., 2021). The central role of the primary cilium as a cellular signaling hub suggests that PTMs regulate core ciliary functions. In addition to phosphorylation and ubiquitylation, ciliary proteins are targets of diverse modifications, such as acetylation (Kerek et al., 2021), SUMOylation (McIntyre et al., 2015), and methylation (Yeyati et al., 2017). Several lipid modifications (including acylation, myristoylation, palmitoylation, and prenylation) of ciliary proteins have also been involved in protein trafficking, membrane tethering, and protein stability (Roy and Marin, 2019). Moreover, ciliary microtubules are extensively acetylated, detyrosinated, glutamylated, and glycylated, which reflects axoneme maturation and affects axoneme assembly, protein interaction, and stability (Janke and Magiera, 2020). In the following, we focus on phosphorylation and ubiquitylation and discuss recent findings on their involvement in regulating cilia formation and signaling.

CILIARY SIGNALING

Conceptually, primary cilia are believed to function as cell type-specific micro-compartments with diverse compositions including receptors to receive, mediators to process, and effectors to transmit signals to the rest of the cell (Sung and Leroux, 2013; Nachury and Mick, 2019). Despite a large variety of receptors, far fewer mediators are commonly used in cellular signaling processes. Cyclic nucleotides or calcium ions are second messengers, the concentrations of which are interpreted by specific enzymes to further transmit signals via PTMs (Hilgendorf et al., 2019; Sherpa et al., 2019; Tajhya and Delling, 2020). To communicate with the rest of the cell, effectors are transported into and out of cilia in a dynamic fashion, which allows their modification according to the signaling status (Niewiadomski et al., 2019). This general principle highlights the tight connection between cilia signaling and protein trafficking. Apart from the IFT complexes, cilia require a multitude of additional factors to convey ciliary signals, which involves not only common protein trafficking components, such as β-arrestins, but also cilia-specific machinery, including the BBSome or the Tubby family of proteins (Mukhopadhyay and Jackson, 2011). While the inventory of primary cilia continues to expand (Mick et al., 2015; Kohli et al., 2017; May et al., 2021), the number of enzymes, which catalyze PTMs and have been unambiguously shown to localize to primary cilia, is limited. Nonetheless, we are beginning to unravel how ciliary signaling dynamics can be established as we identify more and more targets of PTMs in cilia.

Hedgehog Signaling

One hallmark ciliary signaling pathway that highlights the dynamics in PTMs is Hedgehog signaling in vertebrates (**Figure 1**; Gigante and Caspary, 2020). An elegantly orchestrated interplay of positive and negative regulators in Hedgehog signaling allows for the correct patterning of the developing embryo, in addition to maintaining adult tissue homeostasis (Shimada et al., 2019). Gradients of the hedgehog morphogens ultimately result in finely tuned levels of active GLI transcription factors that determine target gene expression (Briscoe and Novitch, 2008). In the absence of Hedgehog morphogens, their receptor Patched (PTCH1) localizes to the primary cilium (Rohatgi et al., 2007), while the key Hedgehog effector and G protein-coupled receptor (GPCR) Smoothened (SMO) surveys the primary cilium by shuttling in and out without appreciable local accumulation (**Figure 1A**; Kim et al., 2009; Goetz and Anderson, 2010). A second GPCR, the constitutively active GPR161, stimulates ciliary adenylyl cyclases to increase cAMP levels within cilia and thereby activates the cAMP-dependent

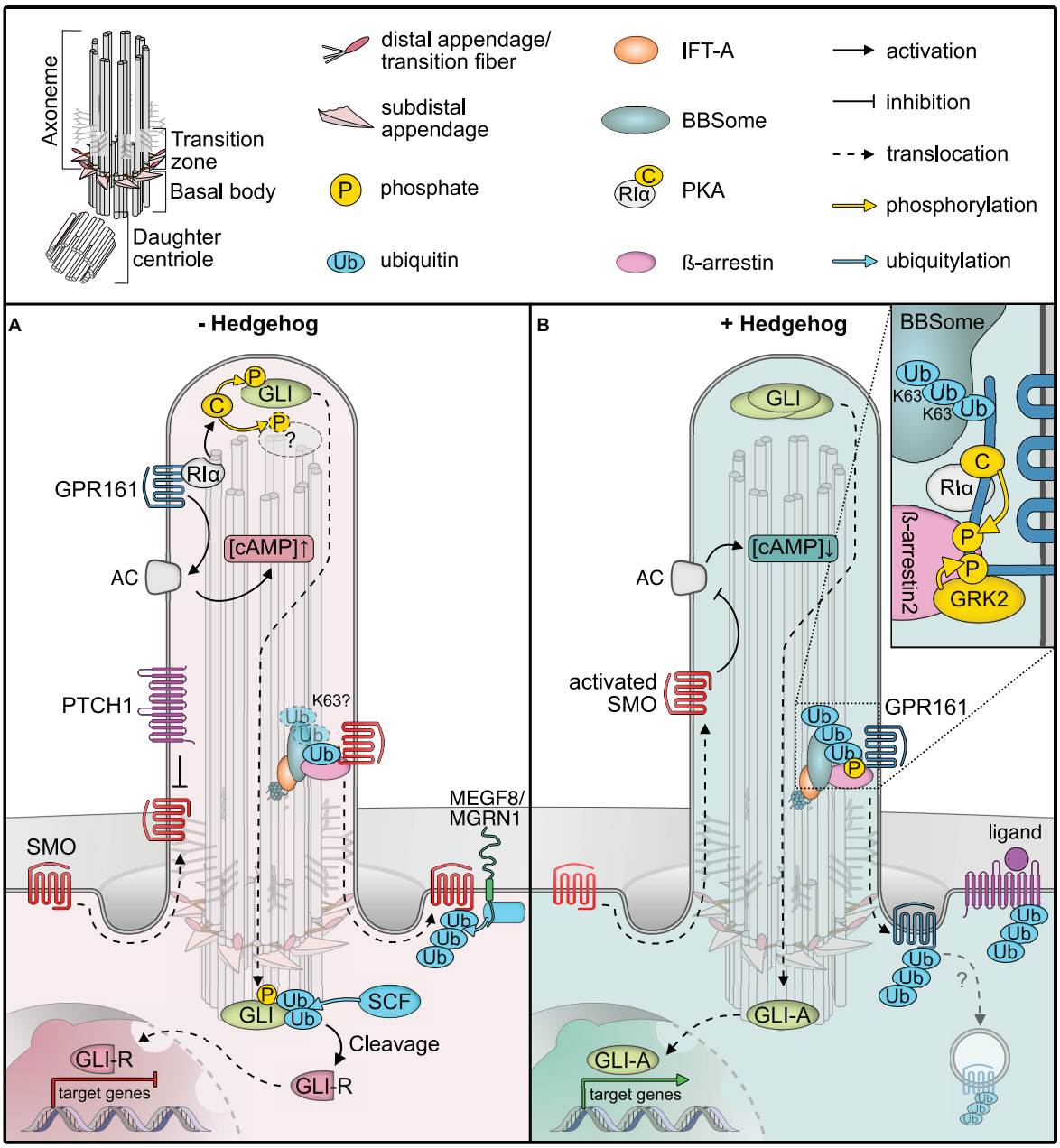

FIGURE 1 | Post-translational modifications (PTMs) regulating Hedgehog signaling. **(A)** In unstimulated cells, the GPCR SMO constantly surveys the cilium without accumulation, due to constant removal in a ubiquitin (Ub) and BBSome-dependent manner. The Hedgehog receptor PTCH1 suppresses SMO, and the constitutively active GPCR GPR161 is retained in cilia. GPR161 stimulates adenylyl cyclases (AC) to generate cAMP. High cAMP is sensed by the regulatory PKA subunit Iα (RIα), which releases the PKA catalytic subunit (C) to phosphorylate target proteins, such as GLI transcription factors. GLI phosphorylation leads to ubiquitylation and proteolytic cleavage to GLI repressor forms (GLI-R) that repress target gene expression in the nucleus. The ubiquitin ligase MEGF is recruited to the plasma membrane by MGRN1 where it ubiquitinylates SMO for subsequent degradation. **(B)** In the presence of Hedgehog ligands, PTCH1 exits the primary cilium, presumably in a Ub-dependent fashion, leading to SMO activation and accumulation. GPR161 in turn is phosphorylated by GRK2 (and PKA). GPR161 phosphorylation is sensed by β-arrestin2, which leads to ubiquitylation and BBSome-mediated removal of GPR161 together with PKA from the primary cilium. Together with a drop in cAMP levels, GLIs are no longer phosphorylated and full-length GLIs activate target genes in the nucleus. After removal from cilia, the mechanism by which GPR161 is internalized remains unclear.

protein kinase (PKA) (Mukhopadhyay et al., 2013). GPR161 also fulfills a second function in PKA signaling, as it serves as an atypical A-kinase anchoring protein (AKAP) that targets PKA to cilia (Bachmann et al., 2016). Here, it tethers to the cilia-resident PKA regulatory subunit RIα that senses ciliary cAMP (Mick et al., 2015). At high ciliary cAMP levels in unstimulated cells,

PKA-RIα binds cAMP and releases the catalytic PKA-C subunit (**Figure 1A**; Taylor et al., 2004). Free PKA-C can phosphorylate and regulate target proteins, such as the GLI transcription factors that convey the signaling status to the nucleus (Tuson et al., 2011; Niewiadomski et al., 2014). PKA-mediated phosphorylation of GLIs is a pre-requisite for their proteolytical cleavage to yield repressor forms that block the transcription of target genes (**Figure 1A**). GLI transcription factors are precisely regulated by a variety of activating and deactivating PTMs, which include activating phosphorylations at the N-terminal repressor domain, and two clusters of PKA phosphorylation sites on the activator domain. PKA phosphorylation precedes further phosphorylation by CK1 and GSK3β, which in turn recruits the SCF E3 ubiquitin ligase that marks GLIs for proteolytic processing by the proteasome (Kong et al., 2019; Niewiadomski et al., 2019).

Upon Hedgehog ligand binding, PTCH1 exits the primary cilium and SMO is activated and retained in cilia, whereas GPR161 is removed (Rohatgi et al., 2007; Gigante and Caspary, 2020). As the adenylyl cyclase inhibitory SMO replaces the stimulating GPR161, ciliary cAMP decreases (Mukhopadhyay et al., 2013). Consequently, PKA activity ceases and the GLI transcription factors are no longer phosphorylated and further processed, such that they can function as activators to initiate target gene expression in the nucleus (**Figure 1B**).

One central element in Hedgehog signaling is the dynamic re-localization of the components involved. Similar to other cellular protein trafficking mechanisms, PTMs control the localization of Hedgehog signaling proteins, which is particularly well-studied for GPR161 (Mukhopadhyay et al., 2013; Pal et al., 2016). GPR161's C-terminal tail not only contains the AKAP binding domain for PKA but also several protein kinase consensus sites, including one for PKA (Bachmann et al., 2016). Upon Hedgehog pathway activation, the C-terminal tail of GPR161 is phosphorylated by GRK2 and presumably PKA (Bachmann et al., 2016; Pal et al., 2016; May et al., 2021). GRK-mediated phosphorylation recruits the molecular sensor of activated GPCRs, specifically β-arrestin2, which is required for the removal of activated GPCRs from cilia (**Figure 1B**; Pal et al., 2016). Consequently, GPR161 exits cilia together with its binding partner PKA (May et al., 2021). Thereby, PKA activity in cilia is inhibited by two mechanisms: (i) reducing cAMP levels and (ii) removing PKA itself.

As exemplified by the GLI transcription factors and GPR161, specific phosphorylations are often catalyzed by individual kinases; however, our knowledge of specific protein phosphatases that antagonize these phosphorylations in cilia is still rudimentary. The protein phosphatases PP1 and PP2A have been reported to dephosphorylate SMO to dampen Hh signaling in *Drosophila* (Su et al., 2011; Liu et al., 2020). However, since primary cilia are dispensable for *Drosophila* Hh signal transduction, it remains unclear whether PP1 and PP2A also function within primary cilia. Mass spectrometric analyses have identified PP1 subunits in isolated *Chlamydomonas* cilia (Pazour et al., 2005) and PP2A subunits in primary cilia of kidney epithelial cells (Ishikawa et al., 2012), but these findings still await confirmation by independent methods. In contrast, lipid phosphatases, such as the inositol polyphosphate-5-phosphatase E, have been unambiguously shown to localize to primary cilia, where they modulate ciliary signal transduction by regulating protein trafficking (Chávez et al., 2015; Garcia-Gonzalo et al., 2015). Ciliary lipid phosphatase activities create a specific phosphatidylinositide phosphate environment that is required for efficient ciliary signaling.

A recent study investigated the involvement of ubiquitin in Hedgehog signaling by fusing mono-ubiquitin to the C-terminus of SMO (Desai et al., 2020). The SMO-Ub fusion accumulated in cilia in the absence of stimulation in IFT and BBSome mutants but failed to accumulate in cilia after Hedgehog pathway activation in wild type cells (Desai et al., 2020). These findings indicate that ubiquitin is required for the removal of SMO from cilia by a process involving IFT and the BBSome. Moreover, β-arrestin2 was shown to mediate the ubiquitylation of GPR161 in response to Hedgehog pathway activation (Shinde et al., 2020), before GPR161 exits the primary cilium in a BBSome-dependent fashion (Ye et al., 2018). More evidence for the central role of ubiquitylation for cilia trafficking comes from mutational analysis of the Hedgehog receptor PTCH1. PTCH1 harbors two E3 ubiquitin ligase recognition motifs and remains in the cilium when both motifs are mutated, even upon stimulation with Hedgehog ligands (Kim J.C. et al., 2015). SMO has been reported to be a target of the ubiquitin ligase HERC4 (Jiang et al., 2019). Furthermore, ubiquitylation of SMO by a complex of the E3 ubiquitin ligase MGRN1 and the plasma membrane protein MEGF8 serves as a signal for proteasomal degradation (Kong et al., 2020). Yet, whether these ubiquitin ligases are directly involved in the IFT-dependent retrieval of SMO awaits experimental validation.

Molecular dissection of ubiquitylation may help to decipher the different functions of ubiquitin in regulating ciliary proteins. Upon Hedgehog pathway activation, specifically K63-linked ubiquitin chains increase in primary cilia upon GPCR activation or in BBSome mutants (Shinde et al., 2020). This suggests that K63 ubiquitin chains function as export signals for ciliary proteins, which are recognized by the BBSome (Desai et al., 2020; Shinde et al., 2020). In BBSome mutant mice, photoreceptor outer segments, which are uniquely modified cilia that harbor the entire signaling cascade for visual phototransduction, accumulate more than 100 proteins that are absent in wild types (Datta et al., 2015). Based on these findings, the BBSome has been proposed to mediate the removal of unwanted proteins from cilia and, therefore, may function as an important mediator of a ciliary protein quality control network (Shinde et al., 2020). Additional components, such as the AAA-ATPase VCP or the ubiquitin-regulatory X domain protein UBXN10, have been shown to localize to primary cilia (Mick et al., 2015; Raman et al., 2015). While data from trypanosomes indicate that the BBSome may directly recognize ubiquitin as it can be enriched on ubiquitin-agarose resin (Langousis et al., 2016), it does not contain canonical ubiquitin binding domains. How ubiquitylated proteins are recognized in cilia on a molecular level and what enzymatic activities regulate ubiquitylation within cilia remains to be established. The E3 ubiquitin ligase CBL is recruited to cilia in response to PDGFRα signaling (Schmid et al., 2018) and the deubiquitylase UBPY/USP8 has been reported to antagonize SMO ubiquitylation in *Drosophila* (Ma et al., 2016).

These findings seem promising starting points for future studies elucidating the cilia-specific ubiquitylation network.

CILIUM DYNAMICS

Cilium Assembly—A Primary Cilium Is (Re)born

Ciliogenesis, i.e., the formation of cilia, is another dynamic process that is regulated by specific phosphorylation and ubiquitylation events (Cao et al., 2009; Shearer and Saunders, 2016). A specialized maternal centriole, the so-called basal body, templates the cilium. Yet, mother and daughter centrioles also form centrosomes required for spindle apparatus formation and chromosome segregation in metaphase. These two alternative roles of the mother centriole necessitate a cell cycle-dependent assembly and disassembly of primary cilia (Wang and Dynlacht, 2018; Breslow and Holland, 2019). Depending on cell type, the mother centriole takes one of two different routes to form a cilium, starting either directly at the plasma membrane (termed extracellular pathway) or within the cell (Bernabé-Rubio and Alonso, 2017; Kumar and Reiter, 2021). Here, we will be focusing on the intracellular pathway, which occurs in several steps (see **Figure 2**): (i) maturation of the mother centriole and acquisition of so-called distal and subdistal appendages, (ii) recruitment of a growing ciliary vesicle (the future ciliary membrane) to the mother centriole, (iii) separation of the ciliary compartment by the formation of the transition zone, (iv) extension of the ciliary axoneme, and (v) docking of the basal body and final fusion with the plasma membrane. While this process has been described on an ultrastructural level more than half a century ago (Sorokin, 1968), we are still discovering an increasing number of the required factors such as RABs and EHD family proteins that are involved in membrane recruitment (Lu et al., 2015; Blacque et al., 2018) and are just beginning to understand their regulation.

A central kinase that determines cilium formation is the Tau tubulin kinase 2 (TTBK2) (Tomizawa et al., 2001; Goetz et al., 2012). TTBK2 loss was originally reported to allow basal body docking to the plasma membrane, while blocking transition zone formation and ciliary shaft elongation. In actively proliferating cells, the distal ends of both mother and daughter centrioles are capped by protein complexes of CP110 and CEP97 that suppress cilia formation (Spektor et al., 2007; Schmidt et al., 2009). Recruitment of these caps seems to follow a hierarchical scheme, the precise order of which awaits clarification (Ye et al., 2014; Tsai et al., 2019). One central component involved in ciliogenesis is the microtubule-depolymerizing kinesin KIF24 (Kobayashi et al., 2011). KIF24 recruits the M-Phase phosphoprotein MPP9, which is required for the assembly of CEP97–CP110 complexes at the distal ends of centrioles (**Figure 2A**; Huang et al., 2018). The specific removal of the CEP97–CP110 complex relies on TTBK2 phosphorylation (**Figures 2B,C**; Goetz et al., 2012; Čajánek and Nigg, 2014; Huang et al., 2018). To ensure specificity of distal end uncapping and thereby cilium formation at the mother centriole, it is the distal appendage protein CEP164 that recruits TTBK2 (Schmidt et al., 2012; Čajánek and Nigg, 2014). TTBK2 has recently been shown to phosphorylate distal appendage proteins, such as CEP164 and CEP83 (Bernatik et al., 2020), which is required for efficient vesicle recruitment (**Figure 2B**; Lo et al., 2019). Notably, TTBK2 phosphorylates MPP9 resulting in the loss of MPP9 and the CEP97–CP110 complex from the distal centriolar end (**Figure 2C**; Huang et al., 2018). Moreover, with the onset of cilia formation, MPP9 is ubiquitylated and degraded by the proteasome. Although the precise ubiquitin linkage type has not been determined yet, many molecular details of MPP9 PTM have been resolved. Intriguingly, one identified ubiquitylation site in MPP9 is flanked by two phosphorylation sites. Phosphorylation-deficient mutants show reduced ubiquitylation and consequently stabilize MPP9 (Huang et al., 2018). This finding highlights a typical PTM cascade and suggests that the phosphorylation status determines MPP9 stability. Similar to MPP9, the CEP97–CP110 complex is subject to proteasomal degradation when ciliation is initiated (Spektor et al., 2007; Nagai et al., 2018). CP110 has been shown to be a target of the SCF ubiquitin ligase complex and a substrate of the E3 ubiquitin ligase UBR5 in an *in vitro* ubiquitylation assay (D'Angiolella et al., 2010; Hossain et al., 2017). Additionally, CEP97 degradation is suppressed after knockdown of the CUL3 E3 ligase, and therefore, it remains bound to CP110 at centrioles and inhibits ciliogenesis (Nagai et al., 2018). UBR5 has been found at centrosomes and CUL3 has been suggested to localize specifically to mother centrioles (Moghe et al., 2012; Nagai et al., 2018), where it may ubiquitylate Aurora kinase A, a central regulator of the cell cycle and promoter of cilium disassembly (Pugacheva et al., 2007). It will be interesting to investigate whether these ubiquitin ligases converge on the same targets and whether ubiquitylation is the cause or consequence of CEP97–CP110 removal. Also, how precisely ubiquitylation can be regulated and what role DUBs, such as USP33 that targets CP110 (Li et al., 2013), are playing in ciliogenesis need to be addressed in future studies.

Cilium Disassembly

In contrast to cilia formation, we are just beginning to understand the molecular details of how cilia are dismantled to allow cell cycle re-entry (Liang et al., 2016; Breslow and Holland, 2019). NEK2, a kinase predominantly expressed in the S and G2 phases of the cell cycle, has been proposed to promote cilium disassembly (**Figure 2D**; Kim S. et al., 2015). Among several targets, NEK2 phosphorylates and stimulates the microtubule-depolymerizing KIF24 at the distal centriolar ends (Kim S. et al., 2015). This may not only block unwanted cilium assembly but also shift the balance toward disassembly when resting cells re-enter the cell cycle (Kim S. et al., 2015; Viol et al., 2020). In support of a central role for KIF24 in cilium disassembly, a recent study identified FLS2 as a CDK-like kinase that phosphorylates the KIF24 ortholog CrKIF13 in *Chlamydomonas*, allowing efficient cilia disassembly (**Figure 2D**; Zhao et al., 2020). In turn, phosphorylated FLS2 showed lower activity and appears to be dephosphorylated upon cilia disassembly when it enters cilia by binding to the IFT-B component IFT70 (Zhao et al., 2020). While the precise mechanisms of regulation still need to be established, it is tempting to speculate that dephosphorylation of FLS2 may not only alter its kinase activity but also unmask targeting signals for IFT. This suggests a mechanism by which an

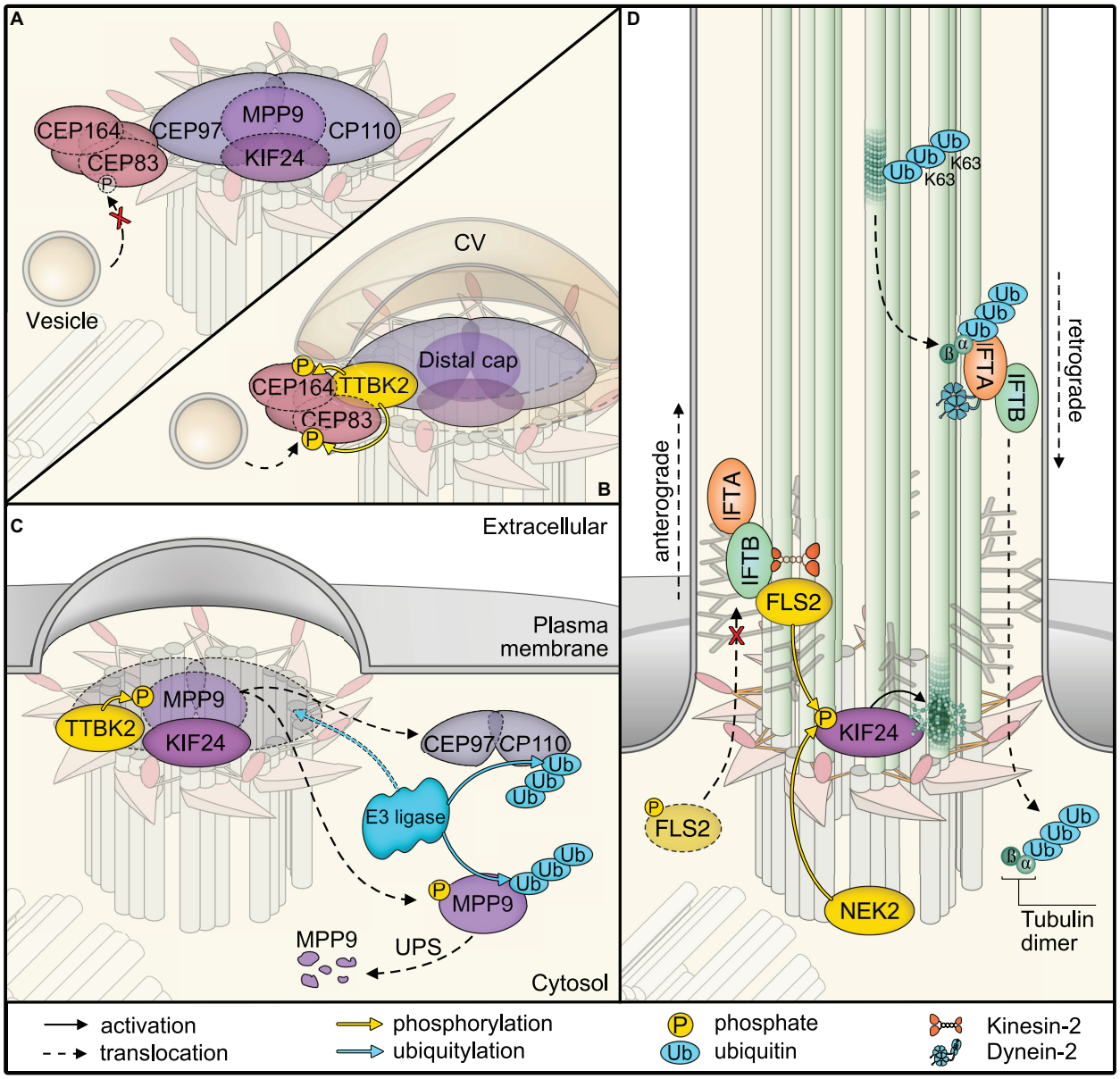

FIGURE 2 | Post-translational modifications (PTMs) in primary cilia assembly and disassembly. **(A)** Mother centriolar distal appendage components CEP164 and CEP83 are shown in red. The distal end proteins KIF24 and MPP9 recruit the capping protein complex CEP97–CP110 to block axoneme extension. Note that only one cap is shown for simplicity, while each microtubule triplet is capped by one complex. Unphosphorylated CEP83 diminishes ciliary vesicle recruitment **(B)** CEP164 recruits the kinase TTBK2 that phosphorylates CEP164 and CEP83. Recruitment and activity of TTBK2 enables subsequent steps of cilia assembly such as formation of the ciliary vesicle (CV). **(C)** TTBK2 phosphorylates MPP9, which results in ubiquitylation and dissociation of MPP9 and the remaining CEP97–CP110 complex from the distal centriolar end. Several E3 ubiquitin ligase complexes have been implicated in modifying distal cap components, while the precise location of ubiquitylation has not been determined (see text for details). Ultimately, MPP9, CEP97, and CP110 are degraded by the proteasome (UPS) and ciliary growth can be initiated. **(D)** Diagram of fully assembled primary cilium. The microtubule depolymerizing kinesin KIF24 has been implicated in microtubule disassembly. Phosphorylation of KIF24 by NEK2 stimulates KIF24 activity. In *Chlamydomonas*, dephosphorylated FLS2 enters cilia by binding to IFT-B and phosphorylates the KIF24 homolog. Upon disassembly, tubulins are ubiquitylated by unknown mechanisms. IFT-A binds to K63-linked ubiquitin chains and mediates removal.

active kinase can be directed into cilia to promote disassembly by phosphorylating specific targets such as the microtubule-depolymerizing kinesin KIF24.

In cilia of *Chlamydomonas*, a ubiquitin conjugation system has been identified more than a decade ago (Huang et al., 2009), yet the involvement of ubiquitin in cilia disassembly has only recently been demonstrated. Despite a massive rise in the ubiquitin levels in shortening cilia, semi-quantitative mass spectrometric analysis of a temperature-sensitive *Chlamydomonas* model has only detected an increase in ubiquitylation of α-tubulin and ubiquitin itself (Wang et al., 2019). The study further revealed α-tubulin poly-ubiquitylation

by K63 chains, which allows binding to the IFT-A subunit IFT139 for tubulin removal via retrograde IFT (**Figure 2D**; Wang et al., 2019). Intriguingly, the authors also observed an increase in K11 and K48 chains in response to cilia shortening. K11 chains are also assembled by the anaphase-promoting complex to drive proteasomal degradation of substrates during mitosis, suggesting potential mechanisms for cell cycle-dependent regulation (Matsumoto et al., 2010).

OUTLOOK

As we are gathering increasing evidence for the existence of a ciliary ubiquitylation machinery involved in protein trafficking, signaling, disassembly, and potentially protein quality control, its identity remains elusive. Similarly, antagonistic cilia-specific DUBs as well as protein phosphatases that counterbalance known kinases await their identification. Powerful unbiased genetic and proteomic screening technologies have been applied to primary cilia (Mick et al., 2015; Kohli et al., 2017; Breslow et al., 2018; Pusapati et al., 2018) and promise to reveal the missing links that modulate manifold dynamic processes in cilia by PTM.

AUTHOR CONTRIBUTIONS

EM wrote the first draft of the manuscript. TS conceptualized and prepared the figures. DM wrote sections of the manuscript. All authors contributed to the conception of the article, manuscript revision, and read and approved the submitted version.

FUNDING

The authors acknowledge support by the Deutsche Forschungsgemeinschaft (DFG, German Research Foundation) and Saarland University within the funding programme Open Access Publishing. This work was supported by the DFG grant SFB894/TPA-22 (to DM).

ACKNOWLEDGMENTS

The authors thank D. Breslow and B. Schrul for comments on the manuscript and N. Byers and V. Chaumet for critically reading the manuscript. They apologize to all colleagues whose work could not be mentioned due to length restrictions.

REFERENCES

Anvarian, Z., Mykytyn, K., Mukhopadhyay, S., Pedersen, L. B., and Christensen, S. T. (2019). Cellular signalling by primary cilia in development, organ function and disease. *Nat. Rev. Nephrol.* 15, 199–219. doi: 10.1038/s41581-019-0116-9

Bachmann, V. A., Mayrhofer, J. E., Ilouz, R., Tschaikner, P., Raffeiner, P., Röck, R., et al. (2016). Gpr161 anchoring of PKA consolidates GPCR and cAMP signaling. *Proc. Natl. Acad. Sci. U.S.A.* 113, 7786–7791. doi: 10.1073/pnas.1608061113

Baker, K., and Beales, P. L. (2009). Making sense of cilia in disease: The human ciliopathies. *Am. J. Med. Genet. C Semin. Med. Genet.* 151, 281–295. doi: 10.1002/ajmg.c.30231

Bernabé-Rubio, M., and Alonso, M. A. (2017). Routes and machinery of primary cilium biogenesis. *Cell. Mol. Life Sci. CMLS* 74, 4077–4095. doi: 10.1007/s00018-017-2570-5

Bernatik, O., Pejskova, P., Vyslouzil, D., Hanakova, K., Zdrahal, Z., and Cajanek, L. (2020). Phosphorylation of multiple proteins involved in ciliogenesis by Tau Tubulin kinase 2. *Mol. Biol. Cell* 31, 1032–1046. doi: 10.1091/mbc.E19-06-0334

Bertolotti, A. (2018). The split protein phosphatase system. *Biochem. J.* 475, 3707–3723. doi: 10.1042/BCJ20170726

Blacque, O. E., Scheidel, N., and Kuhns, S. (2018). Rab GTPases in cilium formation and function. *Small GTPases* 9, 76–94. doi: 10.1080/21541248.2017.1353847

Breslow, D. K., and Holland, A. J. (2019). Mechanism and regulation of centriole and cilium biogenesis. *Annu. Rev. Biochem.* 88, 691–724. doi: 10.1146/annurev-biochem-013118-111153

Breslow, D. K., Hoogendoorn, S., Kopp, A. R., Morgens, D. W., Vu, B. K., Kennedy, M. C., et al. (2018). A CRISPR-based screen for Hedgehog signaling provides insights into ciliary function and ciliopathies. *Nat. Genet.* 50, 460–471. doi: 10.1038/s41588-018-0054-7

Briscoe, J., and Novitch, B. G. (2008). Regulatory pathways linking progenitor patterning, cell fates and neurogenesis in the ventral neural tube. *Philos. Trans. R. Soc. Lond. B. Biol. Sci.* 363, 57–70. doi: 10.1098/rstb.2006.2012

Čajánek, L., and Nigg, E. A. (2014). Cep164 triggers ciliogenesis by recruiting Tau tubulin kinase 2 to the mother centriole. *Proc. Natl. Acad. Sci. U.S.A.* 111, E2841–E2850. doi: 10.1073/pnas.1401777111

Cao, M., Li, G., and Pan, J. (2009). "Regulation of cilia assembly, disassembly, and length by protein phosphorylation," in *Methods in Cell Biology Primary Cilia*, Chap. 17, ed. R. D. Sloboda (Cambridge, MA: Academic Press), 333–346. doi: 10.1016/S0091-679X(08)94017-6

Chávez, M., Ena, S., Van Sande, J., de Kerchove d'Exaerde, A., Schurmans, S., and Schiffmann, S. N. (2015). Modulation of ciliary phosphoinositide content regulates trafficking and sonic hedgehog signaling output. *Dev. Cell* 34, 338–350. doi: 10.1016/j.devcel.2015.06.016

Clague, M. J., Urbé, S., and Komander, D. (2019). Breaking the chains: deubiquitylating enzyme specificity begets function. *Nat. Rev. Mol. Cell Biol.* 20, 338–352. doi: 10.1038/s41580-019-0099-1

D'Angiolella, V., Donato, V., Vijayakumar, S., Saraf, A., Florens, L., Washburn, M. P., et al. (2010). SCF Cyclin F controls centrosome homeostasis and mitotic fidelity through CP110 degradation. *Nature* 466, 138–142. doi: 10.1038/nature09140

Datta, P., Allamargot, C., Hudson, J. S., Andersen, E. K., Bhattarai, S., Drack, A. V., et al. (2015). Accumulation of non-outer segment proteins in the outer segment underlies photoreceptor degeneration in Bardet-Biedl syndrome. *Proc. Natl. Acad. Sci. U.S.A.* 112, E4400–E4409. doi: 10.1073/pnas.1510111112

Desai, P. B., Stuck, M. W., Lv, B., and Pazour, G. J. (2020). Ubiquitin links smoothened to intraflagellar transport to regulate Hedgehog signaling. *J. Cell Biol.* 219:e201912104. doi: 10.1083/jcb.201912104

Forsythe, E., Kenny, J., Bacchelli, C., and Beales, P. L. (2018). Managing bardet-biedl syndrome-now and in the future. *Front. Pediatr.* 6:23. doi: 10.3389/fped.2018.00023

Garcia, G., Raleigh, D. R., and Reiter, J. F. (2018). How the ciliary membrane is organized inside-out to communicate outside-in. *Curr. Biol.* 28, R421–R434. doi: 10.1016/j.cub.2018.03.010

Garcia-Gonzalo, F. R., Phua, S. C., Roberson, E. C., Garcia, G., Abedin, M., Schurmans, S., et al. (2015). Phosphoinositides regulate ciliary protein trafficking to modulate hedgehog signaling. *Dev. Cell* 34, 400–409. doi: 10.1016/j.devcel.2015.08.001

Garcia-Gonzalo, F. R., and Reiter, J. F. (2017). Open sesame: how transition fibers and the transition zone control ciliary composition. *Cold Spring Harb. Perspect. Biol.* 9:a028134. doi: 10.1101/cshperspect.a028134

Gigante, E. D., and Caspary, T. (2020). Signaling in the primary cilium through the lens of the Hedgehog pathway. *Wiley Interdiscip. Rev. Dev. Biol.* 9:e377. doi: 10.1002/wdev.377

Goetz, S. C., and Anderson, K. V. (2010). The primary cilium: a signaling center during vertebrate development. *Nat. Rev. Genet.* 11, 331–344. doi: 10.1038/nrg2774.The

Goetz, S. C., Liem, K. F. J., and Anderson, K. V. (2012). The spinocerebellar ataxia-associated gene Tau tubulin kinase 2 controls the initiation of ciliogenesis. *Cell* 151, 847–858. doi: 10.1016/j.cell.2012.10.010

Gonçalves, J., and Pelletier, L. (2017). The ciliary transition zone: finding the pieces and assembling the gate. *Mol. Cells* 40, 243–253. doi: 10.14348/molcells.2017.0054

Hilgendorf, K. I., Johnson, C. T., Mezger, A., Rice, S. L., Norris, A. M., Demeter, J., et al. (2019). Omega-3 fatty acids activate ciliary FFAR4 to control adipogenesis. *Cell* 179, 1289–1305.e21. doi: 10.1016/j.cell.2019.11.005

Hossain, D., Javadi Esfehani, Y., Das, A., and Tsang, W. Y. (2017). Cep78 controls centrosome homeostasis by inhibiting EDD-DYRK2-DDB1VprBP. *EMBO Rep.* 18, 632–644. doi: 10.15252/embr.201642377

Huang, K., Diener, D. R., and Rosenbaum, J. L. (2009). The ubiquitin conjugation system is involved in the disassembly of cilia and flagella. *J. Cell Biol.* 186, 601–613. doi: 10.1083/jcb.200903066

Huang, N., Zhang, D., Li, F., Chai, P., Wang, S., Teng, J., et al. (2018). M-Phase Phosphoprotein 9 regulates ciliogenesis by modulating CP110-CEP97 complex localization at the mother centriole. *Nat. Commun.* 9:4511. doi: 10.1038/s41467-018-06990-9

Ishikawa, H., Thompson, J. III, Yates, J. R., and Marshall, W. F. (2012). Proteomic analysis of mammalian primary cilia. *Curr. Biol.* 22, 414–419. doi: 10.1016/j.cub.2012.01.031

Janke, C., and Magiera, M. M. (2020). The tubulin code and its role in controlling microtubule properties and functions. *Nat. Rev. Mol. Cell Biol.* 21, 307–326. doi: 10.1038/s41580-020-0214-3

Jiang, W., Yao, X., Shan, Z., Li, W., Gao, Y., and Zhang, Q. (2019). E3 ligase Herc4 regulates Hedgehog signalling through promoting Smoothened degradation. *J. Mol. Cell Biol.* 11, 791–803. doi: 10.1093/jmcb/mjz024

Jin, H., White, S. R., Shida, T., Schulz, S., Aguiar, M., Gygi, S. P., et al. (2010). The conserved Bardet-Biedl syndrome proteins assemble a coat that traffics membrane proteins to cilia. *Cell* 141, 1208–1219. doi: 10.1016/j.cell.2010.05.015

Kerek, E. M., Yoon, K. H., Luo, S. Y., Chen, J., Valencia, R., Julien, O., et al. (2021). A conserved acetylation switch enables pharmacological control of tubby-like protein stability. *J. Biol. Chem.* 296:100073. doi: 10.1074/jbc.RA120.015839

Kim, J., Kato, M., and Beachy, P. A. (2009). Gli2 trafficking links Hedgehog-dependent activation of Smoothened in the primary cilium to transcriptional activation in the nucleus. *Proc. Natl. Acad. Sci. U.S.A.* 106, 21666–21671. doi: 10.1073/pnas.0912180106

Kim, J. C., Hsia, E. Y., Brigui, A., Plessis, A., Beachy, P. A., and Zheng, X. (2015). The role of ciliary trafficking in Hedgehog receptor signaling. *Sci. Signal.* 8, ra55–ra55. doi: 10.1126/scisignal.aaa5622

Kim, S., Lee, K., Choi, J.-H., Ringstad, N., and Dynlacht, B. D. (2015). Nek2 activation of Kif24 ensures cilium disassembly during the cell cycle. *Nat. Commun.* 6:8087. doi: 10.1038/ncomms9087

Kobayashi, T., Tsang, W. Y., Li, J., Lane, W., and Dynlacht, B. D. (2011). Centriolar kinesin Kif24 interacts with CP110 to remodel microtubules and regulate ciliogenesis. *Cell* 145, 914–925. doi: 10.1016/j.cell.2011.04.028

Kohli, P., Höhne, M., Jüngst, C., Bertsch, S., Ebert, L. K., Schauss, A. C., et al. (2017). The ciliary membrane-associated proteome reveals actin-binding proteins as key components of cilia. *EMBO Rep.* 18, 1521–1535. doi: 10.15252/embr.201643846

Kong, J. H., Siebold, C., and Rohatgi, R. (2019). Biochemical mechanisms of vertebrate hedgehog signaling. *Development* 146:dev166892. doi: 10.1242/dev.166892

Kong, J. H., Young, C. B., Pusapati, G. V., Patel, C. B., Ho, S., Krishnan, A., et al. (2020). A ubiquitin-based mechanism for the oligogenic inheritance of heterotaxy and heart defects. *bioRxiv [Preprint]* doi: 10.1101/2020.05.25.113944

Kumar, D., and Reiter, J. (2021). How the centriole builds its cilium: of mothers, daughters, and the acquisition of appendages. *Curr. Opin. Struct. Biol.* 66, 41–48. doi: 10.1016/j.sbi.2020.09.006

Langousis, G., Shimogawa, M. M., Saada, E. A., Vashisht, A. A., Spreafico, R., Nager, A. R., et al. (2016). Loss of the BBSome perturbs endocytic trafficking and disrupts virulence of Trypanosoma brucei. *Proc. Natl. Acad. Sci. U.S.A.* 113, 632–637. doi: 10.1073/pnas.1518079113

Li, J., D'Angiolella, V., Seeley, E. S., Kim, S., Kobayashi, T., Fu, W., et al. (2013). USP33 regulates centrosome biogenesis via deubiquitination of the centriolar protein CP110. *Nature* 495, 255–259. doi: 10.1038/nature11941

Liang, Y., Meng, D., Zhu, B., and Pan, J. (2016). Mechanism of ciliary disassembly. *Cell. Mol. Life Sci.* 73, 1787–1802. doi: 10.1007/s00018-016-2148-7

Liu, M., Liu, A., Wang, J., Zhang, Y., Li, Y., Su, Y., et al. (2020). Competition between two phosphatases fine-tunes Hedgehog signaling. *J. Cell Biol.* 220:e202010078. doi: 10.1083/jcb.202010078

Lo, C.-H., Lin, I.-H., Yang, T. T., Huang, Y.-C., Tanos, B. E., Chou, P.-C., et al. (2019). Phosphorylation of CEP83 by TTBK2 is necessary for cilia initiation. *J. Cell Biol.* 218, 3489–3505. doi: 10.1083/jcb.201811142

Lu, Q., Insinna, C., Ott, C., Stauffer, J., Pintado, P. A., Rahajeng, J., et al. (2015). Early steps in primary cilium assembly require EHD1/EHD3-dependent ciliary vesicle formation. *Nat. Cell Biol.* 17, 228–240. doi: 10.1038/ncb3109

Ma, G., Li, S., Han, Y., Li, S., Yue, T., Wang, B., et al. (2016). Regulation of smoothened trafficking and hedgehog signaling by the SUMO pathway. *Dev. Cell* 39, 438–451. doi: 10.1016/j.devcel.2016.09.014

Matsumoto, M. L., Wickliffe, K. E., Dong, K. C., Yu, C., Bosanac, I., Bustos, D., et al. (2010). K11-Linked polyubiquitination in cell cycle control revealed by a K11 linkage-specific antibody. *Mol. Cell* 39, 477–484. doi: 10.1016/j.molcel.2010.07.001

May, E. A., Kalocsay, M., Galtier, D., Auriac, I., Schuster, P. S., Gygi, S. P., et al. (2021). Time-resolved proteomics profiling of the ciliary Hedgehog response. *J. Cell Biol.* doi: 10.1083/jcb.202007207 [Epub ahead of print].

McIntyre, J. C., Joiner, A. M., Zhang, L., Iñiguez-Lluhí, J., and Martens, J. R. (2015). SUMOylation regulates ciliary localization of olfactory signaling proteins. *J. Cell Sci.* 128, 1934–1945. doi: 10.1242/jcs.164673

Mick, D. U., Rodrigues, R. B., Leib, R. D., Adams, C. M., Chien, A. S., Gygi, S. P., et al. (2015). Proteomics of primary cilia by proximity labeling. *Dev. Cell* 35, 497–512. doi: 10.1016/j.devcel.2015.10.015

Miller, C. J., and Turk, B. E. (2018). Homing in: mechanisms of substrate targeting by protein kinases. *Trends Biochem. Sci.* 43, 380–394. doi: 10.1016/j.tibs.2018.02.009

Moghe, S., Jiang, F., Miura, Y., Cerny, R. L., Tsai, M.-Y., and Furukawa, M. (2012). The CUL3−KLHL18 ligase regulates mitotic entry and ubiquitylates Aurora-A. *Biol. Open* 1, 82–91. doi: 10.1242/bio.2011018

Mukhopadhyay, S., and Jackson, P. K. (2011). The tubby family proteins. *Genome Biol.* 12:225. doi: 10.1186/gb-2011-12-6-225

Mukhopadhyay, S., Wen, X., Ratti, N., Loktev, A., Rangell, L., Scales, S. J., et al. (2013). The ciliary G-protein-coupled receptor Gpr161 negatively regulates the Sonic hedgehog pathway via cAMP signaling. *Cell* 152, 210–223. doi: 10.1016/j.cell.2012.12.026

Nachury, M. V., and Mick, D. U. (2019). Establishing and regulating the composition of cilia for signal transduction. *Nat. Rev. Mol. Cell Biol.* 20, 389–405. doi: 10.1038/s41580-019-0116-4

Nagai, T., Mukoyama, S., Kagiwada, H., Goshima, N., and Mizuno, K. (2018). Cullin-3-KCTD10-mediated CEP97 degradation promotes primary cilium formation. *J. Cell Sci.* 131:jcs219527. doi: 10.1242/jcs.219527

Niewiadomski, P., Kong, J. H., Ahrends, R., Ma, Y., Humke, E. W., Khan, S., et al. (2014). Gli protein activity is controlled by multisite phosphorylation in vertebrate hedgehog signaling. *Cell Rep.* 6, 168–181. doi: 10.1016/j.celrep.2013.12.003

Niewiadomski, P., Niedziółka, S. M., Markiewicz, Ł, Uśpieński, T., Baran, B., and Chojnowska, K. (2019). Gli proteins: regulation in development and cancer. *Cells* 8:147. doi: 10.3390/cells8020147

Pal, K., Hwang, S., Somatilaka, B., Badgandi, H., Jackson, P. K., DeFea, K., et al. (2016). Smoothened determines β-arrestin–mediated removal of the G protein–coupled receptor Gpr161 from the primary cilium. *J. Cell Biol.* 212, 861–875. doi: 10.1083/jcb.201506132

Patwardhan, A., Cheng, N., and Trejo, J. (2021). Post-translational modifications of G Protein–Coupled receptors control cellular signaling dynamics in space and time. *Pharmacol. Rev.* 73, 120–151. doi: 10.1124/pharmrev.120.000082

Pazour, G. J., Agrin, N., Leszyk, J., and Witman, G. B. (2005). Proteomic analysis of a eukaryotic cilium. *J. Cell Biol.* 170, 103–113. doi: 10.1083/jcb.200504008

Pugacheva, E. N., Jablonski, S. A., Hartman, T. R., Henske, E. P., and Golemis, E. A. (2007). HEF1-dependent aurora a activation induces disassembly of the primary cilium. *Cell* 129, 1351–1363. doi: 10.1016/j.cell.2007.04.035

Pusapati, G. V., Kong, J. H., Patel, B. B., Krishnan, A., Sagner, A., Kinnebrew, M., et al. (2018). CRISPR screens uncover genes that regulate target cell sensitivity to the morphogen sonic hedgehog. *Dev. Cell* 44, 113–129.e8. doi: 10.1016/j.devcel.2017.12.003

Raman, M., Sergeev, M., Garnaas, M., Lydeard, J. R., Huttlin, E. L., Goessling, W., et al. (2015). Systematic proteomics of the VCP–UBXD adaptor network identifies a role for UBXN10 in regulating ciliogenesis. *Nat. Cell Biol.* 17, 1356–1369. doi: 10.1038/ncb3238

Reiter, J. F., and Leroux, M. R. (2017). Genes and molecular pathways underpinning ciliopathies. *Nat. Rev. Mol. Cell Biol.* 18, 533–547. doi: 10.1038/nrm.2017.60

Rohatgi, R., Milenkovic, L., and Scott, M. P. (2007). Patched1 regulates hedgehog signaling at the primary cilium. *Science* 317, 372–376. doi: 10.1126/science.1139740

Roy, K., and Marin, E. P. (2019). Lipid modifications in cilia biology. *J. Clin. Med.* 8, 921–921. doi: 10.3390/jcm8070921

Sánchez, I., and Dynlacht, B. D. (2016). Cilium assembly and disassembly. *Nat. Cell Biol.* 18, 711–717. doi: 10.1038/ncb3370

Satir, P., and Christensen, S. T. (2007). Overview of structure and function of mammalian cilia. *Annu. Rev. Physiol.* 69, 377–400. doi: 10.1146/annurev.physiol.69.040705.141236

Schmid, F. M., Schou, K. B., Vilhelm, M. J., Holm, M. S., Breslin, L., Farinelli, P., et al. (2018). IFT20 modulates ciliary PDGFRα signaling by regulating the stability of Cbl E3 ubiquitin ligases. *J. Cell Biol.* 217, 151–161. doi: 10.1083/jcb.201611050

Schmidt, K. N., Kuhns, S., Neuner, A., Hub, B., Zentgraf, H., and Pereira, G. (2012). Cep164 mediates vesicular docking to the mother centriole during early steps of ciliogenesis. *J. Cell Biol.* 199, 1083–1101. doi: 10.1083/jcb.201202126

Schmidt, T. I., Kleylein-Sohn, J., Westendorf, J., Le Clech, M., Lavoie, S. B., Stierhof, Y.-D., et al. (2009). Control of centriole length by CPAP and CP110. *Curr. Biol. CB* 19, 1005–1011. doi: 10.1016/j.cub.2009.05.016

Shearer, R. F., and Saunders, D. N. (2016). Regulation of primary cilia formation by the ubiquitin-proteasome system. *Biochem. Soc. Trans.* 44, 1265–1271. doi: 10.1042/BST20160174

Sherpa, R. T., Mohieldin, A. M., Pala, R., Wachten, D., Ostrom, R. S., and Nauli, S. M. (2019). Sensory primary cilium is a responsive cAMP microdomain in renal epithelia. *Sci. Rep.* 9:6523. doi: 10.1038/s41598-019-43002-2

Shimada, I. S., Somatilaka, B. N., Hwang, S.-H., Anderson, A. G., Shelton, J. M., Rajaram, V., et al. (2019). Derepression of sonic hedgehog signaling upon Gpr161 deletion unravels forebrain and ventricular abnormalities. *Dev. Biol.* 450, 47–62. doi: 10.1016/j.ydbio.2019.03.011

Shinde, S. R., Nager, A. R., and Nachury, M. V. (2020). Ubiquitin chains earmark GPCRs for BBSome-mediated removal from cilia. *J. Cell Biol.* 219:e202003020. doi: 10.1083/jcb.202003020

Sorokin, S. P. (1968). Centriole formation and ciliogenesis. *Aspen Emphysema Conf.* 11, 213–216.

Spektor, A., Tsang, W. Y., Khoo, D., and Dynlacht, B. D. (2007). Cep97 and CP110 suppress a cilia assembly program. *Cell* 130, 678–690. doi: 10.1016/j.cell.2007.06.027

Su, Y., Ospina, J. K., Zhang, J., Michelson, A. P., Schoen, A. M., and Zhu, A. J. (2011). Sequential phosphorylation of smoothened transduces graded hedgehog signaling. *Sci. Signal.* 4:ra43. doi: 10.1126/scisignal.2001747

Sung, C.-H., and Leroux, M. R. (2013). The roles of evolutionarily conserved functional modules in cilia-related trafficking. *Nat. Cell Biol.* 15, 1387–1397. doi: 10.1038/ncb2888

Swatek, K. N., and Komander, D. (2016). Ubiquitin modifications. *Cell Res.* 26, 399–422. doi: 10.1038/cr.2016.39

Tajhya, R., and Delling, M. (2020). New insights into ion channel-dependent signalling during left-right patterning. *J. Physiol.* 598, 1741–1752. doi: 10.1113/JP277835

Taylor, S. S., Yang, J., Wu, J., Haste, N. M., Radzio-Andzelm, E., and Anand, G. (2004). PKA: a portrait of protein kinase dynamics. *Biochim. Biophys. Acta BBA Proteins Proteom.* 1697, 259–269. doi: 10.1016/j.bbapap.2003.11.029

Tomizawa, K., Omori, A., Ohtake, A., Sato, K., and Takahashi, M. (2001). Tau-tubulin kinase phosphorylates tau at Ser-208 and Ser-210, sites found in paired helical filament-tau. *FEBS Lett.* 492, 221–227. doi: 10.1016/S0014-5793(01)02256-6

Tsai, J.-J., Hsu, W.-B., Liu, J.-H., Chang, C.-W., and Tang, T. K. (2019). CEP120 interacts with C2CD3 and Talpid3 and is required for centriole appendage assembly and ciliogenesis. *Sci. Rep.* 9:6037. doi: 10.1038/s41598-019-42577-0

Tuson, M., He, M., and Anderson, K. V. (2011). Protein kinase A acts at the basal body of the primary cilium to prevent Gli2 activation and ventralization of the mouse neural tube. *Dev. Camb. Engl.* 138, 4921–4930. doi: 10.1242/dev.070805

Viol, L., Hata, S., Pastor-Peidro, A., Neuner, A., Murke, F., Wuchter, P., et al. (2020). Nek2 kinase displaces distal appendages from the mother centriole prior to mitosis. *J. Cell Biol.* 219:e201907136. doi: 10.1083/jcb.201907136

Vu, L. D., Gevaert, K., and De Smet, I. (2018). Protein language: post-translational modifications talking to each other. *Trends Plant Sci.* 23, 1068–1080. doi: 10.1016/j.tplants.2018.09.004

Wang, L., and Dynlacht, B. D. (2018). The regulation of cilium assembly and disassembly in development and disease. *Dev. Camb. Engl.* 145:dev151407. doi: 10.1242/dev.151407

Wang, Q., Peng, Z., Long, H., Deng, X., and Huang, K. (2019). Polyubiquitylation of α-tubulin at K304 is required for flagellar disassembly in Chlamydomonas. *J. Cell Sci.* 132:jcs229047. doi: 10.1242/jcs.229047

Webb, S., Mukhopadhyay, A. G., and Roberts, A. J. (2020). Intraflagellar transport trains and motors: insights from structure. *Semin. Cell Dev. Biol.* 107, 82–90. doi: 10.1016/j.semcdb.2020.05.021

Yang, T. T., Su, J., Wang, W.-J., Craige, B., Witman, G. B., Tsou, M.-F. B., et al. (2015). Superresolution pattern recognition reveals the architectural map of the ciliary transition zone. *Sci. Rep.* 5:14096. doi: 10.1038/srep14096

Yau, R., and Rape, M. (2016). The increasing complexity of the ubiquitin code. *Nat. Cell Biol.* 18, 579–586. doi: 10.1038/ncb3358

Ye, F., Nager, A. R., and Nachury, M. V. (2018). BBSome trains remove activated GPCRs from cilia by enabling passage through the transition zone. *J. Cell Biol.* 217, 1847–1868. doi: 10.1083/jcb.201709041

Ye, X., Zeng, H., Ning, G., Reiter, J. F., and Liu, A. (2014). C2cd3 is critical for centriolar distal appendage assembly and ciliary vesicle docking in mammals. *Proc. Natl. Acad. Sci. U.S.A.* 111, 2164–2169. doi: 10.1073/pnas.1318737111

Yeyati, P. L., Schiller, R., Mali, G., Kasioulis, I., Kawamura, A., Adams, I. R., et al. (2017). KDM3A coordinates actin dynamics with intraflagellar transport to regulate cilia stability. *J. Cell Biol.* 216, 999–1013. doi: 10.1083/jcb.201607032

Zhao, Q., Li, S., Shao, S., Wang, Z., and Pan, J. (2020). FLS2 is a CDK-like kinase that directly binds IFT70 and is required for proper ciliary disassembly in Chlamydomonas. *PLoS Genet.* 16:e1008561. doi: 10.1371/journal.pgen.1008561

Conflict of Interest: The authors declare that the research was conducted in the absence of any commercial or financial relationships that could be construed as a potential conflict of interest.

frontiers in Cell and Developmental Biology

ORIGINAL RESEARCH
published: 22 April 2021
doi: 10.3389/fcell.2021.656273

Colchicine Blocks Tubulin Heterodimer Recycling by Tubulin Cofactors TBCA, TBCB, and TBCE

Sofia Nolasco[1,2], Javier Bellido[3†], Marina Serna[4], Bruno Carmona[2,5], Helena Soares[2,5] and Juan Carlos Zabala[3]**

[1] Faculdade de Medicina Veterinária, CIISA – Centro de Investigação Interdisciplinar em Sanidade Animal, Universidade de Lisboa, Lisbon, Portugal, [2] Escola Superior de Tecnologia da Saúde de Lisboa, Instituto Politécnico de Lisboa, Lisbon, Portugal, [3] Departamento de Biología Molecular, Facultad de Medicina, Universidad de Cantabria, Santander, Spain, [4] Spanish National Cancer Research Center, CNIO, Madrid, Spain, [5] Centro de Química Estrutural – Faculdade de Ciências da Universidade de Lisboa, Lisbon, Portugal

OPEN ACCESS

Edited by:
Pedro Roda-Navarro,
Universidad Complutense de Madrid, Spain

Reviewed by:
Richard Luduena,
The University of Texas Health Science Center at San Antonio, United States
Nagaraj Balasubramanian,
Indian Institute of Science Education and Research, Pune, India

***Correspondence:**
Helena Soares
mhsoares@fc.ul.pt
Juan Carlos Zabala
juan.zabala@unican.es

†Present address:
Javier Bellido,
Departamento de Ámbito Científico Tecnológico, Centro de Educación de Personas Adultas (CEPA), Santoña, Spain

Specialty section:
This article was submitted to Cell Adhesion and Migration, a section of the journal Frontiers in Cell and Developmental Biology

Received: 20 January 2021
Accepted: 29 March 2021
Published: 22 April 2021

Citation:
Nolasco S, Bellido J, Serna M, Carmona B, Soares H and Zabala JC (2021) Colchicine Blocks Tubulin Heterodimer Recycling by Tubulin Cofactors TBCA, TBCB, and TBCE. Front. Cell Dev. Biol. 9:656273. doi: 10.3389/fcell.2021.656273

Colchicine has been used to treat gout and, more recently, to effectively prevent autoinflammatory diseases and both primary and recurrent episodes of pericarditis. The anti-inflammatory action of colchicine seems to result from irreversible inhibition of tubulin polymerization and microtubule (MT) assembly by binding to the tubulin heterodimer, avoiding the signal transduction required to the activation of the entire NLRP3 inflammasome. Emerging results show that the MT network is a potential regulator of cardiac mechanics. Here, we investigated how colchicine impacts in tubulin folding cofactors TBCA, TBCB, and TBCE activities. We show that TBCA is abundant in mouse heart insoluble protein extracts. Also, a decrease of the TBCA/β-tubulin complex followed by an increase of free TBCA is observed in human cells treated with colchicine. The presence of free TBCA is not observed in cells treated with other anti-mitotic agents such as nocodazole or cold shock, neither after translation inhibition by cycloheximide. *In vitro* assays show that colchicine inhibits tubulin heterodimer dissociation by TBCE/TBCB, probably by interfering with interactions of TBCE with tubulin dimers, leading to free TBCA. Manipulation of TBCA levels, either by RNAi or overexpression results in decreased levels of tubulin heterodimers. Together, these data strongly suggest that TBCA is mainly receiving β-tubulin from the dissociation of pre-existing heterodimers instead of newly synthesized tubulins. The TBCE/TBCB+TBCA system is crucial for controlling the critical concentration of free tubulin heterodimers and MT dynamics in the cells by recycling the tubulin heterodimers. It is conceivable that colchicine affects tubulin heterodimer recycling through the TBCE/TBCB+TBCA system producing the known benefits in the treatment of pericardium inflammation.

Keywords: colchicine, tubulin cofactors, TBCA, TBCB, TBCE, tubulin heterodimer dissociation, microtubule cytoskeleton

INTRODUCTION

Microtubules (MTs) are dynamic polymers of heterodimers of α- and β-tubulin that grow and shrink by the addition and removal of tubulin heterodimers at their ends. MT arrays are present in almost all eukaryotic cells constituting, together with actin and intermediate filaments, the cytoskeleton. MTs, in crosstalk with other cytoskeleton members, play many roles in cell spatial

organization, the establishment of cellular asymmetries and polarity, intracellular transport, cell migration, and morphogenesis (Dogterom and Koenderink, 2019). These polymers are also the main constituents of complex structures such as the mitotic and meiotic spindles, centrioles/basal bodies, and the ciliary axoneme, being involved in cell division, motility, and signaling. The diversity of MT functions depends on the biochemical variety of tubulin pools generated either by the constitutive or tissue-specific expression patterns of the tubulin gene family members and by tubulin post-translational modifications (Roll-Mecak, 2020). Additionally, MTs are modulated by a vast number of MT-binding proteins with multiple activities (for review, Goodson and Jonasson, 2018).

In vivo, the dynamic behavior of MTs relies on the existence of competent tubulin heterodimers originated either from *de novo* synthesis or MTs recycling (for review Gonçalves et al., 2010). For this, eukaryotic cells are equipped with a few molecular chaperones (cytosolic chaperonin CCT (cytosolic chaperonin-containing TCP1) and its cochaperone prefoldin) (Cowan and Lewis, 2001; Lopez et al., 2015), and a group of specific tubulin cofactors (TBCA-E) (Lewis et al., 1997; Lopez-Fanarraga et al., 2001). Along with tubulin folding, tubulin cofactors assist tubulin heterodimer assembly/dissociation, as well as tubulin degradation (Lewis et al., 1997; Lopez-Fanarraga et al., 2001; Kortazar et al., 2007; Voloshin et al., 2010). Therefore, *in vivo*, tubulin cofactors play pivotal roles in maintaining tubulin pools and tubulin heterodimers recycling/degradation by controlling their native structure's quality. This also indicates that TBCs can be involved in MT cytoskeleton remodeling and the assembly/disassembly of specific MT populations and structures. The overexpression of TBCD and TBCE completely disrupts the MT cytoskeleton (Martín et al., 2000; Kortazar et al., 2006). TBCD and TBCE are capable of dissociating the tubulin heterodimer by themselves, but in the case of TBCE, its dissociation activity is highly increased by the presence of TBCB (Serna and Zabala, 2016). In fact, TBCB and TBCE stabilize the α-tubulin subunit after dimer dissociation originating a ternary complex TBCE/TBCB/α-tubulin (Carranza et al., 2013; Serna et al., 2015). Both TBCB and TBCE share a CAP-Gly and a UBL (ubiquitin-like) domain in their primary structures, but in inverted order (Serna and Zabala, 2016). The dissociation complex may also be involved in α-tubulin degradation. The UBL domains of TBCE and TBCB present a protruding arrangement suggesting the possibility of interacting with the proteasome (Serna et al., 2015), as mechanistically detailed in the review by Serna and Zabala (2016).

After tubulin heterodimer dissociation, cells avoid the toxic effect of β-tubulin (Archer et al., 1995; Abruzzi et al., 2002) by stabilizing it through the association with TBCD or/and TBCA (Carranza et al., 2013; Serna et al., 2015). In budding yeast, TBCA (Rbl2p) can rescue cells from β-tubulin overexpression and is required for meiosis (Archer et al., 1995). In contrast, in fission yeast, TBCA (Alp31) is necessary for the integrity of MTs and consequently for growth polarity (Radcliffe et al., 2000). *In vitro*, TBCA is dispensable for tubulin folding (Abruzzi et al., 2002), which contrasts with the observation that, in human cell lines, TBCA is encoded by an essential gene (Nolasco et al., 2005). Depletion of TBCA in human cells causes a decrease in soluble tubulin, modifications in MT and actin cytoskeletons organization, and G1 cell cycle arrest. Similarly, TBCA mutants in *Schizosaccharomyces pombe* and *Arabidopsis thaliana* present unstable and defective MTs structures, compromised MT organization, and cell morphology alterations (Archer et al., 1995; Radcliffe et al., 2000; Kirik et al., 2002; Steinborn et al., 2002).

Although the molecular mechanisms underlying the role of tubulin cofactors in tubulin heterodimers' maturation, tubulin recycling, and tubulin degradation have been progressively elucidated, the complete scenario of their roles *in vivo* is far from being completely understood. Different tubulin cofactors seem to play critical roles in invertebrate and vertebrate brain function/maintenance, development, and morphogenesis (Shern et al., 2003; Okumura et al., 2015; Chen et al., 2016), which is highlighted by their association with diverse neurodegenerative diseases like the giant axonal neuropathy (GAN) (Wang et al., 2005; Yang et al., 2007), amyotrophic lateral sclerosis (Helferich et al., 2018), motor neuronopathy (Martin et al., 2002; Schaefer et al., 2007; Bellouze et al., 2014), progressive neurodegenerative encephalopathy with distal spinal muscular atrophy (Sferra et al., 2016) and eventually with tauopathies (Fujiwara et al., 2020). Other syndromes, such as the recessive disorder Sanjad-Sakati syndrome (SSS), and the autosomal recessive Kenny-Caffey syndrome, were associated with TBCE mutations (Parvari et al., 2002). In general, the cells from patients with these syndromes show lower MT density/disrupted MT networks, perturbed MT polarity, and Golgi apparatus fragmentation (Martin et al., 2002; Schaefer et al., 2007; Bellouze et al., 2014; Sferra et al., 2016). TBCs have also been involved in breast cancer development suggesting that dysregulation of the tubulin heterodimer pool may impact tumor cell phenotypes and response to chemotherapy (Vadlamudi et al., 2005; Hage-Sleiman et al., 2010). The activity of tubulin cofactors has also been associated with cilia biology (Grayson et al., 2002; Lopez-Fanarraga et al., 2007; Fanarraga et al., 2010a). The complexity of the roles of tubulin cofactors indicates that these proteins may also have non-tubulin-folding activities. For example, TBCB and TBCD localize at the centrosome, and changes in these cofactors affect centrosomal γ-tubulin (Vadlamudi et al., 2005; Cunningham and Kahn, 2008; Fanarraga et al., 2010a). In *S. pombe*, genetic interactions between TBCD mutant forms with the kinetochore CENP-B-like protein and spindle components (Fedyanina et al., 2006) suggest that TBCD may play essential functions at these structures. Also, disassembly of tight and adherent junctions followed by cell dissociation from the epithelial monolayer is observed in TBCD overexpression backgrounds (Shultz et al., 2008). The study of the complexity of regulatory mechanisms involving tubulin cofactors has been neglected. Still, the activity of TBCB is regulated by post-translational modifications like phosphorylation by a p21-activated kinase (Pak1) that is essential for the polymerization of new MTs (Vadlamudi et al., 2005). Similar to *tau* and α-tubulin, TBCB also undergoes nitration, which inhibits the polymerization of new MTs (Rayala et al., 2007) by inhibiting TBCB phosphorylation. TBCB also seems to be regulated by

the non-coding micro RNA miR-1825 (Helferich et al., 2018), whereas a non-coding antisense RNA regulates TBCA during testis maturation (Nolasco et al., 2012).

MTs and/or tubulin are the targets for many small molecules that act as anti-mitotic agents. However, how these compounds interfere with the *in vivo* activities of TBCs is unknown. The importance of investigating this putative interplay relies not only on the fact that valuable information about the mechanisms underlying MT dynamics *in vivo* can be acquired but primarily because these molecules are clinically significant. For example, the anti-mitotic drug colchicine has been used as an anti-inflammatory and anti-fibrotic drug (for review, Roberts, 1987; Dalbeth et al., 2014). The uses for colchicine include chronic inflammatory diseases as gouty arthritis (Roberts, 1987; Dalbeth et al., 2014), the familial Mediterranean fever (FMF) (Goldfinger, 1972), the Behcet's disease (Yurdakul et al., 2001), a variety of dermatological conditions (e.g., epidermolysis bullosa acquisita and aphthous stomatitis), and other fibro-inflammatory diseases (Addrizzo-Harris et al., 2002; Martínez et al., 2015; Solak et al., 2017). In the last years, colchicine has also been emerging as a first-line drug to treat pericardial diseases. The anti-inflammatory properties of colchicine and the absence of effective drugs to treat COVID-19 lead to the idea that the use of colchicine may be efficient in COVID-19 treatment (Corral et al., 2020; Nasiripour et al., 2020). Therefore, several colchicine randomized controlled trials in COVID-19 are ongoing[1].

The anti-inflammatory action of colchicine seems to result from a compromised MT cytoskeleton that affects several inflammatory pathways in cells that mediate immune response like the adhesion and recruitment of neutrophils, superoxide production, inflammasome activation, the RhoA/Rho effector kinase (ROCK) pathway, and the tumor necrosis factor-alpha (TNF-α)-induced nuclear factor κB (NF-κB) pathway (for review Angelidis et al., 2018).

Virtually nothing is known about colchicine's impact on the recycling cycle and quality control of tubulin heterodimers conducted by TBCs. Here we show that the exposure of human cells to colchicine causes a decrease of the TBCA/β-tubulin complex to vestigial levels followed by an increase of free TBCA. Free TBCA was never observed in human control cells nor in cells exposed to other anti-mitotic MT depolymerizing agents like nocodazole and cold-shock, or even after translation inhibition by cycloheximide. The appearance of free TBCA is accompanied by an increase in free soluble tubulin heterodimers due to MT depolymerization. We show, in *in vitro* assays, that colchicine inhibits tubulin heterodimer dissociation by TBCE/TBCB, affecting heterodimer recycling/quality control. This result strongly suggests that MT depolymerization by colchicine treatment is not only due to the conformational alteration of the tubulin heterodimer but also to the inability of cofactors to recycle these heterodimers, which also explains the irreversible colchicine action. The manipulation of TBCA levels, either by RNAi or by overexpression, causes the decrease of tubulin heterodimers. Collectively, our data strongly suggest that TBCA is mainly receiving β-tubulin from the dissociation of pre-existing heterodimers instead of newly synthesized tubulins, which is supported by the observations using the translation inhibitor cycloheximide. Thus, we show that the system TBCE/TBCB+TBCA is crucial for the control of the critical concentration of free tubulin heterodimers and MT dynamics in the cells. The finding that colchicine affects the tubulin heterodimer recycling/degradation system TBCE/TBCB+TBCA should be taken into account in the context of colchicine's therapeutic benefits as an anti-inflammatory drug.

[1]https://clinicaltrials.gov/ct2/results?cond=COVID&term=colchicine&cntry=&state=&city=&dist

RESULTS

Colchicine Causes the Decrease of the TBCA/β-Tubulin Complex and the Detection of Free TBCA in HeLa Cells

In addition to tubulin folding, TBCs are also involved in tubulin heterodimer recycling and degradation, regulating MT dynamics by controlling the tubulin heterodimer pool competent to polymerize (Serna et al., 2015). MTs and/or tubulin are targets for many small molecules that can stabilize or destabilize these polymers due to their ability to increase or decrease MT assembly at high concentrations. These molecules also strongly compromise MT dynamics at concentrations 10- to 100-fold lower than those required to affect MT mass (for review, see Dumontet and Jordan, 2010).

Previously, we showed that TBCA knockdown causes a decreased amount of α- and β-tubulin, G1 cell cycle arrest, and cell death in human cell lines (Nolasco et al., 2005). Contrary to TBCB, TBCE, and TBCD, TBCA is not able to dissociate the native tubulin heterodimer by itself (Martín et al., 2000; Kortazar et al., 2006, 2007; Carranza et al., 2013), but after tubulin heterodimer dissociation, TBCA forms a stable complex with β-tubulin, being responsible for its recycling/degradation (Kortazar et al., 2007).

To investigate how the *in vivo* activities of TBCA are affected by MT depolymerizing agents, we treated HeLa cells with: a) colchicine (5 μM), a tubulin-binding anti-mitotic drug, with clinical relevance, that depolymerizes MTs irreversibly; b) nocodazole (30 μM), a tubulin-binding anti-mitotic drug, a rapid and reversible inhibitor of MT polymerization (De Brabander et al., 1976); and c) cold shock, low temperature, that is well-established to promote MT depolymerization (Weisenberg, 1972; Shelanski et al., 1973). The exposure of cells to all different treatments was performed for 15, 30, and 60 min after which soluble native protein extracts were prepared and analyzed by 6% (w/v) non-denaturing-PAGE. As migration markers, purified α/β-tubulin heterodimers and TBCA were simultaneously analyzed with the protein extracts of cells treated with distinct MT depolymerizing agents (**Figure 1**). These analyses were followed by western blot using antibodies against TBCA and β-tubulin (**Figure 1**). As expected for purified TBCA (free TBCA), we observed a unique band in the lane (**Figures 1A1,B1,C1**). However, according to Llosa et al. (1996) when protein extracts from cells are analyzed in this type of

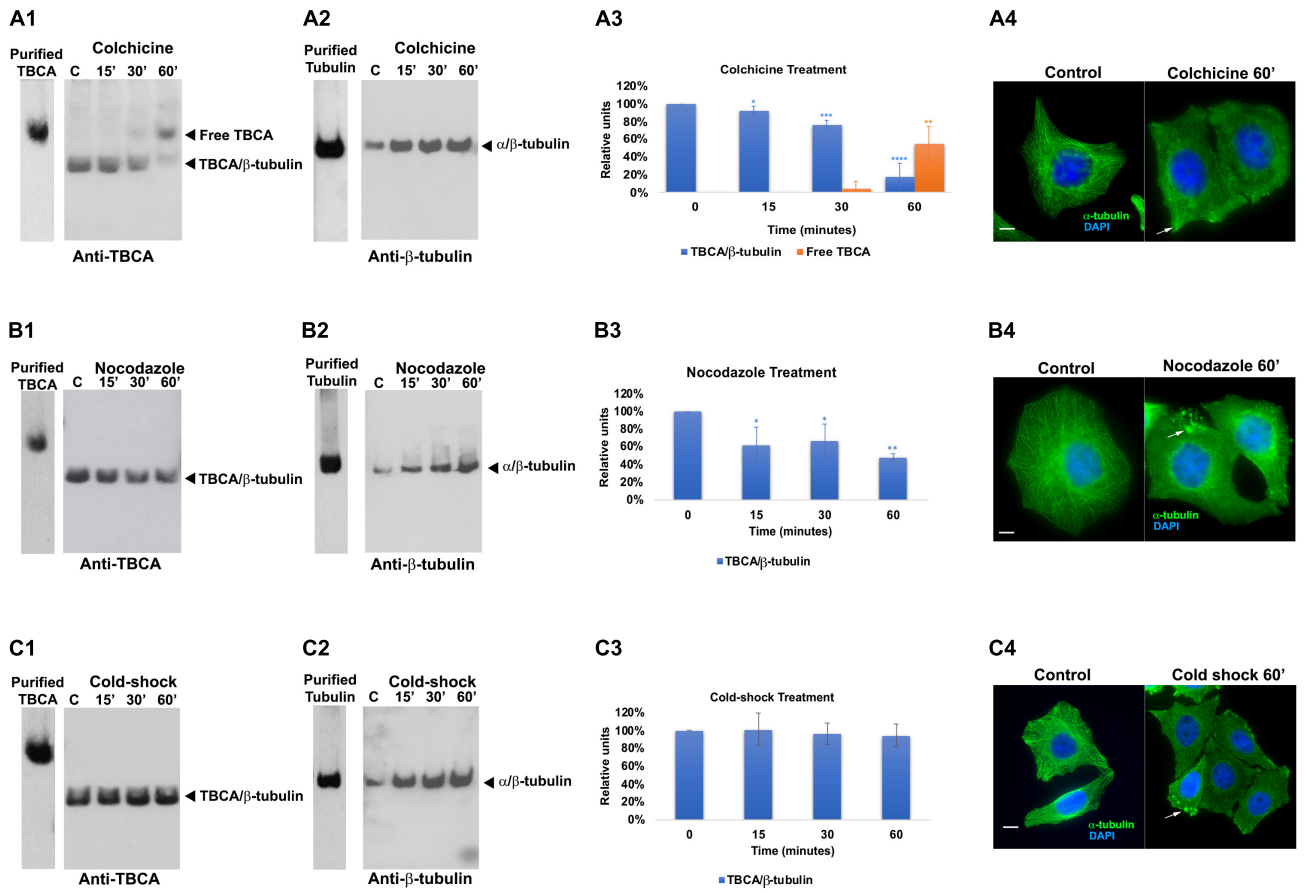

FIGURE 1 | Colchicine treatment triggers the appearance of free TBCA in HeLa cells. HeLa cells were treated with different microtubule depolymerizing agents (colchicine, nocodazole, and cold shock) for 15, 30, and 60 min. After each treatment, native protein extracts were prepared, and equal amounts of soluble protein extracts (30 μg) were analyzed by non-denaturing gel electrophoresis (6% native-PAGE) followed by western blot with antibodies directed to TBCA **(A1,B1,C1)** and β-tubulin **(A2,B2,C2)**. Representative images of the native-PAGE show that: free TBCA was not detected in all-control cells (untreated) **(A1,B1,C1)**; upon colchicine treatment, the amount of TBCA/β-tubulin complex progressively decreases over the indicated time-frames reaching the lowest level at 60 min which is accompanied by the detection of free TBCA in the cell extract (**A1,A3**: $^{*}p < 0.05$, $^{**}p < 0.01$, $^{***}p < 0.005$, and $^{****}p < 0.001$); under nocodazole treatment TBCA/β-tubulin complex also decreases at 60 min to exposure of cells to this anti-mitotic drug, but free TBCA is never detected (**B1,B3**: $^{*}p < 0.05$ and $^{**}p < 0.0001$); and under cold shock treatment the levels of the TBCA/β-tubulin complex are maintained **(C1,C3)**. The soluble α/β-tubulin levels increase in response to MT depolymerization **(A2,B2,C2)**. The graphs in panels **(A3)** (colchicine), **(B3)** (nocodazole), and **(C3)** (cold-shock), show the relative units in percentage of TBCA/β-tubulin complex and free TBCA levels in comparison to control cells (100%). Statistical significance was calculated using a *t*-test and the *p*-values were determined in comparison to the time 0 min (control). The graphic bars are the mean ± s.d. (error bars) of three independent assays. For each treatment, the MT depolymerization was confirmed by indirect immunofluorescence using an antibody against α-tubulin **(A4,B4,C4)** (the DNA was stained with DAPI, scale bar 10 μm).

native gels, it is expected that the anti-TBCA sera will be able to detect not only the free TBCA but also a faster migrating band corresponding to the TBCA/β-tubulin complex.

Interestingly, in control extracts from HeLa cells (**Figures 1A1,B1,C1**; lane C), the band corresponding to free TBCA is never observed. A faster migrating band, probably corresponding to the TBCA/β-tubulin complex, is clearly visible. To demonstrate that in our analysis, we could not use the antibody against β-tubulin as this only detects the α/β-tubulin heterodimer but not the TBCA/β-tubulin complex (**Figures 1A2,B2,C2**). This is probably a consequence of the β-tubulin epitope, recognized by this antibody, being hidden in the quaternary structure of the TBCA/β-tubulin complex. Therefore, to prove that the faster migrating band corresponds to the TBCA/β-tubulin complex, we excised this band from a 6% (w/v) Native-PAGE stained with Coomassie Brilliant Blue and re-analyzed it on a 16.5% (w/v) Tricine–SDS–PAGE. Then western-blot analysis was performed using specific antibodies to TBCA and β-tubulin. This analysis showed that the extracted band possesses β-tubulin and TBCA, confirming that it corresponds to the TBCA/β-tubulin complex (**Supplementary Figure 1**).

Curiously, these results clearly show that, in HeLa control cells, most TBCA is in a complex with β-tubulin, and these cells do not seem to contain a free pool of TBCA. The results in HeLa cells exposed for different times to cold shock 4°C (**Figure 1C1**) are like those observed in control cells, and the amount of the TBCA/β-tubulin complex does not significantly change over the

studied time lapse (see panel C3). On the contrary, the amount of soluble tubulin heterodimer increases reaching the highest level at 60 min after exposure to 4°C (**Figure 1C2**), suggesting that depolymerized MTs contribute to the rise of the soluble tubulin pool (heterodimers). In fact, the detection of α-tubulin by immunofluorescence (IF) microscopy in HeLa control cells and cells exposed to cold shock for 60 min show that in cells subject to 4°C the MT arrays are dismantled, even though their regular shape is maintained (**Figure 1C4**). In some cells, soluble free tubulin concentrates at specific sites of the cytoplasm (**Figure 1C4** arrows). Noteworthy, depolymerization of MTs caused by nocodazole or colchicine as revealed by IF microscopy analysis (see **Figures 1A4,B4**) is accompanied by the decrease of the amount of the TBCA/β-tubulin complex (**Figures 1A1,B1**). However, this decrease is much more accentuated in HeLa cells subjected to colchicine treatment (18 ± 16%) than in those subjected to nocodazole (48 ± 4%) for the same period (**Figures 1A3,B3**).

Moreover, the reduction of the amount of TBCA/β-tubulin complex initiates at 15 min of colchicine and nocodazole treatment (**Figures 1A1,A3**). Strikingly, in cells treated with colchicine, the decrease of the amount of TBCA/β-tubulin complex is closely followed by the gradual appearance of a band corresponding to free TBCA (**Figures 1A1,A3**). This band is not observed in HeLa cells treated with nocodazole, indicating a specific effect of the colchicine action in HeLa cells. Moreover, in agreement with the IF microscopy data, a progressive increase in the amount of α/β-tubulin heterodimer is observed either in nocodazole or colchicine HeLa treated cells during the studied time course (see **Figures 1A3,B3**). Thus, the interesting observation that colchicine dramatically increases the levels of free TBCA is not a direct consequence of MT depolymerization.

For all conditions the soluble protein extracts previously tested in native gels were subjected to 16.5% (w/v) Tricine–SDS–PAGE followed by detection with anti-TBCA and β-tubulin antibodies upon western blot analysis. The results (**Supplementary Figure 2**) show no significant alterations of TBCA levels and a slight increase in β-tubulin levels compared to the levels of these proteins in control cells. Of note, the increase of α/β-tubulin heterodimers, in response to the MT depolymerization, is not as clearly observed as in native gels, since in these we analyze the amount of all β-tubulin polypeptides regardless of its origin (α/β-tubulin, TBCA/β-tubulin or other). Therefore, the variations in the amount of free TBCA and the TBCA/β-tubulin complex observed in colchicine and nocodazole treated cells (**Figures 1A1,B1**) do not correspond to changes in the total amount of soluble TBCA and β-tubulin proteins in HeLa cells treated with these different MT depolymerizing agents in the indicated time-frames. These data clearly show that the decreased amounts of the TBCA/β-tubulin complex are not the result of reduced levels of any of the two proteins in HeLa cells. Moreover, in the time course of all the conditions studied, the soluble β-tubulin levels do not change significantly (see **Supplementary Figure 2**), but the native analysis indicates that the soluble α/β-tubulin heterodimer amount clearly increases (see **Figures 1A2,B2,C2**). This strongly suggests that at least β-tubulin may be displaced to a complex not visible in our conditions.

Free TBCA Is Not a Consequence of Protein Translation Inhibition

Since there is evidence that low doses of colchicine prevent mRNA translation by promoting polysome disaggregation (Walker and Whitfield, 1984), we put forward the hypothesis that the appearance of free TBCA in cells treated with colchicine could be related to the absence of newly synthesized tubulin. To assess this hypothesis, we analyzed the effect of the eukaryotic translational elongation inhibitor cycloheximide in the amounts of TBCA/β-tubulin complex as well as free TBCA. Thus, HeLa cells were treated with cycloheximide (50 μg/ml) for 15 min, 30 min, and 60 min, and soluble protein extracts were analyzed by 6% native-PAGE. We expected that the absence of input of newly synthesized tubulin to TBCA, due to protein synthesis inhibition, would mimic the effect of colchicine. However, we did not observe a decrease in the TBCA/β-tubulin complex levels nor in the free TBCA protein's appearance during the time course of cycloheximide treatment (**Figure 2C**). So, translation blockage does not affect TBCA/β-tubulin complex levels and does not cause the appearance of free TBCA. These results indicate that the decrease in the amount of TBCA/β-tubulin in HeLa cells treated with colchicine or nocodazole is not a consequence of the inhibition of protein translation caused by the increase in soluble tubulin as a consequence of the loss of the MTs network. Also, the detection of free TBCA in cells treated with colchicine cannot be ascribed to the absence of newly synthesized β-tubulin. Thus, to further unequivocally show that the appearance of the free TBCA protein observed is essentially the result of colchicine treatment, we analyzed the soluble protein extracts of HeLa cells simultaneously treated with cycloheximide and colchicine. For this, we treated HeLa cells with cycloheximide (50 μg/ml) for 15 min before colchicine was added. This period provided the time to inhibit protein synthesis prior to the action of colchicine. From these cells, soluble protein extracts were prepared after 15, 30, and 60 min of exposure to both compounds and analyzed in a 6% native-PAGE followed by western blot analysis using specific antibodies against TBCA and β-tubulin (**Figure 2**). The pattern of variation of TBCA/β-tubulin complex levels and free TBCA protein appearance were like those obtained in cells only treated with colchicine (compare **Figures 1A1**, 2A,C). Therefore, colchicine causes the appearance of free TBCA. As anticipated, protein synthesis inhibition does not interfere with colchicine's ability to promote MT depolymerization, which was confirmed by indirect IF microscopy (**Figure 2D**). All samples analyzed by non-denaturing gel electrophoresis (6% native-PAGE) were simultaneously analyzed by 16.5% (w/v) Tricine–SDS–PAGE followed by western blot analysis with antibodies directed to TBCA and β-tubulin. As observed in **Supplementary Figure 2**, colchicine in the presence of the translation inhibitor does not cause dramatic changes in the levels of soluble TBCA and β-tubulin (**Supplementary Figure 3**).

Overall, these results show that the absence of protein synthesis and consequently the absence of an input of newly

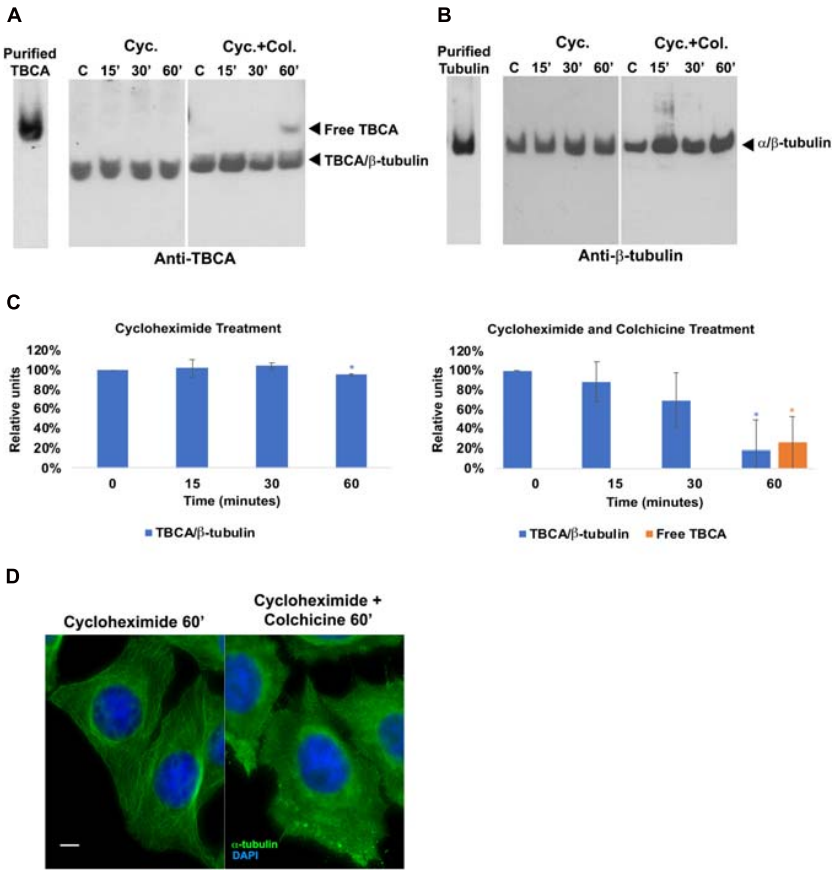

FIGURE 2 | Protein translation inhibition by cycloheximide does not lead to the detection of free TBCA in the cell extract. HeLa cells were treated with cycloheximide to inhibit the protein translation and also with cycloheximide plus colchicine for 15, 30, and 60 min. In both treatments, time 0 min (control) corresponds to 15 min after the cycloheximide addition. After each treatment, native protein extracts were prepared, and equal amounts of soluble protein (30 μg) were analyzed by non-denaturing gel electrophoresis (6% Native-PAGE) followed by western blot with antibodies directed to TBCA **(A)** and β-tubulin **(B)**. Representative images of the native-PAGE show that under the cycloheximide treatment, free TBCA was not detected, and the levels of TBCA/β-tubulin are maintained but, the addition of colchicine to cycloheximide leads to a decrease in TBCA/β-tubulin levels and detection of free TBCA after 60 min of colchicine treatment (**A,C**: for cycloheximide treatment $^*p < 0.005$, and for cycloheximide and colchicine treatment $^*p < 0.002$). The graphs in panel **(C)** (cycloheximide and cycloheximide plus colchicine), show the relative units in percentage of TBCA/β-tubulin complex and free TBCA levels in comparison to control (100%) cells. Statistical significance was calculated using a *t*-test. And the *p*-values were determined in comparison to the time 0 min (control). The graphic bars are the mean s.d. (error bars) of three independent assays. The α/β-tubulin levels are maintained during cycloheximide treatment but increase after addition of colchicine **(B)**. For each treatment, the MT depolymerization was confirmed by indirect immunofluorescence **(D)** using an antibody against α-tubulin (the DNA was stained with DAPI, scale bar 10 μm). The results observed in panel **(B)** agree with the results showed in panel **(C)**, where MTs can be detected with cycloheximide treatment but not with cycloheximide plus colchicine **(C)**.

synthesized β-tubulin in the tubulin folding pathway does not lead to the appearance of free TBCA nor affects the levels of the TBCA/β-tubulin complex. This is the first indication that TBCA is involved in heterodimer recycling from MT depolymerization. This observation may finally elucidate the apparent incongruent observations that TBCA is not essential for tubulin folding *in vitro* (Tian et al., 1996) while its depletion causes cell death (Nolasco et al., 2005).

TBCB and TBCE Are Not Able to Dissociate Tubulin Heterodimers Bound to Colchicine

Next, we aimed at elucidating the intriguing observation that 60 min of colchicine treatment leads to the appearance of free TBCA. It is well-established that *in vitro*, TBCA is able to accept β-tubulin from native tubulin heterodimers in the presence of TBCE and TBCB (Kortazar et al., 2006, 2007). Additionally, TBCB and TBCE cooperate to dissociate the tubulin dimer and stabilize α-tubulin (Kortazar et al., 2007). Also, colchicine binds irreversibly to tubulin dimers (Bhattacharyya et al., 2008; Bhattacharya et al., 2016). Together, these data strongly suggest that TBCA cannot interact with β-tubulin from colchicine-bound to tubulin heterodimers, probably because colchicine affects the ability of TBCB/TBCE to dissociate the heterodimer. To test this hypothesis, we performed *in vitro* tubulin dissociation assays in the presence of purified tubulin cofactors: TBCE, TBCE plus TBCB, and TBCE plus TBCB plus TBCA. In these assays, we incubated these cofactors with native purified tubulin or with native tubulin purified after

colchicine treatment. In the last case, tubulin was incubated with colchicine for 1 h at room temperature in a proportion of 2 μM:48.2 μM, respectively (Banerjee and Luduena, 1992). After incubating with colchicine, we purified the tubulin heterodimer-colchicine complex by gel filtration chromatography to remove the unbound colchicine. A similar purification protocol was applied to tubulin not incubated with colchicine (control). **Figure 3A** shows the chromatograms of the tubulin and tubulin-colchicine gel filtration purification. The separation profiles are very similar, indicating that colchicine did not affect tubulin heterodimer behavior through gel filtration chromatographic analysis. The tubulin heterodimer elutes at the second peak (fractions 17–19) in accordance with its expected size (Fanarraga et al., 2010b). Tubulin also appears in the column's void volume (first peak; fractions 6–9), suggesting the formation of large aggregates (Fanarraga et al., 2010b). In each case, fractions corresponding to tubulin heterodimers peak (17–19 fractions in both cases) were pooled. These fractions were used to perform tubulin heterodimer dissociation assays (Kortazar et al., 2006). For this purified tubulin and tubulin-colchicine heterodimers (2.2 μg/reaction) were incubated with or without TBCE (1.5 μg/reaction), TBCB (0.6 μg/reaction) and TBCA (5 μg/reaction), according to the table in **Figure 3B**. The products of tubulin heterodimer dissociation assays were analyzed by native-PAGE, and the gel was stained with Coomassie brilliant blue. Under these conditions, tubulin incubation with TBCE and TBCB leads to decreased tubulin heterodimers' concentration due to tubulin heterodimer dissociation, which agrees with what was previously described by Kortazar et al. (2006). As expected (Kortazar et al., 2006; Carranza et al., 2013), when TBCA is included in the reaction, a new band corresponding to TBCA/β-tubulin complex is detected in the gel. However, when a similar assay is performed using tubulin pre-incubated with colchicine, the decrease in the α/β-tubulin heterodimer is not observed (**Figure 3B**). Consequently, in the presence of TBCA, we did not detect the TBCA/β-tubulin complex. These results clearly indicate that the binding of colchicine to tubulin heterodimer blocks the ability of TBCE and TBCB to dissociate the tubulin heterodimer, which leaves TBCA free.

These data are supported by a structural prediction based on the comparison between the α/β-tubulin-colchicine and α/β-tubulin 3D structure in association with TBCB and TBCE as presented in **Figure 4**. This analysis was based on the fact that the tubulin dimer dissociation by TBCB/TBCE involves a ternary complex TBCE/TBCB/α-tubulin (Carranza et al., 2013; Serna et al., 2015). TBCE and TBCB have a cytoskeleton-associated protein glycine-rich (CAP-Gly) and a UBL domain (Grynberg et al., 2003; Serna and Zabala, 2016). The TBCB intermediate region has a short coiled-coil region (CC), whereas that of TBCE has a leucine-rich repeat (LRR) domain. The molecular architecture of this complex proposed by Serna et al. (2015), predicts that the TBCE-TBCB complex, hold by the interaction between the CAP-Gly domains, bind the α-tubulin monomer of the α/β-tubulin heterodimer and dissociate it presumably by pushing the TBCE LRR domain toward the β-tubulin monomer and distorting the α/β-tubulin interface. Also, the colchicine molecule binds at the α/β-tubulin interface, next to the α-tubulin GTP binding pocket (Prota et al., 2014). The comparative analysis of α/β-tubulin-colchicine and α/β-tubulin 3D structures show that, in the presence of the colchicine, the α/β-tubulin interface adopts a closer conformation (**Figure 4C**). This agrees with the experimental observations that colchicine binding induces a conformational change of tubulin (Garland, 1978; Detrich et al., 1981; Andreu and Timasheff, 1982). Therefore, the presence of the colchicine could impair the α/β-tubulin heterodimer dissociation by TBCB/TBCE by stabilizing the α/β-tubulin interface and make it resist the mechanical force applied by the LRR domain of TBCE (**Figure 4D**).

Again, the overall data strongly supports that an important role of TBCA in HeLa cells is to accept β-tubulin resulting from α/β-tubulin heterodimer that arises from MT depolymerization and is dissociated by the TBCB/TBCE machine or by the TBCD cofactor (Martín et al., 2000). Therefore, *in vivo*, TBCA's role is articulated with TBCB/TBCE activity to recycle the tubulin heterodimers and most probably to control their quality. The three tubulin cofactors also probably manage tubulin degradation, with TBCA avoiding the toxic effect of β-tubulin during the recycling process. These data also explain why the depolymerization of MTs by colchicine is irreversible in the presence of saturated doses of this molecule. Tubulin-colchicine heterodimers are condemned to be part of a pool of heterodimers that cannot polymerize because they cannot be dissociated and then recycled.

Studies of Overexpression and Depletion Support TBCA Main Role in β-Tubulin Recycling

The observation that an important role of TBCA is to bind β-tubulin during tubulin heterodimer recycling raised the question of whether TBCA levels may affect the tubulin dissociation rate by TBCB/TBCE, regulating, therefore, the availability of tubulin heterodimers competent to polymerize and also MT dynamics. It is conceivable, therefore, that if *in vivo* TBCA concentration is critical, it would regulate the efficiency of tubulin heterodimer dissociation by TBCB/TBCE. On other words, low levels of TBCA in the context of accentuated MT depolymerization could impair tubulin heterodimer dissociation by TBCB/TBCE since β-tubulin cannot be accepted, becoming toxic. This would implicate that in this background β-tubulin is driven to degradation. Consequently, we performed experiments where we modulated TBCA levels either by promoting its overexpression via pcDNA3-TBCA transfection (**Figures 5A,B**) or by knocking down the TBCA gene with a specific siRNA (as in Nolasco et al., 2005; **Figures 5C,D**). Western blot analysis of TBCA levels in control and TBCA siRNA-treated cells shows that TBCA levels decreased by about 48 ± 8% in TBCA-silenced cells. Hsp70 was used as loading control (**Figure 5D**). 24 h after transfections, native soluble protein extracts were prepared from control and TBCA overexpressing or depleted cells and analyzed either by native-PAGE or Tricine–SDS–PAGE followed by western blot using antibodies against TBCA, α- and β-tubulin (**Figure 5**). TBCA overexpression results show a dramatic

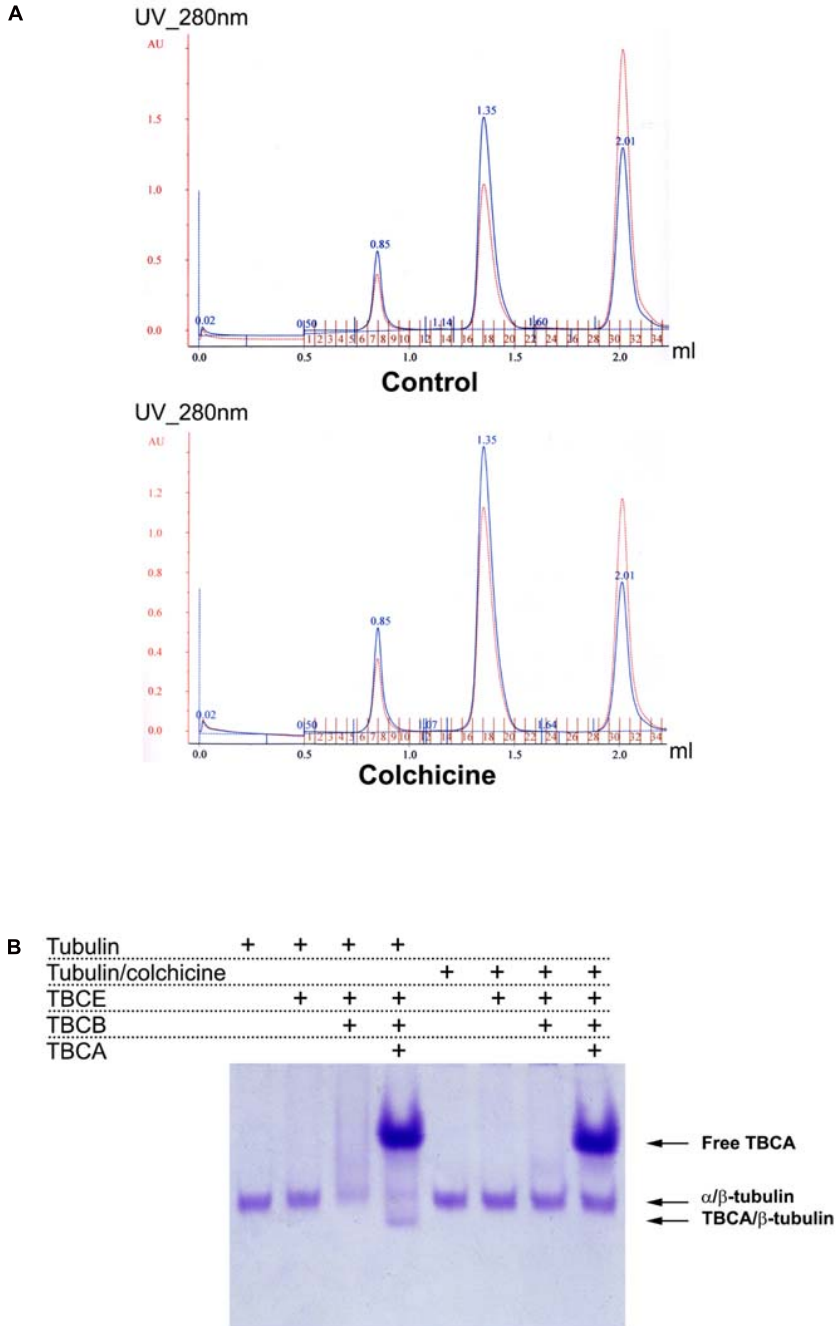

FIGURE 3 | *In vitro* dissociation assays reveal that TBCB and TBCE are not able to dissociate the tubulin-colchicine heterodimer which leaves TBCA free. **(A)** After the assay of colchicine binding to tubulin, tubulin-colchicine heterodimers were purified by gel filtration to remove the unbounded colchicine molecules and aggregated misfolded tubulin. As a control the same amount of tubulin was also incubated without colchicine and purified by gel filtration. Chromatographic elution profiles obtained at 280 nm of absorbance from a gel filtration analysis of control and tubulin heterodimers incubated with colchicine are very similar, presenting three prominent peaks: the first one corresponds to tubulin aggregates, the second one to tubulin heterodimers, and the third one to small molecules. The colchicine molecule bound to tubulin heterodimer did not affect the behavior of tubulin heterodimer in gel filtration. Each peak of tubulin and tubulin-colchicine heterodimers were pooled (17–19 fractions). **(B)** Purified tubulin and tubulin-colchicine heterodimers, from pooled fractions (2.2 μg/reaction), were incubated at 30°C for 30 min with or without TBCE (1.5 μg/reaction), TBCB (0.6 μg/reaction) and TBCA (5 μg/reaction), according to the table, to perform tubulin heterodimer dissociation assays. The tubulin heterodimer dissociation assays were analyzed by non-denaturing gel electrophoresis (6% native-PAGE) and stained with Coomassie brilliant blue. The tubulin incubation with TBCE and/or TBCB lead to a decrease in the tubulin heterodimers amount due to tubulin heterodimer dissociation, as previously described (Kortazar et al., 2006; Carranza et al., 2013). When TBCA is also present, we detected a new band in the gel that corresponds to TBCA/β-tubulin (Kortazar et al., 2006; Carranza et al., 2013). When colchicine is bound to tubulin, TBCE and/or TBCB cannot dissociate the tubulin heterodimer. Consequently, in the presence of TBCA, we did not detect the presence of TBCA/β-tubulin complex. Colchicine impairs the tubulin dissociate activity of TBCE/TBCB, leaving TBCA free.

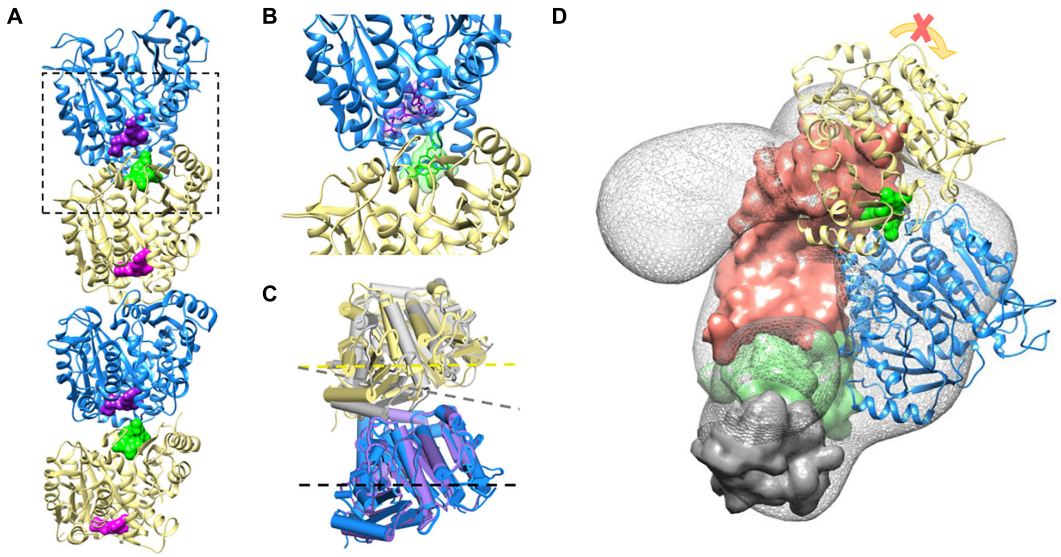

FIGURE 4 | Colchicine could impair TBCE-TBCB complex function in the α/β-tubulin heterodimer dissociation process by stabilizing the α-tubulin/β-tubulin interface. **(A)** Two associated α/β-tubulin heterodimers stabilized by the colchicine molecule (green surface). The GTP form of the α-tubulin monomer and the GDP form of the β-tubulin are displayed in blue and yellow (GTP and GDP surfaces are shown in purple and magenta, respectively), PDB ID 4O2B. **(B)** Zoom-in view of colchicine (green) at the α/β-tubulin interface, next to the α-tubulin GTP binding pocket, PDB ID 4O2B (Prota et al., 2014). **(C)** Comparison of the free α/β-tubulin heterodimer (α-tubulin in purple and β-tubulin in gray, PDB ID 1JFF; Löwe et al., 2001), with the α/β-tubulin heterodimer stabilized by colchicine (α-tubulin in blue and β-tubulin in yellow, PDB ID 4O2B; Prota et al., 2014) by aligning the α-tubulin monomers. The presence of colchicine affects the α/β-tubulin interface geometry, as shown with the dash lines. **(D)** The complex TBCE-TBCB, hold by the interaction between the CAP-Gly domains (TBCE CAP-Gly domain surface in green and TBCB CAP-Gly domain surface in gray), binds the α-tubulin monomer of the α/β-tubulin heterodimer (blue, EMDB-2447; Serna et al., 2015) pushing the TBCE LRR domain (domain surface in coral) toward the β-tubulin monomer (yellow) and distorting the α/β-tubulin interface. The presence of colchicine (green surface) could impair α/β-tubulin heterodimer dissociation by stabilizing the α/β-tubulin interface, making it resistant to the mechanical force applied by the LRR domain.

increase in free TBCA and TBCA/β-tubulin complex levels in native gels (**Figure 5A**) and a clear increase in total soluble TBCA amount can be observed in SDS denaturing gels (**Figure 5B**).

On the other hand, the levels of α/β-tubulin heterodimer slightly decrease in response to the increased TBCA levels (**Figure 5A**). This small decrease in heterodimer may result from an increased dissociation rate of the heterodimer by TBCB/TBCE, which agrees with the increased levels of TBCA/β-tubulin complex (see **Figure 5A**) and absence of variation of total soluble β-tubulin levels. However, the results did not support the observation that TBCA improves the *in vitro* dimerization rate of α/β-tubulin (Fanarraga et al., 1999) since we do not observe an increase in tubulin heterodimer. This observation confirms once more that TBCA plays a critical role in heterodimer recycling but not in the tubulin folding route. On the other hand, TBCA siRNA significantly decreases the amount of native α/β-tubulin heterodimer (**Figure 5C**) in line with our previous results showing an accentuated decrease of α- and β-tubulin in HeLa and MCF-7 cell lines extracts in response to TBCA depletion (Nolasco et al., 2005). Probably this is due to the continuous tubulin heterodimer dissociation by TBCB/TBCE to be recycled. Since there is not enough TBCA to accept β-tubulin, both tubulins are probably destined to degradation. Altogether, these results indicate that the levels of TBCA are essential to regulate the rate of tubulin heterodimer dissociation/recycling by TBCB/TBCE. These results also strengthen the role of TBCA as a major component of the recycling/degradation pathway of the α/β-tubulin heterodimer, weakening its eventual role in the folding of newly synthesized β-tubulin *in vivo*.

TBCA Is Abundant in Insoluble Protein Extracts of the Heart

Colchicine has been consistently used in the treatment of acute and recurrent pericarditis (Adler et al., 2015). Moreover, other potential therapeutic uses for colchicine are the prevention of Atrial Fibrillation (AF) reappearance after cardiac surgery or AF ablation (Calkins et al., 2017), as well as in patients with coronary artery disease (Nidorf et al., 2014, 2020; Deftereos et al., 2015) and chronic heart failure. In this view and guided by our results showing that: (i) colchicine impairs tubulin heterodimer dissociation by TBCB/TBCE, leaving TBCA free of β-tubulin; (ii) TBCA has a regulatory role in tubulin heterodimer recycling and (iii) altered levels of TBCA have been associated with human diseases (see **Table 1**), we analyzed the pattern of TBCA expression in different mouse organs. Previous analyses showed that TBCA is a soluble protein highly expressed in testis and in brain (Fanarraga et al., 1999) but no information is available regarding expression of TBCA in the heart. Therefore, we have prepared total protein extracts from the heart, brain, kidney, liver, lung, and testis of adult mice. The extracts were fractionated in soluble and insoluble fractions and analyzed by 16.5% (w/v) Tricine–SDS–PAGE followed by western blot using specific antibodies against TBCA, α-tubulin, and β-actin

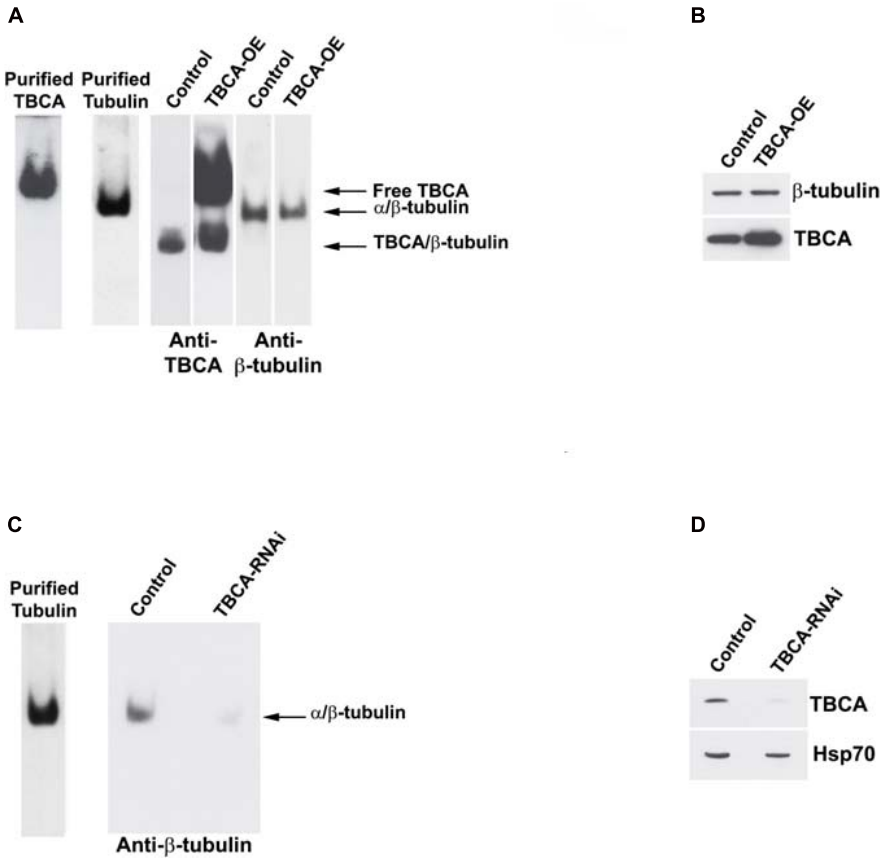

FIGURE 5 | Native tubulin heterodimers levels decrease in response to TBCA overexpression and TBCA siRNA. HeLa cells were transfected with TBCA-pcDNA3 (TBCA-OE), and control cells were transfected with empty pcDNA3. 24 h after transfection, native protein extracts were prepared. Equivalent amounts of protein soluble fraction (30 μg) were analyzed by non-denaturing gel electrophoresis Native-PAGE) **(A)** and by 16.5% Tricine–SDS–PAGE **(B)** followed by Western blot with antibodies directed to TBCA and β-tubulin. **(A)** In native gels, TBCA overexpression is clearly detected by the increase of the amount of free TBCA and the TBCA/β-tubulin complex. Tubulin heterodimer levels decrease when TBCA is overexpressed. **(B)** The denaturing analysis using Tricine–SDS–PAGE showed that β-tubulin levels do not change in response to TBCA overexpression. 24 h after TBCA siRNA transfection (see Nolasco et al., 2005 for details and controls), protein extracts were prepared. Equal amounts of protein soluble fraction (30 μg) were analyzed by non-denaturing gel electrophoresis (6% Native-PAGE) **(C)** and by 16.5% Tricine–SDS–PAGE **(D)**, to check the TBCA knockdown efficiency, followed by western blot with antibodies against β-tubulin, TBCA and Hsp70. **(C)** TBCA knockdown also causes a decrease in the tubulin heterodimer amount. **(D)** Cells transfected for 24 h with TBCA siRNAs show a reduction in levels of TBCA. Hsp70 protein levels were used as a loading control.

(**Figure 6**). Similar to what was observed by Fanarraga et al. (1999), TBCA is extremely abundant in the soluble fraction of testis followed by the brain, and α-tubulin and β-actin are detected in all tissue-specific samples (**Figure 6A**). However, in the insoluble fraction, TBCA is extremely abundant in the heart, followed by the testis. As expected, α-tubulin is mainly detected in the brain and testis, and β-actin is present in all samples but much more abundant in the heart, followed by the lung. These results are surprising because TBCA is assumed to be a soluble protein pinpointing for a possible contamination of the insoluble fraction with soluble proteins. This hypothesis is, however, discarded by the observation that in the heart TBCA is barely detected in the soluble fraction. We could still consider that our protein extraction was inefficient in heart cells lysates, explaining the low levels of TBCA observed in the soluble fraction and its retention in the insoluble extract. However, the detection of α-tubulin and even actin excludes this hypothesis (**Figures 6A,B**). Therefore, TBCA should be associated with membranes and/or cellular organelles present in insoluble extracts.

DISCUSSION

The dynamic behavior of MTs is critical for the myriad functions these polymers play in eukaryotic cells. MT functions require a pool of tubulin heterodimers competent to polymerize from newly synthesized tubulins and from recycling tubulin heterodimers from pre-existing MTs. These processes are complex and assisted by a dedicated set of tubulin cofactors. Colchicine is a natural anti-mitotic agent with clinical relevance in treating inflammatory diseases that is known to irreversibly affect MT polymerization and dynamics. Although anti-mitotic agents' action in MT assembly is well-established, their impact on tubulin heterodimers' recycling pathway is mainly unknown.

TABLE 1 | Altered TBCA expression in several diseases.

Disease	Organ	TBCA expression	Molecule	Reference
Cancer	Kidney	Overexpression	Protein	Zhang et al., 2013
	Skin (cell culture)	Overexpression (SIRT knock-down)	Protein	Wilking-Busch et al., 2018
	Breast	Overexpression	Protein	Fonseca-Sánchez et al., 2012
	Stomach	Overexpression	mRNA	Malta-Vacas et al., 2009
Alzheimer	Brain	Underexpression	Protein	Zhang et al., 2018
Parkinson	Brain	Overexpression	Protein	Werner et al., 2008
Osteoporosis	Bone	Underexpression	mRNA	Xia et al., 2017
Ankylosing spondylitis	Blood	Hypomethylation	DNA	Coit et al., 2019

In the present work, we report that colchicine treatment of HeLa cells, but not cold-shock or nocodazole, causes the appearance of free TBCA in protein extracts (**Figure 1**). This is an unexpected observation since, in all situations that we have studied, we have always found TBCA in a complex with β-tubulin. Moreover, this was accompanied by a marked decrease of the TBCA/β-tubulin complex. Our data also shows that the appearance of free TBCA cannot be ascribed to the interruption of the tubulin folding pathway. Indeed, protein translation inhibition by cycloheximide does not lead to free TBCA, and colchicine is still able to cause the appearance of free TBCA in its presence (**Figure 2**). These assays clearly show that not only colchicine interferes with TBCA's role, but TBCA seems to receive β-tubulin polypeptides mostly from the tubulin heterodimer recycling pathway. The current model of α/β-tubulin heterodimer assembly (Lopez-Fanarraga et al., 2001; Serna and Zabala, 2016) predicts that, if the input of newly synthesized β-tubulin is inhibited by the absence of translation, TBCA becomes free, at least partially. In the recycling pathway of the α/β-tubulin heterodimers, their dissociation by TBCE and TBCB leads to a ternary complex of TBCB/TBCE/α-tubulin, whereas β-tubulin is stabilized by TBCD or TBCA (Carranza et al., 2013; Serna et al., 2015). Noteworthy, *in vitro*, the TBCA/β-tubulin complex is stable and easy to be detected (Kortazar et al., 2006). Therefore, the appearance of free TBCA is probably the result of compromised TBCB/TBCE dissociation activity due to colchicine. Our tubulin heterodimer dissociation *in vitro* assays (**Figure 3**) unequivocally confirm this hypothesis, showing that, in the presence of colchicine, the TBCB/TBCE dissociation machine is unable to dissociate the tubulin heterodimer (**Figure 3**). Given these results, the decrease in the amount of TBCA/β-tubulin complex during the colchicine treatment is easily explained by the absence of β-tubulin that cannot be released by tubulin cofactors from the dimer, resulting in the detection of free TBCA.

Colchicine and nocodazole are both microtubule binding drugs that targets the β-tubulin subunit at a pocket close to the α-tubulin/β-tubulin heterodimer interface. It has been proposed that both compounds disrupt the MT dynamics by preventing the curve-to-straight conformational change of the α/β-tubulin heterodimer upon GTP hydrolysis (Wang et al., 2016). Our structural prediction of the α/β-tubulin-colchicine 3D structure associated with TBCB/TBCE (**Figure 4**), indicates that, in the presence of the colchicine, the α/β-tubulin interface might adopt a closer and more stable conformation, able to resist the mechanical force applied by the LRR domain of TBCE, which could explain the inability of TBCB/TBCE to dissociate the tubulin heterodimer. In the case of nocodazole, the molecule is structurally very different of colchicine and show different binding dynamics. Firstly, the nocodazole molecule is

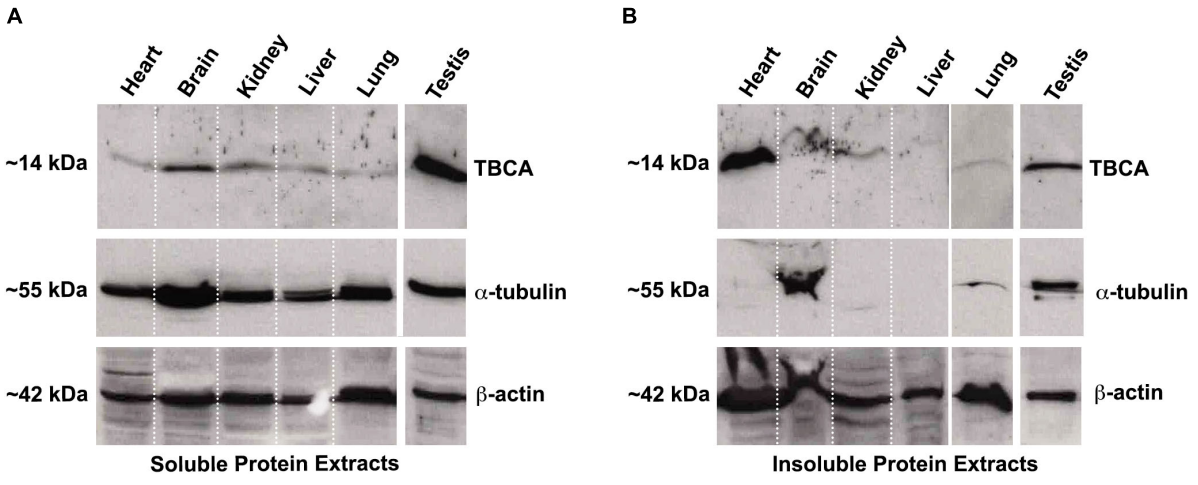

FIGURE 6 | TBCA is present in a high amount in mouse insoluble protein extracts from the heart. Soluble **(A)** and insoluble **(B)** protein extracts from mouse organs (heart, brain, kidney, liver, lung, and testis) were prepared and analyzed on 16.5% (w/v) Tricine–SDS–PAGE followed by western blot with antibodies against TBCA, α-tubulin, and β-actin. Soluble protein extracts were quantified, and equal protein amounts (100 μg) were analyzed. Insoluble protein extracts were solubilized with 8 M urea and diluted 1:2 in loading buffer and, 20 out of 200 μl were analyzed. **(A)** The analysis showed that TBCA was more abundant in testis and brain. α-tubulin and β-actin are detected in all organs. **(B)** The insoluble protein extracts show that TBCA is more abundant in the heart and testis. α-tubulin is mainly detected in testis and brain, and β-actin is detected in all organs. The approximate molecular mass of the proteins is indicated on the left side of the panels.

placed deeper in the β-tubulin monomer than the colchicine and it does not seem to interact with the α-tubulin monomer (Aguayo-Ortiz et al., 2013; Wang et al., 2016). Secondly, while colchicine is irreversibly bound to the β-tubulin and its effects on MT polymerization is also irreversible; nocodazole is a rapidly reversible inhibitor. Because the α/β-tubulin heterodimer conformation in the presence of colchicine is very similar to that in the presence of nocodazole, it is tempting to think that the nocodazole bound-heterodimer would be also resistant to the TBCE, TBCB dissociation activity. However, nocodazole results are distinct from those originated by colchicine (**Figure 1**). It is plausible that the resistance to the mechanical force applied to the heterodimer by the tubulin cofactors might require a more stable drug binding-state of it to be evaluated. Although the α/β-tubulin heterodimer dissociation kinetics remains to be quantified, it is reasonable to propose that the dissociation activity of the TBCE and TBCB cofactors may be slower than the binding kinetics of nocodazole. In bulk, the dissociation activity taking place on free heterodimers would hinder detection of the activity on nocodazole bound heterodimers.

It was known that in *in vitro* tubulin dissociation assays performed in the presence of TBCB and TBCE, but in the absence of TBCA, β-tubulin becomes unstable and aggregates (Kortazar et al., 2006). The formation of those aggregates might be avoided by the addition of TBCA (Kortazar et al., 2006). These results motivated us to investigate how excess or deficiency in TBCA levels affect tubulin heterodimer dissociation by analyzing the levels of the TBCA/β-tubulin complex. Interestingly, and contrary to our prediction, TBCA overexpression leads to a decrease of the α/β-tubulin heterodimer levels (**Figure 5A**). Strikingly, TBCA depletion (**Figure 5C**) also causes the decrease of α/β-tubulin heterodimer (Nolasco et al., 2005) and present work). TBCA overexpression results support the evidence that TBCA plays an important role in the recycling pathway of the tubulin heterodimer. Indeed, excess TBCA does not lead to an increase in tubulin dimerization. The observed decrease of α/β-tubulin heterodimer amounts, together with the increase in the TBCA/β-tubulin complex, strongly suggests that, when more TBCA is available, the tubulin heterodimer proceeds through the recycling route. In the case of cells treated with TBCA siRNA, the diminished levels of the α/β-tubulin heterodimer are possibly the consequence of driving tubulin to degradation, since the recycling pathway cannot be completed due to low TBCA levels. Therefore, it is conceivable that, *in vivo*, TBCA concentration determines tubulin fate being it recycling or degradation. It was proposed that the UBL domains of both TBCE and TBCB in the dissociation complex remain free and exposed, protruding from opposite positions in the central mass of the complex (Serna et al., 2015). This observation strongly suggests that both domains could be involved in the degradation of α-tubulin subunit by the proteasome, while no degradation mechanism was previously described for β-tubulin. In our study we show that β-tubulin is degraded in cells depleted of TBCA, indicating that TBCD, known to dissociate the α/β-tubulin heterodimer by itself and to stabilize the β-tubulin (Martín et al., 2000), does not seem to have a prominent role in its recycling pathway.

In the last years, numerous studies have shown that altered levels of TBCA expression are associated with human diseases like cancer, neurodegenerative diseases, osteoporosis, and Ankylosing spondylitis (**Table 1**). Strikingly the human diseases associated with the other TBCs are mainly due to mutations in genes encoding these proteins (review Serna and Zabala, 2016). According to our results, the altered levels of TBCA will affect the α/β-tubulin heterodimer recycling/degradation, which will impact MT cytoskeleton dynamics and remodeling. Nothing is known about the role of TBCs in the incorporation of distinct tubulin isotypes in different MT classes, or alternatively in response to specific signals. We envisage that the recycling pathway of tubulins will have a prominent role in altering the biochemical/biophysical properties of MTs by allowing the polymerization of different tubulin isotypes.

Our results also show that TBCA is enriched in insoluble protein extracts obtained from adult heart mice (**Figure 6**). At first glance, this observation is unexpected, but a detailed analysis of the cardiomyocyte cytoskeleton reveals that MTs in crosstalk with actin and intermediate filaments play specific roles in sustaining the cardiac contractile function (Kuznetsov et al., 2020). In cardiomyocytes, MTs are known to be involved in the intracellular traffic and the transmission of mechanical signals, in the shaping of membrane systems, and in the spatial organization of myofibrils and organelles (Caporizzo et al., 2019). Probably, the demanding roles of MTs in these cells, such as mechanical transduction, may require intense recycling of tubulin heterodimers, explaining the abundance of TBCA. In fact, it was recently shown that MTs exchange tubulin dimers at lattice defects sites induced by mechanical stress (Schaedel et al., 2015; Aumeier et al., 2016). Indeed, TBCD was downregulated by arterial shear stress (Schubert et al., 2000). These events may occur spontaneously during MT polymerization due to MT-severing enzymes or other unknown factors (Schaedel et al., 2015; Aumeier et al., 2016). The specific roles of TBCs, including the role of TBCA shown in this work, indicate that these molecules are excellent candidates to be involved in these stress responses.

It is still intriguing the observation of high levels of TBCA in the insoluble protein extracts of the heart tissue. In cardiac cells, MTs are located close to the nuclear envelope, in the transverse (T)-tubules membrane, and at the mitochondrial membrane (Caporizzo et al., 2019). It was observed that tubulin heterodimers are bound to and regulate the voltage-dependent anion channel (VDAC) in mitochondria (Carré et al., 2002). This attachment that seems to be established through a specific β-tubulin isotype (βII-tubulin), is strong enough to maintain β-tubulin in an ordered striated distribution pattern that colocalizes with the mitochondria, even after MT depolymerization and cells permeabilization (Rappaport and Samuel, 1988; Guerrero et al., 2010). Moreover, it was described that in cardiomyocytes, about 70% of total tubulin is present in MTs, whereas 30% occurs as free tubulin heterodimers (Tagawa et al., 1998; Hein et al., 2000; Kostin et al., 2000). Therefore, we can speculate that TBCA may be associated with β-tubulin in these localizations playing an unknown function, which could justify the enrichment of TBCA in the insoluble fraction. Alternatively, the canonical role of TBCA/β-tubulin

complex in β-tubulin recycling may be performed *in situ* in close association with membranes.

Colchicine is a therapeutical hallmark in pericardial diseases characterized by densification of the MT network, leading to increased cell stiffness (Hein et al., 2000). It has been assumed that colchicine has a beneficial role in cardiomyocytes via decreasing MT mass and altering MT dynamics (Hein et al., 2000). Our work shows, for the first time, that colchicine affects the tubulin recycling process by inhibiting tubulin heterodimer dissociation, which leads to the decrease in the amount of TBCA/β-tubulin complex, resulting in free TBCA in the cell. As such, our results open the possibility that TBCA/β-tubulin complex may have unknown roles in cardiomyocytes. Future studies are required to elucidate the consequences of free TBCA in cells and overall colchicine mechanism of action.

From this work, TBCA emerges as an important protein in the recycling/degradation of β-tubulin and, consequently, in the regulation of MT dynamics. Indeed, this idea is strongly supported by the fact that TBCA has been associated with different human diseases where its levels are altered (**Table 1**). Although providing an important contribution, our results suggest that the role of TBCA and/or TBCA-tubulin complex's role in eukaryotic cells require further validation from *in vitro*, and, most importantly, *in vivo* studies.

MATERIALS AND METHODS

Cell Culture

HeLa human tumor cell line, was cultured in a 5% CO_2 humidified atmosphere at 37°C as exponentially growing sub-confluent monolayers in Dulbecco's modified Eagle's medium (DMEM) with Glutamax (Invitrogen; Thermo Fisher Scientific, Inc., Waltham, MA, United States), supplemented with 10% fetal calf serum (Invitrogen; Thermo Fisher Scientific, Inc., Waltham, MA, United States) and non-essential amino acids (Invitrogen; Thermo Fisher Scientific, Inc., Waltham, MA, United States).

The MT depolymerizing experiments were done after 15, 30, and 60 min incubation with either 5 μM colchicine (Sigma, St. Louis, United States), or 30 μM nocodazole (Sigma, St. Louis, United States) or with cold shock (culture media at 4°C was added to the cells and the cell plates were put on ice during the treatment (Weisenberg, 1972; Shelanski et al., 1973). The concentrations of colchicine and nocodazole used in this work aimed at causing an accentuated and rapid increase of tubulin heterodimers due to MT depolymerization and are similar to those already used in other cell lines (Breitfeld et al., 1990; Karbowski et al., 2001). Translation inhibition was carried out by the cycloheximide (Sigma, St. Louis, United States) treatment (50 μ g/ml).

TBCA siRNA and TBCA overexpression transfection experiments were performed according to our previous results (Nolasco et al., 2005; Kortazar et al., 2007).

Protein Extraction From HeLa Cells

For native protein extracts, cells were rinsed twice with PBS. During the second PBS wash, cells were removed from culture plates by scraping and then centrifuged at 3,500 *g* for 5 min at room temperature (RT). Then, PBS was discarded, and the cell pellets were resuspended in lysis buffer (100 mM MES, pH 6.7 (Sigma, St. Louis, United States); 1 mM $MgCl_2$ (Merck, Darmstadt, Germany); 1 mM EGTA (Sigma, St. Louis, United States); 0.1 mM GTP (Sigma, St. Louis, United States); 0.2 mM DTT (Sigma, St. Louis, United States) and 0.1 mM PMSF (Sigma, St. Louis, United States), containing a protease inhibitors cocktail (Thermo Fisher Scientific, Inc., Waltham, MA, United States). Total protein extracts were obtained by homogenizing samples at room temperature or 4°C mechanically, using a potter-homogenizer. Cellular lysates were centrifuged at 14,000 *g* for 30 min at RT. The supernatants were recovered (soluble fraction). An important note is that, except for samples submitted to cold shock, all protein extracts were prepared at RT and RT solutions/buffers to avoid MT depolymerization due to cold solutions/buffers normally used to prevent protein degradation.

After protein quantification by Bradford (Bio-Rad, California, United States), equal amounts of soluble protein extracts (30 μg) were separated on non-denaturing gel electrophoresis [6% (w/v) Native-PAGE] (Zabala and Cowan, 1992; Fontalba et al., 1993). Protein extracts from TBCA siRNA and TBCA overexpression experiments were also analyzed on a 16.5% (w/v) Tricine–SDS–PAGE (Schägger and von Jagow, 1987).

Protein Extraction From Different Mouse Organs

Mouse organs were pulverized cryogenically in liquid nitrogen using a mortar and pestle for grinding frozen tissue. 200 μl of lysis buffer [1% NP40; 50 mM HEPES, pH 8 (Sigma, St. Louis, United States); 200 mM NaCl (Sigma, St. Louis, United States); 5 mM EDTA (Sigma, St. Louis, United States); 0.2 mM DTT (Sigma, St. Louis, United States) and 0.1 mM PMSF (Sigma, St. Louis, United States)], containing a protease inhibitors cocktail (Thermo Fisher Scientific, Inc., Waltham, MA, United States) were added to 150 mg of the pulverized organ and homogenized using a potter-homogenizer. Cellular lysates were removed and centrifuged at 14,000 × *g* for 90 min at 4°C. After protein quantification by Bradford (Bio-Rad, California, United States), equal amounts of soluble protein extracts (100 μg) were separated on 16.5% (w/v) Tricine–SDS–PAGE (Schägger and von Jagow, 1987). 100 μl of 8 M urea were added to the pellets of the insoluble fraction. The insoluble protein extracts were diluted 1:2 in loading buffer, and 20 μl were analyzed on 16.5% (w/v) Tricine–SDS–PAGE (Schägger and von Jagow, 1987).

Western Blot Analysis

Westerns blots were performed using the rabbit polyclonal serum against TBCA (1:5,000) (Llosa et al., 1996), the mouse monoclonal antibody against β-tubulin (1:1,000) (clone TUB 2.1, Sigma, St. Louis, United States), the mouse monoclonal antibody against α-tubulin (1:1,000) (clone DM1A, Sigma, St. Louis, United States) and the rabbit monoclonal antibody against β-actin (1:2,000) (Sigma, St. Louis, United States). Secondary antibodies against rabbit and mouse (Jackson Immuno Research)

were used at 1:4,000. The immunostaining was carried out using the ECL technique (GE Healthcare). The presented results are representative of at least three independent experiments.

Fluorescence Microscopy

For immunofluorescence microscopy studies, cells were washed twice with PBS (Invitrogen; Thermo Fisher Scientific, Inc., Waltham, MA, United States) and then fixed in 3.7% (w/v) paraformaldehyde (Merck, Darmstadt, Germany) in PBS for 10 min at room temperature. They were then washed twice with PBS for 5 min and permeabilized for 2 min using 0.1% (v/v) Triton X-100 (Sigma, St. Louis, United States) in PBS. After rinsing twice for 5 min in PBS and once in PBS-0.1% (v/v) Tween-20 (Merck, Darmstadt, Germany), cells were blocked in 3% (w/v) BSA (Calbiochem; Sigma, St. Louis, United States) for 15 min. Next, cells were incubated with the mouse monoclonal α-tubulin antibody (clone DM1A, Sigma, St. Louis, United States) at 1:200 in the same solution for 60 min. Samples were washed twice in PBS for 5 min and once in PBS-0.1% (v/v) Tween-20. Secondary antibody Alexa Fluor 488-conjugated goat anti-mouse IgG at 1:500 (Molecular Probes; Invitrogen; Thermo Fisher Scientific, Inc., Waltham, MA, United States) was incubated for 60 min in the same solution. The preparations were washed twice in PBS for 5 min and once in PBS-0.1% (v/v) Tween-20. DNA was stained with DAPI (1 μg/μl) in PBS for 1 min. The preparations were washed in PBS and mounted in MOWIOL 4-88 (Calbiochem; Sigma, St. Louis, United States) mounting medium supplemented with 2.5% (w/v) DABCO (Sigma, St. Louis, United States). Cells were examined with a fluorescence microscope (Leica DMRA2), and image acquisition was performed with a cooled CCD camera and MetaMorph Imaging Software (Universal Imaging Corporation). Image processing was carried out with ImageJ Software.

Protein Production for *in vitro* Assay

Human TBCA was cloned and purified from *Escherichia coli* cells (Llosa et al., 1996). Human TBCE and TBCB were purified from insect cells infected with recombinant baculovirus and *E. coli* cells, respectively (Kortazar et al., 2007). Tubulin dimers were isolated and purified from bovine brain (Avila et al., 2008).

Tubulin Purification After Colchicine Incubation

The *in vitro* assay of colchicine binding to tubulin was done under conditions where the drug was present in large excess over tubulin (Banerjee and Luduena, 1992). Bovine brain purified tubulin (60 μM) was incubated with colchicine (1.4 mM) for 1 h at room temperature, and tubulin-colchicine heterodimers were purified by gel filtration (Superdex 200 PC 3.2/30) using a Smart System (Amersham Pharmacia Biotech) to remove unbounded colchicine. The elution buffer used was 0.1 M MES pH 6.7, 1 mM $MgCl_2$, 1 mM EGTA, 25 mM KCl and 0.1 mM GTP. Fractions of 50 μl were eluted at 40 μl/min. As a control, the same amount of bovine brain purified tubulin was also incubated for 1 h at room temperature, without colchicine, followed by gel filtration purification. Each peak of tubulin and tubulin-colchicine heterodimers were pooled (17–19 fractions).

Tubulin Dimer Dissociation Assay

Purified tubulin and tubulin-colchicine heterodimers, from pooled fractions (2.2 μg), were incubated at 30°C for 30 min with or without TBCE (1.5 μg/reaction), TBCB (0.6 μg/reaction) and TBCA (5 μg/reaction) in buffer 0.1 M MES pH 6.7, 1 mM $MgCl_2$ and 0.1 mM GTP, to perform tubulin heterodimer dissociation assays. These assays were analyzed on 6% (w/v) native-PAGE (Zabala and Cowan, 1992; Kortazar et al., 2007) and stained with Coomassie brilliant blue.

Statistical Analysis

The experiments were performed at least three times and the results were expressed as means ± S.D. Differences between the data were tested for statistical significance by t-test. $P < 0.05$ were considered statistically significant.

DATA AVAILABILITY STATEMENT

The original contributions presented in the study are included in the article/**Supplementary Material**, further inquiries can be directed to the corresponding author/s.

ETHICS STATEMENT

The animal study was reviewed and approved by the Comite de Bioetica de la Universidad de Cantabria.

AUTHOR CONTRIBUTIONS

SN: conceptualization, resources, funding acquisition, data curation (molecular and cell biology and transfection, fluorescence microscopy, western blot), image composition, and writing (original draft, review and editing). JB: conceptualization, resources, and data curation (protein purification, protein analysis, westerns, antibodies production, and purification). MS and BC: data curation and analysis, writing (original) image, and table composition. HS and JZ: conceptualization, resources, funding acquisition, and writing (original draft, review and editing). All authors contributed to the article and approved the submitted version.

FUNDING

This work was supported by the Fundação para a Ciência e a Tecnologia (FCT), project UID/QUI/00100/2019, Portugal, to HS and BC, and project UIDB/00276/2020, Portugal, to SN and the Spanish Ministry of Science and Innovation, grant number BFU2010-18948 to JZ.

ACKNOWLEDGMENTS

We acknowledge the contribution of Anita Gomes (ESTeSL/IMM; Portugal) and João Gonçalves (Deep Genomics, Canada) for their critical review of the manuscript.

SUPPLEMENTARY MATERIAL

The Supplementary Material for this article can be found online at: https://www.frontiersin.org/articles/10.3389/fcell.2021.656273/full#supplementary-material

REFERENCES

Abruzzi, K. C., Smith, A., Chen, W., and Solomon, F. (2002). Protection from free beta-tubulin by the beta-tubulin binding protein Rbl2p. *Mol. Cell. Biol.* 22, 138–147. doi: 10.1128/mcb.22.1.138-147.2002

Addrizzo-Harris, D. J., Harkin, T. J., Tchou-Wong, K. M., McGuinness, G., Goldring, R., Cheng, D., et al. (2002). Mechanisms of colchicine effect in the treatment of asbestosis and idiopathic pulmonary fibrosis. *Lung* 180, 61–72. doi: 10.1007/s004080000083

Adler, Y., Charron, P., Imazio, M., Badano, L., Barón-Esquivias, G., Bogaert, J., et al. (2015). 2015 ESC Guidelines for the diagnosis and management of pericardial diseases: the task force for the diagnosis and management of pericardial diseases of the European Society of Cardiology (ESC)endorsed by: the European association for cardio-thoracic surg. *Eur. Heart J.* 36, 2921–2964. doi: 10.1093/eurheartj/ehv318

Aguayo-Ortiz, R., Méndez-Lucio, O., Medina-Franco, J. L., Castillo, R., Yépez-Mulia, L., Hernández-Luis, F., et al. (2013). Towards the identification of the binding site of benzimidazoles to β-tubulin of *Trichinella spiralis*: insights from computational and experimental data. *J. Mol. Graph. Model.* 41, 12–19. doi: 10.1016/j.jmgm.2013.01.007

Andreu, J. M., and Timasheff, S. N. (1982). Conformational states of tubulin liganded to colchicine, tropolone methyl ether, and podophyllotoxin. *Biochemistry* 21, 6465–6476. doi: 10.1021/bi00268a023

Angelidis, C., Kotsialou, Z., Kossyvakis, C., Vrettou, A.-R., Zacharoulis, A., Kolokathis, F., et al. (2018). Colchicine pharmacokinetics and mechanism of action. *Curr. Pharm. Des.* 24, 659–663. doi: 10.2174/1381612824666180123110042

Archer, J. E., Vega, L. R., and Solomon, F. (1995). Rbl2p, a yeast protein that binds to beta-tubulin and participates in microtubule function in vivo. *Cell* 82, 425–434. doi: 10.1016/0092-8674(95)90431-x

Aumeier, C., Schaedel, L., Gaillard, J., John, K., Blanchoin, L., and Théry, M. (2016). Self-repair promotes microtubule rescue. *Nat. Cell Biol.* 18, 1054–1064. doi: 10.1038/ncb3406

Avila, J., Soares, H., Fanarraga, M. L., and Zabala, J. C. (2008). Isolation of microtubules and microtubule proteins. *Curr. Protoc. Cell Biol.* Chapter 3:Unit3.29. doi: 10.1002/0471143030.cb0329s39

Banerjee, A., and Luduena, R. F. (1992). Kinetics of colchicine binding to purified beta-tubulin isotypes from bovine brain. *J. Biol. Chem.* 267, 13335–13339.

Bellouze, S., Schäfer, M. K., Buttigieg, D., Baillat, G., Rabouille, C., and Haase, G. (2014). Golgi fragmentation in pmn mice is due to a defective ARF1/TBCE cross-talk that coordinates COPI vesicle formation and tubulin polymerization. *Hum. Mol. Genet.* 23, 5961–5975. doi: 10.1093/hmg/ddu320

Bhattacharya, S., Das, A., Datta, S., Ganguli, A., and Chakrabarti, G. (2016). Colchicine induces autophagy and senescence in lung cancer cells at clinically admissible concentration: potential use of colchicine in combination with autophagy inhibitor in cancer therapy. *Tumour Biol.* 37, 10653–10664. doi: 10.1007/s13277-016-4972-7

Bhattacharyya, B., Panda, D., Gupta, S., and Banerjee, M. (2008). Anti-mitotic activity of colchicine and the structural basis for its interaction with tubulin. *Med. Res. Rev.* 28, 155–183. doi: 10.1002/med.20097

Breitfeld, P. P., McKinnon, W. C., and Mostov, K. E. (1990). Effect of nocodazole on vesicular traffic to the apical and basolateral surfaces of polarized MDCK cells. *J. Cell Biol.* 111, 2365–2373. doi: 10.1083/jcb.111.6.2365

Calkins, H., Hindricks, G., Cappato, R., Kim, Y.-H., Saad, E. B., Aguinaga, L., et al. (2017). 2017 HRS/EHRA/ECAS/APHRS/SOLAECE expert consensus statement on catheter and surgical ablation of atrial fibrillation. *Hear. Rhythm* 14, e275–e444. doi: 10.1016/j.hrthm.2017.05.012

Caporizzo, M. A., Chen, C. Y., and Prosser, B. L. (2019). Cardiac microtubules in health and heart disease. *Exp. Biol. Med. (Maywood)* 244, 1255–1272. doi: 10.1177/1535370219868960

Carranza, G., Castaño, R., Fanarraga, M. L., Villegas, J. C., Gonçalves, J., Soares, H., et al. (2013). Autoinhibition of TBCB regulates EB1-mediated microtubule dynamics. *Cell. Mol. Life Sci.* 70, 357–371. doi: 10.1007/s00018-012-1114-2

Carré, M., André, N., Carles, G., Borghi, H., Brichese, L., Briand, C., et al. (2002). Tubulin is an inherent component of mitochondrial membranes that interacts with the voltage-dependent anion channel. *J. Biol. Chem.* 277, 33664–33669. doi: 10.1074/jbc.M203834200

Chen, K., Koe, C. T., Xing, Z. B., Tian, X., Rossi, F., Wang, C., et al. (2016). Arl2–and Msps-dependent microtubule growth governs asymmetric division. *J. Cell Biol.* 212, 661–676. doi: 10.1083/jcb.201503047

Coit, P., Kaushik, P., Caplan, L., Kerr, G. S., Walsh, J. A., Dubreuil, M., et al. (2019). Genome-wide DNA methylation analysis in ankylosing spondylitis identifies HLA-B*27 dependent and independent DNA methylation changes in whole blood. *J. Autoimmun.* 102, 126–132. doi: 10.1016/j.jaut.2019.04.022

Corral, P., Corral, G., and Diaz, R. (2020). Colchicine and COVID-19. *J. Clin. Pharmacol.* 60:978. doi: 10.1002/jcph.1684

Cowan, N. J., and Lewis, S. A. (2001). Type II chaperonins, prefoldin, and the tubulin-specific chaperones. *Adv. Protein Chem.* 59, 73–104. doi: 10.1016/s0065-3233(01)59003-8

Cunningham, L. A., and Kahn, R. A. (2008). Cofactor D functions as a centrosomal protein and is required for the recruitment of the gamma-tubulin ring complex at centrosomes and organization of the mitotic spindle. *J. Biol. Chem.* 283, 7155–7165. doi: 10.1074/jbc.M706753200

Dalbeth, N., Lauterio, T. J., and Wolfe, H. R. (2014). Mechanism of action of colchicine in the treatment of gout. *Clin. Ther.* 36, 1465–1479. doi: 10.1016/j.clinthera.2014.07.017

De Brabander, M. J., Van de Veire, R. M., Aerts, F. E., Borgers, M., and Janssen, P. A. (1976). The effects of methyl (5-(2-thienylcarbonyl)-1H-benzimidazol-2-yl) carbamate, (R 17934; NSC 238159), a new synthetic antitumoral drug interfering with microtubules, on mammalian cells cultured in vitro. *Cancer Res.* 36, 905–916.

Deftereos, S., Giannopoulos, G., Angelidis, C., Alexopoulos, N., Filippatos, G., Papoutsidakis, N., et al. (2015). Anti-inflammatory treatment with colchicine in acute myocardial infarction: a pilot study. *Circulation* 132, 1395–1403. doi: 10.1161/CIRCULATIONAHA.115.017611

Detrich, H. W., Wilson, L., Williams, R. C., Macdonald, T. L., and Puett, D. (1981). Changes in the circular dichroic spectrum of colchicine associated with its binding to tubulin. *Biochemistry* 20, 5999–6005. doi: 10.1021/bi00524a012

Dogterom, M., and Koenderink, G. H. (2019). Actin–microtubule crosstalk in cell biology. *Nat. Rev. Mol. Cell Biol.* 20, 38–54. doi: 10.1038/s41580-018-0067-1

Dumontet, C., and Jordan, M. A. (2010). Microtubule-binding agents: a dynamic field of cancer therapeutics. *Nat. Rev. Drug Discov.* 9, 790–803. doi: 10.1038/nrd3253

Fanarraga, M. L., Bellido, J., Jaén, C., Villegas, J. C., and Zabala, J. C. (2010a). TBCD links centriologenesis, spindle microtubule dynamics, and midbody abscission in human cells. *PLoS One* 5:e8846. doi: 10.1371/journal.pone.0008846

Fanarraga, M. L., Carranza, G., Castaño, R., Nolasco, S., Avila, J., and Zabala, J. C. (2010b). Nondenaturing electrophoresis as a tool to investigate tubulin complexes. *Methods Cell Biol.* 95, 59–75. doi: 10.1016/S0091-679X(10)95005-X

Fanarraga, M. L., Párraga, M., Aloria, K., Del Mazo, J., Avila, J., and Zabala, J. C. (1999). Regulated expression of p14 (cofactor A) during spermatogenesis. *Cell Motil. Cytoskeleton* 43, 243–254. doi: 10.1002/(SICI)1097-0169199943:3<243::AID-CM7<3.0.CO;2-0

Fedyanina, O. S., Mardanov, P. V., Tokareva, E. M., McIntosh, J. R., and Grishchuk, E. L. (2006). Chromosome segregation in fission yeast with mutations in the tubulin folding cofactor D. *Curr. Genet.* 50, 281–294. doi: 10.1007/s00294-006-0095-9

Fonseca-Sánchez, M. A., Cuevas, S. R., Mendoza-Hernández, G., Bautista-Piña, V., Ocampo, E. A., Hidalgo-Miranda, A., et al. (2012). Breast cancer proteomics

reveals a positive correlation between glyoxalase 1 expression and high tumor grade. *Int. J. Oncol.* 41, 670–680. doi: 10.3892/ijo.2012.1478

Fontalba, A., Paciucci, R., Avila, J., and Zabala, J. C. (1993). Incorporation of tubulin subunits into dimers requires GTP hydrolysis. *J. Cell Sci.* 106(Pt 2), 627–632.

Fujiwara, H., Watanabe, S., Iwata, M., Ueda, S., Nobuhara, M., Wada-Kakuda, S., et al. (2020). Inhibition of microtubule assembly competent tubulin synthesis leads to accumulation of phosphorylated tau in neuronal cell bodies. *Biochem. Biophys. Res. Commun.* 521, 779–785. doi: 10.1016/j.bbrc.2019.10.191

Garland, D. L. (1978). Kinetics and mechanism of colchicine binding to tubulin: evidence for ligand-induced conformational change. *Biochemistry* 17, 4266–4272. doi: 10.1021/bi00613a024

Goldfinger, S. E. (1972). Colchicine for familial mediterranean fever. *N. Engl. J. Med.* 287:1302. doi: 10.1056/NEJM197212212872514

Gonçalves, J., Tavares, A., Carvalhal, S., and Soares, H. (2010). Revisiting the tubulin folding pathway: new roles in centrosomes and cilia. *Biomol. Concepts* 1, 423–434. doi: 10.1515/bmc.2010.033

Goodson, H. V., and Jonasson, E. M. (2018). Microtubules and microtubule-associated proteins. *Cold Spring Harb. Perspect. Biol.* 10:a022608. doi: 10.1101/cshperspect.a022608

Grayson, C., Bartolini, F., Chapple, J. P., Willison, K. R., Bhamidipati, A., Lewis, S. A., et al. (2002). Localization in the human retina of the X-linked retinitis pigmentosa protein RP2, its homologue cofactor C and the RP2 interacting protein Arl3. *Hum. Mol. Genet.* 11, 3065–3074. doi: 10.1093/hmg/11.24.3065

Grynberg, M., Jaroszewski, L., and Godzik, A. (2003). Domain analysis of the tubulin cofactor system: a model for tubulin folding and dimerization. *BMC Bioinform.* 4:46. doi: 10.1186/1471-2105-4-46

Guerrero, K., Monge, C., Brückner, A., Puurand, U., Kadaja, L., Käämbre, T., et al. (2010). Study of possible interactions of tubulin, microtubular network, and stop protein with mitochondria in muscle cells. *Mol. Cell. Biochem.* 337, 239–249. doi: 10.1007/s11010-009-0304-1

Hage-Sleiman, R., Herveau, S., Matera, E. L., Laurier, J. F., and Dumontet, C. (2010). Tubulin binding cofactor C (TBCC) suppresses tumor growth and enhances chemosensitivity in human breast cancer cells. *BMC Cancer* 10:135. doi: 10.1186/1471-2407-10-135

Hein, S., Kostin, S., Heling, A., Maeno, Y., and Schaper, J. (2000). The role of the cytoskeleton in heart failure. *Cardiovasc. Res.* 45, 273–278. doi: 10.1016/s0008-6363(99)00268-0

Helferich, A. M., Brockmann, S. J., Reinders, J., Deshpande, D., Holzmann, K., Brenner, D., et al. (2018). Dysregulation of a novel miR-1825/TBCB/TUBA4A pathway in sporadic and familial ALS. *Cell. Mol. Life Sci.* 75, 4301–4319. doi: 10.1007/s00018-018-2873-1

Karbowski, M., Spodnik, J. H., Teranishi, M., Wozniak, M., Nishizawa, Y., Usukura, J., et al. (2001). Opposite effects of microtubule-stabilizing and microtubule-destabilizing drugs on biogenesis of mitochondria in mammalian cells. *J. Cell Sci.* 114, 281–291.

Kirik, V., Grini, P. E., Mathur, J., Klinkhammer, I., Adler, K., Bechtold, N., et al. (2002). The *Arabidopsis* TUBULIN-FOLDING COFACTOR A gene is involved in the control of the alpha/beta-tubulin monomer balance. *Plant Cell* 14, 2265–2276. doi: 10.1105/tpc.003020

Kortazar, D., Carranza, G., Bellido, J., Villegas, J. C., Fanarraga, M. L., and Zabala, J. C. (2006). Native tubulin-folding cofactor E purified from baculovirus-infected Sf9 cells dissociates tubulin dimers. *Protein Expr. Purif.* 49, 196–202. doi: 10.1016/j.pep.2006.03.005

Kortazar, D., Fanarraga, M. L., Carranza, G., Bellido, J., Villegas, J. C., Avila, J., et al. (2007). Role of cofactors B (TBCB) and E (TBCE) in tubulin heterodimer dissociation. *Exp. Cell Res.* 313, 425–436. doi: 10.1016/j.yexcr.2006.09.002

Kostin, S., Hein, S., Arnon, E., Scholz, D., and Schaper, J. (2000). The cytoskeleton and related proteins in the human failing heart. *Heart Fail. Rev.* 5, 271–280. doi: 10.1023/A:1009813621103

Kuznetsov, A. V., Javadov, S., Grimm, M., Margreiter, R., Ausserlechner, M. J., and Hagenbuchner, J. (2020). Crosstalk between mitochondria and cytoskeleton in cardiac cells. *Cells* 9:222. doi: 10.3390/cells9010222

Lewis, S. A., Tian, G., and Cowan, N. J. (1997). The alpha- and beta-tubulin folding pathways. *Trends Cell Biol.* 7, 479–484. doi: 10.1016/S0962-8924(97)01168-9

Llosa, M., Aloria, K., Campo, R., Padilla, R., Avila, J., Sánchez-Pulido, L., et al. (1996). The beta-tubulin monomer release factor (p14) has homology with a region of the DnaJ protein. *FEBS Lett.* 397, 283–289. doi: 10.1016/s0014-5793(96)01198-2

Lopez, T., Dalton, K., and Frydman, J. (2015). The mechanism and function of group ii chaperonins. *J. Mol. Biol.* 427, 2919–2930. doi: 10.1016/j.jmb.2015.04.013

Lopez-Fanarraga, M., Avila, J., Guasch, A., Coll, M., and Zabala, J. C. (2001). Review: postchaperonin tubulin folding cofactors and their role in microtubule dynamics. *J. Struct. Biol.* 135, 219–229. doi: 10.1006/jsbi.2001.4386

Lopez-Fanarraga, M., Carranza, G., Bellido, J., Kortazar, D., Villegas, J. C., and Zabala, J. C. (2007). Tubulin cofactor B plays a role in the neuronal growth cone. *J. Neurochem.* 100, 1680–1687. doi: 10.1111/j.1471-4159.2006.04328.x

Löwe, J., Li, H., Downing, K. H., and Nogales, E. (2001). Refined structure of alpha beta-tubulin at 3.5 A resolution. *J. Mol. Biol.* 313, 1045–1057. doi: 10.1006/jmbi.2001.5077

Malta-Vacas, J., Nolasco, S., Monteiro, C., Soares, H., and Brito, M. (2009). Translation termination and protein folding pathway genes are not correlated in gastric cancer. *Clin. Chem. Lab. Med.* 47, 427–431. doi: 10.1515/CCLM.2009.091

Martín, L., Fanarraga, M. L., Aloria, K., and Zabala, J. C. (2000). Tubulin folding cofactor D is a microtubule destabilizing protein. *FEBS Lett.* 470, 93–95. doi: 10.1016/s0014-5793(00)01293-x

Martin, N., Jaubert, J., Gounon, P., Salido, E., Haase, G., Szatanik, M., et al. (2002). A missense mutation in Tbce causes progressive motor neuronopathy in mice. *Nat. Genet.* 32, 443–447. doi: 10.1038/ng1016

Martínez, G. J., Robertson, S., Barraclough, J., Xia, Q., Mallat, Z., Bursill, C., et al. (2015). Colchicine acutely suppresses local cardiac production of inflammatory cytokines in patients with an acute coronary syndrome. *J. Am. Heart Assoc.* 4:e002128. doi: 10.1161/JAHA.115.002128

Nasiripour, S., Zamani, F., and Farasatinasab, M. (2020). Can colchicine as an old anti-inflammatory agent be effective in COVID-19? *J. Clin. Pharmacol.* 60, 828–829. doi: 10.1002/jcph.1645

Nidorf, S. M., Eikelboom, J. W., and Thompson, P. L. (2014). Colchicine for secondary prevention of cardiovascular disease. *Curr. Atheroscler. Rep.* 16:391. doi: 10.1007/s11883-013-0391-z

Nidorf, S. M., Fiolet, A. T. L., Mosterd, A., Eikelboom, J. W., Schut, A., Opstal, T. S. J., et al. (2020). Colchicine in patients with chronic coronary disease. *N. Engl. J. Med.* 383, 1838–1847. doi: 10.1056/NEJMoa2021372

Nolasco, S., Bellido, J., Gonçalves, J., Tavares, A., Zabala, J. C., and Soares, H. (2012). The expression of tubulin cofactor A (TBCA) is regulated by a noncoding antisense Tbca RNA during testis maturation. *PLoS One* 7:e42536. doi: 10.1371/journal.pone.0042536

Nolasco, S., Bellido, J., Gonçalves, J., Zabala, J. C., and Soares, H. (2005). Tubulin cofactor A gene silencing in mammalian cells induces changes in microtubule cytoskeleton, cell cycle arrest and cell death. *FEBS Lett.* 579, 3515–3524. doi: 10.1016/j.febslet.2005.05.022

Okumura, M., Sakuma, C., Miura, M., and Chihara, T. (2015). Linking cell surface receptors to microtubules: tubulin folding cofactor D mediates Dscam functions during neuronal morphogenesis. *J. Neurosci.* 35, 1979–1990. doi: 10.1523/JNEUROSCI.0973-14.2015

Parvari, R., Hershkovitz, E., Grossman, N., Gorodischer, R., Loeys, B., Zecic, A., et al. (2002). Mutation of TBCE causes hypoparathyroidism-retardation-dysmorphism and autosomal recessive Kenny-Caffey syndrome. *Nat. Genet.* 32, 448–452. doi: 10.1038/ng1012

Prota, A. E., Danel, F., Bachmann, F., Bargsten, K., Buey, R. M., Pohlmann, J., et al. (2014). The novel microtubule-destabilizing drug BAL27862 binds to the colchicine site of tubulin with distinct effects on microtubule organization. *J. Mol. Biol.* 426, 1848–1860. doi: 10.1016/j.jmb.2014.02.005

Radcliffe, P. A., Garcia, M. A., and Toda, T. (2000). The cofactor-dependent pathways for alpha- and beta-tubulins in microtubule biogenesis are functionally different in fission yeast. *Genetics* 156, 93–103.

Rappaport, L., and Samuel, J. L. (1988). Microtubules in cardiac myocytes. *Int. Rev. Cytol.* 113, 101–143. doi: 10.1016/s0074-7696(08)60847-5

Rayala, S. K., Martin, E., Sharina, I. G., Molli, P. R., Wang, X., Jacobson, R., et al. (2007). Dynamic interplay between nitration and phosphorylation of tubulin cofactor B in the control of microtubule dynamics. *Proc. Natl. Acad. Sci. U.S.A.* 104, 19470–19475. doi: 10.1073/pnas.0705149104

Roberts, W. N. (1987). Colchicine in acute gout. *JAMA* 257:1920. doi: 10.1001/jama.1987.03390140090033

Roll-Mecak, A. (2020). The tubulin code in microtubule dynamics and information encoding. *Dev. Cell* 54, 7–20. doi: 10.1016/j.devcel.2020.06.008

Schaedel, L., John, K., Gaillard, J., Nachury, M. V., Blanchoin, L., and Théry, M. (2015). Microtubules self-repair in response to mechanical stress. *Nat. Mater.* 14, 1156–1163. doi: 10.1038/nmat4396

Schaefer, M. K. E., Schmalbruch, H., Buhler, E., Lopez, C., Martin, N., Guénet, J.-L., et al. (2007). Progressive motor neuronopathy: a critical role of the tubulin chaperone TBCE in axonal tubulin routing from the Golgi apparatus. *J. Neurosci.* 27, 8779–8789. doi: 10.1523/JNEUROSCI.1599-07.2007

Schägger, H., and von Jagow, G. (1987). Tricine-sodium dodecyl sulfate-polyacrylamide gel electrophoresis for the separation of proteins in the range from 1 to 100 kDa. *Anal. Biochem.* 166, 368–379. doi: 10.1016/0003-2697(87)90587-2

Schubert, A., Cattaruzza, M., Hecker, M., Darmer, D., Holtz, J., and Morawietz, H. (2000). Shear stress-dependent regulation of the human beta-tubulin folding cofactor D gene. *Circ. Res.* 87, 1188–1194. doi: 10.1161/01.res.87.12.1188

Serna, M., Carranza, G., Martín-Benito, J., Janowski, R., Canals, A., Coll, M., et al. (2015). The structure of the complex between α-tubulin, TBCE and TBCB reveals a tubulin dimer dissociation mechanism. *J. Cell Sci.* 128, 1824–1834. doi: 10.1242/jcs.167387

Serna, M., and Zabala, J. C. (2016). "Tubulin folding and degradation," in *ELS* (Chichester: John Wiley & Sons, Ltd), 1–9. doi: 10.1002/9780470015902.a0026333

Sferra, A., Baillat, G., Rizza, T., Barresi, S., Flex, E., Tasca, G., et al. (2016). TBCE mutations cause early-onset progressive encephalopathy with distal spinal muscular atrophy. *Am. J. Hum. Genet.* 99, 974–983. doi: 10.1016/j.ajhg.2016.08.006

Shelanski, M. L., Gaskin, F., and Cantor, C. R. (1973). Microtubule assembly in the absence of added nucleotides. *Proc. Natl. Acad. Sci. U.S.A.* 70, 765–768. doi: 10.1073/pnas.70.3.765

Shern, J. F., Sharer, J. D., Pallas, D. C., Bartolini, F., Cowan, N. J., Reed, M. S., et al. (2003). Cytosolic Arl2 is complexed with cofactor D and protein phosphatase 2A. *J. Biol. Chem.* 278, 40829–40836. doi: 10.1074/jbc.M308678200

Shultz, T., Shmuel, M., Hyman, T., and Altschuler, Y. (2008). Beta-tubulin cofactor D and ARL2 take part in apical junctional complex disassembly and abrogate epithelial structure. *FASEB J.* 22, 168–182. doi: 10.1096/fj.06-7786com

Solak, Y., Siriopol, D., Yildiz, A., Yilmaz, M. I., Ortiz, A., Covic, A., et al. (2017). Colchicine in renal medicine: new virtues of an ancient friend. *Blood Purif.* 43, 125–135. doi: 10.1159/000454669

Steinborn, K., Maulbetsch, C., Priester, B., Trautmann, S., Pacher, T., Geiges, B., et al. (2002). The *Arabidopsis* PILZ group genes encode tubulin-folding cofactor orthologs required for cell division but not cell growth. *Genes Dev.* 16, 959–971. doi: 10.1101/gad.221702

Tagawa, H., Koide, M., Sato, H., Zile, M. R., Carabello, B. A., and Cooper, G. (1998). Cytoskeletal role in the transition from compensated to decompensated hypertrophy during adult canine left ventricular pressure overloading. *Circ. Res.* 82, 751–761. doi: 10.1161/01.res.82.7.751

Tian, G., Huang, Y., Rommelaere, H., Vandekerckhove, J., Ampe, C., and Cowan, N. J. (1996). Pathway leading to correctly folded β-tubulin. *Cell* 86, 287–296. doi: 10.1016/S0092-8674(00)80100-2

Vadlamudi, R. K., Barnes, C. J., Rayala, S., Li, F., Balasenthil, S., Marcus, S., et al. (2005). p21-activated kinase 1 regulates microtubule dynamics by phosphorylating tubulin cofactor B. *Mol. Cell. Biol.* 25, 3726–3736. doi: 10.1128/MCB.25.9.3726-3736.2005

Voloshin, O., Gocheva, Y., Gutnick, M., Movshovich, N., Bakhrat, A., Baranes-Bachar, K., et al. (2010). Tubulin chaperone E binds microtubules and proteasomes and protects against misfolded protein stress. *Cell. Mol. Life Sci.* 67, 2025–2038. doi: 10.1007/s00018-010-0308-8

Walker, P. R., and Whitfield, J. F. (1984). Colchicine prevents the translation of mRNA molecules transcribed immediately after proliferative activation of hepatocytes in regenerating rat liver. *J. Cell. Physiol.* 118, 179–185. doi: 10.1002/jcp.1041180210

Wang, W., Ding, J., Allen, E., Zhu, P., Zhang, L., Vogel, H., et al. (2005). Gigaxonin interacts with tubulin folding cofactor B and controls its degradation through the ubiquitin-proteasome pathway. *Curr. Biol.* 15, 2050–2055. doi: 10.1016/j.cub.2005.10.052

Wang, Y., Zhang, H., Gigant, B., Yu, Y., Wu, Y., Chen, X., et al. (2016). Structures of a diverse set of colchicine binding site inhibitors in complex with tubulin provide a rationale for drug discovery. *FEBS J.* 283, 102–111. doi: 10.1111/febs.13555

Weisenberg, R. C. (1972). Microtubule formation in vitro in solutions containing low calcium concentrations. *Science* 177, 1104–1105. doi: 10.1126/science.177.4054.1104

Werner, C. J., Heyny-von Haussen, R., Mall, G., and Wolf, S. (2008). Proteome analysis of human substantia nigra in Parkinson's disease. *Proteome Sci.* 6, 3943–3952. doi: 10.1186/1477-5956-6-8

Wilking-Busch, M. J., Ndiaye, M. A., Liu, X., and Ahmad, N. (2018). RNA interference-mediated knockdown of SIRT1 and/or SIRT2 in melanoma: identification of downstream targets by large-scale proteomics analysis. *J. Proteomics* 170, 99–109. doi: 10.1016/j.jprot.2017.09.002

Xia, B., Li, Y., Zhou, J., Tian, B., and Feng, L. (2017). Identification of potential pathogenic genes associated with osteoporosis. *Bone Joint Res.* 6, 640–648. doi: 10.1302/2046-3758.612.BJR-2017-0102.R1

Yang, Y., Allen, E., Ding, J., and Wang, W. (2007). Giant axonal neuropathy. *Cell. Mol. Life Sci.* 64, 601–609. doi: 10.1007/s00018-007-6396-4

Yurdakul, S., Mat, C., Tüzün, Y., Ozyazgan, Y., Hamuryudan, V., Uysal, O., et al. (2001). A double-blind trial of colchicine in Behçet's syndrome. *Arthritis Rheum.* 44, 2686–2692. doi: 10.1002/1529-0131(200111)44:11<2686::aid-art448<3.0.co;2-h

Zabala, J. C., and Cowan, N. J. (1992). Tubulin dimer formation via the release of alpha- and beta-tubulin monomers from multimolecular complexes. *Cell Motil. Cytoskeleton* 23, 222–230. doi: 10.1002/cm.970230306

Zhang, P., Ma, X., Song, E., Chen, W., Pang, H., Ni, D., et al. (2013). Tubulin cofactor A functions as a novel positive regulator of ccRCC progression, invasion and metastasis. *Int. J. Cancer* 133, 2801–2811. doi: 10.1002/ijc.28306

Zhang, Q., Ma, C., Gearing, M., Wang, P. G., Chin, L. S., and Li, L. (2018). Integrated proteomics and network analysis identifies protein hubs and network alterations in Alzheimer's disease. *Acta Neuropathol. Commun.* 6:19. doi: 10.1186/s40478-018-0524-2

Conflict of Interest: The authors declare that the research was conducted in the absence of any commercial or financial relationships that could be construed as a potential conflict of interest.

frontiers in Cell and Developmental Biology

MINI REVIEW
published: 07 May 2021
doi: 10.3389/fcell.2021.673973

Nitric Oxide and Electrophilic Cyclopentenone Prostaglandins in Redox signaling, Regulation of Cytoskeleton Dynamics and Intercellular Communication

Ángel Bago[1], Miguel A. Íñiguez[1,2†] and Juan M. Serrador[1*†]*

[1] Interactions with the Environment Program, Immune System Development and Function Unit, Centro de Biología Molecular "Severo Ochoa" (CBMSO), CSIC-UAM, Madrid, Spain, [2] Departamento de Biología Molecular, Universidad Autónoma de Madrid, Madrid, Spain

OPEN ACCESS

Edited by:
Pedro Roda-Navarro, Universidad Complutense de Madrid, Spain

Reviewed by:
Pieta Mattila, University of Turku, Finland
Lidija Radenovic, University of Belgrade, Serbia

***Correspondence:**
Miguel A. Íñiguez
mainiguez@cbm.csic.es
Juan M. Serrador
jmserrador@cbm.csic.es

† These authors have contributed equally to this work and share senior authorship

Specialty section:
This article was submitted to Cell Adhesion and Migration, a section of the journal Frontiers in Cell and Developmental Biology

Received: *28 February 2021*
Accepted: *01 April 2021*
Published: *07 May 2021*

Citation:
Bago Á, Íñiguez MA and Serrador JM (2021) Nitric Oxide and Electrophilic Cyclopentenone Prostaglandins in Redox signaling, Regulation of Cytoskeleton Dynamics and Intercellular Communication. Front. Cell Dev. Biol. 9:673973. doi: 10.3389/fcell.2021.673973

Nitric oxide (NO) and electrophilic cyclopentenone prostaglandins (CyPG) are local mediators that modulate cellular response to oxidative stress in different pathophysiological processes. In particular, there is increasing evidence about their functional role during inflammation and immune responses. Although the mechanistic details about their relationship and functional interactions are still far from resolved, NO and CyPG share the ability to promote redox-based post-translational modification (PTM) of proteins that play key roles in cellular homeostasis, signal transduction and transcription. NO-induced S-nitrosylation and S-glutathionylation as well as cyclopentenone-mediated adduct formation, are a few of the main PTMs by which intra- and inter-cellular signaling are regulated. There is a growing body of evidence indicating that actin and actin-binding proteins are susceptible to covalent PTM by these agents. It is well known that the actin cytoskeleton is key for the establishment of interactions among leukocytes, endothelial and muscle cells, enabling cellular activation and migration. In this review we analyze the current knowledge about the actions exerted by NO and CyPG electrophilic lipids on the regulation of actin dynamics and cytoskeleton organization, and discuss some open questions regarding their functional relevance in the regulation of intercellular communication.

Keywords: nitric oxide, cyclopentenone prostaglandins, S-nitrosylation, S-glutathionylation, actin cytoskeleton

INTRODUCTION

Nitric oxide (NO) and cyclopentenone prostaglandins (CyPGs) are inflammation-related agents of importance for cell and tissue homeostasis. NO is synthesized enzymatically from L-Arg by the action of nitric oxide synthases (neuronal: nNOS/NOS1, inducible: iNOS/NOS2 and endothelial: eNOS/NOS3). On the other hand, cyclooxygenase 1 (COX-1) and COX-2 catalyze the committed step in formation of prostaglandins (PGs) from arachidonic acid (AA) or dihomo-γ-linolenic

acid (DGLA). Dehydration of PGs such as PGE_1 and PGD_2 results in the formation of CyPGs PGA_1 and 15-deoxy-Δ12,14-PGJ_2 (15-$dPGJ_2$), respectively (Hobbs et al., 1999; Straus and Glass, 2001; Simmons et al., 2004; Oeste and Perez-Sala, 2014). Unlike precursor PGs, CyPGs are highly reactive bioactive lipids with anti-inflammatory, anti-tumoral, and anti-angiogenic features (Diez-Dacal and Perez-Sala, 2010; Surh et al., 2011). In the inflammatory process, NO and CyPGs can reach significant concentrations as a consequence of the inducible expression of NOS2 and COX-2, participating in modulation of the inflammatory process and immune response (Hernansanz-Agustin et al., 2013; Delmastro-Greenwood et al., 2014; Garcia-Ortiz and Serrador, 2018).

Evidence of a functional interplay between NO and PG has been reported; they often act simultaneously, with essential roles in similar pathophysiological conditions. Interaction between NO and PG occurs at multiple levels. NO can either stimulate or inhibit PG production depending on cell type, the source and levels of NO and on its selective activity on COX-1 or COX-2 expression (Salvemini et al., 2013). CyPG can also regulate the cellular levels of NO. In platelets and tumoral cells, selective inhibition of COX-2 reduces the synthesis of NO whereas in macrophages, 15-$dPGJ_2$ reduces expression of iNOS either through inhibition of IKKβ or activation of PPAR-γ (Chen et al., 1997; Li et al., 2000).

Moreover, beyond the reciprocal regulation of NO and CyPG at the transcriptional level, these agents can also cross-talk by means of their ability to promote post-translational modification (PTM) of various proteins. These PTMs occur mainly through binding to redox sensitive Cys and can be mediated by NO-derived reactive nitrogen species (RNS) or by covalent thiol adduction of CyPG. There are many examples of proteins modified by both NO and CyPG: the transcription factor NF-κB; Ras; and Kelch-like ECH-associated protein 1 (Keap1), a sensor protein for oxidative stress that allows nuclear factor erythroid 2-related factor 2 (Nrf2) activation, promoting transcriptional activation and expression of antioxidant phase II genes (Straus et al., 2000; Cernuda-Morollon et al., 2001; Oliva et al., 2003; Renedo et al., 2007; Ibiza et al., 2008; Anta et al., 2016; Unoki et al., 2020).

Of note, another common target of NO and CyPG is the actin cytoskeleton. An increasing number of studies have identified actin and actin-binding proteins (ABPs) as major targets of RNS and CyPG in both physiological and oxidative pathophysiological conditions, resulting in alterations of actin network rearrangements by disturbing filament growth and stabilization (Gayarre et al., 2006; Horenberg et al., 2019; Varland et al., 2019).

In this review, we summarize the previous findings and more recent reports on the potential role of NO and CyPG in organization of the actin cytoskeleton and their involvement in regulation of cell signaling and gene expression during intercellular communication. We discuss the mechanisms by which these agents exert their functions, focusing on the interaction among leukocytes, endothelial and muscular cells as the paradigm of how NO and electrophilic CyPG may regulate homocellular and heterocellular communication in the immune and vascular systems.

NO- AND CYPG-MEDIATED POST-TRANSLATIONAL MODIFICATIONS OF ACTIN

The best-recognized pathway for NO mediated cell signaling is through binding to the heme prosthetic group of soluble guanylate cyclase and the activation of protein kinase G by cGMP. However, NO also mediates other biologically significant actions by redox-based PTM including S-nitrosylation and S-glutathionylation of Cys (**Figure 1A**), interrelated reversible processes that can occur both spontaneously and enzymatically (Martinez-Ruiz et al., 2011; Seth et al., 2018; Wolhuter et al., 2018). S-nitrosylation can take place enzymatically through a complex formed between iNOS and the S100 calcium binding proteins A8 (S100A8) and A9 (S100A9), and also through S-nitroso-CoA, which can transfer the nitrosative activity of NO from eNOS (Jia et al., 2014; Zhou et al., 2019). S-nitrosylated proteins become denitrosylated by thioredoxin (Trx/TrxR), S-nitrosoglutathione (GSH/GSNOR) and S-nitroso-CoA (SNO-CoA-SCOR) reductase systems (Garcia-Ortiz and Serrador, 2018). S-glutathionylation occurs by mixed disulfide bonds between glutathione (GSH) and Cys. Glutathione transferase (e.g., GSTP1-1 and GSTM1-1) and glutaredoxin (Grx1 and Grx2) are the main systems of enzymatic glutathionylation and deglutathionylation, respectively. S-nitrosylated proteins can also react with GSH and become denitrosylated by a nitrosyl to glutathionyl radical shift. This reaction competes *in vivo* with transnitrosylation, the transference of nitrosyl groups between proteins, producing denitrosylated proteins and free GSNO, which, in turn, can either glutathionylate or S-nitrosylate other proteins (West et al., 2006). Likewise, electrophilic CyPG can signal in cells by covalent binding to the nucleophilic thiol group of redox-sensitive Cys, a reaction that takes place through Michael addition of the α,β-unsaturated carbonyl group in the cyclopentane ring of the CyPG (Oeste and Perez-Sala, 2014; **Figure 1A**).

Proteomics studies have consistently shown that actin can be modified by S-nitrosylation, S-glutathionylation and adduct formation with the CyPGs PGA_1 and 15-$dPGJ_2$ in a remarkable number of tissues and cell types expressing β and γ non-muscular actin (e.g., leukocytes and endothelial cells) or α muscular actin (e.g., smooth muscle cells) (Fratelli et al., 2002; Gayarre et al., 2006; Nardo et al., 2009; Su et al., 2013).

S-nitrosylation of actin promotes changes in actin polymerization, and Cys217, 257, 272, 285, and 374 have all been identified as targets of S-nitrosylation in muscle cells and neutrophils. These Cys residues are located nearest to the C-terminus of actin, an important region for the establishment of actin inter-monomer contacts and association with profilin, gelsolin and cofilin among other regulatory ABPs (Thom et al., 2008; Su et al., 2013). Moreover, a number of ABPs are also S-nitrosylated on redox-sensitive thiols. Thus, the interaction of actin with cofilin, α-actinin, drebrin, filamin, tropomyosin, and

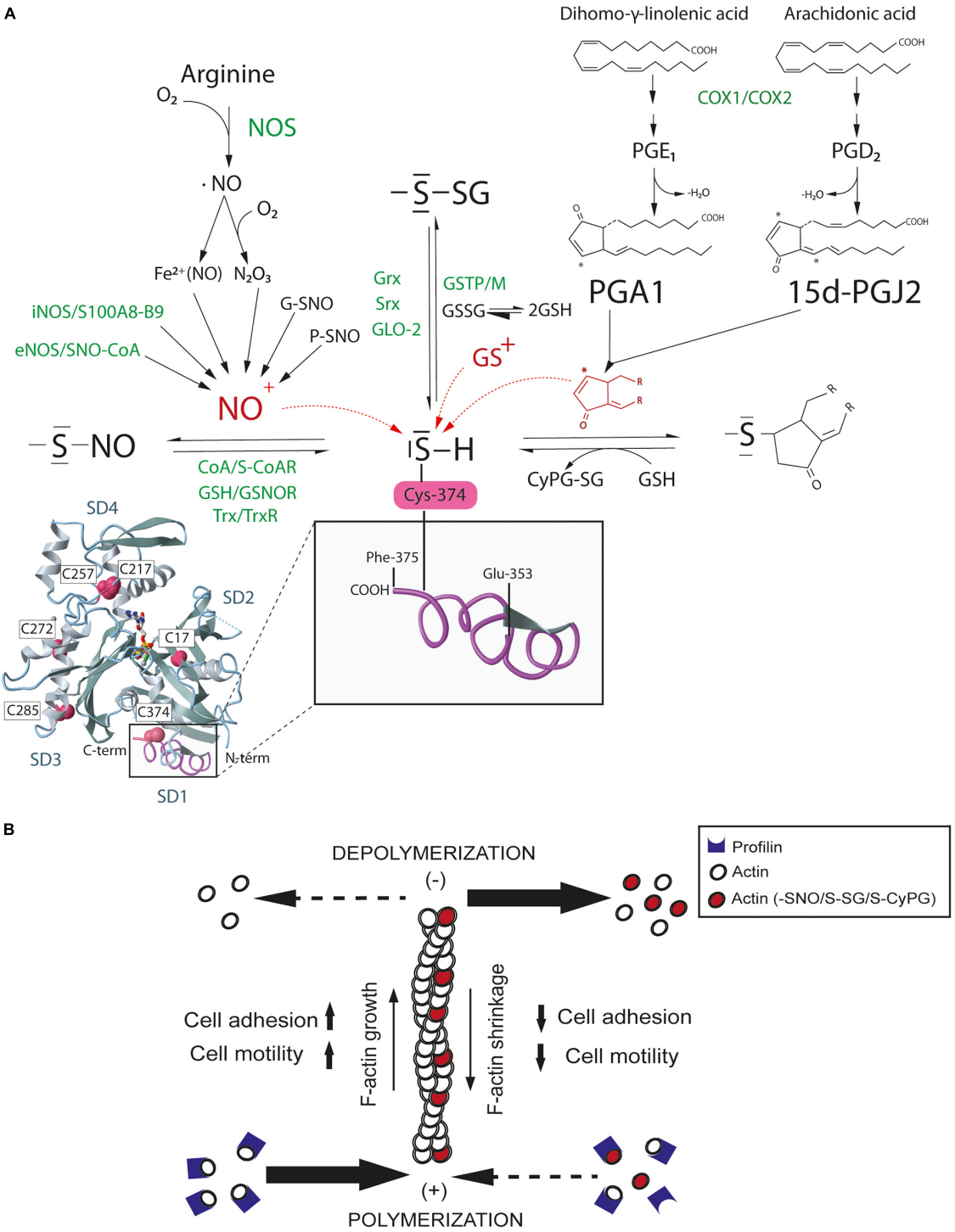

FIGURE 1 | S-nitrosylation, S-glutathionylation, and CyPG adduction of actin Cys374. **(A)** Nitric oxide (NO) produced by NO synthases (NOS) spontaneously and enzymatically S-nitrosylates actin. S-nitrosylation mainly occurs through the electrophilic attack of the nitrosonium cation (NO^+) on the sulfhydryl group of Cys, a reaction reversed by denitrosilases. Oxidized glutathione (GSSG) and glutathione-S-transferases (GSTP-M) glutathionylate actin whereas some reductases (e.g., Grx) promote actin deglutathionylation. Actin forms adducts with PGA_1 and 15-$dPGJ_2$, which can be reduced by glutathione (GSH). Spontaneous (black) and enzymatic (green) processes are shown. In red, electrophilic NO+, glutathionyl (GS+) and cyclopentenyl ring reactive species against the nucleophilic Cys sulfhydryl group of actin for S-nitrosylation, S-glutathionylation and CyPG adduction. Monomeric actin structure with subdomains (SD1-4) and redox sensitive Cys has been modified from MMDB ID:67242 using the NCBI Molecular Modeling Database (Madej et al., 2014). The inset shows the C-terminal region of actin in subdomain 1 (SD1) from Glu353 to Phe375. **(B)** Graphical abstract of actin filament shortening by redox-based post-translational modifications. S-nitrosylation, S-glutathionylation, and CyPG adduction of actin may disturb cell adhesion and motility likewise by reducing actin binding to profilin and polymerization at the barbed-end (+) and/or enhancing actin depolymerization from the pointed-end (–), which eventually induces F-actin shrinkage and actin cytoskeleton reorganization.

plastin/fimbrin may be regulated by S-nitrosylation (Martinez-Ruiz and Lamas, 2005; Ulrich et al., 2012; Figueiredo-Freitas et al., 2015). Ezrin and moesin, which are plasma membrane organizers that link the actin cytoskeleton to the cytoplasmic tail of transmembrane proteins, are also S-nitrosylated on Cys117 and 284 in response to iNOS-derived NO, increasing actin cytoskeleton tension and cell migration (Fernando et al., 2019; Zhang et al., 2019).

Actin is also a target for S-glutathionylation on Cys17, 217, and 374 (Wang et al., 2001; Hamnell-Pamment et al., 2005). S-glutathionylation impairs actin polymerization and destabilizes F-actin, in part by reducing the interaction between actin and tropomyosin, which triggers morphological changes that are reverted by Grx-mediated deglutathionylation (Pastore et al., 2003; Wang et al., 2003). Glyoxilase II (Glo2), sulfiredoxin 1 (Srx1) and protein disulfide isomerase (PDI) are other redox enzymes that could catalyze deglutathionylation of actin in eukaryotic cells (Findlay et al., 2006; Sobierajska et al., 2014; Ercolani et al., 2016). Interestingly, S-glutathionylation of the elastic protein titin on Cys47 and 63 at the F-actin-rich sarcomere regulates stiffness in both skeletal and cardiac muscle through inhibition of titin refolding (Herrero-Galan et al., 2019).

CyPGs are also redox regulators of actin. Several studies have shown that, PGA_1 and 15-$dPGJ_2$ bind covalently to actin on Cys374, inducing morphological changes in the actin cytoskeleton of neuroblastoma and mesangial cells by interfering with the formation of F-actin, with less abundant filaments, shorter length and altered structure (Gayarre et al., 2006; Stamatakis et al., 2006; Aldini et al., 2007). CyPG also regulate the interaction of actin with vimentin. PGA_1 and 15-$dPGJ_2$ directly bind to vimentin on Cys328, promoting cytoskeletal rearrangements that impair mitosis progression by interfering with its association with actin at the cell cortex (Duarte et al., 2019; Monico et al., 2019). In this regard, although both S-nitrosylation and S–glutathionylation on Cys328 have been reported to affect vimentin elongation (Kaus-Drobek et al., 2020), whether some of these redox-based PTMs disrupt the association between vimentin and actin at the cell cortex remains unknown.

Therefore, a large body of evidence supports Cys374 as the residue most sensitive to redox in actin, undergoing mild oxidation by RNS, GSH/GSSG or CyPG. The high reactivity of Cys374 may be in part due to its position as the penultimate amino acid residue in the C-terminal domain of actin, leaving it to be partially solvent-exposed and thus accessible to PTM. In addition, its proximity to Tyr133 (aromatic ring) and Arg116 (basic) in actin subdomain 1 would favor the reactivity of the Cys374 sulfhydryl group (Lassing et al., 2007). Moreover, Cys374 contributes to F-actin intra- and inter-strand contacts between actin subunits, fostering actin polymerization and F-actin stability (Oda et al., 2009; Dominguez and Holmes, 2011). In this regard, S-nitrosylation, S-glutathionylation and CyPG adduction on Cys374 similarly disturb the organization of the actin cytoskeleton, reducing cell adhesion and motility (**Figure 1B**). Nevertheless, the functional relationship between these actin PTMs remains an open question. It is plausible that S-nitrosylation and CyPG adduction of Cys374 do not represent end-effector PTMs but rather intermediate stages of actin oxidation, as observed previously (Giustarini et al., 2005; Gayarre et al., 2007; Wolhuter and Eaton, 2017). Changes in the GSH/GSSG ratio may switch these PTMs to glutathionylation, as a protective modification to preserve actin functions from harmful nitrosative and oxidative stress.

NO- AND CYPG-MEDIATED REDOX POST-TRANSLATIONAL MODIFICATIONS IN ENDOTHELIAL CELL JUNCTIONS

Regulation of F-actin dynamics is essential for the endothelial barrier function of the adherens junctions (AJs). Homophilic extracellular adhesion between vascular endothelial (VE)-cadherin molecules and anchorage to the actin cytoskeleton through α-/β-catenin complexes associated with the cytoplasmic tail of VE-cadherin are needed to stabilize AJs between endothelial cells. Recent studies have shown that S-nitrosylation regulates AJ and vascular permeability at different levels (**Figure 2A**). Activation of endothelial cells with platelet-activating factor (PAF) S-nitrosylates VE-cadherin solely on its transmembrane-localized Cys, promoting VE-cadherin phosphorylation on Tyr, dissociation from actin-cytoskeleton–linked β-catenin and internalization (Guequen et al., 2016). Moreover, β-catenin is S-nitrosylated on Cys619 in response to eNOS activation by VEGF, PAF, or TNF-α, inducing dissociation from VE-cadherin (Thibeault et al., 2010; Marin et al., 2012). Release of F-actin-linked α-/β-catenin complexes from VE-cadherin increases permeability through the dissociation of the actin cytoskeleton from the AJ. S-nitrosylation of T-plastin also disturbs AJs; angiotensin-II-induced iNOS expression in aortic endothelial cells S-nitrosylates T-plastin on Cys566, increasing the F-actin-severing activity of cofilin at the AJ, which may be involved in the pathophysiological basis of thoracic aortic dissection, a disease in which aortic tissues from patients show high levels of S-nitrosylation (Pan et al., 2020). Rac-1, a small Rho GTPase of importance for the actin cytoskeletal rearrangements that orchestrate AJ formation in endothelial cells, is also a redox target of S-nitrosylation, S-glutathionylation and 15-$dPGJ_2$ adduction. S-glutathionylation and 15-$dPGJ_2$ adduction on Cys157 inhibits actin polymerization by Rac-1, disrupting the AJ and increasing endothelial permeability, whereas S-nitrosylation on Cys157 has also been observed in muscular cells, although the functional relevance of this PTM remains unknown (Su et al., 2013; Wall et al., 2015; Han et al., 2016). In contrast, *in vitro* studies with GSSG have shown that Rac-1 can be S-glutathionylated on Cys18, a PTM that accelerates nucleotide exchange and activation (Hobbs et al., 2015).

Tight junctions (TJ) and gap junctions (GJ) are also targets of oxidative and nitrosative stress. In Friedich ataxia, frataxin deficiency increases S-glutathionylation of actin, disrupting actin cytoskeleton anchorage to TJ proteins in micro VE cells of the blood–brain barrier, a PTM that is also characteristic of aortic valve sclerosis in humans (Valerio et al., 2019; Smith and Kosman, 2020). Coordinated S-nitrosylation/denitrosylation

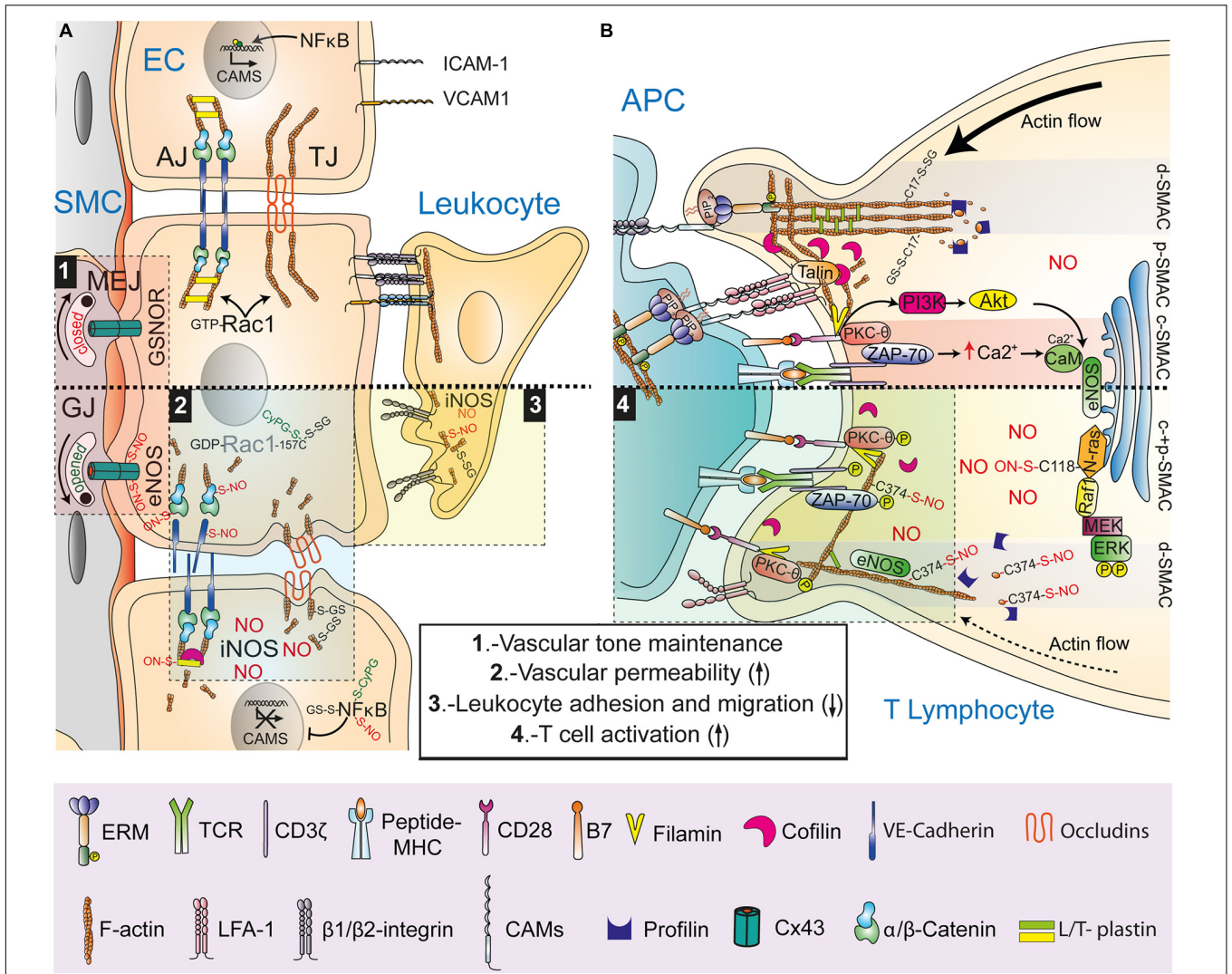

FIGURE 2 | NO- and CyPG-mediated redox post-translational modifications of actin at cell-cell interactions. **(A)** Regulation of endothelial cell junctions and leukocyte-endothelial cell interactions. Upper part, Rac-1-mediated formation of actin-based adherens junctions (AJ) and tight junctions (TJ), NF-κB-promoted induction of cell adhesion molecules (CAMs) expression on activated endothelial cells (EC), integrin-mediated formation of leukocyte-EC docking structures, and closure of gap junctions (GJ) by GSNOR-mediated Cx45 denitrosylation at myoendothelial junctions (MEJ) are depicted. Lower part, Nitric oxide (NO) synthesized by eNOS opens GJ to control vascular SMC tone through S-nitrosylation of Cx45 (1) and disrupts AJ through S-nitrosylation of β-catenin and VE-cadherin increasing vascular permeability (2). Rac-1 inhibition by S-glutathionylation and CyPG adduction on Cys157 interferes with AJ and TJ formation whereas iNOS-derived NO interferes with AJ and TJ formation through cofilin activation by S-nitrosylation of T-plastin and S-glutathionylation of actin, respectively (2). NO produced by iNOS in ECs downregulates CAMs by either S-nitrosylation, S-glutathionylation, or CyPG adduction of NF-κB and in leukocytes interferes with β2 integrin activation by actin S-nitrosylation and S-glutathionylation, reducing leukocyte adhesion to ECs and migration (3). **(B)** Regulation of the immune synapse (IS). Upper part, retrograde actin flow in a mature IS showing ICAM-associated ERM, L-plastin-bundled F-actin and actin S-glutathionylated on Cys17 at the d-SMAC; cofilin and clusters of talin-associated LFA-1 at the p-SMAC; and signaling complexes between filamin-associated CD28 and PKC-θ and between TCR and ZAP-70 at the c-SMAC. Lower part, reduced retrograde actin flow upon full eNOS activation on the Golgi complex and the d-SMAC, where actin binding to profilin and polymerization is disturbed by S-nitrosylation on Cys374. Inactivated LFA-1 and mislocalization of cofilin are depicted. Enhanced phosphorylation of dispersed CD28-filamin-PKC- and TCR-ZAP-70 microclusters increases T cell activation (4).

of GJ connexin (Cx)43 on Cys271 by compartmentalized activation of eNOS and GSNOR on the endothelial side of myoendothelial junctions (MEJ), controls smooth vascular muscle contraction and relaxation (Straub et al., 2011). The pathophysiological significance of Cx43 S-nitrosylation is illustrated in a mouse experimental model of Duchenne muscular dystrophy in which the opening of Cx43 hemichannels by NO-mediated S-nitrosylation led to cardiac stress-induced arrhythmias (Lillo et al., 2019).

Therefore, ample evidence exists to consider endothelial cell junctions as hot-spots of oxidative and nitrosative stress, with actin cytoskeleton-associated proteins anchored to them as important redox targets for the regulation of leukocyte homeostasis and inflammation.

NO- AND CYPG-MEDIATED REDOX POST-TRANSLATIONAL MODIFICATIONS IN LEUKOCYTE-ENDOTHELIAL INTERACTIONS

In the vascular system, NO and CyPG regulate leukocyte adhesion to endothelial cells, thus working as anti-inflammatory agents. Expression of the adhesion molecules ICAM-1, VCAM-1, and E- and P- selectin on activated endothelial cells is modulated at the transcriptional level by RNS- and CyPG-mediated PTM of NF-κB. S-nitrosylation, glutathionylation and 15-dPGJ$_2$ adduction of IKKβ, p50, and p65 reduce the transcriptional activity of NF-κB by targeting Cys62, 38, and 179, respectively (Straus et al., 2000; Cernuda-Morollon et al., 2001; Pineda-Molina et al., 2001; Castrillo et al., 2003; Reynaert et al., 2004, 2006; Lin et al., 2012). However, the regulation exerted on leukocyte-endothelial interactions by NO and CyPG is not restricted to endothelial cells (**Figure 2A**). For instance, 15-dPGJ$_2$ abrogates ICAM-1 expression on endothelial cells in mesenteric vessels through an NO-dependent mechanism, but disturbs actin cytoskeleton rearrangements and migration in renal carcinoma cells and neutrophils likely through formation of adducts with actin (Aldini et al., 2007; Napimoga et al., 2008; Yamamoto et al., 2020). Similarly, S-nitrosylation, and S-glutathionylation of actin regulate adhesion to endothelial cells and migration of neutrophils by interfering with cytoskeleton dynamics. In this way, hyperoxia- and hyperglycemia-induced nitrosative stress by iNOS-synthesized NO S-nitrosylates β-actin on Cys 257, 272, 285, and 374, leading to a subset of short actin filaments that bind NLRP3 and disturbs β_2 integrin clustering and adhesion of neutrophils to ICAM-1, which activates inflammasomes (Thom et al., 2008, 2017). This process is transient and followed by association of FAK, Trx/TrxR, VASP, and Rac with S-nitrosylated actin for subsequent denitrosylation and reorganization of F-actin to restore clustering and activation of β_2 integrins (Thom et al., 2012, 2013). Impairment of adhesion via β_2 integrins has also been reported in N-formylmethionyl-leucyl-phenylalanine (fMLF)-mediated migration of neutrophils from Grx1-deficient mice, which show reduced actin polymerization and increased S-glutathionylation of actin on Cys374, a PTM that also occurs upon oxidative stress by NADPH oxidase (Sakai et al., 2012).

Therefore, dynamic coordination between actin S-nitrosylation and S-glutathionylation seems necessary for the actin cytoskeleton rearrangements that regulate neutrophil chemotaxis.

S-NITROSYLATION AND S-GLUTATHIONYLATION AT THE T CELL IMMUNE SYNAPSE

S-nitrosylation also plays a key role in the regulation of T cell cognate interactions. The development of T lymphocytes is compromised in GSNOR-deficient mice whereas induction of GSNOR expression increases T cell activation by reducing S-nitrosylation of Akt on Cys224, which allows phosphorylation on Ser473 and Akt signaling (Yang et al., 2010; Li et al., 2018). On the other hand, compartmentalized production of NO by eNOS on the Golgi complex of T cells stimulated with antigen-pulsed antigen-presenting cells (APCs) activates N-Ras by S-nitrosylation on Cys118, leading to Ras-Raf-MEK-ERK signaling and activation-induced cell death (AICD) (Ibiza et al., 2008). Despite the ability of S-nitrosylation to regulate signaling targets downstream of the T cell receptor (TCR), a more general mechanism involving S-nitrosylation of actin for regulation of TCR-triggered signal transmission at the immune synapse (IS) can be considered (**Figure 2B**). NO synthesized by eNOS near the F-actin ring at the distal supramolecular activation clusters (d-SMAC) disturbs the coalescence of signaling microclusters of CD3, PKC-θ and CD28 in the central (c-)SMAC. These molecules show increased phosphorylation, which leads to a stronger activation of NF-κB (Ibiza et al., 2006; Garcia-Ortiz et al., 2017). Changes exerted by NO on signaling microclusters depend on the S-nitrosylation of actin on Cys374, which interferes with the formation of profilin-actin complexes, the main cellular source of ATP-activated actin used by formins and Arp 2/3 to nucleate filaments (Garcia-Ortiz et al., 2017). By interfering with binding between profilin and actin, S-nitrosylation reduces actin polymerization and retrograde flow toward the c-SMAC, the proposed main force driving movement of microclusters of TCR-associated signaling receptors, kinases and adaptors from the d-SMAC to the c-SMAC, where they dissociate from the TCR and signaling is attenuated (Hammer et al., 2019).

S-glutathionylation also plays an important function in T cell activation and IS formation. Sulphoraphane and piperlongumine, natural plant-derived prooxidative compounds that lower intracellular GSH levels, reduce the S-glutathionylation of actin, the expression of the activation markers CD69 and CD25, the secretion of IL-2 and T cell proliferation. Low GSH inhibits differentiation of proinflammatory Th17 but not Th1 and Th2 cells by reducing the production of IL-22, IL-17A, and IL-17F through inhibition of the transcription factors RORγt, HIF-1α, and STAT-3 (Liang et al., 2018, 2020). Interestingly, depletion of GSH by piperlongumine interferes with the enrichment of CD3 and the β_2 integrin LFA-1 at the c- and peripheral (p)-SMAC, respectively, switching S-glutathionylation of actin on Cys17 to irreversible sulfinylation and sulfonylation (Liang et al., 2020).

In addition, some evidence suggests that S-nitrosylation and/or glutathionylation may also regulate the function of ABPs in the T cell IS. Cofilin, an F-actin severing ABP localized at the p-SMAC, is a target of oxidative stress and RNS. H_2O_2 impairs cofilin function through formation of an intramolecular disulfide bridge between Cys39 and 80. This PTM inhibits dephosphorylation-induced activation of cofilin on Ser3 and disturbs F-actin depolymerization in the IS, which is necessary for localization of LFA-1 and cofilin itself at the p-SMAC. On the other hand, S-nitrosylation and S-glutathionylation of cofilin on both Cys80 and 139 by eNOS-derived NO and by expression of GSTP1, respectively, have been described to reduce the F-actin-severing activity of cofilin (Zhang et al., 2015; Kruyer et al., 2019). L-plastin, an F-actin-bundling ABP whose phosphorylation on Ser5 facilitates the actin-dependent organization of LFA-1 at the

p-SMAC (Wabnitz et al., 2010; Wang et al., 2010), also forms an intramolecular disulfide bridge between Cys42 and 101 when T cells are exposed to oxidative stress with H_2O_2. Oxidation of L-plastin is reversed by the Trx/TrxR system, which targets Cys101 as the most redox sensitive Cys residue of L-plastin in T cells (Balta et al., 2019). In this regard, recent reports have shown that iNOS-mediated nitrosative oxidation in neutrophils induces S-glutathionylation of L-plastin on Cys460, leading to the compartmentalized dissociation of F-actin bundles at the leading edge (Dubey et al., 2015). The actions that these NO-mediated cofilin and plastin PTMs exert on the reorganization of the actin cytoskeleton raises the possibility that other ABPs localized within the IS and susceptible to S-nitrosylation/S-glutathionylation (e.g., α-actinin, drebrin, dynamin, catenin or ezrin) may also work as redox sensors for the regulation of T cell activation.

CONCLUSION

Increasing evidence demonstrates that RNS- and CyPG-mediated redox PTMs on reactive Cys residues promote changes in the structure and function of actin cytoskeleton regulatory proteins thus playing an essential role in cell function. In physiological conditions, NO is produced at basal steady-state levels, and reversible S-nitrosylation/denitrosylation controls cell homeostasis. However, higher levels of NO and PGs are released simultaneously in inflammatory conditions, mainly due to the inducible expression of iNOS and COX-2, respectively. RNS- and CyPG-mediated PTM contribute to the actin cytoskeleton-associated outcome of intercellular interactions between immune and vascular cells, controlling leukocyte activation, migration and vascular permeability (**Figure 2**). This is of importance from a pathophysiological perspective, as NO and CyPGs are redox regulators of development and resolution of the inflammatory process. How reversibility of S-nitrosylation and CyPG adduction is preserved during increasing inflammation-induced oxidative stress is still an unanswered question. In this regard, glutathionylation is now also considered to be a physiologically important PTM by which intracellular redox changes are transduced into functional responses (Klatt and Lamas, 2000). Although the mechanisms involved in protein glutathionylation are not yet fully understood, they may take place in part through RNS- and CyPG-mediated PTMs as intermediate products of oxidation on protein thiols. A better understanding of how NO- and CyPG–mediated PTMs cooperate to regulate actin polymerization and stability may provide new insights into the regulation of vascular dysfunction and inflammatory immune responses.

AUTHOR CONTRIBUTIONS

All authors listed have made a substantial, direct and intellectual contribution to the work, and approved it for publication.

FUNDING

This work was supported by grant RTI2018-100815-B-I00 (MICIU/FEDER) to MÍ and JS. We acknowledge support of the publication fee by the Spanish Research Council (CSIC) Open Access Publication Support Initiative.

ACKNOWLEDGMENTS

The professional editing service NB Revisions was used for technical preparation of the text prior to submission. We apologize to any authors and work that was not cited due to restrictions in the size of the manuscript.

REFERENCES

Aldini, G., Carini, M., Vistoli, G., Shibata, T., Kusano, Y., Gamberoni, L., et al. (2007). Identification of actin as a 15-deoxy-Delta12,14-prostaglandin J2 target in neuroblastoma cells: mass spectrometric, computational, and functional approaches to investigate the effect on cytoskeletal derangement. *Biochemistry* 46, 2707–2718. doi: 10.1021/bi0618565

Anta, B., Perez-Rodriguez, A., Castro, J., Garcia-Dominguez, C. A., Ibiza, S., Martinez, N., et al. (2016). PGA1-induced apoptosis involves specific activation of H-Ras and N-Ras in cellular endomembranes. *Cell Death Dis.* 7:e2311. doi: 10.1038/cddis.2016.219

Balta, E., Hardt, R., Liang, J., Kirchgessner, H., Orlik, C., Jahraus, B., et al. (2019). Spatial oxidation of L-plastin downmodulates actin-based functions of tumor cells. *Nat. Commun.* 10:4073.

Castrillo, A., Traves, P. G., Martin-Sanz, P., Parkinson, S., Parker, P. J., and Bosca, L. (2003). Potentiation of protein kinase C zeta activity by 15-deoxy-delta(12,14)-prostaglandin J(2) induces an imbalance between mitogen-activated protein kinases and NF-kappa B that promotes apoptosis in macrophages. *Mol. Cell. Biol.* 23, 1196–1208. doi: 10.1128/mcb.23.4.1196-1208.2003

Cernuda-Morollon, E., Pineda-Molina, E., Canada, F. J., and Perez-Sala, D. (2001). 15-Deoxy-Delta 12,14-prostaglandin J2 inhibition of NF-kappaB-DNA binding through covalent modification of the p50 subunit. *J. Biol. Chem.* 276, 35530–35536. doi: 10.1074/jbc.m104518200

Chen, L., Salafranca, M. N., and Mehta, J. L. (1997). Cyclooxygenase inhibition decreases nitric oxide synthase activity in human platelets. *Am. J. Physiol.* 273, H1854–H1859.

Delmastro-Greenwood, M., Freeman, B. A., and Wendell, S. G. (2014). Redox-dependent anti-inflammatory signaling actions of unsaturated fatty acids. *Ann. Rev. Physiol.* 76, 79–105. doi: 10.1146/annurev-physiol-021113-170341

Diez-Dacal, B., and Perez-Sala, D. (2010). Anti-inflammatory prostanoids: focus on the interactions between electrophile signaling and resolution of inflammation. *Sci. World J.* 10, 655–675. doi: 10.1100/tsw.2010.69

Dominguez, R., and Holmes, K. C. (2011). Actin structure and function. *Annu. Rev. Biophys.* 40, 169–186.

Duarte, S., Viedma-Poyatos, A., Navarro-Carrasco, E., Martinez, A. E., Pajares, M. A., and Perez-Sala, D. (2019). Vimentin filaments interact with the actin cortex in mitosis allowing normal cell division. *Nat. Commun.* 10:4200.

Dubey, M., Singh, A. K., Awasthi, D., Nagarkoti, S., Kumar, S., Ali, W., et al. (2015). L-Plastin S-glutathionylation promotes reduced binding to beta-actin and affects neutrophil functions. *Free Rad. Biol. Med.* 86, 1–15. doi: 10.1016/j.freeradbiomed.2015.04.008

Ercolani, L., Scire, A., Galeazzi, R., Massaccesi, L., Cianfruglia, L., Amici, A., et al. (2016). A possible S-glutathionylation of specific proteins by glyoxalase II: an in vitro and in silico study. *Cell Biochem. Funct.* 34, 620–627. doi: 10.1002/cbf.3236

Fernando, V., Zheng, X., Walia, Y., Sharma, V., Letson, J., and Furuta, S. (2019). S-nitrosylation: an emerging paradigm of redox signaling. *Antioxidants* 8:404. doi: 10.3390/antiox8090404

Figueiredo-Freitas, C., Dulce, R. A., Foster, M. W., Liang, J., Yamashita, A. M., Lima-Rosa, F. L., et al. (2015). S-nitrosylation of sarcomeric proteins depresses myofilament Ca2+)sensitivity in intact Cardiomyocytes. *Antioxid. Redox Signal.* 23, 1017–1034. doi: 10.1089/ars.2015.6275

Findlay, V. J., Townsend, D. M., Morris, T. E., Fraser, J. P., He, L., and Tew, K. D. (2006). A novel role for human sulfiredoxin in the reversal of glutathionylation. *Cancer Res.* 66, 6800–6806. doi: 10.1158/0008-5472.can-06-0484

Fratelli, M., Demol, H., Puype, M., Casagrande, S., Eberini, I., Salmona, M., et al. (2002). Identification by redox proteomics of glutathionylated proteins in oxidatively stressed human T lymphocytes. *Proc. Natl. Acad. Sci. U.S.A.* 99, 3505–3510. doi: 10.1073/pnas.052592699

Garcia-Ortiz, A., Martin-Cofreces, N. B., Ibiza, S., Ortega, A., Izquierdo-Alvarez, A., Trullo, A., et al. (2017). eNOS S-nitrosylates beta-actin on Cys374 and regulates PKC-theta at the immune synapse by impairing actin binding to profilin-1. *PLoS Biol.* 15:e2000653. doi: 10.1371/journal.pbio.2000653

Garcia-Ortiz, A., and Serrador, J. M. (2018). Nitric oxide signaling in T cell-mediated immunity. *Trends Mol. Med.* 24, 412–427. doi: 10.1016/j.molmed.2018.02.002

Gayarre, J., Avellano, M. I., Sanchez-Gomez, F. J., Carrasco, M. J., Canada, F. J., and Perez-Sala, D. (2007). Modification of proteins by cyclopentenone prostaglandins is differentially modulated by GSH in vitro. *Ann. N. Y. Acad. Sci.* 1096, 78–85. doi: 10.1196/annals.1397.072

Gayarre, J., Sanchez, D., Sanchez-Gomez, F. J., Terron, M. C., Llorca, O., and Perez-Sala, D. (2006). Addition of electrophilic lipids to actin alters filament structure. *Biochem. Biophys. Res. Commun.* 349, 1387–1393. doi: 10.1016/j.bbrc.2006.09.005

Giustarini, D., Milzani, A., Aldini, G., Carini, M., Rossi, R., and Dalle-Donne, I. (2005). S-nitrosation versus S-glutathionylation of protein sulfhydryl groups by S-nitrosoglutathione. *Antioxid. Redox Signal.* 7, 930–939. doi: 10.1089/ars.2005.7.930

Guequen, A., Carrasco, R., Zamorano, P., Rebolledo, L., Burboa, P., Sarmiento, J., et al. (2016). S-nitrosylation regulates VE-cadherin phosphorylation and internalization in microvascular permeability. *Am. J. Physiol.* 310, H1039–H1044.

Hammer, J. A., Wang, J. C., Saeed, M., and Pedrosa, A. T. (2019). Origin, organization, dynamics, and function of actin and actomyosin networks at the T cell immunological synapse. *Annu. Rev. Immunol.* 37, 201–224. doi: 10.1146/annurev-immunol-042718-041341

Hamnell-Pamment, Y., Lind, C., Palmberg, C., Bergman, T., and Cotgreave, I. A. (2005). Determination of site-specificity of S-glutathionylated cellular proteins. *Biochem. Biophys. Res. Commun.* 332, 362–369. doi: 10.1016/j.bbrc.2005.04.130

Han, J., Weisbrod, R. M., Shao, D., Watanabe, Y., Yin, X., Bachschmid, M. M., et al. (2016). The redox mechanism for vascular barrier dysfunction associated with metabolic disorders: glutathionylation of Rac1 in endothelial cells. *Redox Biol.* 9, 306–319. doi: 10.1016/j.redox.2016.09.003

Hernansanz-Agustin, P., Izquierdo-Alvarez, A., Garcia-Ortiz, A., Ibiza, S., Serrador, J. M., and Martinez-Ruiz, A. (2013). Nitrosothiols in the immune system: signaling and protection. *Antioxid. Redox Signal.* 18, 288–308. doi: 10.1089/ars.2012.4765

Herrero-Galan, E., Martinez-Martin, I., and Alegre-Cebollada, J. (2019). Redox regulation of protein nanomechanics in health and disease: lessons from titin. *Redox Biol.* 21:101074. doi: 10.1016/j.redox.2018.101074

Hobbs, A. J., Higgs, A., and Moncada, S. (1999). Inhibition of nitric oxide synthase as a potential therapeutic target. *Annu. Rev. Pharmacol. Toxicol.* 39, 191–220. doi: 10.1146/annurev.pharmtox.39.1.191

Hobbs, G. A., Mitchell, L. E., Arrington, M. E., Gunawardena, H. P., DeCristo, M. J., Loeser, R. F., et al. (2015). Redox regulation of Rac1 by thiol oxidation. *Free Rad. Biol. Med.* 79, 237–250. doi: 10.1016/j.freeradbiomed.2014.09.027

Horenberg, A. L., Houghton, A. M., Pandey, S., Seshadri, V., and Guilford, W. H. (2019). S-nitrosylation of cytoskeletal proteins. *Cytoskeleton* 76, 243–253. doi: 10.1002/cm.21520

Ibiza, S., Perez-Rodriguez, A., Ortega, A., Martinez-Ruiz, A., Barreiro, O., Garcia-Dominguez, C. A., et al. (2008). Endothelial nitric oxide synthase regulates N-Ras activation on the Golgi complex of antigen-stimulated T cells. *Proc. Natl. Acad. Sci. U.S.A.* 105, 10507–10512. doi: 10.1073/pnas.0711062105

Ibiza, S., Victor, V. M., Bosca, I., Ortega, A., Urzainqui, A., O'Connor, J. E., et al. (2006). Endothelial nitric oxide synthase regulates T cell receptor signaling at the immunological synapse. *Immunity* 24, 753–765. doi: 10.1016/j.immuni.2006.04.006

Jia, J., Arif, A., Terenzi, F., Willard, B., Plow, E. F., Hazen, S. L., et al. (2014). Target-selective protein S-nitrosylation by sequence motif recognition. *Cell* 159, 623–634. doi: 10.1016/j.cell.2014.09.032

Kaus-Drobek, M., Mucke, N., Szczepanowski, R. H., Wedig, T., Czarnocki-Cieciura, M., Polakowska, M., et al. (2020). Vimentin S-glutathionylation at Cys328 inhibits filament elongation and induces severing of mature filaments in vitro. *FEBS J.* 287, 5304–5322. doi: 10.1111/febs.15321

Klatt, P., and Lamas, S. (2000). Regulation of protein function by S-glutathiolation in response to oxidative and nitrosative stress. *Eur. J. Biochem.* 267, 4928–4944. doi: 10.1046/j.1432-1327.2000.01601.x

Kruyer, A., Ball, L. E., Townsend, D. M., Kalivas, P. W., and Uys, J. D. (2019). Post-translational S-glutathionylation of cofilin increases actin cycling during cocaine seeking. *PLoS One* 14:e0223037. doi: 10.1371/journal.pone.0223037

Lassing, I., Schmitzberger, F., Bjornstedt, M., Holmgren, A., Nordlund, P., Schutt, C. E., et al. (2007). Molecular and structural basis for redox regulation of beta-actin. *J. Mol. Biol.* 370, 331–348. doi: 10.1016/j.jmb.2007.04.056

Li, J., Zhang, Y., Lu, S., Miao, Y., Yang, J., Huang, S., et al. (2018). GSNOR modulates hyperhomocysteinemia-induced T cell activation and atherosclerosis by switching Akt S-nitrosylation to phosphorylation. *Redox Biol.* 17, 386–399. doi: 10.1016/j.redox.2018.04.021

Li, M., Pascual, G., and Glass, C. K. (2000). Peroxisome proliferator-activated receptor gamma-dependent repression of the inducible nitric oxide synthase gene. *Mol. Cell. Biol.* 20, 4699–4707. doi: 10.1128/mcb.20.13.4699-4707.2000

Liang, J., Jahraus, B., Balta, E., Ziegler, J. D., Hubner, K., Blank, N., et al. (2018). Sulforaphane inhibits inflammatory responses of primary human T-cells by increasing ROS and depleting glutathione. *Front. Immunol.* 9:2584. doi: 10.3389/fimmu.2018.02584

Liang, J., Ziegler, J. D., Jahraus, B., Orlik, C., Blatnik, R., Blank, N., et al. (2020). Piperlongumine acts as an immunosuppressant by exerting prooxidative effects in human T cells resulting in diminished TH17 but enhanced Treg differentiation. *Front. Immunol.* 11:1172. doi: 10.3389/fimmu.2020.01172

Lillo, M. A., Himelman, E., Shirokova, N., Xie, L. H., Fraidenraich, D., and Contreras, J. E. (2019). S-nitrosylation of connexin43 hemichannels elicits cardiac stress-induced arrhythmias in duchenne muscular dystrophy mice. *JCI Insight* 4:e130091.

Lin, Y. C., Huang, G. D., Hsieh, C. W., and Wung, B. S. (2012). The glutathionylation of p65 modulates NF-kappaB activity in 15-deoxy-Delta(1)(2),(1)(4)-prostaglandin J(2)-treated endothelial cells. *Free Radic. Biol. Med.* 52, 1844–1853. doi: 10.1016/j.freeradbiomed.2012.02.028

Madej, T., Lanczycki, C. J., Zhang, D., Thiessen, P. A., Geer, R. C., Marchler-Bauer, A., et al. (2014). MMDB and VAST+: tracking structural similarities between macromolecular complexes. *Nucleic Acids Res.* 42, D297–D303.

Marin, N., Zamorano, P., Carrasco, R., Mujica, P., Gonzalez, F. G., Quezada, C., et al. (2012). S-Nitrosation of beta-catenin and p120 catenin: a novel regulatory mechanism in endothelial hyperpermeability. *Circ. Res.* 111, 553–563. doi: 10.1161/circresaha.112.274548

Martinez-Ruiz, A., Cadenas, S., and Lamas, S. (2011). Nitric oxide signaling: classical, less classical, and nonclassical mechanisms. *Free Radic. Biol. Med.* 51, 17–29. doi: 10.1016/j.freeradbiomed.2011.04.010

Martinez-Ruiz, A., and Lamas, S. (2005). Nitrosylation of thiols in vascular homeostasis and disease. *Curr. Atheroscler. Rep.* 7, 213–218. doi: 10.1007/s11883-005-0009-1

Monico, A., Duarte, S., Pajares, M. A., and Perez-Sala, D. (2019). Vimentin disruption by lipoxidation and electrophiles: role of the cysteine residue and filament dynamics. *Redox Biol.* 23:101098. doi: 10.1016/j.redox.2019.101098

Napimoga, M. H., Souza, G. R., Cunha, T. M., Ferrari, L. F., Clemente-Napimoga, J. T., Parada, C. A., et al. (2008). 15d-prostaglandin J2 inhibits inflammatory hypernociception: involvement of peripheral opioid receptor. *J. Pharmacol. Exper. Therap.* 324, 313–321. doi: 10.1124/jpet.107.126045

Nardo, G., Pozzi, S., Mantovani, S., Garbelli, S., Marinou, K., Basso, M., et al. (2009). Nitroproteomics of peripheral blood mononuclear cells from patients and a rat model of ALS. *Antioxid. Redox Signal.* 11, 1559–1567. doi: 10.1089/ars.2009.2548

Oda, T., Iwasa, M., Aihara, T., Maeda, Y., and Narita, A. (2009). The nature of the globular- to fibrous-actin transition. *Nature* 457, 441–445. doi: 10.1038/nature07685

Oeste, C. L., and Perez-Sala, D. (2014). Modification of cysteine residues by cyclopentenone prostaglandins: interplay with redox regulation of protein function. *Mass. Spectrom. Rev.* 33, 110–125. doi: 10.1002/mas.21383

Oliva, J. L., Perez-Sala, D., Castrillo, A., Martinez, N., Canada, F. J., Bosca, L., et al. (2003). The cyclopentenone 15-deoxy-delta 12,14-prostaglandin J2 binds to and activates H-Ras. *Proc. Natl. Acad. Sci. U.S.A.* 100, 4772–4777. doi: 10.1073/pnas.0735842100

Pan, L., Lin, Z., Tang, X., Tian, J., Zheng, Q., Jing, J., et al. (2020). S-Nitrosylation of Plastin-3 exacerbates thoracic aortic dissection formation via endothelial barrier dysfunction. *Arterioscleros. Thrombos. Vasc. Biol.* 40, 175–188. doi: 10.1161/atvbaha.119.313440

Pastore, A., Tozzi, G., Gaeta, L. M., Bertini, E., Serafini, V., Di Cesare, S., et al. (2003). Actin glutathionylation increases in fibroblasts of patients with Friedreich's ataxia: a potential role in the pathogenesis of the disease. *J. Biol. Chem.* 278, 42588–42595. doi: 10.1074/jbc.m301872200

Pineda-Molina, E., Klatt, P., Vazquez, J., Marina, A., Garcia de Lacoba, M., Perez-Sala, D., et al. (2001). Glutathionylation of the p50 subunit of NF-kappaB: a mechanism for redox-induced inhibition of DNA binding. *Biochemistry* 40, 14134–14142. doi: 10.1021/bi011459o

Renedo, M., Gayarre, J., Garcia-Dominguez, C. A., Perez-Rodriguez, A., Prieto, A., Canada, F. J., et al. (2007). Modification and activation of Ras proteins by electrophilic prostanoids with different structure are site-selective. *Biochemistry* 46, 6607–6616. doi: 10.1021/bi602389p

Reynaert, N. L., Ckless, K., Korn, S. H., Vos, N., Guala, A. S., Wouters, E. F., et al. (2004). Nitric oxide represses inhibitory kappaB kinase through S-nitrosylation. *Proc. Natl. Acad. Sci. U.S.A.* 101, 8945–8950. doi: 10.1073/pnas.0400588101

Reynaert, N. L., van der Vliet, A., Guala, A. S., McGovern, T., Hristova, M., Pantano, C., et al. (2006). Dynamic redox control of NF-kappaB through glutaredoxin-regulated S-glutathionylation of inhibitory kappaB kinase beta. *Proc. Natl. Acad. Sci. U.S.A.* 103, 13086–13091. doi: 10.1073/pnas.0603290103

Sakai, J., Li, J., Subramanian, K. K., Mondal, S., Bajrami, B., Hattori, H., et al. (2012). Reactive oxygen species-induced actin glutathionylation controls actin dynamics in neutrophils. *Immunity* 37, 1037–1049. doi: 10.1016/j.immuni.2012.08.017

Salvemini, D., Kim, S. F., and Mollace, V. (2013). Reciprocal regulation of the nitric oxide and cyclooxygenase pathway in pathophysiology: relevance and clinical implications. *Am. J. Physiol.* 304, R473–R487.

Seth, D., Hess, D. T., Hausladen, A., Wang, L., Wang, Y. J., and Stamler, J. S. (2018). A multiplex enzymatic machinery for cellular protein S-nitrosylation. *Mol. Cell* 69, 451–464.e456.

Simmons, D. L., Botting, R. M., and Hla, T. (2004). Cyclooxygenase isozymes: the biology of prostaglandin synthesis and inhibition. *Pharmacol. Rev.* 56, 387–437. doi: 10.1124/pr.56.3.3

Smith, F. M., and Kosman, D. J. (2020). Molecular defects in Friedreich's Ataxia: convergence of oxidative stress and cytoskeletal abnormalities. *Front. Mol. Biosci.* 7:569293. doi: 10.3389/fmolb.2020.569293

Sobierajska, K., Skurzynski, S., Stasiak, M., Kryczka, J., Cierniewski, C. S., and Swiatkowska, M. (2014). Protein disulfide isomerase directly interacts with beta-actin Cys374 and regulates cytoskeleton reorganization. *J. Biol. Chem.* 289, 5758–5773. doi: 10.1074/jbc.m113.479477

Stamatakis, K., Sanchez-Gomez, F. J., and Perez-Sala, D. (2006). Identification of novel protein targets for modification by 15-deoxy-Delta12,14-prostaglandin J2 in mesangial cells reveals multiple interactions with the cytoskeleton. *J. Am. Soc. Nephrol.* 17, 89–98. doi: 10.1681/asn.2005030329

Straub, A. C., Billaud, M., Johnstone, S. R., Best, A. K., Yemen, S., Dwyer, S. T., et al. (2011). Compartmentalized connexin 43 s-nitrosylation/denitrosylation regulates heterocellular communication in the vessel wall. *Arterioscleros. Thrombos. Vasc. Biol.* 31, 399–407. doi: 10.1161/atvbaha.110.215939

Straus, D. S., and Glass, C. K. (2001). Cyclopentenone prostaglandins: new insights on biological activities and cellular targets. *Med. Res. Rev.* 21, 185–210. doi: 10.1002/med.1006

Straus, D. S., Pascual, G., Li, M., Welch, J. S., Ricote, M., Hsiang, C. H., et al. (2000). 15-deoxy-delta 12,14-prostaglandin J2 inhibits multiple steps in the NF-kappa B signaling pathway. *Proc. Natl. Acad. Sci. U.S.A.* 97, 4844–4849. doi: 10.1073/pnas.97.9.4844

Su, D., Shukla, A. K., Chen, B., Kim, J. S., Nakayasu, E., Qu, Y., et al. (2013). Quantitative site-specific reactivity profiling of S-nitrosylation in mouse skeletal muscle using cysteinyl peptide enrichment coupled with mass spectrometry. *Free Radic. Biol. Med.* 57, 68–78. doi: 10.1016/j.freeradbiomed.2012.12.010

Surh, Y. J., Na, H. K., Park, J. M., Lee, H. N., Kim, W., Yoon, I. S., et al. (2011). 15-Deoxy-Delta(1)(2),(1)(4)-prostaglandin J(2), an electrophilic lipid mediator of anti-inflammatory and pro-resolving signaling. *Biochem. Pharmacol.* 82, 1335–1351. doi: 10.1016/j.bcp.2011.07.100

Thibeault, S., Rautureau, Y., Oubaha, M., Faubert, D., Wilkes, B. C., Delisle, C., et al. (2010). S-nitrosylation of beta-catenin by eNOS-derived NO promotes VEGF-induced endothelial cell permeability. *Mol. Cell* 39, 468–476. doi: 10.1016/j.molcel.2010.07.013

Thom, S. R., Bhopale, V. M., Mancini, D. J., and Milovanova, T. N. (2008). Actin S-nitrosylation inhibits neutrophil beta2 integrin function. *J. Biol. Chem.* 283, 10822–10834. doi: 10.1074/jbc.m709200200

Thom, S. R., Bhopale, V. M., Milovanova, T. N., Yang, M., and Bogush, M. (2012). Thioredoxin reductase linked to cytoskeleton by focal adhesion kinase reverses actin S-nitrosylation and restores neutrophil beta(2) integrin function. *J. Biol. Chem.* 287, 30346–30357. doi: 10.1074/jbc.m112.355875

Thom, S. R., Bhopale, V. M., Milovanova, T. N., Yang, M., Bogush, M., and Buerk, D. G. (2013). Nitric-oxide synthase-2 linkage to focal adhesion kinase in neutrophils influences enzyme activity and beta2 integrin function. *J. Biol. Chem.* 288, 4810–4818. doi: 10.1074/jbc.m112.426353

Thom, S. R., Bhopale, V. M., Yu, K., Huang, W., Kane, M. A., and Margolis, D. J. (2017). Neutrophil microparticle production and inflammasome activation by hyperglycemia due to cytoskeletal instability. *J. Biol. Chem.* 292, 18312–18324. doi: 10.1074/jbc.m117.802629

Ulrich, C., Quillici, D. R., Schegg, K., Woolsey, R., Nordmeier, A., and Buxton, I. L. (2012). Uterine smooth muscle S-nitrosylproteome in pregnancy. *Mol. Pharmacol.* 81, 143–153. doi: 10.1124/mol.111.075804

Unoki, T., Akiyama, M., and Kumagai, Y. (2020). Nrf2 activation and its coordination with the protective defense systems in response to electrophilic stress. *Intern. J. Mol. Sci.* 21:545. doi: 10.3390/ijms21020545

Valerio, V., Myasoedova, V. A., Moschetta, D., Porro, B., Perrucci, G. L., Cavalca, V., et al. (2019). Impact of oxidative stress and protein S-Glutathionylation in aortic valve sclerosis patients with overt atherosclerosis. *J. Clin. Med.* 8:552. doi: 10.3390/jcm8040552

Varland, S., Vandekerckhove, J., and Drazic, A. (2019). Actin post-translational modifications: the cinderella of cytoskeletal control. *Trends Biochem. Sci.* 44, 502–516. doi: 10.1016/j.tibs.2018.11.010

Wabnitz, G. H., Lohneis, P., Kirchgessner, H., Jahraus, B., Gottwald, S., Konstandin, M., et al. (2010). Sustained LFA-1 cluster formation in the immune synapse requires the combined activities of L-plastin and calmodulin. *Eur. J. Immunol.* 40, 2437–2449. doi: 10.1002/eji.201040345

Wall, S. B., Oh, J. Y., Mitchell, L., Laube, A. H., Campbell, S. L., Renfrow, M. B., et al. (2015). Rac1 modification by an electrophilic 15-deoxy Delta(12,14)-prostaglandin J2 analog. *Redox Biol.* 4, 346–354. doi: 10.1016/j.redox.2015.01.016

Wang, C., Morley, S. C., Donermeyer, D., Peng, I., Lee, W. P., Devoss, J., et al. (2010). Actin-bundling protein L-plastin regulates T cell activation. *J. Immunol.* 185, 7487–7497. doi: 10.4049/jimmunol.1001424

Wang, J., Boja, E. S., Tan, W., Tekle, E., Fales, H. M., English, S., et al. (2001). Reversible glutathionylation regulates actin polymerization in A431 cells. *J. Biol. Chem.* 276, 47763–47766. doi: 10.1074/jbc.c100415200

Wang, J., Tekle, E., Oubrahim, H., Mieyal, J. J., Stadtman, E. R., and Chock, P. B. (2003). Stable and controllable RNA interference: Investigating the physiological function of glutathionylated actin. *Proc. Natl. Acad. Sci. U.S.A.* 100, 5103–5106. doi: 10.1073/pnas.0931345100

West, M. B., Hill, B. G., Xuan, Y. T., and Bhatnagar, A. (2006). Protein glutathiolation by nitric oxide: an intracellular mechanism regulating redox protein modification. *FASEB J.* 20, 1715–1717. doi: 10.1096/fj.06-5843fje

Wolhuter, K., and Eaton, P. (2017). How widespread is stable protein S-nitrosylation as an end-effector of protein regulation? *Free Radic. Biol. Med.* 109, 156–166. doi: 10.1016/j.freeradbiomed.2017.02.013

Wolhuter, K., Whitwell, H. J., Switzer, C. H., Burgoyne, J. R., Timms, J. F., and Eaton, P. (2018). Evidence against stable protein s-nitrosylation as a widespread mechanism of post-translational regulation. *Mol. Cell* 69, 438–450.e435.

Yamamoto, Y., Koma, H., and Yagami, T. (2020). 15-Deoxy-Delta(12,14)-prostaglandin J2 inhibits cell migration on renal cell carcinoma via down-regulation of focal adhesion kinase signaling. *Biol. Pharm. Bull.* 43, 153–157. doi: 10.1248/bpb.b19-00748

Yang, Z., Wang, Z. E., Doulias, P. T., Wei, W., Ischiropoulos, H., Locksley, R. M., et al. (2010). Lymphocyte development requires S-nitrosoglutathione reductase. *J. Immunol.* 185, 6664–6669. doi: 10.4049/jimmunol.1000080

Zhang, H. H., Wang, W., Feng, L., Yang, Y., Zheng, J., Huang, L., et al. (2015). S-nitrosylation of Cofilin-1 serves as a novel pathway for VEGF-stimulated endothelial cell migration. *J. Cell. Physiol.* 230, 406–417. doi: 10.1002/jcp.24724

Zhang, X., Li, G., Guo, Y., Song, Y., Chen, L., Ruan, Q., et al. (2019). Regulation of ezrin tension by S-nitrosylation mediates non-small cell lung cancer invasion and metastasis. *Theranostics* 9, 2555–2571. doi: 10.7150/thno.32479

Zhou, H. L., Zhang, R., Anand, P., Stomberski, C. T., Qian, Z., Hausladen, A., et al. (2019). Metabolic reprogramming by the S-nitroso-CoA reductase system protects against kidney injury. *Nature* 565, 96–100. doi: 10.1038/s41586-018-0749-z

Conflict of Interest: The authors declare that the research was conducted in the absence of any commercial or financial relationships that could be construed as a potential conflict of interest.

frontiers in Cell and Developmental Biology

MINI REVIEW
published: 14 June 2021
doi: 10.3389/fcell.2021.673986

WIP, YAP/TAZ and Actin Connections Orchestrate Development and Transformation in the Central Nervous System

Inés M. Antón[1,2]* *and Francisco Wandosell*[2,3]*

[1] Departamento de Biología Molecular y Celular, Centro Nacional de Biotecnología (CNB-CSIC), Madrid, Spain, [2] Centro de Investigación Biomédica en Red de Enfermedades Neurodegenerativas (CIBERNED), Madrid, Spain, [3] Departamento de Neuropatología Molecular, Centro de Biología Molecular "Severo Ochoa", Universidad Autónoma de Madrid – Consejo Superior de Investigaciones Científicas, Madrid, Spain

OPEN ACCESS

Edited by:
Francisco Sanchez-Madrid, Autonomous University of Madrid, Spain

Reviewed by:
Miguel Vicente-Manzanares, Consejo Superior de Investigaciones Científicas, Spanish National Research Council (CSIC), Spain
Mary C. Farach-Carson, University of Texas Health Science Center at Houston, United States

***Correspondence:**
Inés M. Antón
ianton@cnb.csic.es
Francisco Wandosell
fwandosell@cbm.csic.es

Specialty section:
This article was submitted to Cell Adhesion and Migration, a section of the journal Frontiers in Cell and Developmental Biology

Received: *28 February 2021*
Accepted: *12 May 2021*
Published: *14 June 2021*

Citation:
Antón IM and Wandosell F (2021) WIP, YAP/TAZ and Actin Connections Orchestrate Development and Transformation in the Central Nervous System. Front. Cell Dev. Biol. 9:673986. doi: 10.3389/fcell.2021.673986

YAP (Yes-associated protein) and TAZ (transcriptional coactivator with PDZ-binding motif) are transcription co-regulators that make up the terminal components of the Hippo signaling pathway, which plays a role in organ size control and derived tissue homeostasis through regulation of the proliferation, differentiation and apoptosis of a wide variety of differentiated and stem cells. Hippo/YAP signaling contributes to normal development of the nervous system, as it participates in self-renewal of neural stem cells, proliferation of neural progenitor cells and differentiation, activation and myelination of glial cells. Not surprisingly, alterations in this pathway underlie the development of severe neurological diseases. In glioblastomas, YAP and TAZ levels directly correlate with the amount of the actin-binding molecule WIP (WASP interacting protein), which regulates stemness and invasiveness. In neurons, WIP modulates cytoskeleton dynamics through actin polymerization/depolymerization and acts as a negative regulator of neuritogenesis, dendrite branching and dendritic spine formation. Our working hypothesis is that WIP regulates the YAP/TAZ pools using a Hippo-independent pathway. Thus, in this review we will present some of the data that links WIP, YAP and TAZ, with a focus on their function in cells from the central and peripheral nervous systems. It is hoped that a better understanding of the mechanisms involved in brain and nervous development and the pathologies that arise due to their alteration will reveal novel therapeutic targets for neurologic diseases.

Keywords: glioblastoma, cytoskeleton, neuritogenesis, axonogenesis, nuclear actin, Hippo pathway

INTRODUCTION

Proper neuritogenesis in post-mitotic neurons is a requisite for dendritic arborization and neuronal function. Neurite extension, sprouting and axonal polarization is directed by microtubule (MT) dynamics and polymerized actin microfilaments (MF), which form actin-rich structures (lamellipodia and filopodia) in the tip of the growth cone. The tip of the growth cone is more

a filamentous actin (F-actin) field whereas the intermediate and proximal regions of the growth cone are MT filled (Black and Baas, 1989). These two major cytoskeletal elements have some opposing functions; as a general rule, MT depolymerization prevents or retracts the initial neuritic extension and growth, whereas MF depolymerization leads to generation of multiple axons (Bradke and Dotti, 1999).

In almost all cell types, including neurons, the dynamics of branched MF rely on actin polymerization controlled by the Arp2/3 (actin-related protein) complex and by NPF (nucleation-promoting factors) such as cortactin and N-WASP/WASP (neural/Wiskott-Aldrich syndrome protein) (Padrick and Rosen, 2010). Much less is known about the role of the actin regulator WIP (WASP Interacting Protein) in neuritogenesis, though we recently showed that WIP had unexpected functions in neurons and glia. In the present review we will summarize some of the data linking WIP function with new regulatory aspects of neuritogenesis and its contribution to transformation of astrocytes, another essential component of the nervous system. In addition to the older regulatory functions of WIP in actin polymerization, a few new players have been identified: Yes-associated protein (YAP) and transcriptional coactivator with PDZ-binding motif (TAZ).

WIP and Actin

WIP was initially described as a regulator of the formation of actin-rich cerebriform projections in B lymphocytes (Ramesh et al., 1997). It is very abundant in hematopoietic cells like lymphocytes and dendritic cells, while lower levels are found in astrocytes, neurons and fibroblasts, where it regulates formation of lamellipodia and filopodia (Antón et al., 2007). WIP binds actin as well as N-WASP and cortactin, regulating their actin-nucleation capability through Arp2/3 (Paunola et al., 2002). Binding of the N-terminal domain of WASP by the WIP C-terminal domain was demonstrated in initial descriptions of the complex (Ramesh et al., 1997), and its contribution to shield WASP proteasome-mediated degradation was identified soon after (Sasahara et al., 2002). Advanced nuclear magnetic resonance structures of purified co-expressed fragments from WASP (a.a. 20–158) and WIP (a.a. 442–492) have confirmed these results and unraveled WIP's wrapping around WASP (Halle-Bikovski et al., 2018). WIP residues a.a. 454–456 are the major contributor to WASP affinity, while residues a.a. 449–451 have the greatest effect on WASP phosphorylation, and likely its degradation.

WIP binds monomeric globular actin (G-actin) and polymerized F-actin with different affinities (Martinez-Quiles et al., 2001), and their direct interaction depends on the residues ^{45}KLKK^{48}. In lymphocytes, around 80% of cellular WIP exists in a constitutive complex with WASP, which itself directly binds actin (Koduru et al., 2007). The WIP sequence contains a large number of prolines, which potentiates contact with other proteins including SH3 (src homology 3) domains, which are very common among actin-binding elements. The links between the WIP/WASP complex and the actin cytoskeleton and derived structures are therefore multiple and very relevant. Some of the described WIP-dependent cellular functions such as fibroblast chemotaxis toward PDGF (platelet-derived growth factor) are dependent on WIP's ability to bind actin, since mutations in the KLKK domain prevent actin co-precipitation, formation of actin-rich dorsal ruffles and impede fibroblast-directed migration (Antón et al., 2003).

We reported WIP expression in the adult mouse brain (cortex, hippocampus and olfactory bulb) and cultured embryonic cortical and hippocampal neurons. We demonstrated that WIP acts as a negative regulator of early neurite emission and branching: development of WIP-deficient cortical neurons from knockout embryos was accelerated, whereas neurite protrusion was retarded by WIP-overexpression. In contrast, WIP-deficient neurons did not have modified axon formation, number or complexity (Franco et al., 2012). The observed phenotype was accompanied by mislocalization of actin NPFs such as N-WASP and cortactin. Thus, our results support that a cooperative action of WIP/N-WASP/cortactin and the Arp2/3 complex are essential for control of actin polymerization, a process required in the initial steps of neuritogenesis for proper neuronal morphogenesis and neuronal network formation. Therefore, we could propose that the growth cone of WIP-deficient neurons may have a more active polymerization dynamic, and this activity could be translated into more robust integrin-associated signaling, locally. This could explain the effect of better initiation of neurite protrusion and axonogenesis of WIP-deficient neurons, although these initial differences with the wild-type neurons, it smoothest out over time, WIP-knockdown dissociated hippocampal neurons maintained both the number of primary neurites and total neuritic length higher than wild-type neurons (Franco et al., 2012).

From these data, several working hypotheses may be proposed about how WIP controls the process of neuritogenesis. A structure-related option based on the regulatory role of actin dynamics points to WIP as a negative regulator of the actin polymerization complex Arp2/3 cortactin-N-WASP. A second option focuses on signaling, with WIP modulating cytoplasmic pathways that control neuritic outgrowth and promote axonal polarity, such as PI3K-Akt-GSK3 pathway, Par3/Par6/aPKC or the multiprotein complex mTORC1 (Jiang and Rao, 2005; Garrido et al., 2007).

One of the main cytoplasmic regulators of actin polymerization is the Rho-GTPase superfamily, which is regulated by the PI3K-Akt pathway, among others. For example, RhoA, Rac1, and Cdc42 are major modulators of the cytoskeleton that act through actin-binding proteins such as N-WASP and WIP (Antón et al., 2020). It has been reported that active Cdc42-GTP interacts with WASP and N-WASP, thereby increasing its nucleation activity (Aspenström et al., 1996; Martinez-Quiles et al., 2001). In neurons, a lack of WIP increased dendritic spine size and filamentous actin content in a RhoA-dependent manner (Franco-Villanueva et al., 2014). Furthermore, stimulated by several growth factors the Akt-mTORC1-S6K pathway is involved in actin cytoskeleton reorganization (Jaworski and Sheng, 2006) and S6K promotes actin filament crosslinking and stabilization by directly binding F-actin, depending on the level of S6K phosphorylation (Moresco et al., 2005). WIP not only plays a cytoskeletal role, but also governs signaling

through mTORC1- and Abl-dependent modulation of the S6K pathway, which controls neuritic extension and branching (Franco-Villanueva et al., 2015).

All these data strongly suggest that WIP may play two complementary roles in neurogenesis: regulating actin polymerization levels through N-WASP and by modulating the signaling activity of mTORC1.

YAP/TAZ and Actin

Actin dynamics regulate axonogenesis and neuronal polarity, as demonstrated by the generation of multi-axons in primary neurons subjected to actin depolymerization, favored either by latrunculin or cytochalasin D (Bradke and Dotti, 1999; Inagaki et al., 2001). Actin dynamics are controlled by well-characterized extracellular signaling pathways including tyrosine kinase receptors, adhesion molecules and neurotransmitter receptors, which use Rho-GTPases as downstream elements in almost all cases. Subsequently, Rho-GTPases exert functions via a plethora of conserved protein effectors, which can be general or quite specific to the particular GTPase (Hall, 2012). More recently, it has been described how extracellular stimuli are mechanotransduced and regulated by a new set of elements: YAP and TAZ (Chan et al., 2005). YAP/TAZ are transcription co-regulatory proteins that respond to physical signals by activating transcription, particularly that of genes involved in extracellular matrix remodeling and cytoskeleton reorganization. YAP/TAZ were initially described as the final effectors of the Hippo pathway (highly conserved from *Drosophila* to mammals), although they can also perform Hippo-independent activities. In contrast to ordinary transduction signaling based on single ligand-receptor interaction, the Hippo pathway integrates multiple upstream stimuli ignited by soluble factors, activation of adhesion molecules and forces driven by the actin cytoskeleton. Therefore, there is a strong cooperative effect among Hippo signaling with cytoskeletal regulation and a combination of extracellular cues, initiating directed migration and mechanotransduction.

YAP/TAZ Phosphorylation, Quantity, and Subcellular Localization Regulate Their Activity

In the Hippo pathway, two conserved kinases regulate the activity of YAP/TAZ, designated as serine/threonine-protein kinases 4 and 3 (STK4/3, usually referred to as MST1/2) (**Figure 1**). These kinases form heterodimers with Salvador homolog 1 (SAV1), an interaction that is required for MST1/2 to phosphorylate not only SAV1 but also MOB kinase activator 1A protein and the serine/threonine-protein kinase LATS1/2 (Chan et al., 2005). Afterward, when the Hippo pathway is activated, LATS1/2 directly phosphorylates YAP and TAZ at multiple sites, preventing their nuclear localization (Ma et al., 2019). This cytoplasmic retention is mostly regulated by the binding of 14–3–3 protein to phosphorylated YAP/TAZ, resulting in YAP/TAZ inhibition. Live multiphoton microscopy showed that during cellular interphase, endogenously tagged Yki (YAP homolog in *Drosophila*) rapidly fluctuates between the cytosol and the nucleus, where it locates to mitotic chromatin (Manning et al., 2018). The Hippo pathway regulates Yki subcellular distribution by regulating its rate of nuclear import. It is tempting to suggest that Yki/YAP may perform nuclear roles in addition to transcriptional regulation, opening up the search for exclusively nuclear binding partners. Regulation of the amount and half-life of YAP/TAZ relies on the successive phosphorylation by casein kinase 1, which leads to β-TrCP–mediated ubiquitination and proteasomal degradation (Liu et al., 2010; Zhao et al., 2010).

In the cytoplasm, YAP/TAZ have been associated with adhesion molecules such as cadherin, or linked to cytoplasmic actin or actin-binding proteins such as the angiomotin family (AMOT) (Zhao et al., 2011). YAP/TAZ enter the nucleus through mechanical stretching of the nuclear membrane and nuclear pore regulation (Elosegui-Artola et al., 2017). When YAP/TAZ are dephosphorylated and translocate into the nucleus (i.e., when the Hippo pathway is inactive), they can act as transcriptional co-regulators. Neither of these proteins contain DNA-binding domains, and consequently they must interact with direct transcription factors. Although their main binding partners are TEAD family transcription factors, some of which differentially regulate brain cortical development (Mukhtar et al., 2020), YAP/TAZ are capable of forming complexes with other transcription factors such as SMAD, RUNX1/2, p63/p73, or OCT4 (Yu et al., 2015).

YAP/TAZ regulate and are regulated by the actin cytoskeleton. For instance, CYR61 and CTGF, two genes whose transcription is usually induced by the complex YAP/TAZ-TEAD, encode extracellular matrix proteins that work as integrin ligands and are functionally important for cell adhesion to the extracellular matrix (Jedsadayanmata et al., 1999). As a general rule, YAP/TAZ control a set of matrix proteins or cytoskeleton remodeling genes and, in addition, the actin cytoskeleton plays an essential role in regulating YAP/TAZ activity by controlling their cytoplasmic–nuclear shuttling.

A second cytoplasmic element that regulates actin and YAP/TAZ activity is the GTPase RhoA. While the conventional regulation of RhoA–mediated actin polymerization is broadly documented, the detailed mechanism of how RhoA specifically inhibits the Hippo kinase cascade is not completely understood. It is known that ROCK (Rho-associated protein kinase) is partially involved, and that F-actin mediates the effect of Rho on Hippo regulation since the disruption/depolymerization of F-actin by latrunculin or cytochalasin D strongly induces LATS1/2-mediated phosphorylation, preventing the nuclear shuttling of YAP/TAZ (Aragona et al., 2013).

YAP/TAZ–Actin, Nuclear and/or Cytoplasmic Interactions?

In almost all cell types, actin polymerization is regulated by a variety of G- and F-actin-binding, actin-capping and actin-severing proteins (actin regulatory proteins; ARPs), such as gelsolin, CapZ, profilin, cofilin, thymosin β-4, and formins (Lee and Dominguez, 2010). Although the vast majority of actin is cytoplasmic, there is also a nuclear actin component with numerous ARPs (Treisman, 2013) that has long been understudied. Considering all these actin-binding proteins, it is important to remember that YAP/TAZ transcription is regulated

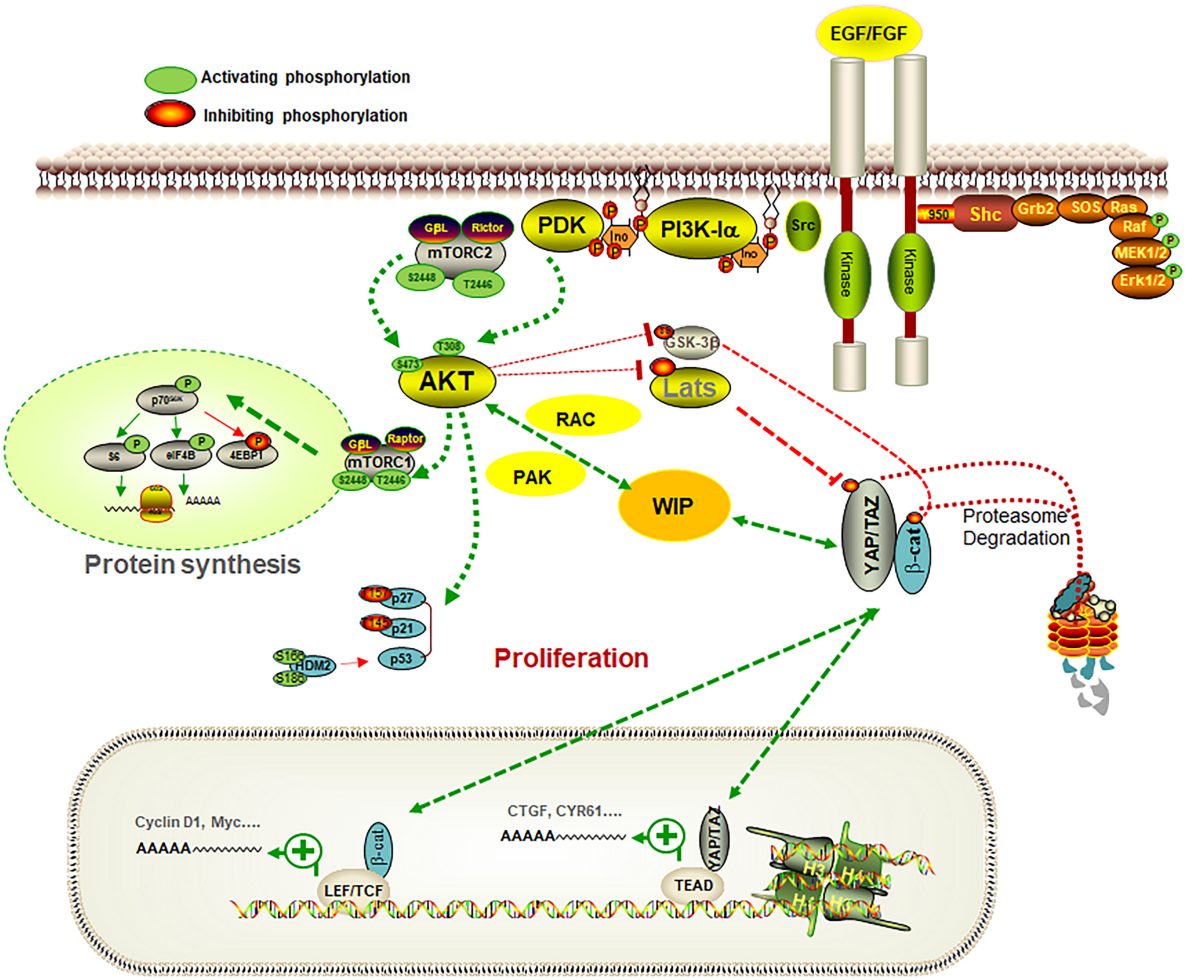

FIGURE 1 | Pathways controlling the glia-glioma transformation. The scheme represents some of the signaling pathways involved in the regulation of the role of WIP in gliomas. WIP drives a mechanism that stimulates growth signals, promoting YAP/TAZ and β-catenin stability in a Hippo-independent fashion, and allows cells to coordinate processes such as proliferation, stemness, and invasiveness, which are key factors in cancer progression. When gliomas were grown in a defined medium containing EGF and FGF as growth factors, PI3K inhibition or Akt knockdown reduced their proliferation. WIP is overexpressed in gliomas and its downregulation decreased YAP/TAZ levels and their targets (such as CTGF or CYR61), in parallel with a reduction in proliferation and stem markers such as nestin. The effect of WIP reduction was compensated, at least in part, by over-expression of Rac or PAK. Some elements of the PI3K-Akt-mTORC1 pathway and the connection of Akt with WIP and YAP/TAZ, are represented in this scheme.

by F-actin-capping and -severing proteins such as capZ, cofilin, and gelsolin. Accordingly, knockdown of any of these proteins increases the expression of YAP/TAZ target genes, such as CYR61 or CTGF (Aragona et al., 2013). In many cell types, nuclear actin primarily acts in complex with other proteins of the ARP family, such as the Arp2/3 complex (Goley et al., 2006; Yoo et al., 2007), formins (Parisis et al., 2017), or N-WASP, which participates not only as a structural/cytoskeletal element but also regulates RNA polymerase II-dependent transcription (Wu et al., 2006).

Interestingly, the pool of nuclear F-actin may exert a role in cell cycle regulation through control of chromatin organization at mitotic exit (Baarlink et al., 2017), and it may combine its regulatory effect with the contribution of branched actin networks from the cell cortex to control cell cycle progression in mammary epithelial cells (Molinie et al., 2019). Therefore, considering that numerous ARPs controlling actin dynamics are present both in the cytoplasm and nucleus, some questions about the exact role of nuclear actin in the regulatory activity of YAP/TAZ have not been fully addressed. It is well established that YAP/TAZ nuclear transit is mediated by the actin polymerization stage, however cytochalasin D and latrunculin treatment can simultaneously affect cytoplasmic and nuclear actin. Thus, the question about whether actin is only necessary for the nuclear shuttling of YAP/TAZ, or is playing an additional role in the transcriptional activity of YAP/TAZ is still an open question (Piccolo et al., 2014).

It appears that YAP/TAZ regulation is not directed by the total levels of F-actin, but rather by its subcellular organization, fine structure, tension and resistance offered by the cytoskeleton

and by the whole nucleus. This dual cytoplasmic/nuclear role is not exclusive to YAP/TAZ, as other similar co-transcriptional regulators have been described, for instance β-catenin or myocardin-related transcription factor (MRTF), through the TCF family of transcription factors and the transcription mediator serum response factor (SRF), respectively (Olson and Nordheim, 2010; Nusse and Clevers, 2017).

The MRTF and YAP transcriptional pathways contribute to the response to cell proliferation and mechanotransduction. Several observations suggest that MRTFs and YAP/TAZ may functionally interact despite not sharing a common DNA targeting factor. In cancer-associated fibroblasts (CAFs), the MRTF–SRF and YAP pathways are required for the contractile and pro-invasive properties of these cells. It has been reported that in CAFs, expression of direct MRTF–SRF genomic targets is also dependent on YAP–TEAD activity and, conversely, YAP–TEAD target gene expression depends on MRTF–SRF signaling. In normal fibroblasts, expression of activated MRTF versions induces YAP, while activated YAP stimulates MRTF. Cross-talk between the pathways requires recruitment of MRTF and YAP to DNA via their respective DNA-binding partners (SRF and TEAD), and is therefore indirect. However, YAP/TAZ mechanotransduction differs substantially from actin regulation of the MRTF family, as a sensor of F-actin/G-actin ratio binds directly to free nuclear G-actin in a manner that inhibits its association with SRF (Foster et al., 2017).

It has also been reported that WIP can promote nuclear transit of MRTF-SRF via actin polymerization (Ramesh et al., 2014), similar to YAP/TAZ. As both transcription factors depend on actin polymerization to reach the nucleus and WIP contributes to modify the ratio G/F-actin, we considered the possibility that WIP regulates the subcellular distribution of YAP/TAZ through an indirect mechanism based on the levels of cellular F-actin. In contrast, the interaction β-catenin/TCF with YAP/TAZ is direct; some initial data indicate that the Hippo pathway genetically and functionally interacts with Wnt/β-catenin signaling (Varelas et al., 2010). Reports demonstrated a novel mechanism through which Hippo signaling inhibits Wnt/β-catenin input; YAP/TAZ binds to β-catenin, thereby suppressing Wnt-target gene expression. YAP phosphorylation stimulated by the activated Hippo pathway induces cytoplasmic retention of YAP, which is required for the YAP-mediated inhibition of Wnt/β-catenin signaling (Imajo et al., 2012). More recently, an "alternative Wnt-YAP/TAZ signaling axis" was based on Wnt5a/b and Wnt3a, which are potent activators of the critical mediators YAP/TAZ (Park et al., 2015). Moreover, another report indicated that YAP could directly interact with β-catenin in the nucleus, thus forming a transcriptional YAP/β-catenin/TCF4 complex. This transcriptional complex was confirmed by target genes of this complex Lgr5 and cyclin D1 (Deng et al., 2018).

Several data support common regulatory steps between YAP/TAZ and β-catenin. When the Wnt pathway is inactive, YAP/TAZ are sequestered in the β-catenin destruction complex where they recruit βTrCP, which is needed for β-catenin inactivation. In contrast, when Wnt is activated, YAP/TAZ are released from the complex and accumulate in the nucleus (Azzolin et al., 2014).

YAP/TAZ and Neuronal Development

The extracellular matrix protein/integrin interaction serves as a first responder to collect mechanosignals and transmit the information to the regulatory machinery of YAP/TAZ, possibly not only through the Hippo pathway (Hu J. K. H. et al., 2017). It is tantalizing to propose that YAP/TAZ may play a role in the regulation of axonogenesis induced by the extracellular matrix. However, the exact mechanism underlying how YAP/TAZ are regulated by various mechanical/extracellular signals in neurogenesis is far from known.

Current data indicate an important role of YAP/TAZ in neuronal development. Development of the nervous system is based on proliferation of neural stem cells (NSCs) and posterior differentiation into diverse neural lineages. NSCs are the group of self-renewing cells that can generate neurons and several glial cell types during embryonic development (Beattie and Hippenmeyer, 2017). Recently, several studies have suggested an essential role of the Hippo signaling pathway in regulation of NSC proliferation. For instance, downregulated Hippo signaling ensured translocation of YAP inside the nucleus, thereby transcribing genes associated with cellular proliferation. Prolonged YAP/TAZ activation also enhances the stemness (Panciera et al., 2016) and delays differentiation of NSCs. In a mouse model and a murine primary neuronal culture system, it has been reported that overexpression of YAP/TAZ promotes NSC characteristics *in vivo* in the stem cell niche, and increases the size of cultured neurospheres. Moreover, this YAP/TAZ function restricting differentiation is dependent on the transcriptional co-activator TEAD (Han et al., 2015; Robledinos-Antón et al., 2020).

Considering the previously described interaction between YAP/TAZ and β-catenin and the role of the Wnt pathway in neuronal development, it is tempting to speculate that some of the neuronal actions of Wnt signaling might be a combination of YAP/TAZ and β-catenin-dependent effects. Besides Hippo, pathways including Notch, Shh, FGFs, TGF-β, retinoic acid, and reelin are well-known to regulate NSC proliferation, neurogenesis and gliogenesis. Consequently, the crosstalk between Hippo and some of these signaling pathways and the final impact of these signals on target genes is an open question (Paridaen and Huttner, 2014; Mukhtar and Taylor, 2018; **Figure 2**).

YAP/TAZ not only conditioned the cell fate of the NSC throughout several signaling pathways, but also reprogrammed the energy metabolism. For instance it has been reported that the Hippo pathway can also affect nucleotide biosynthesis and lipid metabolism through the regulation of *de novo* purine/pyrimidine biosynthesis, gluconeogenesis, amino acid uptake, and cholesterol and lipid biosynthesis (Hu Y. et al., 2017; Santinon et al., 2018).

All the gathered knowledge underlines the need for future studies to clarify how any of these metabolic pathways and their integration with signaling and mechanotransduction cues exert an impact on neuritogenesis, axonal elongation and neuronal maturation.

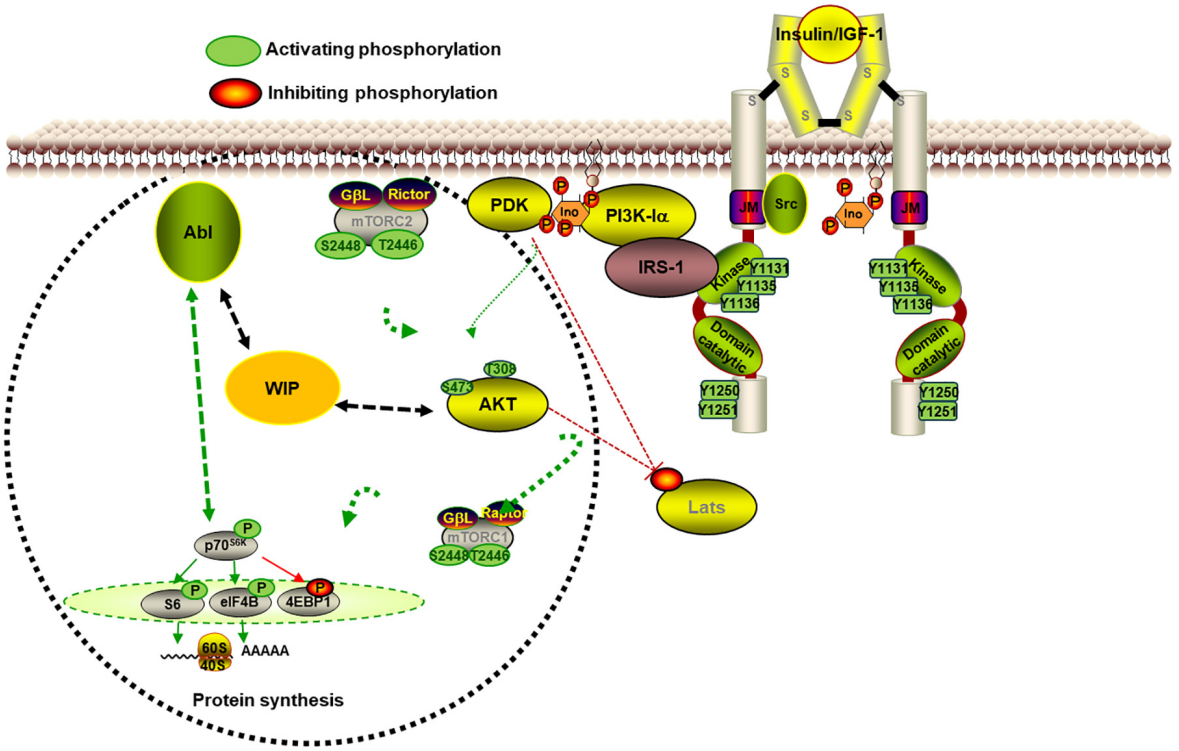

FIGURE 2 | WIP controls neurite initiation and extension in primary neurons. The scheme represents some of the signaling involved in the contribution of WIP in neurite extension. The WIP knockdown increased neurite protrusion and elongation in a neuronal model in which the high level of insulin is the main growth factor. WIP not only has a cytoskeleton dependent role, but also governs signaling through mTORC1- and Abl family kinases-dependent modulation of the S6K pathway, which controls neuritic extension and branching.

Neuritogenesis and NSCs, WIP-YAP/TAZ and Actin

In almost all mammalian cells analyzed, actin forms complexes with other proteins like cofilin or profilin, and they can actively be transported into and out of the nucleus by some members of the importin β superfamily and modulated by Ran GTP (Dopie et al., 2012). Also, as previously mentioned, Arp2/3 and WASP are present in the nucleus where they regulate RNA polymerase II-dependent transcription. In fibroblasts, WIP may localize in the nucleus, and its co-expression with N-WASP caused redistribution of N-WASP, reducing its main nuclear expression and leading to co-localization with WIP in the perinuclear areas (Vetterkind et al., 2002). Whether WIP has a similar effect on WASP subcellular distribution in hematopoietic cells is a relevant question that remains unsolved.

Recently we demonstrated that WIP drives a new mechanism that stimulates growth signals in tumor cells, promoting YAP/TAZ stability that allows cells to coordinate key activities in cancer progression, such as proliferation, stemness and invasiveness. This protein stabilization appears to be Hippo-independent (a LATS mutant did not modify it) and actin-independent (it was not modified by either actin depolymerization or polymerization agents) (Gargini et al., 2016). The specific cellular machinery that determines how actin controls YAP/TAZ activity and whether the cellular effects of WIP expression are solely due to the consequent increase in YAP/TAZ remain open questions. The nuclear transit of MRTF-SRF promoted by WIP is regulated by actin polymerization (Ramesh et al., 2014). However, the question of whether WIP might locally regulate YAP/TAZ transcriptional activity in the nucleus is far from resolved.

In contrast to the pro-oncogenic version of WIP-YAP/TAZ in glioma, WASP and WIP act as onco-suppressor proteins in ALK-dependent lymphomas (Menotti et al., 2019). ALK transforming activity leads to down-regulation of WASP and WIP through transcriptional repression, mediated by STAT3 and C/EBP-b. Interestingly, YAP's expression and tumoral effects run in parallel to those of WIP: YAP is markedly downregulated in hematological malignancies, including lymphomas, leukemias and multiple myeloma, and is upregulated in cell lines from solid tumors of epithelial origin (Cottini et al., 2014).

As previously indicated, prolonged activation of YAP/TAZ enhances stemness (Han et al., 2015; Panciera et al., 2016). However, the expression of YAP/TAZ in the postnatal brain opens several questions about whether the YAP/TAZ–TEAD complex plays a role beyond maintaining NSC phenotypes, and whether in this context WIP/N-WASP affect the biological/physiological activity of YAP/TAZ, since only limited reports on WIP's contribution to neuronal development are available. A low number of babies and children suffering a

severe immunodeficiency similar to Wiskott-Aldrich syndrome due to mutations in the *WIPF1* gene have been identified (Lanzi et al., 2012; Mansour et al., 2020). Studies related to these patients focused on their immunological alterations and the corresponding therapies, but they did not address the potential neurological consequences derived from mutant WIP malfunction. Interestingly, the *WIPF1* gene was the only common genomic region shared by 6–8 patients suffering from neurological diseases (Mitter et al., 2010). WIP-KO mice provide a useful and relevant model to analyze the potential contribution of WIP to cortical or hippocampal development, as well as its participation in the function of the olfactory bulb, since these three murine brain regions have been shown to express the protein (Franco et al., 2012). Mouse behavioral tests may also shed light on the role of WIP in the reduced reproductive success observed in WIP-KO animals.

Despite a limited understanding of WIP's contribution to the functionality of the nervous system, the role of WIP-YAP/TAZ in the brain is still an open question. A potentially relevant player is the phosphatase PP2AC, suggested to support cortical neuronal growth and cognitive function by modulating the Hippo-p73 signaling cascade and the glutamate/glutamine cycle (Liu et al., 2018). PP2AC may connect the new WIP-YAP/TAZ pathway, which is heavily activated in some p53 mutant tumor cells and modulated by integrins and Akt signaling (Escoll et al., 2017). Although the putative role of YAP/TAZ in the brain under stressful or disease conditions has barely been studied, it is an important issue to explore, considering the role of the p53 family of proteins in several pathologies. For instance, despite its recognition as a cytoplasmic activator of Arp2/3, WASP has been shown to colocalize in the nucleus with the damage marker γH2AX after DNA-chemical insult (Schrank et al., 2018). Whether WIP also cooperates with WASP in this activity is an attractive research question to pursue.

FUTURE PERSPECTIVES

Neuronal functional morphogenesis relies on coordinated modulation of the reorganization of the actin cytoskeleton by actin-binding proteins like N-WASP and WIP, with the activity of transcriptional co-regulators such as YAP and TAZ, whose nuclear distribution depends on actin. The multiple intertwined connections between these players provide a fascinating working niche with many relevant questions that need to be addressed. For example, is the predominant role of WIP in actin dynamics in complete cellular systems universal, or does it depend on the cell type? Is phosphorylation status of YAP/TAZ the master regulator of their subcellular distribution in mature neurons, astrocytes or glioblastomas? Is the WIP-mediated control of YAP/TAZ stability stronger than the actin-dependent modulation of YAP/TAZ activity? Does WIP indirectly contribute to YAP/TAZ nuclear distribution through actin depolymerization? How is actin and YAP/TAZ crosstalk regulated in a two-way manner? Future work in the field will provide clear answers and, hopefully, lead to novel diagnostic and therapeutic tools for neurological diseases or nervous system tumors.

AUTHOR CONTRIBUTIONS

IA and FW: conceived the manuscript, writing of the manuscript, approved its final content, conceptualization, and writing—review and editing. FW: writing original draft preparation. Both authors contributed to the article and approved the submitted version.

FUNDING

This research was funded by grants to IA and FW from the Fundación Ramón Areces (CIVP18A3861) and Spanish Ministerio de Ciencia e Innovación (RTI2018-096303-B-C31), which was in part granted with FEDER funding (EC), corresponding to the Programa Estatal de Investigación, Desarrollo e Innovación Orientada a los Retos de la Sociedad.

ACKNOWLEDGMENTS

We apologize if any relevant references were not included due to space limitations. We acknowledge all the past and present members of both laboratories for their generous contribution. We also acknowledge the support of the publication fee by the CSIC Open Access Publication Support Initiative through its Unit of Information Resources for Research (URICI). The professional editing service NB Revisions was used for technical preparation of the text prior to this submission.

REFERENCES

Antón, I. M., Gómez-Oro, C., Rivas, S., and Wandosell, F. (2020). Crosstalk between WIP and Rho family GTPases. *Small GTPases* 11, 160–166. doi: 10.1080/21541248.2017.1390522

Antón, I. M., Jones, G. E., Wandosell, F., Geha, R., and Ramesh, N. (2007). WASP-interacting protein (WIP): working in polymerisation and much more. *Trends Cell Biol.* 17, 555–562. doi: 10.1016/j.tcb.2007.08.005

Antón, I. M., Saville, S. P., Byrne, M. J., Curcio, C., Ramesh, N., Hartwig, J. H., et al. (2003). WIP participates in actin reorganization and ruffle formation induced by PDGF. *J. Cell Sci.* 116(Pt 12), 2443–2451. doi: 10.1242/jcs.00433

Aragona, M., Panciera, T., Manfrin, A., Giulitti, S., Michielin, F., Elvassore, N., et al. (2013). A mechanical checkpoint controls multicellular growth through YAP/TAZ regulation by actin-processing factors. *Cell* 154, 1047–1059. doi: 10.1016/j.cell.2013.07.042

Aspenström, P., Lindberg, U., and Hall, A. (1996). Two GTPases, Cdc42 and Rac, bind directly to a protein implicated in the immunodeficiency disorder Wiskott-Aldrich syndrome. *Curr. Biol.* 6, 70–75. doi: 10.1016/S0960-9822(02)00423-2

Azzolin, L., Panciera, T., Soligo, S., Enzo, E., Bicciato, S., Dupont, S., et al. (2014). YAP/TAZ incorporation in the β-catenin destruction complex orchestrates the Wnt response. *Cell* 158, 157–170. doi: 10.1016/j.cell.2014.06.013

Baarlink, C., Plessner, M., Sherrard, A., Morita, K., Misu, S., Virant, D., et al. (2017). A transient pool of nuclear F-actin at mitotic exit controls chromatin organization. *Nat. Cell Biol.* 19, 1389–1399. doi: 10.1038/ncb3641

Beattie, R., and Hippenmeyer, S. (2017). Mechanisms of radial glia progenitor cell lineage progression. *FEBS Lett.* 591, 3993–4008. doi: 10.1002/1873-3468.12906

Black, M. M., and Baas, P. W. (1989). The basis of polarity in neurons. *Trends Neurosci.* 12, 211–214. doi: 10.1016/0166-2236(89)90124-0

Bradke, F., and Dotti, C. C. (1999). The role of local actin instability in axon formation. *Science* 283, 1931–1934. doi: 10.1126/science.283.5409.1931

Chan, E. H. Y., Nousiainen, M., Chalamalasetty, R. B., Schäfer, A., Nigg, E. A., and Sillje, H. H. W. (2005). The Ste20-like kinase Mst2 activates the human large tumor suppressor kinase Lats1. *Oncogene* 24, 2076–2086. doi: 10.1038/sj.onc.1208445

Cottini, F., Hideshima, T., Xu, C., Sattler, M., Dori, M., Agnelli, L., et al. (2014). Rescue of Hippo coactivator YAP1 triggers DNA damage-induced apoptosis in hematological cancers. *Nat. Med.* 20, 599–606. doi: 10.1038/nm.3562

Deng, F., Peng, L., Li, Z., Tan, G., Liang, E., Chen, S., et al. (2018). YAP triggers the Wnt/β-catenin signalling pathway and promotes enterocyte self-renewal, regeneration and tumorigenesis after DSS-induced injury. *Cell Death Dis.* 9:153. doi: 10.1038/s41419-017-0244-8

Dopie, J., Skarp, K. P., Rajakylä, E. K., Tanhuanpää, K., and Vartiainen, M. K. (2012). Active maintenance of nuclear actin by importin 9 supports transcription. *Proc. Natl. Acad. Sci. U.S.A.* 109, E544–E552. doi: 10.1073/pnas.1118880109

Elosegui-Artola, A., Andreu, I., Beedle, A. E. M., Lezamiz, A., Uroz, M., Kosmalska, A. J., et al. (2017). Force triggers YAP nuclear entry by regulating transport across nuclear pores. *Cell* 171, 1397.e14–1410.e14. doi: 10.1016/j.cell.2017.10.008

Escoll, M., Gargini, R., Cuadrado, A., Antón, I. M., and Wandosell, F. (2017). Mutant p53 oncogenic functions in cancer stem cells are regulated by WIP through YAP/TAZ. *Oncogene* 36, 3515–3527. doi: 10.1038/onc.2016.518

Foster, C. T., Gualdrini, F., and Treisman, R. (2017). Mutual dependence of the MRTF-SRF and YAP-TEAD pathways in cancer-associated fibroblasts is indirect and mediated by cytoskeletal dynamics. *Genes Dev.* 31, 2361–2375. doi: 10.1101/gad.304501.117

Franco, A., Knafo, S., Banon-Rodriguez, I., Merino-Serrais, P., Fernaud-Espinosa, I., Nieto, M., et al. (2012). WIP is a negative regulator of neuronal maturation and synaptic activity. *Cereb. Cortex* 22, 1191–1202. doi: 10.1093/cercor/bhr199

Franco-Villanueva, A., Fernández-López, E., Gabandé-Rodríguez, E., Bañón-Rodríguez, I., Esteban, J. A., Antón, I. M., et al. (2014). WIP modulates dendritic spine actin cytoskeleton by transcriptional control of lipid metabolic enzymes. *Hum. Mol. Genet.* 23, 4383–4395. doi: 10.1093/hmg/ddu155

Franco-Villanueva, A., Wandosell, F., and Antón, I. M. (2015). Neuritic complexity of hippocampal neurons depends on WIP-mediated mTORC1 and Abl family kinases activities. *Brain Behav.* 5:e00359. doi: 10.1002/brb3.359

Gargini, R., Escoll, M., García, E., García-Escudero, R., Wandosell, F., and Antón, I. M. (2016). WIP drives tumor progression through YAP/TAZ-dependent autonomous cell growth. *Cell Rep.* 17, 1962–1977. doi: 10.1016/j.celrep.2016.10.064

Garrido, J. J., Simón, D., Varea, O., and Wandosell, F. (2007). GSK3 alpha and GSK3 beta are necessary for axon formation. *FEBS Lett.* 581, 1579-86. doi: 10.1016/j.febslet.2007.03.018

Goley, E. D., Ohkawa, T., Mancuso, J., Woodruff, J. B., D'Alessio, J. A., Canda, W. Z., et al. (2006). Dynamic nuclear actin assembly by Arp2/3 complex and a baculovirus WASP-like protein. *Science* 314, 464–467. doi: 10.1126/science.1133348

Hall, A. (2012). Rho family GTPases. *Biochem. Soc. Trans.* 40, 1378–1382. doi: 10.1042/BST20120103

Halle-Bikovski, A., Fried, S., Rozentur-Shkop, E., Biber, G., Shaked, H., Joseph, N., et al. (2018). New structural insights into formation of the key actin regulating WIP-WASp complex determined by NMR and molecular imaging. *ACS Chem. Biol.* 13, 100–109. doi: 10.1021/acschembio.7b00486

Han, D., Byun, S. H., Park, S., Kim, J., Kim, I., Ha, S., et al. (2015). YAP/TAZ enhance mammalian embryonic neural stem cell characteristics in a Tead-dependent manner. *Biochem. Biophys. Res. Commun.* 458, 110–116. doi: 10.1016/j.bbrc.2015.01.077

Hu, J. K. H., Du, W., Shelton, S. J., Oldham, M. C., DiPersio, C. M., and Klein, O. D. (2017). An FAK-YAP-mTOR signaling axis regulates stem cell-based tissue renewal in mice. *Cell Stem Cell* 21, 91.e6–106.e6. doi: 10.1016/j.stem.2017.03.023

Hu, Y., Shin, D. J., Pan, H., Lin, Z., Dreyfuss, J. M., Camargo, F. D., et al. (2017). YAP suppresses gluconeogenic gene expression through PGC1α. *Hepatology* 66, 2029–2041. doi: 10.1002/hep.29373

Imajo, M., Miyatake, K., Iimura, A., Miyamoto, A., and Nishida, E. (2012). A molecular mechanism that links Hippo signalling to the inhibition of Wnt/β-catenin signalling. *EMBO J.* 31, 1109–1122. doi: 10.1038/emboj.2011.487

Inagaki, N., Chihara, K., Arimura, N., Ménager, C., Kawano, Y., Matsuo, N., et al. (2001). CRMP-2 induces axons in cultured hippocampal neurons. *Nat. Neurosci.* 4, 781–782. doi: 10.1038/90476

Jaworski, J., and Sheng, M. (2006). The growing role of mTOR in neuronal development and plasticity. *Mol. Neurobiol.* 34, 205–219. doi: 10.1385/MN:34:3:205

Jedsadayanmata, A., Chen, C. C., Kireeva, M. L., Lau, L. F., and Lam, S. C. T. (1999). Activation-dependent adhesion of human platelets to Cyr61 and Fisp12/mouse connective tissue growth factor is mediated through integrin α(IIb)β3. *J. Biol. Chem.* 274, 24321–24327. doi: 10.1074/jbc.274.34.24321

Jiang, H., and Rao, Y. (2005). Axon formation: fate versus growth. *Nat. Neurosci.* 8, 544–546. doi: 10.1038/nn0505-544

Koduru, S., Massaad, M., Wilbur, C., Kumar, L., Geha, R., and Ramesh, N. (2007). A novel anti-WIP monoclonal antibody detects an isoform of WIP that lacks the WASP binding domain. *Biochem. Biophys. Res. Commun.* 353, 875–881. doi: 10.1016/j.bbrc.2006.12.079

Lanzi, G., Moratto, D., Vairo, D., Masneri, S., Delmonte, O., Paganini, T., et al. (2012). A novel primary human immunodeficiency due to deficiency in the WASP-interacting protein WIP. *J. Exp. Med.* 209, 29–34. doi: 10.1084/jem.20110896

Lee, S. H., and Dominguez, R. (2010). Regulation of actin cytoskeleton dynamics in cells. *Mol. Cells* 29, 311–325. doi: 10.1007/s10059-010-0053-8

Liu, B., Sun, L. H., Huang, Y. F., Guo, L. J., and Luo, L. S. (2018). Protein phosphatase 2ACα gene knock-out results in cortical atrophy through activating hippo cascade in neuronal progenitor cells. *Int. J. Biochem. Cell Biol.* 95, 53–62. doi: 10.1016/j.biocel.2017.12.015

Liu, C. Y., Zha, Z. Y., Zhou, X., Zhang, H., Huang, W., Zhao, D., et al. (2010). The hippo tumor pathway promotes TAZ degradation by phosphorylating a phosphodegron and recruiting the SCFβ-TrCP E3 ligase. *J. Biol. Chem.* 285, 37159–37169. doi: 10.1074/jbc.M110.152942

Ma, S., Meng, Z., Chen, R., and Guan, K. L. (2019). The hippo pathway: biology and pathophysiology. *Annu. Rev. Biochem.* 88, 577–604. doi: 10.1146/annurev-biochem-013118-111829

Manning, S. A., Dent, L. G., Kondo, S., Zhao, Z. W., Plachta, N., and Harvey, K. F. (2018). Dynamic fluctuations in subcellular localization of the hippo pathway effector yorkie in vivo. *Curr. Biol.* 28, 1651.e4–1660.e4. doi: 10.1016/j.cub.2018.04.018

Mansour, R., El-Orfali, Y., Saber, A., Noun, D., Youssef, N., Youssef, Y., et al. (2020). Wiskott-aldrich syndrome in four male siblings from a consanguineous family from Lebanon. *Clin. Immunol.* 219:108573. doi: 10.1016/j.clim.2020.108573

Martinez-Quiles, N., Rohatgi, R., Antón, I. M., Medina, M., Saville, S. P., Miki, H., et al. (2001). WIP regulates N-WASP-mediated actin polymerization and filopodium formation. *Nat. Cell Biol.* 3, 484–491. doi: 10.1038/35074551

Menotti, M., Ambrogio, C., Cheong, T. C., Pighi, C., Mota, I., Cassel, S. H., et al. (2019). Wiskott–aldrich syndrome protein (WASP) is a tumor suppressor in T cell lymphoma. *Nat. Med.* 25, 130–140. doi: 10.1038/s41591-018-0262-9

Mitter, D., Chiaie, B. D., Lüdecke, H.-J., Gillessen-Kaesbach, G., Bohring, A., Kohlhase, J., et al. (2010). Genotype-phenotype correlation in eight new patients with a deletion encompassing 2q31.1. *Am. J. Med. Genet. Part A* 152A, 1213–1224. doi: 10.1002/ajmg.a.33344

Molinie, N., Rubtsova, S. N., Fokin, A., Visweshwaran, S. P., Rocques, N., Polesskaya, A., et al. (2019). Cortical branched actin determines cell cycle progression. *Cell Res.* 29, 432–445. doi: 10.1038/s41422-019-0160-9

Moresco, E. M., Donaldson, S., Williamson, A., and Koleske, A. J. (2005). Integrin-mediated dendrite branch maintenance requires Abelson (Abl) family kinases. *J. Neurosci.* 25, 6105–6118. doi: 10.1523/JNEUROSCI.1432-05.2005

Mukhtar, T., Breda, J., Grison, A., Karimaddini, Z., Grobecker, P., Iber, D., et al. (2020). Tead transcription factors differentially regulate cortical development. *Sci. Rep.* 10, 1–19. doi: 10.1038/s41598-020-61490-5

Mukhtar, T., and Taylor, V. (2018). Untangling cortical complexity during development. *J. Exp. Neurosci.* 12:1179069518759332. doi: 10.1177/1179069518759332

Nusse, R., and Clevers, H. (2017). Wnt/β-catenin signaling, Dise1. Nusse R, Clevers H. Wnt/β-catenin signaling, disease, and emerging therapeutic modalities. *Cell* 169, 985–999. doi: 10.1016/j.cell.2017.05

Olson, E. N., and Nordheim, A. (2010). Linking actin dynamics and gene transcription to drive cellular motile functions. *Nat. Rev. Mol. Cell Biol.* 11, 353–365. doi: 10.1038/nrm2890

Padrick, S. B., and Rosen, M. K. (2010). Physical mechanisms of signal integration by WASP family proteins. *Annu. Rev. Biochem.* 79, 707–735. doi: 10.1146/annurev.biochem.77.060407.135452

Panciera, T., Azzolin, L., Fujimura, A., di Biagio, D., Frasson, C., Bresolin, S., et al. (2016). Induction of expandable tissue-specific stem/progenitor cells through transient expression of YAP/TAZ. *Cell Stem Cell* 19, 725–737. doi: 10.1016/j.stem.2016.08.009

Paridaen, J. T., and Huttner, W. B. (2014). Neurogenesis during development of the vertebrate central nervous system. *EMBO Rep.* 15, 351–364. doi: 10.1002/embr.201438447

Parisis, N., Krasinska, L., Harker, B., Urbach, S., Rossignol, M., Camasses, A., et al. (2017). Initiation of DNA replication requires actin dynamics and formin activity. *EMBO J.* 36, 3212–3231. doi: 10.15252/embj.201796585

Park, H. W., Kim, Y. C., Yu, B., Moroishi, T., Mo, J. S., Plouffe, S. W., et al. (2015). Alternative Wnt signaling activates YAP/TAZ. *Cell* 162, 780–794. doi: 10.1016/j.cell.2015.07.013

Paunola, E., Mattila, P. K., and Lappalainen, P. (2002). WH2 domain: a small, versatile adapter for actin monomers. *FEBS Lett.* 513, 92–97. doi: 10.1016/S0014-5793(01)03242-2

Piccolo, S., Dupont, S., and Cordenonsi, M. (2014). The biology of YAP/TAZ: hippo signaling and beyond. *Physiol. Rev.* 94, 1287–1312. doi: 10.1152/physrev.00005.2014

Ramesh, N., Antón, I. M., Hartwig, J. H., and Geha, R. S. (1997). WIP, a protein associated with Wiskott-Aldrich syndrome protein, induces actin polymerization and redistribution in lymphoid cells. *Proc. Natl. Acad. Sci. U.S.A.* 94, 14671–14676. doi: 10.1073/pnas.94.26.14671

Ramesh, N., Massaad, M. J., Kumar, L., Koduru, S., Sasahara, Y., Anton, I., et al. (2014). Binding of the WASP/N-WASP-interacting protein WIP to actin regulates focal adhesion assembly and adhesion. *Mol. Cell. Biol.* 34, 2600–2610. doi: 10.1128/mcb.00017-14

Robledinos-Antón, N., Escoll, M., Guan, K. L., and Cuadrado, A. (2020). TAZ represses the neuronal commitment of neural stem cells. *Cells* 9:2230. doi: 10.3390/cells9102230

Santinon, G., Brian, I., Pocaterra, A., Romani, P., Franzolin, E., Rampazzo, C., et al. (2018). d NTP metabolism links mechanical cues and YAP / TAZ to cell growth and oncogene-induced senescence. *EMBO J.* 37:e97780. doi: 10.15252/embj.201797780

Sasahara, Y., Rachid, R., Byrne, M. J., de la Fuente, M. A., Abraham, R. T., Ramesh, N., et al. (2002). Mechanism of recruitment of WASP to the immunological synapse and of its activation following TCR ligation. *Mol. Cell* 10, 1269–1281. doi: 10.1016/S1097-2765(02)00728-1

Schrank, B. R., Aparicio, T., Li, Y., Chang, W., Chait, B. T., Gundersen, G. G., et al. (2018). Nuclear ARP2/3 drives DNA break clustering for homology-directed repair. *Nature* 559, 61–66. doi: 10.1038/s41586-018-0237-5

Treisman, R. (2013). Shedding light on nuclear actin dynamics and function. *Trends Biochem. Sci.* 38, 376–377. doi: 10.1016/j.tibs.2013.06.004

Varelas, X., Miller, B. W., Sopko, R., Song, S., Gregorieff, A., Fellouse, F. A., et al. (2010). The hippo pathway regulates Wnt/β-Catenin signaling. *Dev. Cell* 18, 579–591. doi: 10.1016/j.devcel.2010.03.007

Vetterkind, S., Miki, H., Takenawa, T., Klawitz, I., Scheidtmann, K. H., and Preuss, U. (2002). The rat homologue of Wiskott-Aldrich syndrome protein (WASP)-interacting protein (WIP) associates with actin filaments, recruits N-WASP from the nucleus, and mediates mobilization of actin from stress fibers in favor of filopodia formation. *J. Biol. Chem.* 277, 87–95. doi: 10.1074/jbc.M104555200

Wu, X., Yoo, Y., Okuhama, N. N., Tucker, P. W., Liu, G., and Guan, J. L. (2006). Regulation of RNA-polymerase-II-dependent transcription by N-WASP and its nuclear-binding partners. *Nat. Cell Biol.* 8, 756–763. doi: 10.1038/ncb1433

Yoo, Y., Wu, X., and Guan, J. L. (2007). A novel role of the actin-nucleating Arp2/3 complex in the regulation of RNA polymerase II-dependent transcription. *J. Biol. Chem.* 282, 7616–7623. doi: 10.1074/jbc.M607596200

Yu, F. X., Zhao, B., and Guan, K. L. (2015). Hippo pathway in organ size control, tissue homeostasis, and cancer. *Cell* 163, 811–828. doi: 10.1016/j.cell.2015.10.044

Zhao, B., Li, L., Lu, Q., Wang, L. H., Liu, C. Y., Lei, Q., et al. (2011). Angiomotin is a novel Hippo pathway component that inhibits YAP oncoprotein. *Genes Dev.* 25, 51–63. doi: 10.1101/gad.2000111

Zhao, B., Li, L., Tumaneng, K., Wang, C. Y., and Guan, K. L. (2010). A coordinated phosphorylation by Lats and CK1 regulates YAP stability through SCFβ-TRCP. *Genes Dev.* 24, 72–85. doi: 10.1101/gad.1843810

Conflict of Interest: The authors declare that the research was conducted in the absence of any commercial or financial relationships that could be construed as a potential conflict of interest.

frontiers in Cell and Developmental Biology

BRIEF RESEARCH REPORT
published: 17 June 2021
doi: 10.3389/fcell.2021.671887

Syne2b/Nesprin-2 Is Required for Actin Organization and Epithelial Integrity During Epiboly Movement in Zebrafish

Yu-Long Li[1†], Xiao-Ning Cheng[2†], Tong Lu[1†], Ming Shao[1] and De-Li Shi[3,4*]*

[1] School of Life Sciences, Shandong University, Qingdao, China, [2] Central People's Hospital of Zhanjiang, Zhanjiang, China, [3] Affiliated Hospital of Guangdong Medical University, Zhanjiang, China, [4] Laboratory of Developmental Biology, CNRS-UMR 7622, Institut de Biologie Paris-Seine (IBPS), Sorbonne University, Paris, France

OPEN ACCESS

Edited by:
Noa B. Martin-Cofreces, Princess University Hospital, Spain

Reviewed by:
Pierre-Olivier Angrand, Lille University of Science and Technology, France
Enrique Martin-Blanco, Instituto de Biología Molecular de Barcelona (IBMB), Spain
Qiuping Zhang, King's College London, United Kingdom

***Correspondence:**
Ming Shao
shaoming@sdu.edu.cn
De-Li Shi
de-li.shi@upmc.fr

[†] These authors have contributed equally to this work

Specialty section:
This article was submitted to Cell Adhesion and Migration, a section of the journal Frontiers in Cell and Developmental Biology

Received: 24 February 2021
Accepted: 28 May 2021
Published: 17 June 2021

Citation:
Li Y-L, Cheng X-N, Lu T, Shao M and Shi D-L (2021) Syne2b/Nesprin-2 Is Required for Actin Organization and Epithelial Integrity During Epiboly Movement in Zebrafish. Front. Cell Dev. Biol. 9:671887. doi: 10.3389/fcell.2021.671887

Syne2b/nesprin-2 is a giant protein implicated in tethering the nucleus to the cytoskeleton and plays an important role in maintaining cellular architecture. Epiboly is a conserved morphogenetic movement that involves extensive spreading and thinning of the epithelial blastoderm to shape the embryo and organize the three germ layers. Dynamic cytoskeletal organization is critical for this process, but how it is regulated remains elusive. Here we generated a zebrafish *syne2b* mutant line and analyzed the effects of impaired Syne2b function during early development. By CRISPR/Cas9-mediated genome editing, we obtained a large deletion in the *syne2b* locus, predicted to cause truncation of the nuclear localization KASH domain in the translated protein. Maternal and zygotic *syne2b* embryos showed delayed epiboly initiation and progression without defects in embryonic patterning. Remarkably, disruption of Syne2b function severely impaired cytoskeletal organization across the embryo, leading to aberrant clustering of F-actin at multiple cell contact regions and abnormal cell shape changes. These caused disintegration of the epithelial blastoderm before the end of gastrulation in most severely affected embryos. Moreover, the migration of yolk nuclear syncytium also became defective, likely due to disorganized cytoskeletal networks at the blastoderm margin and in the yolk cell. These findings demonstrate an essential function of Syne2b in maintaining cytoskeletal architecture and epithelial integrity during epiboly movement.

Keywords: Syne2b, nesprin, zebrafish, epiboly, morphogenetic movement, actin cytoskeleton, epithelial integrity

INTRODUCTION

Nesprins (Nuclear Envelope SPectrin Repeat proteINS) are outer nuclear membrane resident macromolecules that constitute the LINC (LInker of the Nucleoskeleton and Cytoskeleton) complex (Zhang et al., 2001; Rajgor and Shanahan, 2013; Davidson and Cadot, 2020). Nesprin-1 and –2 are giant proteins containing an N-terminal actin-binding domain, followed by a long central domain composed of spectrin repeats, and a C-terminal nuclear localization KASH

(Klarsicht/ANC-1/Syne Homology) domain, thus connecting the nucleus to the cytoplasmic actin cytoskeleton (Crisp et al., 2006; Noegel and Neumann, 2011). In humans, these proteins are encoded by *SYNE* (*synaptic nuclear envelope*) *–1* and *–2* loci, whose mutations cause various diseases, such as muscular dystrophy, dilated cardiomyopathy, neurological disorders and hearing loss (Cartwright and Karakesisoglou, 2014; Janin and Gache, 2018; Zhou et al., 2018a). Mutant mouse models for nesprins that mimic different human diseases have provided insights into their tissue-specific postnatal functions (Zhou et al., 2018b). However, the implication of nesprins in morphogenetic movements remains unclear.

Epiboly is a conserved morphogenetic process in vertebrates (Solnica-Krezel, 2005). In the zebrafish embryo, it is initiated in the blastula and progresses in the gastrula. By the mid-blastula stage, the embryo becomes organized into a superficial monolayer known as the enveloping layer (EVL), a deep cell multilayer (DEL), and a yolk syncytial layer (YSL) consisting of nuclei (YSN) and non-yolky cytoplasm located on the yolk cell (Kimmel et al., 1995). Epiboly initiates when the large yolk cell domes upward into the blastoderm. During epiboly progression, the blastoderm and YSL move toward the vegetal pole to engulf the yolk cell by the end of gastrulation (Warga and Kimmel, 1990; Bruce, 2016). Dynamic cytoskeletal changes across the embryo are important for epiboly movement. Cortical F-actin belt is organized in EVL cells from the early blastula stage onward; punctate F-actin rings form ahead of the leading edge of the E-YSL at more late stages of epiboly; F-actin bundles are also present in the vegetal cortex of the yolk cell until before the end of gastrulation (Lee, 2014). These actin networks play essential roles in modulating cellular behavior changes and cell rearrangements during epiboly progression (Köppen et al., 2006; Li et al., 2017; Sun et al., 2017). Thus, cytoskeletal organization is closely linked to epithelial morphogenesis, but how it is regulated remains largely elusive.

Here we report a role for Syne2b (also called nesprin-2) during epiboly in zebrafish. By CRISPR/Cas9-mediated genome editing, we generated a deletion mutation in the zebrafish *syne2b* locus that should impair the attachment of Syne2b to the nuclear membrane. Maternal and zygotic *syne2b* mutants displayed severely disorganized actin cytoskeleton and delayed epiboly movement. Strikingly, cortical F-actin belt in the EVL was reduced and abnormally concentrated to multiple cell contact regions, resulting in aberrant cell shape changes and disrupted epithelial integrity. These results demonstrate a requirement for Syne2b in regulating cytoskeletal organization to maintain cell shape and integrity of the epithelial blastoderm. They provide insights into the implication of nesprins in morphogenetic movements during vertebrate early development.

METHODS

Zebrafish

Adult zebrafish were maintained in standard housing systems. Embryos were microinjected using a PLI-100A picoliter microinjector (Harvard Apparatus).

Ethics Statement

All experiments were approved by the Ethics Committee for Animal Research of Life Science of Shandong University (SYDWLL-2018–05), and performed by following the ARRIVE guidelines.

Genome Editing of *Syne2b* Locus

DNA templates for *in vitro* transcription of sgRNAs were cloned into p-T7-gRNA vector. The two sgRNAs (200 pg each) were mixed with Cas9 protein (300 pg) and injected into 1-cell stage embryos. Fish were screened by sequencing PCR products amplified from tail fin genomic DNA as described previously (Shao et al., 2020).

Expression Constructs and mRNA Synthesis

The sequence encoding the last 69 amino acids of zebrafish Syne1a was amplified by PCR (**Supplementary Table 1**) and cloned inframe with the myc-coding sequence in the pCS2 vector, to generate the dominant negative Syne1a KASH (Tsujikawa et al., 2007). Life-Act-GFP was cloned in the pCS2 vector, and mGFP and H2B-RFP were described previously (Cheng et al., 2017). Capped mRNAs were *in vitro* transcribed using mMESSAGE mMACHINE SP6 kit (Ambion).

Phalloidin and DAPI Staining

Stage-matched wild-type and MZ*syne2b* embryos were fixed in 4% paraformaldehyde for 1 h at room temperature. They were stained with rhodamine-conjugated phalloidin and counterstained with DAPI (Sigma-Aldrich). Images were acquired using a confocal microscope (Zeiss LSM700). Z-stack projections were generated using the z-projection function.

Time-Lapse Imaging

Embryos were mounted in a cavity microscope slide in 1% low-melting agarose. Cell shape changes in the EVL and vegetal movements of YSN were recorded for 1 h and 30 min, respectively, at 5 min intervals. Time-lapse movies were generated using ImageJ software (NIH Image). The experiments were repeated twice using 6 wild-type or MZ*syne2b* embryos from different batches.

Immunofluorescence

Embryos were fixed in 4% paraformaldehyde and rinsed in phosphate-buffered saline. They were incubated with rabbit polyclonal antibodies against ß-tubulin (1/1,000, Sigma-Aldrich), followed by fluorescein-conjugated secondary antibody. The samples were analyzed under a confocal microscope (Zeiss, LSM700).

qRT-PCR

Total RNA was extracted using TRIzol Reagent (Invitrogen) and reverse transcribed using M-MLV reverse transcriptase (Invitrogen) in the presence of random primer. Gene-specific primers are listed in **Supplementary Table 1**.

Whole-Mount *in situ* Hybridization

DNA templates for generating *syne2b*, *goosecoid*, *chordin* and *tbxta* probes were obtained by PCR amplification of embryonic cDNAs (**Supplementary Table 1**). PCR products were cloned in pBluescript or pGEM-T easy vector and antisense probes were synthesized using appropriate RNA polymerases and digoxigenin-11-UTP (Roche Diagnostics). *In situ* hybridization was performed according to published protocol (Thisse and Thisse, 2008). Embryos after 24 hpf (hours post-fertilization) were treated with proteinase K (10 μg/mL) for 15 min.

Statistical Analyses

Data from two to three independent experiments were statistically analyzed using unpaired Student's *t*-test, with *p*-values indicated in the corresponding figures and legends.

RESULTS

Expression of *Syne2b* During Early Development

We first performed *in situ* hybridization to analyze *syne2b* expression pattern. Maternal *syne2b* transcripts were enriched in the blastodisc, but were also weakly present in the yolk region at least at 1-cell stage (**Figures 1A–D**). During gastrulation, *syne2b* expression was detected in the blastoderm, particularly in the dorsal region (**Figures 1E,F**). As development proceeds, *syne2b* transcripts became predominantly localized to dorsal structures, such as neural keel in the anterior region, lateral edges of neural keel in the posterior region, and primary neurons (**Figures 1G–J**). At 18-somite stage, *syne2b* expression was also evident in the tail bud (**Figures 1K,L**). Thus, Syne2b may be involved in early developmental processes before and after zygotic genome activation beginning around 512-cell stage.

Generation of *Syne2b* Deletion Mutants

Zebrafish *syne2b* locus (NCBI gene ID: 559348) comprises 131 exons and is predicated to encode a giant protein consisting of 9,853 amino acids. As human SYNE2/Nesprin-2, zebrafish Syne2b contains an N-terminal actin-binding domain, followed by spectrin repeats and a C-terminal KASH domain. To disrupt *syne2b* gene by CRISPR/Cas9, we synthesized two sgRNAs targeting exons 120 and 129, respectively. PCR-based genotyping of genomic DNA (**Supplementary Figure 1**) in F1 and F2 offspring detected a large deletion of the intervening region (**Figures 2A,B**). Sequencing of PCR products indicated that this caused a frameshift and the premature termination of translation after amino acid position 9383, predicting the expression of a truncated protein without attachment to the nuclear membrane due to the absence of the nuclear localization KASH domain (**Figures 2C,D**). Analysis by qRT-PCR using primers that are specific for each isoform of *syne* genes showed a less than twofold decreased expression of *syne2b* mutant transcripts in MZ*syne2b* embryos at 10 hpf, probably caused by nonsense-mediated decay. The expression of *syne2a* and *syne3*, but not of *syne1a* and *syne1b*, was also slightly but significantly decreased (**Supplementary Figure 2**). Thus, this mutation may affect the function of Syne2b protein and the expression of *syne2a* and *syne3* genes.

Disruption of Syne2b Function Delays Epiboly Initiation and Progression

The phenotype of *syne2b* mutants was examined in comparison with time-matched wild-type embryos. To avoid possible variations in the exact timing of fertilization, which may introduce fluctuations in embryonic development, we collected eggs spawned within 10 min intervals and monitored the number of blastomeres from 8 to 32-cell stages. Heterozygous and zygotic homozygous *syne2b* mutants showed no developmental defects. Maternal-zygotic *syne2b* (MZ*syne2b*) embryos developed

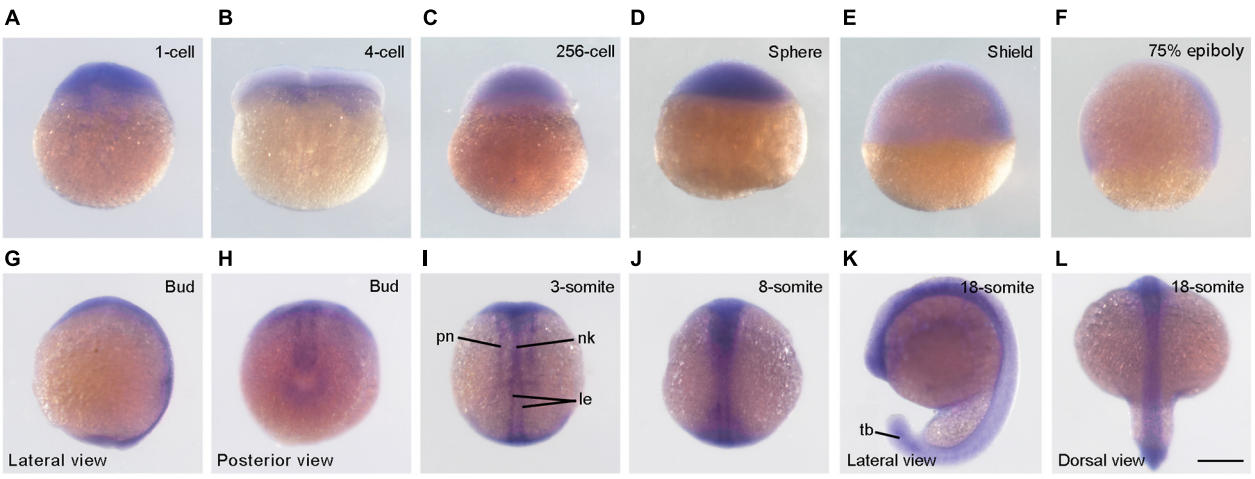

FIGURE 1 | Expression pattern of *syne2b* during early development. **(A–D)** At cleavage and blastula stages, *syne2b* transcripts are enriched in the blastodisc. Animal pole region is on the top. **(E,F)** Predominant expression of *syne2b* in the dorsal region during gastrulation. Lateral view with animal pole region on the top and dorsal region to the right. **(G,H)** Expression of *syne2b* along the anteroposterior axis at bud stage. **(I,J)** Dorsal views show *syne2b* expression in axial structures, including neural keel (nk), lateral edges (le) of neural keel and primary neurons (pn). **(K,L)** Expression of *syne2b* in the neural tissue and tail bud (tb). Scale bar: **(A–L)** 200 μm.

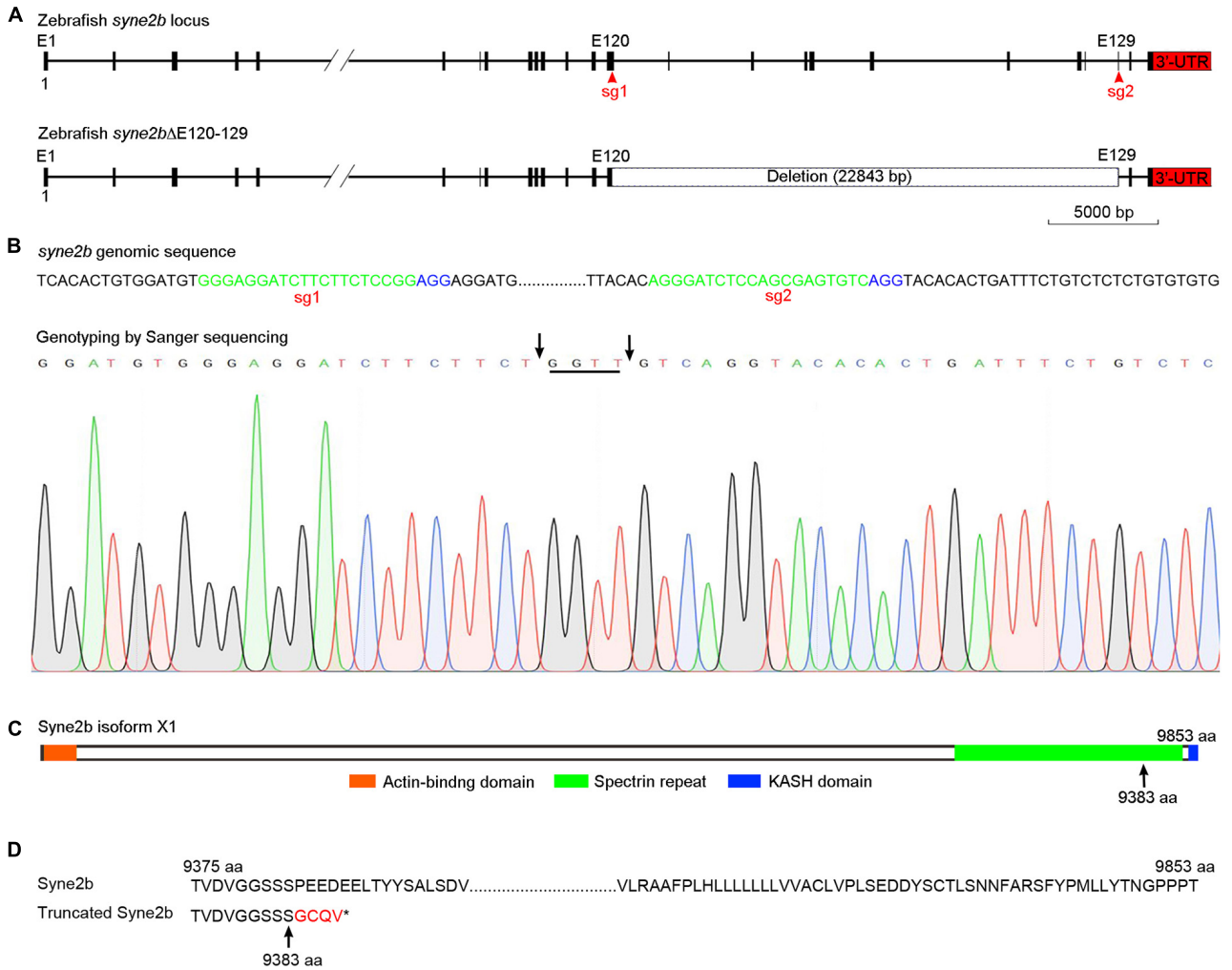

FIGURE 2 | Generation of *syne2b* mutation by CRISPR/Cas9-mediated genome editing. **(A)** Organization of the zebrafish *syne2b* locus. Shown are the sgRNA targeting sites (sg1 and sg2) and the deleted intervening region. **(B)** Genotyping of *syne2b* mutation. The sgRNA recognition sequences are green colored, and the PAM regions are shown in blue. Arrows indicate the positions of deletion in exons 120 and 129. Nucleotides inserted as a result of DNA repair are underlined. **(C)** Syne2b protein domains. Arrow indicates the position after which truncation occurs in the translated Syne2b protein. **(D)** Alignment of the C-terminal regions from wild-type and truncated Syne2b proteins. Residues translated after frameshift are indicated in red.

normally during early cleavage stages, but they were transiently higher from 128 to 512-cell stages (**Supplementary Figure 3**). After resuming a spherical shape at 4 hpf, the subsequent development showed delayed epiboly initiation and progression, with 100% penetrance.

At 4.25 hpf when epiboly initiated in wild-type embryos with the yolk cell doming into the blastoderm, there was still a flat border between the blastoderm and the yolk cell in MZ*syne2b* embryos (**Figures 3A,B**). At 5 hpf, the blastoderm became thinner in wild-type embryos, whereas it remained thicker in MZ*syne2b* embryos (**Figures 3C,D,O**), indicating delayed yolk cell doming. From 6 to 10 hpf, there was obviously a delayed epiboly progression in MZ*syne2b* embryos, as judged by the slowed spreading of the blastoderm toward the vegetal pole (**Figures 3E–L,P,Q**). As a result, when wild-type embryos completed gastrulation at 10 hpf (**Figure 3K**), MZ*syne2b* embryos only reached about 80% epiboly (**Figure 3L**). At 11.5 hpf, although most MZ*syne2b* embryos could complete epiboly, they presented a shortened anteroposterior axis compared to time-matched wild-type embryos (**Figures 3M,N**). Thus, MZ*syne2b* embryos showed a delay of about 1.5 h in epiboly progression. This is significant given that the period from the initiation to the end of epiboly normally lasts 6 h when embryos develop at 28.5°C (Kimmel et al., 1995).

We also observed a proportion of more severely affected embryos that could not complete gastrulation due to disintegration of the blastoderm, usually occurring around the animal pole region (**Supplementary Figure 4**). From two independent batches, about 12% (n = 65) of MZ*syne2b* embryos from young homozygous female parents displayed most severely delayed epiboly, with multiple disintegrated regions in the blastoderm before the end of gastrulation. This variation may

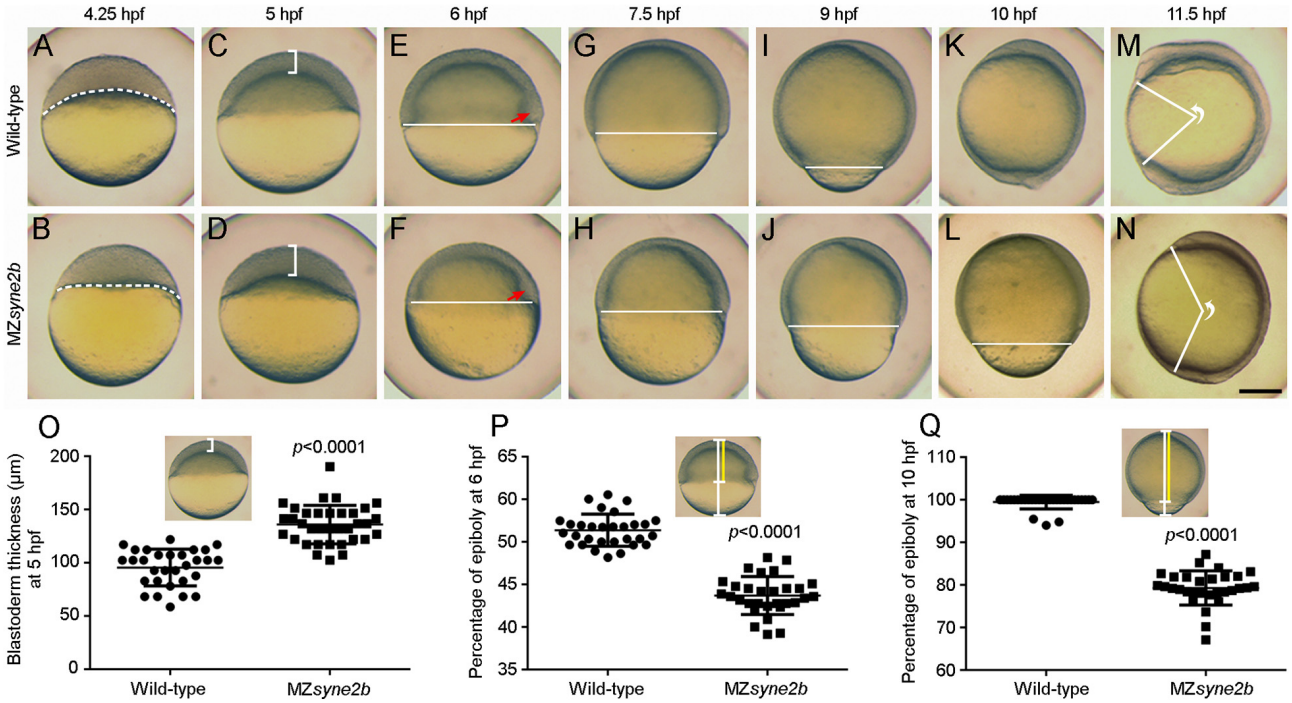

FIGURE 3 | Disruption of Syne2b function impairs epiboly movement and anteroposterior axis elongation. Live images show epiboly initiation and progression in time-matched embryos. Lateral views with animal pole or anterior region on the top. **(A,B)** At 4.25 hpf, yolk cell domes into the blastoderm in wild-type embryos, while the border between the blastoderm and the yolk cell (broken lines) remains flat in MZ*syne2b* embryos. **(C,D)** At 5 hpf, the blastoderm in MZ*syne2b* embryos is thicker compared with wild-type embryos (brackets). **(E,F)** At 6 hpf, MZ*syne2b* embryos show delayed epiboly compared with wild-type embryos (horizontal lines). Red arrows indicate the embryonic shield. **(G–J)** At 7.5 and 9 hpf, delayed epiboly progression is evident in MZ*syne2b* embryos. **(K,L)** At 10 hpf, wild-type embryos complete gastrulation, whereas MZ*syne2b* embryos only reach about 80% epiboly. **(M,N)** At 11.5 hpf, wild-type embryos develop a long anteroposterior axis, while MZ*syne2b* embryos only complete gastrulation. The angle formed between the most anterior end and the most posterior end of the anteroposterior axis, with vertex at the geometric center of the embryo, reflects the extent of axis elongation. **(O)** Scatter plot compares blastoderm thickness between wild-type and MZ*syne2b* embryos. **(P,Q)** Scatter plots compare epiboly progression between wild-type and MZ*syne2b* embryos. Scale bars: **(A–N)** 200 μm.

result from the differential expressivity and the maternal age of mutant fish. There is also a possibility that other nesprins with similar functions may compensate for the loss of Syne2b. Indeed, expression of the dominant negative Syne1a KASH in MZ*syne2b* embryos further delayed epiboly (**Supplementary Figure 5**). Together, these analyses suggest that interference with maternal Syne2b function delays epiboly initiation and progression.

Disrupted Cytoskeletal Organization in MZ*syne2b* Mutants

Analysis of the expression pattern of dorsal mesoderm markers *chordin* and *goosecoid* and the pan-mesoderm marker *tbxta* indicated that mesoderm patterning was not affected in MZ*syne2b* embryos. Nevertheless, the expression domain of *chordin* and *goosecoid* at shield stage became expanded laterally, while that of *tbxta* at 9 hpf was reduced along the anteroposterior axis, suggesting delayed convergence of lateral cells toward the embryonic shield at early stages of epiboly and reduced extension of axial mesoderm during late stages of gastrulation (**Supplementary Figure 6**). Given the binding activity of Syne2b to actin and the requirement of cytoskeletal dynamics for epiboly movement, we examined F-actin organization and YSN behaviors in stage-matched embryos ($n = 6$ from three independent batches for each condition).

At 30% epiboly, strong and regular cortical F-actin, as revealed by phalloidin staining, could be observed in the cortex of EVL cells in wild-type embryos (**Figures 4A–A″**). However, weak and disrupted cortical F-actin was present in MZ*syne2b* embryos (**Figures 4B–B″**). Particularly, F-actin was concentrated at multiple cell contact regions (arrows in **Figure 4B′**). By this stage, DAPI-stained YSN were present ahead of the blastoderm margin in wild-type embryos (**Figures 4A,A″**), whereas they were rarely observed in MZ*syne2b* embryos (**Figures 4B,B″**). At 50% epiboly, besides the defective localization of cortical F-actin belt in EVL cells, F-actin bundles in the yolk cell was also disorganized in MZ*syne2b* embryos (**Figures 4D–E″**). The abnormal vegetal migration of YSN was evident, as further demonstrated by time-lapse imaging at 50% epiboly (**Figures 4I–J″**). This defect may be also correlated with a disorganization of microtubule arrays in the yolk cell (**Supplementary Figure 7**). At 70% epiboly when wild-type embryos formed a thick marginal actin ring (**Figures 4E–E″**), MZ*syne2b* embryos displayed a generalized F-actin disorganization, with strongly reduced F-actin in front of the EVL margin (**Figures 4F–F″**). Moreover, EVL cells in wild-type embryos displayed uniform cortical F-actin belt

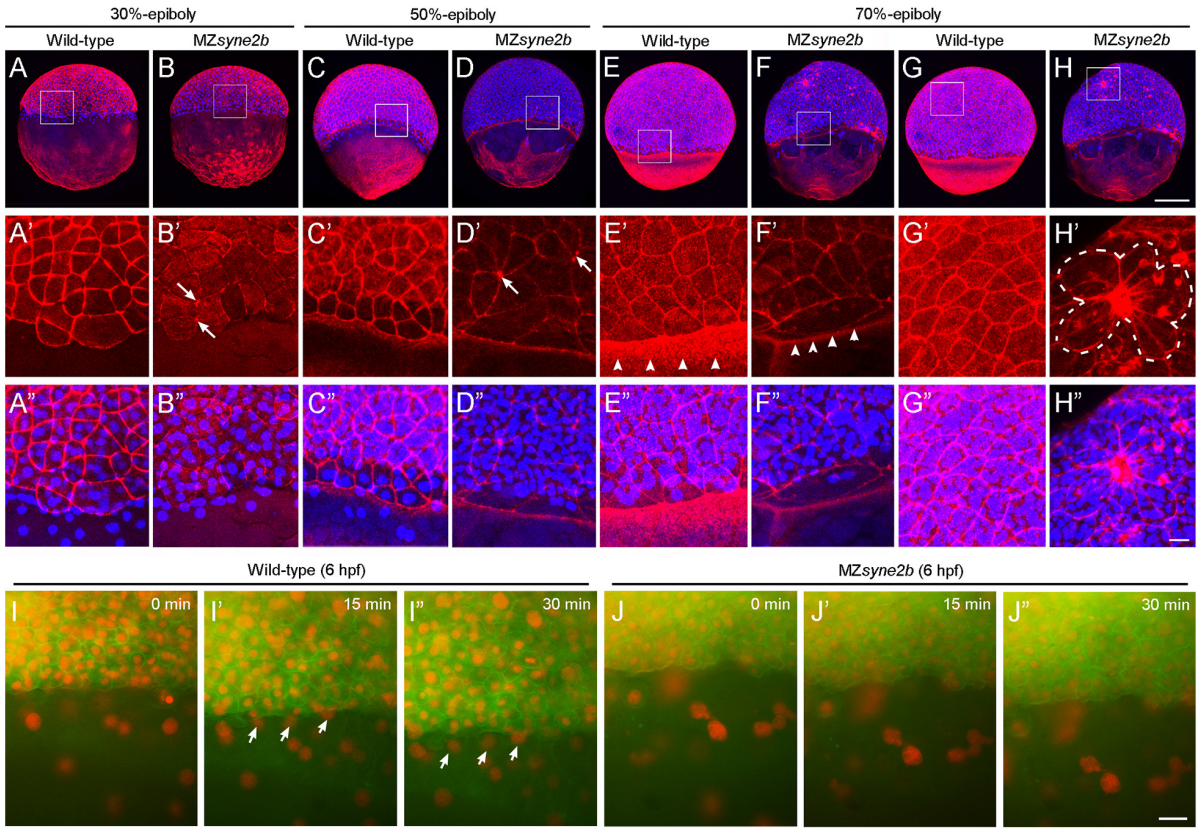

FIGURE 4 | Disruption of Syne2b function affects F-actin organization, EVL cell shape and YSN movements. Phalloidin and DAPI staining of stage-matched embryos. **(A–A′′)** Wild-type embryos at 30% epiboly show strong phalloidin staining in the cortex of EVL cells. A ring of YSN are apparent at the EVL margin. **(B–B′′)** MZ*syne2b* embryos at 30% epiboly show reduced and clustered (arrows) phalloidin staining in EVL cells. Few YSN are present at the EVL margin. **(C–C′′)** In wild-type embryos at 50% epiboly, phalloidin staining is present strongly in the cortex of EVL cells and uniformly in the yolk cell. YSN are still present at the EVL margin. **(D–D′′)** In MZ*syne2b* embryos at 50% epiboly, phalloidin staining is clustered at multiple cell contact regions in the blastoderm (arrows) and is disrupted in the yolk cell. Few YSN are scattered in the yolk cell. **(E–E′′)** In wild-type embryos at 70% epiboly, thick actin rings are formed around the blastoderm margin (arrowheads). **(F–F′′)** MZ*syne2b* embryos at 70% epiboly form weak and thin marginal actin rings (arrowheads). YSN remain scattered in the yolk cell. **(G–G′′)** Regular cortical F-actin and cell shape in the blastoderm of wild-type embryos. **(H–H′′)** Severely disrupted cell shape and rearrangements in the blastoderm of MZ*syne2b* embryos, with the occurrence of rosette structures (broken lines). **(I,J′′)** Still frames from time-lapse imaging show YSN movements at 50% epiboly. Note that YSN emerge from the front of the EVL margin during epiboly in wild-type embryos (arrows). Scale bars: **(A–H)** 200 μm; **(A′–H′′)** 20 μm; **(I–J′′)** 100 μm.

and took a polygonal shape (**Figures 4G–G′′**), whereas F-actin became further concentrated at multiple cell contact regions in the blastoderm of MZ*syne2b* embryos (**Figures 4H–H′′**). Strikingly, this caused the appearance of "actin-rich plaques," which appeared to attach surrounding EVL cells, forming multiple pinwheel-like or rosette structures (**Figures 4H′,H′′** and **Supplementary Figure 8**). These defects could lead to reduced cellular cohesion, because blastoderm disintegration likely occurred at these regions in most severely affected MZ*syne2b* embryos (**Supplementary Figure 8**). The severe disruption of cortical F-actin associated with abnormal EVL cell shape changes and loss of epithelial integrity in MZ*syne2b* embryos was further confirmed by time-lapse recording at 70% epiboly using LifeAct-GFP (**Supplementary Movies 1, 2**). From mid-gastrula stage onward, some YSN recede from the marginal zone and converge toward dorsal and anterior regions (D'Amico and Cooper, 2001), thus no YSN could be observed in front of the EVL margin in wild-type embryos. However, scattered YSN were still present in the yolk cell of MZ*syne2b* embryos (**Figures 4E,F** and **Supplementary Figures 8A′,B′**), indicating abnormal dorsal convergence and anterior migration. Altogether, our results suggest that loss of maternal Syne2b function disrupts F-actin organization across the embryo, resulting in reduced epithelial integrity in the blastoderm and impaired YSN movements. All these defects contribute to delayed epiboly initiation and progression.

DISCUSSION

We have created *syne2b* gene mutation that should disrupt the nuclear localization KASH domain and nuclear-cytoskeletal connections. MZ*syne2b* embryos exhibited delayed epiboly initiation and progression, resulting in reduced elongation of the anteroposterior axis. Mechanistically, loss of maternal Syne2b function caused F-actin disorganization across the embryo.

Particularly, abnormal accumulation of F-actin at multiple cell contact regions led to aberrant cell shape changes and impaired epithelial integrity. Moreover, YSN also showed defective migration during epiboly. Thus, our results demonstrate an important role for Syne2b in cytoskeletal organization during morphogenetic movements.

We showed that maternal *syne2b* transcripts are highly expressed in the blastodisc of cleavage stage embryos. During gastrulation, the expression of *syne2b* in the blastoderm and in the dorsal and ventral regions is consistent with a function in epiboly (Kudoh et al., 2001). Indeed, all MZ*syne2b* mutants displayed epiboly defects. A small proportion of embryos, generally derived from young female parents, also showed blastoderm disintegration at late stages of gastrulation. There is a possibility that variations or changes in phenotype expressivity with maternal age may result from genetic compensation by paralogous genes (El-Brolosy and Stainier, 2017). Syne1 and Syne3 are also anchored to the nuclear membrane and display similar functions as Syne2 (Ketema et al., 2007; Postel et al., 2011). Thus, they may have redundant activity as Syne2b in epiboly. Consistently, expression of the dominant negative Syne1a KASH in MZ*syne2b* embryos enhanced epiboly delay. A decline in the severity of embryonic phenotypes with maternal age has been also observed in other situations, such as *ichabod* mutants with defective dorsoanterior development (Kelly et al., 2000).

Interference with Syne2b function severely affected F-actin localization across the embryo, including disrupted cortical F-actin in EVL cells, reduced marginal F-actin ring, and disorganized F-actin bundles in the yolk cell. Most significantly, F-actin in EVL cells of MZ*syne2b* mutants was progressively accumulated at multiple cell contact regions. These "actin-rich plaques" likely caused abnormal local constriction of surrounding EVL cells, resulting in the formation of rosette structures. Thus, the disrupted cell arrangements impaired epithelial integrity and caused disintegration of the blastoderm during epiboly. Deletion of the C-terminal KASH domain likely disrupts Syne2b function to link different subcellular compartments, but further analyses are needed to examine the subcellular localization of the truncated protein. Given the binding activity of nesprins to actin, it is conceivable that perturbation of Syne2b function and localization should disrupt the organization of actin cytoskeleton, and as a consequence, cause abnormal cell shape changes. This is consistent with the intracellular scaffolding functions of nesprins in maintaining cellular architecture (Rajgor et al., 2012). Our *in vivo* observations are supported by previous studies showing that knockdown of Nesprin-1 and Nesperin-2 in human umbilical vein endothelial cells affects F-actin distribution and cell shape (King et al., 2014).

Removal of the KASH domain in nesprins also affects nuclear positioning and migration in mice (Zhang et al., 2007). Although it is unclear whether nuclear behaviors in EVL cells were also affected in MZ*syne2b* embryos, defective movements of YSN were apparent during epiboly. Through interaction with cytoskeleton, YSN pull the EVL toward the vegetal pole to cover the yolk cell during gastrulation (Kimmel et al., 1995; Li et al., 2017). Syne2b/nesprin-2 has been shown to regulate nuclear migration during retina development in mice (Yu et al., 2011). Interestingly, YSN in front of the EVL margin were absent or abnormally clustered in MZ*syne2b* embryos, suggesting impaired migration. It is likely caused by a disrupted cytoskeleton-nuclear membrane anchor activity. Besides F-actin bundles, microtubule arrays formed in the YSL and in the yolk cell are critical for driving the vegetal migration of YSN (Solnica-Krezel and Driever, 1994). Thus, disruption of microtubule networks in the yolk cell of MZ*syne2b* mutants may also contribute to impaired YSN movements during epiboly. This observation is consistent with a previous report showing that overexpression of the dominant negative Syne2a KASH slows migration speeds of YSN (Fei et al., 2019). Thus, our results further illustrate an important role of the LINC complex in coordinating nuclear movements.

In summary, we demonstrate for the first time that zebrafish maternal Syne2b is required for epithelial integrity and nuclear migration through regulation of cytoskeleton during morphogenetic movements. This study provides insights into different cytoplasmic and nuclear roles of Syne2b during early development.

DATA AVAILABILITY STATEMENT

The original contributions presented in the study are included in the article/**Supplementary Material**, further inquiries can be directed to the corresponding authors.

ETHICS STATEMENT

The animal study was reviewed and approved by the Ethics Committee for Animal Research of Life Science of Shandong University.

AUTHOR CONTRIBUTIONS

Y-LL, X-NC, and TL performed the experiments, data collections and analyses. MS and D-LS designed and managed this study. D-LS wrote the manuscript. All authors approved the submitted version.

FUNDING

This work was supported by the National Natural Science Foundation of China (Grant Nos. 32070813, 31900577, and 31871451), the National Key R&D Project of China (Grant No. 2018YFA0801000), the Centre National de la Recherche Scientifique (CNRS), and the Sorbonne University.

SUPPLEMENTARY MATERIAL

The Supplementary Material for this article can be found online at: https://www.frontiersin.org/articles/10.3389/fcell.2021.671887/full#supplementary-material

REFERENCES

Bruce, A. E. E. (2016). Zebrafish epiboly: spreading thin over the yolk. *Dev. Dyn.* 245, 244–258. doi: 10.1002/dvdy.24353

Cartwright, S., and Karakesisoglou, I. (2014). Nesprins in health and disease. *Semin. Cell Dev. Biol.* 29, 169–179. doi: 10.1016/j.semcdb.2013.12.010

Cheng, X. N., Shao, M., Li, J. T., Wang, Y. F., Qi, J., Xu, Z. G., et al. (2017). Leucine repeat adaptor protein 1 interacts with Dishevelled to regulate gastrulation cell movements in zebrafish. *Nat. Commun.* 8:1353.

Crisp, M., Liu, Q., Roux, K., Rattner, J. B., Shanahan, C., Burke, B., et al. (2006). Coupling of the nucleus and cytoplasm: role of the LINC complex. *J. Cell Biol.* 172, 41–53. doi: 10.1083/jcb.200509124

D'Amico, L. A., and Cooper, M. S. (2001). Morphogenetic domains in the yolk syncytial layer of axiating zebrafish embryos. *Dev. Dyn.* 222, 611–624. doi: 10.1002/dvdy.1216

Davidson, P. M., and Cadot, B. (2020). Actin on and around the nucleus. *Trends Cell Biol.* 31, 211–223. doi: 10.1016/j.tcb.2020.11.009

El-Brolosy, M. A., and Stainier, D. Y. R. (2017). Genetic compensation: a phenomenon in search of mechanisms. *PLoS Genet.* 13:e1006780. doi: 10.1371/journal.pgen.1006780

Fei, Z., Bae, K., Parent, S. E., Wan, H., Goodwin, K., Theisen, U., et al. (2019). A cargo model of yolk syncytial nuclear migration during zebrafish epiboly. *Development* 146:dev169664.

Janin, A., and Gache, V. (2018). Nesprins and lamins in health and diseases of cardiac and skeletal muscles. *Front. Physiol.* 9:1277. doi: 10.3389/fphys.2018.01277

Kelly, C., Chin, A. J., Leatherman, J. L., Kozlowski, D. J., and Weinberg, E. S. (2000). Maternally controlled (beta)-catenin-mediated signaling is required for organizer formation in the zebrafish. *Development* 127, 3899–3911. doi: 10.1242/dev.127.18.3899

Ketema, M., Wilhelmsen, K., Kuikman, I., Janssen, H., Hodzic, D., and Sonnenberg, A. (2007). Requirements for the localization of nesprin-3 at the nuclear envelope and its interaction with plectin. *J. Cell Sci.* 120, 3384–3394. doi: 10.1242/jcs.014191

Kimmel, C. B., Ballard, W. W., Kimmel, S. R., Ullmann, B., and Schilling, T. F. (1995). Stages of embryonic development of the zebrafish. *Dev. Dyn.* 203, 253–310.

King, S. J., Nowak, K., Suryavanshi, N., Holt, I., Shanahan, C. M., and Ridley, A. J. (2014). Nesprin-1 and nesprin-2 regulate endothelial cell shape and migration. *Cytoskeleton* 71, 423–434. doi: 10.1002/cm.21182

Köppen, M., Fernandez, B. G., Carvalho, L., Jacinto, A., and Heisenberg, C. P. (2006). Coordinated cell-shape changes control epithelial movement in zebrafish and *Drosophila*. *Development* 133, 2671–2681. doi: 10.1242/dev.02439

Kudoh, T., Tsang, M., Hukriede, N. A., Chen, X., Dedekian, M., Clarke, C. J., et al. (2001). A gene expression screen in zebrafish embryogenesis. *Genome Res.* 11, 1979–1987. doi: 10.1101/gr.209601

Lee, S. J. (2014). Dynamic regulation of the microtubule and actin cytoskeleton in zebrafish epiboly. *Biochem. Biophys. Res. Commun.* 452, 1–7. doi: 10.1016/j.bbrc.2014.08.005

Li, Y. L., Shao, M., and Shi, D. L. (2017). Rac1 signalling coordinates epiboly movement by differential regulation of actin cytoskeleton in zebrafish. *Biochem. Biophys. Res. Commun.* 490, 1059–1065. doi: 10.1016/j.bbrc.2017.06.165

Noegel, A. A., and Neumann, S. (2011). The role of nesprins as multifunctional organizers in the nucleus and the cytoskeleton. *Biochem. Soc. Trans.* 39, 1725–1728. doi: 10.1042/bst20110668

Postel, R., Ketema, M., Kuikman, I., de Pereda, J. M., and Sonnenberg, A. (2011). Nesprin-3 augments peripheral nuclear localization of intermediate filaments in zebrafish. *J. Cell Sci.* 124, 755–764. doi: 10.1242/jcs.081174

Rajgor, D., Mellad, J. A., Autore, F., Zhang, Q., and Shanahan, C. M. (2012). Multiple novel nesprin-1 and nesprin-2 variants act as versatile tissue-specific intracellular scaffolds. *PLoS One* 7:e40098. doi: 10.1371/journal.pone.0040098

Rajgor, D., and Shanahan, C. M. (2013). Nesprins: from the nuclear envelope and beyond. *Expert. Rev. Mol. Med.* 15:e5.

Shao, M., Lu, T., Zhang, C., Zhang, Y. Z., Kong, S. H., and Shi, D. L. (2020). Rbm24 controls poly(A) tail length and translation efficiency of crystallin mRNAs in the lens via cytoplasmic polyadenylation. *Proc. Natl. Acad. Sci. U.S.A.* 117, 7245–7254. doi: 10.1073/pnas.1917922117

Solnica-Krezel, L. (2005). Conserved patterns of cell movements during vertebrate gastrulation. *Curr. Biol.* 15, R213–R228.

Solnica-Krezel, L., and Driever, W. (1994). Microtubule arrays of the zebrafish yolk cell: organization and function during epiboly. *Development* 120, 2443–2455. doi: 10.1242/dev.120.9.2443

Sun, Q., Liu, X., Gong, B., Wu, D., Meng, A., and Jia, S. (2017). Alkbh4 and atrn act maternally to regulate zebrafish epiboly. *Int. J. Biol. Sci.* 13, 1051–1066. doi: 10.7150/ijbs.19203

Thisse, C., and Thisse, B. (2008). High-resolution in situ hybridization to whole-mount zebrafish embryos. *Nat. Protoc.* 3, 59–69. doi: 10.1038/nprot.2007.514

Tsujikawa, M., Omori, Y., Biyanwila, J., and Malicki, J. (2007). Mechanism of positioning the cell nucleus in vertebrate photoreceptors. *Proc. Natl. Acad. Sci. U.S.A.* 104, 14819–14824. doi: 10.1073/pnas.0700178104

Warga, R. M., and Kimmel, C. B. (1990). Cell movements during epiboly and gastrulation in zebrafish. *Development* 108, 569–580. doi: 10.1242/dev.108.4.569

Yu, J., Lei, K., Zhou, M., Craft, C. M., Xu, G., Xu, T., et al. (2011). KASH protein Syne-2/Nesprin-2 and SUN proteins SUN1/2 mediate nuclear migration during mammalian retinal development. *Hum. Mol. Genet.* 20, 1061–1073. doi: 10.1093/hmg/ddq549

Zhang, Q., Skepper, J. N., Yang, F., Davies, J. D., Hegyi, L., Roberts, R. G., et al. (2001). Nesprins: a novel family of spectrin-repeat-containing proteins that localize to the nuclear membrane in multiple tissues. *J. Cell Sci.* 114, 4485–4498. doi: 10.1242/jcs.114.24.4485

Zhang, X., Xu, R., Zhu, B., Yang, X., Ding, X., Duan, S., et al. (2007). Syne-1 and Syne-2 play crucial roles in myonuclear anchorage and motor neuron innervation. *Development* 134, 901–908. doi: 10.1242/dev.02783

Zhou, C., Rao, L., Shanahan, C. M., and Zhang, Q. (2018a). Nesprin-1/2: roles in nuclear envelope organisation, myogenesis and muscle disease. *Biochem. Soc. Trans.* 46, 311–320. doi: 10.1042/bst20170149

Zhou, C., Rao, L., Warren, D. T., Shanahan, C. M., and Zhang, Q. (2018b). Mouse models of nesprin-related diseases. *Biochem. Soc. Trans.* 46, 669–681. doi: 10.1042/bst20180085

Conflict of Interest: The authors declare that the research was conducted in the absence of any commercial or financial relationships that could be construed as a potential conflict of interest.

frontiers in Cell and Developmental Biology

REVIEW
published: 24 June 2021
doi: 10.3389/fcell.2021.670882

F-Actin Dynamics in the Regulation of Endosomal Recycling and Immune Synapse Assembly

Nagaja Capitani and Cosima T. Baldari**

Department of Life Sciences, University of Siena, Siena, Italy

Membrane proteins endocytosed at the cell surface as vesicular cargoes are sorted at early endosomes for delivery to lysosomes for degradation or alternatively recycled to different cellular destinations. Cargo recycling is orchestrated by multimolecular complexes that include the retromer, retriever, and the WASH complex, which promote the polymerization of new actin filaments at early endosomes. These endosomal actin pools play a key role at different steps of the recycling process, from cargo segregation to specific endosomal subdomains to the generation and mobility of tubulo-vesicular transport carriers. Local F-actin pools also participate in the complex redistribution of endomembranes and organelles that leads to the acquisition of cell polarity. Here, we will present an overview of the contribution of endosomal F-actin to T-cell polarization during assembly of the immune synapse, a specialized membrane domain that T cells form at the contact with cognate antigen-presenting cells.

Keywords: vesicular trafficking, endosome, WASH complex, retromer, retriever, polarized recycling, actin dynamics

OPEN ACCESS

Edited by:
Francisco Sanchez-Madrid, Autonomous University of Madrid, Spain

Reviewed by:
Andres Alcover, Institut Pasteur, France
Esteban Veiga, Consejo Superior de Investigaciones Científicas (CSIC), Spain

****Correspondence:***
Nagaja Capitani
capitani2@unisi.it
Cosima T. Baldari
baldari@unisi.it

Specialty section:
This article was submitted to Cell Adhesion and Migration, a section of the journal Frontiers in Cell and Developmental Biology

Received: *22 February 2021*
Accepted: *24 May 2021*
Published: *24 June 2021*

Citation:
Capitani N and Baldari CT (2021) F-Actin Dynamics in the Regulation of Endosomal Recycling and Immune Synapse Assembly. Front. Cell Dev. Biol. 9:670882. doi: 10.3389/fcell.2021.670882

INTRODUCTION

Surface expression of plasma membrane (PM)-associated receptors is dynamically regulated through constitutive or ligand-dependent endocytosis. Receptor internalization, which occurs in a clathrin-dependent or clathrin-independent manner (Doherty and McMahon, 2009), results in their targeting to the endocytic pathway. This pathway is orchestrated by a series of intracellular membrane-bound compartments that allow for the sorting of these molecules, referred to as cargoes, for one of two alternative fates: delivery to lysosomes or vacuoles for degradation by the endosomal sorting complex required for transport (ESCRT) and the multivesicular bodies (MVBs) compartment (Vietri et al., 2020) or targeting to the trans-Golgi network (TGN) or to the PM for reuse (Johannes and Wunder, 2011; Hsu et al., 2012). In this second route, the cargo is first recognized by a retrieval complex and routed away from the degradative pathway, then is pinched off from the endosome as a vesicle and coupled to cytoskeletal motor proteins for delivery to the target compartment (Burd and Cullen, 2014; Wang et al., 2018).

Sorting of endosomal cargo for recycling relies on a number of multiprotein complexes spatially and temporally regulated. The two main complexes responsible for endosomal retrieval are the retromer complex (Burd and Cullen, 2014) and the more recently identified retriever complex acting together with the CCC complex (Phillips-Krawczak et al., 2015; McNally et al., 2017). The Wiskott–Aldrich syndrome protein and SCAR homologue (WASH) complex plays essential roles in both retromer- and retriever-dependent pathways by promoting branched actin polymerization on

endosomes (Gomez and Billadeau, 2009; Phillips-Krawczak et al., 2015; McNally et al., 2017). These complexes are not only important for the trafficking of molecules from the PM to the compartments of destination but also play a key role in polarized recycling of specific molecules to specialized areas of the cell as observed, for example, in T lymphocytes undergoing immune synapse (IS) formation. Indeed, upon T-cell receptor (TCR) engagement, endosomal trafficking is redirected toward the contact area of the T cell with the antigen-presenting cell (APC) by local F-actin pools that act in concert with microtubules and endosomal traffic regulators (Soares et al., 2013; Martín-Cófreces and Sánchez-Madrid, 2018; Onnis and Baldari, 2019). Here, we will review the role of the main molecular complexes involved in endosomal cargo recycling and the related actin dynamics, with a focus on polarized recycling to the T-cell IS.

SORTING OF RECYCLING CARGO AT EARLY ENDOSOMES BY THE RETROMER, RETRIEVER, AND CCC COMPLEXES

Endosomes are cellular hubs where internalized cargoes are sorted toward different trafficking pathways. Some cargoes are routed to the PM by recycling endosomes, a process known as endosome-to-plasma membrane recycling; others are transported to the TGN through an endosome-to-TGN retrieval or retrograde transport. Cargo recycling back to the cell surface can occur either via a fast recycling pathway controlled by the small GTPase Rab4 or via a slow recycling pathway in a Rab11-dependent manner (Galvez et al., 2012; Wandinger-Ness and Zerial, 2014; **Figure 1A**).

Endosomal sorting is accompanied by endosomal maturation. Early endosomes (EEs) are the main sorting station in the cell. EEs are characterized by specific markers such as Rab5 and early endosome antigen 1 (EEA1) and by the presence of large domains enriched in phosphatidylinositol(3,4,5)-triphosphate (PIP3) and sortin nexin (SNX) family members. A remarkable mosaicism in the EE membrane has emerged with the finding that cargoes, once they have reached the EEs, are targeted for degradation or recycling through the formation of specialized membrane subdomains that allow for cargo sorting and routing to the respective trafficking pathways through the local recruitment of specific molecular assemblies (Sönnichsen et al., 2000; Puthenveedu et al., 2010). The molecular machinery essential for cargo sorting in the recycling pathway is represented by three main complexes: retromer, retriever, and the CCC complex.

Retromer

The retromer complex was first identified in *Saccharomyces cerevisiae* as a heteropentameric assembly consisting of a SNX heterodimer composed of vacuolar protein sorting (VPS), VPS5 and VPS17, and a heterotrimer composed of VPS26, VPS29, and VPS35, also known as "core" (Gallon and Cullen, 2015; Simonetti and Cullen, 2019; **Figure 1C**). SNXs are a large family of proteins containing a PX (phox homology) domain, which is responsible for binding to specific phosphoinositides (PIs) (Carlton and Cullen, 2005; Teasdale and Collins, 2012). In addition to the PX domain, SNXs may contain other domains and, on this basis, can be classified into five subfamilies: the SNX-PX subfamily, whose members are only endowed with a PX domain (e.g., SNX3) (Strochlic et al., 2007); the SNX-BAR subfamily, whose members comprise a BAR (Bin/Amphiphysin/Rvs) domain (e.g., the yeast VPS5-VPS17 and mammalian SNX1/2-SNX5/6) (Rojas et al., 2007; Wassmer et al., 2007); the SNX-FERM subfamily, whose members comprise PDZ (PSD95/Dlg/ZO) and FERM (protein 4.1/ezrin/radixin/moesin) domains (e.g., SNX27) (Temkin et al., 2011; Steinberg et al., 2013); the SNX–PXA–RGS–PXC (PX-associated domain A/regulator of G-protein signaling/PX-associated domain C) subfamily with a central PX domain flanked by several conserved domains (e.g., SNX13, SNX14, SNX19, and SNX25); and the SNX–MIT subfamily characterized by a microtubule interacting and transport domain (e.g., SNX15) (Teasdale and Collins, 2012). The core complex of retromer is conserved across all eukaryotes (Seaman, 2007), while the exact composition of the SNX dimer in mammals is less defined, with SNX1/SNX2 and SNX5/SNX6 as the mammalian orthologues of VPS5 and VPS17, respectively (Griffin et al., 2005; Wassmer et al., 2007). In mammals, the SNX dimer is responsible for the recruitment of the retromer to endosomes (Griffin et al., 2005), while the core complex is thought to participate in cargo binding and is therefore referred to as the "cargo recognition complex" (CRC) (Strochlic et al., 2007; Harterink et al., 2011; Temkin et al., 2011; Zhang et al., 2011; Steinberg et al., 2013).

Recent studies have revealed that SNXs play a central role in cargo recognition (Lucas et al., 2016). While some cargoes have been reported to directly bind to the CRC, recognition of other cargoes that recycle to the TGN or to the PM is mediated by SNX3 or SNX27 cargo adaptors, respectively (Strochlic et al., 2007; Harterink et al., 2011; Zhang et al., 2011). The retromer can directly interact with SNX3, resulting in the generation of a binding site for a canonical ØX(L/M) motif (where Ø is an aromatic amino acid) present in a variety of receptors, including the cation-independent mannose 6-phosphate receptor (CI-MPR) (Rojas et al., 2007; Seaman, 2007), the glycoprotein sortilin (Seaman, 2007; Canuel et al., 2008), the divalent metal transporter DMT1–II (Tabuchi et al., 2010), the G-protein-coupled receptor Wntless (Harterink et al., 2011; Zhang et al., 2011), and others. On the other hand, SNX27 recognizes, through its FERM and PDZ domains, the cytosolic domain of integral membrane proteins containing NPXY motifs or a carboxy-terminal class I PDZ-binding motif. Examples of this type of cargo include the β2 adrenergic receptor (β2AR), the glucose transporter GLUT1, the copper transporter ATP7A, and the glutamate receptors (Lauffer et al., 2010; Ghai et al., 2013; Steinberg et al., 2013; Gallon et al., 2014; McGough et al., 2014; Clairfeuille et al., 2016; Shinde and Maddika, 2017). Following retromer recruitment to endosomal membranes and cargo recognition via either SNX27 or SNX3, SNX-BAR proteins induce membrane deformation, generating endosomal tubules for cargo recycling to either the PM or the Golgi apparatus (Carlton and Cullen, 2005; Burd and Cullen, 2014; **Figure 1B**).

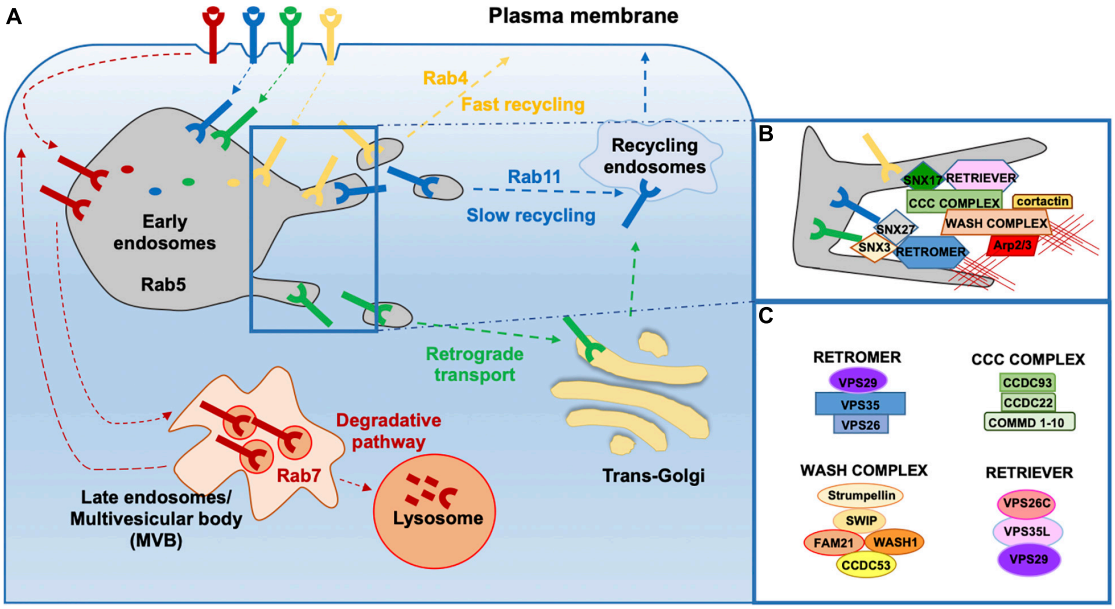

FIGURE 1 | Overview of endosomal sorting and associated molecular machineries. **(A)** Following internalization, transmembrane proteins can be delivered to the degradative pathway through late endosomes and finally lysosomes or can be destined for recycling. Delivery of cargo back to the cell surface can occur directly through the fast recycling pathway or indirectly through the slow recycling pathway involving the pericentrosomal recycling compartment. Some cargo proteins can undergo retrograde transport from endosome to the Trans Golgi Network (TGN). **(B,C)** Multiprotein complexes involved in the retrieval and recycling of cargo proteins on **(B)** endosomes and the **(C)** components of each complex.

Retriever

Not all cargoes transiting through the endosomal system require retromer for their trafficking (Steinberg et al., 2012; Kvainickas et al., 2017; Simonetti et al., 2017). Recently, McNally et al. (2017) identified and characterized a new protein complex, named retriever, required for sorting of a subgroup of transmembrane proteins. Retriever is a heterotrimer consisting of VPS26C (DSCR3), VPS35L (C16orf62), and VPS29, the latter shared with the retromer complex (**Figure 1C**). To fulfill its function in cargo recycling, the retriever, similar to retromer, needs to couple to an SNX protein, namely, SNX17 (**Figure 1B**). SNX17 interacts through its C-terminal tail with the VPS26C subunit of retriever, which is important for endosomal localization, while its FERM domain binds NPxY/NxxY motif-containing cargo proteins, such as the heterodimeric β1 integrins, the low-density lipoprotein receptor-related protein 1 (LRP1), the low-density lipoprotein receptor (LDLR), the epidermal growth factor receptor (EGFR), and others (Stockinger et al., 2002; Burden et al., 2004; Böttcher et al., 2012; Steinberg et al., 2012; Farfán et al., 2013; McNally et al., 2017). Interestingly, the interaction of retriever with SNX17 is not required for its association with endosomes. Similar to retromer, the retriever is not predicted to bind membranes; its endosomal recruitment depends on interactions with another complex, the CCC complex (McNally et al., 2017).

The CCC Complex

The CCC complex consists of coiled-coil domain-containing proteins 22 (CCDC22) and 93 (CCDC93) and 10 members of the copper metabolism MURR1 domain-containing (COMMD) protein family (Maine and Burstein, 2007; **Figure 1C**). The CCC complex colocalizes with the retromer, retriever, and the WASH complex on endosomes (Phillips-Krawczak et al., 2015). CCC deficiency in human and mouse cells causes defective recycling of both SNX17/retriever-dependent (Bartuzi et al., 2016; McNally et al., 2017; Fedoseienko et al., 2018) and SNX27/retromer-dependent cargoes (Vonk et al., 2011; Phillips-Krawczak et al., 2015), indicating that CCC is required for both retromer- and retriever-dependent protein trafficking. Similar to retromer (Harbour et al., 2012), the CCC complex itself does not associate with endosomes but relies on its interaction with a component of the WASH complex, FAM21, for its correct localization (Phillips-Krawczak et al., 2015).

THE WASH COMPLEX AND CORTACTIN COORDINATE F-ACTIN NUCLEATION AT ENDOSOMES

The WASH complex is a pentameric complex composed of WASH1 (WASHC1), Strumpellin (WASHC5), the Strumpellin and WASH-interacting protein SWIP (also known as KIAA1033 or WASHC4), FAM21A/C (family with sequence similarity 21A and C, also known as WASHC2A/C), and coiled-coil domain containing protein 53 (CCDC53 or WASHC3) (Derivery et al., 2009; Gomez and Billadeau, 2009; Jia et al., 2010; Alekhina et al., 2017; **Figure 1C**). Among these, FAM21 is an important structural component of the WASH complex for its key role in interacting with other protein complexes through its long,

unstructured C-terminal tail containing multiple functional binding sites consisting of 21 copies of the LFa motif, rich in leucine, phenylalanine, and several acidic residues (Derivery and Gautreau, 2010). FAM21 associates with multiple VPS35 retromer subunits (Harbour et al., 2012; Jia et al., 2012; Helfer et al., 2013), as well as with the CCDC93 subunit of the CCC complex (Phillips-Krawczak et al., 2015), thereby coupling both retromer and retriever to endosomes. FAM21 also contains two regions within its tail that are able to bind with intermediate affinity to PI3P and with strong affinity to PI(3,5)P2 (Singla et al., 2019). Moreover, FAM21 can associate with the CAPZα/β heterodimer, known as capping protein (CP). CP binds to the barbed end of the actin protofilament, thereby controlling filament growth by inhibiting monomer addition or loss from that end. FAM21 interacts directly with CAPZ and impairs its actin-capping activity (Hernandez-Valladares et al., 2010).

WASH1 is another important component of the WASH complex that serves as nucleation-promoting factor (NPF) by activating Arp2/3-dependent actin polymerization on endosomal membranes (Derivery et al., 2009; Gomez and Billadeau, 2009; Jia et al., 2010). Arp2/3 is a heptameric protein complex, so called because of its two main components, actin-related proteins (Arp) 2 and 3. It is the first actin nucleator identified in eukaryotic cells and is highly conserved among species (Pizarro-Cerdá et al., 2017). The ability of WASH to activate the Arp2/3 complex is finely tuned by ubiquitination (Hao et al., 2013). The E3 ubiquitin ligase TRIM27 and its enhancer MAGE-L2 are recruited by the retromer subunit VPS35 to WASH1, resulting in its K63-linked polyubiquitination, which leads to a conformational change that enhances actin nucleation (Hao et al., 2013). WASH ubiquitination is further regulated by the USP7 enzyme, which has a dual activity: to promote WASH ubiquitination by preventing TRIM27 auto-ubiquitination and degradation and, concomitantly, to limit WASH ubiquitination through its direct deubiquitination (Hao et al., 2015).

Another activator of the Arp2/3 complex that has been described to associate with endosomes is cortactin (Kaksonen et al., 2000; Lladó et al., 2008). Cortactin controls a wide range of processes including the maturation of late endosomes and lysosomes, the retrograde transport to the Golgi apparatus, and actin dynamics at endosomes. Cortactin is a class II NPF that promotes actin assembly both by inducing Arp2/3-dependent actin polymerization and by binding and stabilizing pre-existing branched F-actin nucleated by the WASH complex. Cortactin is in turn regulated by PI(3,5)P2, which directly interacts with its actin-binding domain, preventing F-actin binding and leading to the inhibition of cortactin-mediated branched F-actin nucleation and stabilization (Hong et al., 2015). Interestingly, the ability of PIs to regulate F-actin dynamics is not limited to PI(3,5)P2. For instance, PI(4,5)P2, the best characterized actin regulator, interacts with and modulates N-WASP and actin-binding proteins such as cofilin, CAPZ, filamin, vinculin, talin, and others (Yin and Janmey, 2003). On the other hand, PI(3,4,5)P3 regulates the activation of the WASP family member WAVE2 to control lamellipodial protrusion (Suetsugu et al., 2006), highlighting a pleiotropic role of PIs in actin cytoskeleton regulation (Saarikangas et al., 2010).

CYTOSKELETAL REGULATION OF ENDOSOMAL TRAFFICKING

Endosome sorting and maturation is accompanied by continuous membrane remodeling that requires the participation of both the actin and microtubule cytoskeletons. F-Actin is implicated in this process starting from the earliest steps, participating in defining endosomal subdomains to establish cargo destination. F-Actin associates with recycling microdomains and prevents the loss of recycling cargo to the degradative machinery (Simonetti and Cullen, 2019). In addition, F-actin polymerization at endosomes is essential for cargo sorting to recycling endosomes. Until recently, cargo recycling was believed to occur through sequence-independent "bulk" flow, as in the case of the transferrin receptor (Maxfield and McGraw, 2004). However, a large variety of cargoes have been demonstrated to recycle through a sequence-dependent pathway tightly regulated by actin dynamics (Puthenveedu et al., 2010; Temkin et al., 2011; Burd and Cullen, 2014). Cargoes to be recycled through this pathway are first recognized by a retrieval complex (retromer or retriever) and then packaged into tubulo-vesicular transport carriers enriched in F-actin and actin-related proteins (Puthenveedu et al., 2010). At this stage, microtubules join the game, with the microtubule-associated motor dynein and its partner dynactin, allowing for the extension of the nascent carriers. The WASH complex participates also in this step, exploiting its ability to interact with tubulin to stabilize the carriers on microtubule tracks. Subsequently, WASH-dependent F-actin nucleation at the apical portion of the tubular carriers provides the pushing force necessary for membrane fission. Following their detachment, F-actin regulates the short-distance mobility of tubular carriers mainly through actin motors such as myosin (Derivery et al., 2009; Harbour et al., 2010; **Figure 2**). This is exemplified by the β2AR receptor, which is recycled via tubular profiles enriched in F-actin and actin-related machineries (Bowman et al., 2016). A key role in this process is played by cortactin, which participates in the signaling cascade that regulates recycling (Vistein and Puthenveedu, 2014), the actin binding protein filamin A (FLNa) responsible for cargo entry into the tubular recycling domains (Pons et al., 2017), and other actin regulators including formins (Gong et al., 2018).

Following sorting at EEs, other recycling cargoes, such as the CI-MPR or sortilin, undergo retrograde trafficking to the TGN (Tu et al., 2020). In this process, cargoes are recognized by the SNX3–retromer complex, SNX-BARs, or clathrin and the adapter protein AP1, confined to specific endosomal subdomains and, following endosomal fission, transported by tubulo-vesicular transport carriers toward the TGN along microtubule tracks (Lu and Hong, 2014; Cheung and Pfeffer, 2016; Saimani and Kim, 2017). Once they arrive close to the TGN compartment, cargoes are captured by TGN-localized golgin proteins, such as golgin-97, golgin-245, GCC88, and GCC185 (Lowe, 2019). This process

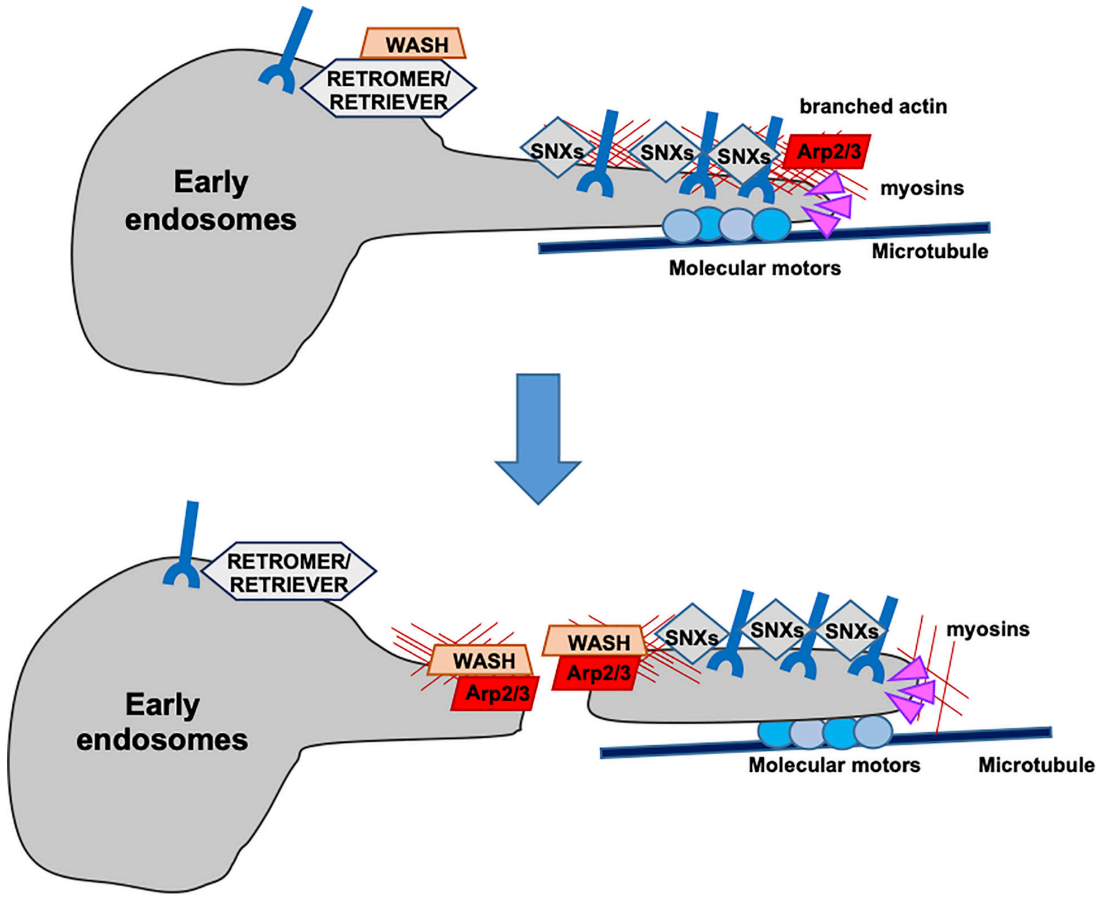

FIGURE 2 | Recycling of receptors through actin-rich tubular domains. Sequence-dependent recycling of cargoes is tightly regulated by actin dynamics at the surface of endosomes. The retrieving machineries (retromer or retriever), together with the WASH complex, allow for the entry of the receptors into tubular profiles enriched in F-actin and actin-related proteins. Microtubule motors drive the stabilization and extension of the tubular profiles and branched F-actin contributes to vesicle fission.

also involves TBC1D23, a protein that acts as a bridging protein by binding simultaneously to golgins and to the WASH complex subunit FAM21 on endosomal vesicles (Shin et al., 2017). Finally, carrier fusion with the Golgi membrane is mediated by four different vSNARE–tSNARE complexes (Lu and Hong, 2014).

INTERPLAY BETWEEN Rab GTPases AND MOLECULAR COMPLEXES IMPLICATED IN ACTIN-MEDIATED MEMBRANE TRAFFICKING

Membrane trafficking is orchestrated by a variety of Rab GTPases that control different steps of the process, from cargo sorting to vesicle budding, motility, and fusion, through the recruitment of effector molecules, including the actin regulators mentioned in the previous paragraphs (Stenmark, 2009). Rab proteins are important regulators of retromer-mediated vesicular transport, not only in mammals but also in other organisms. For example, the core complex of retromer was found to interact with the GTP-bound form of Rab7 (Rab7-GTP) in yeast, plants, and mammalian cells (Rojas et al., 2008; Liu et al., 2012; Zelazny et al., 2013), leading to retromer recruitment to late endosomes (Priya et al., 2015). Rab32 regulates the retrograde trafficking of the CI-MPR to the TGN by directly interacting with SNX6 (Waschbüsch et al., 2019), while Rab21 is implicated in cargo sorting by establishing a complex with WASH and retromer to regulate endosomal F-actin (Del Olmo et al., 2019). Additionally, Rab9, together with retromer, WASH, and F-actin, has been recently reported to form an endosomal retrieval machinery that regulates selective recycling of the luminal protein Serpentine in the *Drosophila* trachea (Dong et al., 2013). Although little is known about the interplay between Rab GTPases and the retriever and CCC and WASH complexes, a recent proteomic study focused on SNARE and Rab proteins identified functional clusters, such as a correlation between Rab10 and the SNARE Syntaxin4 (STX4) or between Rab7/Rab21 and the WASH and CCC complexes (Clague and Urbé, 2020).

Rab GTPases also participate in tethering of the vesicles carrying recycling cargo to the target membrane through the recruitment of tethering factors (Stenmark, 2009). Rab32 and

Rab38 were found to be implicated in the trafficking of the glucose transporter GLUT1 to the PM by regulating the effector molecule VARP, which in turn binds to the R-SNARE VAMP7 to facilitate membrane fusion between recycling endosomes carrying GLUT1 and the PM (Hesketh et al., 2014). SNX1 has been reported to interact with Rab6IP, a Rab6-interacting protein localized at the Golgi compartment and involved in the tethering of endosome-derived transport carriers to the TGN (Miserey-Lenkei et al., 2007). A similar function was observed for the *Drosophila* orthologue of TBC1D23, tbc1, a Rab GTPase-activating protein that couples endosome-derived vesicles to their target membrane at the TGN (Johnson and Andrew, 2019).

Although the specific identities and roles of Rab GTPases during receptor recycling are only beginning to be investigated, these findings underscore a tight functional interplay of these membrane trafficking regulators with the sorting, transport, and tethering machineries at all critical steps in receptor recycling. While the link between these Rabs and the cargo sorting complexes supports their implication in the local regulation of F-actin dynamics, the underlying mechanisms remain to be directly addressed.

ACTIN DYNAMICS IN POLARIZED ENDOSOMAL TRAFFICKING: FOCUS ON THE IMMUNE SYNAPSE

The molecular complexes described above and the associated actin dynamics participate in cell polarization by regulating the recycling-dependent accumulation of receptors, adhesion molecules, and signaling mediators at specialized areas of the PM. This is exemplified by the formation of apical membrane specializations including primary cilia and apical microvilli of ciliated cells (Goldenring, 2015), the polarization of epithelial or neuronal cells (Vergés, 2016), or immune synapse (IS) formation in T lymphocytes and other immune cells.

The IS can be described as a highly polarized structure that forms at the T-cell interface with an APC carrying cognate MHC-bound antigen and allows the communication between the two cells to ensure efficient TCR signal transduction and T-cell activation (Dustin and Choudhuri, 2016). The typical "bull's eye" structure of the mature IS features three concentric regions, referred to as supramolecular activation clusters (SMACs) that can be distinguished based on the specific partitioning of TCRs, costimulatory molecules, and integrins: the TCR-enriched central SMAC (cSMAC), the integrin-enriched peripheral SMAC (pSMAC), and the distal SMAC (dSMAC), where molecules with large ectodomains and negative regulators of TCR signaling are confined. IS assembly is coordinated by both the actin and the microtubule cytoskeletons, which drive the accumulation and partitioning of the synaptic components throughout the extended timeframe required for T-cell activation (Ritter et al., 2013; Martín-Cófreces and Sánchez-Madrid, 2018; Hammer et al., 2019).

The actin cytoskeleton plays a key role beginning from the first step of IS formation, which involves the assembly of TCR microclusters that move centripetally from the periphery to the center of the IS using F-actin as driving force (Ritter et al., 2013). In addition, actin promotes the activation of integrins to stabilize the T cell–APC contact and forms a ring-like seal at the inner side of the dSMAC (Hammer et al., 2019). However, the role of F-actin in IS assembly and function extends beyond the rearrangement and signaling events that occur at the PM. Early upon TCR activation, the centrosome translocates toward the IS in a process that is in part regulated by centrosomal F-actin dynamics (Ritter et al., 2013). Centrosome polarization is coordinated with F-actin clearance to generate a central F-actin-free area that facilitates the polarized release of effector molecules, such as cytokines produced by helper or cytotoxic T cells or the cytotoxic contents of the lytic granules of CTLs (Hivroz et al., 2012; Ritter et al., 2015; de la Roche et al., 2016; Kabanova et al., 2018; Herranz et al., 2019; Sanchez et al., 2019). Synaptic F-actin dynamics is also essential for the polarized release of vesicles carrying bioactive molecules, including synaptic ectosomes, which are assembled and released directly from the PM (Saliba et al., 2019), and exosomes, which are released upon the fusion of MVBs with the PM (Mittelbrunn et al., 2015; Bello-Gamboa et al., 2020).

Following polarization, the centrosome rapidly generates a network of microtubules both irradiating from the centrosome toward the periphery of the IS and converging from the periphery toward the center of IS to guide the polarized transport of vesicular components and organelles (Martín-Cófreces and Sánchez-Madrid, 2018). The identity of the vesicle-associated molecules that undergo polarized exocytosis to the IS depends on the type of T lymphocyte and APC, with helper T cells ($CD4^+$ cells) secreting cytokines at the IS formed with cognate MHC-II-bearing cell targets to promote their maturation and function and cytotoxic T lymphocytes ($CD8^+$ cells) releasing the toxic contents of their lytic granules at the IS formed with MHC-I-bearing cell targets for specific killing (Hivroz et al., 2012; de la Roche et al., 2016). Directional vesicular trafficking is, however, also the main mechanism by which T lymphocytes ensure the continuous availability of a functional pool of TCRs at the IS to sustain signaling during cell activation (Soares et al., 2013; Onnis et al., 2016; Finetti et al., 2017). This is achieved through the delivery to the synaptic membrane of TCRs associated with a pool of endosomes that undergo polarized recycling in a process regulated by both the tubulin and actin cytoskeletons (Martín-Cófreces and Sánchez-Madrid, 2018; Mastrogiovanni et al., 2020).

TCR Endocytosis in Polarized Recycling to the IS

Receptor internalization is dependent on local actin polymerization to provide force for local membrane deformation and carrier budding (Hinze and Boucrot, 2018). The pathways that regulate both constitutive and ligand-dependent TCR internalization have been extensively investigated but are still debated (see Alcover et al., 2018 for an exhaustive coverage of TCR endocytosis). Two distinct endocytic routes of TCR endocytosis have been identified based on the requirement for the coat protein clathrin (Onnis and Baldari, 2019). In the clathrin-dependent endocytosis pathway, internalized TCRs are incorporated into a network of endosomal compartments defined

by clathrin and the AP2 complex (Dietrich et al., 1994; von Essen et al., 2002; Crotzer et al., 2004). In the clathrin-independent endocytosis pathway, which appears as the main player in TCR recycling, internalized TCRs are incorporated into a dynamic endocytic network demarcated by the membrane-organizing proteins flotillins. Although flotillins are not required for TCR internalization, they are essential for the recycling of internalized TCRs to the IS and for full T-cell activation (Compeer et al., 2018). A third pathway involves the arrestin-dependent internalization of non-engaged, bystander TCRs for polarized recycling to the IS (Fernández-Arenas et al., 2014). Routing of TCR–CD3 complexes toward these alternative pathways of endocytosis and their subsequent targeting to recycling or late endosomes for subsequent degradation is dictated, at least in part, by the type of posttranslational modifications of the cytosolic domains of the CD3 complex components (Alcover et al., 2018).

Cargo Sorting and Retrieval in Polarized Recycling to the IS

Consistent with the role of F-actin in the process of endosome recycling described in the previous sections, proteins controlling actin polymerization and branching, such as the Arp2/3 component ARPC2 (Zhang et al., 2017) and WASH (Piotrowski et al., 2013), together with the retrieval complexes responsible for cargo recycling, regulate endosomal TCR trafficking and its polarization to IS. The interaction of retromer with WASH at EEs promotes F-actin nucleation, allowing for the generation of TCR carriers that undergo retrograde transport to the IS along microtubule tracks, to which they become coupled exploiting the tubulin-binding ability of WASH (Derivery et al., 2009; Gomez and Billadeau, 2009). We recently identified the ciliary protein coiled-coil domain containing 28B (CCDC28B) (Cardenas-Rodriguez et al., 2013), as a new component of the TCR retrieval machinery essential for polarized TCR recycling. We found that CCDC28B regulates actin polymerization at EEs carrying recycling TCRs by recruiting the FAM21–WASH complex to EE-associated retromer (Capitani et al., 2020; **Figure 3**). Consistent with the key role of WASH in regulating the recycling-dependent events occurring during IS formation, WASH deficiency in T lymphocytes results in a decrease in the surface levels not only of the TCR but also of the integrin LFA-1, the costimulatory receptor CD28, and the glucose transporter GLUT1 due to defective recycling (Piotrowski et al., 2013). Similarly, we observed defective TCR accumulation and signaling at the IS of CCDC28B-deficient cells downstream of early signaling and centrosome polarization caused by impaired TCR recycling (Capitani et al., 2020). Additionally, the Arp2/3 subunit ARPC1B was found to participate in IS formation in cytotoxic T lymphocytes by inducing receptor recycling to the PM via the retromer and WASH complexes. These include the TCR and the coreceptor CD8, as well as GLUT1 (Randzavola et al., 2019).

Recently, the retromer-associated SNX family member, SNX27, was found to be associated in resting T cells to early and recycling endosomes, largely through the interaction of its PX domain with PI3P. Upon T-cell engagement by APC, SNX27-enriched endosomes rapidly polarize toward the IS, accumulating at the cSMAC and pSMAC. The polarization of SNX27$^+$ endosomes toward the IS is also regulated by PI binding, with the PX domain binding to PI3P-enriched membrane domains and the FERM domain to PI(4,5)P2- and/or PI(3,4,5)P3-enriched membrane domains (Rincón et al., 2011; Ghai et al., 2015). In support of the importance of PIs in SNX27 function, impaired PIP recognition by the SNX27 FERM domain affected its localization at the endosomal recycling compartment and impaired its correct distribution during initial steps of IS formation (Tello-Lafoz et al., 2014). In addition, proteomic analysis of the SNX27 interactome in activated T cells confirmed that SNX27-mediated trafficking involves the retromer and WASH complexes and also revealed additional cargoes that associate with SNX27 in polarized recycling to IS (Tello-Lafoz et al., 2017). Among these are the lipid second messenger diacylglycerol (DAG) (Rincón et al., 2007); the protein zonula occludens-2 (ZO-2), a tight junction scaffold protein recently identified in T lymphocytes; the centromere protein J (CENPJ), which acts as a microtubule plus-end tracking protein; and the Rho guanine nucleotide exchange factor 7 (ARHGEF7) (González-Mancha and Mérida, 2020). These results indicate that other receptors or membrane-associated signaling components that participate in IS assembly may exploit the retromer-regulated pathway for EEs sorting and redirection to the synaptic membrane.

While a role for retromer in IS formation is well established, less is known about the contribution of retriever and the CCC complex to this process, although the identification of retriever-associated SNX17 bound to TCR complexes at the IS suggests that multiple retrieval complexes coexist during polarized recycling of endosomal synaptic components. Interestingly, SNX17 silencing affects TCR and LFA-1 expression at the T-cell surface, suggesting that SNX17 is required to maintain functional surface pools of activating receptors and integrins to allow for IS formation and T-cell activation (Osborne et al., 2015).

Multiple Recycling Pathways Regulate IS Assembly

In addition to the TCR, two membrane-bound molecules essential for TCR signaling also undergo polarized recycling to the IS: the initiating lymphocyte-specific protein tyrosine kinase Lck (Ehrlich et al., 2002) and the transmembrane adaptor linker for activation of T cells (LAT) (Bonello et al., 2004). Similar to the TCR, these molecules form two different pools within the cell, one associated with the plasma membrane and the other with the endosomal and Golgi compartments, which are sequentially delivered to the IS to sustain signaling (**Figure 3**). The polarized trafficking of these molecules occurs through distinct routes within the "classical" recycling pathway regulated by the Rab5 and Rab11. Polarized TCR recycling to the IS involves additional Rab GTPases, which include Rab8, Rab29, and Rab35 (Finetti et al., 2015; Onnis et al., 2015; Patino-Lopez et al., 2018) and the intraflagellar transport (IFT) system components IFT20, IFT54, IFT57, and IFT88 (Finetti et al., 2009, 2014). Similar to the TCR, Lck associates with Rab11$^+$ endosomal compartments, and its transport to the IS and sorting to the cSMAC is regulated by

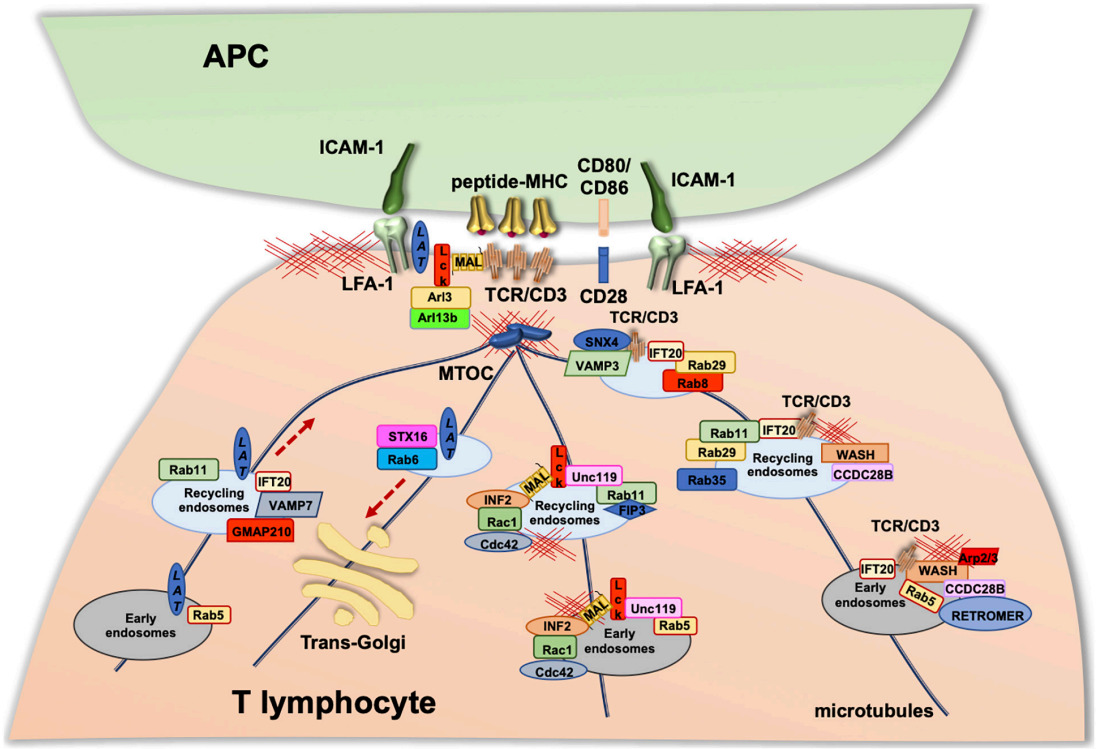

FIGURE 3 | Vesicular trafficking in the regulation of IS formation. Upon TCR stimulation, the T-cell receptor, as well as associated signaling molecules (e.g., LAT and Lck), are delivered to the IS via endosomal vesicles. The polarized trafficking of different molecules occurs through distinct trafficking routes within the "classical" recycling pathway regulated by the Rab5 and Rab11. TCR-polarized trafficking to the IS involves additional Rab GTPases, some components of the intraflagellar transport (IFT) system, and the ciliogenesis protein CCDC28B that is essential for WAS-dependent actin polymerization on TCR^+ endosomes. Lck associates with $Rab11^+$ endosomal compartments, and its transport to the IS and sorting to the cSMAC are regulated by the uncoordinated 119 protein (Unc119), the membrane protein MAL, and Rab11-FIP3. LAT trafficking to the IS occurs through the classical Rab5 and Rab11 route, where anterograde transport is specifically regulated by GMAP210, IFT20, and VAMP7 and retrograde transport by Rab6 and Syntaxin-16.

a variety of molecules. Among these are the uncoordinated 119 protein (Unc119), which extracts PM-bound Lck by sequestering its hydrophobic myristoyl group and releases the kinase at the synaptic membrane under the control of the ARL3/ARL13B complex (Stephen et al., 2018); the membrane protein MAL that, together with the formin INF2, generates specific carriers for Lck targeting to the IS in a Cdc42-Rac1-dependent manner (Andrés-Delgado et al., 2010; Antón et al., 2011); and the Rab11 effector FIP3 (Rab11 family interacting protein-3), which plays a key role in the regulation of the subcellular localization and function of Lck (Bouchet et al., 2017). LAT trafficking to the IS occurs through the classical Rab5 and Rab11 route, where anterograde transport is specifically regulated by the golgin GMAP210, the intraflagellar transport protein IFT20 and the SNARE VAMP7 and retrograde transport by Rab6 and SNARE Syntaxin-16 (Larghi et al., 2013; Vivar et al., 2016; Carpier et al., 2018; Zucchetti et al., 2019; Saez et al., 2021).

Although the role of endosomal actin in IS assembly and T-cell activation has been well established, the underlying mechanisms remain to be fully understood. As detailed in *Cargo sorting and retrieval in polarized recycling to the IS*, actin polymerization at TCRs undergoing sorting at early endosomes is mediated by both the retromer and retrieval complexes through the WASH-dependent recruitment of Arp2/3. CCDC28B plays a key role in this process by coupling the FAM21 component of the WASH complex to the retromer at endosomes carrying recycling TCRs (Capitani et al., 2020). Interestingly, $Rab11^+$ endosomes indirectly regulate actin dynamics at the synaptic membrane by allowing for the polarized transport of the Rac GTPase Rac1, which associates with Rab11 through its effector FIP3 (Bouchet et al., 2016, 2018). MVBs that are delivered to the synaptic membrane also contribute to local actin polymerization through the clathrin-dependent recruitment of proteins that are implicated in this process, such as dynamin-2, Arp2/3, and CD2AP (Calabia-Linares et al., 2011). In this emerging scenario, endosomal and plasma membrane actin dynamics establish a tight interplay to sustain IS architecture and signaling during T-cell activation.

CONCLUSION

The striking architecture of the IS was described over 20 years ago. Not surprisingly, rearrangements of TCRs, adhesion molecules, costimulatory receptors, and membrane-associated signaling mediators occurring at the region of the T-cell plasma

membrane at the contact with cognate APC have been extensively investigated. Only more recently has vesicular trafficking entered the picture with the finding that intracellular pools of the TCR and other components of the IS play a key role in this process beyond the known function of polarized delivery of effectors in differentiated T cells. From the initial finding that intracellular TCRs are delivered to the synaptic membrane through polarized recycling, it has become clear that the TCR is by no means unique in this respect. A wide array of other membrane-associated molecules, including receptors such as CD28 and signaling mediators such as Lck and LAT, have been demonstrated to undergo polarized recycling (Onnis and Baldari, 2019). Strikingly, with the identification of new regulators of the traffic of these molecules, achieved with essential input from the fields of vesicular trafficking and ciliogenesis (Cassioli and Baldari, 2019), it is now clear that a diversity of recycling pathways characterized by unique combinations of Rab GTPases and respective GEFs, v- and t-SNAREs, and tethering proteins coexist within the classical recycling pathways defined by Rab11 (Onnis et al., 2016).

While a role for microtubules and microtubule motors for the movement of these endosomes was expected, the identification of endosomal F-actin as a key player in the sorting of recycling molecules and their coupling to microtubules has brought a new layer of complexity to the process of polarized recycling to the IS. The identification of the retromer, retriever, and the CCC complex as a different means to achieve the polymerization of new actin filaments at endosome subdomains enriched in specific receptors that are destined for recycling has highlighted a diversity also at this step of the pathway (Wang et al., 2018; Simonetti and Cullen, 2019). Further work will be required to unravel the mechanisms and molecular machineries responsible for the specificity in the selection of both the receptors to be sorted for recycling and the respective actin-nucleating complex on which their transit from early to recycling endosomes depends. Additionally, how membrane subdomains are generated at early endosomes to serve as hubs for the accumulation of individual receptors and associated regulators remains elusive, as do the fine details of local force generation for the abscission of vesicles that will mature to recycling endosomes. We expect that a multidisciplinary approach to these questions capitalizing on converging new knowledge and new technologies gleaned from immunology, cell biology, and biophysics will be crucial to unravel the increasing complexity of the process of IS assembly.

AUTHOR CONTRIBUTIONS

NC and CB wrote the manuscript. NC prepared the artwork. Both the authors contributed to the article and approved the submitted version.

FUNDING

Part of the work described in this review was carried out with the support of Associazione Italiana per la Ricerca sul Cancro (Grant IG 20148), Fondazione Telethon, Italy (Grant GGP16003), and Ministero dell'Istruzione, dell'Università e della Ricerca (Grant PRIN bando 2017—2017FS5SHL) to CB.

REFERENCES

Alcover, A., Alarcón, B., and Di Bartolo, V. (2018). Cell biology of T cell receptor expression and regulation. *Annu. Rev. Immunol.* 36, 103–125. doi: 10.1146/annurev-immunol-042617-053429

Alekhina, O., Burstein, E., and Billadeau, D. D. (2017). Cellular functions of WASP family proteins at a glance. *J. Cell Sci.* 130, 2235–2241. doi: 10.1242/jcs.199570

Andrés-Delgado, L., Antón, O.-M., Madrid, R., Byrne, J. A., and Alonso, M. A. (2010). Formin INF2 regulates MAL-mediated transport of Lck to the plasma membrane of human T lymphocytes. *Blood* 116, 5919–5929. doi: 10.1182/blood-2010-08-300665

Antón, O. M., Andrés-Delgado, L., Reglero-Real, N., Batista, A., and Alonso, M. A. (2011). MAL protein controls protein sorting at the supramolecular activation cluster of human T lymphocytes. *J. Immunol.* 186, 6345–6356. doi: 10.4049/jimmunol.1003771

Bartuzi, P., Billadeau, D. D., Favier, R., Rong, S., Dekker, D., Fedoseienko, A., et al. (2016). CCC- and WASH-mediated endosomal sorting of LDLR is required for normal clearance of circulating LDL. *Nat. Commun.* 7:10961. doi: 10.1038/ncomms10961

Bello-Gamboa, A., Velasco, M., Moreno, S., Herranz, G., Ilie, R., Huetos, S., et al. (2020). Actin reorganization at the centrosomal area and the immune synapse regulates polarized secretory traffic of multivesicular bodies in T lymphocytes. *J. Extracell. Vesicles* 9:1759926. doi: 10.1080/20013078.2020.1759926

Bonello, G., Blanchard, N., Montoya, M. C., Aguado, E., Langlet, C., He, H. T., et al. (2004). Dynamic recruitment of the adaptor protein LAT: LAT exists in two distinct intracellular pools and controls its own recruitment. *J. Cell Sci.* 117, 1009–1016. doi: 10.1242/jcs.00968

Böttcher, R. T., Stremmel, C., Meves, A., Meyer, H., Widmaier, M., Tseng, H. Y., et al. (2012). Sorting nexin 17 prevents lysosomal degradation of β1 integrins by binding to the β1-integrin tail. *Nat. Cell Biol.* 14, 584–592. doi: 10.1038/ncb2501

Bouchet, J., Del Río-Iñiguez, I., Lasserre, R., Agüera-Gonzalez, S., Cuche, C., Danckaert, A., et al. (2016). Rac1-Rab11-FIP3 regulatory hub coordinates vesicle traffic with actin remodeling and T-cell activation. *EMBO J.* 35, 1160–1174. doi: 10.15252/embj.201593274

Bouchet, J., Del Río-Iñiguez, I., Vázquez-Chávez, E., Lasserre, R., Agüera-González, S., Cuche, C., et al. (2017). Rab11-FIP3 regulation of Lck endosomal traffic controls TCR signal transduction. *J. Immunol.* 198, 2967–2978. doi: 10.4049/jimmunol

Bouchet, J., McCaffrey, M. W., Graziani, A., and Alcover, A. (2018). The functional interplay of Rab11, FIP3 and Rho proteins on the endosomal recycling pathway controls cell shape and symmetry. *Small GTPases.* 9, 310–315. doi: 10.1080/21541248.2016.1224288

Bowman, S. L., Shiwarski, D. J., and Puthenveedu, M. A. (2016). Distinct G protein-coupled receptor recycling pathways allow spatial control of downstream G protein signaling. *J. Cell Biol.* 214, 797–806. doi: 10.1083/jcb.201512068

Burd, C., and Cullen, P. J. (2014). Retromer: a master conductor of endosome sorting. *Cold Spring Harb. Perspect. Biol.* 6:a016774. doi: 10.1101/cshperspect.a016774

Burden, J. J., Sun, X. M., García García, A. B., and Soutar, A. K. (2004). Sorting motifs in the intracellular domain of the low density lipoprotein receptor interact with a novel domain of sorting Nexin-17. *J. Biol. Chem.* 279, 16237–16245. doi: 10.1074/jbc.M313689200

Calabia-Linares, C., Robles-Valero, J., de la Fuente, H., Perez-Martinez, M., Martín-Cofreces, N., Alfonso-Pérez, M., et al. (2011). Endosomal clathrin drives actin

accumulation at the immunological synapse. *J. Cell Sci.* 124, 820–830. doi: 10.1242/jcs.078832

Canuel, M., Lefrancois, S., Zeng, J., and Morales, C. R. (2008). AP-1 and retromer play opposite roles in the trafficking of sortilin between the Golgi apparatus and the lysosomes. *Biochem. Biophys. Res. Commun.* 366, 724–730. doi: 10.1016/j.bbrc.2007.12.015

Capitani, N., Onnis, O., Finetti, F., Cassioli, C., Plebani, A., Brunetti, J., et al. (2020). A CVID-associated variant in the ciliogenesis protein CCDC28B disrupts immune synapse assembly. *Res. Square [Preprint]* doi: 10.21203/rs.3.rs-86351/v1

Cardenas-Rodriguez, M., Osborn, D. P. S., Irigoín, F., Graña, M., Romero, H., Beales, P. L., et al. (2013). Characterization of CCDC28B reveals its role in ciliogenesis and provides insight to understand its modifier effect on Bardet-Biedl syndrome. *Hum. Genet.* 132, 91–105. doi: 10.1007/s00439-012-1228-5

Carlton, J. G., and Cullen, P. J. (2005). Sorting nexins. *Curr. Biol.* 15, R819–R820. doi: 10.1016/j.cub.2005.10.012

Carpier, J. M., Zucchetti, A. E., Bataille, L., Dogniaux, S., Shafaq-Zadah, M., Bardin, S., et al. (2018). Rab6-dependent retrograde traffic of LAT controls immune synapse formation and T cell activation. *J. Exp. Med.* 215, 1245–1265. doi: 10.1084/jem.20162042

Cassioli, C., and Baldari, C. T. (2019). A ciliary view of the immunological synapse. *Cells* 8:789. doi: 10.3390/cells8080789

Cheung, P. Y., and Pfeffer, S. R. (2016). Transport vesicle tethering at the trans Golgi network: coiled coil proteins in action. *Front. Cell. Dev. Biol.* 4:18. doi: 10.3389/fcell.2016.00018

Clague, M. J., and Urbé, S. (2020). Data mining for traffic information. *Traffic* 21, 162–168. doi: 10.1111/tra.12702

Clairfeuille, T., Mas, C., Chan, A. S. M., Yang, Z., Tello-Lafoz, M., Chandra, M., et al. (2016). A molecular code for endosomal recycling of phosphorylated cargos by the SNX27-retromer complex. *Nat. Struct. Mol. Biol.* 23, 921–932. doi: 10.1038/nsmb.3290

Compeer, E. B., Kraus, F., Ecker, M., Redpath, G., Amiezer, M., Rother, N., et al. (2018). A mobile endocytic network connects clathrin-independent receptor endocytosis to recycling and promotes T cell activation. *Nat. Commun.* 9:1597. doi: 10.1038/s41467-018-04088-w

Crotzer, V. L., Mabardy, A. S., Weiss, A., and Brodsky, F. M. (2004). T cell receptor engagement leads to phosphorylation of clathrin heavy chain during receptor internalization. *J. Exp. Med.* 199, 981–991. doi: 10.1084/jem.20031105

de la Roche, M., Asano, Y., and Griffiths, G. M. (2016). Origins of the cytolytic synapse. *Nat. Rev. Immunol.* 16, 421–432. doi: 10.1038/nri.2016.54

Del Olmo, T., Lauzier, A., Normandin, C., Larcher, R., Lecours, M., Jean, D., et al. (2019). APEX2-mediated RAB proximity labeling identifies a role for RAB21 in clathrin-independent cargo sorting. *EMBO Rep.* 20:e47192. doi: 10.15252/embr.201847192

Derivery, E., and Gautreau, A. (2010). Evolutionary conservation of the WASH complex, an actin polymerization machine involved in endosomal fission. *Commun. Integr. Biol.* 3, 227–230. doi: 10.4161/cib.3.3.11185

Derivery, E., Sousa, C., Gautier, J. J., Lombard, B., Loew, D., and Gautreau, A. (2009). The Arp2/3 activator WASH controls the fission of endosomes through a large multiprotein complex. *Dev. Cell.* 17, 712–723. doi: 10.1016/j.devcel.2009.09.010

Dietrich, J., Hou, X., Wegener, A. M., and Geisler, G. (1994). CD3 gamma contains a phosphoserine-dependent di-leucine motif involved in down-regulation of the T cell receptor. *EMBO J.* 13, 2156–2166. doi: 10.1002/j.1460-2075.1994

Doherty, G. J., and McMahon, H. T. (2009). Mechanisms of endocytosis. *Annu. Rev. Biochem.* 78, 857–902. doi: 10.1146/annurev.biochem.78.081307.110540

Dong, B., Kakihara, K., Otani, T., Wada, H., and Hayashi, S. (2013). Rab9 and retromer regulate retrograde trafficking of luminal protein required for epithelial tube length control. *Nat. Commun.* 4:1358. doi: 10.1038/ncomms2347

Dustin, M. L., and Choudhuri, K. (2016). Signaling and polarized communication across the T cell immunological synapse. *Annu. Rev. Cell Dev. Biol.* 32, 303–325. doi: 10.1146/annurev-cellbio-100814-125330

Ehrlich, L. I. R., Ebert, P. J. R., Krummel, M. F., Weiss, A., and Davis, M. M. (2002). Dynamics of p56lck translocation to the T cell immunological synapse following agonist and antagonist stimulation. *Immunity* 17, 809–822. doi: 10.1016/S1074-7613(02)00481-8

Farfán, P., Lee, J., Larios, J., Sotelo, P., Bu, G., and Marzolo, M. P. (2013). A sorting Nexin 17-binding domain within the LRP1 cytoplasmic tail mediates receptor recycling through the basolateral sorting endosome. *Traffic* 14, 823–838. doi: 10.1111/tra.12076

Fedoseienko, A., Wijers, M., Wolters, J. C., Dekker, D., Smit, M., Huijkman, N., et al. (2018). The COMMD family regulates plasma LDL levels and attenuates atherosclerosis through stabilizing the CCC complex in endosomal LDLR traffcking. *Circ. Res.* 122, 1648–1660. doi: 10.1161/CIRCRESAHA.117.312004

Fernández-Arenas, E., Calleja, E., Martínez-Martín, N., Gharbi, S. I., Navajas, R., García-Medel, N., et al. (2014). β-Arrestin-1 mediates the TCR-triggered re-routing of distal receptors to the immunological synapse by a PKC-mediated mechanism. *EMBO J.* 33, 559–577. doi: 10.1002/embj.201386022

Finetti, F., Cassioli, C., and Baldari, C. T. (2017). Transcellular communication at the immunological synapse: a vesicular traffic-mediated mutual exchange. *F1000 Res.* 6:1880. doi: 10.12688/f1000research.11944.1

Finetti, F., Paccani, S. R., Riparbelli, M. G., Giacomello, E., Perinetti, G., Pazour, G. J., et al. (2009). Intraflagellar transport is required for polarized recycling of the TCR/ CD3 complex to the immune synapse. *Nat. Cell Biol.* 11, 1332–1339. doi: 10.1038/ncb1977

Finetti, F., Patrussi, L., Galgano, D., Cassioli, C., Perinetti, G., Pazour, G. J., et al. (2015). The small GTPase Rab8 interacts with VAMP-3 to regulate the delivery of recycling T-cell receptors to the immune synapse. *J. Cell Sci.* 128, 2541–2552. doi: 10.1242/jcs.171652

Finetti, F., Patrussi, L., Masi, G., Onnis, A., Galgano, D., Lucherini, O. M., et al. (2014). Specific recycling receptors are targeted to the immune synapse by the intraflagellar transport system. *J. Cell Sci.* 127, 1924–1937. doi: 10.1242/jcs.139337

Gallon, M., and Cullen, P. J. (2015). Retromer and sorting nexins in endosomal sorting. *Biochem. Soc. Trans.* 43, 33–47. doi: 10.1042/BST20140290

Gallon, M., Clairfeuille, T., Steinberg, F., Mas, C., Ghai, R., Sessions, R. B., et al. (2014). A unique PDZ domain and arrestin-like fold interaction reveals mechanistic details of endocytic recycling by SNX27-retromer. *Proc. Natl. Acad. Sci. U.S.A.* 111, E3604–E3613. doi: 10.1073/pnas.1410552111

Galvez, T., Gilleron, J., Zerial, M., and O'Sullivan, G. A. (2012). SnapShot: mammalian Rab proteins in endocytic trafficking. *Cell* 151, 234–234.e2. doi: 10.1016/j.cell.2012.09.013

Ghai, R., Bugarcic, A., Liu, H., Norwood, S. J., Skeldal, S., Coulson, E. J., et al. (2013). Structural basis for endosomal trafficking of diverse transmembrane cargos by PX-FERM proteins. *Proc. Natl. Acad. Sci. U.S.A.* 110, E643–E652. doi: 10.1073/pnas.1216229110

Ghai, R., Tello-Lafoz, M., Norwood, S. J., Yang, Z., Clairfeuille, T., Teasdale, R. D., et al. (2015). Phosphoinositide binding by the SNX27 FERM domain regulates its localization at the immune synapse of activated T-cells. *J. Cell Sci.* 128, 553–565. doi: 10.1242/jcs.158204

Goldenring, J. R. (2015). Recycling endosomes. *Curr. Opin. Cell Biol.* 35, 117–122. doi: 10.1016/j.ceb.2015.04.018

Gomez, T. S., and Billadeau, D. D. (2009). A FAM21-containing WASH complex regulates retromer-dependent sorting. *Dev. Cell.* 17, 699–711. doi: 10.1016/j.devcel.2009.09.009

Gong, T., Yan, Y., Zhang, J., Liu, S., Liu, H., Gao, J., et al. (2018). PTRN -1/ CAMSAP promotes CYK -1/formin-dependent actin polymerization during endocytic recycling. *EMBO J.* 37:e98556. doi: 10.15252/embj.201798556

González-Mancha, N., and Mérida, I. (2020). Interplay between snx27 and dag metabolism in the control of trafficking and signaling at the IS. *Int. J. Mol. Sci.* 21:4254. doi: 10.3390/ijms21124254

Griffin, C. T., Trejo, J. A., and Magnuson, T. (2005). Genetic evidence for a mammalian retromer complex containing sorting nexins 1 and 2. *Proc. Natl. Acad. Sci. U.S.A.* 102, 15173–15177. doi: 10.1073/pnas.0409558102

Hammer, J. A., Wang, J. C., Saeed, M., and Pedrosa, A. T. (2019). Origin, organization, dynamics, and function of actin and actomyosin networks at the T cell immunological synapse. *Annu. Rev. Immunol.* 37, 201–224. doi: 10.1146/annurev-immunol-042718-041341

Hao, Y. H., Doyle, J. M., Ramanathan, S., Gomez, T. S., Jia, D., Xu, M., et al. (2013). Regulation of WASH-dependent actin polymerization and protein trafficking by ubiquitination. *Cell* 152, 1051–1064. doi: 10.1016/j.cell.2013.01.051

Hao, Y. H., Fountain, M. D., Fon Tacer, K., Xia, F., Bi, W., Kang, S. H. L., et al. (2015). USP7 acts as a molecular rheostat to promote WASH-dependent

endosomal protein recycling and is mutated in a human neurodevelopmental disorder. *Mol. Cell* 59, 956–969. doi: 10.1016/j.molcel.2015.07.033

Harbour, M. E., Breusegem, S. Y. A., Antrobus, R., Freeman, C., Reid, E., and Seaman, M. N. J. (2010). The cargo-selective retromer complex is a recruiting hub for protein complexes that regulate endosomal tubule dynamics. *J. Cell Sci.* 123, 3703–3717. doi: 10.1242/jcs.071472

Harbour, M. E., Breusegem, S. Y., and Seaman, M. N. J. (2012). Recruitment of the endosomal WASH complex is mediated by the extended "tail" of Fam21 binding to the retromer protein Vps35. *Biochem. J.* 442, 209–220. doi: 10.1042/BJ20111761

Harterink, M., Port, F., Lorenowicz, M. J., McGough, I. J., Silhankova, M., Betist, M. C., et al. (2011). A SNX3-dependent retromer pathway mediates retrograde transport of the Wnt sorting receptor Wntless and is required for Wnt secretion. *Nat. Cell Biol.* 13, 914–923. doi: 10.1038/ncb2281

Helfer, E., Harbour, M. E., Henriot, V., Lakisic, G., Sousa-Blin, C., Volceanov, L., et al. (2013). Endosomal recruitment of the WASH complex: active sequences and mutations impairing interaction with the retromer. *Biol. Cell* 105, 191–207. doi: 10.1111/boc.201200038

Hernandez-Valladares, M., Kim, T., Kannan, B., Tung, A., Aguda, A. H., Larsson, M., et al. (2010). Structural characterization of a capping protein interaction motif defines a family of actin filament regulators. *Nat. Struct. Mol. Biol.* 17, 497–503. doi: 10.1038/nsmb.1792

Herranz, G., Aguilera, P., Dávila, S., Sánchez, A., Stancu, B., Gómez, J., et al. (2019). Protein kinase C δ regulates the depletion of actin at the immunological synapse required for polarized exosome secretion by T cells. *Front. Immunol.* 10:851. doi: 10.3389/fimmu.2019.00851

Hesketh, G. G., Perez-Dorado, I., Jackson, L. P., Wartosch, L., Schafer, I. B., Gray, S. R., et al. (2014). VARP is recruited on to endosomes by direct interaction with retromer, where together they function in export to the cell surface. *Dev. Cell* 29, 591–606. doi: 10.1016/j.devcel.2014.04.010

Hinze, C., and Boucrot, E. (2018). Local actin polymerization during endocytic carrier formation. *Biochem. Soc. Trans.* 46, 565–576. doi: 10.1042/BST20170355

Hivroz, C., Chemin, K., Tourret, M., and Bohineust, A. (2012). Crosstalk between T lymphocytes and dendritic cells. *Crit. Rev. Immunol.* 32, 139–155. doi: 10.1615/critrevimmunol.v32.i2.30

Hong, N. H., Qi, A., and Weaver, A. M. (2015). PI(3,5)P2 controls endosomal branched actin dynamics by regulating cortactin-Actin interactions. *J. Cell Biol.* 210, 753–769. doi: 10.1083/jcb.201412127

Hsu, V. W., Bai, M., and Li, J. (2012). Getting active: protein sorting in endocytic recycling. *Nat. Rev. Mol. Cell Biol.* 3, 323–328. doi: 10.1038/nrm3332

Jia, D., Gomez, T. S., Billadeau, D. D., and Rosen, M. K. (2012). Multiple repeat elements within the FAM21 tail link the WASH actin regulatory complex to the retromer. *Mol. Biol. Cell* 23, 2352–2361. doi: 10.1091/mbc.E11-12-1059

Jia, D., Gomez, T. S., Metlagel, Z., Umetani, J., Otwinowski, Z., Rosen, M. K., et al. (2010). WASH and WAVE actin regulators of the Wiskott-Aldrich syndrome protein (WASP) family are controlled by analogous structurally related complexes. *Proc. Natl. Acad. Sci. U.S.A.* 107, 10442–10447. doi: 10.1073/pnas.0913293107

Johannes, L., and Wunder, C. (2011). Retrograde transport: two (or more) roads diverged in an endosomal tree? *Traffic* 12, 956–962. doi: 10.1111/j.1600-0854.2011.01200.x

Johnson, D. M., and Andrew, D. J. (2019). Role of tbc1 in *Drosophila* embryonic salivary glands. *BMC Mol. Cell Biol.* 20:19. doi: 10.1186/s12860-019-0198-z

Kabanova, A., Zurli, V., and Baldari, C. T. (2018). Signals controlling lytic granule polarization at the cytotoxic immune synapse. *Front. Immunol.* 9:307. doi: 10.3389/fimmu.2018.00307

Kaksonen, M., Peng, H. B., and Rauvala, H. (2000). Association of cortactin with dynamic actin in lamellipodia and on endosomal vesicles. *J. Cell Sci.* 113, 4421–4426.

Kvainickas, A., Jimenez-Orgaz, A., Nägele, H., Hu, Z., Dengjel, J., and Steinberg, F. (2017). Cargo-selective SNX-BAR proteins mediate retromer trimer independent retrograde transport. *J. Cell Biol.* 216, 3677–3693. doi: 10.1083/jcb.201702137

Larghi, P., Williamson, D. J., Carpier, J. M., Dogniaux, S., Chemin, K., Bohineust, A., et al. (2013). VAMP7 controls T cell activation by regulating the recruitment and phosphorylation of vesicular Lat at TCR-activation sites. *Nat. Immunol.* 14, 723–731. doi: 10.1038/ni.2609

Lauffer, B. E. L., Melero, C., Temkin, P., Lei, C., Hong, W., Kortemme, T., et al. (2010). SNX27 mediates PDZ-directed sorting from endosomes to the plasma membrane. *J. Cell Biol.* 90, 565–574. doi: 10.1083/jcb.201004060

Liu, T., Gomez, T. S., Sackey, B. K., Billadeau, D. D., and Burd, C. G. (2012). Rab GTPase regulation of retromer-mediated cargo export during endosome maturation. *Mol. Biol. Cell* 23, 2505–2515. doi: 10.1091/mbc.E11-11-0915

Lladó, A., Timpson, P., Vilà De Muga, S., Moretó, J., Pol, A., Grewal, T., et al. (2008). Protein kinase Cδ and calmodulin regulate epidermal growth factor receptor recycling from early endosomes through Arp2/3 complex and cortactin. *Mol. Biol. Cell* 19, 17–29. doi: 10.1091/mbc.E07-05-0411

Lowe, M. (2019). The physiological functions of the golgin vesicle tethering proteins. *Front. Cell Dev. Biol.* 7:94. doi: 10.3389/fcell.2019.00094

Lu, L., and Hong, W. (2014). From endosomes to the trans-Golgi network. *Semin. Cell Dev. Biol.* 31, 30–39. doi: 10.1016/j.semcdb.2014.04.024

Lucas, M., Gershlick, D. C., Vidaurrazaga, A., Rojas, A. L., Bonifacino, J. S., and Hierro, A. (2016). Structural mechanism for cargo recognition by the retromer complex. *Cell* 167, 1623–1635.e14. doi: 10.1016/j.cell.2016.10.056

Maine, G. N., and Burstein, E. (2007). COMMD proteins: COMMing to the scene. *Cell. Mol. Life Sci.* 64, 1997–2005. doi: 10.1007/s00018-007-7078-y

Martín-Cófreces, N. B., and Sánchez-Madrid, F. (2018). Sailing to and docking at the immune synapse: role of tubulin dynamics and molecular motors. *Front. Immunol.* 9:1174. doi: 10.3389/fimmu.2018.01174

Mastrogiovanni, M., Juzans, M., Alcover, A., and Di Bartolo, V. (2020). Coordinating cytoskeleton and molecular traffic in T Cell migration, activation, and effector functions. *Front. Cell Dev. Biol.* 8:591348. doi: 10.3389/fcell.2020.591348

Maxfield, F. R., and McGraw, T. E. (2004). Endocytic recycling. *Nat. Rev. Mol. Cell Biol.* 5, 121–132. doi: 10.1038/nrm1315

McGough, I. J., Steinberg, F., Gallon, M., Yatsu, A., Ohbayashi, N., Heesom, K. J., et al. (2014). Identification of molecular heterogeneity in SNX27-retromermediated endosome-to-plasma-membrane recycling. *J. Cell Sci.* 127, 4940–4953. doi: 10.1242/jcs.156299

McNally, K. E., Faulkner, R., Steinberg, F., Gallon, M., Ghai, R., Pim, D., et al. (2017). Retriever is a multiprotein complex for retromer-independent endosomal cargo recycling. *Nat. Cell Biol.* 9, 1214–1225. doi: 10.1038/ncb3610

Miserey-Lenkei, S., Waharte, F., Boulet, A., Cuif, M. H., Tenza, D., El Marjou, A., et al. (2007). Rab6-interacting protein 1 links Rab6 and Rab11 function. *Traffic* 8, 1385–1403. doi: 10.1111/j.1600-0854.2007.00612.x

Mittelbrunn, M., Vicente Manzanares, M., and Sánchez-Madrid, F. (2015). Organizing polarized delivery of exosomes at synapses. *Traffic* 16, 327–337. doi: 10.1111/tra.12258

Onnis, A., and Baldari, C. T. (2019). Orchestration of immunological synapse assembly by vesicular trafficking. *Front. Cell Dev. Biol.* 7:110. doi: 10.3389/fcell.2019.00110

Onnis, A., Finetti, F., and Baldari, C. T. (2016). Vesicular trafficking to the immune synapse: how to assemble receptor-tailored pathways from a basic building set. *Front. Immunol.* 7:50. doi: 10.3389/fimmu.2016.00050

Onnis, A., Finetti, F., Patrussi, L., Gottardo, M., Cassioli, C., Spanò, S., et al. (2015). The small GTPase Rab29 is a common regulator of immune synapse assembly and ciliogenesis. *Cell Death Differ.* 22, 1687–1699. doi: 10.1038/cdd.2015.17

Osborne, D. G., Piotrowski, J. T., Dick, C. J., Zhang, J. S., and Billadeau, D. D. (2015). SNX17 Affects T cell activation by regulating TCR and integrin recycling. *J. Immunol.* 194, 4555–4566. doi: 10.4049/jimmunol.1402734

Patino-Lopez, G., Dong, X., Ben-Aissa, K., Bernot, K. M., Itoh, T., Fukuda, M., et al. (2018). Rab35 and its GAP EPI64C in T cells regulate receptor recycling and immunological synapse formation. *J. Biol. Chem.* 283, 18323–18330. doi: 10.1074/jbc.M800056200

Phillips-Krawczak, C. A., Singla, A., Starokadomskyy, P., Deng, Z., Osborne, D. G., Li, H., et al. (2015). COMMD1 is linked to the WASH complex and regulates endosomal trafficking of the copper transporter ATP7A. *Mol. Biol. Cell.* 26, 91–103. doi: 10.1091/mbc.E14-06-1073

Piotrowski, J. T., Gomez, T. S., Schoon, R. A., Mangalam, A. K., and Billadeau, D. D. (2013). WASH knockout T Cells demonstrate defective receptor trafficking, proliferation, and effector function. *Mol. Cell. Biol.* 33, 958–973. doi: 10.1128/mcb.01288-12

Pizarro-Cerdá, J., Chorev, D. S., Geiger, B., and Cossart, P. (2017). The diverse family of Arp2/3 complexes. *Trends Cell Biol.* 27, 93–100. doi: 10.1016/j.tcb.2016.08.001

Pons, M., Izquierdo, I., Andreu-Carbó, M., Garrido, G., Planagumà, J., Muriel, O., et al. (2017). Phosphorylation of filamin A regulates chemokine receptor CCR2 recycling. *J. Cell Sci.* 130, 490–501. doi: 10.1242/jcs.193821

Priya, A., Kalaidzidis, I. V., Kalaidzidis, Y., Lambright, D., and Datta, S. (2015). Molecular insights into Rab7-mediated endosomal recruitment of core retromer: deciphering the role of Vps26 and Vps35. *Traffic* 16, 68–84. doi: 10.1111/tra.12237

Puthenveedu, M. A., Lauffer, B., Temkin, P., Vistein, R., Carlton, P., Thorn, K., et al. (2010). Sequence-dependent sorting of recycling proteins by actin-stabilized endosomal microdomains. *Cell* 143, 761–773. doi: 10.1016/j.cell.2010.10.003

Randzavola, L. O., Strege, K., Juzans, M., Asano, Y., Stinchcombe, J. C., Gawden-Bone, C. M., et al. (2019). Loss of ARPC1B impairs cytotoxic T lymphocyte maintenance and cytolytic activity. *J. Clin. Invest.* 129, 5600–5614. doi: 10.1172/JCI129388

Rincón, E., De Guinoa, J. S., Gharbi, S. I., Sorzano, C. O. S., Carrasco, Y. R., and Mérida, I. (2011). Translocation dynamics of sorting nexin 27 in activated T cells. *J. Cell Sci.* 124, 776–788. doi: 10.1242/jcs.072447

Rincón, E., Santos, T., Ávila-Flores, A., Albar, J. P., Lalioti, V., Lei, C., et al. (2007). Proteomics identification of sorting nexin 27 as a diacyglycerol kinase ζ-associated protein: new diacylglycerol kinase roles in endocytic recycling. *Mol. Cell. Prot.* 6, 1073–1087. doi: 10.1074/mcp.M700047-MCP200

Ritter, A. T., Angus, K. L., and Griffiths, G. M. (2013). The role of the cytoskeleton at the immunological synapse. *Immunol. Rev.* 256, 107–117. doi: 10.1111/imr.12117

Ritter, A. T., Asano, Y., Stinchcombe, J. C., Dieckmann, N. M., Chen, B. C., Gawden-Bone, C., et al. (2015). Actin depletion initiates events leading to granule secretion at the immunological synapse. *Immunity* 42, 864–876. doi: 10.1016/j.immuni.2015.04.013

Rojas, R., Kametaka, S., Haft, C. R., and Bonifacino, J. S. (2007). Interchangeable but essential functions of SNX1 and SNX2 in the association of retromer with endosomes and the trafficking of mannose 6-phosphate receptors. *Mol. Cell. Biol.* 27, 1112–1124. doi: 10.1128/mcb.00156-06

Rojas, R., van Vlijmen, T., Mardones, G. A., Prabhu, Y., Rojas, A. L., and Mohammed, S. (2008). Regulation of retromer recruitment to endosomes by sequential action of Rab5 and Rab7. *J. Cell Biol.* 183, 513–526. doi: 10.1083/jcb.200804048

Saarikangas, J., Zhao, H., and Lappalainen, P. (2010). Regulation of the actin cytoskeleton-plasma membrane interplay by phosphoinositides. *Physiol. Rev.* 90, 259–289. doi: 10.1152/physrev.00036.2009

Saez, J. J., Dogniaux, S., Sharaq-Zadah, M., Ludger, J., Hivroz, C., and Zucchetti, A. E. (2021). Retrograde and anterograde transport of lat-vesicles during the immunological synapse formation: defining the finely-tuned mechanism. *Cells* 10:359. doi: 10.3390/cells10020359

Saimani, U., and Kim, K. (2017). Traffic from the endosome towards trans-Golgi network. *Eur. J. Cell Biol.* 96, 198–205. doi: 10.1016/j.ejcb.2017.02.005

Saliba, D. G., Céspedes-Donoso, P. F., Bálint, S., Compeer, E. B., Korobchevskaya, K., Valvo, S., et al. (2019). Composition and structure of synaptic ectosomes exporting antigen receptor linked to functional CD40 ligand from helper T cells. *Elife* 8:e47528. doi: 10.7554/eLife.47528

Sanchez, E., Liu, X., and Huse, M. (2019). Actin clearance promotes polarized dynein accumulation at the immunological synapse. *PLoS One* 14:e0210377. doi: 10.1371/journal.pone.0210377

Seaman, M. N. J. (2007). Identification of a novel conserved sorting motif required for retromer-mediated endosome-to-TGN retrieval. *J.Cell.Sci.* 120, 2378–2389. doi: 10.1242/jcs.009654

Shin, J. J. H., Gillingham, A. K., Begum, F., Chadwick, J., and Munro, S. (2017). TBC1D23 is a bridging factor for endosomal vesicle capture by golgins at the trans-Golgi. *Nat. Cell Biol.* 19, 1424–1432. doi: 10.1038/ncb3627

Shinde, S. R., and Maddika, S. (2017). PTEN regulates glucose transporter recycling by impairing SNX27 retromer assembly. *Cell Rep.* 21, 1655–1666. doi: 10.1016/j.celrep.2017.10.053

Simonetti, B., and Cullen, P. J. (2019). Actin-dependent endosomal receptor recycling. *Curr. Opin. Cell Biol.* 56, 22–33. doi: 10.1016/j.ceb.2018.08.006

Simonetti, B., Danson, C. M., Heesom, K. J., and Cullen, P. J. (2017). Sequence-dependent cargo recognition by SNX-BARs mediates retromer-independent transport of CI-MPR. *J. Cell Biol.* 216, 3695–3712. doi: 10.1083/jcb.201703015

Singla, A., Fedoseienko, A., Giridharan, S. S. P., Overlee, B. L., Lopez, A., Jia, D., et al. (2019). Endosomal PI(3)P regulation by the COMMD/CCDsC22/CCDC93 (CCC) complex controls membrane protein recycling. *Nat. Commun.* 10:4271. doi: 10.1038/s41467-019-12221-6

Soares, H., Lasserre, R., and Alcover, A. (2013). Orchestrating cytoskeleton and intracellular vesicle traffic to build functional immunological synapses. *Immunol. Rev.* 256, 118–132. doi: 10.1111/imr.12110

Sönnichsen, B., De Renzis, S., Nielsen, E., Rietdorf, J., and Zerial, M. (2000). Distinct membrane domains on endosomes in the recycling pathway visualized by multicolor imaging of Rab4, Rab5, and Rab11. *J. Cell Biol.* 149, 901–914. doi: 10.1083/jcb.149.4.901

Steinberg, F., Gallon, M., Winfield, M., Thomas, E. C., Bell, A. J., Heesom, K. J., et al. (2013). A global analysis of SNX27-retromer assembly and cargo specificity reveals a function in glucose and metal ion transport. *Nat. Cell Biol.* 15, 461–471. doi: 10.1038/ncb2721

Steinberg, F., Heesom, K. J., Bass, M. D., and Cullen, P. J. (2012). SNX17 protects integrins from degradation by sorting between lysosomal and recycling pathways. *J. Cell Biol.* 97, 219–230. doi: 10.1083/jcb.201111121

Stenmark, H. (2009). Rab GTPases as coordinators of vesicle traffic. *Nat. Rev. Mol. Cell Biol.* 10, 513–525. doi: 10.1038/nrm2728

Stephen, L. A., ElMaghloob, Y., McIlwraith, M. J., Yelland, T., Castro Sanchez, P., Roda-Navarro, P., et al. (2018). The ciliary machinery is repurposed for T cell immune synapse trafficking of LCK. *Dev. Cell* 47, 122–132.e4. doi: 10.1016/j.devcel.2018.08.012

Stockinger, W., Sailler, B., Strasser, V., Recheis, B., Fasching, D., Kahr, L., et al. (2002). The PX-domain protein SNX17 interacts with members of the LDL receptor family and modulates endocytosis of the LDL receptor. *EMBO J.* 21, 4259–4267. doi: 10.1093/emboj/cdf435

Strochlic, T. I., Setty, T. G., Sitaram, A., and Burd, C. G. (2007). Grd19/Snx3p functions as a cargo-specific adapter for retromer-dependent endocytic recycling. *J. Cell Biol.* 177, 115–125. doi: 10.1083/jcb.200609161

Suetsugu, S., Kurisu, S., Oikawa, T., Yamazaki, D., Oda, A., and Takenawa, T. (2006). Optimization of WAVE2 complex-induced actin polymerization by membrane-bound IRSp53, PIP3, and Rac. *J. Cell Biol.* 173, 571–585. doi: 10.1083/jcb.200509067

Tabuchi, M., Yanatori, I., Kawai, Y., and Kishi, F. (2010). Retromer-mediated direct sorting is required for proper endosomal recycling of the mammalian iron transporter DMT1. *J. Cell Sci.* 123, 756–766. doi: 10.1242/jcs.060574

Teasdale, R. D., and Collins, B. M. (2012). Insights into the PX (phox-homology) domain and SNX (sorting nexin) protein families: Structures, functions and roles in disease. *Biochem. J.* 441, 39–59. doi: 10.1042/BJ20111226

Tello-Lafoz, M., Ghai, R., Collins, B., and Mérida, I. (2014). A role for novel lipid interactions in the dynamic recruitment of SNX27 to the T-cell immune synapse. *Bioarchitecture* 4, 215–220. doi: 10.1080/19490992.2015.1031950

Tello-Lafoz, M., Martínez-Martínez, G., Rodríguez-Rodríguez, C., Albar, J. P., Huse, M., Gharbi, S., et al. (2017). Sorting nexin 27 interactome in T-lymphocytes identifies zona occludens-2 dynamic redistribution at the immune synapse. *Traffic* 18, 491–504. doi: 10.1111/tra.12492

Temkin, P., Lauffer, B., Jäger, S., Cimermancic, P., Krogan, N. J., and Von Zastrow, M. (2011). SNX27 mediates retromer tubule entry and endosome-to-plasma membrane trafficking of signalling receptors. *Nat. Cell Biol.* 13, 715–721. doi: 10.1038/ncb2252

Tu, Y., Zhao, L., Billadeau, D. D., and Jia, D. (2020). Endosome-to-TGN trafficking: organelle-vesicle and organelle-organelle interactions. *Front. Cell Dev. Biol.* 8:163. doi: 10.3389/fcell.2020.00163

Vergés, M. (2016). Retromer in polarized protein transport. *Int. Rev. Cell Mol. Biol.* 323, 129–179. doi: 10.1016/bs.ircmb.2015.12.005

Vietri, M., Radulovic, M., and Stenmark, H. (2020). The many functions of ESCRTs. *Nat. Rev. Mol. Cell Biol.* 21, 25–42. doi: 10.1038/s41580-019-0177-4

Vistein, R., and Puthenveedu, M. A. (2014). Src regulates sequence-dependent beta-2 adrenergic receptor recycling via cortactin phosphorylation. *Traffic* 15, 1195–1205. doi: 10.1111/tra.12202

Vivar, O., Masi, G., Carpier, J. M., Magalhaes, J. G., Galgano, D., Pazour, G. J., et al. (2016). IFT20 controls LAT recruitment to the immune synapse and T-cell activation in vivo. *Proc. Natl. Acad. Sci. U.S.A.* 113, 386–391. doi: 10.1073/pnas.1513601113

von Essen, M., Menne, C., Nielsen, B. L., Lauritsen, J. P., Dietrich, J., Andersen, P. S., et al. (2002). The CD3 gamma leucine-based receptor-sorting motif is required for efficient ligand-mediated TCR down-regulation. *J. Immunol.* 168, 4519–4523. doi: 10.4049/jimmunol.168.9.4519

Vonk, W. I. M., Bartuzi, P., de Bie, P., Kloosterhuis, N., Wichers, C. G. K., Berger, R., et al. (2011). Liver-specific Commd1 knockout mice are susceptible to hepatic copper accumulation. *PLoS One* 6:e29183. doi: 10.1371/journal.pone.0029183

Wandinger-Ness, A., and Zerial, M. (2014). Rab proteins and the compartmentalization of the endosomal system. *Cold Spring Harb. Perspect. Biol.* 6:a022616. doi: 10.1101/cshperspect.a022616

Wang, J., Fedoseienko, A., Chen, B., Burstein, E., Jia, D., and Billadeau, D. D. (2018). Endosomal receptor trafficking: Retromer and beyond. *Traffic* 19, 578–590. doi: 10.1111/tra.12574

Waschbüsch, D., Hübel, N., Ossendorf, E., Lobbestael, E., Baekelandt, V., Lindsay, A. J., et al. (2019). Rab32 interacts with SNX6 and affects retromer-dependent Golgi trafficking. *PLoS One* 14:e0208889. doi: 10.1371/journal.pone.0208889

Wassmer, T., Attar, N., Bujny, M. V., Oakley, J., Traer, C. J., and Cullen, P. J. (2007). A loss-of-function screen reveals SNX5 and SNX6 as potential components of the mammalian retromer. *J. Cell Sci.* 120, 45–54. doi: 10.1242/jcs.03302

Yin, H. L., and Janmey, P. A. (2003). Phosphoinositide regulation of the actin cytoskeleton. *Annu. Rev. Physiol.* 65, 761–789. doi: 10.1146/annurev.physiol.65.092101.142517

Zelazny, E., Santambrogio, M., Pourcher, M., Chambrier, P., Berne-Dedieu, A., Fobis-Loisy, I., et al. (2013). Mechanisms governing the endosomal membrane recruitment of the core retromer in *Arabidopsis*. *J. Biol. Chem.* 288, 8815–8825. doi: 10.1074/jbc.M112.440503

Zhang, P., Wu, Y., Belenkaya, T. Y., and Lin, X. (2011). SNX3 controls Wingless/Wnt secretion through regulating retromer-dependent recycling of Wntless. *Cell Res.* 21, 1677–1690. doi: 10.1038/cr.2011.167

Zhang, Y., Shen, H., Liu, H., Feng, H., Liu, Y., Zhu, X., et al. (2017). Arp2/3 complex controls T cell homeostasis by maintaining surface TCR levels via regulating TCR+ endosome trafficking. *Sci. Rep.* 7:8952. doi: 10.1038/s41598-017-08357-4

Zucchetti, A. E., Bataille, L., Carpier, J. M., Dogniaux, S., San Roman-Jouve, M., Maurin, M., et al. (2019). Tethering of vesicles to the Golgi by GMAP210 controls LAT delivery to the immune synapse. *Nat. Commun.* 10:2864. doi: 10.1038/s41467-019-10891-w

Conflict of Interest: The authors declare that the research was conducted in the absence of any commercial or financial relationships that could be construed as a potential conflict of interest.

frontiers in Cell and Developmental Biology

ORIGINAL RESEARCH
published: 30 June 2021
doi: 10.3389/fcell.2021.655773

3D-STED Super-Resolution Microscopy Reveals Distinct Nanoscale Organization of the Hematopoietic Cell-Specific Lyn Substrate-1 (HS1) in Normal and Leukemic B Cells

Marta Sampietro[1,2,3], Moreno Zamai[3], Alfonsa Díaz Torres[3], Veronica Labrador Cantarero[3], Federica Barbaglio[1], Lydia Scarfò[4,5], Cristina Scielzo[1†] and Valeria R. Caiolfa[3,6*†]*

[1] Malignant B Cells Biology and 3D Modeling Unit, Division of Experimental Oncology, IRCCS Ospedale San Raffaele, Milan, Italy, [2] Nanomedicine Center NANOMIB, School of Medicine and Surgery, Università di Milano Bicocca, Milan, Italy, [3] Unit of Microscopy and Dynamic Imaging, Centro Nacional de Investigaciones Cardiovasculares (CNIC), Madrid, Spain, [4] B-Cell Neoplasia Unit and Strategic Research Program on CLL, Division of Experimental Oncology, IRCCS Ospedale San Raffaele, Milan, Italy, [5] School of Medicine, Università Vita-Salute San Raffaele, Milan, Italy, [6] Experimental Imaging Center, IRCCS Ospedale San Raffaele, Milan, Italy

HS1, the hematopoietic homolog of cortactin, acts as a versatile actin-binding protein in leucocytes. After phosphorylation, it is involved in GTPase and integrin activation, and in BCR, TCR, and CXCR4 downstream signaling. In normal and leukemic B cells, HS1 is a central cytoskeletal interactor and its phosphorylation and expression are prognostic factors in chronic lymphocytic leukemia (CLL) patients. We here introduce for the first time a super-resolution imaging study based on single-cell 3D-STED microscopy optimized for revealing and comparing the nanoscale distribution of endogenous HS1 in healthy B and CLL primary cells. Our study reveals that the endogenous HS1 forms heterogeneous nanoclusters, similar to those of YFP-HS1 overexpressed in the leukemic MEC1 cell line. HS1 nanoclusters in healthy and leukemic B cells form bulky assemblies at the basal sides, suggesting the recruitment of HS1 for cell adhesion. This observation agrees with a phasor-FLIM-FRET and STED colocalization analyses of the endogenous MEC1-HS1, indicating an increased interaction with Vimentin at the cell adhesion sites. In CLL cells isolated from patients with poor prognosis, we observed a larger accumulation of HS1 at the basal region and a higher density of HS1 nanoclusters in the central regions of the cells if compared to good-prognosis CLL and healthy B cells, suggesting a different role for the protein in the cell types analyzed. Our 3D-STED approach lays the ground for revealing tiny differences of HS1 distribution, its functionally active forms, and colocalization with protein partners.

Keywords: HS1, CLL, B cells, super-resolution, STED, phasor-FLIM, FRET

OPEN ACCESS

Edited by:
Noa B. Martin-Cofreces, Princess University Hospital, Spain

Reviewed by:
Michael Schnoor, Instituto Politécnico Nacional de México, Mexico
Jorge Bernardino De La Serna, National Heart and Lung Institute, United Kingdom

****Correspondence:***
Cristina Scielzo
cristina.scielzo@hsr.it
Valeria R. Caiolfa
valeria.caiolfa@hsr.it

† These authors have contributed equally to this work and share last authorship

Specialty section:
This article was submitted to Cell Adhesion and Migration, a section of the journal Frontiers in Cell and Developmental Biology

Received: *19 January 2021*
Accepted: *01 June 2021*
Published: *30 June 2021*

Citation:
Sampietro M, Zamai M, Díaz Torres A, Labrador Cantarero V, Barbaglio F, Scarfò L, Scielzo C and Caiolfa VR (2021) 3D-STED Super-Resolution Microscopy Reveals Distinct Nanoscale Organization of the Hematopoietic Cell-Specific Lyn Substrate-1 (HS1) in Normal and Leukemic B Cells. Front. Cell Dev. Biol. 9:655773. doi: 10.3389/fcell.2021.655773

INTRODUCTION

The hematopoietic cell-specific lyn substrate-1 (HS1) protein is the hematopoietic homologue of cortactin (Schnoor et al., 2018), belonging to the class II nucleation-promoting factor (NPF) family able to initiate branched actin network assembly by activating the Arp2/3 complex (Helgeson and Nolen, 2013).

The multi-domain sequence of HS1 is responsible for the recruitment of the protein in different mechanisms such as the activation of GTPases and integrins and the downstream signaling of BCR and TCR, and is indispensable for signaling events leading to actin assembly during immunological synapse (IS) formation (reviewed in Gomez et al., 2006; Castro-Ochoa et al., 2019). The HS1 sequence contains also a nuclear localization signal (van Rossum et al., 2005), for shuttling the transcription factor LEF-1 to the nucleus of myeloid cells (Skokowa et al., 2012). The N-terminal acidic region of HS1 mediates the connection of the Arp2/3 complex to actin intermediate filaments (IF), stabilizing newly formed branched actin networks (Uruno et al., 2003; Scherer et al., 2018). In response to various stimuli, a proline-rich domain interacts with SH2/SH3 domain-containing proteins, with phosphorylation of several tyrosine residues (Ruzzene et al., 1996).

HS1 functions are strictly regulated by posttranslational modifications. In B cells, HS1 is phosphorylated at residues Y378 and Y397 by BCR-activated Syk and Lyn kinases, followed by B-cell apoptosis (Yamanashi et al., 1997). Upon BCR-induced cross-linking and Syk activation, HS1 is localized in membrane lipid rafts, suggesting an adapter role in the recruitment and assembly of actin (Hao et al., 2004). In T cells, phosphorylation links HS1 to multiple signaling proteins, including Lck, PLCγ1, and Vav1, and is essential for the stable recruitment of Vav1 to the IS (Gomez et al., 2006).

Chronic lymphocytic leukemia (CLL) is the most common leukemia in the Western world and affects mainly elderly patients (Tausch et al., 2014). Most patients with CLL are diagnosed with this disease at the early stage and managed with active surveillance; however, the individual course of patients is very heterogeneous, and their probability of needing treatment is difficult to be anticipated at diagnosis. For this reason, different prognostic factors have been explored over time (Chen and Puvvada, 2016). Recently, the immunoglobulin heavy variable gene (IGHV) unmutated status has been defined as the biomarker with the strongest effect on time to first treatment prognostication (Condoluci et al., 2020).

CLL cells are clonal $CD5^+$ B lymphocytes that accumulate, progressively expand, and traffic between peripheral blood, bone marrow, and secondary lymphoid organs (Burger and Gribben, 2014; Caligaris-Cappio et al., 2014), where they proliferate by sensing and reacting to the microenvironment (i.e., stromal, endothelial, and immune cells), likely undergoing a major cytoskeleton rearrangement (Calissano et al., 2009; Herishanu et al., 2011; Ponzoni et al., 2011). The continuous trafficking of CLL cells from tissue back to circulation induces a phenotype that possibly contributes to disease progression and chemo-resistance (Burger, 2010; Herishanu et al., 2011; Ponzoni et al., 2011).

The implication of the cytoskeleton in the dynamic behavior of CLL cells was first observed in early studies showing that CLL cells manifest anomalous motility, cap formation (Stark et al., 1984), and aberrant cytoskeleton rearrangement (Caligaris-Cappio et al., 1986).

These mechanisms are controlled by cytoskeleton regulatory molecules, as HS1, which we reported to be able to interact with cytoskeleton adapters such as Vimentin and HIP-55 in normal and leukemic B cells (Muzio et al., 2007). Moreover, HS1 was identified as a prognostic marker in CLL (Scielzo et al., 2005) depending on its activation status; active/inactive forms correlate with favorable or adverse prognosis, respectively (Yamanashi et al., 1993, 1997; Scielzo et al., 2010).

We demonstrated that downregulation of HS1 expression interferes with CLL cell secondary lymphoid organ infiltration and leads to increased bone marrow homing, which is associated with impaired cytoskeletal activity (Scielzo et al., 2010; ten Hacken et al., 2013). Further underlining the potential clinical significance of HS1, more recently, it has been also shown that its association with ROR1 enhances CLL cell migration (Hasan et al., 2017).

These mechanisms imply an intracellular dynamics and redistribution of HS1 and its active/inactive forms that have not been studied in detail to date in B cells. Confocal microscopy studies have given only an overall visualization of HS1 in the extranuclear space. However, up to now little is known about the nanostructural features of HS1 in primary CLL cells obtained from patients with diverse prognoses. It is also missing a direct comparison with the HS1 patterns in model cell lines that, in contrast to primary CLL cells, are prone to genetic manipulation and, therefore, allow studies on the dynamics of HS1 relocations and interactions. The prerequisite for approaching this level of investigation is to determine how and where the total endogenous HS1 distributes in primary CLL cells and whether we find differences between normal B cells and CLL cells originated from patients with diverse prognoses. As a second step, we also aim at comparing the HS1 nanostructure organization in leukemic MEC1 cells, since this cell line can be used for controlling the expression of specific active/inactive HS1 forms and follow their intracellular dynamics.

In this work, we show for the first time that a 3D-STED super-resolution approach is instrumental for revealing HS1 clustering in primary CLL and B cells and a concentration gradient of the protein toward the adhesion sites, features that are well recapitulated in the MEC1 CLL cell line.

MATERIALS AND METHODS

Cells and Human Primary Sample Purification

CD19 cells were negatively selected from fresh pheripheral blood from patients or healthy donors using the RosetteSep B-lymphocyte enrichment kit (StemCell Technologies, Vancouver, Canada). Human healthy cells were further negatively selected using B-lymphocyte enrichment kit (StemCell Technologies, Canada). The purity of all preparations was always higher than 99%, and the cells co-expressing CD19 and CD5 on their surface as assayed by flow cytometry (Navios Beckman Coulter Life Science, Indianapolis IL, United States)

preparations were virtually devoid of natural killer cells, T lymphocytes, and monocytes.

The MEC1 cell line was obtained from Deutsche Sammlung von Mikroorganismen und Zellkulturen GmbH (DSMZ) and cultured in RPMI 1640 medium (Euroclone, Milan, Italy) supplemented with 10% volume/volume (v/v) fetal bovine serum (FBS) and 15 mg/ml gentamicin (complete RPMI) at 37°C and 5% CO_2. MEC1-HS1-YFP was generated by transfecting MEC1 cells, taking advantage of Nucleofector Technology (AMAXA) with the use of the program X-001, solution V.

The Vivid Colors^{TM} pcDNA^{TM}6.2/N-YFP-DEST Vector expressing the HS1 gene (Thermo Fisher Scientific, Waltham, MA, United States) was used for transfection and blasticidin (Thermo Fisher Scientific, United States) for the antibiotic selection.

Immunofluorescence Staining

Primary cells and cell lines (3×10^6) were seeded in medium on polyornithine:PBS (1:5)-coated coverslips (22 × 22-mm high-precision glass, code: 0101050, Marienfeld, Germany) and incubated for 2 h at 37°C and 5% CO_2. For single immunostaining of endogenous HS1, after removing the incubation medium, cells were washed with PBS, fixed with PFA 4%, incubated 15 min in the dark, and permeabilized in blocking buffer (blocking buffer: 0.1% w/v BSA, 10% v/v FBS in PBS), containing 0.3% v/v Triton-X 100 (Sigma-Aldrich, Merck, Germany), to limit unspecific antibody binding. Samples were incubated overnight at 4°C with a primary monoclonal anti-mouse HS1 Ab:PBS solution (code: 610541, BD Biosciences, San Jose, CA, United States) then labeled with an anti-mouse-Alexa 488 (code: A11001, Invitrogen, Thermo Fisher Scientific, United States) or anti-mouse-Alexa 568 (code: A11004, Invitrogen, Thermo Fisher Scientific, Waltham, MA, United States) for 2 h at RT and in the dark. The lack of cross-reactivity for cortactin was checked by applying the immunostaining protocol to fibroblasts, which have a high expression of cortactin but lack HS1 (**Supplementary Figure 1**).

For double HS1-Vimentin immunolabeling in MEC1-YFP-HS1 cells, we followed the above protocol modifying the fixation step to PFA 1% for 15 min. Samples were incubated overnight at 4°C with primary anti-goat YFP (600-101-215M, Thermo Fisher Scientific, United States) and monoclonal anti-mouse Vimentin (code: SC 6260, Santa Cruz Biotechnology, Santa Cruz, CA, United States), followed by incubation for 2 h at RT, in the dark with anti-goat-Alexa 568 (code: A11057, Invitrogen, Thermo Fisher Scientific, United States) and anti-mouse-Alexa 532 (code: A11002, Invitrogen, Thermo Fisher Scientific, United States).

For FRET experiments, MEC1 cells (4×10^6) were co-immunostained for endogenous HS1 and Vimentin. Fixation was in PFA 1% for 30 min at RT. Samples were blocked and incubated as above with a primary monoclonal anti-Vimentin-mouse (Santa Cruz Biotechnology, Inc., Santa Cruz, CA, United States) and anti-HS1-goat Abs, then labeled with anti-mouse-Alexa 546 and anti-goat-Alexa 488.

For microscopy, we used ProLong Gold or Diamond antifade reagents (Invitrogen, Thermo Fisher Scientific, United States) for B and CLL or Diamond for MEC1-HS1-YFP cells as mounting media.

Super-Resolution 3D-STED Microscopy

We used a gated STED-3X-WLL SP8 microscope (Leica Microsystems, Wetzlar, Germany) and a HC Pl Apo CS2 100x/1.40 oil objective for all experiments. The microscope was equipped with 592- and 660-nm depletion lasers, and the excitation was provided by a pulsed white laser. The acquisition software was LAS X 3.5.6.21594.

For cluster analysis on Alexa 488 immunolabeled HS1 in CLL and B cells, X,Y,Z depletion was obtained by a STED 592-nm laser set at 100% output in X, Y, and Z. Excitation at 489 nm was performed by a white laser fixed at 3%, applying a gated unidirectional resonant scanning mode with a 16-line average and 8-frame accumulation at 8,000 Hz scan speed. Fluorescence (508–555 nm) was collected using a HyD spectral detector in standard mode and a gating of 0.1. A zoom 2 was applied to acquire Z-stacks of 13 optical sections of 968 × 968 pixels at the center of the cells with a voxel size of 60 × 60 × 100 nm. This setting was chosen among others to maximize axial resolution and minimize photobleaching, autofluorescence, and reflections, keeping the white laser excitation at the minimum yet being capable of maintaining the same settings for all cells, which showed variable intensities (i.e., amount of stained HS1). Depletion laser power, image format, zoom, and scanning conditions were optimized according to the same principle to obtain minimal photobleaching and Z-distortion and define conditions applicable to all samples for a total of 220 cells. The image resolution under the conditions optimized for our samples was determined by measuring the X,Y,Z PSF in a 23-nm nanobead sample coated with the Alexa 488 fluorophore (GATTAquant GmbH, Germany) (**Supplementary Figure 2**).

To reconstruct the total intracellular distribution of Alexa 488 immunolabeled HS1 in primary CLL and B cell and in YFP-HS1 MEC1 samples, we acquired Z-stacks of about 4–7 μm under the above conditions. For Alexa 568-endogenous HS1 MEC1 cells, we depleted the samples at 660 nm. Line and frame accumulation was adapted to the Z-stack depth to minimize photobleaching by testing forward and backward scanning (**Supplementary Movie 1**), and voxel size was optimized for deconvolution.

For 2D-STED HS1-Vimentin colocalization in MEC1 cells, we worked with the 660-nm depletion line between frames, at 700 Hz unidirectional speed. A summary of the super-resolution acquisition conditions is given in **Supplementary Table 1**.

Image Analysis

For cluster analysis, undeconvolved STED Z-stacks were divided in single-cell ROIs. Each ROI was analyzed individually and, when necessary, postprocessed for bleaching by exponential fit Fiji (ImageJ) plugin. ROI Z-stacks with ≥10% bleaching were discarded. Cluster size was determined by IMARIS software (9.1.2 Oxford Instruments plc, Oxon OX13 5QX, United Kingdom). The lowest detectable limit was set equal to four voxels, based on the X,Y,Z resolution obtained for the 23-nm Alexa 488 beads (**Supplementary Figure 2**). The total volume

of each Z-stack was determined by local intensity thresholding above the background.

Deconvolution was performed on single-labeled whole-cell STED Z-stacks of primary CLL, B (Alexa 488-endogenous HS1) and MEC1 (Alexa 568-endogenous HS1 or YFP-HS1) cells and on the 2D-STED images of double immunolabeled MEC1 cells (Alexa 568-endogenous HS1 + Alexa 532-endogenous Vimentin). For deconvolution, we used the Huygens software (Scientific Volume Imaging BV, Hilversum, The Netherlands), applying the GMLE algorithm to the STED Z-stacks and the CLME algorithm to the 2D-STED images.

Colocalization analysis was performed by the ImageJ-Fiji Coloc 2 plugin software, and statistical analysis by GraphPad Prism software (GraphPad Software, San Diego, CA, United States).

FRET by Two Photon Phasor-FLIM

The two-photon laser scanning fluorescence microscope for FLIM experiments was assembled at the Laboratory for Fluorescence Dynamics (Irvine University, CA, United States) and was described in detail previously (Caiolfa et al., 2007; Digman et al., 2008). A 40 × 1.2 NA oil-immersion objective (Carl Zeiss, Inc., Germany) was used to acquire fluorescence and lifetime decays at 905-nm excitation. Before measurement, a slide with concentrated fluorescein, pH 9.0, was measured as the standard lifetime and compared with that of 4.04 ns, determined separately in a photoncounting spectrofluorometer (PC1; ISS Inc., Champaign, IL, United States). Images were collected with 0.75 and 1.84 mW laser power at the sample, in 256 × 256 pixel format, equivalent to 32 × 32 μm^2, with a pixel residence time of 16 or 64 μs, depending on the experiment. The total frame acquisition time was 1–4 s to avoid photobleaching. Several frames (10–30) were acquired and averaged for the analysis by SimFCS software (Laboratory for Fluorescence Dynamics Irvine University, CA, United States). FLIM analysis for deriving the FRETeff was performed using the phasor method (Caiolfa et al., 2007; Digman et al., 2008). Statistical analysis was performed by GraphPad Prism software (GraphPad Software, San Diego, CA, United States).

RESULTS

Immunolabeled Endogenous HS1 Is Recognized in Clusters in Primary CLL and Normal B Cells

We isolated primary leukemic B cells from PB samples obtained from patients (n = 11) (**Supplementary Table 2**; Hallek et al., 2008) with CLL and from healthy donors (n = 6) for determining the endogenous HS1 localization at the increased resolution of the 3D-STED imaging. To evaluate possible differences in HS1 activity linked to its localization and intracellular nanostructure in CLL, we stratified the patients based on the mutational status of the IGHV being HS1 downstream the B cell receptor (Castro-Ochoa et al., 2019). We considered that, in CLL patients managed with active surveillance, the IGHV unmutated status is the biomarker with the strongest effect on time to first treatment prognostication (Condoluci et al., 2020). Accordingly, mutated IGHV was associated with patients with good prognosis (mCLL, n = 6), and unmutated IGHV identified patients with poor prognosis (uCLL, n = 5).

Endogenous immunolabeled-Alexa 488 HS1 in B and CLL cells was compared by confocal and STED microscopy (**Figure 1A**), examining sagittal sections of 1.3 μm. Confocal images depict a rough distribution, heavily distorted along the Z-axis of the protein that accumulates in the extranuclear volume. In these images, however, we can detect disperse clusters penetrating in the nucleus with an apparent volume of about 0.001 μm^3, suggesting that the protein would have a cluster-like distribution all over the cell. From this initial observation, we concluded that the information attainable by conventional 2D-STED, although at the highest X,Y resolution, is biased by the lack of resolution along the Z-axis, merging the signal spread perpendicularly inside the cell. Moreover, considering that primary CLL cells are roundish and small (about 5–7 micron), with the nucleus that occupies most of the intracellular space, and that we expect inter- and intra-patient heterogeneity, a single X,Y 2D-STED plane would give insufficient information to derive conclusions about the distribution of the HS1 protein from a single patient, and from different patients. Therefore, we accepted the compromise of reducing X,Y resolution and introduced depletion along the Z-axis, obtaining a more isotropic 3D-STED voxel (**Supplementary Figure 2**) that moderates the imaging distortions, allows to collect optical sections, and increases the significance of our analysis. **Figure 1A** shows the related 3D-STED images in which the HS1 clustering is evident throughout the cell section. The discrete distribution of HS1 in the example in **Figure 1A** was quantified by the number of identified clusters per imaged volume in 3D-STED Z-stacks in **Figure 1B**.

We compared the results from primary cells, with the distribution of the immunolabeled endogenous HS1 in MEC1 cells, observing a similar pattern of discrete clusters (**Figure 1C**). Additionally, to exclude that HS1 clustering was, to some extent, induced by the immunostaining protocol, we also investigated the distribution of a YFP-labeled HS1 overexpressed in MEC1 cells. The genetically labeled protein was found again in clusters, recapitulating the nanostructural features observed in primary CLL cells (**Figure 1D**).

On the one hand, these results provide the first high-resolution visualization of endogenous HS1 recruited in distinct clusters in primary normal and leukemic B cells. On the other hand, they also suggest that MEC1 cells might be a suitable model for characterizing the role of the active protein by means of genetically modified lines.

Endogenous HS1 Clusters Differentiate uCLL From mCLL and Normal B Cells

We pursued an analysis of single cells in single-patient samples, applying a 3D-STED protocol optimized as above to characterize HS1 clusters in B, uCLL, and mCLL cells and assess in-sample and interpatient heterogeneity. Primary cells were plated on precoated polyornithine coverslips and

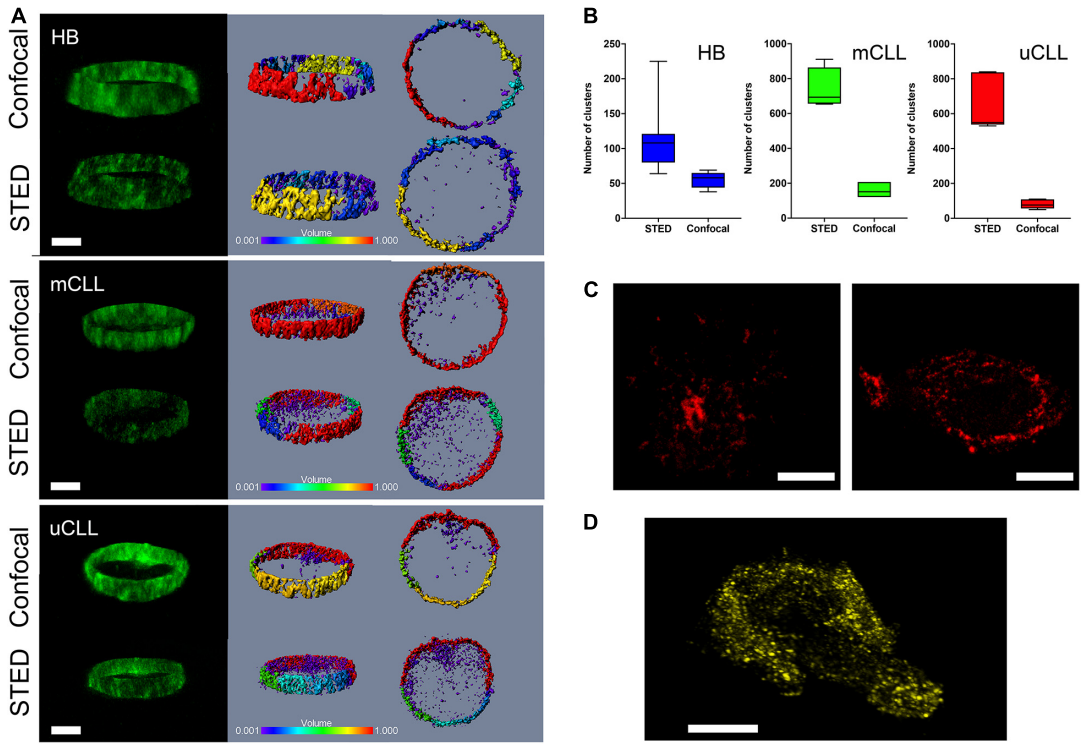

FIGURE 1 | Immunolabeled endogenous HS1 is recognized in clusters in primary CLL and normal B cells. **(A)** Comparison of confocal and STED Z-stacks acquired in central cell regions of Alexa 488-endogenous HS1 in HB, mCLL, and uCLL cells. Fluorescence intensity X,Z stereo view (green pseudo color, left), cluster size stereo view X,Z and X,Y (rainbow pseudo color in μm^3, middle and right). Scale bar 4 μm. **(B)** Histogram of cluster number determined by the IMARIS software in the three confocal and STED examples shown in **(A)**. **(C)** HS1 clusters detected by STED in two representative MEC1 cells stained for Alexa 568-endogenous HS1. Scale bar 4 μm. **(D)** STED Z-stack stereo view of a representative MEC1 cell overexpressing YFP-HS1. Scale bar 4 μm.

Alexa 488-immunostained for HS1. Firstly, each sample was inspected by tiled confocal microscopy to estimate the number of cells in the sample, cellular integrity, density, and dispersion on the coverslip (**Supplementary Figure 3**). We detected a minor number of cell contacts that were easily distinguishable from rare immune-synapse-like events, possibly due to minor T cell contamination (**Supplementary Figure 3**). In both cases, cells engaged in pairs were excluded from the analysis.

For cluster analysis, we standardized data collection by acquiring a fixed volume above and below the center of each single cell (**Figure 2A**) and used the Imaris software for calculating the cluster number, size (**Figure 2B**, top), and volume of the imaged cellular section (**Figure 2B**, bottom).

In all cells, cluster size followed a non-parametric distribution which is well represented by a median value (**Supplementary Figure 4**). **Figure 2C** illustrates these results from the analysis of nine cells from patient P4 in a log-Y scatter plot (**Supplementary Table 2**). In these cells, cluster size varied from a minimum of 0.0002 μm^3 to a maximum of 1 μm^3, giving median values ranging from 0.0015 to 0.0053 μm^3 (red bars in **Figure 2C**). The analysis was repeated on all single cells in patient samples, and the median values were compared (**Figure 2D**). In the group of patients P4, P5, P6, P7, and P11 associated with poor CLL prognosis (**Supplementary Table 2**), HS1 clusters were small and less variable in size, except for patient P4. Despite the unmuted IGHV identity, cells from patient P4 showed a large variability of HS1 clusters, which was not observed in patient P6 that had the same IGHV identity (**Figure 2D** and **Supplementary Table 2**). This discrepancy is likely due to our approach of identifying the patients' groups without considering other prognostic factors (Chen and Puvvada, 2016). Nevertheless, in the primary CLL cells from this group of patients, we found significantly smaller HS1 clusters (**Figure 2E**), which were clearly distinguishable from the HS1 clusters identified in mCLL patients with good prognosis and B cells from healthy donors. HS1 cluster size in the latter two groups, mCLL cells (patients P1, P2, P3, P8, P9, P10) and normal B cells (healthy H1, H2, H3, H4, H5, H6), was largely scattered (**Figure 2D**) and did not allow to distinguish the two groups (**Figure 2E**).

In addition to the size, we also counted the number of HS1 clusters in single-cell sections and found that HS1 forms not only smaller but also more numerous clusters in uCLL cells as compared to mCLL and normal B cells (**Figure 2F**). Because of these differences, the density per volume unit of the HS1 protein is higher in uCLL cells (**Figure 2G**).

Altogether, the results indicate that endogenous HS1 has a distinct distribution in uCLL derived from patients with poor prognosis. Only in these cells, the protein is packed in a high

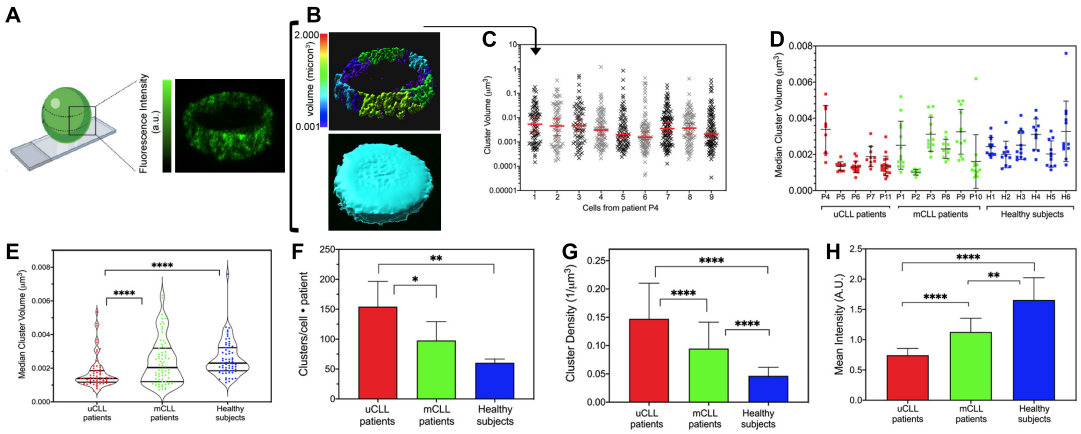

FIGURE 2 | Cluster analysis in primary CLL and healthy B cells. **(A)** Schematic representation created by www.biorender.com that illustrates the position chosen for the analysis of Alexa 488-immunolabeled HS1 clusters (right) and a representative single-cell STED Z-stack (left). **(B)** Example of the IMARIS cluster analysis (rainbow volume scale, top) and of the total volume enclosing the clusters used for data normalization (turquoise, bottom). Size is expressed in μm^3. **(C)** Representative clusters measured in nine primary cells from patient P4. Data are plotted in log-Y scale, and the median and interquartile ranges are shown (red bars). **(D)** Scatter plot illustrating the median cluster size resulting from the analysis of the cells of each patient. Each dot is the median cluster size in a single cell. Black bars indicate the mean (±SD) value for each patient sample. Patients with poor prognosis, uCLL: P4, P5, P6, P7, P11; patients with good outcome, mCLL: P1, P2, P3, P8, P9, P10; normal subjects, HB1–HB6. **(E)** Violin plot resuming the cluster size distribution per group of patients and healthy subjects. Each dot is the median cluster size in a single cell and patient. Black lines: median distribution with quartiles. uCLL vs. HB: $^{****}P < 0.0001$; uCLL vs. mCLL: $^{****}P < 0.0007$; mCLL vs. Healthy: not significant. **(F)** Histogram of total number of clusters normalized by the number of cells and number of subjects included in each group (mean ± SD). uCLL vs. Healthy: $^{**}P < 0.0012$; uCLL vs. mCLL: $^{*}P < 0.0193$; mCLL vs. Healthy: not significant. **(G)** Histogram of cluster densities (mean ± SD) per group of subjects. Data are normalized for the volume of the Z-stack of each cell, for the number of cells, and for the number of patients/subjects in each group. uCLL vs. Healthy: $^{****}P < 0.0001$; uCLL vs. mCLL: $^{****}P < 0.0001$; mCLL vs. Healthy: $P < 0.0001$. **(H)** Histogram of the fluorescence intensities (mean ± SD) Data are normalized for the number of cells and number of patients/subjects in each group. uCLL vs. Healthy: $^{****}P < 0.0001$; uCLL vs. mCLL: $^{****}P < 0.0013$; mCLL vs. Healthy: $^{**}P < 0.0001$. See **Supplementary Table 1** for patients' details. Two-way ANOVA was applied for the statistical significance in **(E–H)**. uCLL 64 cells from 5 patients; mCLL 60 cells from 6 patients; Healthy 66 cells from 6 normal subjects.

number of very small clusters forming a dense, punctuate filling of the extranuclear regions. Interestingly, the fluorescence intensity of the Alexa488-HS1 clusters in uCLL is much lower than in mCLL and normal B cells, suggesting that overall the concentration of the protein in the analyzed regions is lower (**Figure 2H**).

With this analysis, we can also point out to some differences between mCLL and normal B cells. Although at the level of the HS1 cluster size these two groups are not clearly different, the number of clusters (**Figure 2F**) and the density of the protein in the central cell regions (**Figure 2G**) are higher in mCLL cells than in normal B cells. Finally, also in mCLL cells, the intensity of the immunolabeled HS1 is lower than in normal B cells, indicating again a different organization of the protein among the three groups (**Figure 2H**).

HS1 Clusters Form a Concentration Gradient Toward the Adhesion Sites

The differences of HS1 clustering observed in central regions of primary uCLL, mCLL, and normal B cells might be indicative of differences in the total intracellular distribution of the protein among the three groups of subjects. Thus, based on previous evidences on the role of HS1 in cell adhesion and its implication in cytoskeleton rearrangements in CLL cells (Scielzo et al., 2010), we asked whether the HS1 distribution would change toward the adhesion sites of normal B and CLL cells.

We examined regions in contact with the cell support and observed an accumulation of HS1 clusters in healthy B cells (**Figure 3A**, top, **Figure 3B**, left). In uCLL cells, HS1 accumulate more toward the adhesion site, coalescing in large assemblies (**Figure 3A**, bottom, **Figure 3B**, right). According to the volume analysis (**Figure 3C**), the accumulation of the protein at the adhesion sites is much higher in CLL cells in comparison to healthy B cells (**Figure 3D**).

The whole-cell 3D rendering of STED Z-stacks gives an overall view of the HS1 cluster distribution (**Figure 3E** and **Supplementary Movies 2–4**). It is noteworthy that the cellular volume delineated by the distribution of immunolabeled HS1 is comparable to that obtained in SEM (**Supplementary Figure 5**), demonstrating how the 3D-STED protocol developed in this work minimizes the volumetric distortions typical of fluorescence microscopy, which have detrimental effects on the analysis of protein clusters and small aggregates.

The 3D-STED images show, at unprecedented resolution, how the endogenous protein clusters fill the tiny volume surrounding the nucleus. In uCLL cells (**Figure 3E**, right), HS1 clusters become an unresolved and dense surface toward the basal side, adhering to the coverslip. A similar concentration gradient is not observed in healthy B cells (**Figure 3E**, left) and in mCLL cells (**Figure 3E**, middle).

These results agree with the previous observations suggesting the recruitment of HS1 for cell adhesion, and its co-actor role in the cytoskeleton rearrangement. Moreover, the results also

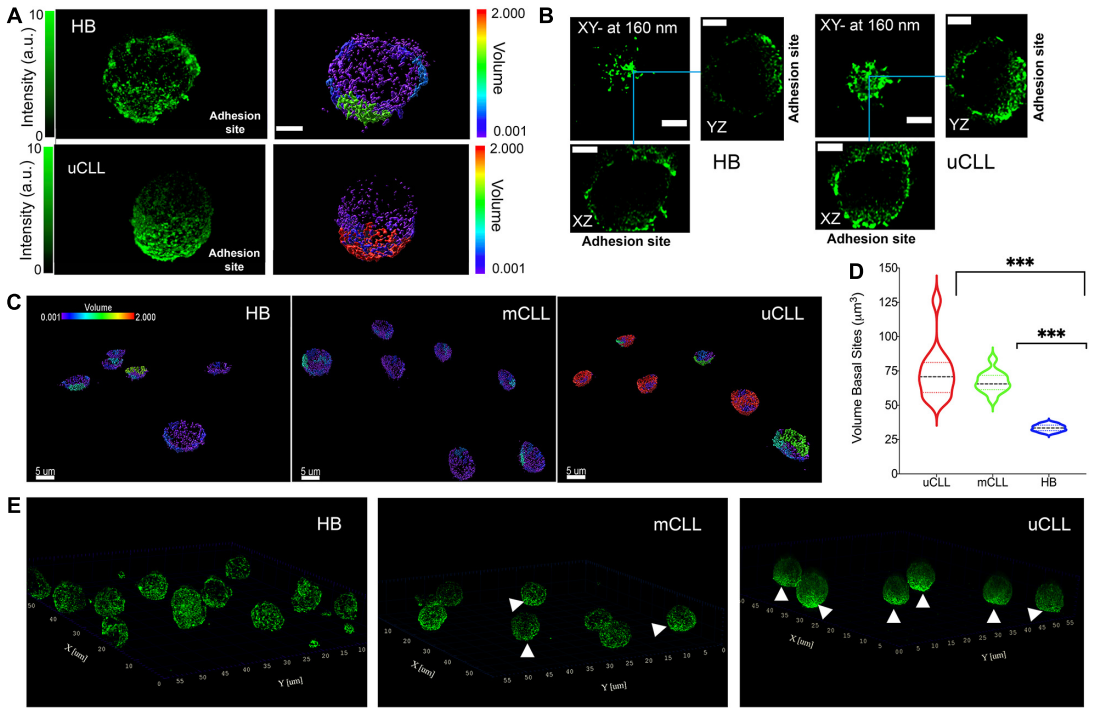

FIGURE 3 | Concentration gradient of HS1 clusters toward the adhesion sites. **(A)** Representative 3D rendering of STED Z-stacks acquired on a single HB and uCLL cells. The fluorescence intensity (green pseudo color) is compared with the cluster size reconstruction by IMARIS software (rainbow pseudo color in μm^3). Scale bar 2 μm. **(B)** Orthogonal projections of the cells shown in **(A)** from 0 to 160 nm above the basal side. Blue lines indicate the orthogonal cross. Scale bar 2 μm. **(C)** Representative 3D rendering of STED Z-stacks acquired at the lowest planes above the coverslip and over a field of view of six or seven cells in parallel experiments. HS1 accumulates in unresolved assemblies in cells obtained from a patient with poor prognosis (uCLL) compared to the more homogeneous cluster distribution of the protein in healthy B cells (HB) and in CLL cells from a patient with good outcome (mCLL). The volume pseudo rainbow scale is in μm^3. **(D)** Violin plot distributions of the cluster size at basal side. HB 7 cells, median 33.5, interquartile 31.6/35.6; mCLL cells 13 from two patients, median 65.5, interquartile 61.4/71.8; uCLL cells 13 from two patients, median 77.8, interquartile 59.3/81.2. Two way ANOVA ***P = 0.0003. **(E)** Whole-cell 3D-rendering of STED Z-stacks showing the distribution of endogenous HS1 in healthy B (HB) and CLL cells obtained from patients with good (mCLL) or poor (uCLL) prognosis. The white arrows point to the HS1 accumulation.

highlight tiny differences at the level of the total endogenous HS1 distribution, distinguishing a clear concentration gradient in uCLL cells from patients with unfavorable prognosis.

MEC1 Cell Line Is a Valid Model to Recapitulate the Activity of Endogenous HS1 in Primary CLL Cells

With HS1 being involved in cytoskeleton dynamics, there is the need of valid cellular models expressing fluorescent HS1 variants, which cannot be obtained in primary cells. With this aim, we validated the MEC1 CLL line as a suitable model for live cell studies. Our results demonstrate that the tiny cluster distribution of endogenous HS1 observed in primary cells is maintained in immunolabeled MEC1, and it is similar to the distribution of YFP-HS1 overexpressed in these cells (**Figure 1**). We have also shown a concentration gradient of HS1 in primary cells toward the adhesion sites, supporting the role of HS1 as a cytoskeleton adapter. Therefore, we investigated the distribution of endogenous HS1 in comparison with Vimentin by co-immunolabeling MEC1 cells (**Figure 4**). 2D-STED images were acquired at the top plane (**Figure 4A**, top) and nearby the coverslip (**Figure 4A**, bottom). Our results suggest higher HS1-Vimentin colocalization toward the adhesion sites. Colocalization was also evident in the whole-cell stack (**Figure 4B**, left), and it was replicated in a high number of cells (**Figure 4B**, right).

We have also asked whether the colocalization of HS1 and Vimentin reports on a direct interaction between the two proteins, as previously suggested (Muzio et al., 2007). For this purpose, we used the two-photon phasor FLIM-FRET approach (representative experiment in **Figures 4C–H** and **Supplementary Figure 6**). Cells were immunolabeled for HS1 (FRET donor Alexa488) and Vimentin (FRET acceptor Alexa 546), and the fluorescence intensity image of a double-stained cell was recorded at the adhesion and top sites (**Figure 4C**). The fluorescence intensity image of a cell stained only for the unquenched HS1-Alexa 488 donor was acquired as control (**Figure 4D**). In parallel, the fluorescence lifetime decays were recorded and the entire distributions of the donor fluorescence lifetime in double (**Figures 4F,G**) or single-stained (control **Figures 4E,H**) cells were reported by a contour plot in polar coordinates. In these plots, the green lines represent the calibration obtained by measuring the lifetime distributions of donor-only cells at decreasing staining intensities in the presence of autofluorescence

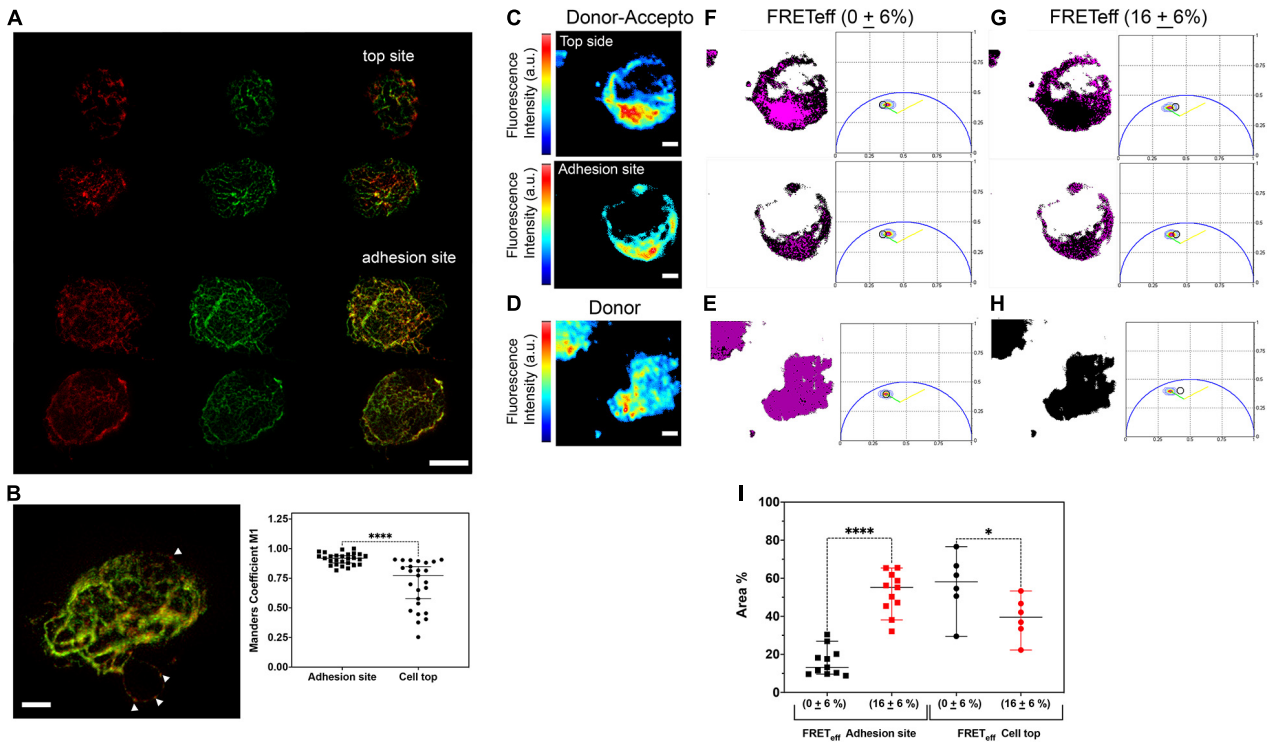

FIGURE 4 | MEC1 cells recapitulate the HS1 gradient of primary CLL cells. **(A)** Immunofluorescence 2D-STED images taken at the top and adhesion sites of representative MEC1 cells showing a colocalization gradient of endogenous HS1 and Vimentin. AntiHS1Ab568 (red), antiVimentinAb532 (green), and merged panels. Scale bar 4 μm. **(B)** Representative 3D rendering of a Z-stack of a double HS1-Vimentin-immunostained MEC1 whole cell (left, white arrows point to the HS1 accumulation), and plot of Manders' coefficients M1, proportional to the amount of fluorescence of the red channel (HS1) co-localizing with the green channel (Vimentin) in cell sections taken at the adhesion and top sites (right). Adhesion site 27 cells, top site 30 cells. Bars: mean ± SD. Mann–Whitney test $P < 0.0001$. Scale bar 2 μm. **(C–H)** Representative two-photon phasor-FLIM-FRET analysis of immunostained endogenous HS1-Alexa488 (donor) and endogenous Vimentin-Alexa 546 (acceptor) in an MEC1 cell. Scale bars 4 μm. **(I)** Scatter plot of the normalized cell areas with FRETeff either negligible (0 ± 6%) or equal to 16 ± 6% measured at the adhesion and top sites in single cells. Areas are reported as % ratio between number of pixels with FRET (pink mask as in panels **E–H**) over the total image area (black mask as in panels **E–H**) at the adhesion and top sites. Bars: mean ± SD. $^{****}P < 0.0001$; $^{*}P = 0.0466$. Adhesion site (0 ± 6%) and (16 ± 6%): 11 cells; Top site (0 ± 6%) and (16 ± 6%): 6 cells.

(unstained cells). The calibration measures the decrease of the donor lifetime due to photobleaching. When donor quenching is due to FRET, the phasor distribution moves outside the green line, and the yellow lines in the phasor plots mark the position expected for 50% FRET efficiency in the presence of variable donor intensities as previously illustrated (Caiolfa et al., 2007).

In each phasor plot, the total fluorescence lifetime distribution is explored by a round cursor. The size of the round cursor was set according to the dispersion of the lifetime in the control cells which, in our experiments, was 6% (**Figure 4E**). The pixels selected inside the round cursor were then localized in the associated images by pink masks. As represented in this example of a double-stained cell (**Figures 4F,G**), pixels that fall into the uncertainty area (control pure donor, **Figure 4E**) were considered to give a negligible value of FRETeff = 0 + 6%. In contrast, pixels outside the area of the control (**Figure 4H**) gave an average FRETeff = 16 + 6%. While at the top of the cells FRETeff was mostly negligible, large areas occupied by interacting HS1 and Vimentin were again detected at the cell adhesion sites, indicating an interaction gradient that support the recruitment of HS1 in the cytoskeleton reorganization for cell adhesion (**Figure 4I**).

Thus, the results in MEC1 cells parallel the unique observations in primary CLL cells and validate this CLL line as a suitable tool for dissecting the specific role of the active/inactive HS1 forms.

DISCUSSION

CLL, the most common adult leukemia in the Western countries, is clinically very heterogeneous and is still uncured. It may express a pre-leukemic form (Caligaris-Cappio and Ghia, 2008; Dagklis et al., 2009; Rawstron, 2009) or appear with an indolent clinical course or as a progressive disease that in some cases transforms into an aggressive high-grade lymphoma (Dagklis et al., 2009; Rawstron, 2009; Fazi et al., 2011). CLL clinical course reflects biological heterogeneity, and patients are usually classified in two main subsets depending on good or poor prognosis, which are based on a set of prognostic factors for the disease outcome and survival. Several studies have demonstrated that differences in the clinical course of the disease can be partially explained by the presence (activation) or absence (inactivation) of

some biological markers with a prognostic value, including HS1 (Damle et al., 1999; Lanham et al., 2003; Wiestner et al., 2003; Apollonio et al., 2014).

HS1 has emerged as a key molecule involved in B-cell migration and specific organ homing especially to the bone marrow. HS1 acts as an actin regulator of the immune synapse in T cells (Gomez et al., 2006) and regulates adhesion, lytic synapse formation, cytolytic activity, and chemotaxis in NK cells (Butler et al., 2008). In both normal and leukemic B cells, HS1 interacts with cytoskeleton adapter proteins involved in cytoskeleton reorganization (Muzio et al., 2007). By dissecting HS1 molecular function in CLL cells, it was established that HS1 takes part in the formation of a complex together with the ZAP-70 kinase and several cytoskeleton adapters (HIP-55 and cortactin) and that it co-localizes with F-actin and Vimentin, thereby showing an enrolment in regulation of the B-cell cytoskeleton (Muzio et al., 2007). While a low Vimentin content of CLL cells correlates with an increased survival, the phosphorylation levels of HS1 relate to the clinical course of patients with CLL, with the hyperphosphorylated form of HS1 being associated with a more aggressive disease (Scielzo et al., 2005). Yet, it is still unclear to what extent HS1 has different functions in CLL and healthy B cells and what determines its prognostic value. Moreover, unraveling HS1 expression and activation could have potential implications also in other leukaemias and lymphomas in particular for T cell leukaemias, and for novel immune/cell therapies, such as CAR-T (El Hajj et al., 2020) and cell therapy (Cerrano et al., 2020), all these aspects have not been explored so far.

Thus, it is important to develop state-of-the-art approaches for complementing the study of HS1 as a structural adapter and signaling molecule related to immune response, migration, adhesion, transendothelial migration, and antigen recognition. With this objective in mind, we obtained a high-resolution visualization of HS1 in primary normal and leukemic cells, and then we compared the results with the distribution of the protein in the MEC1 cell line, also by overexpressing the YFP-HS1 fluorescent variant. Our goal has been twofold: to provide the first refined structural pattern of the protein in primary cells and to investigate whether the MEC1 leukemic cell line can be considered a suitable model in which it is possible to dissect the functions of the specific phosphorylated forms of HS1 by genetically modified expression. Moreover, we divided CLL cells according to the IGHV mutational status of the donor patients in mCLL and uCLL and established a quantitative protocol that has allowed to detect significant differences in the distribution and organization of endogenous HS1 among cells from the two groups of patients and in comparison with normal B cells.

Our results reveal with an unprecedented level of details that endogenous HS1 in primary CLL cells forms nanoclusters all over the extranuclear cell body, with a density gradient toward the adhesion site of the cells. We were able to correlate the HS1 clustering with the mutational state of IGHV and show that in uCLL cells from patients with adverse outcome HS1 clusters are distinguishably smaller, yet highly packed and recruited at the cell adhesion plane. In contrast, in mCLL, cells from patients manifesting a mild prognosis, HS1 clustering in terms of size, number, and concentration gradient showed intermediate values between the extreme features of uCLL cells and the normal features of healthy B cells.

HS1 nanoclusters were recognized also in the MEC1 CLL line, either by immunofluorescence labeling of the endogenous protein or by overexpression of the YFP-HS1 fluorescent variant, demonstrating that the peculiar HS1 clustering is not antibody-induced or dependent on the overexpression of a YFP-tagged form. At the same time, these parallel experiments also validated the MEC1 line as a suitable model for genetic induction of specific HS1 forms, which cannot be performed in primary cells. Since the coalescence of HS1 clusters at the basal side of primary cells alluded to the binding of the protein to the cytoskeleton as previously described, we further tested the MEC1 model by evaluating the positive co-localization at the STED resolution and the direct interaction with Vimentin by a phasor-FLIM-FRET analysis, which showed an increased interaction at the basal sides.

In the present work, we describe a pioneer approach in the field of B cell biology that paves the way to improve the functional characterization of the active/inactive forms of HS1, their intracellular distribution, nanoscale colocalization, and direct molecular interactions.

Thereby, we decided to limit the present study to cells adhered on polyornithine dishes only, to overcome the complexity of CLL adhesion processes and intrinsic adhesive capacity variability (ten Hacken et al., 2013). Further analysis with other types of ECM components, stromal cell cocultures, and/or selected antigens will be addressed in the future to explore the effect of specific microenvironments on the possible re-localization of HS1 clustering and to study its phosphorylations known to be activated following BCR stimulation.

Ultimately, the future combination of super-resolution 3D imaging with biochemical analyses might provide a robust and quantitative approach for determining whether different cellular distributions of the protein and its phosphorylated forms are associated with distinctive functions, further exploring the difference between leukemic cells and healthy B cells first in CLL and later in other leukaemias and lymphomas, engaging other cytoskeleton adaptors and modulators.

DATA AVAILABILITY STATEMENT

The raw data supporting the conclusions of this article will be made available by the authors, without undue reservation.

ETHICS STATEMENT

The studies involving human participants were reviewed and approved by the Ospedale San Raffaele (OSR) ethics committee under the protocol VIVI-CLL entitled: "*In vivo* and *in vitro* characterization on CLL." The buffy coats study was approved by the Ospedale San Raffaele (OSR) ethics committee under the protocol Leu-Buffy coat entitled: "Characterization of leukocyte subpopulations from buffy coats." The patients/participants provided their written informed consent to participate in this study.

AUTHOR CONTRIBUTIONS

MS performed the STED experiments and image analysis. AD did the confocal microscopy and helped in image analysis. MZ developed the IMARIS analysis method and did the FLIM experiments with the analysis. VLC contributed to the STED colocalization experiments. FB prepared the samples. LS provided the patients' cells and clinical information. CS provided all the reagents and cells and contributed to the experimental plan. VRC supervised the experiments and wrote the manuscript. CS, MZ, and MS revised the manuscript. All authors contributed to the article and approved the submitted version.

FUNDING

This project was supported in part by Associazione Italiana per la Ricerca sul Cancro AIRC (Special Program on Metastatic Disease—5 per mille #21198) and first grant AIRC (#17006) P.I. CS. The research leading to these results has received funding from AIRC under IG 2018–ID. 21332 project—P.I. CS. CNIC was supported by the Ministerio de Ciencia, Innovación y Universidades, and the Pro CNIC Foundation. VRC acknowledges the support of FEDER "Una manera de hacer Europa" for the project *In Vivo Advanced Nanoscopy at the ICTS—ReDib—TRIMA—CNIC* 2018–2021.

ACKNOWLEDGMENTS

We thank Elvira Arza (Microscopy and Dynamic Unit at CNIC) for helpful suggestions and technical support. We also thank Barbara Vergani and Antonello Villa (Milano Bicocca University) for providing the SEM image.

SUPPLEMENTARY MATERIAL

The Supplementary Material for this article can be found online at: https://www.frontiersin.org/articles/10.3389/fcell.2021.655773/full#supplementary-material

REFERENCES

Apollonio, B., Bertilaccio, M. T., Restuccia, U., Ranghetti, P., Barbaglio, F., Ghia, P., et al. (2014). From a 2DE-gel spot to protein function: lesson learned from HS1 in chronic lymphocytic leukemia. *J. Vis. Exp.* 92:e51942.

Burger, J. A. (2010). Chemokines and chemokine receptors in chronic lymphocytic leukemia (CLL): from understanding the basics towards therapeutic targeting. *Semin. Cancer Biol.* 20, 424–430. doi: 10.1016/j.semcancer.2010.09.005

Burger, J. A., and Gribben, J. G. (2014). The microenvironment in chronic lymphocytic leukemia (CLL) and other B cell malignancies: insight into disease biology and new targeted therapies. *Semin. Cancer Biol.* 24, 71–81. doi: 10.1016/j.semcancer.2013.08.011

Butler, B., Kastendieck, D. H., and Cooper, J. A. (2008). Differently phosphorylated forms of the cortactin homolog HS1 mediate distinct functions in natural killer cells. *Nat. Immunol.* 9, 887–897. doi: 10.1038/ni.1630

Caiolfa, V. R., Zamai, M., Malengo, G., Andolfo, A., Madsen, C. D., Sutin, J., et al. (2007). Monomer dimer dynamics and distribution of GPI-anchored uPAR are determined by cell surface protein assemblies. *J. Cell Biol.* 179, 1067–1082. doi: 10.1083/jcb.200702151

Caligaris-Cappio, F., Bergui, L., Tesio, L., Corbascio, G., Tousco, F., and Marchisio, P. C. (1986). Cytoskeleton organization is aberrantly rearranged in the cells of B chronic lymphocytic leukemia and hairy cell leukemia. *Blood* 67, 233–239. doi: 10.1182/blood.v67.1.233.bloodjournal671233

Caligaris-Cappio, F., Bertilaccio, M. T., and Scielzo, C. (2014). How the microenvironment wires the natural history of chronic lymphocytic leukemia. *Semin. Cancer Biol.* 24, 43–48. doi: 10.1016/j.semcancer.2013.06.010

Caligaris-Cappio, F., and Ghia, P. (2008). Novel insights in chronic lymphocytic leukemia: are we getting closer to understanding the pathogenesis of the disease? *J. Clin. Oncol.* 26, 4497–4503. doi: 10.1200/jco.2007.15.4393

Calissano, C., Damle, R. N., Hayes, G., Murphy, E. J., Hellerstein, M. K., Moreno, C., et al. (2009). In vivo intraclonal and interclonal kinetic heterogeneity in B-cell chronic lymphocytic leukemia. *Blood* 114, 4832–4842. doi: 10.1182/blood-2009-05-219634

Castro-Ochoa, K. F., Guerrero-Fonseca, I. M., and Schnoor, M. (2019). Hematopoietic cell-specific lyn substrate (HCLS1 or HS1): a versatile actin-binding protein in leukocytes. *J. Leukoc Biol.* 105, 881–890. doi: 10.1002/jlb.mr0618-212r

Cerrano, M., Ruella, M., Perales, M. A., Vitale, C., Faraci, D. G., Giaccone, L., et al. (2020). The advent of CAR T-cell therapy for lymphoproliferative neoplasms: integrating research into clinical practice. *Front. Immunol.* 11:888.

Chen, C., and Puvvada, S. (2016). Prognostic factors for chronic lymphocytic leukemia. *Curr. Hematol. Malig. Rep.* 11, 37–42. doi: 10.1007/s11899-015-0294-x

Condoluci, A., Terzi di Bergamo, L., Langerbeins, P., Hoechstetter, M. A., Herling, C. D., Paoli, L. De, et al. (2020). International prognostic score for asymptomatic early-stage chronic lymphocytic leukemia. *Blood* 135, 1859–1869.

Dagklis, A., Fazi, C., Scarfo, L., Apollonio, B., and Ghia, P. (2009). Monoclonal B lymphocytosis in the general population. *Leuk. Lymphoma* 50, 490–492. doi: 10.1080/10428190902763475

Damle, R. N., Wasil, T., Fais, F., Ghiotto, F., Valetto, A., Allen, S. L., et al. (1999). Ig V gene mutation status and CD38 expression as novel prognostic indicators in chronic lymphocytic leukemia. *Blood* 94, 1840–1847. doi: 10.1182/blood.v94.6.1840.418k06_1840_1847

Digman, M. A., Caiolfa, V. R., Zamai, M., and Gratton, E. (2008). The phasor approach to fluorescence lifetime imaging analysis. *Biophys. J.* 94, L14–L16.

El Hajj, H., Tsukasaki, K., Cheminant, M., Bazarbachi, A., Watanabe, T., and Hermine, O. (2020). Novel treatments of adult T cell leukemia lymphoma. *Front. Microbiol.* 11:1062.

Fazi, C., Scarfo, L., Pecciarini, L., Cottini, F., Dagklis, A., Janus, A., et al. (2011). General population low-count CLL-like MBL persists over time without clinical progression, although carrying the same cytogenetic abnormalities of CLL. *Blood* 118, 6618–6625. doi: 10.1182/blood-2011-05-357251

Gomez, T. S., McCarney, S. D., Carrizosa, E., Labno, C. M., Comiskey, E. O., Nolz, J. C., et al. (2006). HS1 functions as an essential actin-regulatory adaptor protein at the immune synapse. *Immunity* 24, 741–752. doi: 10.1016/j.immuni.2006.03.022

Hallek, M., Cheson, B. D., Catovsky, D., Caligaris-Cappio, F., Dighiero, G., Dohner, H., et al. (2008). Guidelines for the diagnosis and treatment of chronic lymphocytic leukemia: a report from the International workshop on chronic lymphocytic leukemia updating the national cancer institute-working group 1996 guidelines. *Blood* 111, 5446–5456. doi: 10.1182/blood-2007-06-093906

Hao, J. J., Carey, G. B., and Zhan, X. (2004). Syk-mediated tyrosine phosphorylation is required for the association of hematopoietic lineage cell-specific protein 1 with lipid rafts and B cell antigen receptor signalosome complex. *J. Biol. Chem.* 279, 33413–33420. doi: 10.1074/jbc.m313564200

Hasan, M. K., Yu, J., Chen, L., Cui, B., Widhopf Ii, G. F., Rassenti, L., et al. (2017). Wnt5a induces ROR1 to complex with HS1 to enhance migration of chronic lymphocytic leukemia cells. *Leukemia* 31, 2615–2622. doi: 10.1038/leu.2017.133

Helgeson, L. A., and Nolen, B. J. (2013). Mechanism of synergistic activation of Arp2/3 complex by cortactin and N-WASP. *Elife* 2:e00884.

Herishanu, Y., Perez-Galan, P., Liu, D., Biancotto, A., Pittaluga, S., Vire, B., et al. (2011). The lymph node microenvironment promotes B-cell receptor signaling, NF-kappaB activation, and tumor proliferation in chronic lymphocytic leukemia. *Blood* 117, 563–574. doi: 10.1182/blood-2010-05-284984

Lanham, S., Hamblin, T., Oscier, D., Ibbotson, R., Stevenson, F., and Packham, G. (2003). Differential signaling via surface IgM is associated with VH gene mutational status and CD38 expression in chronic lymphocytic leukemia. *Blood* 101, 1087–1093. doi: 10.1182/blood-2002-06-1822

Muzio, M., Scielzo, C., Frenquelli, M., Bachi, A., De Palma, M., Alessio, M., et al. (2007). HS1 complexes with cytoskeleton adapters in normal and malignant chronic lymphocytic leukemia B cells. *Leukemia* 21, 2067–2070. doi: 10.1038/sj.leu.2404744

Ponzoni, M., Doglioni, C., and Caligaris-Cappio, F. (2011). Chronic lymphocytic leukemia: the pathologist's view of lymph node microenvironment. *Semin. Diagn. Pathol.* 28, 161–166. doi: 10.1053/j.semdp.2011.02.014

Rawstron, A. C. (2009). Monoclonal B-cell lymphocytosis. *Hematol. Am. Soc. Hematol. Educ. Program*. 9, 430–439. doi: 10.1182/asheducation-2009.1.430

Ruzzene, M., Brunati, A. M., Marin, O., Donella-Deana, A., and Pinna, L. A. (1996). SH2 domains mediate the sequential phosphorylation of HS1 protein by p72syk and Src-related protein tyrosine kinases. *Biochemistry* 35, 5327–5332. doi: 10.1021/bi9528614

Scherer, A. N., Anand, N. S., and Koleske, A. J. (2018). Cortactin stabilization of actin requires actin-binding repeats and linker, is disrupted by specific substitutions, and is independent of nucleotide state. *J. Biol. Chem.* 293, 13022–13032. doi: 10.1074/jbc.ra118.004068

Schnoor, M., Stradal, T. E., and Rottner, K. (2018). Cortactin: cell functions of a multifaceted actin-binding protein. *Trends Cell Biol.* 28, 79–98. doi: 10.1016/j.tcb.2017.10.009

Scielzo, C., Bertilaccio, M. T., Simonetti, G., Dagklis, A., ten Hacken, E., Fazi, C., et al. (2010). HS1 has a central role in the trafficking and homing of leukemic B cells. *Blood* 116, 3537–3546. doi: 10.1182/blood-2009-12-258814

Scielzo, C., Ghia, P., Conti, A., Bachi, A., Guida, G., Geuna, M., et al. (2005). HS1 protein is differentially expressed in chronic lymphocytic leukemia patient subsets with good or poor prognoses. *J. Clin. Invest.* 115, 1644–1650. doi: 10.1172/jci24276

Skokowa, J., Klimiankou, M., Klimenkova, O., Lan, D., Gupta, K., Hussein, K., et al. (2012). Interactions among HCLS1, HAX1 and LEF-1 proteins are essential for G-CSF-triggered granulopoiesis. *Nat. Med.* 18, 1550–1559. doi: 10.1038/nm.2958

Stark, R. S., Liebes, L. F., Shelanski, M. L., and Silber, R. (1984). Anomalous function of vimentin in chronic lymphocytic leukemia lymphocytes. *Blood* 63, 415–420. doi: 10.1182/blood.v63.2.415.bloodjournal632415

Tausch, E., Mertens, D., and Stilgenbauer, S. (2014). Advances in treating chronic lymphocytic leukemia. *F1000Prime Rep.* 6:65.

ten Hacken, E., Scielzo, C., Bertilaccio, M. T., Scarfo, L., Apollonio, B., Barbaglio, F., et al. (2013). Targeting the LYN/HS1 signaling axis in chronic lymphocytic leukemia. *Blood* 121, 2264–2273. doi: 10.1182/blood-2012-09-457119

Uruno, T., Zhang, P., Liu, J., Hao, J. J., and Zhan, X. (2003). Haematopoietic lineage cell-specific protein 1 (HS1) promotes actin-related protein (Arp) 2/3 complex-mediated actin polymerization. *Biochem. J.* 371, 485–493. doi: 10.1042/bj20021791

van Rossum, A. G., Schuuring-Scholtes, E., van Buuren-van Seggelen, V., Kluin, P. M., and Schuuring, E. (2005). Comparative genome analysis of cortactin and HS1: the significance of the F-actin binding repeat domain. *BMC Genomics* 6:15.

Wiestner, A., Rosenwald, A., Barry, T. S., Wright, G., Davis, R. E., Henrickson, S. E., et al. (2003). ZAP-70 expression identifies a chronic lymphocytic leukemia subtype with unmutated immunoglobulin genes, inferior clinical outcome, and distinct gene expression profile. *Blood* 101, 4944–4951. doi: 10.1182/blood-2002-10-3306

Yamanashi, Y., Fukuda, T., Nishizumi, H., Inazu, T., Higashi, K., Kitamura, D., et al. (1997). Role of tyrosine phosphorylation of HS1 in B cell antigen receptor-mediated apoptosis. *J. Exp. Med.* 185, 1387–1392. doi: 10.1084/jem.185.7.1387

Yamanashi, Y., Okada, M., Semba, T., Yamori, T., Umemori, H., Tsunasawa, S., et al. (1993). Identification of HS1 protein as a major substrate of protein-tyrosine kinase(s) upon B-cell antigen receptor-mediated signaling. *Proc. Natl. Acad. Sci. U.S.A.* 90, 3631–3635. doi: 10.1073/pnas.90.8.3631

Conflict of Interest: The authors declare that the research was conducted in the absence of any commercial or financial relationships that could be construed as a potential conflict of interest.

frontiers in Cell and Developmental Biology

MINI REVIEW
published: 02 August 2021
doi: 10.3389/fcell.2021.679500

The Actin Cytoskeleton at the Immunological Synapse of Dendritic Cells

José Luis Rodríguez-Fernández and Olga Criado-García*

Department of Cellular and Molecular Biology, Centro de Investigaciones Biológicas Margarita Salas, Consejo Superior de Investigaciones Científicas, Madrid, Spain

Dendritic cells (DCs) are considered the most potent antigen-presenting cells. DCs control the activation of T cells (TCs) in the lymph nodes. This process involves forming a specialized superstructure at the DC-TC contact zone called the immunological synapse (IS). For the sake of clarity, we call IS(DC) and IS(TC) the DC and TC sides of the IS, respectively. The IS(DC) and IS(TC) seem to organize as multicentric signaling hubs consisting of surface proteins, including adhesion and costimulatory molecules, associated with cytoplasmic components, which comprise cytoskeletal proteins and signaling molecules. Most of the studies on the IS have focused on the IS(TC), and the information on the IS(DC) is still sparse. However, the data available suggest that both IS sides are involved in the control of TC activation. The IS(DC) may govern activities of DCs that confer them the ability to activate the TCs. One key component of the IS(DC) is the actin cytoskeleton. Herein, we discuss experimental data that support the concept that actin polarized at the IS(DC) is essential to maintaining IS stability necessary to induce TC activation.

Keywords: dendritic cell, immunological synapse, actin, T cell activation, cytoskeleton

Lord Carnarvon: "Can you see anything?"
Howard Carter: "Yes, wonderful things!"

An exchange between wealthy patron Carnavon and archeologist Carter after the latter peered through a hole into Tutankhamun's tomb.

OPEN ACCESS

Edited by:
Noa B. Martin-Cofreces, Princess Royal University Hospital, Spain

Reviewed by:
Lidija Radenovic, University of Belgrade, Serbia
Vincenzo Di Bartolo, Institut Pasteur, France

****Correspondence:***
José Luis Rodríguez-Fernández
rodrifer@cib.csic.es

Specialty section:
This article was submitted to Cell Adhesion and Migration, a section of the journal Frontiers in Cell and Developmental Biology

Received: *11 March 2021*
Accepted: *05 July 2021*
Published: *02 August 2021*

Citation:
Rodríguez-Fernández JL and Criado-García O (2021) The Actin Cytoskeleton at the Immunological Synapse of Dendritic Cells. Front. Cell Dev. Biol. 9:679500. doi: 10.3389/fcell.2021.679500

INTRODUCTION

Dendritic cells (DCs) are the most potent antigen-presenting cells (APCs; Banchereau and Steinman, 1998). There are two main groups of DCs: conventional and plasmacytoid (Banchereau and Steinman, 1998; Merad et al., 2013). DCs are found in tissues in the immature differentiation stage. In the presence of pathogens, they undergo a process of differentiation called maturation, which involves multiple phenotypical changes, including the upregulation of major histocompatibility complex class I (MHC-I) and class II (MHC-II) and costimulatory molecules, like CD80 and CD86. Mature DCs migrate to the lymph nodes (LNs), where they present pathogen-derived peptides *via* MHC-I to $CD8^+$ T cells (TCs) or *via* MHC-II to $CD4^+$ TCs, resulting in the activation of these lymphocytes. Hereafter, unless otherwise indicated, when we use the word DCs, we refer to the conventional mature DCs. Several studies have shown that activation of naïve TCs in the LNs involves, first, brief serial DC-TC encounters, which are antigen independent, followed by prolonged and stable antigen-dependent contacts that last several hours (Delon et al., 1998; Iezzi et al., 1998;

Stoll et al., 2002; Bajenoff et al., 2003; Bousso and Robey, 2003; Mempel et al., 2004; Miller et al., 2004; Shakhar et al., 2005; Celli et al., 2007). Finally, the TCs recover their motility and proliferate (Mempel et al., 2004; Celli et al., 2007; Scholer et al., 2008). The region of tight adhesion that connects DCs and TCs when they establish stable interactions is called the immunological synapse (IS). We call the DC and TC sides of the IS the IS(DC) and IS(TC), respectively. Most studies on the IS have centered on the IS(TC), and analyses of the IS(DC) are sparse (Riol-Blanco et al., 2009; Rodriguez-Fernandez et al., 2010a,b; Benvenuti, 2016; Verboogen et al., 2016; Gomez-Cabanas et al., 2019; Alcaraz-Serna et al., 2021). Herein, we analyze the role of the filamentous-actin (F-actin) cytoskeleton of the IS(DC) in TC activation.

ORGANIZATION OF THE PLASMA MEMBRANE PROTEINS COMPONENTS OF THE IS(DC)

The first studies on the IS focused on the IS(TC) (Monks et al., 1998; Grakoui et al., 1999). In one of the experimental models used, the $CD4^+$ TCs were plated on a glass-supported lipid bilayer that was converted into a surrogate APC by inserting the intercellular adhesion molecule 1 (ICAM-1), the ligand of the integrin lymphocyte function-associated antigen (LFA-1), and peptides bound to MHC (pMHC; Grakoui et al., 1999). In another model, the $CD4^+$ TCs were allowed to form IS with B cells (BCs; Monks et al., 1998; Grakoui et al., 1999). Following the binding of the TCs either to the glass-supported lipid bilayer or to the BCs, the costimulatory molecule CD28 and the TC receptor (TCR) clustered together in a region called the central supramolecular activation cluster (cSMAC). Contiguous to this region are found LFA-1 molecules that form a ring called peripheral SMAC (pSMAC). Large negatively charged molecules like CD43 and CD45 organize in an outermost ring called distal SMAC (dSMAC; Monks et al., 1998; Grakoui et al., 1999; Freiberg et al., 2002). Interestingly, when the DCs form the IS with TCs (naïve or activated) at the IS(TC), instead of the monocentric organization described above, surface proteins form multiple protein clusters that include TCRs, adhesion proteins, and costimulatory molecules (Brossard et al., 2005; Rothoeft et al., 2006; Reichardt et al., 2007; Fisher et al., 2008; Tseng et al., 2008; Thauland and Parker, 2010). The ability of the DCs to promote multicentric IS(TC) could contribute to explain why they are such potent APCs. Numerous clusters of CD3 and costimulatory molecules multiply the signaling from these receptors, resulting in robust TC activation (Leithner et al., 2021). Supporting this concept, TCs plated on surrogate-patterned APCs that promote TCR or CD28 clusters show enhanced functionality (Mossman et al., 2005; Shen et al., 2008).

POLARIZATION OF F-ACTIN AT THE IS(DC)

The following examples, in which fixed cells were stained with phalloidin, show that F-actin polarizes in the IS(DC) upon allogeneic or antigen-specific DC-TC formation. Allogenic conjugates include (i) bone marrow-derived DCs (BM-DCs) (BALB/c genetic background) and $CD4^+$ TCs (C57BL/6 genetic background) (Al-Alwan et al., 2001b) and (ii) human monocyte-derived DCs and allogeneic lymphoblasts (Riol-Blanco et al., 2009). Antigen-specific conjugates include (i) OVA peptide-loaded BM-DC, from BALB/c or C57BL/6 mice, and DO11.10 or OTII $CD4^+$ TCs, respectively (Al-Alwan et al., 2003; Eun et al., 2006; Riol-Blanco et al., 2009), and (ii) OVA peptide-loaded BM-DCs and OTI $CD8^+$ TCs (Tanizaki et al., 2010). A drawback of these fluorescence microscopy analyses performed with fixed conjugates is that it is difficult to know for certain whether the phalloidin-stained F-actin belongs to the IS(TC) or the IS(DC). However, recently, the use of Lifeact, an amino acid fragment of the protein ABP140 that binds selectively to F-actin, has solved this problem (Riedl et al., 2008; Leithner et al., 2021). High-resolution confocal microscopy analysis of Lifeact-green fluorescent protein (Lifeact-GFP)-expressing DCs that form IS with OTII $CD4^+$ TCs shows that F-actin displays at the IS(DC) a multifocal organization, with foci of different sizes separated by regions where actin is sparse (Leithner et al., 2021). Finally, fluorescence recovery after photobleaching (FRAP) experiments performed with mCherry-labeled actin-transfected BM-DCs that interact with OTII TCs showed a slower recovery at the IS(DC) compared with the cortex, suggesting a higher stability and specific molecular features of the F-actin network at the IS(DC) (Malinova et al., 2016).

SURFACE PROTEINS THAT INDUCE ACTIN ACCUMULATION IN THE IS(DC)

Engagement of MHC-II, MHC-I, or LFA-1 with specific antibodies bound to polystyrene beads induces F-actin accumulation only in DCs that bind to beads associated with anti-MHC-II antibodies (Al-Alwan et al., 2003). The lack of effect of MHC-I was unexpected because F-actin accumulates at the IS(DC) in DC-OTI $CD8^+$ TC conjugates (Tanizaki et al., 2010). Moreover, engagement of MHC-I on the membrane of endothelial cells with antibodies induces activation of the F-actin regulator ras homolog family member A (RhoA) (Coupel et al., 2004; Lepin et al., 2004) and actin organization (Lepin et al., 2004; Jin et al., 2007; Ziegler et al., 2012a,b). Hence, other experimental strategies, including different anti-MHC-I antibodies, should be used before ruling out that MHC-I controls F-actin accumulation in DCs. An analysis of wild-type (WT)-BM-DCs or CD80/86 knock-out (KO)-BM-DCs interacting with DO11.10 CD4 + TCs suggests that CD80/CD86 induces actin polarization at the IS(DC) (Rothoeft et al., 2006). However, actin failed to accumulate at the IS(DC) upon engagement of CD86 on DCs with antibodies or when BM-DCs, expressing that the CD28 receptors CD80 and CD86 interact with human Jurkat cells expressing murine CD28 (Al-Alwan et al., 2003; Rothoeft et al., 2006). Therefore, stimulation of CD80 or CD86 is not sufficient to promote F-actin aggregation. Finally, the semaphorin receptor Plexin-A1, which is localized at the IS(DC), can also induce RhoA activation and F-actin polarization in this region (Eun et al., 2006).

ROLE OF F-ACTIN AND ACTIN-REGULATORY PROTEINS AT THE IS(DC) ON TC ACTIVATION

Below, we analyze reports that provide information on the role of DC's F-actin and actin-regulatory proteins on TC activation (**Figure 1** and **Table 1**). When analyzing these experimental data, it is important to take into consideration several points. First, the focus of most of the studies available on this issue was not the IS(DC). Second, the proteins analyzed can be expressed in the IS(DC) and elsewhere in DCs, like the DCs' cortex (e.g., F-actin, WRC, WASP, and Myo9b), implying that these proteins may exert their regulatory effects inside and/or outside the IS(DC) (e.g., WASP, Rac1/2, and mDia also regulate migration). Third, actin-regulatory proteins can also govern actin-independent functions (e.g., HS1). Fourth, the experimental strategies employed to study the role of these molecules, namely, the use of pharmacological agents to inhibit F-actin or DCs deficient in actin-regulatory proteins, do not discriminate between the IS(DC) and other intracellular regions.

Filamentous Actin

To analyze the role of F-actin at the IS(DC), pharmacological agents have been used that alter actin stability, including cytochalasin D, latrunculin A, and mycalolide B (MycB), which disrupt F-actin, and Jasplakinolide, which stabilizes it (Fenteany and Zhu, 2003). When DCs treated with any of these inhibitors interact with DO11.10 or OTII $CD4^+$ TCs, the activation and proliferation of these lymphocytes is inhibited (Al-Alwan et al., 2001b; Leithner et al., 2021; **Table 1**). These results emphasize the importance of the integrity of the DCs' actin cytoskeleton for TC activation (Al-Alwan et al., 2001b; Leithner et al., 2021). Confocal microscopic analyses of DCs that interact with Lifeact-GFP expressing OTII $CD4^+$ TCs show that IS(TC) form multiple actin foci (Leithner et al., 2021). However, when DCs pretreated with MycB to disrupt F-actin were allowed to interact with the Lifeact-GFP OTII $CD4^+$ TCs, ∼50% of the IS(TC) present a ring of F-actin surrounding an actin-free circle, instead of a multifocal actin organization (Leithner et al., 2021; **Table 1**). Hence, multifocal actin at the IS(DC) contributes partially to stabilizing multifocal actin at the IS(DC) and predictably also to

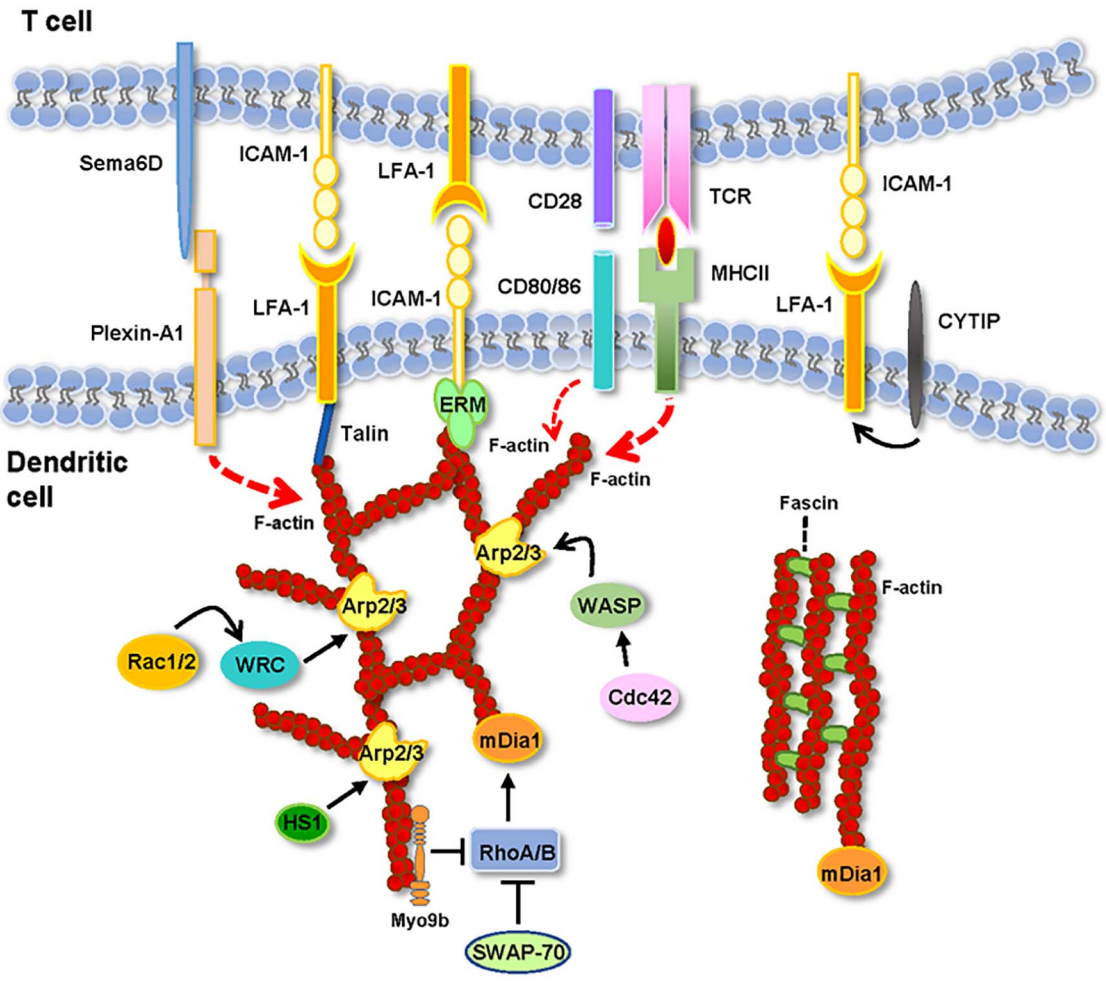

FIGURE 1 | Actin and actin-regulatory proteins at the IS(DC). In the figure are depicted the molecules described in the text. See the text for details.

TABLE 1 | Effects of the perturbation of F-actin and actin-regulatory molecules in the DCs. In the table are presented the effects observed following the interaction between TCs and either pharmacologically inhibited or KO-DCs, which are compared with the results obtained with TCs that interact with uninhibited or WT-DCs controls.

DC protein	Role of the target protein in the DCs	Tool used to inhibit the target protein in the DCs	Type of the IS formed		Effect of inhibition of the DC target after inducing IS formation		References
			Antigen-specific (interacting cells)	Allogeneic (interacting cells)	TC activation and/or proliferation	Other effects in the TCs or DCs	
F-Actin	**Cytoskeletal protein**	Cytochalasin D Jasplakinolide Latrunculin A	Inhibited BM-DCs (BALB/c) and DO11.10 CD4$^+$ TCs Inhibited BM-DCs (C57BL/6) and OTII CD4$^+$ TCs	Inhibited BM-DCs (BALB/c) and CD4$^+$ TCs (C57BL/6)	Reduced	-Reduced production of IL-2 in the DO11.10 and OTII CD4$^+$ TCs	Al-Alwan et al., 2001b
		Mycalolide B	Inhibited BM-DCs and OTII CD4$^+$ TCs Inhibited Lifeact-GFP BM-DCs and OTII CD4$^+$ TCs		Reduced	-Reduction (−50%) in the number of IS(TC) that display multifocal actin organization -Inhibition of early activation markers CD62L and CD69 and IL-2 production in the OTII CD4$^+$ TCs	Leithner et al., 2021
WASP	**Arp2/3 nucleation-promoting factor**	WASP-KO BM-DCs	WASP-KO BM-DCs and OTII CD4$^+$ TCs		Reduced	-WASP-KO DCs are less motile -Unstable IS -Altered signaling at the IS(TC) - Inhibition IL-2 production in the activated OTII CD4$^+$ TC	
		WASP-Y293F BM-DCs	WASP Y293F BM-DCs and OTII CD4$^+$ TCs		Reduced	-Reduction in IS formation and priming ability -Inhibition IL-2 production in the activated OTII CD4$^+$ TCs	Bouma et al., 2011
		Human WASP-/- BM-CD34$^+$ DCs		Human WASP-/-BM-CD34$^+$ DCs and human PBMCs	Reduced	-Reduced production of interferon-γ (IFN-γ) in the TCs	
		WASP-KO BM-DCs	WASP-KO BM-DCs and OTI CD8$^+$ TCs		Reduced	-Reduced duration of DC and CD8$^+$ TC contacts -Reduced levels of CD69 in the OTI CD8$^+$ TCs -Reduced cross-presentation *in vivo*	Pulecio et al., 2008
HS1	**Arp2/3 nucleation-promoting factor**	HS1-KO BM-DCs (BALB/c)	HS1-KO BM-DCs and DO11.10 CD4$^+$ TCs		Reduced	-Maturation, pinocytosis, and phagocytosis, not affected in the HS1-KO DCs -Receptor-mediated endocytosis selectively reduced in the HS1-KO DCs -Reduced production of IL-2 in the DO11.10 CD4$^+$ TCs and OTII CD4$^+$ TCs	Huang et al., 2011
		HS1-KO BM-DCs (C57BL/6)	HS1-KO BM-DC and OTII CD4$^+$ TCs				
WRC	**Arp2/3 nucleation-promoting factor**	WRC-deficient BM-DCs	WRC-deficient BM-DCs and OTII CD4$^+$ TCs		Reduced	-DC-TC contacts last longer -Reduced production of IL-2 in the OTII CD4$^+$ TCs.	Leithner et al., 2021

(Continued)

TABLE 1 | Continued

DC protein	Role of the target protein in the DCs	Tool used to inhibit the target protein in the DCs	Type of the IS formed		Effect of inhibition of the DC target after inducing IS formation		References
			Antigen-specific (interacting cells)	Allogeneic (interacting cells)	TC activation and/or proliferation	Other effects in the TCs or DCs	
mDia	**Actin nucleation factor**	mDia-KO BM-DCs		mDia-KO BM-DCs (C57BL/6) and $CD4^+$ TCs (BALB/c)	Reduced	-Reduced production of IFN-γ in the $CD4^+$ TCs	Tanizaki et al., 2010
		mDia-KO BM-DCs	mDia-KO BM-DCs and OTII $CD4^+$ TCs mDia-KO BM-DCs and OTI $CD8^+$ TCs		Reduced	-Shorter duration contacts between DCs and OTII $CD4^+$ or OTI $CD8^+$ TCs -Lower levels of IFN-γ in the TCs	
Fascin	**Actin bundling protein**	Fascin antisense oligonucleotides		Inhibited BM-DCs (BALB/c) and TCs (C57BL/6)	Reduced	-Fascin antisense-treated BM-DCs present fewer and smaller dendrites but not changes in MHC-II or costimulatory CD86 molecules	Al-Alwan et al., 2001a
SWAP-70	**Rac-GEF* Actin bundling protein**	SWAP-70-KO BM-DCs	SWAP-70-KO BM-DCs and TC hybridoma (BO97.10) SWAP-70-KO SPDCs and TC hybridoma (1H3.1)		Reduced	-Total levels of MHC-II are not altered, however, its location is reduced in the SWAP-70-KO DCs –SWAP-70-KO DCs display lower F-actin density at the IS(DC) -WT and SWAP-70 DCs show similar migration -Reduced production of IL-2 in TC hybridomas	Regnault et al., 1999; Blander and Medzhitov, 2006; Ocana-Morgner et al., 2009
Myo9b	**Rho-GAP***	Myo9b-KO BM-DC	Myo9b-KO BM-DCs and OTII $CD4^+$ TCs		Reduced	-Lower number of interactions, which last longer, between DCs and TCs -Increased levels of F-actin at the IS(DC) -Early TC activation marker CD69 inhibited within 3D-collagen matrices, but not in liquid cultures	Xu et al., 2014
Rac1/2	**Small GTPases***	Rac1/2-KO BM-DC	Rac1/2-KO BM-DCs and Marilyn $CD4^+$ TCs		Reduced	-Brief contacts between DC and $CD4^+$ TCs -Inhibition of the early TC activation marker CD69	Benvenuti et al., 2004
CYTIP	**Cytohesin-interacting protein**	CYTIP siRNA	Inhibited Human mono-DCs and Human $CD8^+$ TCs		Reduced	-CYTIP siRNA-treated DCs display increased adhesion onto TCs -Lower TC activation when siRNA-CYTIP treated DCs partially loaded with A2.1 restricted EBV peptide interact with antigen-specific $CD8^+$ TCs	Hofer et al., 2006
		CYTIP-KO BM-DC	CYTIP-KO BM-DCs and OTII CD4 + TCs CYTIP-KO BM-DCs and OTI CD8 + TCs		Increased	-WT and CYTIP-KO DCs express similar levels of costimulatory molecules -Increased proliferation, measured after 4 days of culture by ^{3}H-thymidine incorporation	Heib et al., 2012

A short note on the regulation of the small GTPases shown in this table and in **Figure 1. These proteins cycle between inactive (GDP-bound) and active (GTP-bound) states, which can interact with effector proteins that relay downstream signaling. This cycle is regulated by specific guanine nucleotide exchange factors (GEFs), which catalyze the release of the bound GDP that is replaced by GTP, and by GTPase-activating proteins (GAPs), which induce GTP hydrolysis.*

the formation of the multicentric IS(TC) (Brossard et al., 2005; Rothoeft et al., 2006; Reichardt et al., 2007; Fisher et al., 2008; Tseng et al., 2008; Thauland and Parker, 2010), although this has to be confirmed in future studies because, in the experiments described, the authors did not stain the surface proteins, such as CD3, and other molecules, which organize in foci in the IS(TC) (Leithner et al., 2021). Finally, F-actin at the IS(DC) can also control DC-TC adhesion by selectively regulating the lateral mobility on the plasma membrane of ICAM-1 (Comrie et al., 2015). Immobilized ICAM-1 at the IS(DC) can promote LFA-1 activation on the IS(TC) and increase DC-TC adhesion (Feigelson et al., 2010).

Wiskott–Aldrich Syndrome Protein

Wiskott–Aldrich syndrome protein (WASP) is a nucleation-promoting factor (NPF) that activates the actin-related protein 2/3 (Arp2/3) complex (**Figure 1**). Arp2/3 is an actin-nucleation factor (ANF) that assembles actin dimers or trimers that serve as nuclei that subsequently polymerize into Y-branched actin networks (Schonichen and Geyer, 2010). WASP organize in foci within the IS(DC) (Leithner et al., 2021). WASP-KO BM-DCs show reduced motility and lower F-actin levels (Bouma et al., 2011; Malinova et al., 2016). WASP-KO BM-DCs that interact with OTII $CD4^+$ TCs *in vitro* present a high number of transient interactions and reduced DC-TC contact areas, suggesting that in the DCs, WASP may stabilize the interactions with the TCs (Bouma et al., 2011; Malinova et al., 2016; **Table 1**). Similar conclusions have been obtained in *in vitro* and *in vivo* studies that analyze the interactions between WASP-KO BM-DCs and OTI $CD8^+$ TCs (Pulecio et al., 2008). At the IS(DC) formed by the WASP-KO BM-DCs, the levels of ICAM-1 and MHC-II are reduced (Malinova et al., 2016). The levels of TCR, LFA-1, F-actin, and talins are also reduced at the IS(TC). Moreover, TCR-dependent signaling was also altered, resulting in reduced IL-2 production, and TC proliferation (Bouma et al., 2011; Malinova et al., 2016). Further supporting a role for the WASP/Arp2/3 axis in IS formation, DCs that express Y293F-WASP (a mutation that impairs WASP's ability to activate Arp2/3) display a low number of IS with TCs and reduced priming ability (Bouma et al., 2011). Finally, in FRAP experiments performed with Cherry-labeled actin-transfected WASP-KO, Y293F-WASP, and WT-BM-DCs that formed IS with OTII $CD4^+$ TCs, actin recovery at the IS(DC) was slower in the WT DCs compared with the WASP-KO and Y293F-WASP DCs, suggesting that WASP-Arp2/3-mediated formation of branched actin stabilizes the actin network at the IS(DC) (Malinova et al., 2016).

Hematopoietic Lineage Cell-Specific Protein 1

Hematopoietic lineage cell-specific protein 1 (HS1) is a NPF that induces Arp2/3-dependent branched actin networks, and, moreover, it can also bind and stabilize this network (Weaver et al., 2001; Uruno et al., 2003; Hao et al., 2005; Dehring et al., 2011; **Figure 1**). Since HS1 expression increases during DC maturation (Huang et al., 2011), it is interesting to study whether this molecule could regulate actin organization at the IS(DC) and DCs' priming ability (**Table 1**). WT and HS1-KO BM-DCs bind and present OVA peptides equally as well with DO11.10 $CD4^+$ TCs (Huang et al., 2011). However, HS1-KO BM-DCs loaded with intact OVA protein display a reduced ability to activate the $CD4^+$ TCs (Huang et al., 2011). WT and HS1-KO BM-DCs present the MHC-I-restricted VSV8 peptide equally as well with the $CD8^+$ TC hybridoma N15. However, when VSV8 was complexed with the protein GRP94, which also uses the MHC-I pathway of antigen presentation, the priming ability of the HS1-KO BM-DCs was impaired. It was observed that receptor-mediated endocytosis was selectively inhibited in the HS1-KO BM-DCs, preventing antigen uptake (Huang et al., 2011). It was also found that HS1 is required for antigen uptake because it participates, together with dynamin 2, in the scission of the endocytic vesicles (Huang et al., 2011). Hence, although HS1 is a NPF, it apparently regulates antigen presentation through the control of antigen endocytosis.

WAVE Regulatory Complex

WASP-family verprolin homologous proteins (WAVE) regulatory complex (WRC) is an NPF that activates Arp2/3 and induces branched actin (Buracco et al., 2019; **Figure 1**). WRC is found in the IS(DC), but it also associates with F-actin at the DC cortex (Leithner et al., 2021). Upon interaction of WRC-deficient BM-DCs (Park et al., 2008) with OTII $CD4^+$ TCs, F-actin displays a multifocal organization in the IS(TC), like the IS(TC) formed by the WT BM-DCs (Leithner et al., 2021; **Table 1**). However, F-actin levels at the IS(DC) are reduced, suggesting that WRC promotes actin accumulation in this region. WRC-deficient DC-TC contacts last longer and display larger areas of contact (Leithner et al., 2021). These prolonged interactions are associated with an increase in the levels of the phospho-ezrin-radixin-moesin (ERM), suggesting a higher anchoring of ICAM-1 to cortical F-actin, which may result in the immobilization of this ligand and increased LFA-1-mediated DC-TC adhesion (Comrie et al., 2015; Leithner et al., 2021). These abnormal long-lasting interactions between WRC-deficient DCs and TCs may explain the observed reduction in the activation of the TCs (Leithner et al., 2021).

Mammalian Homolog of Diaphanous

Mammalian homolog of diaphanous (mDia1) is an ANF of the formin family that promotes F-actin elongation (Schonichen and Geyer, 2010; **Figure 1**). The mDia-KO-BM-DCs display reduced adhesion and impaired migration (Tanizaki et al., 2010). $CD4^+$ TCs that establish alloreactive interactions with mDia-KO BM-DC also presented reduced proliferation and low interferon-γ (IFN-γ) production (**Table 1**). Two-photon microscopy analysis shows that mDia-KO BM-DCs that interact with OTII $CD4^+$ TCs or with OTI CD8 + TCs establish brief contacts within the LNs, indicating that DCs' mDia is important for keeping stable ISs (Tanizaki et al., 2010). Hence, correct TC activation requires of mDia1 expression in the DCs.

Fascin

Fascin is an actin-bundling protein whose expression is increased during DC maturation (Mosialos et al., 1996; Al-Alwan et al., 2001a; Yamashiro, 2012). In mature DCs, fascin, which can localize to the IS(DC), controls dendrite formation (Al-Alwan

et al., 2001a,b; Rothoeft et al., 2006; **Figure 1**). In antigen-specific models of IS formation, accumulation of fascin and F-actin correlates with more extended contacts between DCs and TCs, increased TC proliferation, and $CD4^+$ Th1 TC-dependent responses (Rothoeft et al., 2006). Using an allogeneic model of IS formation, it is observed that the levels of fascin in DCs correlate with the ability of these cells to stimulate the TCs (Al-Alwan et al., 2001a; **Table 1**). Finally, in an alloreactive IS model, it was observed that a reduction of fascin levels in the BM-DCs with antisense oligonucleotides inhibits their ability to allostimulate the TCs (Al-Alwan et al., 2001a). Therefore, fascin-mediated bundling of F-actin in DCs contributes to TC priming.

Switch-Associated Protein 70

Switch-associated protein 70 (SWAP-70) is a Rac GEF (see **Table 1** and legend) that also controls F-actin bundling (Gomez-Cambronero, 2012; Chacon-Martinez et al., 2013; **Figure 1**). Although WT and SWAP-70-KO DCs express similar total MHC-II levels, SWAP-70-KO BM-DCs show a reduced expression of MHC-II on the plasma membrane (Ocana-Morgner et al., 2009). OVA peptide-loaded SWAP-70-KO DCs' ability to prime TCs is impaired (Ocana-Morgner et al., 2009), as shown by their reduced ability to activate two different MHC-II-restricted TC hybridomas (Regnault et al., 1999; Blander and Medzhitov, 2006). In SWAP-70-KO DCs, the actin regulatory GTPases RhoA and RhoB are constitutively activated, resulting in an increase in the amount of F-actin in these cells (Ocana-Morgner et al., 2009; Sit and Manser, 2011). Inhibition of RhoA and RhoB in the SWAP-70-KO DCs with *Clostridium botulinum* increased MHC-II on their plasma membrane and helped recover their ability to activate the TCs. Hence, it is suggested that the high F-actin levels prevent the correct MHC-II localization on the plasma membrane (Bretou et al., 2016). Therefore, SWAP-70 may inhibit RhoA and RhoB activation, which prevents an abnormal increase in F-actin and allows MHC-II localization on the membrane of the DCs (Ocana-Morgner et al., 2009).

Myosin IXb

Myosin IXb (Myo9b) is a cytoskeletal motor that displays Rho-GTPase-activating protein (GAP) activity (see **Table 1** and legend). Myo9b colocalizes with F-actin in DCs (Hanley et al., 2010; Xu et al., 2014; **Figure 1**). Compared to WT-BM-DCs, KO-Myo9B BM-DCs present a low number interaction with OTII $CD4^+$ TCs, although these interactions last longer (Xu et al., 2014). F-Actin is highly increased in the IS(DC) of the KO-Myo9B BM-DCs that form IS with OTII $CD4^+$ TCs. However, KO-Myo9B BM-DC-OTII $CD4^+$ TCs' interactions resulted in reduced proliferation within 3D-collagen matrices but not in liquid co-cultures (Xu et al., 2014). These results could be due to the different spatiotemporal organization of F-actin in the IS(DC) of the KO-Myo9B DCs under both conditions (Xu et al., 2014).

RhoA, Rac1 and Rac 2

RhoA, Rac1, and Rac 2 belong to the Rho GTPase subfamily, which are critical regulators of the actin cytoskeleton (see **Figure 1**, and **Table 1** and legend) (Sit and Manser, 2011). Treatment of the DCs with epidermal cell differentiation inhibitor (EDIN) toxin, which inactivates RhoA, or inhibition of its downstream target, the Rho-associated protein kinase (ROCK), with Y27632, failed to affect IS formation between BM-DCs and OTII $CD4^+$ TCs (Benvenuti et al., 2004). These results suggest that the effects of knocking down SWAP-70 on F-actin discussed above could be mediated by RhoB, instead of RhoA. DCs deficient in Rac1 and Rac2 show alterations in the F-actin organization, resulting in the absence of dendrites and reduced motility. *In vitro* analyses show that Rac1/2-KO BM-DCs do not form stable contacts with $CD4^+$ TCs. Consistent with these results, the Rac1/2-KO BM-DCs show a reduced ability to activate OTII $CD4^+$ TCs. It was suggested that this inhibition was due to deficient actin dynamics in the Rac1/2-KO DCs that prevent these cells from engulfing and establishing full contacts with TCs (Benvenuti et al., 2004).

Cytohesin-Interacting Protein (CYTIP)

Although CYTIP is not an actin-regulatory protein, we have included it in this review because it regulates LFA-1, which is an important molecule at the IS(DC) (**Figure 1**). In resting DCs, LFA-1 remains on the plasma membrane in an inactive state; that is, it cannot bind to its ligand ICAM-1. DCs express cytohesin-1, which interacts with the cytoplasmic β-subunit of LFA-1, resulting in its activation and binding to ICAM-1. CYTIP binds to cytohesin-1, which translocates from the membrane to the cytoplasm, leaving LFA-1 inactivated. During DC maturation, CYTIP levels increase and localize to the IS(DC) (Hofer et al., 2006). Studies on CYTIP in DCs are controversial (**Table 1**). In experiments in which CYTIP was reduced with siRNA in human DCs (Hofer et al., 2006), these cells showed a diminished ability to induce proliferation of autologous antigen-specific $CD8^+$ TCs (Hofer et al., 2006). Other studies show that knocking down CYTIP with siRNA in BM-DCs extends antigen-specific contacts with OTII $CD4^+$ TCs or OTI $CD8^+$ TCs and reduces the activation and proliferation of these cells (Balkow et al., 2010). In contrast, in experiments performed with DCs obtained from CYTIP KO mice (Coppola et al., 2006), CYTIP KO BM-DCs enhanced antigen-specific activation OTI and OTII TCs (Heib et al., 2012).

CONCLUDING REMARKS

The study of the role of F-actin at the IS(DCs) is at its inception. The data discussed above suggest that F-actin polarization at the IS(DC) maintain IS stability necessary to induce TC activation. A network of actin-regulatory proteins controls F-actin organization at the IS(DC) (**Figure 1**). The pharmacological disruption of F-actin, the knockdown of Rac1/2, or the increase of F-actin levels after knocking down Myo9b reduce the ability of the DCs to activate the TCs. Knockdown of WASP or WRC, which promotes branched actin through Arp2/3, or mDia, which regulates linear F-actin, or fascin, a bundling protein, results in inhibition of TC activation. Deletion of WASP, mDia, fascin, and Rac1/2 reduces the number and/or the duration of DC-TC contacts. In contrast, knockdown of WRC or Myo9b results in extended DC-TC contacts and inhibition of TC activation. In summary, perturbation of F-actin dynamics at the IS(DC) leads to the inhibition of TC activation. Multiple

aspects of the F-actin regulation and functions at the IS(DC) need to be addressed in the future. For this purpose, it is very important to develop experimental strategies that selectively target F-actin and its regulatory proteins at the IS(DC). Many wonderful things remain to be discovered at the IS(DC).

AUTHOR CONTRIBUTIONS

JR-F designed the work and wrote the manuscript with the help of OC-G. OC-G prepared the table and the figure. Both authors contributed to manuscript revision, and read and approved the submitted version.

FUNDING

JR-F was supported by grants awarded by Ministerio de Economía y Competitividad (SAF2014-53151-R, SAF2017-83306-R, and 2020AEP158 Ayuda Extra.2020TEC2017-85059-C3-3-R), RIER (RETICS Program/Instituto de Salud Carlos III) (RD08/0075), and Consejería de Educación y Empleo from Comunidad de Madrid (Raphyme, S2010/BMD-2350).

REFERENCES

Al-Alwan, M. M., Liwski, R. S., Haeryfar, S. M., Baldridge, W. H., Hoskin, D. W., Rowden, G., et al. (2003). Cutting edge: dendritic cell actin cytoskeletal polarization during immunological synapse formation is highly antigen-dependent. *J. Immunol.* 171, 4479–4483. doi: 10.4049/jimmunol.171.9.4479

Al-Alwan, M. M., Rowden, G., Lee, T. D., and West, K. A. (2001b). The dendritic cell cytoskeleton is critical for the formation of the immunological synapse. *J. Immunol.* 166, 1452–1456. doi: 10.4049/jimmunol.166.3.1452

Al-Alwan, M. M., Rowden, G., Lee, T. D., and West, K. A. (2001a). Fascin is involved in the antigen presentation activity of mature dendritic cells. *J. Immunol.* 166, 338–345. doi: 10.4049/jimmunol.166.1.338

Alcaraz-Serna, A., Bustos-Moran, E., Fernandez-Delgado, I., Calzada-Fraile, D., Torralba, D., Marina-Zarate, E., et al. (2021). Immune synapse instructs epigenomic and transcriptomic functional reprogramming in dendritic cells. *Sci. Adv.* 7:eabb9965.

Bajenoff, M., Granjeaud, S., and Guerder, S. (2003). The strategy of T cell antigen-presenting cell encounter in antigen-draining lymph nodes revealed by imaging of initial T cell activation. *J. Exp. Med.* 198, 715–724. doi: 10.1084/jem.20030167

Balkow, S., Heinz, S., Schmidbauer, P., Kolanus, W., Holzmann, B., Grabbe, S., et al. (2010). LFA-1 activity state on dendritic cells regulates contact duration with T cells and promotes T-cell priming. *Blood* 116, 1885–1894. doi: 10.1182/blood-2009-05-224428

Banchereau, J., and Steinman, R. M. (1998). Dendritic cells and the control of immunity. *Nature* 392, 245–252. doi: 10.1038/32588

Benvenuti, F. (2016). The dendritic cell synapse: a life dedicated to T cell activation. *Front. Immunol.* 7:70. doi: 10.3389/fimmu.2016.00070

Benvenuti, F., Hugues, S., Walmsley, M., Ruf, S., Fetler, L., Popoff, M., et al. (2004). Requirement of Rac1 and Rac2 expression by mature dendritic cells for T cell priming. *Science* 305, 1150–1153. doi: 10.1126/science.1099159

Blander, J. M., and Medzhitov, R. (2006). Toll-dependent selection of microbial antigens for presentation by dendritic cells. *Nature* 440, 808–812. doi: 10.1038/nature04596

Bouma, G., Mendoza-Naranjo, A., Blundell, M. P., de Falco, E., Parsley, K. L., Burns, S. O., et al. (2011). Cytoskeletal remodeling mediated by WASp in dendritic cells is necessary for normal immune synapse formation and T-cell priming. *Blood* 118, 2492–2501. doi: 10.1182/blood-2011-03-340265

Bousso, P., and Robey, E. (2003). Dynamics of CD8+ T cell priming by dendritic cells in intact lymph nodes. *Nat. Immunol.* 4, 579–585. doi: 10.1038/ni928

Bretou, M., Kumari, A., Malbec, O., Moreau, H. D., Obino, D., Pierobon, P., et al. (2016). Dynamics of the membrane-cytoskeleton interface in MHC class II-restricted antigen presentation. *Immunol. Rev.* 272, 39–51. doi: 10.1111/imr.12429

Brossard, C., Feuillet, V., Schmitt, A., Randriamampita, C., Romao, M., Raposo, G., et al. (2005). Multifocal structure of the T cell – dendritic cell synapse. *Eur. J. Immunol.* 35, 1741–1753. doi: 10.1002/eji.200425857

Buracco, S., Claydon, S., and Insall, R. (2019). Control of actin dynamics during cell motility. *F1000 Res.* 8:F1000 Faculty Rev–1977.

Celli, S., Lemaitre, F., and Bousso, P. (2007). Real-time manipulation of T cell-dendritic cell interactions in vivo reveals the importance of prolonged contacts for CD4+ T cell activation. *Immunity* 27, 625–634. doi: 10.1016/j.immuni.2007.08.018

Chacon-Martinez, C. A., Kiessling, N., Winterhoff, M., Faix, J., Muller-Reichert, T., and Jessberger, R. (2013). The switch-associated protein 70 (SWAP-70) bundles actin filaments and contributes to the regulation of F-actin dynamics. *J. Biol. Chem.* 288, 28687–28703. doi: 10.1074/jbc.m113.461277

Comrie, W. A., Li, S., Boyle, S., and Burkhardt, J. K. (2015). The dendritic cell cytoskeleton promotes T cell adhesion and activation by constraining ICAM-1 mobility. *J. Cell Biol.* 208, 457–473. doi: 10.1083/jcb.201406120

Coppola, V., Barrick, C. A., Bobisse, S., Rodriguez-Galan, M. C., Pivetta, M., Reynolds, D., et al. (2006). The scaffold protein Cybr is required for cytokine-modulated trafficking of leukocytes in vivo. *Mol. Cell Biol.* 26, 5249–5258. doi: 10.1128/mcb.02473-05

Coupel, S., Leboeuf, F., Boulday, G., Soulillou, J. P., and Charreau, B. (2004). RhoA activation mediates phosphatidylinositol 3-kinase-dependent proliferation of human vascular endothelial cells: an alloimmune mechanism of chronic allograft nephropathy. *J. Am. Soc. Nephrol.* 15, 2429–2439. doi: 10.1097/01.asn.0000138237.42675.45

Dehring, D. A., Clarke, F., Ricart, B. G., Huang, Y., Gomez, T. S., Williamson, E. K., et al. (2011). Hematopoietic lineage cell-specific protein 1 functions in concert with the Wiskott-Aldrich syndrome protein to promote podosome array organization and chemotaxis in dendritic cells. *J. Immunol.* 186, 4805–4818. doi: 10.4049/jimmunol.1003102

Delon, J., Bercovici, N., Raposo, G., Liblau, R., and Trautmann, A. (1998). Antigen-dependent and -independent Ca2+ responses triggered in T cells by dendritic cells compared with B cells. *J. Exp. Med.* 188, 1473–1484. doi: 10.1084/jem.188.8.1473

Eun, S. Y., O'Connor, B. P., Wong, A. W., van Deventer, H. W., Taxman, D. J., Reed, W., et al. (2006). Cutting edge: rho activation and actin polarization are dependent on plexin-A1 in dendritic cells. *J. Immunol.* 177, 4271–4275. doi: 10.4049/jimmunol.177.7.4271

Feigelson, S. W., Pasvolsky, R., Cemerski, S., Shulman, Z., Grabovsky, V., Ilani, T., et al. (2010). Occupancy of lymphocyte LFA-1 by surface-immobilized ICAM-1 is critical for TCR- but not for chemokine-triggered LFA-1 conversion to an open headpiece high-affinity state. *J. Immunol.* 185, 7394–7404. doi: 10.4049/jimmunol.1002246

Fenteany, G., and Zhu, S. (2003). Small-molecule inhibitors of actin dynamics and cell motility. *Curr. Top. Med. Chem.* 3, 593–616. doi: 10.2174/1568026033452348

Fisher, P. J., Bulur, P. A., Vuk-Pavlovic, S., Prendergast, F. G., and Dietz, A. B. (2008). Dendritic cell microvilli: a novel membrane structure associated with the multifocal synapse and T-cell clustering. *Blood* 112, 5037–5045. doi: 10.1182/blood-2008-04-149526

Freiberg, B. A., Kupfer, H., Maslanik, W., Delli, J., Kappler, J., Zaller, D. M., et al. (2002). Staging and resetting T cell activation in SMACs. *Nat. Immunol.* 3, 911–917. doi: 10.1038/ni836

Gomez-Cabanas, L., Lopez-Cotarelo, P., Criado-Garcia, O., Murphy, M. P., Boya, P., and Rodriguez-Fernandez, J. L. (2019). Immunological synapse formation induces mitochondrial clustering and mitophagy in dendritic cells. *J. Immunol.* 202, 1715–1723. doi: 10.4049/jimmunol.1800575

Gomez-Cambronero, J. (2012). Structure analysis between the SWAP-70 RHO-GEF and the newly described PLD2-GEF. *Small GTPases* 3, 202–208. doi: 10.4161/sgtp.20887

Grakoui, A., Bromley, S. K., Sumen, C., Davis, M. M., Shaw, A. S., Allen, P. M., et al. (1999). The immunological synapse: a molecular machine controlling T cell activation. *Science* 285, 221–227. doi: 10.1126/science.285.5425.221

Hanley, P. J., Xu, Y., Kronlage, M., Grobe, K., Schon, P., Song, J., et al. (2010). Motorized RhoGAP myosin IXb (Myo9b) controls cell shape and motility. *Proc. Natl. Acad. Sci. U. S. A.* 107, 12145–12150. doi: 10.1073/pnas.0911986107

Hao, J. J., Zhu, J., Zhou, K., Smith, N., and Zhan, X. (2005). The coiled-coil domain is required for HS1 to bind to F-actin and activate Arp2/3 complex. *J. Biol. Chem.* 280, 37988–37994. doi: 10.1074/jbc.m504552200

Heib, V., Sparber, F., Tripp, C. H., Ortner, D., Stoitzner, P., and Heufler, C. (2012). Cytip regulates dendritic-cell function in contact hypersensitivity. *Eur. J. Immunol.* 42, 589–597. doi: 10.1002/eji.201041286

Hofer, S., Pfeil, K., Niederegger, H., Ebner, S., Nguyen, V. A., Kremmer, E., et al. (2006). Dendritic cells regulate T-cell deattachment through the integrin-interacting protein CYTIP. *Blood* 107, 1003–1009. doi: 10.1182/blood-2005-01-0425

Huang, Y., Biswas, C., Klos Dehring, D. A., Sriram, U., Williamson, E. K., Li, S., et al. (2011). The actin regulatory protein HS1 is required for antigen uptake and presentation by dendritic cells. *J. Immunol.* 187, 5952–5963. doi: 10.4049/jimmunol.1100870

Iezzi, G., Karjalainen, K., and Lanzavecchia, A. (1998). The duration of antigenic stimulation determines the fate of naive and effector T cells. *Immunity* 8, 89–95. doi: 10.1016/s1074-7613(00)80461-6

Jin, Y. P., Korin, Y., Zhang, X., Jindra, P. T., Rozengurt, E., and Reed, E. F. (2007). RNA interference elucidates the role of focal adhesion kinase in HLA class I-mediated focal adhesion complex formation and proliferation in human endothelial cells. *J. Immunol.* 178, 7911–7922. doi: 10.4049/jimmunol.178.12.7911

Leithner, A., Altenburger, L. M., Hauschild, R., Assen, F. P., Rottner, K., Stradal, T. E. B., et al. (2021). Dendritic cell actin dynamics control contact duration and priming efficiency at the immunological synapse. *J. Cell Biol.* 220:e202006081.

Lepin, E. J., Jin, Y. P., Barwe, S. P., Rozengurt, E., and Reed, E. F. (2004). HLA class I signal transduction is dependent on Rho GTPase and ROK. *Biochem. Biophys. Res. Commun.* 323, 213–217. doi: 10.1016/j.bbrc.2004.08.082

Malinova, D., Fritzsche, M., Nowosad, C. R., Armer, H., Munro, P. M., Blundell, M. P., et al. (2016). WASp-dependent actin cytoskeleton stability at the dendritic cell immunological synapse is required for extensive, functional T cell contacts. *J. Leukoc. Biol.* 99, 699–710. doi: 10.1189/jlb.2a0215-050rr

Mempel, T. R., Henrickson, S. E., and Von Andrian, U. H. (2004). T-cell priming by dendritic cells in lymph nodes occurs in three distinct phases. *Nature* 427, 154–159. doi: 10.1038/nature02238

Merad, M., Sathe, P., Helft, J., Miller, J., and Mortha, A. (2013). The dendritic cell lineage: ontogeny and function of dendritic cells and their subsets in the steady state and the inflamed setting. *Annu. Rev. Immunol.* 31, 563–604. doi: 10.1146/annurev-immunol-020711-074950

Miller, M. J., Safrina, O., Parker, I., and Cahalan, M. D. (2004). Imaging the single cell dynamics of CD4+ T cell activation by dendritic cells in lymph nodes. *J. Exp. Med.* 200, 847–856. doi: 10.1084/jem.20041236

Monks, C. R., Freiberg, B. A., Kupfer, H., Sciaky, N., and Kupfer, A. (1998). Three-dimensional segregation of supramolecular activation clusters in T cells. *Nature* 395, 82–86. doi: 10.1038/25764

Mosialos, G., Birkenbach, M., Ayehunie, S., Matsumura, F., Pinkus, G. S., Kieff, E., et al. (1996). Circulating human dendritic cells differentially express high levels of a 55-kd actin-bundling protein. *Am. J. Pathol.* 148, 593–600.

Mossman, K. D., Campi, G., Groves, J. T., and Dustin, M. L. (2005). Altered TCR signaling from geometrically repatterned immunological synapses. *Science* 310, 1191–1193. doi: 10.1126/science.1119238

Ocana-Morgner, C., Wahren, C., and Jessberger, R. (2009). SWAP-70 regulates RhoA/RhoB-dependent MHCII surface localization in dendritic cells. *Blood* 113, 1474–1482. doi: 10.1182/blood-2008-04-152587

Park, H., Staehling-Hampton, K., Appleby, M. W., Brunkow, M. E., Habib, T., Zhang, Y., et al. (2008). A point mutation in the murine Hem1 gene reveals an essential role for Hematopoietic protein 1 in lymphopoiesis and innate immunity. *J. Exp. Med.* 205, 2899–2913. doi: 10.1084/jem.20080340

Pulecio, J., Tagliani, E., Scholer, A., Prete, F., Fetler, L., Burrone, O. R., et al. (2008). Expression of Wiskott-Aldrich syndrome protein in dendritic cells regulates synapse formation and activation of naive CD8+ T cells. *J. Immunol.* 181, 1135–1142. doi: 10.4049/jimmunol.181.2.1135

Regnault, A., Lankar, D., Lacabanne, V., Rodriguez, A., Thery, C., Rescigno, M., et al. (1999). Fcgamma receptor-mediated induction of dendritic cell maturation and major histocompatibility complex class I-restricted antigen presentation after immune complex internalization. *J. Exp. Med.* 189, 371–380. doi: 10.1084/jem.189.2.371

Reichardt, P., Dornbach, B., Rong, S., Beissert, S., Gueler, F., Loser, K., et al. (2007). Naive B cells generate regulatory T cells in the presence of a mature immunologic synapse. *Blood* 110, 1519–1529. doi: 10.1182/blood-2006-10-053793

Riedl, J., Crevenna, A. H., Kessenbrock, K., Yu, J. H., Neukirchen, D., Bista, M., et al. (2008). Lifeact: a versatile marker to visualize F-actin. *Nat. Methods* 5, 605–607. doi: 10.1038/nmeth.1220

Riol-Blanco, L., Delgado-Martin, C., Sanchez-Sanchez, N., Alonso, C. L., Gutierrez-Lopez, M. D., Del Hoyo, G. M., et al. (2009). Immunological synapse formation inhibits, via NF-kappaB and FOXO1, the apoptosis of dendritic cells. *Nat. Immunol.* 10, 753–760. doi: 10.1038/ni.1750

Rodriguez-Fernandez, J. L., Riol-Blanco, L., and Delgado-Martin, C. (2010b). What is the function of the dendritic cell side of the immunological synapse? *Sci. Signal.* 3:re2. doi: 10.1126/scisignal.3105re2

Rodriguez-Fernandez, J. L., Riol-Blanco, L., and Delgado-Martin, C. (2010a). What is an immunological synapse? *Microbes Infect.* 12, 438–445.

Rothoeft, T., Balkow, S., Krummen, M., Beissert, S., Varga, G., Loser, K., et al. (2006). Structure and duration of contact between dendritic cells and T cells are controlled by T cell activation state. *Eur. J. Immunol.* 36, 3105–3117. doi: 10.1002/eji.200636145

Scholer, A., Hugues, S., Boissonnas, A., Fetler, L., and Amigorena, S. (2008). Intercellular adhesion molecule-1-dependent stable interactions between T cells and dendritic cells determine CD8+ T cell memory. *Immunity* 28, 258–270. doi: 10.1016/j.immuni.2007.12.016

Schonichen, A., and Geyer, M. (2010). Fifteen formins for an actin filament: a molecular view on the regulation of human formins. *Biochim. Biophys. Acta* 1803, 152–163. doi: 10.1016/j.bbamcr.2010.01.014

Shakhar, G., Lindquist, R. L., Skokos, D., Dudziak, D., Huang, J. H., Nussenzweig, M. C., et al. (2005). Stable T cell-dendritic cell interactions precede the development of both tolerance and immunity in vivo. *Nat. Immunol.* 6, 707–714. doi: 10.1038/ni1210

Shen, K., Thomas, V. K., Dustin, M. L., and Kam, L. C. (2008). Micropatterning of costimulatory ligands enhances CD4+ T cell function. *Proc. Natl. Acad. Sci. U. S. A.* 105, 7791–7796. doi: 10.1073/pnas.0710295105

Sit, S.-T., and Manser, E. (2011). Rho GTPases and their role in organizing the actin cytoskeleton. *J. Cell Sci.* 124(Pt 5), 679–683. doi: 10.1242/jcs.064964

Stoll, S., Delon, J., Brotz, T. M., and Germain, R. N. (2002). Dynamic imaging of T cell-dendritic cell interactions in lymph nodes. *Science* 296, 1873–1876. doi: 10.1126/science.1071065

Tanizaki, H., Egawa, G., Inaba, K., Honda, T., Nakajima, S., Moniaga, C. S., et al. (2010). Rho-mDia1 pathway is required for adhesion, migration, and T-cell stimulation in dendritic cells. *Blood* 116, 5875–5884. doi: 10.1182/blood-2010-01-264150

Thauland, T. J., and Parker, D. C. (2010). Diversity in immunological synapse structure. *Immunology* 131, 466–472. doi: 10.1111/j.1365-2567.2010.03366.x

Tseng, S. Y., Waite, J. C., Liu, M., Vardhana, S., and Dustin, M. L. (2008). T cell-dendritic cell immunological synapses contain TCR-dependent CD28-CD80 clusters that recruit protein kinase C theta. *J. Immunol.* 181, 4852–4863. doi: 10.4049/jimmunol.181.7.4852

Uruno, T., Zhang, P., Liu, J., Hao, J. J., and Zhan, X. (2003). Haematopoietic lineage cell-specific protein 1 (HS1) promotes actin-related protein (Arp) 2/3 complex-mediated actin polymerization. *Biochem. J.* 371(Pt 2), 485–493. doi: 10.1042/bj20021791

Verboogen, D. R., Dingjan, I., Revelo, N. H., Visser, L. J., ter Beest, M., and van den Bogaart, G. (2016). The dendritic cell side of the immunological synapse. *Biomol. Concepts* 7, 17–28. doi: 10.1515/bmc-2015-0028

Weaver, A. M., Karginov, A. V., Kinley, A. W., Weed, S. A., Li, Y., Parsons, J. T., et al. (2001). Cortactin promotes and stabilizes Arp2/3-induced actin filament network formation. *Curr. Biol.* 11, 370–374. doi: 10.1016/s0960-9822(01)00098-7

Xu, Y., Pektor, S., Balkow, S., Hemkemeyer, S. A., Liu, Z., Grobe, K., et al. (2014). Dendritic cell motility and T cell activation requires regulation of Rho-cofilin signaling by the Rho-GTPase activating protein myosin IXb. *J. Immunol.* 192, 3559–3568. doi: 10.4049/jimmunol.1300695

Yamashiro, S. (2012). Functions of fascin in dendritic cells. *Crit. Rev. Immunol.* 32, 11–21. doi: 10.1615/critrevimmunol.v32.i1.20

Ziegler, M. E., Jin, Y. P., Young, S. H., Rozengurt, E., and Reed, E. F. (2012a). HLA class I-mediated stress fiber formation requires ERK1/2 activation in the absence of an increase in intracellular Ca2+ in human aortic endothelial cells. *Am. J. Physiol. Cell Physiol.* 303, C872–C882.

Ziegler, M. E., Souda, P., Jin, Y. P., Whitelegge, J. P., and Reed, E. F. (2012b). Characterization of the endothelial cell cytoskeleton following HLA class I ligation. *PLoS One* 7:e29472. doi: 10.1371/journal.pone.0029472

Conflict of Interest: The authors declare that the research was conducted in the absence of any commercial or financial relationships that could be construed as a potential conflict of interest.

Publisher's Note: All claims expressed in this article are solely those of the authors and do not necessarily represent those of their affiliated organizations, or those of the publisher, the editors and the reviewers. Any product that may be evaluated in this article, or claim that may be made by its manufacturer, is not guaranteed or endorsed by the publisher.

Advantages of publishing in Frontiers

OPEN ACCESS
Articles are free to read for greatest visibility and readership

FAST PUBLICATION
Around 90 days from submission to decision

HIGH QUALITY PEER-REVIEW
Rigorous, collaborative, and constructive peer-review

TRANSPARENT PEER-REVIEW
Editors and reviewers acknowledged by name on published articles

Frontiers
Avenue du Tribunal-Fédéral 34
1005 Lausanne | Switzerland

Visit us: www.frontiersin.org
Contact us: frontiersin.org/about/contact

REPRODUCIBILITY OF RESEARCH
Support open data and methods to enhance research reproducibility

DIGITAL PUBLISHING
Articles designed for optimal readership across devices

FOLLOW US
@frontiersin

IMPACT METRICS
Advanced article metrics track visibility across digital media

EXTENSIVE PROMOTION
Marketing and promotion of impactful research

LOOP RESEARCH NETWORK
Our network increases your article's readership